Investigating the role of short-chain fatty acids in programming the differentiation and function of enteroendocrine L-cells

A thesis submitted to Imperial College London for the degree of Doctor of Philosophy

Aanya Vinod Hirdaramani

Section of Nutrition Research
Department of Metabolism, Digestion & Reproduction
Imperial College London

May 2024

Abstract

Enteroendocrine L-cells in the intestinal epithelium are central in initiating communication along the gut-brain axis by the secretion of the anorectic peptide hormones, Peptide YY (PYY) and Glucagon-like peptide 1 (GLP-1). Clinically, the action of these hormones has been harnessed and gut peptide hormone analogues are rising in popularity as anti-obesity therapies. However, there are outstanding limitations to these pharmacological agents, such as the incidence of associated gastrointestinal-related side effects and their inconvenient routes of administration. The G-protein coupled receptor (GPCR) Free fatty acid receptor 2 (FFAR2) has been implicated in mediating the release of GLP-1 and PYY in mouse L-cells by binding to the microbial metabolites, short chain fatty acids (SCFAs). This thesis aimed to characterise SCFA-activated signalling profiles of FFAR2 in human colonic L-cells, and the endocrine functions that these pathways underlie. Firstly, novel spatial- and context-dependent complexities to SCFA-mediated FFAR2 signalling in human L-cells were uncovered. In addition, the SCFA butyrate exerted prominent transcriptional and morphological effects of the in human L-cells which were indicative of the induction of Notch-sensitive enteroendocrine differentiation to a 'PYY-bias' phenotype. By developing a pH-sensitive fluorescent reporter system, this thesis also demonstrated an upregulatory effect of butyrate on PYY secretion at single-event resolution. The findings in this thesis also demonstrated a dependence on FFAR2-mediated activation of Gαi signalling in the SCFA-mediated effects on human L-cell enterohormone profiles and differentiation, and the use of selective receptor agonists further illuminated the functionalities of the FFAR2-Gαi axis in this system. In Notch-reporter and Lgr5-lineage tracer mouse colonic organoid cultures, butyrate modulated Notch activity and stem-cell like properties of heterogeneous populations in the intestinal epithelium. Together, the findings in this thesis uncovered novel effects of SCFAs and the SCFA-binding GPCR FFAR2 in supporting the nutrient-sensing functions and differentiation of human colonic L-cells.

Statement of originality

This thesis is an original work by the author. No part of this thesis has been submitted elsewhere for any degree or qualification. All research and writing were conducted by the author, and all sources have been cited appropriately to ensure academic integrity.

Copyright declaration

This work is licensed under Creative Commons Attribution-NonCommercial-NoDerivatives 4.0 International.

‘The copyright of this thesis rests with the author. Unless otherwise indicated, its contents are licensed under a Creative Commons Attribution-Non Commercial-No Derivatives 4.0 International Licence (CC BY-NC-ND). Under this licence, you may copy and redistribute the material in any medium or format on the condition that; you credit the author, do not use it for commercial purposes and do not distribute modified versions of the work. When reusing or sharing this work, ensure you make the licence terms clear to others by naming the licence and linking to the licence text. Please seek permission from the copyright holder for uses of this work that are not included in this licence or permitted under UK Copyright Law.’

Declaration of contributors:

The work presented in this thesis was all carried out by the author with the exceptions of collaborations listed below:

Chapter 4: All radioimmunoassays were carried out under the supervision of Professor Kevin Murphy.

Chapter 5: Cervical dislocation of mice was carried out under the supervision of Namrata Pokharel

Table of contents

Statement of originality 2

Copyright declaration 4

Declaration of contributors: 5

Awards & Publications: 9

Acknowledgements 10

List of Abbreviations 15

List Of Figures 12

List Of Tables 14

Abstract 5

1. Introduction 22

1.1 Appetite Regulation **22**
1.1.1 Central pathways of appetite regulation 22
1.1.2 Peripheral regulation of appetite 25

1.2 Obesity **32**
1.2.1 The global obesity landscape 32
1.2.2 Current and emerging anti-obesity agents 32

1.3 The Gut Microbiota & Short Chain Fatty Acids **34**
1.3.1 The gut microbiome 34
1.3.2 The production of Short Chain Fatty Acids 35
1.3.3 The functions of SCFAs 36

1.1 G-protein coupled receptors **37**
1.3.4 An overview of G-protein coupled receptors (GPCRs) 37
1.3.5 GPCR Classification & Structure 38
1.3.6 G-protein dependent signalling pathways 39
1.3.7 GPCR Activation 41
1.3.8 GPCR Desensitisation 42
1.3.9 Intracellular trafficking of GPCRs 43
1.3.10 GPCR signalling at the endomembrane 45
1.3.11 Functional diversification by GPCR endosomal signalling 48

1.4 Free Fatty Acid Receptor 2 & 3 ..... **49**
1.4.1 The Free Fatty Acid Receptor family 49
1.4.2 FFAR1 50
1.4.3 FFAR4 51
1.4.4 FFAR2 & FFAR3 52

1.5 The cellular repertoire of the intestinal epithelium **60**
1.5.1 Intestinal Stem Cell Niche 60
1.5.2 Notch in intestinal epithelial cell fate 62
1.5.3 GPCRs in the intestinal stem cell niche 65

1.6 Enteroendocrine cells **65**
1.6.1 EEC Classification & Function 65
1.6.2 EEC Differentiation 66
1.6.3 The L-cell 67
1.6.4 EEC Plasticity 71

1.7 Summary and Project Aims **73**

b) Uncover the canonical functions of SCFAs in driving acute anorectic peptide hormone release from human L-cells and the involvement of FFAR2 signalling in driving these effects. ..73

2. Materials & Methods 74

2.1 Materials 75
2.1.1 Primary Antibodies 75
2.1.2 Secondary Antibodies 75
2.1.3 Plasmids & Gene Fragments 75
2.1.4 Primers & siRNA 76
2.1.5 Inhibitors & Activators 77
2.1.6 Enzymes 78
2.1.7 Chemical Reagents 78
2.1.8 Cell Culture Reagents 79
2.1.9 Kits 80
1.1.1 Miscellaneous 80
2.1.10 Buffers and solutions 81

2.2 Methods 84
2.2.1 Intestinal Organoids 84
2.2.2 Cell line Culture 85
2.2.3 Transfections 88
2.2.4 Cloning 90
2.2.5 qPCR 92
2.2.6 Protein detection 95
2.2.7 Cell Signalling Assays 96
2.2.8 Microscopy 98
2.2.9 Immunoassays 104
2.2.10 Flow cytometry 107
2.2.11 NanoBit 108
2.2.12 Bioinformatics analysis 109
2.2.13 Statistical analysis 109

3. FFAR2 signalling and trafficking profiles activated by short chain fatty acids in human EECs 111

3.1 Introduction 112

3.2 Results 113
3.2.1 Propionate activates both human FFAR2-Gαi and -Gαq pathways in a heterologous expression system 113
3.2.2 NCI-H716 cells as a model for investigating FFAR2 signalling in human colonic L-cells 115
3.2.3 SCFAs activate heterogeneous Gαi and Gαq signalling profiles in NCI-H716 cells 116
3.2.4 SCFA-activated Gαi responses are mediated by FFAR2 in NCI-H716 cells 121
3.2.5 SCFA promote phosphorylation of ERK 1/2 in NCI-H716 cells 122
3.2.6 FFAR2 undergoes constitutive and SCFA-induced internalisation in NCI-H716 cells and FLAG-hFFAR2 HEK-293 cells *via* a dynamin-dependent mechanism 124
3.2.7 hFFAR2 demonstrates constitutive Gαq but not Gαi activity in NCI-H716 cells 127
3.2.8 SCFA-mediated FFAR2 signalling responses show differential dependence on receptor internalisation in NCI-H716 cells 128
3.2.9 Propionate-activated FFAR2 Gαi and Gαq responses are insensitive to knockdown of very early endosomal marker APPL1 in NCI-H716 cells 132
3.2.10 SCFAs encourage FFAR2 trafficking to EEs in NCI-H716 cells 134
3.2.11 Propionate promotes sustained G□q recruitment from the early endosomal compartment in NCI-H716 cells 137

3.3 Discussion 139

4. Canonical roles of short chain fatty acids in acutely driving anorectic hormone release in human EECs 148

4.1 Introduction 149

4.2 Results 150
4.2.1 SCFAs acutely stimulate GLP-1 secretion in NCI-H716 cells 150
4.2.2 FFAR2-Gαi agonist AZ 1729 stimulates acute GLP-1 release 156
4.2.3 SCFAs may not acutely stimulate PYY secretion in NCI-H716 cells 160
4.2.4 GLP-1 and PYY are poorly co-localised in NCI-H716 cells 161

4.3 Discussion 165

5. Non-canonical actions of short chain fatty acids on human EECs 171

5.1 Introduction 172

5.2 Results 174
5.2.1 SCFAs upregulate the gene expression of PYY but not GCG in human EECs 174
5.2.2 Butyrate upregulates *Pyy* expression *via* FFAR2-Gαi signalling at the plasma membrane 175
5.2.3 SCFAs appear to downregulate the gene expression of *Gcg* in human EECs in an FFAR2-independent manner 179
5.2.4 Butyrate might selectively enhance PYY secretory tone in NCI-H716 cells 181
5.2.5 Butyrate causes cells to adopt a spindle-like shape characteristic of colonic EECs 183
5.2.6 PYY granules are enriched in the cytoplasmic processes of cells chronically treated with butyrate 186
5.2.7 Chronic butyrate treatment may not stimulate secretion of intestinotrophic GLP-2 188
5.2.8 SCFAs modulate the gene expression of markers of L-cell differentiation in NCI-H716 cells 189
5.2.9 The FFAR2-Gαi agonist AZ-1729 upregulates *Pax6* expression in NCI-H716 cells 195
5.2.10 Monitoring butyrate-mediated Notch activity using Hes1-GFP mouse colonic organoids 196
5.2.11 Butyrate downregulates the expression of Lgr5 in Lgr5 lineage-tracing mouse colonic organoids 206

5.3 Discussion 208
5.3.1 NCI-H716 cells 208
5.3.2 Mouse intestinal organoid systems 219

6. Employing a pH-sensitive fluorescent biosensor of PYY secretion in human L-cells 222

6.1 Introduction 223

6.2 Results 223
6.2.1 Cloning a pH sensitive fluorescent PYY biosensor 223
6.2.2 SEP-PYY exhibits a granular structure in NCI-H716 but not HEK-293 cells 231
6.2.3 Chronic butyrate treatment upregulates the production and secretion of SEP-PYY in NCI-H716 cells 233
6.2.4 Chronic butyrate treatment stimulates SEP-PYY exocytosis observed by total internal reflection fluorescence microscopy (TIRFM) 237

6.3 Discussion 239

7. General Discussion 245

8. Appendix 254

8.1 Appendix 1. Marker genes of pre-defined Cell ontology classifications in the sc-RNAseq database 'Tabula Muris' 254

8.2 Appendix 2. Expression of candidate transcription factors from scRNA-seq datasets of the human 'Large Intestine' or 'Colon' grouped by publication 255

8.3 Appendix 3 – Expression of L-cell differentiation markers in NCI-H716 cells in suspension and following plating on extracellular matrix (ECM) substrate. 258

9. References 259

Awards & Publications:

UK Society of Endocrinology BES 2022 Best Basic Science Abstract:

Hirdaramani, A. (2022) Characterising the G-protein signalling mechanisms activated by short chain fatty acids in human enteroendocrine cells which mediate production and release of the anorectic gut hormones peptide YY (PYY) and glucagon-like peptide-1 (GLP-1). *Endocrine Abstracts*.
86 EC1.4 | DOI: 10.1530/endoabs.86.EC1.4:

£25,000 award to pursue research fellowship at Columbia University Stem Cell Initiative.

£5000 award as Imperial Dean of Medicine's Scholar 2022.
£20,000 from Flexible Talent Mobility Award by UK Biotechnology and Biological Sciences Research Council.

Literature Review published in collaboration with colleagues at Columbia University during research fellowship:

Ho J, Puoplo N, Pokharel N, Hirdaramani A, Hanyaloglu AC and Cheng C-W (2024) Nutrigenomic underpinnings of intestinal stem cells in inflammatory bowel disease and colorectal cancer development. *Frontiers of Genetics*
15:1349717. doi: 10.3389/fgene.2024.1349717

Acknowledgements

This thesis would not have come to fruition without the help of several inspirational and kind individuals.

Firstly, I would like to thank my supervisors Professor Gary Frost and Professor Aylin Hanyaloglu. Gary, your words of encouragement have been a constant driving force of my efforts throughout this project. I thank you especially for supporting every new idea I bring to the table with excitement and your invaluable knowledge in the field. Dear Aylin, you have been so much more than a supervisor to me. It has been easy to admire your work ethic, your emphasis on collaboration, and your willingness to help, always. I cannot thank you enough. I would also like to thank Dr. Chia-Wei Cheng for taking me under her wing and enabling an enriching and unforgettable placement at the Columbia Stem Cell Institute. Thank you for challenging my ideas and encouraging me to think big. I am ultimately a better scientist because of you.

To all the past and present members of the Hanyaloglu lab, thank you for making every day in the lab (even the long ones), fun. Thanks goes out in particular to Abbie and Annabelle. Abbie, you have been a mentor and big-sister to me, I am in awe of your creativity and intelligence but more importantly your ability to give world-class advice in cell culture on a Friday night. Annabelle, it has been an honour to grow together over the course of our PhDs, and I can't thank you enough for being a shoulder of support in the lab and always making me smile. To several other of my colleagues in Hammersmith Hospital, Katie, Yurui, Konstantinos, Chandler, Priya, Chiharu and Anke, thank you for putting up with my frantic questions, always offering your insight, and being there for a chat. A special thanks also goes to Claudio in IRDB for being able to fix absolutely everything, anytime, anywhere. I would also like to thank the members of the Cheng lab, Namrata and Jennifer, for being so warm and making New York feel like a second home.

To my parents, I am forever grateful for your unconditional love over these last 4 years. To my father, with your advice and support, you have consistently helped me get over the line when I need it the most. To my mother, thank you for being my rock through all the 6am starts and late-night finishes and for all the hugs. You have both made me

feel strong and put things into perspective even in the face of failure. To my darling brother Arvind, I thank you for making everything so much easier with your unparalleled humour and kindness.

Finally, to my best friend and other half, Nikhil. I don’t know where to begin. I have approached every problem with: ‘What would Nikhil do?’; I look up to your intelligence, your creativity and determination. I knew I had met my person when I compared the length of our ‘to-do’ lists. This thesis quite literally couldn’t have come to life without your kindness, love and understanding. Thank you, for everything.

List Of Figures

Figure 1.1 Schematic of central and peripheral pathways of appetite regulation. 24
Figure 1.2 Schematic of the simplified structure of a GPCR. 38
Figure 1.3 Canonical G-protein-dependent signalling pathways induced by GPCR activation. 41
Figure 1.4 Schematic of the canonical life-cycle of a GPCR. 44
Figure 1.5 Snake plot of FFAR2 and FFAR3 highlighting key residues in facilitating SCFA binding. 58
Figure 1.6 The architecture and cellular heterogeneity of the human intestinal colonic crypt 62
Figure 1.7 Lateral Inhibition by Notch in ISCs and TA cells. 64
Figure 1.8 Classical molecular mechanisms of peptide hormone secretion from EECs which are modulated by nutrient sensing GPCRs. 69
Figure 2.1 Basal cAMP levels vary with passage number in NCI-H716 cells. 87
Figure 2.2 Optimisation of siRNA knockdown of APPL1 in NCI-H716 cells. 89
Figure 2.3 Validation of primers for detection of human FFAR2 expression by qPCR melt curve analysis 94
Figure 2.4 Creating binary masks that were representative of cellular outlines on ImageJ. 101
Figure 2.5 Quantification of fluorescence in HES1-GFP organoids by ImageJ. 103
Figure 3.1 Propionate activates Gαi and Gαq signalling in HEK-293 cells transiently transfected with FLAG-hFFAR2. 115
Figure 3.2 The human colonic NCI-H716 cell line express nutrient-sensing machinery and hormone products characteristic of L-cells. 116
Figure 3.3 SCFAs activate Gαi signalling in NCI-H716 cells in a concentration dependent manner. 117
Figure 3.4 SCFAs activate Gαq signalling in NCI-H716 cells. 119
Figure 3.5 FFAR2 mediates SCFA-activated Gαi signalling in NCI-H716 cells. 122
Figure 3.6 SCFAs promote phosphorylation of ERK 1/2 in NCI-H716 cells. 123
Figure 3.7 FFAR2 undergoes both constitutive and SCFA-induced dynamin-dependent endocytosis in NCI-H716 cells and HEK-293 cells transiently transfected HEK-293 cells. 127
Figure 3.8 hFFAR2 exhibits basal Gαq but not Gαi activity in NCI-H716 cells. 127
Figure 3.9 SCFA-mediated signalling responses show differential dependencies on receptor internalisation in NCI-H716 cells. 129
Figure 3.10 Propionate-activated Gαi and Gαq signalling in HEK-293 cells transiently transfected FLAG-hFFAR2 cells are restricted to the plasma membrane. 131
Figure 3.11 SCFA-activated Gαi and Gαq signalling responses appear to be insensitive to knockdown of very early endosomal marker APPL1. 133
Figure 3.12 Acetate and propionate drive FFAR2 internalisation to early endosomes in NCI-H716 cells. 137
Figure 3.13 Propionate activates sustained Gαq responses localised to the early endosome in NCI-H716 cells. 138
Figure 4.1 Basal and ligand-induced acute GLP-1 secretion by NCI-H716 cells may be affected by glucose content of secretion buffer and culturing media. 154
Figure 4.2 SCFAs acutely stimulate GLP-1 secretion in NCI-H716 cells. 155

Figure 4.3 AZ-1729 is an allosteric FFAR2-Gαi agonist and GLP-1 secretagogue in NCI-H716 cells. 157
Figure 4.4 Propionate may acutely stimulate GLP-1 release in a Gαi-dependent manner in NCI-H716 cells. 160
Figure 4.5 SCFAs may not acutely stimulate PYY secretion in NCI-H716 cells 161
Figure 4.6 GLP-1 and PYY poorly co-localise in NCI-H716 cells. 164
Figure 5.1 Chronic SCFA treatments affect the expression of *Gcg* and *Pyy* in NCI-H716 cells. 175
Figure 5.2 Butyrate upregulates *Pyy* expression *via* activation of a FFAR2-Gαi pathway at the plasma membrane. 177
Figure 5.3 The biased FFAR2-Gαiactivator AZ-1729 enhances the effect of butyrate on *Pyy* expression. 179
Figure 5.4 SCFAs appears to downregulate *Gcg* expression in an FFAR2-independent manner. 180
Figure 5.5 Chronic SCFA treatments may induce distinct effects on PYY and GLP-1 production and secretion. 182
Figure 5.6 Chronic incubation with propionate and butyrate cause unique morphological changes characteristic of colonic L-cells. 184
Figure 5.7 Chronic incubation with butyrate increase cell area and feret diameter. 186
Figure 5.8 PYY granules are enriched in the cytoplasmic processes of cells chronically treated with butyrate. 187
Figure 5.9 Chronic SCFA treatments may not affect GLP-2 secretion 188
Figure 5.10 Chronic butyrate treatment affects the expression of L-cell differentiation markers. 192
Figure 5.11 Butyrate upregulates the gene expression of *Lgr5* in NCI-H716 cells. 194
Figure 5.12 AZ-1729 upregulates the gene expression of *Pax6* but not *NeuroD1* in NCI-H716 cells. 195
Figure 5.13 Employing a Hes1-GFP reporter mouse model. 199
Figure 5.14 A ɣ-secretase inhibitor diminished GFP fluorescence in Hes1-GFP reporter mice. 200
Figure 5.15 Butyrate modulates the GFP fluorescence and area of Hes1-GFP cystic organoids. 203
Figure 5.16 Butyrate downregulates the GFP fluorescence of budding Hes1-GFP organoids in a time-dependent manner. 205
Figure 5.17 Butyrate appears to upregulate the expression of PYY in mouse Hes1-GFP colonic organoids.. 206
Figure 5.18 Butyrate decreases the abundance of Lgr5+ cells in cystic organoids. 207
Figure 5.19 Schematic illustrating potential FFAR2-independent and FFAR2-Gαi-dependent pathways underlying butyrate's effects on the maturation and endocrine function of human L-cells based on findings in NCI-H716 cells. 217
Figure 6.1 Schematic of post-translational processing cascade of PYY in EECs. . 226
Figure 6.2 In silico structural predictions of SEP-PYY by AlphaFold2 50) (*yellow).* 227
Figure 6.3 Structures of human PYY(1-36) and SEP-PYY visualised on PyMOL. . 229
Figure 6.4 *In silico* predictions of signal peptide cleavage sites in endogenous preproPYY and SEP-PYY by SignalP5.0. 230
Figure 6.5 SEP-PYY may be packaged into secretory granules in NCI-H716 but not HEK-293 cells.. 233
Figure 6.6 Chronic butyrate treatment enhances the production of SEP-PYY in NCI-H716 cells. 234

Figure 6.7 Chronic butyrate treatment promotes SEP-PYY secretion in NCI-H716 cells. 236
Figure 6.8 Visualisation of SEP-PYY exocytosis with single event resolution by TIR-FM. 239

List Of Tables

Table 3.1 pIC50 and pEC50 values of SCFAs in NCI-H716 cells. 120
Table 4.1 Culturing conditions used for 24 hours prior to assaying and secretion buffer used to measure GLP-1 in NCI-H716 cell supernatants by RIA. 151
Table 4.2 pIC50 values of SCFA concentration-responses in the presence of 1μM AZ-1729 or DMSO vehicle NCI-H716 cells. 158

List of Abbreviations

3D	Three-Dimensional
Å	Angstrom
ADRA2	α-2 Adrenergic receptor
ADRA1A	α-1A Adrenergic Receptor
AgRP	Agouti-related peptide
AI	Artificial Intelligence
ANOVA	Analysis of Variance
APPL1	Adaptor protein, Phosphotyrosine interacting with Pleckstrin homology Domain and Leucine Zipper 1
ARC	Arcuate Nucleus
ARX	Aristaless related homeobox gene
ATM	Adipose Tissue Macrophage
ATOH1	Atonal bHLH transcription factor 1
AUC	Area under the curve
BBB	Blood-brain Barrier
bHLH	Basic Helix-Loop-Helix
BMI	Body Mass Index
BMP	Bone morphogenetic protein
BRET	Bioluminescence Resonance Energy Transfer
C2	Acetate
C3	Propionate
C4	Butyrate
CAAX	CAAX motif
cAMP	Cyclic adenosine monophosphate
CART	Cocaine-and-Amphetamine-Regulated Transcript
CBC	Crypt Base Columnar Cells
CCK	Cholecystokinin
CD	Crohn's Disease
cDNA	Complementary DNA
CGPR	Calcitonin Gene-Related Peptide Receptor

ChgA Chromogranin A

CNS Central Nervous System

COOH C-terminus

CRC Colorectal Cancer

CRISPR/Cas9
Clustered Regularly Interspaced Short Palindromic Repeats and CRISPR-associated protein 9

DC Dendritic Cells

DCS Deep Crypt Secretory Cells

DH5α Escherichia coli strain DH5α

DMH Dorsomedial Hypothalamus

DMSO Dimethyl Sulfoxide

Dnase I Deoxyribonuclease I

DOPr Delta-Opioid Receptor

DPP IV Dipeptidyl-peptidase 4

EC Epithelial Cells

ECL Extracellular loop

ECM Extracellular Matrix

EE Early Endosome

EEA1 Early Endosomal Antigen 1

EEC Enteroendocrine cell

EGF Epidermal growth factor

EIF4F Eukaryotic Initiation Factor 4F

ELISA Enzyme-linked immunosorbent assay

EM Electron Microscopy

ENR Epidermal growth factor, Noggin, R-spondin

ERK Extracellular signal-Regulated Kinase

FFAR Free Fatty Acid Receptor

FFAR2 Free Fatty Acid Receptor 2

FFAR4 Free Fatty Acid Receptor 4

FIG Forskolin, IBMX, and Glucose

FMRI Functional MRI

FP Fluorescent protein

FSHR Follicle-Stimulating Hormone Receptor

FSK	Forskolin
FVYE	FYVE zinc finger domain
GABA	ɣ-aminobutyric acid
GCG	Glucagon
GFP	Green fluorescent protein
GHS-R	Growth Hormone Secretagogue Receptor
GI	Gastrointestinal
GLP-1	Glucagon-like peptide 1
GLP-2	Glucagon-like peptide 2
GLP1-RA	Glucagon-Like Peptide 1 Receptor Agonist
GPBAR1	G protein-coupled bile acid receptor 1
GPCR	G protein-coupled receptor
GPR109A	G Protein-Coupled Receptor 109A
GPR119	G Protein-Coupled Receptor 119
GPR142	G Protein-Coupled Receptor 142
GPR43	G protein-coupled receptor 43
GPR84	G Protein-Coupled Receptor 84
GSIS	Glucose-Stimulated Insulin Secretion
GTPase	Guanosine Triphosphatase
HDAC	Histone Deacetylase
HDACi	HDAC inhibitor
HEK-293	Human Embryonic Kidney 293 cell line
HF-DIO	High fat-diet induced obesity
HFD	High Fat Diet
hFFAR2	Human Free Fatty Acid Receptor 2
hTAS2R50	Human Taste Receptor Type 2 Member 50
HTRF	Homogeneous time-resolved fluorescence
IBD	Inflammatory Bowel Disease
IBS	Irritable Bowel Syndrome
ICL	Intracellular loop
IE-IGF-1R	Intestinal Epithelial Insulin-like Growth Factor 1 Receptor
IEC	Intestinal Epithelial Cells
IGF-1	Insulin-like Growth Factor 1
IHC	Immunohistochemistry

IP1	Inositol monophosphate
IP3	Inositol trisphosphate
iPE	Inulin-Propionate Ester
iPSC	Induced Pluripotent Stem Cells
IR	Insulin Receptor
ISC	Intestinal Stem Cell
KB	Krebs-Ringer Buffer
LCFA	Long Chain Fatty Acid
LEPR	Leptin Receptor
LG	Low-Glucose DMEM
Lgbit	Large BiT fragment
LGR5	Leucine-Rich Repeat-Containing G Protein-Coupled Receptor 5
LH	Lateral Hypothalamus
LHR	Luteinizing Hormone Receptor
M	Molar
MAPK	Mitogen-Activated Protein Kinase
MCFA	Medium Chain Fatty Acid
MCR3/4	Melanocortin 3 and 4 Receptor
ME	Median Eminence
MFI	Mean Fluorescence Intensity
mg	Milligram
ml	Millilitre
mM	Millimolar
MSH	Melanocyte Stimulating Hormone
MVB	Multivesicular Body
NAC	N-acetyl-L-cysteine
NAc	Nucleus Accumbens
Nanobit	NanoLuc Binary Technology
NCI-H716	Colorectal Adenocarcinoma cell line
NDC	Non-Digestible Carbohydrate
NEUROD1	Neurogenic differentiation 1
NEUROG3	Neurogenin 3
NF-κB	Nuclear factor kappa-light-chain-enhancer of activated B cells
NH2	N-terminus

NICD	Notch Intracellular Domain
NK1R	Neurokinin 1 receptor
NLuc	NanoLuc
ng	Nanogram
nl	Nanolitre
nm	Nanometre
nM	Nanomolar
NMR	Nuclear Magnetic Resonance
NPY	Neuropeptide Y
NTS	Nucleus Tractus Solitarius
OR51E1	Olfactory Receptor 51E1
OR51E2	Olfactory Receptor 51E2
ORF	Open reading frame
OXM	Oxyntomodulin
PAE	Predicted Aligned Error
PAM	Peptidylglycine-a-amidating Monooxygenase
PAR2	Protease-activated Receptor 2
PAX4	Paired box 4 gene
PAX6	Paired Box 6 gene
PC 1/3	Prohormone Convertase 1/3
PCR	Polymerase chain reaction
PDB	Protein Data Bank
pEC50	Negative logarithm of the half maximal effective concentration
PFC	Prefrontal Cortex
pIC50	Negative logarithm of the half maximal inhibitory concentration
pKa	Acid Dissociation Constant
PKD	Protein Kinase D
pLDDT	Predicted Local Distance Difference Test
pmol	Picomole
pM	Picomolar
POMC	Pro-opiomelanocortin
PP	Pancreatic Polypeptide
PP family	Pancreatic Polypeptide Family

PP-fold	Pancreatic Polypeptide Fold
PPG	Preproglucagon
preproPYY	Prepropeptide of Human PYY
PTX	Pertussis Toxin
PVN	Paraventricular Nucleus
PYY	Peptide YY
qPCR	Quantitative Polymerase Chain Reaction
R-spondin	R-spondin protein
RA	Receptor agonist
RBP	Recombinant Binding Protein
RFP	Red Fluorescent Protein
RIA	Radioimmunoassay
RIPA	Radioimmunoprecipitation assay
RP	RPMI-1640
RPL12	Ribosomal protein L12
RT	Reverse Transcriptase
RYGB	Roux-en-Y Gastric Bypass
sc-RNAseq	Single-Cell RNA Sequencing
SCFA	Short Chain Fatty Acid
scRNAseq	Single-cell RNA sequencing
Sct	Secretin
SEM	Standard Error of the Mean
SEP	Super-Ecliptic Phluorin
SEP-LHR	SEP-Tagged Luteinizing Hormone Receptor
SEP-PYY	SEP-Tagged Peptide YY
siAPPL1	Small interfering RNA targeting APPL1
siRNA	Small Interfering RNA
Smbit	Small BiT fragment
SNARE	Soluble N-ethylmaleimide-sensitive factor activating protein receptor
SPase	Signal Peptidase
STC-1	Secretin Tumor cell line
T1R2/T1R3	Sweet Taste Receptor
T2D	Type 2 diabetes
TA	Transit Amplifying

TAS2R	Taste Receptor Type 2
TF	Transcription factor
TIRF	Total Internal Reflection Fluorescence
TIR-FM	TIRF Microscopy
tPA	Tissue-Plasminogen Activator
Treg	Regulatory T Cells
TRPC	Transient Receptor Potential Canonical channel
V2R	Vasopressin receptor 2
VEE	Very Early Endosome
VIPR	Vasoactive intestinal peptide receptor
VMH	Ventromedial Hypothalamus
VTA	Ventral Tegmental Area
Y1R	Neuropeptide Y receptor Y1
Y2R	Neuropeptide Y receptor Y2
β1AR	β-1 adrenergic receptor
β2AR	β-2 adrenergic receptor
β-OHB	Beta-Hydroxybutyrate
µg	Microgram
µl	Microlitre
µm	Micrometre
µM	Micromolar

1. Introduction

1.1 Appetite Regulation

1.1.1 Central pathways of appetite regulation

Our feelings of hunger and satiety are orchestrated by complex homeostatic and hedonistic neuronal circuits that are responsive to organism nutritional and metabolic status behaviours (Cummings & Overduin, 2007). The vagus nerve, the longest of the twelve cranial nerves, is a pivotal usher to the extensive neuroendocrine communicative pathways between the brain and the gastrointestinal (GI) tract (Berthoud & Neuhuber, 2000). Vagal sensory neurons densely innervate the mucosal and submucosal layers of the digestive tract and afferent endings host diverse repertoires of receptors involved in sensing mechanical and chemical cues associated with ingestion and digestion (Williams et al., 2016). Such peripheral stimuli are converted to vagus nerve signals that are primarily received by the nucleus tractus solitarus (NTS) (*Figure 1.1)* (Cummings & Overduin, 2007). The NTS ultimately relays this information to higher forebrain centers where signals are integrated to effect involuntary and voluntary eating behaviours (Cummings & Overduin, 2007). Briefly, brain to gut communication is transmitted by efferent fibres of hindbrain neurons, and links cognitive and emotional centres in the brain to peripheral motor, endocrine and immune functions in the GI tract (Carabotti et al., 2015).

The hypothalamus is classically considered the central hub for the CNS-dependent regulation of energy homeostasis and food intake (Elmquist et al., 1999). In numerous pioneering studies, a variety of aberrant and contrasting bodyweight and feeding phenotypes were observed by lesions affecting specific hypothalamic nuclei (Elmquist et al., 1999). Amongst these nuclei, the arcuate nucleus (ARC) in particular, exerts executive effects on satiety and hunger *via* the action of two functionally antagonistic neuronal populations in the central melanocortin pathway (Timper & Brüning, 2017) (*Figure 1.1)*. Activation of the anorexigenic pro-opiomelanocortin (POMC) and

cocaine-and-amphetamine-regulated transcript (CART) -expressing (POMC/CART) neurons or orexigenic agouti-related peptide (AgRP)-expressing and neuropeptide Y (NPY) -expressing neurons, identified as AgRP/NPY neurons, stimulates a decrease or an increase in food intake (Balthasar et al., 2005; Gropp et al., 2005).

Following nutrient ingestion, POMC/CART neurons are stimulated and the POMC precursor polypeptide is cleaved to α-melanocyte stimulating hormone (α-MSH). α-MSH activates melanocortin 3 and 4 (MCR3/4) receptors on second-order neurons, particularly neurons in the paraventricular nucleus (PVN) but also in the dorsomedial hypothalamus (DMH), the lateral hypothalamus (LH) and the ventromedial hypothalamus (VMH) (*Figure 1.1)* (Millington, 2007). Importantly, several loss-of-function variants of human MCR4 are associated with higher obesity risk (Wen et al., 2022; Farooqi et al., 2000). The ARC is proximal to the median eminence (ME), a circumventricular organ that enables the facilitated diffusion of nutrients and hormonal signals *via* fenestrated capillaries and their direct sensing by POMC/CART neurons (Cone et al., 2001). As such, POMC/CART neurons integrate both peripheral and central inputs in the post-prandial state to provide an appropriate feedback response. In contrast, AgRP/NPY neurons are acutely activated by caloric need and promote food intake by the co-release of NPY and AgRP. NPY stimulates hunger predominantly by activation of Y1 and Y5 receptors on neurons in the PVN and LH (*Figure 1.1)* (Zhang et al., 2011). The neuropeptide AgRP behaves as both an inverse agonist of MC3/4R, thereby overriding the orexigenic effects of α-MSH, and direct antagonist of POMC/CART neurons via inhibitory Ɣ-aminobutyric acid (GABA)-ergic action (Tong et al., 2008; Breit et al., 2006).

There is increasing evidence demonstrating the contribution of dopaminergic reward-related circuitry to the hedonic control of food intake, particularly in the motivation to consume 'hyper-palatable' foods even after energy requirements have been met (Baik, 2021). Dopaminergic neurons originating in the ventral tegmental area (VTA) project onto both mesolimbic and mesocortical pathways, innervating brain regions such as the nucleus accumbens (NAc) and the prefrontal cortex (PFC) (Baik, 2021). Functional MRI (fMRI) studies have demonstrated a positive correlation in the postprandial activation of dopaminergic reward-related regions of the brain and the caloric intake

of food (De Silva et al., 2012). In addition, given that the activity of this reward circuity is highly responsive to neuroendocrine modulators of food intake, dopaminergic-mediated hedonic feeding behaviours might have amplifying or inhibiting effects on hypothalamic-mediated involuntary feeding behaviours (Baik, 2021; De Silva et al., 2012).

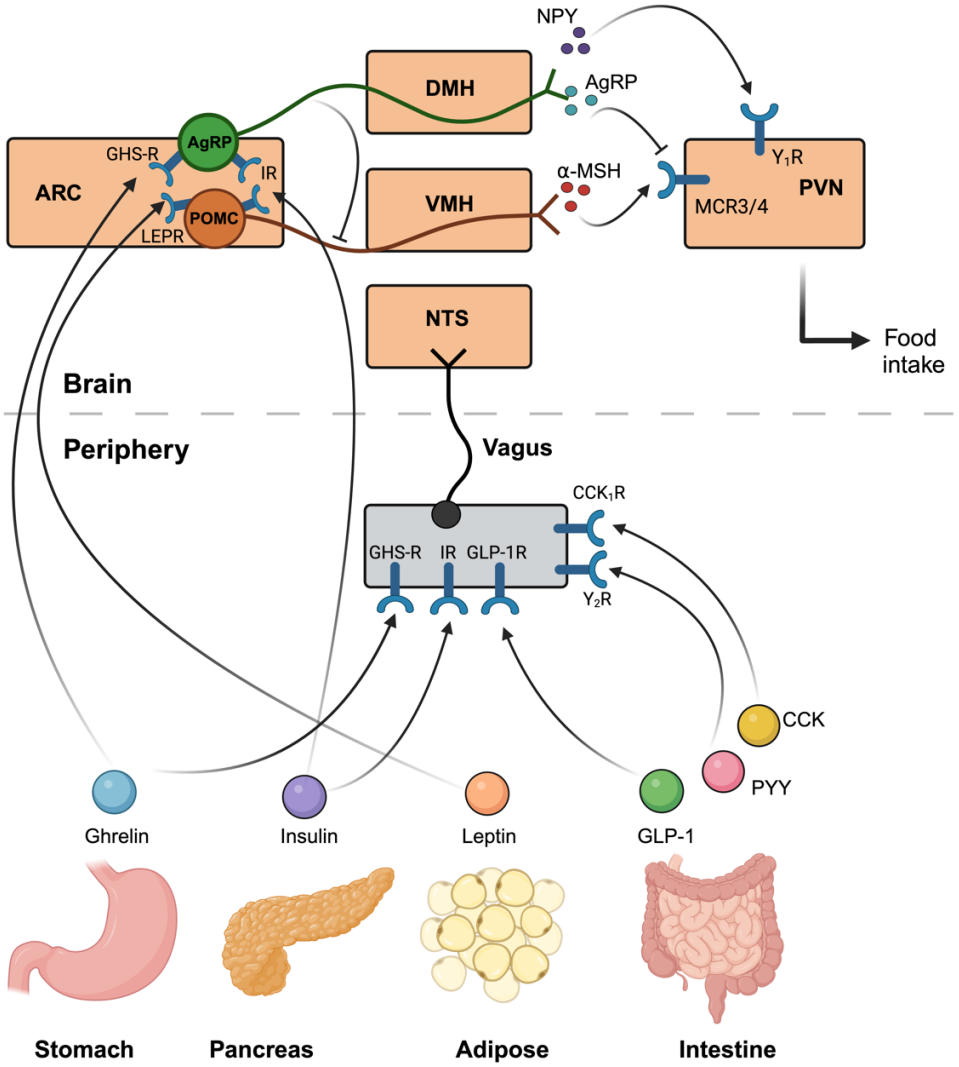


Figure 1.1 Schematic of central and peripheral pathways of appetite regulation. Schematic representation of the actions of endocrine and neural pathways along the gut-brain axis in regulating appetite and energy expenditure. Peripheral organs secrete metabolically active hormones; ghrelin is derived from the stomach, insulin from the pancreas, leptin from adipose tissue, and glucagon-like peptide 1 (GLP-1), peptide YY (PYY) and cholecystokinin (CCK) from the intestine. These hormones interact with their cognate receptors on vagal afferent nerve endings, which transduces these stimuli to the nucleus of the solitary tract (NTS) in the hindbrain, which relays these signals to higher brain centres. Some peripheral signals

such as ghrelin, leptin and insulin are able to cross the blood-brain barrier and directly bind to receptors on hypothalamic neurons. In the hypothalamus, the arcuate nucleus (ARC) contains two functionally antagonistic neuronal populations that are central to appetite regulation and energy homeostasis; cocaine-and-amphetamine-regulated transcript (CART)-expressing (POMC/CART) neurons and agouti-related peptide (AgRP)-expressing and neuropeptide Y (NPY) -expressing neurons. These neurons project onto hypothalamic nuclei such as dorosomedial nucleus of the nucleus (DMH), the ventromedial nucleus of the hypothalamus (VMH) and the paraventricular nucleus (PVN). POMC/CART produce α-melanocyte stimulating hormone (α-MSH), whereas AgRP/NPY neurons produce agouti-related peptide (AgRP) and neuropeptide Y (NPY). Hypothalamic centres integrate signals derived from POMC/CART and AgRP/NPY neuronal populations to regulate food intake and expenditure.

1.1.2 Peripheral regulation of appetite

Acute and chronic changes in energy balance are conveyed to the aforementioned central homeostatic apparatuses by the action of peripherally derived peptide hormones (*Figure 1.1)* (Cummings & Overduin, 2007). Scattered across the gastrointestinal epithelium are specialised peptide hormone-secreting cells known as enteroendocrine cells (EECs). EEC-mediated hormone release is orchestrated by nutrient-sensing receptors and transporters localised to EEC membrane domains that are highly responsive to luminal and circulating nutrient stimuli (Latorre et al., 2016). Outside of the GI tract, the peptide hormones insulin and leptin, produced by pancreatic β-cells and adipocytes respectively, relay nutrient-related information to integrative CNS mechanisms (Wachsmuth, Weninger & Duca, 2022).

1.1.2.1 Insulin

Insulin is a peptide hormone produced from pancreatic β-cells in the islets of Langerhans, that works in conjunction with glucagon to tightly circulating glucose levels (Petersen & Shulman, 2018). Following food intake, insulin promotes the uptake and utilisation of blood glucose into peripheral tissues and inhibits hepatic gluconeogenesis (Petersen & Shulman, 2018). Moreover, multiple lines of evidence from mice and non-human primates demonstrated that insulin is able to promote satiety by crossing the blood-brain barrier (BBB) and influencing central feeding

neurocircuitry (Woods et al., 1979; Scherer et al., 2021). The insulin receptor (IR) is widely distributed across neuronal and non-neuronal populations in the mammalian brain, and the specific ablation of IR in the brain of mice has promoted overeating and the development of obesity in parallel with systemic insulin resistance (Brüning et al., 2000; Scherer, Sakamoto & Buettner, 2021; Schulingkamp et al., 2000). Insulin receptor signalling in mice hypothalamic astrocytes has been shown to link glucose uptake in the CNS with systemic glucose homeostasis *in vivo* (García-Cáceres et al., 2016). Neuroimaging techniques have related impaired insulin signalling *i.e.* insulin resistance in the brain to contribute to the pathophysiology of obesity and type 2 diabetes (T2D) as well as in cognitive disturbances (Kullmann et al., 2016).

1.1.2.2 Leptin

Leptin is an adipocyte-derived hormone encoded by a gene named *obese (ob),* owing to its relevance to long-term body weight regulation (Zhang et al., 1994). Leptin is primarily secreted by white adipose tissue and behaves as a peripheral reporter of body fat status to central melanocortin pathways (Elias et al., 1999). Serum levels of leptin are positively correlated with adipocyte size and lipid content, constructing an important negative feedback mechanism between food intake and body mass (Obradovic et al., 2021). The leptin receptor (LEPR) is expressed POMC hypothalamic neurons, and its activation by leptin leads to the inhibition of AgRP circuitry, inducing satiety (Elias et al., 1999)**.** Numerous mutations in both leptin and LEPR have been associated with hyperphagia and clinical phenotypes of early-onset obesity (Pigeyre et al., 2016; Clément et al., 1998)**.**

1.1.2.3 Ghrelin

Ghrelin is a peptide hormone secreted by the gastric EEC subtype known as P/D1 cells (equivalent to X/A-like cells in rats) that stimulates hunger and the release of growth hormone (Müller et al., 2015). P/D1 cells are found largely in the fundus of the stomach and produce ghrelin under conditions associated with negative energy balance *i.e* in the fasting or long-term calorie restriction (Inui et al., 2004)**.** Ghrelin crosses the BBB and primarily activates hypothalamic AgRP/NPY neurons which

express its cognate receptor, Growth Hormone Secretagogue Receptor (GHS-R) (Sun et al., 2004). In humans, intravenous ghrelin administration has previously been shown to increase hunger by influencing the responsiveness of hypothalamic regions as well as extra-hypothalamic reward circuitry (Müller et al., 2015). Ghrelin levels are inversely proportional to BMI and obesity is associated with both reduced ghrelin levels and impaired AgRP/NPY neuron responses to ghrelin in humans and mice (Cui, López & Rahmouni, 2017). Interestingly, CNS-mediated ghrelin resistance has also been observed in eating disorders, as ghrelin-brain activity relationships have been shown to be dampened in in patients with *anorexia nervosa* despite high circulating ghrelin levels (Müller et al., 2015). The preproghrelin gene from which ghrelin is derived, additionally encodes for the peptide obestatin (Müller et al., 2015). Obestatin has been implicated as the antagonistic 'sibling' of ghrelin, with *in vivo* rodent studies reporting suppressive effects of obestatin on appetite and weight gain (Villarreal et al., 2022). However, much is yet to be understood about the function of obestatin in humans.

1.1.2.4 CCK

Cholecystokinin (CCK) is secreted by the EEC I-cell subtype that line the mucosa of the duodenum and jejunum, as well as central and peripheral neurons (Liddle, 1997; Buffa et al., 1976). Circulating CCK levels are rapidly increased within 15 minutes after a meal and can remain elevated for up to 5 hours, with the primary stimulators of CCK secretion being the digested products of dietary fat and protein (Chaudhri, Small & Bloom, 2006). CCK acts acutely to suppress appetite a postprandially by the activation of POMC/CART hypothalamic circuitry, relying on its paracrine interactions with CCK receptors on vagal afferent fibres in the small intestine in addition to direct activation of CCK receptors in the brain (Raybould, 2007). CCK activation of peripheral vagal afferents has also been coupled to the discharge of vagal efferent fibres and enteric neurons that regulate digestive processes in the gut (Sternini et al., 1999). In both humans and rodents, CCK has been shown to regulate digestion by stimulating contractions of the pyloric sphincter, as well as the production of hepatic bile and pancreatic hydrolases (Chaudhri, Small & Bloom, 2006).

1.1.2.5 Proglucagon-derived peptides: GLP-1

GLP-1 is a peptide hormone secreted by the EEC L-cell subtype in the ileum and colon (Spreckley & Murphy, 2015). GLP-1 is encoded by the preproglucagon (GCG) gene, and GCG-expressing L-cells density increases distally along the gut and are most abundant in ileum and the proximal colon (Larsson et al, 1975; Bryant et al, 1983; Eissele et al, 1992; Gribble & Reimann, 2019; Burclaff et al., 2022). Within intestinal L-cells, post-translationally processing of the proglucagon peptide by prohormone convertase 1/3 (PC1/3) liberates GLP-1, oxyntomodulin (OXM), glucagon-like peptide 2 (GLP-2), and glicentin. L-cell mediated secretion of GLP-1 is stimulated in response to feeding in a biphasic pattern of release: the first peak appears within 10 to 15 minutes after eating, and the latter and larger peak occurs at 90-120 mins (Müller et al., 2019).

A predominant role of GLP-1 is as an incretin, augmenting pancreatic secretion of insulin postprandially *via* its cognate GLP receptor (GLP-R) on β-cells (Mojsov et al., 1987; Holst et al., 1987). GLP-1 also improves postprandial glucose responses by inhibition of gastric emptying and motility, thereby decelerating the rate at which blood glucose enters the circulation (Müller et al., 2019).

GLP1-R is also expressed on vagal afferent neurons (VANs) that terminate in proximity to L-cells in the lamina propria of the gut mucosa, and knockdown of VAN-specific GLP-R *in vivo* has been shown to disrupt the satiating effects of peripherally administered GLP-1 (Krieger et al., 2016). In addition, extensive *in vivo* studies employing pharmacological and genetic manipulations of neuronal populations in the mouse brain have shown GLP-1 to promote satiety by the activation of both anorexigenic hypothalamic POMC/CART circuitry and mesolimbic reward centres (Trapp & Brierley, 2022). GLP-1R expression in the brain spans across multiple hypothalamic regions including the PVN, the DMH, and the AN and is highly conserved between rodents and primates (Merchenthaler et al., 1999; Heppner et al., 2015). GLP-1R activity in the brain has also been implicated in important neuroprotective pathways in mouse models of Parkinson's and Alzheimer's disease, including enhancing learning and memory by stimulating hippocampal synaptic plasticity,

promoting neurogenesis and survival, and attenuating neuroinflammation (Diz-Chaves et al., 2022).

However, L-cell derived GLP-1 is unlikely to exert profound effects on brain GLP-1R activity independent of vagus activation due to the rapid degradation of GLP-1 in the circulation by the ubiquitous blood-borne enzyme dipeptidyl-peptidase 4 (DPP IV) (Mentlein, 1999). Over half of the secreted GLP-1 pool is degraded before it reaches the hepatic portal vein, and less than 20% exits the liver (Mentlein, 1999). As early as 1988, GLP-1 was shown to be synthesised in the CNS itself, deriving from preproglucagon (PPG) neurons located mainly in the NTS of the brainstem (Jin et al., 1988; Williams, 2022). Although PPG axons innervate hypothalamic feeding centres, ablation of NTS-PGG neurons in the mice brain has been shown to significantly affect the regulation of food intake and blood glucose only during psychogenic stress and large meals, but not under physiological conditions (Holt et al., 2019). As such, the activity of brain-derived GLP-1 is suggested to operate secondary to peripheral GLP-1 in response to food intake but may be important in managing satiety and glycaemic control in the stressed brain (Holt et al., 2019).

1.1.2.6 Proglucagon-derived peptides: OXM & GLP-2

Apart from GLP-1, the post-translation processing of proglucagon in L-cells by prohormone convertase (PC 1/3) gives rise to other bioactive products including oxyntomodulin (OXM) and glucagon-like peptide 2 (GLP-2) (Spreckley & Murphy, 2015).

OXM is secreted in response to nutrient intake and activates both glucagon receptors (GCGRs) and GLP-1Rs with equal potency (Pocai, 2012). Like GLP-1, OXM has anorexigenic effects, and administration of OXM has reduced *ad libitum* caloric intake of both normal-weight and obese individuals by up to 27% (Cohen et al., 2003; Wynne et al., 2005). The dual agonism of GCGRs and GLP-1Rs by OXM has stirred dubiousness in potential GLP-1-like incretin effects, however some studies have

observed OXM administration to augment insulin secretion in T2D patients (Shankar et al., 2018).

GLP-2 exerts distinct functions to both GLP-1 and OXM, primarily functioning as an intestinotrophic factor along crypt-villus axes in the colon (Drucker et al., 1996). GLP-2 has been shown to support both healthy intestinal barrier function as well as post-injury repair *in vivo* b*y* stimulating the proliferation of crypt cells, suppressing inflammatory cytokine production, enhancing intestinal blood flow, and upregulating tight-junction proteins (Dong et al., 2014; Guan et al., 2006; Brubaker et al., 1997; Drucker et al., 1996; Qi et al., 2015). Some lines of *in vitro* and *in vivo* evidence implicate GLP-2 in the regulation of appetite *via* hypothalamic neurons in mice, however intravenous GLP-2 has not affected hunger levels in humans (Dalvi & Belsham, 2012; Dong et al., 2014; Lovshin et al., 2001; Schmidt et al., 2003).

1.1.2.7 PYY

PYY is an anorexigenic hormone secreted largely by enteroendocrine L-cells in the colonic epithelium, however a fraction of PYY is found in L-cells of the oesophagus, stomach and small intestine (Karra et al, 2009). PYY secretion is stimulated in response to food intake, and increases proportionally with caloric load (Adrian et al., 1985). Circulating PYY levels reaches maximal concentrations post prandially within 60-120 minutes and remains elevated for up to 5 hours (Adrian et al., 1985). PYY, is part of the structurally related pancreatic polypeptide (PP) family, alongside the peptides NPY and PP, which exert their biological actions *via* centrally and peripherally expressed NPY receptors (Ballantyne, 2006).

PYY circulates in two forms which exert biologically distinct effects on metabolism. These are PYY (1-36), and a truncated predominant form called PYY (3-36) which is derived by DPP IV cleavage (Mentlein, 1999). PYY (1-36) targets four NPY receptor subtypes (Y1, Y2, Y4, Y5), whereas N-terminally truncated PYY(3-36) exhibits high affinity for the Y2 subtype (Cabrele & Beck-Sickinger, 2000). Peripheral administration of the PYY(3-36) form to humans has been observed to successfully reduce *ad libitum* food and increase satiety in both fasted and postprandial conditions (Batterham et al.,

2002). fMRI has mapped the satiating effects of PYY(3-36) in humans to neural activity in homeostatic hypothalamic areas, as well as mescorticolimbic reward centres (Batterham et al., 2007). Peripheral PYY crosses the BBB, and PYY-mediated activation of central Y2 receptors (Y2R) in the arcuate nucleus as well as vagal Y2Rs in the periphery have been linked to observed reductions in feeding (Koda et al., 2005; Nonaka et al., 2003). Interestingly, the anorexigenic effects of PYY(3-36) in rodents have been mechanistically associated with the inhibition of hypothalamic AgRP/NPY neurons, rather than the activation of POMC/CART circuitry (Su et al., 2017; Acuna-Goycolea & van den Pol, 2005).

Evidence of the effects of PYY(1-36) isoform on appetite regulation are sparse. Intravenous infusions of PYY(1-36) have stimulated some PYY(3-36)-like satiating effects in rodents, likely due to peripheral DPP IV processing, but no changes from saline control in humans (Ballantyne, 2006; Sloth et al., 2007). Interestingly, the Y1 receptor has been found expressed on the basolateral surface of crypt stem cells in the human colon and has been suggested to mediate intestinotrophic effects of PYY released from neighbouring enteroendocrine cells (Mannon et al., 1999; Wharton et al., 1993). Notably, PYY(1-36)-mediated activation of the Y1 receptor has been shown to promote intestinal epithelial proliferation *in vitro* via coupling to downstream mitogenic signalling pathways (Mannon & Mele, 2000).

PYY also influences several mechanical and chemical aspects of digestion in the GI tract, and this has been linked to its activation of Y-receptors on local enteric neurons as well as hypothalamic-mediated vagal efferent discharge *in vivo* (Pironi et al., 1993; Masuda et al., 1994; Wang et al., 2010). Numerous studies in humans, mice and canines have demonstrated that PYY inhibits gastrointestinal motility, gastric acid secretion, and pancreatic enzyme secretion (Ballantyne, 2006; Masuda et al., 1994; Pironi et al., 1993; Souli et al., 1997; Wang et al., 2010; Wen et al., 1995). As such, PYY is suggested to contribute to the ‘ileal brake’, a distal-proximal negative feedback mechanism which acts to delay the transit of a meal through the gut to optimise nutrient digestion and absorption. (Wen et al., 1995; Pironi et al., 1993).

1.2 Obesity

1.2.1 The global obesity landscape

Obesity is a complex and multifactorial disease, defined by excessive accumulation of body fat in adipose tissue that can impair health (WHO, 2021). As obesity has systemic effects on multiple organ systems, it is unsurprising that an extensive catalogue of obesity-related co-morbidities poses a major burden to public health and the economy worldwide (Pi-Sunyer, 1999). Such co-morbidities are leading causes of global mortality and include T2D, hypertension, dyslipidaemia, chronic kidney disease, and various types of cancer (Pi-Sunyer, 1999). The last few decades have seen a rapid escalation in the global prevalence of obese, defined as a body mass index (BMI) of ≥ 30 kg/m^2, and overweight (BMI 25 – 29.9 kg/m^2) individuals (WHO, 2000). Trends across age-standardised mean BMI from 1975 to 2014 worldwide state a ~ 2.5-fold increase in the prevalence of obese BMIs in the global population, and a BMI increase/decade of 0.63kg/m^2 and 0.59 kg/m^2 for males and females respectively (NCD-RisC, 2016). As the obesity epidemic continues to grow, it is predicted that over 4 billion people worldwide may be overweight or obese by 2035, and the WHO Global Noncommunicable Disease (NCD) targets of halting the rise of obesity by 2025 are unlikely to be met (World Obesity Federation, 2023).

1.2.2 Current and emerging anti-obesity agents

The first-line therapy for obese or overweight individuals is lifestyle modifications, also known as behavioural weight control, and consists of three main strategies: adherence to a hypocaloric or normocaloric diet, increased physical activity and cognitive behavioural therapy (CBT) (Wadden et al., 2012). For individuals who have tried these lifestyle modifications yet continue to have a BMI ≥ 30 kg/m^2 or a BMI ≥ 27 kg/m^2 in the presence of obesity-related condition *e.g* hypertension, pharmacotherapies are commonly prescribed. In more severe forms of obesity (BMI ≥ 40 kg/m^2 or ≥ 35 kg/m^2 in the presence of co-morbidity), bariatric surgery remains an effective, although risk-bearing treatment modality.

Currently, a class of medications known as GLP-1 receptor agonists (GLP-1 RAs) comprise most of the anti-obesity therapeutic landscape (Gores & Rickwood, 2024). GLP-1 RAs harness the incretin and anorectic effects of endogenous GLP-1 by similarly binding to and activating GLP-1 receptors situated in metabolically active tissues in the periphery, as well as in central appetite circuits (Drucker, 2018). After primarily being approved as T2D medications, the weight loss reduction efficacy of these agents gained clinical interest soon after (Drucker, 2018). The first GLP-1 RA to be approved for a weight-loss indication in the UK was liraglutide, sold under the name Saxenda, followed by semaglutide, sold under the name Wegovy (Davies et al., 2015; Lexchin & Mintzes, 2023; Wadden et al., 2013). GLP-1 RAs continue to be a crucial backbone of the pipeline for anti-obesity pharmacotherapies. Assets currently in development include oral GLP-1 RAs (compared to current agents that require subcutaneous administration) and combination treatments of GLP-1 RA with analogues of other entero-pancreatic hormones such as GIP and PYY (Melson et al., 2024). The PYY analogue NNC0165-1875 has recently entered phase III trial testing in combination with semaglutide (ClinicalTrials.gov, 2018). In addition, the PYY analogue Y-14 has successfully passed phase I testing for use as a weight loss monotherapy (Tan et al., 2021). The development of dual-action agonists which simultaneously target multiple pathways e.g. tirzepatide (GLP-1/GIP RA), sold under the name Mounjaro, have further improved the weight-loss reduction efficacy of conventional GLP-1 RAs and are gaining popularity (Jastreboff et al., 2022; Melson et al., 2024). Earlier this year, an additional indication of Wegovy in the reduction of cardiovascular risk associated with obesity was approved in the U.S (Lincoff et al., 2023).

Combination therapies of GLP-1 RA agents with non-entero-pancreatic peptide hormone analogue partners, such as human monoclonal antibody bimagrumab, are currently in developmental stages (Melson et al., 2024). Bimagrumab binds to type II activin receptors on skeletal muscle; in combination with semaglutide, treatment with bimagrumab has successfully achieved significant fat loss whilst promoting increased lean muscle mass in overweight and obese patients (Nunn et al., 2024). Beyond targeting gut peptide hormone axes, data from pre-clinical studies suggests an anti-obesity effect of activating brown adipose tissue (BAT); BAT specialises in expending

energy *via* the uncoupling of respiration and heat production, whereas its counterpart, white adipose tissue (WAT), functions in storing excess energy (Liu et al., 2023). A number of small-molecule agents which elevate the thermogenic activity of BAT have exhibited anti-obesity benefits in mouse models (Lu et al., 2020). By using CRISPR/Cas9-editing technology, scientists from the Harvard Stem Cell Institute have engineered human white preadipocytes with thermogenic functionalities of brown fat-like adipocytes by boosting the expression of uncoupling protein 1 (UCP1); transplantation of these 'HUMBLE' (human brown-like) cells into obese mice have successfully significantly improved biomarkers of metabolism and blood glucose, and suppressed weight gain (Wang et al., 2020). The application of this approach in humans, whereby a small set of a patient's white adipocytes are removed, 'UCP1-boosted' and returned to the body, warrants further study; success of this treatment might pave the way for the development of novel cell therapies in the anti-obesity landscape.

1.3 The Gut Microbiota & Short Chain Fatty Acids

1.3.1 The gut microbiome

The human GI tract is inhabited by a diverse repertoire of bacteria, archaea, eukarya and viruses, collectively defined as the microbiota, which engage in dynamic and influential symbiotic relationships with the host (Ursell et al., 2012). The number of microbes colonising the human GI tract is estimated to exceed 10^{14} and encompasses over 2000 species that are predominated by four bacterial phyla: Firmicutes, Bacteroidetes, Proteobacteria and Actinobacteria (Hugon et al., 2015). Advancements in high-throughput metagenomic sequencing have established a catalogue of over 3 million genes in human gut microbial communities, many of which pertain to the production of microbiota-derived metabolites (Qin et al., 2010). Equipped with an arsenal of unique enzymes that are not encoded by the human genome, the gut microbiota substantially contributes to host metabolism, *via* the *de novo* synthesis of bioactive molecules, as well as the metabolism of dietary-derived macronutrients and micronutrients (Cryan et al., 2019). Many gut bacterial metabolites activate nutrient-sensing EECs, which initiates communication to central homeostatic centres *via*

neural, endocrine and immune pathways; as such, the concept of a gut-microbiome-brain axis exists (Martin et al., 2018).

1.3.2 The production of Short Chain Fatty Acids

Bacteria in the flora of the large intestine ferment carbohydrates that are resistant to digestion in the upper gut, yielding a major class of microbial metabolites known as short chain fatty acids (SCFAs) (Cummings & Macfarlane, 1997). Such non-digestible carbohydrates (NDCs) include non-starch polysaccharides abundant in plant-derived foods, such as cellulose, fructans and β-glucans, and are comprised of 10 or more monomeric units interlinked in complex ways by glycosidic linkages (Cummings & Stephen, 2007). Other NDC substrates for microbial fermentation include resistant starch and shorter non-α glucan oligosaccharides such as raffinose and stachyose (Cummings & Stephen, 2007). The production profile of SCFAs varies with physiochemical properties of different NDCs reaching the colon, including chain length and branching, monosaccharide composition, and glycosidic bond position (Harris, Edwards & Morrison, 2017).

SCFAs are carboxylic acids comprising of aliphatic chains of 6 or less carbons. The most abundant SCFAs are acetate, propionate and butyrate which contain 2, 3 or 4 carbons respectively. Humans lack the appropriate glycosidic hydrolases to release oligosaccharides and monosaccharides from NDCs (Popoola-Akinola, Raji & Olawoye, 2022). Instead, NDCs enter the caecum and colon where they are processed by a large repertoire of carbohydrate-degrading enzymes encoded by the microbiome, to oligosaccharides and then 5- or 6-carbon monosaccharides (Cummings, 1981). The main precursor for SCFAs, pyruvate, is subsequently produced from pentoses *via* the pentose phosphate pathway, and from hexose and deoxy-hexoses *via* glycolysis (Cummings, 1981).

Acetate is a ubiquitous end-product of both anaerobic fermentation and the reductive Wood-Ljungdahl pathway across gut bacterial genera, achieving the highest concentration amongst the SCFAs in the intestinal lumen (Louis & Flint, 2017). In

contrast, the production of propionate and butyrate are substrate- and species-specific. Two pathways are largely responsible for the production of propionate *via* anaerobic bacterial fermentation. The succinate pathway is used by Bacteroidetes and the Negativicutes class of Firmicutes (Reichardt et al., 2014). The propanediol pathway is utilised by the Lachnospiraceae family of Firmicutes, producing propionate from the deoxy sugars rhamnose and fucose (Reichardt et al., 2014). Butyrate production is largely carried out by colonic Firmicutes bacteria and is mediated by two key enzymes, butyryl CoA:acetate CoA transferase and butyrate kinase (Louis & Flint, 2017). The majority of butyrogenic bacteria use the former pathway, such as members of the Ruminococcaceae and Lachnospiraceae families, whereas the Clostridiaceae family use the latter (Louis et al., 2004). Although NDCs are the predominant substrate for SCFA production, acetate, propionate and butyrate are also formed *via* the bacterial fermentation of amino acids by both saccharolytic and asaccharolytic species (Smith & Macfarlane, 1997).

1.3.3 The functions of SCFAs

Acetate, propionate and butyrate exist in a molar ratio of 60:20:20 respectively and decrease in abundance along the length of the large intestine (Cummings et al., 1987). Total SCFA concentration reaches 70-140mM in the proximal colon, and drops to 20-70 mM in the distal colon, with fluctuations subject to total dietary fibre intake(s) as well as the types of fibres consumed (Topping & Clifton, 2001).

Following their production, SCFAs can beneficially interact with the local intestinal environment. SCFAs may be absorbed in the intestine *via* passive diffusion, however uptake is greatly enhanced by solute transporters such as the proton-coupled monocarboxylate transporters (MCT1) and sodium-coupled monocarboxylate transporter (SMCT1) (Den Besten et al., 2013). Butyrate is extensively used as an energy source in colonocytes, undergoing β-oxidation in the mitochondria to Acetyl-CoA which subsequently enters the Krebs cycle (Donohoe et al., 2011). In addition, SCFAs affect immunity, metabolic responses and differentiation in the intestinal milieu by modulating cellular epigenetic states (Krautkramer et al., 2016). SCFAs act as mediators of gene expression via two routes, by the inhibition of histone deacetylases

(HDACs), and by contribution to the production of the histone acetyltransferases (HATs) substrate acetyl-CoA (Donohoe et al., 2012; Sealy & Chalkley, 1978). Alternatively, SCFAs can function as signalling molecules *via* activation of the nutrient-sensing G-protein coupled receptors (GPCR) free fatty acid receptor 2 (FFAR2/GPR43) or free fatty acid receptor 3 (FFAR3/GPR41) expressed on intestinal epithelial and immune cells (Kimura et al., 2020). Butyrate is also an agonist of the GPCR hydroxycarboxylic acid receptor 2 (HCAR2/GPR109A) on intestinal epithelial cells (Thangaraju et al., 2009). Recent studies have uncovered the expression of two other SCFA-binding receptors in the intestinal epithelium: the olfactory GPCRs OR51E1 and OR51E2 (Dinsart et al., 2023; Fleischer et al., 2015; Han et al., 2018; Nishida et al., 2021) .The leftover pool of butyrate and propionate that is unutilised by metabolism in colonocytes are shuttled to the liver *via* the portal circulation and supply gluconeogenic and lipogenic pathways (Schönfeld & Wojtczak, 2016). Although SCFAs further reach the systemic circulation and other tissues in only micromolar quantities, their systemic functions hold high importance to human health and disease (Cummings et al., 1987).

1.1 G-protein coupled receptors

1.3.4 An overview of G-protein coupled receptors (GPCRs)

G-protein coupled receptors (GPCRs) are the largest family of cell surface receptors encoded by the human genome, constituting over 800 genes (Yang et al., 2021). GPCRs bind to a broad repertoire of endogenous ligands including hormones, neurotransmitters, chemokines, odors, nutrients and metabolites and mediate a preponderance of physiological processes (Foster et al., 2019). By recruiting G proteins, β-arrestins or other downstream effectors, GPCRs are able to transduce such extracellular cue, within milliseconds to hours, into diverse intracellular responses (Wootten et al., 2018). GPCRs have been implicated in a number of diseases such as obesity, T2D, cancer, and Alzheimer's disease, and are currently the targets of approximately 34% of FDA-approved drugs (Majumdar et al., 2024). However, a considerable proportion of human GPCRs are still considered orphan receptors because their endogenous ligands remain unknown; the application of

experimental high-throughput screening tools such as PRESTO-TANGO and TRUPATH, coupled with increasingly advancing structure-based computational methods, will undoubtedly continue to advance efforts in uncovering the druggable human GPCRome (Kroeze et al., 2015; Olsen et al., 2020; Szwabowski, Baker & Parrill, 2023).

1.3.5 GPCR Classification & Structure

All GPCRs share a common architecture consisting of an extracellular N-terminus, 7 transmembrane (TM) helices (TM1-TM7) linked by 3 intracellular loops (ICL1-ICL3) and 3 extracellular loops (ECL1-ECL3), and an intracellular C-terminus *(Figure 1.2)* (Filipek et al., 2003).

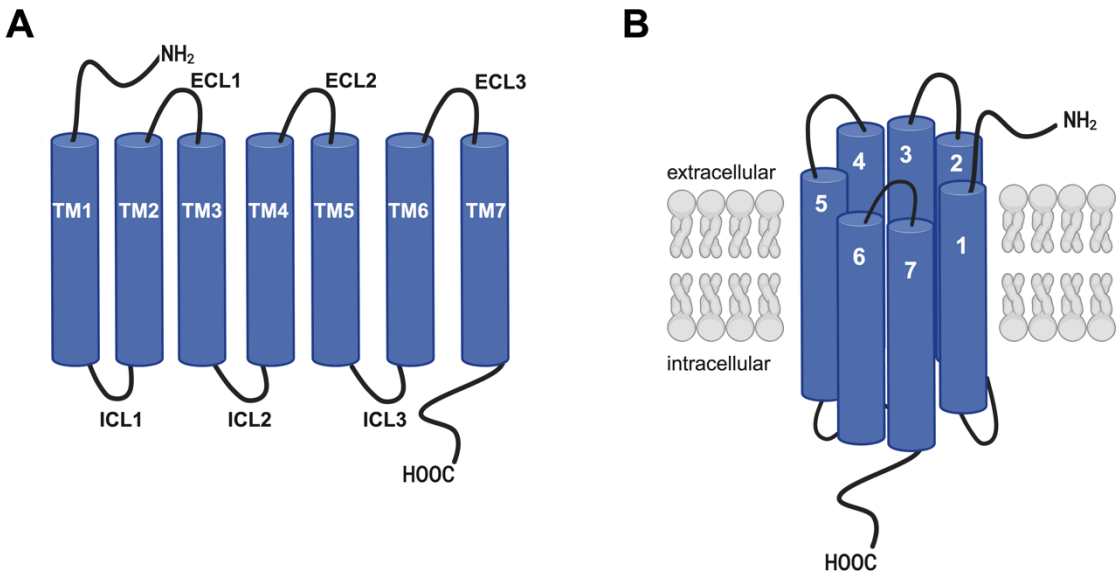


Figure 1.2 Schematic of the simplified structure of a GPCR. (A) The characteristic 7 transmembrane helices of a GPCR are indicated in blue (TM1-7) in addition to the 3 intracellular loops (ICL1-3) and 3 extracellular loops (ECL1-3) by which they are connected. The N- (NH2) and C- (COOH) termini are also indicated. (B) The characteristic topology of a GPCR at the plasma membrane.

Mammalian GPCRs can be grouped into classes based on phylogenetic analysis; A (rhodopsin), B (secretin and adhesion), C (glutamate), F (frizzled), and T (Taste 2)

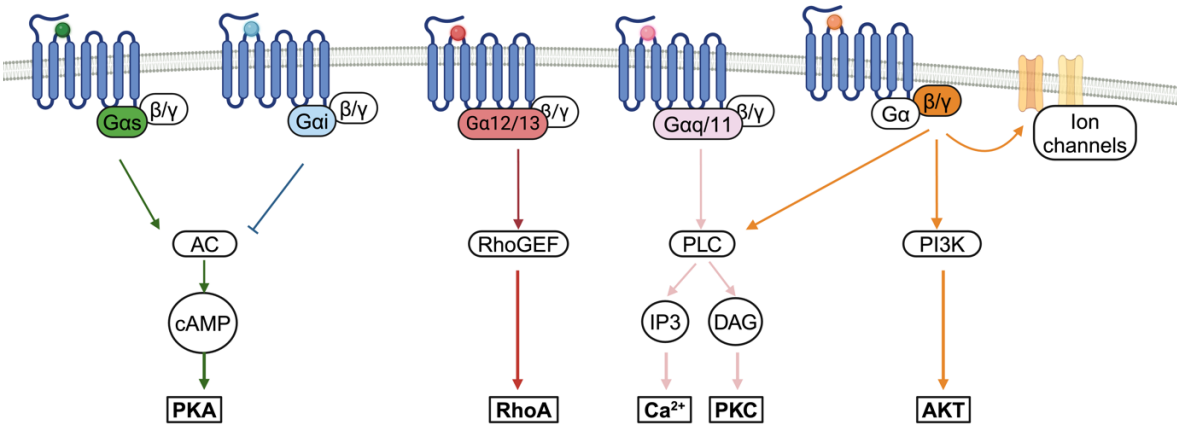
(Hauser et al., 2021). Two other, albeit smaller, classes of GPCRs exist in non-vertebrates; Class D is comprised of fungal pheromone mating receptors, and Class E is comprised of cyclic AMP (cAMP) receptors that mediate chemotactic signalling in slime molds (Prabhu & Eichinger, 2006; Brown et al., 2018). Class A represents the largest and most widely studied class of GPCRs, and the first crystal structure of a GPCR was that of the archetypal class A member rhodopsin in the year 2000 (Palczewski et al., 2000). Since then, the structural determination of GPCRs has massively thrived, particularly accelerated by the advent of cryo-electron microscopy (cryo-EM), with a total of 243 unique structures having been published on the Protein Data Bank as of 2023 (Cheng et al., 2023).

1.3.6 G-protein dependent signalling pathways

Heteromeric guanine-binding proteins, known as G-proteins, are the eponymous coupling partners of GPCRs that mediate intracellular signal transmission (Bokoch et al., 1983). The G-protein is composed of α, β, and ɣ subunits, of which β and ɣ form a stable dimer which can be regarded as one functional unit (Gβɣ) (Syrovatkina et al., 2016). The human genome encodes 16 Gα subunits which are grouped into four subfamilies by their downstream signalling properties: Gαi, Gαq/11, Gαs, and Gα12/13 (Downes & Gautam, 1999). The biological activity of G-proteins is determined by the nucleotide to which the Gα subunit is bound *(Figure 1.3)*. In the absence of a signal, Gα is bound to guanosine diphosphate (GDP); upon GPCR-ligand association, the GDP molecule bound to Gα is exchanged for guanosine trisphosphate (GTP) causing the G-protein to split into two parts, Gβɣ and GTP-bound Gα (Syrovatkina et al., 2016). Both the Gβɣ dimer and GTP-bound Gα can subsequently bind with membrane effector proteins such as enzymes and ion channels, initiating unique signalling cascades (Syrovatkina et al., 2016). Moreover, the majority of GPCRs can couple to more than one type of Gα subunit, endowing an inherent pleiotropy in the physiological responses driven by a single GPCR (Masuho et al., 2023).

Typically, Gαs proteins activate the enzyme adenylyl cyclase (AC), increasing the production of the secondary messenger cyclic adenosine monophosphate (cAMP)

from ATP (*Figure 1.3)* (Wettschureck & Offermanns, 2005). The primary effectors that cAMP activates are cAMP-dependent protein kinase (PKA), which phosphorylates numerous cytosolic enzyme and nuclear transcription factors, cyclic-nucleotide-gated (CNG) ion channels, and cAMP-regulated guanine nucleotide exchange factors (EPAC/cAMP-GEF) (Sassone-Corsi, 2012). In contrast, members of the Gαi family inhibit AC, resulting in a decrease in intracellular cAMP concentrations (Wettschureck & Offermanns, 2005). Gαq/11 proteins activate β-type phospholipase C (PLC- β) which catalyses the hydrolysis of the plasma membrane phospholipid Phosphatidylinositol 4,5-bisphosphate (PIP_2) to inositol triphosphate (IP_3) and diacylglycerol (DAG) (*Figure 1.3)* (Wettschureck & Offermanns, 2005). IP_3 diffuses through the cytoplasm to the endoplasmic reticulum, where it binds to and opens IP_3-gated Ca^{2+} channels leading to intracellular calcium flux, and DAG binds to and activates protein kinase C (PKC) (Wettschureck & Offermanns, 2005). The Gα12/13 family couple GPCRs to the activation of the small monomeric GTPase RhoA by stimulating the activity of RhoGTPase nucleotide exchange factors (RhoGEFs) (*Figure 1.3)* (Siehler, 2009). Finally, the Gβɣ dimer, once separated from GTP-bound Gα, also modulate various cellular signalling effectors; Gβɣ dimers activate proteins at the



membrane such as Kir3 K^+ channels, voltage-dependent Ca_v2 Ca^{2+} channels, PLCs and phosphoinositide 3-kinases (PI3Ks), in addition to associating intracellularly with cytoskeletal elements (*Figure 1.3)* (Khan et al., 2013; Sierra-Fonseca et al., 2018).

Figure 1.3 Canonical G-protein-dependent signalling pathways induced by GPCR activation. Schematic depicting the main intracellular cascades activated by G-proteins downstream of GPCR activation. Upon ligand binding, GPCRs activate G-protein(s) by stimulating conversion from a GDP-bound to a GTP-bound state. This nucleotide exchange causes the Gα subunit to split from the βɣ subunit, both of which can then activate diverse signalling pathways. The four major Gα subunit families are Gαs, Gαi, Gαq/11, and Gα12/13. Gαs stimulates the activity of the enzyme adenylyl cyclase (AC) which catalyses the production of the secondary messenger cyclic adenosine monophosphate (cAMP) from adenosine triphosphate (ATP). Protein kinase A (PKA) is a downstream effector of cAMP. In contrast, the Gαi subunit inhibits the activity of AC. Gα12/13 subunits are activators of RhoGTPase nucleotide exchange factors (RhoGEFs) which in turn activate the small monomeric GTPase RhoA. Gαq/11 stimulates the activation of phospholipase C (PLC) which catalyses the conversion of phospholipid Phosphatidylinositol 4,5-bisphosphate (PIP_2) to inositol triphosphate (IP_3) and diacylglycerol (DAG). IP3 binds to and opens IP3-gated calcium channels on the endoplasmic reticulum, leading to an influx of Ca2+ into the cytoplasm. In addition, DAG activates protein kinase C (PKC). Gβɣ subunits are able to activate a variety of downstream efffectors including PLC, phosphoinositide 3-kinases, and ion channels.

1.3.7 GPCR Activation

The orthosteric ligand-binding site is situated within the TM domain of class A GPCRs, in the extracellular domain of class C GPCRs, and class B and F GPCRs can have one of the two (Hauser et al., 2021). Upon ligand binding, GPCRs undergo a conformational transition that funnels through the hydrophobic helical bundle and promotes a rearrangement of the intracellular C-terminal domain to accommodate transducer binding (Wingler & Lefkowitz, 2020). Across the GPCR superfamily, this conformational switch is characterised by a large outward displacement (7-19Å) and rotation of the intracellular side of TM6, combined with a smaller movement of TM5 (Hauser et al., 2021). Another integral molecular switch in the activation dynamics of Class A GPCRs is called the “ionic lock”; this describes a salt bridge formed between the cytoplasmic domains of TM3 and TM6 that restrains the receptor in its inactive state, and is broken upon activation (Trzaskowski et al., 2012). Importantly, the application of spectroscopic and computer simulation techniques have revealed a

complexity in the conformational landscape of GPCRs that contests a simple binary transition between inactive and active states (Hilger, 2021; Wingler & Lefkowitz, 2020).

1.3.8 GPCR Desensitisation

Several mechanisms exist to fine-tune the duration of GPCR responses to prevent overstimulation (Rajagopal & Shenoy, 2018). Upon prolonged exposure to their activating ligands, GCPRs are absconded from the plasma membrane in a process known as “desensitisation” (Rajagopal & Shenoy, 2018). Canonically, GPCR desensitisation has been categorised as homologous or heterologous in its nature; homologous desensitisation refers to the attenuation of the agonist-specific responsiveness of a GPCR, whereas heterologous desensitisation refers to the synergistic loss of responsiveness of the agonist-activated GPCR as well as heterologous GPCRs subtypes that are activated by unrelated ligands (Bünemann & Hosey, 1999). Pioneering studies on GPCR desensitisation focused on β2AR and uncovered a critical role of receptor phosphorylation in both homologous and heterogeneous mechanisms (Sibley et al., 1984; Stadel et al., 1983; Sibley et al., 1985; Stadel et al., 1983). Heterologous desensitisation is mediated not at the level of the GPCR itself, but rather *via* activation of secondary messenger kinases downstream of another GPCR, and promotes G-protein uncoupling and/or receptor internalisation (Rajagopal & Shenoy, 2018). For example, persistent activation of β2AR has stimulated the desensitisation of members of the muscarinic acetylcholine receptor family (mAChRs) by activation of protein kinase A, and sphingosine 1-phosphate S1P1 receptor (S1P1R) activation has induced desensitisation of the α-1B (ADRA1B) adrenergic receptor *via* PI3K and PKC activation (Pera & Penn, 2014; Lee & Fraser, 1993; Castillo-Badillo et al., 2012).

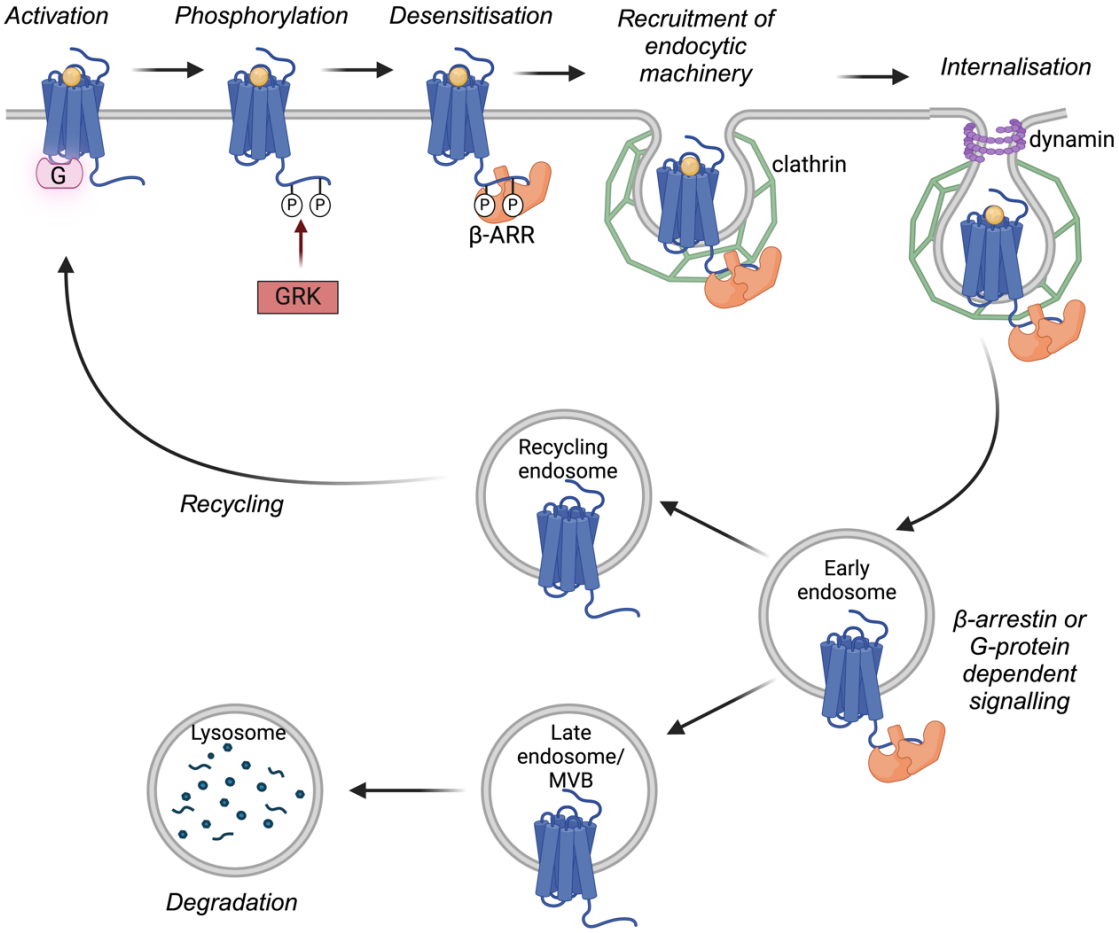
In homologous desensitisation, the agonist-occupied GPCR becomes a substrate for G protein-coupled receptor kinases (GRKs), which phosphorylate serine and threonines on ICL3 or the C-terminus of the receptor (*Figure 1.4)* (Kelly, Bailey & Henderson, 2008). These phosphorylated residues are docking sites for a family of proteins called arrestins, which bind to the receptor and precludes further coupling to G-proteins (Kelly et al., 2008). There are four mammalian members of the arrestin

family which fall into two categories; two members are visual arrestins (arrestin-1 and arrestin-4), which exclusively quench the activity of light-transducing opsins, and two members are β-arrestins (arrestin-2/β-arrestin-1 and arrestin-3/β-arrestin-2), which act on a wide range of GPCRs outside the retina (Gurevich et al., 1995). In addition, arrestins effectively bind key components of endocytic machinery including clathrin and its adaptor AP-2, thereby promoting rapid receptor internalisation via clathrin-coated pits (*Figure 1.4)* (Goodman et al., 1996; Laporte et al., 1999). Clathrin-coated pits undergo scission from the membrane by the GTPase dynamin, thereby forming clathrin-coated vesicles that can traffic their receptor cargo to diverse intracellular locations (Traub, 2009). Beyond this canonical mechanism, there is evidence for a number of clathrin-independent endocytic routes undertaken by specific GPCRs including endothelin receptor type A, the M2 mAChR and the β1-adrenergic receptor (β1AR) (Delaney et al., 2002; Okamoto et al., 2000; Boucrot et al., 2015). Importantly, the internalisation of GPCRs is not exclusively an agonist-dependent phenomenon, and some GPCRs are endocytosed in the absence of agonist known as “constitutive” internalisation (Hendrik Schmidt et al., 2020; Møller et al., 2024; Mohammad et al., 2007; Wolfe, Marchese & Trejo, 2007; Stanasila et al., 2008).

1.3.9 Intracellular trafficking of GPCRs

The early endosome (EE) is the prominent platform in mediating the sorting of GPCRs between lysosomes for degradation, or to the plasma membrane to be recycled (*Figure 1.4)* (Hanyaloglu & Von Zastrow, 2008). The trafficking itinerary of GPCRs is largely dictated by the presence of motifs on intracellular loops or the C-terminal tail which engage key sorting proteins in endosomes (Hanyaloglu & Von Zastrow, 2008). Endo-lysosomal sorting necessitates the covalent attachment of ubiquitin to cytoplasmic lysine residues on target GPCRs *via* the sequential action of three enzymes: ubiquitin-activating enzyme (E1), ubiquitin-conjugating enzyme (E2), and ubiquitin-protein ligase (E3) (Hanyaloglu & Von Zastrow, 2008). Ubiquitinated GPCRs are recognised and bound to by protein complexes that contain Ubiqutin-interating motifs (UIMs) such as the Hrs/STAM complex, GGA3 and the TOM1/Tollip complex (Piper & Luzio, 2007). Subsequently, ubiquitinated cargo are transferred to the endosomal sorting complexes required for sorting machinery (ESCRT), which drives

their internalisation into small intraluminal vesicles of maturing multivesicular bodies (MVBs) (Piper & Luzio, 2007). Mature MVBs ultimately fuse with lysosomes, initiating the degradation of their sequestered contents by acidic hydrolases (Dores & Trejo, 2019). In contrast, C-terminal *cis*-acting sorting sequences known as PDZ ligands typically direct post-endocytic trafficking of GPCRs to the plasma membrane for



recycling *via* binding to PDZ proteins such as SNX27 and Na^+/H^+ exchange regulatory factor 1 (NHERF-1) (Romero, von Zastrow & Friedman, 2011). Importantly, this sequence-directed pathway is mechanistically distinct from GPCR recycling that occurs in the absence of sorting signals and by bulk membrane flow, known as "default" recycling (Hanyaloglu & von Zastrow, 2007; Puthenveedu et al., 2010; Tanowitz & von Zastrow, 2003).

Figure 1.4 Schematic of the canonical life-cycle of a GPCR. GPCRs typically undergo sequential activation, desensitisation and intracellular trafficking towards lysosomal degradation or recycling to the plasma membrane. Following ligand binding and activation of their respective G-protein coupled pathways, GPCR signals are eventually "switched off" by desensitisation. In homologous desensitisation, GPCRs are phosphorylated at their

intracellular domain by GPCR kinases (GRK). These newly phosphorylated hubs attract the binding of β-arrestins (β-ARR) to the receptor. β-ARRs can engage key machinery of clathrin-mediated endocytosis and facilitate receptor internalisation. The primary sorting platform of endocytosed GPCRs is the early endosome, from which receptors can be recycled back to the plasma membrane *via* recycling endosomes or targeted to multi-vesicular bodies which eventually fuse with lysosomes and stimulate receptor degradation. Internalised GPCRs may also activate β-arrestin- or G-protein-dependent responses from intracellular compartments such as the early endosome.

1.3.10 GPCR signalling at the endomembrane

The canonical plasma membrane-centric views of GPCR activation have long since been revised, as a variety of subcellular compartments to which GPCRs traffic also serve as dynamic sites for physiologically unique signalling responses (Thomsen et al., 2018). Initially, endosomal-based signalling of GPCRs was proposed to engage discrete molecular machinery, such as mitogen-activated protein kinases (MAPK) and Src-family kinases, and G-protein activation remained exclusive to the plasma membrane (von Zastrow & Sorkin, 2007; Sorkin & von Zastrow, 2002). Subsequently, seminal studies on the parathyroid hormone receptor (PTHR), the thyroid stimulating hormone receptor (TSHR) and the vasopressin type 2 receptor (V_2R) evidenced the activation of prolonged Gαs-mediated cAMP responses protein from endosomes that outlived transient signalling from the plasma membrane (Calebiro et al., 2009; Feinstein et al., 2011; Ferrandon et al., 2009; Wehbi et al., 2013; Feinstein et al., 2013). Concomitantly, this paradigm of endosomal cAMP signalling was extended to the activation of persistent Gαi responses by S1P1R (Mullershausen et al., 2009). Several GPCRs have also been reported to activate sustained Gαq-mediated responses from endosomes such as the neurokinin 1 receptor (NK1R) and the calcitonin gene-related peptide (CGRP) receptor and the proteinase-activated (PAR2) receptor (Yarwood et al., 2017; Jensen et al., 2017; Gorvin et al., 2018).

Alongside instructing the spatial distribution of GPCRs along the endocytic pathway, β-arrestins are at the crux of endowing temporal pleiotropy in GPCR signalling (Irannejad et al., 2013; Thomsen et al., 2016; Cahill et al., 2017). Importantly, GPCRs

can be characterised based on the nature of their interaction with β-arrestins, which can be transient, termed ‘class A’ GPCRs including β2AR, or of a higher affinity, termed ‘class B GPCRs which includes PTHR, TSHR and V2R (Oakley et al., 1999). As such, Class A GPCRs dissociate quickly following their internalisation, and are recycled back to the plasma membrane, whereas Class B GPCRs complexes with β-arrestin reside in endosomes for longer and favour a second wave of G-protein signalling (Thomsen et al., 2016; Cahill et al., 2017). Contradictory to β-arrestin-mediated obstruction of receptor G-protein binding sites in the traditional models of GPCR signalling, Thomsen et al., revealed the formation of complexes composed of internalised class B receptor, G-protein and β-arrestin, termed “megaplexes”. Championed by the recently resolved cryo-EM structure, the megaplex architecture necessitates a unique “tail” conformation in which β-arrestin is primarily bound to phosphorylated hubs on the C-terminal receptor tail thereby leaving the receptor internal cavity available for G-protein coupling (Nguyen & Lefkowitz, 2021). Moreover, the binding pattern of β-arrestin to class B GPCRs elicits unique functional outcomes; the “tail” conformation mediates sustained G-protein endosomal signalling responses but not receptor desensitisation, which instead relies on the fully engaged “core” conformation consisting of a dual interaction between β-arrestin and the receptor C-terminus, as well as the core (Cahill et al., 2017).

In contrast, endosomal Gαs-mediated cAMP responses of class A GPCRs occur following the dissociation of β-arrestins, and are distinct from sustained class B by their rapid onset within minutes of agonist addition and transient nature (Kotowski et al., 2011; Irannejad et al., 2013). Interestingly, the vasoactive intestinal peptide receptor 1 (VIPR1) has been recently demonstrated to engage in a third mode of endosomal GPCR signalling in which both receptor internalisation and endosomal Gαs activation can proceed in a fully β-arrestin-independent manner (Blythe & von Zastrow, 2023).

The use of fluorescent and bioluminescent biosensors has provided immense spatiotemporal resolution in characterising the real-time activation of GPCRs from subcellular compartments in live cells (Demby & Zaccolo, 2024). In particular, EEs have been shown to host an abundance of GPCR signalling responses which modulate crucial physiological and pathophysiological cellular outcomes. These

include the sustained activation of Gαs (PTHR, GLP-1R), Gαi (μ- and δ-opioid receptors (MORs and DORs)) and Gαq (V2R, calcium sensing receptor (CaSR), as well as the acute activation of Gαs (β2AR) (Wright et al., 2023; Stoeber et al., 2018; Ferrandon et al., 2009; Gorvin et al., 2018; Daly et al., 2023; Irannejad et al., 2013). Notably, pioneering studies by the Hanyaloglu lab have extensively characterised a endosomal compartment distinct from the EEs known as very early endosomes (VEEs), which are host to the endosomal Gαs responses of the luteinising hormone receptor (LHR), the follicle-stimulating hormone receptor (FSHR) and β1AR (Sposini et al., 2020, 2017; Jean-Alphonse et al., 2014). VEEs which is a third of the size (400nm-500nm) of EEs (1200nm-1400nm), and are devoid of classical EE markers such as Rab5 and the early endosome autoantigen 1 (EEA1) (Jean-Alphonse et al., 2014). A subpopulation of VEEs are marked by the presence of Adaptor protein, Phosphotyrosine interacting with Pleckstrin homology Domain and Leucine Zipper 1 (APPL1), which mediates the rapid recycling of receptor-containing VEEs back to the plasma membrane, and additionally functions as a negative regulator of endosomal Gαs signalling (Sposini et al., 2017).

Aside from endosomes, a number GPCRs have been found to signal from diverse subcellular organelles including the endoplasmic reticulum, the Golgi Apparatus, the mitochondria, and the nucleus (Barrios-Rodiles et al., 2005; O'Malley et al., 2003; Valdehita et al., 2010; Hebert-Chatelain et al., 2016; Purgert et al., 2014; Wright et al., 2023; Godbole et al., 2017; Irannejad et al., 2017; Nash et al., 2019). Signalling by GPCRs localised to nuclear membranes include Gαs-mediated cAMP production by VIPRs, and the opening of nuclear IP3-gated Ca^{2+} channels via activation of Gαq by metabotropic glutamate (mGlu5) receptors (O'Malley et al., 2003; Valdehita et al., 2010).Gαs is also recruited and activated at the Golgi Apparatus by internalised receptors that have been retrogradely shuttled from endosomes (Godbole et al., 2017; Wright et al., 2023). Nevertheless, pre-existing Golgi-resident β1AR populations which are activated by endogenous catecholamines that gain access to Golgi by passive diffusion or specialised transporters, are able to activate Gαs/cAMP signalling (Irannejad et al., 2017; Nash et al., 2019).

1.3.11 Functional diversification by GPCR endosomal signalling

The term “biased agonist” in the field of GPCR biology has widely been used to describe ligands which upon engaging their cognate receptor, preferentially activate either G-protein or β-arrestin-mediated downstream signalling (Liu et al., 2015). In the case of “promiscuous” GPCRs that engage more than one G-protein subtypes, ligand bias can also distinguish between activation of G-protein families as is the case for synthetic agonists of FFAR2, V2R, the angiotension II type I (AT1R) and prostaglandin F2$\boldsymbol{\alpha}$ (FP) receptor (Bolognini et al., 2016; Heydenreich et al., 2022; Priyadarshini et al., 2015; Sedki et al., 2022). However, an additional layer of complexity to the functional selectivity of GPCR ligands is the capability to activate signalling from specific subcellular compartments (Klauer, Willette & Tsvetanova, 2024). Importantly, the spatial compartmentalisation of GPCR signalling encodes significant specificity and diversity in downstream cellular responses (Caengprasath & Hanyaloglu, 2019; Sposini & Hanyaloglu, 2017; West & Hanyaloglu, 2015; Klauer, Willette & Tsvetanova, 2024; Thomsen et al., 2018).

Two structurally-related endogenous ligands of the PTHR, PTH and Parathyroid-hormone related peptide (PTHRP) exemplify spatial bias; PTH is able to activate PTHR/Gαs signalling from the plasma membrane as well as a second wave of prolonged endosomal signalling, whereas PTHRP-mediated PTHR/Gαs signalling is restricted to the plasma membrane (Ferrandon et al., 2009). Effective regulation of blood Ca^{2+} levels and vitamin D production by the PTHR requires sustained endosomal cAMP production and explains ligand-specific differences in clinical outcomes from earlier human studies (Horwitz et al., 2005; Ferrandon et al., 2009; White et al., 2021). Notably, the development of an optogenetic strategy, utilising the transgenic expression of a bacteria-derived photoactivatable-adenylyl cyclase (pPAC) fused to organelle-specific targeting motifs, illustrates the importance of the subcellular location of Gαs signalling in dictating an extensive breadth of downstream cAMP-mediated effects on the cellular transcriptome and phosphoproteome (Tsvetanova & von Zastrow, 2014; Tsvetanova et al., 2021).

In addition, endosomal signalling by a number GPCRs has been linked to the control pathophysiological processes and may be leveraged for the development of more precise and effective drugs (Thomsen et al., 2018; Klauer et al., 2024; Sposini & Hanyaloglu, 2017). In particular, the sustained endosomal signalling responses of PAR2 and NK1R have been implicated in the persistent hyperexcitability of nociceptors that underlies chronic pain (Latorre et al., 2022; Jimenez-Vargas et al., 2018; Jensen et al., 2017). Specific blockade of these receptors in endosomes, achieved by antagonist conjugation to membrane lipid anchors or encapsulation into pH-responsive nanoparticles, has provided effective pain relief *in vivo* (Jensen et al., 2017; Jimenez-Vargas et al., 2018; Hegron et al., 2023; Jiménez-Vargas et al., 2022; Jimenez-Vargas et al., 2020; Latorre et al., 2022). In contrast, endosomally targeted agonists of the anti-noicieptive δ-opioid receptor promotes sustained analgesia in mouse models of colitis (Jimenez-Vargas et al., 2020).

1.4 Free Fatty Acid Receptor 2 & 3

1.4.1 The Free Fatty Acid Receptor family

The free fatty acid receptor (FFAR) family of GPCRs consists of members that have been deorphanised as being activated by endogenous free fatty acids, and includes FFAR1-FFAR4.(Briscoe et al., 2003; Brown et al., 2003; Hirasawa et al., 2005; Le Poul et al., 2003). In humans, FFAR2 and FFAR3 are clustered with free fatty acid receptor 1 (FFAR1 / GPR40) at chromosomal locus 19q13.1 and share between 30-40% sequency identity amongst them. In contrast free fatty acid receptor 4 (FFAR4 / GPR120) resides separately on chromosome 10 and exhibits very low sequence similarity to other FFAR family members (Le Poul et al., 2003; Watson et al., 2012). Moreover, primates possess a tandem segmented duplication of the open reading frame (ORF) of FFAR3, known as GPR42 in humans (Sawzdargo et al., 1997). The original classification of GPR42 as a pseudogene has since been questioned, following evidence of human GPR42 functionality in heterologous expression systems (Puhl et al., 2015).

FFAR1 and FFAR4 are activated by both medium chain fatty acids (MCFAs) and long chain fatty acids (LCFAs), which contain 7-12 carbons and ≥13 carbon chains respectively (Briscoe et al., 2003; Hirasawa et al., 2005). FFAR1 and FFAR4 recognise a broad spectrum of both saturated and unsaturated fatty acids, derived from either dietary fats or *de novo* synthesis in the liver. FFAR2 and FFAR3 are endogenously activated by SCFAs produced by the gut microbiota (Le Poul et al., 2003; Brown et al., 2003). Apart from SCFAs, the nutrient-sensing repertoire of FFAR2/3 has more recently been reported to include a class of hepatic metabolites known as ketone bodies (Kimura et al., 2011; Miyamoto et al., 2019; Mårtensson et al., 2023). Ketogenesis is upregulated in response to low blood glucose levels, such as during low-carbohydrate diets, starvation or untreated type I diabetes, to provide an alternative energy source for tissues (Veech et al., 2001). Under such conditions, fatty acids are mobilised from adipose tissue and serve as the primary substrates for ketogenesis in the mitochondria of hepatocytes (Veech et al., 2001). Two primary ketone bodies, acetoacetate and β-OHB, have been shown to modulate the activity of FFAR2 and FFAR3 respectively in both *in vitro* and *in vivo* studies (Kimura et al., 2011; Miyamoto et al., 2019; Mårtensson et al., 2023; Grüter et al., 2023).

FFAR1-4 exhibit functionalities that are therapeutically relevant to diverse facets of metabolism and inflammation, which are reflected in their tissue-specific expression patterns.

1.4.2 FFAR1

The expression of FFAR1 was first characterised to be abundant in pancreatic islets, and subsequent studies have demonstrated an enhancement of glucose-stimulated insulin secretion from pancreatic β-cells by LCFAs *via* activation of FFAR1 (Itoh et al., 2003; Briscoe et al., 2003). FFAR1 is also expressed on neurons across the CNS and contributes to monoaminergic neurotransmission systems underlying antinociceptive and emotional behaviours (Aizawa et al., 2016; Nakamoto et al., 2017). Other sites of FFAR1 expression include the gastrointestinal tract, where FFAR1 is present on various enteroendocrine cell types (Edfalk, Steneberg & Edlund, 2008). Chemosensation of luminal LCFAs by FFAR1 on L, K and I cells has been implicated

in driving the secretion of GLP-1, GIP and CCK respectively (Edfalk, Steneberg & Edlund, 2008; Liou et al., 2011). FFAR1 is expressed in the liver, and FFAR1 agonists have demonstrated hepatoprotective benefits by reducing lipogenesis and fibrosis *in vivo* (Pon`kina et al., 2023; Gagnon et al., 2018; Ookawara et al., 2020). FFAR1 expression has been reported in the heart, bone and muscle, though FFAR1 functionality in these tissues warrants further study (Briscoe et al., 2003; Milligan et al., 2017).

1.4.3 FFAR4

In its initial deorphanisation, FFAR4 was shown to be abundantly expressed in both human and mice in the large intestine and lungs (Hirasawa et al., 2005). Regarding the latter, recent *in vivo* evidence from FFAR4$^{-/-}$ mice has illuminated the role of FFAR4 in regulating innate immune cell infiltration, pulmonary barrier integrity and epithelial dysplasia following immune injury (Sveiven et al., 2023). FFAR4 is expressed on IECs and all major EEC cell types in both rodent and human gastrointestinal tracts and has been implicated in mediating lipid-induced GLP-1, CCK and GIP secretion *in vivo* (Ghislain & Poitout, 2021). In contrast, small molecule agonists of FFAR4 have exhibited inhibitory effects on the secretion of ghrelin and SST from gastric EECs *in vitro* (Lu, Gribble & Reimann, 2018). Interestingly, transcript levels of FFAR4 have been observed to positively correlate with obesity-related markers in humans and mice (Milligan et al., 2017). Moreover, a functionally compromising genetic polymorphism in FFAR4 has been linked to obesity in a European population (Ichimura et al., 2012)

FFAR4 is also expressed across cells of the innate and adaptive immune system and has been shown to mediate several anti-inflammatory benefits of poly-unsaturated omega 3 fatty acids (ω-3 PUFAs) (Duah et al., 2023). ω-3 PUFA-mediated stimulation of FFAR4 has ameliorated inflammation in mouse models of high fat diet (HFD)-induced obesity by reducing adipose tissue macrophage (ATM) infiltration and inflammatory gene expression (Oh et al., 2014). Supplementation with docosahexaenoic acid (DHA) has reduced lymphocytic infiltration and pro-inflammatory cytokine production in the colonic mucosa of mice with experimental colitis, which has been linked to FFAR4-dependent regulation of Nuclear factor kappa-

light-chain-enhancer of activated B cells (NF-κB) activity (Zhao et al., 2017). Moreover, inhibition of NF-κB signalling downstream of FFAR4 activation has been shown to prevent inflammation-driven bone destruction *in vivo* by suppressing osteoclastic resorption (Tsuchiya et al., 2020).

1.4.4 FFAR2 & FFAR3

1.4.4.1 Expression & Function

FFAR2 and FFAR3 influence a plethora of unique functions in immunity and metabolism.

GI tract

Numerous studies have detected the expression of FFAR2 and FFAR3 has been detected in GLP-1 and PYY-positive enteroendocrine L-cell populations derived from rat, mouse and human intestines (Karaki et al., 2006; Karaki et al., 2008; Samuel et al., 2008; Tazoe et al., 2009; Tolhurst et al., 2012). Both FFAR2 and FFAR3 have been shown to drive the secretion of GLP-1 and PYY downstream of SCFA supplementation *in vivo* (Samuel et al., 2008; Tolhurst et al., 2012; Psichas et al., 2015). The secretion of both these hormones, along with their associated metabolic benefits such as protection against HFD-induced obesity and blood glucose control, are compromised in FFAR2$^{-/-}$ and FFAR3$^{-/-}$ mice (Tolhurst et al., 2012; Bellahcene et al., 2013; Shimizu et al., 2019). The selective orthosteric FFAR2 agonist Compound 1 (Cpd1) has demonstrated promising metabolic benefit in HFD-induced obese mice, reducing bodyweight, food intake and GI motility (Forbes et al, 2015). Interestingly, Forbes et al (2015) also demonstrated that Cpd1-driven activation of anorexigenic circuitry in the mouse colonic mucosa was predominantly a PYY-mediated rather than a GLP-1- or dual hormone-mediated response. By employing the selective FFAR3 agonist AR420625, a further study by this group have identified a PYY-independent mechanism of FFAR3 agonism in human and mouse colonic mucosae which relies on

submucosal enteric neuronal activity; their findings discriminate between FFAR2 and FFAR3 signalling in being primarily neuronal- and L-cell derived respectively (Tough et al, 2018).

FFAR2 and FFAR3 are also expressed on intestinal epithelial cells, and are involved in mediating critical anti-bacterial immune responses in the colonic mucosa (Kim et al., 2013) Interestingly, FFAR2 has been associated with the anti-inflammatory effects of SCFAs in the intestinal epithelium of animal models of inflammatory bowel disease (IBD), and is also found to be expressed at lower levels in ileal biopsies of patients with Crohn's disease (CD), when compared to healthy controls (Maslowski et al., 2009; Macia et al., 2015; Agus et al., 2016). FFAR2-knockout mice, as well as germ-free mice which produce little or no SCFAs, display increased inflammation, decreased colon length and greater morbidity in DSS-induced colitis (Maslowski et al., 2009). Interestingly, administration of a synthetic allosteric agonist of FFAR2 has decreased susceptibility to DSS-induced colitis as well as severity of inflammation (Agus et al., 2016). Previous studies have demonstrated a protective role of FFAR2 in the suppression of intestinal carcinogenesis *in vivo* (Tang et al., 2011; Sivaprakasam et al., 2016). Propionate and butyrate have been reported to exert anti-tumour potential by inhibiting cell cycle progression and survival *via* activation of FFAR2 in human colorectal epithelial cells *in vitro* (Tang et al., 2011). Moreover, expression of FFAR2 has been found to be significantly downregulated in human colorectal cancer tissue compared to healthy colonic tissue (Tang et al., 2011).

Aside from the colon, the expression of both FFAR2 and FFAR3 has been detected in the gastric mucosa; acetate and propionate have been found to inhibit the secretion of ghrelin from primary gastric EECs *ex vivo* in and FFAR2- and FFAR3-dependent manner (Engelstoft et al., 2013).

Nervous system

FFAR2 and FFAR3 are also expressed across various peripheral afferents that directly relay gut-derived information to the CNS (Calabrò et al., 2023). FFAR2 and FFAR3 expression has been detected in parasympathetic neurons of the nodose ganglion of mice, and FFAR3 on vagal sensory nerve terminals has been implicated in establishing a direct link between enteric SCFAs and central control of feeding behaviours (Cook et al., 2021; Barki et al., 2022). Genetic ablation of vagal FFAR3 in mice has disrupted the positive effects of propionate supplementation on suppressing food intake and weight gain in response to an obesogenic diet (Cook et al., 2021). In addition, propionate and the ketone body β-OHB have been shown to directly regulate activity of the sympathetic nervous system *via* FFAR3 expressed in super cervical ganglia (SCG) (Kimura et al., 2011). Interestingly, sympathetic outflow was increased by propionate-mediated activation of FFAR3, whereas sympathetic depression was induced by β-OHB antagonism of FFAR3 thereby regulating a protective decrease in energy expenditure during ketogenesis in starvation and diabetes (Kimura et al., 2011). Moreover, FFAR3 expression has also been detected within the CNS in the cerebral endothelium, and there is interest in elucidating the contribution of FFAR3 to the anti-inflammatory effects of propionate in supporting integrity of the blood-brain barrier (BBB) (Hoyles et al., 2018).

In the somatic nervous system of mice, FFAR3 has been found to be functionally expressed on sensory dorsal root neurons and has been suggested to bestow neurons with anti-oxidative defences that might offer much therapeutic promise in treating peripheral inflammatory neuropathies (Nøhr et al., 2015; Barki et al., 2022; Grüter et al., 2023). Both propionate and β-OHB have exerted neuroprotective effects against oxidative stress in root ganglia in a FFAR3-dependent manner *ex vivo* (Grüter et al., 2023). In addition, transgenic mouse models have established the expression of FFAR3 on neurons in the submucosal and myenteric plexuses of the enteric nervous system (Tazoe et al., 2009; Nøhr et al., 2013; Barki et al., 2022). Butyrate has been observed to regulate populations of mouse cholinergic myenteric neurons and cholinergic-mediated contractile activity of colonic muscle *ex vivo*, however whether these effects are FFAR3-dependent warrants further study (Soret et al., 2010).

Pancreatic islets

Expression of both FFAR2 and FFAR3 has been detected in mouse and human pancreatic islet β-cells (Tang et al., 2015). Aside from the indirect effects of FFAR2 and FFAR3 on insulin secretion *via* the incretin effects of GLP-1, both receptors have been shown to directly affect insulin release of glucose-stimulated insulin secretion (GSIS) in mouse and human islets (Oteng & Liu, 2023). SCFA-mediated activation of FFAR3 has been proposed to mediate an inhibition of insulin secretion, with the knockdown of FFAR3 in mice potentiating GSIS from mouse islets *in vitro* (Priyadarshini & Layden, 2015; Tang et al., 2015). In agreement, improvements in glucose tolerance in HFD-fed transgenic mice selectively depleted of pancreatic FFAR3 have been observed (Tang et al., 2015).

SCFA-mediated activation of FFAR2 has been implicating in stimulating GSIS in mouse and human islets in vitro and ex vivo (McNelis et al., 2015; Pingitore et al., 2019). In contrast, the synthetic FFAR2 agonists 4-CMTB and TUG-1375 have been reported to inhibitory GSIS in human pseuodoislet systems (Lorza-Gil et al., 2020). Forbes et al (2015) have also demonstrated an inhibitory effect of the agonist Cpd1 on glucose tolerance and insulin secretion in lean and HF-DIO mice.

Adipose tissue

Numerous studies demonstrated that FFAR2 is expressed in both human and mouse adipose tissue (; Le Poul et al., 2003; Hong et al., 2005; Ge et al., 2008; Zaibi et al., 2010; Dewulf et al., 2013). Acetate and propionate have exhibited anti-lipolytic activity on murine adipocytes *in vitro* which is sensitive to small interfering RNA (siRNA)-mediated suppression of FFAR2 expression (Hong et al., 2005). Propionate-mediated activation of FFAR2 has also been shown to suppress adipogenic differentiation of human mesenchymal stem cells *in vitro,* however the involvement of FFAR2 in human and mice adipogenesis is disputed amongst the conclusions of all studies thus far (Iván et al., 2017; Al Mahri et al., 2022). Given that the adipose tissue is a critical regulator of systemic glucose and energy metabolism, it is unsurprising that the functional significance of adipose FFAR2 has garnered therapeutic interest in potentially treating diabetes and obesity (Al Mahri et al., 2022). Interestingly, contrasting metabolic phenotypes have been observed between FFAR2$^{-/-}$ mice and transgenic mice overexpressing adipose-specific FFAR2 (*aP2-Gpr43TG)* (Kimura et

al., 2013a). FFAR2$^{-/-}$ mice exhibited increased body weights, and enlargement of adipocytes in WAT under HFD conditions, all of which appeared to be attenuated in *aP2-Gpr43TG* littermates (Kimura et al., 2013a). Moreover, activation of FFAR2 by acetate was shown to functionally supress insulin signalling and thereby energy uptake in mouse white adipose tissue, ultimately enhancing systemic insulin sensitivity and energy utilisation by other tissues (Kimura et al., 2013a). Unlike with FFAR2, it is debated whether FFAR3 is expressed at significant levels in adipose tissue, although depletion of FFAR3 in mice has been observed to compromise SCFA-mediated leptin production *in vitro* and *in vivo* (Brown et al., 2003; Samuel et al., 2008; Zaibi et al., 2010; Frost et al., 2014; Inoue, Tsujimoto & Kimura, 2014; Al Mahri et al., 2022).

Immune system

The expression of both receptors was first characterised in white blood cells in humans, and FFAR2 concurrently was shown to encourage neutrophil chemotaxis following activation acetate or propionate *in vitro* (Le Poul et al., 2003). FFAR2 has since been reported to significantly enhance the protective pro-inflammatory responses of a variety of innate immune cells, and FFAR2-knockout mice have demonstrated unresolving inflammation in models of asthma, arthritis, and colitis (Z. Ang et al., 2016; Fachi et al., 2020; Maslowski et al., 2009; Sina et al., 2009). Moreover, a distinct function of FFAR2 on anti-inflammatory M2 macrophages in white adipose tissue has been observed *in vivo*; FFAR2 activation by acetate stimulating the induction of M2 tumour necrosis factor-α (TNF-α) signalling, a crucial agency in supressing fat accumulation and regulating adipose insulin sensitivity (Nakajima, et al., 2017). In addition, the expression and functionality of FFAR2 and FFAR3 on various arms of adaptive immune system have been established across heterogeneous immune niches in transgenic mice *(*Kimura et al., 2020). Propionate-mediated activation of FFAR2 on regulatory T cells (Tregs) populations in the colonic mucosa, has been shown to enhance the local abundance as well of the anti-inflammatory functionalities of these protective cells (Smith et al., 2013). Independent of T cells, activation of FFAR2 by acetate on mouse intestinal dendritic cells has also been shown to promotes IgA class switching of B cells cultures and IgA production *in vitro* (Wu et al., 2017). FFAR3 is abundantly expressed on medullary epithelial cells (ECs) in the thymus and has been shown to mechanistically link butyrate production

by maternal microbiomes and the induction of thymic Treg differentiation in offspring *in vivo* (Nakajima, et al., 2017).

1.4.4.2 Pharmacology

SCFAs exhibit different potencies on FFAR2 and FFAR3 based on the length of their carbon chain (Brown et al., 2003; Le Poul et al., 2003; Nilsson et al., 2003). Both receptors are activated by SCFAs of 1 to 6 carbons in length, most notably acetate (C2), propionate (C3) and butyrate (C4), in the high micromolar to millimolar range (Brown et al., 2003; Le Poul et al., 2003). Using recombinant cell systems, deorphanisation studies of FFAR2 established acetate and propionate to be equipotent at the human ortholog (hFFAR2), followed by valerate (C5) and formate (C1) (C2 =C3 > C4 > C5= C1) (Brown et al., 2003; Le Poul et al., 2003; Nilsson et al., 2003; Milligan, Stoddart & Smith, 2009). In contrast, FFAR3 shows a stronger response to longer SCFAs, exhibiting a rank order of C3 = C4 = C5 > C2 > C1 was observed for FFAR3 (Brown et al., 2003; Le Poul et al., 2003; Milligan, Stoddart & Smith, 2009). That acetate has demonstrated approximately 10 times more potency at hFFAR2 has prompted its use as an FFAR2-selective SCFA (Milligan et al., 2017). In addition, the 6-carbon SCFA caproate has been found to exclusively but weakly activate hFFAR3, and not hFFAR2 (Nilsson et al., 2003; Stoddart et al., 2008).

In probing the structure-activity relationships (SARs) of SCFAs at hFFAR2 and hFFAR3, Stoddart et al., (2008) uncovered four conserved polar residues within their TM regions that facilitate stabilising charge interactions with SCFA carboxylate moieties: two arginine residues, one in in TMD V (5.39), and one in TMD VII (7.35), and two histidine residues, one in TM IV (4.56) and one in VI (6.55) (*Figure 1.5)*.

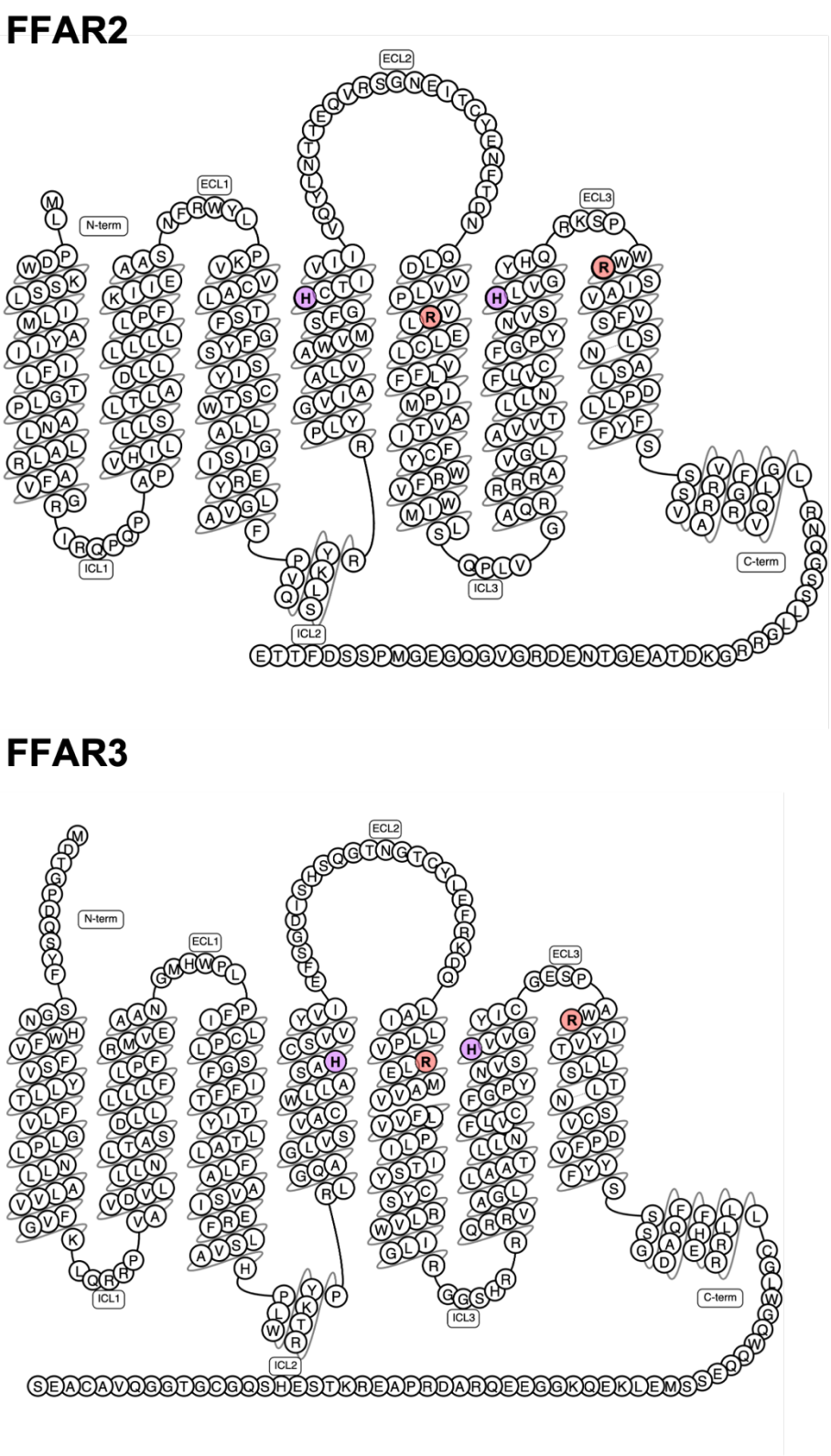


Figure 1.5 Snake plot of FFAR2 and FFAR3 highlighting key residues in facilitating SCFA binding. FFAR2 and FFAR3 snake plots modified from the GPCR database (GPCRdb) showing structural features of the 7TM configuration. Conserved arginine and histidine residues involved in charge-stabilising interactions between receptor and SCFA carboxylate

moieties are highlighted in pink (Arginine 5.39, Arginine 7.35) and purple (Histidine 4.56, Histidine 6.55) respectively.

Although these four residues are conserved in both FFAR2 and FFAR3 across human and mice, SCFAs display distinct selectivity at mouse FFAR2 (mFFAR2) and FFAR3 (mFFAR3) to their human counterparts (Hudson et al., 2012). In contrast to acetate's strong preference for FFAR2 between human orthologs, acetate does not discriminate between mFFAR2 and mFFAR3 (Hudson, et al., 2012). In addition, propionate is approximately 12 times more potent at mFFAR3 than mFFAR2, and butyrate is non-selective between both mouse orthologs (Hudson et al., 2012). The increased potency of SCFAs at hFFAR2 and mFFAR3 has been attributed to a higher level of constitutive receptor activity compared with mFFAR2 and hFFAR3 (Hudson et al., 2012). Mutagenesis studies identified a glutamate residue and (Glu-159) an asparagine residue (Asp-158) in the extracellular loop II of mFFAR2 and hFFAR3 respectively, that by forming ionic interactions with conserved arginines in the SCFA binding pockets can 'lock' mFFAR2 or hFFAR3 in an inactive conformational state with limited ligand-independent activity (Hudson et al., 2012).

1.4.4.3 Signalling Pathways

Despite the overlap of their endogenous SCFA agonists, FFAR2 and FFAR3 display unique G-protein coupling specificities (Nilsson et al., 2003; Le Poul et al., 2003; Brown et al., 2003). Using the well-established pheromone reporter assay in yeast, Brown et al. revealed FFAR2 to couple to multiple yeast/mammalian Gα chimeras from $G\alpha_{i/o}$ and $G\alpha_{q/11}$ families (King et al., 1990). FFAR2 coupling to both $G\alpha_{i/o}$ and $G\alpha_{q/11}$ pathways was also demonstrated by functional assays measuring intracellular cAMP accumulation or Ca^{2+} mobilisation respectively (Le Poul et al., 2003). In contrast, FFAR3 prefers coupling to Gαi (Le Poul et al., 2003; Brown et al., 2003) However, like many Gαi-coupled receptors, FFAR3 can elicit Ca^{2+} release by co-expression with the promiscuous G protein Gα16 (Milligan, Stoddart & Smith, 2009).

Besides G-protein coupling, BRET-based studies have established the interaction of FFAR2 with β-arrestin 2 in response to agonist stimulation (Hudson et al., 2012;

Hudson et al., 2013). Moreover, a β-arrestin dependent signalling pathway has been implicated in the suppression of nuclear translocation of the NF-κB activity by FFAR2 synthetic agonists *in vitro* (Lee et al., 2013). Although studies on FFAR3-arrestin interactions are scarcer, SCFA-induced signalling *via* FFAR3 has not been compromised by siRNA knockdown of β-arrestin 2 *in vitro* (Kimura et al., 2011). In addition, FFAR2 and FFAR3 have been shown to form heteromers, in both primary human phagocytes and heterologous expression systems, with unique pharmacological properties to parent monomers. Interestingly, FFAR2-FFAR3 heteromers display enhanced Ca^{2+} signalling and β-arrestin 2 recruitment, but the inability to inhibit cAMP accumulation via $G\alpha_{i/o}$ (Ang et al., 2018). Both FFAR2 and FFAR3 have also been linked to the activation of various mitogen-activated protein kinase (MAPK) cascades (Seljeset & Siehler, 2012) Notably, regulation of ERK1/2 and p38-MAPK activity by FFAR2 and/or FFAR3 is closely associated with various facets of immune and metabolic homeostasis (Caengprasath et al., 2020; Mishra et al., 2020).

1.5 The cellular repertoire of the intestinal epithelium

1.5.1 Intestinal Stem Cell Niche

The innermost lining of the intestine, known as the epithelium, is a highly dynamic cellular landscape that contributes to immunity, digestion and symbiotic functions of the gut microbiome (van der Flier & Clevers, 2009). The cellular architecture of the human intestinal epithelium replenishes itself every 4-5 days and is compartmentalised into crypts, invaginations into the mesenchyme where proliferating intestinal stem cells (ISCs) reside, and villi, finger-like protrusions into the lumen composed of differentiated cell types (Clevers, 2013). Comparatively, the epithelial lining of the colon is folded into crypts which are wider and flat, and does not form villi (de Santa Barbara, van den Brink & Roberts, 2003). In addition to facilitating the self-renewing capacity of the intestinal epithelium, ISCs are the origin of all differentiated intestinal epithelial cell types owing to their multipotency (Sato et al., 2009; Cheng &

Leblond, 1974). Mature intestinal epithelial cells are categorised as absorptive, known as enterocytes, or secretory which fall into three cell types: antimicrobial peptide-secreting Paneth cells, mucus-secreting goblet cells, and hormone-secreting enteroendocrine cells (Beumer & Clevers, 2021). The dynamics of ISC proliferation and differentiation are instructed by their microenvironment, known as the ISC niche (Gehart & Clevers, 2019). The ISC niche comprises an epithelial and mesenchymal cellular network that provides local niche factors that regulate ISC behaviours such as Wnt, Notch, EGF, BMP and Hippo signals (*Figure 1.6)* (Gehart & Clevers, 2019).

ISCs, which are also called crypt base columnar cells (CBCs), are marked by the presence of the leucine-rich repeat-containing G-protein coupled receptor 5 (Lgr5) (Barker et al., 2007). In the small intestine, CBCs are interspersed at the crypt base between post-mitotic specialised Paneth cells that supply essential niche signals (Sato, van Es, et al., 2011). Paneth cells are absent in the colon and the colonic crypt niche is instead supported by $Reg4^+$ deep crypt secretory cells (DCS) (Sasaki et al., 2016). $Lgr5^+$ ISCs divide once every 24 hours to produce a vigorously proliferating but short-lived subset of progenitors known as transit amplifying (TA) cells (Clevers, 2013). TA cells undergo 4-5 rounds of cell division whilst migrating upwards before terminally differentiating to yield mature absorptive and secretory lineages (*Figure 1.5)* (Marshman, Booth & Potten, 2002). *In vivo* cell lineage tracing experiments have identified a second population of “label-retaining” ISCs, located at the +4 position from the crypt base, with distinct kinetics and functions to $Lrg5^+$ CBCs ((Yan et al., 2012). In contrast to continuously cycling $Lrg5^+$ ISCs, +4 ISCs are quiescent in homeostatic conditions and injury-resistant; +4 ISCs are proposed to represent committed secretory progenitor cells that are capable of de-differentiation to $Lrg5^+$ ISCs during intestinal injury (Yan et al., 2012; Buczacki et al., 2013).

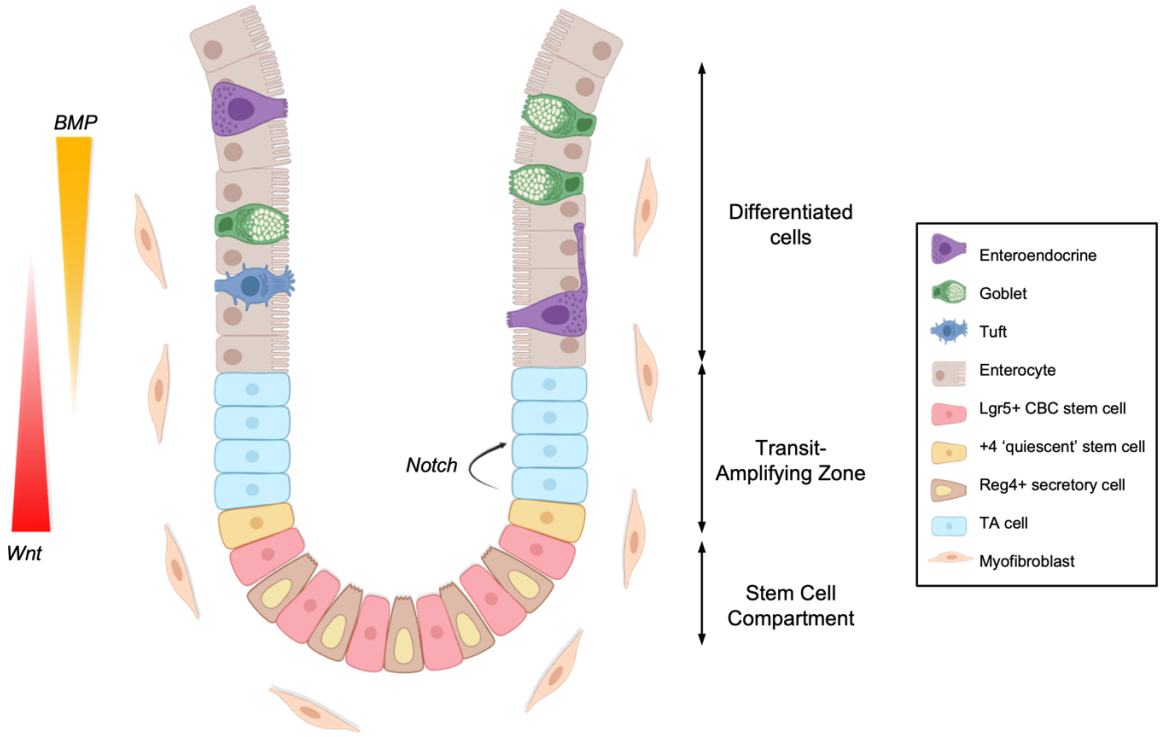


Figure 1.6 The architecture and cellular heterogeneity of the human intestinal colonic crypt. The intestinal crypt can be divided into three zones; a stem cell compartment at the crypt base which is followed by a transit-amplifying zone, and finally a differentiated zone in the upper crypt. The stem cell compartment lies is where proliferative Lgr5+ crypt-base columnar cells (CBCs) reside. In the colon, CBCs are interspersed with Reg4+ secretory cells at the crypt base which provide essential niche signals. Within the stem cell compartment, a quiescent stem-cell population which are mobilised upon intestinal injury are situated at the +4 position from the crypt base: +4 cells. CBCs generate transit amplifying (TA) cells which undergo rapid cell division whilst migrating up the crypt to give rise to mature absorptive (enterocyte) and secretory (goblet, tuft, enteroendocrine) lineages. The intestinal stem cell (ISC) niche is comprised by subepithelial mesenchymal elements such as myofibroblasts, and paracrine signals such as Wnt, Notch and bone morphogenetic protein (BMP).

1.5.2 Notch in intestinal epithelial cell fate

Notch signalling is an evolutionary conserved cell-cell communication pathway that governs cell fate in many aspects of metazoan development and tissue homeostasis

(Bray, 2016). Within the intestinal milieu, Notch machinery serves as both a gatekeeper of ISC proliferation and a binary cell fate determinant between absorptive and secretory lineages (Jensen et al., 2000; Yang et al., 2001).

By a mechanism known as lateral inhibition, Notch is able to specify differential cell fates of adjacent cells, thereby producing the characteristic cellular mosaic patterning of differentiated cell types in the intestinal epithelium (*Figure 1.7)* (Pellegrinet et al., 2011; Fre et al., 2005). Notch is a negative regulator of endocrine differentiation, with first evidence coming from studies in the mouse pancreas reporting the premature differentiation of multipotent progenitor cells into endocrine cells by the blockage of Notch signalling (Apelqvist et al., 1999). Activation of Notch relies on cell-cell contact and is mediated by the binding of with a transmembrane Notch ligand on one cell with a Notch receptor on the surface of an adjacent 'receiving' cell (Fre et al., 2005a; Pellegrinet et al., 2011). In the 'receiving' cell, membrane-tethered Notch undergoes three consecutive cleavages to release the Notch intracellular domain (NICD) (Bray, 2016). NICD translocates to the nucleus where it forms a transcriptional activation complex with the CBF1-Supressor of Hairless-LAG-1 (CSL or RBP-Jκ) to stimulate the expression of Notch target genes including the hairy and enhancer of split-1 (Hes-1) (Jensen et al., 2000; Bray, 2016). Atonal homologue 1 *(Atoh1)* is a bHLH transcription factors antagonised by *Hes1* and is required in committing progenitor cells to secretory enteroendocrine, goblet or Paneth fates (Yang et al., 2001; Shroyer et al., 2007). As such, the status of Notch activity in a crypt progenitor cell specifies an absorptive or secretory fate *via* the action of *Hes1* or *Atoh1* respectively. Intestine-specific knockout *Atoh1* mice causes a secretory-to-absorptive fate switch in crypts, with emerging progenitor cells solely differentiating to enterocytes (Shroyer et al., 2007). Conversely, *Hes1*-knockout mice display secretory cell hyperplasia at the expense of enterocyte development (Jensen et al., 2000; Suzuki et al., 2005). The mechanism of Notch lateral inhibition relies on a positive feedback loop in adjacent cells which reinforces their differential cell fates; The expression of delta-like Notch ligands *Dll1* and *Dll4* is directly upregulated by *Atoh1,* thus repressing secretory differentiation of neighbouring cells (Kim & Shivdasani, 2011).

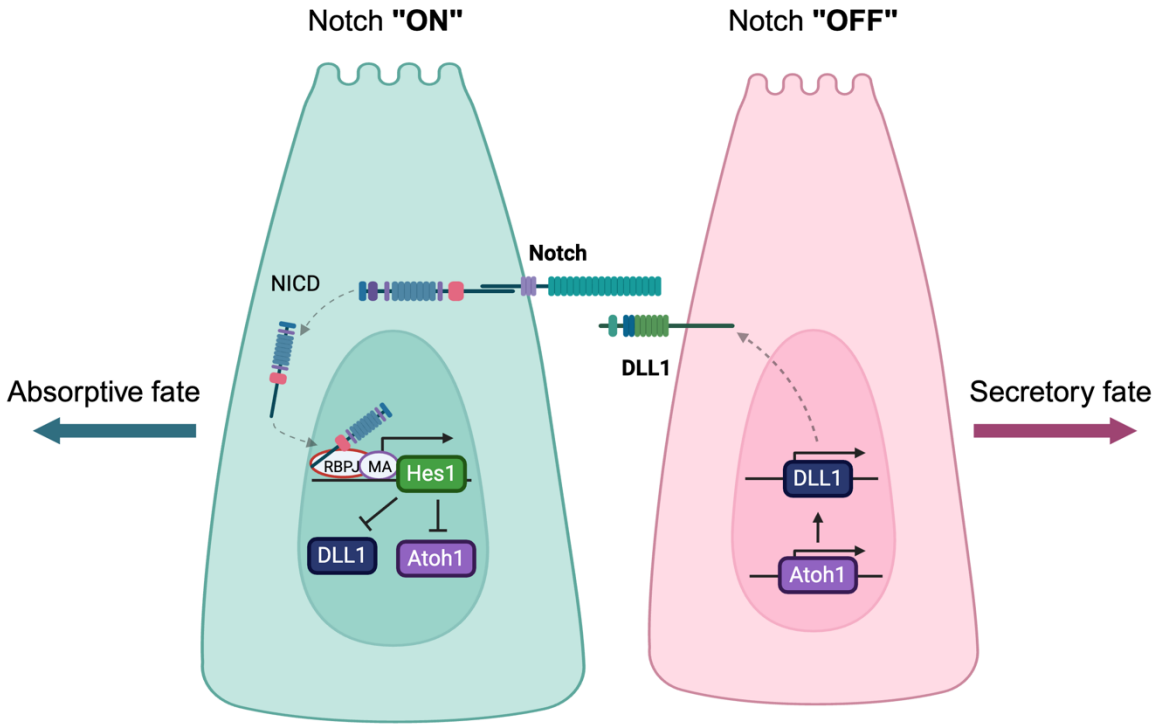


Figure 1.7 Lateral Inhibition by Notch in ISCs and TA cells. Schematic indicating the mechanism of lateral inhibition underlying Notch-mediated cell fate specification in the ISC niche. Notch signalling is initiated when a cell-surface Delta ligand *e.g* (DLL1) binds to a Notch receptor expressed on the surface of a neighbouring cell. The activation of Notch is followed by sequential proteolytic cleavage events which liberate the Notch intracellular domain (NICD). NICD translocates to the nucleus where it forms a transcriptional activation complex with transcription factor CBF1-Supressor of Hairless-LAG-1 (CSL or RBP-Jκ) and a member of the Mastermind family of transcriptional coactivators (MAML1-3). This complex relieves the repression on the gene expression of the downstream Notch effector, hairy and enhancer of split-1 (Hes-1). Hes-1 represses the expression of the secretory lineage differentiation factor, Atonal homologue 1 (Atoh1). In a cell with "low" Notch activity, the expression of Atoh1 is derepressed. Atoh1 is a direct upregulator of Delta ligand transcription in "low" Notch cells, whereas Delta ligand expression is repressed in "high" Notch cells. These mechanisms reinforce the opposing Notch status of neighbouring cells and hence facilitate their progression to divergent cell fates.

1.5.3 GPCRs in the intestinal stem cell niche

Although signalling gradients such as Wnt, Notch and BMP are primarily known to co-ordinate the ISC niche, a number of GPCRs have emerged as important regulators of ISC behaviours during homeostasis, regeneration and tumorigenesis (Ho et al., 2024). For example, activation of GPR81 on Paneth cells and subepithelial stromal cells by the gut microbial metabolite lactate is involved in maintenance of ISC proliferation *in vivo* by upregulation of Wnt signalling. (Lee et al., 2018). The cholecystokinin 2 receptor (CCK2R) upregulates the proliferation of $Lgr5^+$ stem cells in murine colonic crypts upon stimulation with prograstrin (Jin et al., 2009). Notably, Prograstrin-CCK2R interactions appear to stimulate signal transduction by beta-arrestins rather than a classical G-protein dependent mechanism. Progastrin is also a ligand for the GPR56, expressed on colonic stem-progenitor cells, and GPR56-dependent mechanism have been shown to underlie progastrin-stimulated proliferation of intestinal epithelial cells in mouse models of colorectal cancer (Jin et al., 2017). Synthetic agonists of both FFAR2 and FFAR3 have stimulated IEC proliferation and turnover in mouse intestinal organoids *in vitro* (Park et al., 2016). In contrast, the orphan GPCR GPR182 has been shown to negatively regulate the proliferation of small intestinal ISCs during irradiation-induced injury via an upregulation of ERK 1/2; however, this receptor-mediated effect is specific to regeneration and not evident in homeostatic conditions (Kechele et al., 2017).

1.6 Enteroendocrine cells

1.6.1 EEC Classification & Function

Enteroendocrine cells (EECs) are a rare hormone-secreting mature cell type that populate 1% of the intestinal epithelium, but collectively comprise the body's largest endocrine system (Goldspink, Reimann, et al., 2018). EECs express a complement of transporters and GPCRs which sense diverse nutrient, chemical and mechanical cues and respond by activating hormone release (Gribble & Reimann, 2016). Mechanistically, both transporter- and GPCR-mediated signalling cascades drive the exocytosis of hormone-containing secretory granules from EECs in a Ca^{2+} -dependent

manner *via* influx of extracellular Ca^{2+} through voltage- or ligand-gated channels, or mobilisation of Ca^{2+} from intracellular stores (Gribble & Reimann, 2016). Once secreted, EEC-derived hormones impact broad aspects of metabolism and physiology by paracrine action on intrinsic enteric nerves, DRG neurons, vagal afferents or neighbouring cells in the mucosa, or by entering the circulation and activating receptors on organs in the periphery (Schonhoff, Giel-Moloney & Leiter, 2004).

EEC subtypes have historically been categorised by a single letter code based on their principle hormonal product, with the exception of L-cells for which both glucagon- and polypeptide-like immunoreactivity was observed (Fothergill & Furness, 2018; El-Salhy et al., 1983; Buffa et al., 1978). As per the "one cell-one hormone" classification system, the human EEC repertoire consisted of the following subtypes: G cells (gastrin), X/A cells (ghrelin), K cells (gastric inhibitory peptide), D cells (somatostatin), S cells (secretin), I cells (CCK), M cells (motilin), Enterochromaffin cells (serotonin), N cells (neurotensin) & L-cells (GLP-1, PYY) (Fothergill & Furness, 2018). However, an overwhelming body of research in the last decade confirms the existence of multihormonal EECs, and regional-specific differences in secretory repertoires within subtypes (Egerod et al., 2012; Habib et al., 2012; Grunddal et al., 2016; Fothergill et al., 2017; Glass et al., 2017; Haber et al., 2017; Martins et al., 2017; Gehart et al., 2019; Beumer et al., 2020). EECs can be further classified by their morphology as "open type", with an extending apical process bearing microvilli that make immediate contact with luminal contents; in contrast, "close type" EECs, are round in shape and linked to the basal membrane without making contact with the lumen (Gribble & Reimann, 2016). "Close-type" EECs are believed to be activated indirectly by luminal stimuli via neural or hormonal networks (Latorre et al., 2016).

1.6.2 EEC Differentiation

Downstream of *Atoh1,* activity of the bHLH protein Neurogenin 3 *(Neurog3)* is determinative in initiating the segregation of common secretory progenitors to an enteroendocrine lineage, rather than Paneth or goblet cell fates (Schonhoff, Giel-Moloney & Leiter, 2004; Jenny et al., 2002). As such, loss of *Neurog3* in the mouse intestine leads to a depletion of all mature hormone-secreting enteroendocrine

subtypes, whereas neither goblet nor Paneth cell production is compromised (Jenny et al., 2002). A paucity of EECs has been also reported in patients with loss-of-function mutations in *Neurog3* (Wang et al., 2006). *Neurog3*-positive cells represent a transient state common to early endocrine progenitors, and expression of *Neurog3* is switched off post-mitotically as cells begin to differentiate (Jenny et al., 2002; Schwitzgebel et al., 2000). *Neurog3* activates the transcription of Neurogenic Differentiation factor 1 (*NeuroD1*/*Beta2*); *NeuroD1* is required for differentiation and maturation of post-mitotic enteroendocrine progenitors and its expression is retained amongst nearly all mature EEC cell types (Gehart et al., 2019; Jenny et al., 2002; Naya et al., 1997; Mutoh et al., 1997; Huang et al., 2000).

Several studies employing knockout mice have identified transcription factors which may specify the differential hormonal signatures of EEC subtypes in the terminal stages of differentiation *in vivo* including *Pax4, Pax6, Arx, Foxa1/2* and *Isl1* (Larsson et al., 1998; Hill, Asa & Drucker, 1999; Beucher et al., 2012; Ye & Kaestner, 2009; Terry et al., 2014; Du et al., 2012). For example, depletion of *Pax6*, a direct activator of proglucagon gene expression, leads to an absence of GLP-1 and GLP-2 expressing-EECs in the mouse small and large intestine (Hill, Asa & Drucker, 1999). *Pax4* has been associated with the differentiation of serotonin-, secretin-, CCK-, GIP- and PYY-immunoreactive EEC subtypes in particular, but it is unknown whether Pax4 additionally behaves as a modulator of enterohormone gene transcription in these cells (Larsson et al., 1998; Brooks et al., 2017). Moreover, the promoters of *Pax4* and *Pax6* both contain candidate bHLH binding sites, known as ‘E boxes’; *Neurog3* and *NeuroD1* have been shown to activate *Pax4* and *Pax6* respectively *in vitro* (Smith et al., 2003; Marsich et al., 2003). Notably, single-cell transcriptomic studies in recent years by the *Clevers* group have provided immense spatial and temporal resolution to subtype-specific transcriptional cascades of EEC lineages in both the mouse and human intestine (Gehart et al., 2019; Beumer et al., 2020).

1.6.3 The L-cell

L-cells are EECs which are the predominant source of proglucagon-derived peptides (PGPDs), GLP-1, GLP-2, OXM and glicentin, and PYY (Böttcher et al., 1984). L-cell-

mediated hormone release is co-ordinated by membrane transporters and GPCRs which are responsive to a variety of luminal nutrient stimuli including glucose (Parker et al., 2012; Kuhre et al., 2015), artificial sweeteners (Jang et al, 2007), amino acids (Mace et al., 2012), bile acids (Trabelsi et al., 2015), fatty acid derivatives (Ekberg et al., 2016; Hodge et al., 2016), short-chain fatty acids (Psichas et al., 2015), medium- and long-chain fatty acids (Hirasawa et al., 2005; Peiris et al., 2022) ketone bodies (Elebring et al., 2023), non-nutrient food components such as allyl-isothiocyanate (mustard oil) and carvacrol (oregano) (Emery et al., 2015) , bitter tastants (Lee et al., 2023) and odorants (Kim et al, 2017; Y. Wang et al., 2023; Nishida et al., 2021).

Whether nutrient-sensing GPCRs on L-cells reside apically or basolaterally remains largely unknown due to the lack of receptor specificity in GPCR antibodies. However, a few L-cell GPCRs have been suggested to reside on the basolateral surface, including FFAR1 (Christensen et al., 2015; Psichas et al., 2017), MC4R (Panaro et al., 2014), the bile-acid receptor GPBAR1 (Brighton et al., 2015; Tough et al, 2020) and the L-amino acid-sensing calcium-sensing receptor (CasR) (Modvig et al., 2021), which mediate hormone secretion through non-luminal stimuli including stimulation from the ENS, post-absorptive nutrients in the circulation, or enterocyte-derived lipid metabolites. The orphan GPCR GPR119 (Hodge et al, 2016; Psichas et al., 2017), as well as the free fatty acid GPCRs FFAR2 and FFAR3 (Tough et al, 2018) have been proposed to reside on both apical and basolateral epithelial domains.

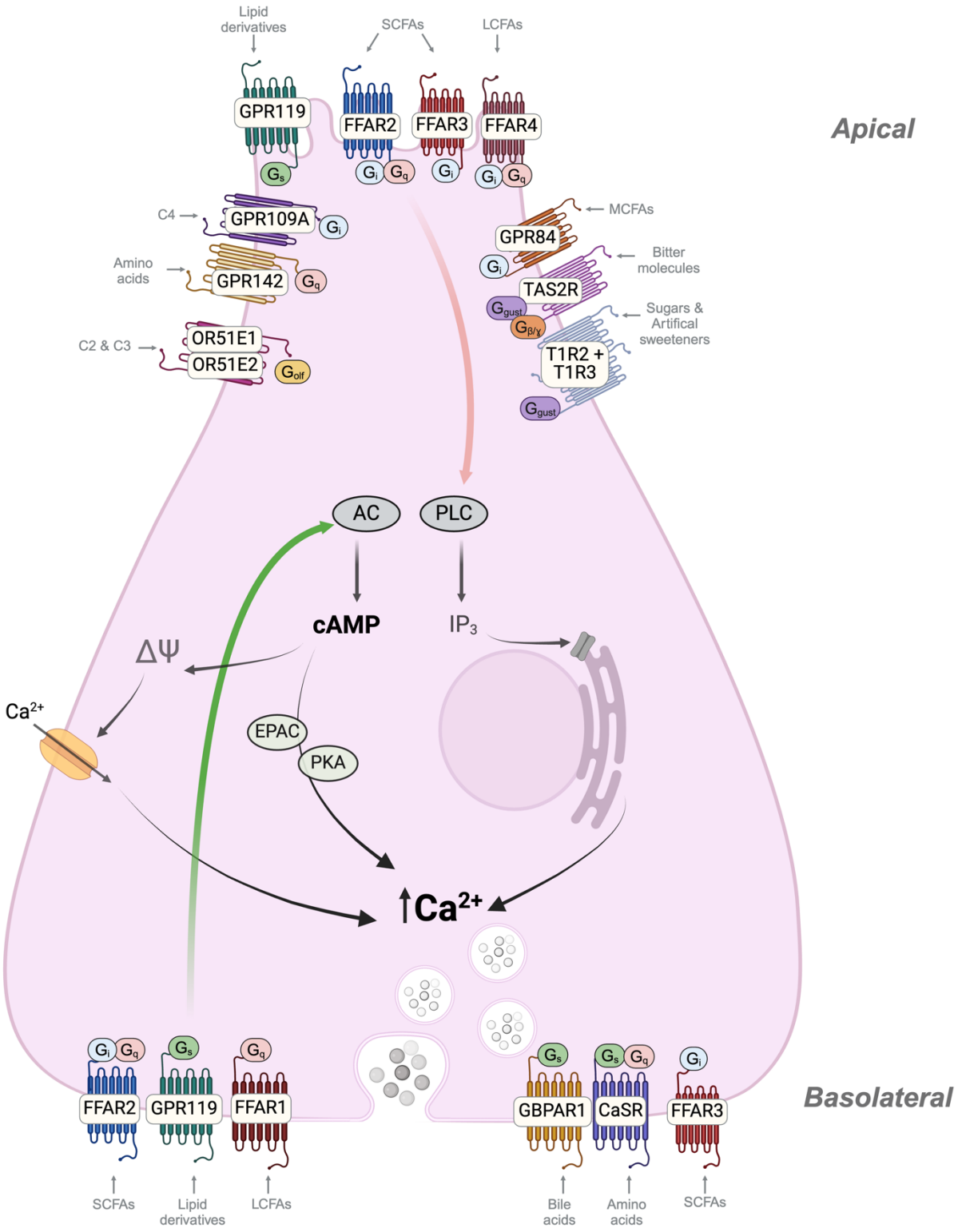


Figure 1.8 Classical molecular mechanisms of peptide hormone secretion from EECs which are modulated by nutrient sensing GPCRs. EECs express a diverse range of nutrient-sensing GPCRs stimulate Ca^{2+}-dependent exocytosis of peptide hormones via G-protein pathways. The action of Gαs-coupled receptors (indicated by a green arrow) stimulate

cAMP production by adenylyl cyclase (AC); cAMP can mediate Ca^{2+} influx via the action of protein kinase A (PKA) or exchange protein directly activated by cAMP (EPAC), in addition to binding to Hyperpolarization-activated cyclic nucleotide-gated channels (HCN). Gαq-coupled receptors (pink arrow) activate phospholipase C (PLC), leading to the production of IP_3 and intracellular calcium flux from IP_3-gated channels in the endoplasmic reticulum. Nutrient-sensing GPCRs that have been implicated in driving EEC gut hormone release are not limited to Gαs and Gαq coupling; examples are the actions of gustducin (G_{gust}) and Gβɣ subunits coupled to taste receptors, Golf pathways downstream of activation of olfactory GPCRs, and Gαi-coupled receptors. EECs can be stimulated to release hormone by the stimulation of GPCRs which are located on their apical or basolateral surface.

Notably, L-cells populations in the small and large intestine greatly differ in their hormonal repertoires; L-cells in the upper small intestine express high transcript levels of CCK and GIP alongside GLP-1, whereas GLP-1 and PYY co-expressing L-cells are enriched in the colon (Habib et al., 2012, 2012; Billing et al., 2019). L-cell secretion of PYY has been measured to increases distally along the length of the intestine, whereas GLP-1 secretion from ileal L-cells is higher than in the colon (Jones et al., 2023; Adrian et al., 1985). Although GLP-1 and PYY have previously been shown to largely co-localise within secretory granules of colonic L-cells, this is contradicted by reports of secretion of only one L-cell hormone upon nutrient challenge (Böttcher et al., 1984; Nilsson et al., 1991; Pironi et al., 1993; Anini et al., 1999; Gerspach et al., 2011; Habib et al., 2013). Moreover, 3D-structured illumination microscopy has resolved subcellular microdomains in human, pig, rat and mouse L-cells in which secretory vesicles harboring only one type of hormone (GLP-1 or PYY) predominate (Cho et al., 2014).

L-cells are often recognised by their “open-type” flask- or bottle-like morphology, consisting of a long microvilli-decorated apical pole reaching the gut lumen, and a capillary-facing basolateral side where hormone-containing granules 200-400nm in diameter are situated (Buffa et al., 1978). Seminal studies using electron microscopy also demonstrated the existence of long and slender basal cytoplasmic processes in PYY-immunoreactive cells that extended along the lamina propria, which were attributed to a potential paracrine action on adjacent goblet cells (Lundberg et al., 1982; El-Salhy et al., 1983; Böttcher et al., 1984). Decades later, Bohorquez unveiled

the 3D ultrastructure of these processes and coined the term “neuropod”, due to their anatomic similarity to a synaptic bouton (Bohórquez et al., 2011, 2014). Neuropods were evident in both ileal and colonic PYY-secreting L-cells, were upto 70µm in length spanning across 10-15 epithelial cells and contained over 70% of the total secretory vesicle pool of each EEC (Bohórquez et al., 2011, 2014, 2015). Interestingly, PYY-positive L-cells are enriched in a cohort of genes associated with synaptic function (Bohórquez et al., 2015). Using viral neuronal tracing, PYY-positive neuropods have been shown to engage in direct synaptic transmission with innervating vagal sensory fibers in the mouse colon (Kaelberer et al., 2018).

1.6.4 EEC Plasticity

A further challenge to the “one cell-one hormone” classification system of EECs is the concept of hormonal plasticity; the ability of mature EEC lineages to shift hormonal repertoires under the influence of local signalling microenvironments in the intestinal millieu (Beumer et al., 2018). Notably, L-cells and EC cells have been shown to exhibit a particular flexibility in hormonal expression, cued by crypt-to-villus gradients of the niche signal bone morphogenetic protein (BMP) *in vivo* (Beumer et al., 2018; Gehart et al., 2019; Beumer & Clevers, 2021). L-cells undergo a decrease in proglucagon (Gcg) expression and simultaneous transition to a transcriptional identity akin to I- or N-cells which coincides with their migration from BMP-low crypts zones to BMP-high villi zones*;* In EC cells, the selective expression of preprotachykinin-1 in crypts is overridden by secretin expression during their trajectory towards villus tips (Beumer et al., 2018; Gehart et al., 2019; Beumer & Clevers, 2021).

The differentiation of ISCs to EEC progeny, and the reversibility of this process, exhibits a high degree of plasticity in response to diet and injury. Both early secretory progenitors and mature EECs have been shown to dedifferentiate and regain Lgr5+ “stemness” during injury-induced regeneration of the intestinal epithelium (van Es et al., 2012; Yan et al., 2017). The effect of dietary patterns on cellular dynamics, fate and function in the ISC niche are widely appreciated, and several reports focus on the nutritional regulation of EEC differentiation in particular (Gribble & Reimann, 2016; Ho et al., 2024). Notably, high fat-diet induced obesity (HF-DIO) has been shown to

enhance the stemness of ISCs and intestinal progenitor cells *in vivo*, and at the expense of the abundance of differentiated secretory populations (Mah et al., 2014; Sakar et al., 2014; Beyaz et al., 2016; Aliluev et al., 2021). Reported effects of HF-DIO on EEC differentiation and functionality in particular are contradictory; inconsistency between the overall macronutrient composition of high-fat diets used in studies is a likely confounding factor (Aranias et al., 2015; Aliluev et al., 2021; Richards et al., 2016).

The consumption of dietary fiber has been shown to boost ISC proliferation *in vivo,* which has been linked with the increased production of SCFAs (Edwards et al., 1992; Lupton & Kurtz, 1993; Zhang & Lupton, 1994; Corrêa et al., 2023). However, both stimulatory and inhibitory effects of SCFA supplementation on ISC dynamics have been observed and highlighted divergent outcomes between epithelium from varying intestinal regions, and with SCFA chain length and concentration (Ichikawa et al., 2002; Boffa et al., 1992; Sakata, 1987; Grouls et al., 2022; Pearce et al., 2020). Notably, Brooks et al., reported that mice fed a diet enriched in the fermentable carbohydrate inulin had an increased abundance of colonic EECs positive for PYY; this effect was dampened in FFAR2-knockout mice, suggesting a potential involvement of an SCFA-FFAR2 axis. In addition, SCFAs have increased the abundance of GLP-1-positive EECs in both mouse and human small intestinal organoids (Petersen et al., 2014). An upregulatory effect by SCFAs on the expression of markers of secretory lineage differentiation has also been observed *in vitro* (Petersen et al., 2014; Grouls et al., 2022). Another GPCR that has been implicated in L-cell differentiation is the G protein-coupled bile acid receptor 1 (GPBAR1); a synthetic GPBAR1 agonist, L3740, has been shown to increase the density of GLP-1-positive EECs and L-cell differentiation markers both *in vitro* in human ileal organoids and *in vivo* within 2-3 days (Lund et al., 2020).

Multiple lines of evidence have demonstrated the prominent effects of metabolic disease on EEC differentiation and function in specific regions of the GI tract (Wölnerhanssen et al., 2017; Osinski et al., 2021; Boese et al., 2020). For instance, Wölnerhanssen et al. have observed a reduction of EECs but increase in goblet cell and enterocyte populations in the duodenum of morbidly obese patients, suggesting a compensatory re-directing of lineage differentiation. Moreover, T2D has been

associated with a lower jejunal abundance of GLP-1 producing EECs in obesity (Osinski et al., 2021). Dysregulated EEC differentiation in the obese intestine is suggested to derive from the reduced expression of transcription factors that are necessary for secretory lineage differentiation (Wölnerhanssen et al., 2017; Osinski et al., 2021; Boese et al., 2020). In agreement, the favourable shift of enterohormone profiles observed in patients following Roux-en-Y gastric bypass surgery has been associated with restored expression of EEC differentiation factors and abundance of selective intestinal EEC populations (Rhee et al., 2015; Nergård et al., 2015; Wölnerhanssen et al., 2017).

1.7 Summary and Project Aims

There is growing clinical interest in harnessing the anorectic functions of the gut peptide hormones GLP-1 and PYY for anti-obesity treatment paradigms. GLP-1 and PYY are secreted from enteroendocrine L-cells, and the SCFA-binding GPCR FFAR2 has previously been implicated in mediating their release. However these findings are limited to mouse models and the molecular mechanisms and functional implications of SCFA-mediated activation of FFAR2 signalling pathways in human L-cells still remain unclear. These pathways could encompass novel targets for the development of anti-obesity agents.

The main aims of this thesis were to:

a) Characterise the SCFA-mediated profiles of FFAR2 activation in human L-cells and how these might be spatially regulated.
b) Uncover the canonical functions of SCFAs in driving acute anorectic peptide hormone release from human L-cells and the involvement of FFAR2 signalling in driving these effects.
c) Uncover the non-canonical functions of SCFAs in modulating the differentiation of human L-cells and the involvement of FFAR2 signalling in driving these effects.

2. Materials & Methods

2.1 Materials

2.1.1 Primary Antibodies

Antibody	Species	Supplier	Catalogue #	Concentration
FLAG M1	Mouse	Sigma-Aldrich	F3040	1:500
EEA1	Rabbit	Cell signalling	3288S	1:500
APPL1	Rabbit	Cell signalling	3858S	1:500
GAPDH	Mouse	Millipore	MAB374	1:1000
GLP-1	Mouse	Abcam	ab23468	1:500
PYY	Rabbit	Abcam	ab22663	1:1000

2.1.2 Secondary Antibodies

Antibody	Source	Target	Supplier	Catalogue #	Final Concentration
Alexafluor 488	Goat	Mouse	Invitrogen	A11001	1:1000
Alexafluor 647	Donkey	Rabbit	Invitrogen	A31753	1:1000
Fluoromount-G with DAPI	N/A	N/A	Invitrogen	0-4959-052	N/A
HCS CellMaskTM Deep Red stain	N/A	N/A	Invitrogen	H32721	1:20,000
Horseradish Peroxidase (HRP) conjugated IgG	Goat	Mouse	Abcam	ab6789	1:5000
Horseradish Peroxidase (HRP) conjugated IgG	Mouse	Rabbit	Santa Cruz	sc-2357	1:1000

2.1.3 Plasmids & Gene Fragments

DNA Construct	Source
FLAG-LHR	Aylin Hanyaloglu
Human GPR43 ORF clone	Origene
FLAG-hFFAR2	Aanya Hirdaramani
mGsq-Lgbit	Aska Inoue

endofin-Smbit	Aska Inoue
SEP-PYY	Aanya Hirdaramani
SEP-LHR	Silvia Sposini
pcDNA 3.1(+)	Invitrogen

Gene Fragment	Sequence	Supplier
SEP-PYY	AAGCTTGCAATGGTGTTTGTGCGCCGCCCGTGGCCGGCG CTGACCACCGTGCTGCTGGCGCTGCTGGTGTGCCTGGGC GCGCTGGTGGATGCGTATAGCAAAGGCGAAGAACTGTTT ACCGGCGTGGTGCCGATTCTGGTGGAACTGGATGGCGAT GTGAACGGCCATAAATTTAGCGTGAGCGGCGAAGGCGAA GGCGATGCGACCTATGGCAAACTGACCCTGAAATTTATTT GCACCACCGGCAAACTGCCGGTGCCGTGGCCGACCCTG GTGACCACCCTGACCTATGGCGTGCAGTGCTTTAGCCGC TATCCGGATCATATGAAACGCCATGATTTTTTTAAAAGCGC GATGCCGGAAGGCTATGTGCAGGAACGCACCATTTTTTTT AAAGATGATGGCAACTATAAAACCCGCGCGGAAGTGAAAT TTGAAGGCGATACCCTGGTGAACCGCATTGAACTGAAAG GCATTGATTTTAAAGAAGATGGCAACATTCTGGGCCATAA ACTGGAATATAACTATAACGATCATCAGGTGTATATTATGG CGGATAAACAGAAAAACGGCATTAAAGCGAACTTTAAAAT TCGCCATAACATTGAAGATGGCGGCGTGCAGCTGGCGGA TCATTATCAGCAGAACACCCCGATTGGCGATGGCCCGGT GCTGCTGCCGGATAACCATTATCTGTTTACCACCAGCACC CTGAGCAAAGATCCGAACGAAAAACGCGATCATATGGTGC TGCTGGAATTTGTGACCGCGGCGGGCATTACCCATGGCA TGGATGAACTGTATAAAACCGGCGATGATGATAAACGCGC GCCGATTAAACCGGAAGCGCCGCGCGAAGATGCGAGCC CGGAAGAACTGAACCGCTATTATGCGAGCCTGCGCCATTA TCTGAACCTGGTGACCCGCCAGCGCTATGGCAAACGCGA TGGCCCGGATACCCTGCTGAGCAAAACCTTTTTTCCGGAT GGCGAAGATCGCCCGGTGCGCAGCCGCAGCGAAGGCCC GGATCTGTGGTAAGGATCC	Twist Bioscience

2.1.4 Primers & siRNA

qPCR primers		5’ - 3’
FFAR2	fwd	GCTACCTGGGAGTGGCTTTC
	rev	CATAACCCAGGCCACCAGAG
FFAR3	fwd	CCAATGGGACCTGCTACCTG
	rev	ATCAGCGGGACCACAAAGAG
PYY	fwd	TCTTTTCCCATACCGCTGCC
	rev	CTCGTCTGCTTCACAAGCTATC
GCG	fwd	TTCAGACCAAAATCACTGAC

	rev	AACATTTCAAACATCCCACG
ATOH1	fwd	CCTTCCAGCAAACAGGTGAAT
	rev	TTGTTGAACGACGGGATAACAT
NGN3	fwd	GCGCCGGTAGAAAGGATGA
	rev	GGTCACTTCGTCTTCCGAGG
NEUROD1	fwd	ATGACCAAATCGTACAGCGAG
	rev	GTTCATGGCTTCGAGGTCGT
ARX	fwd	TGGAAACAGAGGACCAGCAC
	rev	GTTGGAGTTGGAGCGAGGTT
PAX4	fwd	ATACCCGGCAGCAGATTGTG
	rev	AAGACACCTGTGCGGTAGTAA
PAX6	fwd	CAGACACAGCCCTCACAAACAC
	rev	TGGTGAAGCTGGGCATAGG
RPL12	fwd	CATCTCCTTCTCGGCATCA
	rev	AACCCTGTTGTCAATGCCTC

Cloning Primers		**5' - 3'**
FLAG-hFFAR2	fwd	GTCGCGATATCAATGCTTCCAGACTGAAA
	rev	GCTCTAGATTACTCAGTTGTGAAGTCGGATGATGGC

siRNA	**ID**	**Supplier**	**Catalogue #**
siAPPL1	HSS119758	Thermofisher	1299001

2.1.5 Inhibitors & Activators

Inhibitors	**Target**	**Supplier**	**Catalogue #**	**Final Concentration**
3-isobutyl-1-methylxanthine (IBMX)	Phosphodiesterase	Sigma-Aldrich	I5879	0.5mM
Pertussis toxin	Gαi	Tocris	3097	250ng/µl or 500ng/µl
Lithium Chloride	Inositol monophosphatase	Thermo Fisher	199885000	50mM
YM-254890	Gαq	Tocris	7352	10µM
GLPG0974	FFAR2	Sigma-Aldrich	SML2443	1µM
Dyngo-4a	Dynamin	Abcam	Ab120689	50µM
DBZ	ɣ-secretase	StemCell	73092	5µM
cOmplete, Mini, EDTA-free	Proteases	Sigma-Aldrich	11836170001	1 tablet/10ml

Protease inhibitor Cocktail				
Sodium fluoride (NaF)	Serine/threonine phosphatases	NEB	P0759S	1mM
Sodium orthovandate (NaVO3)	Tyrosine phosphatases	Sigma-Aldrich	S6508	1mM
Phenylmethylsulfonyl fluoride (PMSF)	Serine proteases	Sigma-Aldrich	P7626	1mM

Activators	Target	Supplier	Catalogue #	Final Concentration
Forskolin	Adenylyl cylase	Abcam	Ab120058	0.5mM
Isoproterenol hydrochloride	B2AR	Sigma-Aldrich	I6504	10nm
Sodium Acetate	FFAR2	Sigma-Aldrich	S2889	0.1-10mM
Sodium Butyrate				0.1-10mM
Sodium Propionate	FFAR2	Sigma-Aldrich	P1880	0.1-10mM
AZ-1729	FFAR2-Gαi	Tocris	6826	0.001 – 100 μM

2.1.6 Enzymes

Enzyme	Supplier	Catalogue #
AfeI	NEB	R0652S
EcoRV-HF	NEB	R3195S
XbaI	NEB	R0145S
RNase Out	Thermofisher	10777019
Superscript IV Reverse Transcriptase	Thermofisher	18090050
Deoxyribonuclease I (Dnase I)	Thermofisher	EN0521
PowerUp SYBR Green Master Mix	Applied Biosystems	A25742

2.1.7 Chemical Reagents

Reagent	Supplier
2-Mercaptoethanol	Sigma-Aldrich
Absolute ethanol	VWR Chemicals
40% Acrylamide/Bis solution	ThermoFisher
Activated charcoal	Sigma-Aldrich

Ampicllin	Sigma-Aldrich
Agarose Powder	Sigma Aldrich
Ammonium persulfate (APS)	Sigma-Aldrich
Bovine serum albumin (BSA) fatty acid free	Sigma-Aldrich
Bromophenol blue	Sigma-Aldrich
Calcium chloride	Sigma-Aldrich
Chloroform	Sigma-Aldrich
Deoxynucleotide triphosphate (DNTPs)	Invitrogen
Dimethyl sulphoxyde (DMSO)	Sigma-Aldrich
Dithiothereitol (DTT)	Invitrogen
Ethylenediaminetetraacetic acid (EDTA)	Sigma-Aldrich
Gelatine powder	Sigma-Aldrich
Glucose	Sima-Aldrich
HEPES	ThermoFisher
Hydrochloric acid	Sigma-Aldrich
Isopropanol	VWR Chemicals
L-arginine	Sima-Aldrich
Magnesium sulphate	Sigma-Aldrich
Methanol	VWR Chemicals
Monopotassium phosphate	VWR Chemicals
Paraformaldehyde	Sigma-Aldrich
Phosphate buffered saline (PBS)	In-house
PBS with Ca^{2+}/Mg^{2+}	Sigma-Aldrich
Poly-D-lysine hydrobromide	Sigma-Aldrich
Potassium chloride	Sigma-Aldrich
SDS solution 10% w/v	Fisher Scientific
Sodium azide	Sigma-Aldrich
Sodium chloride	Sigma-Aldrich
Sodium deoxycholic acid (monohydrate)	Sigma-Aldrich
Sodium hydroxide	Sigma-Aldrich
Sodium phosphate dibasic dihydrate	VWR Chemicals
Tetramethylethylenediamine (TEMED)	Sigma-Aldrich
Tris base	Sigma-Aldrich
Tris HCl	Sigma-Aldrich
Triton X-100	Sigma-Aldrich
Trizol	ThermoFisher
Tween 20	BioRad

2.1.8 Cell Culture Reagents

Reagent	Supplier
Cultrex Basement Membrane Extract	R&D systems
RPMI-1640 media	Sigma Aldrich
Dulbecco's modified eagles medium (DMEM)	Sigma Aldrich

Phenol-Red Free Dulbecco's modified eagles medium (DMEM)	GIbco
Fetal Bovine Serum	Merck
Pen/Strep	Sigma Aldrich
Lipofectamine 2000	ThermoFisher
Lipofectamine RNAimax	ThermoFisher
Opti-Mem I reduced serum media	Gibco
Matrigel^{TM}	Corning
Advanced DMEM-F12	Gibco
Glutamax	ThermoFisher
Penicillin-Streptomycin	ThermoFisher
Trypsin-EDTA solution	ThermoFisher
Trypan Blue	ThermoFisher
HEPES	ThermoFisher
B27	ThermoFisher
N2	ThermoFisher
NAC (N-acetyl-L-cysteine)	ThermoFisher
Recombinant R-spondin	R&D Systems
Recombinant Noggin	Cedarlane Labs
Recombinant EGF	Sigma-Aldrich

2.1.9 Kits

Kit	Supplier
NanoGlo Live Cell Assay system	Promega
Human PYY ELISA Kit	Merck
Human GLP-2 ELISA Kit	abcam
HiSpeed Maxiprep kit	Qiagen
QIAprep Spin Miniprep kit	Qiagen
Fluo-4 Direct Calcium Assay	Invitrogen
cAMPGαs Dynamic HTRF kit	Cisbio
IP-One –GαqHTRF Kit	CIsbio

1.1.1 Miscellaneous

Item	Supplier
Max EfficiencyTM DH5α competent cells	ThermoFisher
PageRuler Plus prestained protein ladder	ThermoFisher
Western Blot Stripping Buffer	abcam
Hyperladder DNA marker	Bioline
FLuoromount G with DAPI	Thermofisher
Immobilon Forte HRP substrate	Millipore
Immobilon Forte Classico substrate	Millipore
DNA loading dye	Bioline

Plasticware	Corning
Acrylamide/N,N'-Methylenebisacrylamide 37.5:1	ThermoFisher
Non-fat dried milk powder	Sigma-Aldrich
Rnase ZAP	Sigma-Aldrich
SYBR Safe DNA Gel Stain	Invitrogen
Nuclease-Free Water	Ambion
DEPC-treated Water	Sigma Aldrich
0.22μM syringe filter units	Merck
μ-Slide 8 Well Glass Bottome	IBIDI
384 low volume well plate	Greiner
Glass bottomed petri dishes (35mm)	Mattek Corporation
Hybond blotting paper	GE Healthcare
Glass coverslips	Menzel-GLazer
Nitrocellulose blotting membrane	GE Healthcare
96-Well PCR Plate for FAST systems	starlab
Falcon Chambered Cell Culture Slides	Fisher scientific
Hochest 33342	ThermoFisher
Prolong Gold Antifade mountant	ThermoFisher

2.1.10 Buffers and solutions

2.1.10.1 General

a) Phosphate buffered saline (PBS): 140 mM NaCl, 2.5 mM KCl, 1.5 mM KH2PO4, pH 7.2, 1.5 mM Na2HPO4, pH 7.2
b) Tris buffered saline (TBS): 130 mM NaCl, 20 mM Tris pH 7.6,
c) TBS-Tween 20 (TBS-T): 0.2% Tween 20 in TBS in 1x TBS
d) Tris/acetate/EDTA (TAE): 2M Tris Base, 1M EDTA, 1M Acetic Acid

2.1.10.2 Organoid ENR Media

ENR Media: 1% Glutamax, 1% Penicillin-Streptomycin, 10mM HEPES, 1x B27, 1x N2, 1μM NAC, 1μg/ml Recombinant R-spondin, 100ng/ml Recombinant Noggin, 50ng/ml Recombinant EGF in 50ml DMEM-F12. Stored in 4℃ and used within one week.

2.1.10.3 Bacterial Media

a) LB Broth: 1% (w/v) Bacto Tryptone, 0.5% (w/v) Yeast extract, 0.5% (w/v) NaCl. Made up in sterile water and autoclaved.
b) LB Agar*:* LB Broth + 1.5% (w/v) Agar

2.1.10.4 Immunofluorescence

a) FACs buffer: 2% (w/v) FBS in PBS with $Ca^{2+/}Mg^{2+}$
b) Fixation solution: 4% (w/v) paraformaldehyde (PFA) solution in PBS, pH 7.2-7.4. Stored at -4℃ for one week or -20 for long term storage.
c) Anti-FLAG M1 antibody stripping solution: 0.04M EDTA in PBS
d) Permeabilisation solution: 0.2% Triton-X in PBS with $Ca^{2+/}Mg^{2+}$
e) Blocking buffer and antibody dilution buffer: 2% (w/v) FBS in PBS with $Ca^{2+/}Mg^{2+}$
f) Organoid immunofluorescence buffer: 0.2% Triton X-100, 0.05% Tween in PBS
g) Organoid Permeabilisation solution: 0.5% Triton X-100 in PBS
h) Organoid blocking buffer and antibody dilution buffer: 1% BSA in Organoid Immunofluorescence Buffer

2.1.10.5 Western blotting

a) Cell lysis buffer: 10mM Tris-HCL (pH 7.5), 0.5 mM EDTA, 150 mM NaCl, 1% (v/v) Triton X- 100, 1mM PMSF, 1 mM NaF, 1 mM NaV03. Stored at 4℃ for 1 week or -20℃ for one month without PMSF, NaF, NaV03.
b) SDS Tris-Glycine running buffer 10X: 250 mM Tris Base, 1.9 M Glycine pH 8.3, 1% (w/v) SDS
c) Transfer buffer 10x: 250 mM Tris Base, 1.9 M Glycine pH 8.3

d) Transfer buffer 1x: 10x Transfer Buffer, cold distilled water, 20% (w/v) methanol. Made just before use.
e) Laemli buffer 2x: 0.5 M Tris-HCl, pH 6.8, 20% (v/v) Glycerol, 4% (v/v) SDS, 0.002% (w/v) Bromophenol Blue. Stored at -20℃ for 4-6 months. 5% (v/v) β-mercaptoethanol added immediately before use.
f) Blocking buffer and antibody dilution buffer. 5% (w/v) non-fat milk **or** BSA in TBS-Tween

2.1.10.6 SDS Polyacrlamide Gels

a) 12% Separating Gel: 12% (w/v) Acrylamide, 380 mM Tris HCL (pH 8.8), 0.1% (v/v) SDS, 0.1% (w/v) APS, TEMED added at 1:2000.
b) Stacking Gel: 5% (w/v) Acrylamide, 80 mM Tris HCL (pH 6.8), 0.1% (w/v) SDS, 1% (w/v) APS, TEMED added at 1:1000

2.1.10.7 Radioimmunoassay, ELISA & fluorescent supernatant measurements

a) Phosphate buffer: 1L boiled distilled water and allowed to cool, 48 g Na2HPO4.2H2O, 4.14g KHPO4, 18.61g EDTA, 2.5g NaN3. Stored at +4℃ up to a month.

b) Phosphate buffer with gelatin: Same as above, with the addition of 12.5g of gelatin. Stored at +4℃ up to a month.
c) Dextran-coated charcoal buffer: 2.4g Charcoal and 0.24g Dextran dissolved in phosphate buffer with gelatin and placed on magnetic stirrer for 20 mins.
d) Cell lysis buffer (see 2.1.12.5)
e) 1x Kreb's secretion buffer: 128.5mM NaCl, 4.8mM KCl, 1.2mM KH_2PO_4, 1.2mM $MgSO_4$, 5mM $NaHCO_3$, 2.5mM $CaCl_2$, 10mM HEPES dissolved in 1L water and and filter sterilised. Kept at +4℃ in a sealed container and used within 3 weeks. 0.2% (w/v) fatty-acid free BSA added immediately before use.

2.2 Methods

2.2.1 Intestinal Organoids

2.2.1.1 Crypt Isolation

Colonic crypts were isolated from female and male mice with ages ranging from 19-34w. Mice were sacrificed by euthanasia with carbon dioxide asphyxiation, and death was ensured by cervical dislocation. The peritoneal cavity was dissected and the colon was located, distal to the cecum, and excised. Using an oral gavage needle, the colon was flushed twice with ice-cold PBS, slit, and separated into proximal and distal segments. 0.5cm fragments of tissue were cut directly over a tube containing 50ml cold PBS and 1ml of 0.5M disodium EDTA was added to the tube before incubating on a nutating rocker for 45 minutes at 4℃. Fluid was decanted and the tissue was washed thrice with ice-cold PBS. Tubes were refilled with 30ml ice-cold PBS and shaken vigorously in an elliptical motion for 8-10min until tissue fragments were floating and the release of crypts into the supernatant was confirmed under a

microscope. Supernatant was transferred to a fresh tube and spun down at 300 x g for 5 min at 4℃. The pellet was resuspended in crypt media by manual flicking, avoiding pipetting as to not break the crypts and Matrigel was added in a 2:1 dilution of Matrigel:crypt+media. 25µl domes were seeded per well in 48 well plates, and placed for 20 minutes at 37℃ in a humidified incubator with 5% CO_2 to allow polymerisation of Matrigel. After incubation, 250µl of crypt media was added per well and culture plates were left to grow and monitored for formation of organoids at 37℃ for 5-7 days in a humidified incubator with 5% CO_2.

2.2.1.2 Culturing Organoids

Mouse colonic organoids were routinely passaged every 4-6 days by mechanical dissociation. First, Matrigel domes were manually broken up by pipetting up and down approximately 20-30 times, using a p20 pipette tip stacked on top of a p200 pipette tip, and the suspension was transferred to a fresh 1.5ml Eppendorf tube before centrifugation at 300 x g for 5 min at 4℃. A second shorter spin (~6-8 seconds) was performed to ensure proper separation of cellular pellet from residual Matrigel. A chemical dissociation step was carried out at this point exclusively for the first round of passaging following establishing primary cultures. Briefly, the supernatant was carefully removed from pelleted organoids and 200µl of TrypLe Dissociation reagent was added to the tube. The suspension was mixed by flicking and incubated in a sterile 37℃ water bath for 5 minutes. 10ml of cold PBS was added to stop the reaction before centrifugation at 300 x g for 5 min at 4℃. The supernatant was carefully removed. Finally, the pellet was resuspended before plating in crypt media by pipetting up and down and then Matrigel was added to a final a 2:1 dilution of Matrigel:media suspension. Plating conditions were the same as described above. Organoids were maintained for 5-7 passages. Fluorescence of colonic organoids derived from HES1-GFP and LGR5-lineage tracer mice was routinely monitored during culturing by an All-in-One Fluorescence Microscope (Keyence).

2.2.2 Cell line Culture

2.2.2.1 HEK-293 & NCI-H716 cell lines

HEK-293 (ATCC, CRL-1573) were grown as an adherent monolayer in T-75 flasks in DMEM containing 4.5g/L D-glucose and 4mM glutamine supplemented with 10% (v/v) fetal bovine serum (FBS) and 100U/ml penicillin/streptomycin (+/+ DMEM). HEK-293 cells were passaged once weekly, at 80-90% confluency. NCI-H716 cells (ATCC, CCL-251) were maintained in suspension in RPMI-1640 media containing 2g/L D-glucose and 2mM glutamine supplemented with 10% (v/v) fetal bovine serum (FBS) and 100U/ml penicillin/streptomycin (+/+ RPMI), in T-75 flasks placed upright. Both cell lines were maintained at 37℃ in a humidified incubator with 5% CO_2. NCI-H716 were grown in suspension at densities between 2 x 10^5 and 7 x 10^5 cells per ml and passaged every 4-5 days.

Prior to seeding NCI-H716 cells for experiments, cell culture plates required pre-coating with Cultrex Basement Membrane Extract (BME) to achieve cell adherence. BME concentrate (8-10mg/ml) was thawed overnight on ice at 4℃ and diluted in ice-cold serum and antibiotic-free RPMI media (-/- RPMI) to a final concentration of 0.5mg/ml. The volume of BME required for coating was dependent on well surface area (~170μl/cm^2) BME-coated plates were incubated at 37℃ for 90 minutes to set and washed once with warmed serum-free RPMI.

For routine passaging, HEK-293 cells were detached with 0.25% trypsin with EDTA in phosphate-buffered saline. Trypsination was neutralised by addition of +/+ DMEM and cells were the transferred to 15ml falcon. To passage NCI-H716 cells, cell medium from flasks were decanted to 15ml falcon tubes. Both cell lines were spun down by centrifugation at *1118 x g* for 5 minutes. Next, media was aspirated and fresh +/+ media was used to resuspend cell pellets. Cell viability was ascertained by a Trypan blue (%) exclusion test. 10μl of diluted cell suspension:Trypan blue mixture was loaded onto the centre of the haemocytometer and the number of live and blue (dead) cells within the centre 1mm^2 area was counted. Passages were utilised only if cell viability was ≥ 80%.

$$\%\ \text{cell viability} = \frac{\#\ \text{live cells}}{\#\ \text{live cells} + \#\ \text{blue cells}} \times 100$$

The number of live cells was counted across the four outer 1mM squares of the haemocytomer and averaged.

$$\#\ \text{cells/ml} = \text{average live cells}/mm^2 \text{x } 10{,}000 \text{ x dilution factor(s)}$$

The appropriate volumes of cell suspension were diluted in media for plating out onto 96-, 48-, 24-, 12-, and/or 6-well plates for downstream assays to achieve the required cell density for each cell. Passage numbers of HEK-293 cells were between 35 and 45. NCI-H716 cells were cultured and used for downstream assays within a 7–8-week window, after which they were frozen down or discarded. Optimal assay performance for NCI-H716 cells was observed between passages 18 and 37 (*Figure 2.1)*.

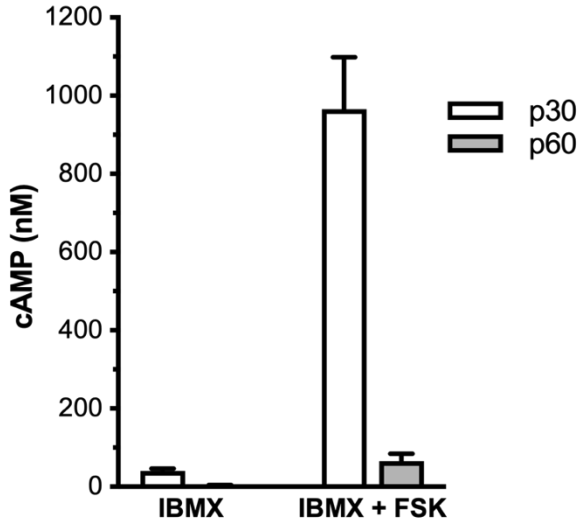


Figure 2.1 Basal cAMP levels vary with passage number in NCI-H716 cells. Intracellular cAMP accumulation in NCI-H716 cells of passage number 30 (p30) or passage number 60 (p60; *grey)* cells following treatment with IBMX (500 nM, 5 min) and then treatment with forskolin (FSK) (3μM, 5 min) or IBMX alone (500 nM, 10 min). Data are presented as mean ± SEM of at least triplicates, n=2 independent experiments.

2.2.2.2 Cryopreservation & Thawing

To cryopreserve cells, NCI-H716 or HEK-293 cells were first spun down at *1118 x g* for 5 minutes and pellets were resuspended in +/+ RPMI containing 5% DMSO or +/+ DMEM containing 10% DMSO respectively. Cell suspensions were quickly added to

cryovial and transferred in a freezing container containing isopropanol, to slow down the rate of freezing, to be placed at -80℃. Cryovials were transferred to liquid nitrogen the following day for long term storage.

To thaw cells, sealed cryovials were placed in an antibiotic-treated water bath at 37℃ for one minute. 1ml of cell suspension was transferred to a 15 ml falcon containing 9ml of fresh complete medium and spun down for 5 minutes at *1118 x g*. Pellets were resuspended in fresh medium at appropriate volumes and seeding density for optimal growth. Doubling rate of NCI-H716 cells was halted after thawing, therefore cells were maintained in T25 flasks for 2 passages following thawing to accelerate growth. NCI-H716 and HEK-293 cells were both passaged twice after thawing before seeding for downstream assaying.

2.2.3 Transfections

2.2.3.1 Transient DNA transfections with Lipofectamine™ 2000 Reagent

NCI-H716 cells were transfected via reverse transfection on the day of plating.
Plasmid DNA (1μg-3μg) and 5μl Lipofectamine 2000 were each diluted in 250μl of Opti-MEM™ I Reduced-Serum Medium and incubated for 5 minutes at room temperature. DNA- and lipofectamine-OPTIMEM mixes were combined and incubated for 15-20 mins at room temperature. 500μl of DNA:Lipofectamine mix was added per well of a 6 well plate, and cell suspension (1 x 106 cells/well of a 6 well plate), diluted in +/- RPMI media was added on top.

HEK-293 cells were plated 24-48 hours onto 6-well plates before transfection and grown to 70-80% confluency. On the day of transfection, media was changed to antibiotic-free DMEM supplemented with 10% FBS (+/- DMEM) and 500μl of the DNA:Lipofectamine mix was added dropwise to each well.

For both NCI-H716 and HEK-293, media was changed back to +/+ RPMI or +/+ DMEM respectively 16-20 hours after transfection. DNA amounts, and volumes of lipofectamine 2000 and OptiMEM were adjusted according to surface area for

transfections on 48-, 24- and 12-well plates. Cells were harvested 48-96 hours after transfection.

2.2.3.2 RNAiMAX for APPL1 knockdown

NCI-H716 were depleted of APPL1 via reverse transfection of siRNA. 2.5µl of Lipofectamine™ RNAiMAX Transfection Reagent were added to 200µl of OptiMEM. siAPPL1 was added to the mixture at a final concentration of 50nM or 200nM, and gently mixed and incubated at room temperature for 20 minutes**.** 200µl of RNAiMax:siAPPL1:OptiMEM mixture was added per well of a 12 well plate, and cell suspension diluted in RPMI-1640 media with 10% FBS was added on top. 16 hours after transfection, media was changed to complete culture medium containing antibiotic. Transfection conditions that were optimised were siRNA concentration (50nM or 200nM) and transfection duration (48h or 96h) (*Figure 2.2).* 48h after transfection, cell lysates were collected for analysis (48h time point) or split into 12- and 96-well plates for protein analysis and signalling assays respectively and lysates were collected 48h later (96h time point). When APPL1 protein abundance in lysateswas assessed by SDS-PAGE, the highest % knockdown was observed by incubation with 200nM siAPPL1 for a total of 96h.

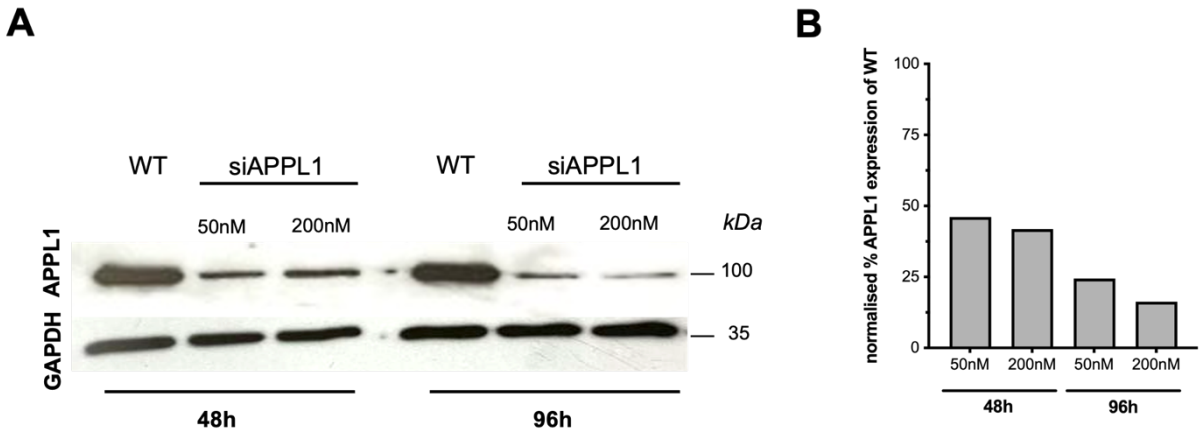


Figure 2.2 Optimisation of siRNA knockdown of APPL1 in NCI-H716 cells. The efficacy of siRNA-mediated knockdown of APPL1 was tested across 2 siRNA concentrations and 2 timepoints. NCI-H716 cells were reverse-transfected with 50nM or 200nM of siAPPL1 at the same time of plating on Matrigel-coated12 well plates. Cellular lysates were collected 48h after transfection, or transfected cells were split again at this time point and lysates were collected 48h later (96h). (A) Representative image of western blot probing for expression of APPL1

and GAPDH loading control in lysates of NCI-H716 cells reverse-transfected with 50nM or 200nM siAPPL1 *vs* wild-type/untreated (WT) cells at 48h or 96 after transfection. (B) Densitometry analysis showing APPL1 protein expression relative to GAPDH in siAPPL1-transfected cells across transfection conditions as % APPL1 expression relative to GAPDH in control cells. Symbols represent APPL1 protein expression in singlet per independent experiment, n=1 independent experiments.

2.2.4 Cloning

2.2.4.1 FLAG-FFAR2

An N-terminally FLAG-tagged human FFAR2 construct was produced by molecular cloning methods. A human FFAR2 plasmid (SC116813, Origene) was used as a template for PCR amplification with Q5 High-Fidelity DNA Polymerase. Primers were designed to add restriction enzyme sites recognised by *EcoRV* and *AfeI* to the 5' and 3' of amplified construct respectively.

Per reaction, 10ng of template DNA was added with 10µl 5x Q5 reaction buffer, 1µl 10mM dNTPs (200µM final concentration), 2.5µl of 10µM Forward Primer and 2.5µl of 10µM Reverse Primer (500nM final concentration), 0.5µl of Q5 enzyme, and nuclease-free water to constitute 50µl final volume. Tubes were placed in a DNA Engine Tetrad 2 Peltier Thermal Cycler (Bio Rad) and the following cycling steps were run: initial denaturation at 98℃ for 30 seconds and 35 cycles of: 30 seconds at 95℃, 2 min at 68℃ and 1 min at 75℃, followed by a 2-minute final extension at 72C.

hFFAR2 was amplified by PCR and fragments were cloned into a pcDNA3.1 carrying FLAG-LHR. The LHR sequence was digested out of the vector by *AfeI* and *XbaI,* and human FFAR2 was digested with *EcoRV* and *XbaI.* For each digest 41µl of amplified FFAR2 PCR product, or 41µl of FLAG-LHR equalling 1µgmade up in nuclease-free water, was incubated with 5µl of CutSmart Buffer and 1µl of each restriction enzyme. The reaction was incubated at 37℃ on a heat block for 2 hours. The digested

fragments were separated by gel electrophoresis on a 2% (w/v) agarose gel containing SYBR Safe DNA Gel Stain (1:10000), which was run for 40 minutes at 100V. The linearised pcDNA3.1 fragment containing the FLAG tag (~ 5.4 kb) and amplified FFAR2 (~ 1kb) were excised from the gel and purified by QIAquick Gel Extraction Kit. DNA concentrations and purity were measured by a ND-1000 Nanodrop spectrophotometer. A 260/280nm absorbance of ~1.7-1.9 was an indicator of acceptable DNA purity.

100ng of purified plasmid was ligated to purified insert in a 1:5 ratio of plasmid:insert using Quick Ligase™. The appropriate amount of vector and insert were mixed with 10µl of Quick Ligase buffer and made upto 20µl with nuclease-free water. 1µl of Quick Ligase was added to the mix before incubation for 5 minutes at room temperature.

2.2.4.2 SEP-PYY

A PYY construct tagged with super-ecliptic pHluorin (SEP) (SEP-PYY*)* were designed and produced by molecular cloning methods. Gene fragments of SEP-PYY (Twist Bioscience) included sequences recognised by *XbaI* and *AfeI* at the 5' and 3' ends respectively, for cloning into pcDNA 3.1 +/+ vector. pcDNA 3.1 +/+ was linearised with *XbaI* and *AfeI.* Proceeding steps were carried out as described above.

2.2.4.3 Transformation of competent bacteria

2µl of ligation mixture was added to 50µl of DH5α Competent Cells (ThermoFisher) thawed on ice and incubated on ice for 30 mins. The mixture was placed at 42℃ for 30 seconds to heat shock before being placed back on ice for 2 minutes. Maintaining aseptic technique, 950µl of LB broth was added and tubes were placed in a 37℃ incubator for 60 minutes with shaking (250rpm). Tubes were centrifuged at *800 x g* 5 minutes to pellet the bacteria. 950µl of supernatant was removed and the pellet was resuspended in 50µl of remaining LB broth. 50µl of each ligation mixture was streaked onto pre-warmed LB agar plates containing 100ug/ml ampicillin for selection and placed in a 37℃ incubator overnight. The next day colonies were selected. Single colonies were inoculated in 5ml or 200ml of LB broth for miniprep and maxiprep

cultures and incubated in a shaking incubator at 37℃ for 14-16h. Bacterial cells were harvested by centrifugation at *6000 x g* for 10 mins at 4℃, supernatant was removed, and plasmid DNA was purified from cell pellets by QIAGEN miniprep or maxiprep kits. DNA concentration and purity were measured ND-1000 Nanodrop spectrophotometer. Samples with a 260/280 ratio value of ~1.7-1.9 and 260/230 ratio value of ~ 2.0-2.2 were accepted as pure.

2.2.5 qPCR

2.2.5.1 Trizol RNA Extraction

NCI-H716 cells were seeded 48h before extraction **(**1.2 – 1.5 X 10^6 cells/well in 6-well plates), and pre-treatments and or ligands were added at mentioned timepoints. RNA was extracted using Trizol Reagent. Plates were kept on ice for all steps. 300µl of Trizol was added directly to each well with pipetting up and down 20 times to encourage homogenisation and incubated for 5 minutes. Lysates were transferred to RNase-free 1.5ml eppendorfs. 60µl of chloroform was added per tube and then mixed thoroughly by inverting the tube several times for 20-30 seconds. Samples were incubated for 2-3 mins at 4℃ and then separated into three phases by centrifugation at *12,000 x g* for 15 mins at 4℃. The upper aqueous phase containing RNA were transferred to a new tube and 150µl of isopropanol was added, Mixtures were incubated for 10 minutes before centrifugation for 10 minutes at *12,000 x g* at 4℃. Supernatant was carefully removed manually with a pipette and the RNA pellet was resuspended in 300µl of 75% ethanol. Samples were vortexed briefly and centrifuged for 5 mins at *7500 x g* for 5 minutes. This washing step was repeated twice more. Finally, the RNA pellet was air-dried for an additional 10 minutes before resuspension in 10µl of nuclease-free water. RNA yield and purity were measured by a ND-1000 Nanodrop spectrophotometer. RNA samples were accepted as pure if both 260/280 and 260/230 ratio values fell between ~ 2.0 – 2.2.

2.2.5.2 Dnase I

RNA samples were treated with Deoxyribonuclease I (DNase I) (Invitrogen) remove any contamination by genomic DNA. 1µgof RNA was made upto 8µlin nuclease-free water and incubated with 1µl of 10x Dnase I buffer and 1µl of Dnase I for 10 mins at room temperature. 1µl of EDTA were added to each tube, and mixtures were heat-inactivated at 65℃ for 10 minutes in a DNA Engine Tetrad 2 Peltier Thermal Cycler (Bio Rad). If samples were not immediately used for cDNA synthesis, they were stored at -80℃ for upto 1 year in aliquots to avoid repeated freeze-thaw cycles.

2.2.5.3 cDNA synthesis

Complementary DNA (cDNA) was synthesised from RNA samples by SuperScript IV Reverse Transcriptase (SSIV RT) (Invitrogen). A DNA Engine Tetrad 2 Peltier Thermal Cycler was used for the heating of samples in the following steps. 1µgof DNase-treated RNA was mixed with 1µl of 10mM dNTPs and 1µl of 50µM Random Hexamers and incubated at 65℃ for 5 minutes. Reactions were placed on ice for at least 60 seconds and 7 µl of the following MasterMix was added: 4µl 5x SSIV buffer, 1µl DTT, 1µl RNAseOUT and 1µl SSIV RT. Next, samples were incubated in the following thermocycling conditions: 23℃ for 10 min, 50℃ for 10 min, 80℃ for 10 min. RT reactions were either used immediately for PCR amplification or stored at -20℃ for upto 48 hours.

2.2.5.4 qPCR

Primers for quantitative real-time PCR (qPCR) of target genes were designed to meet the following criteria: amplification of a 75-200p product, spanning an exon-exon junction to avoid amplification of contaminating genomic DNA, containing <60% GC, and having melting temperature (T_m) within 3C of each other. Designed primers were input into NCBI Primer-BLAST to confirm low probability of primer-dimers (3' self-complementarity score <4) and possible secondary structures between primer itself or primer pairs (self-complementarity score <4) (Ye et al., 2012). Optimal forward (F) and

reverse (R) primer concentrations was determined across a 100nM-900nM range of incremental concentrations which were applied to both template and No Template Control (NTC) wells: Trialled F/R primer concentrations (nM) were 100/100, 200/200, 300/300, 400/400, 500/500, 600/600, 700/700, 800/800, 900/900. If the absence of non-specific amplification from NTC wells was also apparent, the reaction producing the lowest Ct (cycle threshold) and the highest fluorescent reporter value (△Rn) was chosen for proceeding assays. Melt curves were analysed to confirm specific amplification of the target product (*Figure 2.3)*.

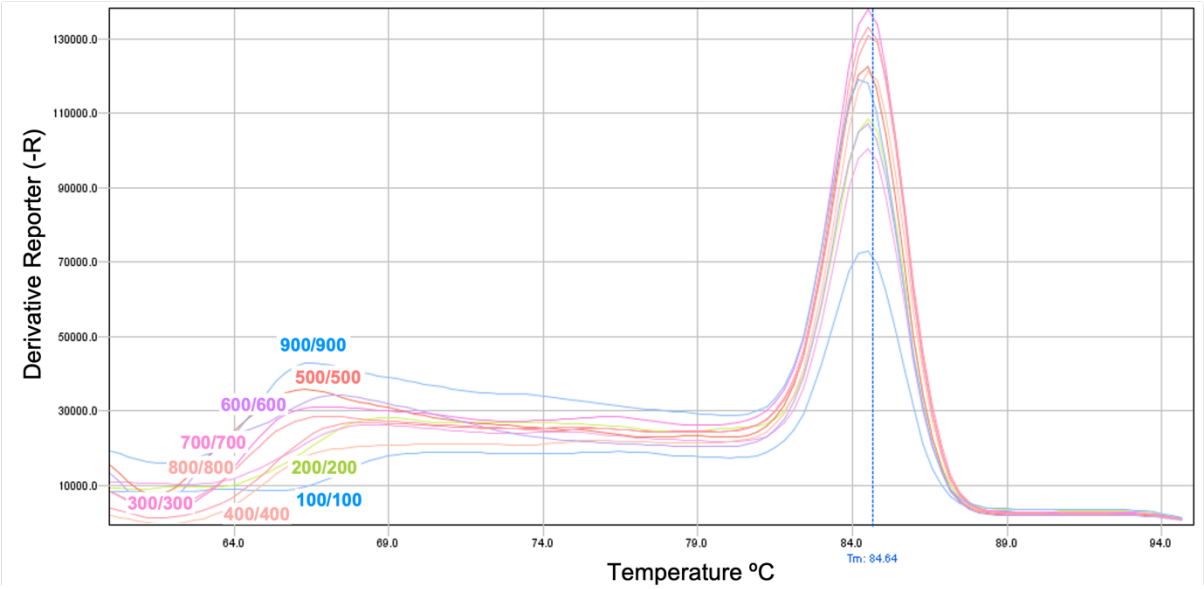


Figure 2.3 Validation of primers for detection of human FFAR2 expression by qPCR melt curve analysis. A melt curve plot of the derivative reporter signal (-R) as a function of temperature (℃) for primer optimisation of human FFAR2. NCI-H716 cells were harvested and RNA was extracted, DNAse-treated and converted to cDNA. RT-qPCR was subsequently carried out using a range of incremental forward and reverse primers concentrations for human FFAR2 (100-900nM each). Following product amplification, melt curve analysis was performed. Primer concentration combinations are coloured and labelled on the melt curve plot.

Each well of a semi-skirted 96 well PCR plate (STARLAB) contained; contained 20ng of cDNA (assuming 100% RNA to cDNA conversion), 100-100nM of forward and reverse primer, 10µl of PowerUp SYBR Master Mix and nuclease-free water to make up a 20µl reaction volume. Plates were run on a StepOne Plus Real-Time PCR system (Applied Biosystems) using the following cycling conditions: 5 minutes at 50℃ for

activation of uracil-DNA glycosylase (UDG), 5 minutes at 95℃ for activation of Dual-Lock DNA Polymerase, and then 40 cycles of: denaturation at 95℃ for 15 seconds followed by annealing and extension at 65℃ for 1 min. Melt-curve analysis immediately followed and consisted of the following; 95℃ for 15 seconds, 60℃ for 1 min, and then temperature was gradually increased by 0.3℃ every 15 seconds to 95℃. The 2-△△Ct method was used calculate relative changes in gene expression (Livak & Schmittgen, 2001):

$$\Delta Ct = Ct\ (\text{gene of interest}) - Ct\ (\text{housekeeping gene})$$

$$\Delta\Delta Ct = \Delta Ct\ (\text{treated sample}) - \Delta Ct\ (\text{untreated sample})$$

$$\textit{Relative gene expression} = 2^{-\Delta\Delta Ct}$$

2.2.6 Protein detection

NCI-H716 cells were plated 48 hours prior to assaying in 12-well plates (7.5 x 10^5 cells/well) and grown to 80-90% confluency. For ERK1/2 blots, cells were serum-starved in -/- RPMI with 0.2% fatty acid-free BSA for 24 hours prior to ligand treatments. To obtain cell lysates, wells were washed with ice-cold PBS, 50μl RIPA lysis buffer was added per well. Wells were then scraped and incubated for 10min at 4℃ before lysates were transferred to 1.5ml eppendorfs and spun down at *16000 x g* for 15 min. A Bradford protein assay was carried out using Coomassie Brilliant Blue dye to establish protein content of lysates. Lysates were normalised to a unform concentration of 1μg/μl diluted using the appropriate volume of lysis buffer. 5x Laemli buffer with 5% β-mercapthoethanol was added to samples before incubating for 10 mins at 90℃ on a heat block. Samples could be stored at -20℃ at this point or used for immediate loading. 40μl of sample was loaded per well of a 10-well polyacrylamide gel, alongside 10μl of PageRuler™ Pre-Stained Protein Ladder using the Mini-PROTEIN Tetra electrophoresis system (Bio-Rad). Tanks were filled with SDS Running Buffer and electrophoresis was carried out at 100V for 20 mins at 100V, and then 140V for a further 90 mins at 140V.

Following electrophoresis, proteins were transferred to a nitrocellulose membrane using a Mini Trans-Blot Electrophoretic Transfer Cell system (Bio-Rad). Gels were

carefully trimmed with a razor blade and equilibrated in transfer buffer before placement in a “transfer sandwich”. The gel sandwich was assembled as follows; blotting paper – gel – membrane – blotting paper and cushioned by sponges at both ends. The sandwich was placed in a tank, the tank was filled with transfer buffer, and a voltage of 100V was applied for 90 minutes at 4℃. Once gels had been electrotransferred, membranes were carefully removed from transfer sandwiches using tweezers and incubated in Blocking buffer for one hour at room temperature with gentle agitation. After washing with TBS-T, membranes were incubated overnight in primary antibody in appropriate dilution at 4℃ with gentle agitation. Membranes were washed thrice with TBS-T, each time for 5 minutes, before incubation with secondary antibody in the appropriate dilution for one hour at room temperature with gentle agitation. Membranes were washed thrice with TBS-T, each time for 15 minutes, and incubated with Luminata Forte chemiluminescent substrate for detection. Chemiluminescence was captured using an ImageQuant LAS 4000 system (GE Healthcare) using the automatic exposure time module.

2.2.7 Cell Signalling Assays

HEK-293 cells (3 x 10^4 cells/well) or NCI-H716 cells (6 x 10^4 cells/well) were plated 48 hours prior to assaying in 96-well plates and grown to 80-90% confluency. For measuring intracellular cAMP accumulation, cells were incubated with 0.5mM IBMX in +/+ media for 5 minutes. If inhibitors were relevant to the assay, these were administered to wells (alongside wells treated with DMSO or H20 vehicle for comparison) before IBMX pre-treatment. Next, cells were incubated with 3μM of forskolin in +/+ media for 5 min in the presence or absence of ligands. For measuring intracellular IP1 accumulation, cells were treated with inhibitor or vehicle (if relevant to the assay) prior to incubation with ligand in the presence of 50mM LiCl in +/+ media. for 2 hours. Treatments were aspirated, and cells were incubated with 30μl of Phospho-total protein lysis buffer 1 (Cisbio) per well for 20 mins at room temperature with gentle agitation. Lysates were scraped and transferred to individual 1.5ml eppendorfs and spun down for 15 minutes at *16000 x g* at room temperature. If not immediately used for HTRF assays, lysates were stored at -20℃ for up to 1 month or at -80℃ for up to 3 months.

cAMP levels were quantified using a cAMP Gαs dynamic HTRF kit (Cisbio) which was reconstituted according to manufacturer's instructions. A standard dose response curve spanning from 0 - 712nM of cAMP was established per kit. 10μl of lysate wad added per well of a 384-well white bottomed plate, followed by 5μl of anti-cAMP Eu cryptate donor antibody and 5μl of d2-labelled cAMP acceptor reagent and incubated for one hour in the dark at room temperature. Negative control wells containing 15μl of lysis buffer and 5μl of cryptate donor antibody only were included.

An IP-One Gαq kit (Cisbio) was used to quantify IP1 levels and was reconstituted according to manufacturer's instructions. Per kit, a standard dose response curve spanning from 0 – 7700nM of IP1 was determined. Per well of a 384-well white bottomed plate, 14μl of lysate wad added followed by 3μl of anti-IP1-cryptate donor antibody and 3μl of d2-labelled IP1 acceptor reagent and incubated for one hour in the dark at room temperature. Negative control wells containing 17μl of lysis buffer and 3μl of cryptate donor antibody only were included.

For cAMP and IP1 assays, A PHERAstar Plus reader (BMG LABTECH) was used to measure 620nm cryptate and 665nm acceptor emissions respectively. The ratio of acceptor and donor emission signals were calculated per well:

$$Ratio = \frac{\text{Signal 665nM}}{\text{Signal 620nM}} \text{ x } 10{,}000$$

Delta F% values were calculated for each sample to account for non-specific background signal:

$$Delta\ F\% = \frac{\text{Ratio}_{\text{sample}} - \text{Ratio}_{\text{negative control}}}{\text{Ratio}_{\text{negative control}}} \text{ x } 100\%$$

Finally, cAMP or IP1 concentrations were interpolated from Delta F% values using relevant standard curves. cAMP values detected for each ligand treatment were normalised to forskolin to represent and inhibition of forskolin-mediated cAMP accumulation:

$$\% FSK = \frac{[cAMP]_{sample}}{[cAMP]_{forskolin}} \; x\, 100$$

2.2.8 Microscopy

2.2.8.1 Fluorescent Calcium Assay

NCI-H716 cells (8 x 10^5 cells/dish) were seeded on 35mm MatTek glass bottom dishes 48h before assaying and grown to 50-60% confluency. Cells were incubated with 990µl of Fluo-4 Direct™ calcium indicator (Invitrogen), diluted 1:1 in -/- RPMI media, for 30 minutes in an incubator at 37℃ in the dark, and 30 minutes at room temperature in the dark. Excitation and emission of Fluo-4 are at 494nm and 516nm respectively. Cells were imaged with a SP5 inverted confocal microscope (Leica) using th LasX software, with excitation at 488nm. Background fluorescence was captured over 1 minute at a frame rate of 1 frame/second. Next, 10µl of ligand, in a 1M working stock to give 10mM final concentration, was added to the dish, and cells were imaged at 1 frame/second until calcium levels re-equilibrated to basal. Fluorescence intensity of at least 50 cells per condition were analysed using the Time series analyser V3 plugin on ImageJ. In each frame, fluorescence intensity was normalised to average background fluorescence per cell:

$$\text{Normalised fluorescence intensity} = \text{Fluorescence intensity} - \frac{\text{fluorescence intensity}_{[\text{frame 1}]} + \ldots \text{fluorescence intensity}_{[\text{frame 60}]}}{60}$$

2.2.8.2 Immunofluorescent staining of Whole-Mount Organoids

Organoids were cultured for 5-6 days in Matrigel domes on 48-well plates. Media was carefully removed, and each well was washed twice with PBS. After breaking up the domes using a blunt P1000 tip, organoids were incubated with 300µl of 4% PFA per well and incubated for 4 hours for fixation at room temperature on a tilting platform. Plates were periodically monitored to ensure both complete dissolving of Matrigel and preserved organoid morphology. The fixative was transferred to a 1.5m Low Adhesion Micro Centrifuge Tube (USA Scientific, #1415-2690). Once the organoids had settled by gravity (10-15 minutes), the fixative was carefully removed without disturbing the pellet. To wash the organoids, 500µl of PBS was added to the tube, organoids were allowed to sink again, and this wash was repeated once more. During the final PBS wash, an 8-well Culture Slide (Falcon, 354118) were coated with a thin layer (50µl/well) of Matrigel in a 1:2 dilution in media. The slide was incubated for 5 mins at 37℃ to allow the coating to partially set. Using a blunt P1000 tip pre-coated with 0.1% BSA, the organoid pellet was finally resuspended in 50µl of PBS. 25µl of suspension was carefully added dropwise per well of the pre-coated chamber slides incubated for 90 minutes at 37℃ to allow the organoids to adhere. Wells were washed once with 300µl of PBS, and then permeabilised in Organoid Permeabiilisation Solution (300µl/well) for 30 minutes at room temperature. Next, organoids were washed once with 300µl of Organoid IF buffer, blocked in Organoid Blocking Buffer (300µl/well) for one hour at room temperature, and then incubated with primary antibody diluted in Organoid Blocking Buffer (150µl/well) at 4℃ overnight. The next day, organoids were washed 3 times with IF buffer for 5 min each and then incubated with Secondary antibody and Hoescht 33342 solution diluted in Organoid Blocking Buffer (150µl/well) for one hour at room temperature in the dark. After secondary incubation, wells were washed similarly to the previous step. After removal of the IF buffer, the chambers were carefully detached using the contained removal kit (Falcon, 354118). 20µl of ProLong Gold AntiFade Mountant (ThermoFisher, P36930) was added to the centre of each well and a coverslip was gently lowered onto the specimen, by starting on one edge, to avoid entry of air bubbles. The edges of the coverslip were sealed using clear nail polish and stored at 4℃ in the dark until imaging. Slides were imaged on a Stellaris 8 Inverted confocal microscope (Leica) using the LasX software.

2.2.8.3 Preparation of fixed slides

HEK-293 (3 x 10^4) or NCI-H716 (7.5 x 10^4) were plated on 13mm coverslips in 24-well plates and grown till 30-40% confluency for 48 hours. For staining with anti-FLAG M1 antibody, cells were incubated with M1 diluted in -/- media for 35 minutes, and relevant ligands were added directly into wells for the final 20 minutes. If inhibitors were used, these were administered to cells at respective timepoints prior to M1 treatment. Next, cells were washed with PBS-Ca^{2+}. For stripping M1 antibody off cell membranes, coverslips were quickly washed three times in 0.04M EDTA in calcium-free PBS, and then three times with PBS-CA^{2+}. Cells were fixed with 4% paraformaldehyde in PBS for 30 minutes at room temperature and washed three times again. For membrane permeabilisation, cells were incubated with 0.2% Triton X-100 in PBS-Ca^{2+} for 15 mins at room temperature. Next, cells were washed again and blocked for one hour at room temperature in 2% FBS PBS-Ca2+ (blocking buffer). Cells were incubated with primary antibody(s) in appropriate dilution(s) in blocking buffer for one hour at room temperature. Next, cells were incubated with Alex secondary antibodies for one hour at room temperature in the dark. Cells were washed thrice with PBS-Ca^{2+} for 15 minutes each. If cells were to be stained with HCS CellMask™ Deep Red, a 30 min incubation with CellMask diluted in blocking buffer was carried out at room temperature in the dark. Finally, coverslips were mounted using Fluoromount G onto clear glass slides and stored at 4℃ in the dark until imaging. Slides were imaged on a Stellaris 8 Inverted confocal microscope (Leica) using the LasX software.

2.2.8.4 Colocalisation analysis

For co-localisation analysis, images were capture on Stellaris 8 Inverted confocal microscope (Leica) with the adaptive deconvolution module Lightning to achieve super-resolution. Images analysed using the JACoP: Just Another Co-localisation plugin on ImageJ. For co-localisation analysis of FLAG-hFFAR2 and EEA1, appropriate thresholds were applied to receptor and EEA1 channels, which were kept constant between treatments, and Manders' overlap coefficients were calculated. Files were renamed arbitrarily to avoid sampling bias in choosing thresholds. For co-

localisation analysis of GLP-1 and PYY, Pearson's correlation coefficient between respective channels. was computed.

2.2.8.5 Cell morphology measurements

In NCI-H716 cells, Automatic particle analysis on ImageJ was carried out to quantify changes in cell size and morphology. To reduce observer bias, blinding of treatment allocation was maintained during the image analysis process. Images were split into individual channels and the Cell Mask channel was manually thresholded (threshold was kept constant across samples within an experiment). After a threshold was determined, binary images were automatically generated in which individual cells were segmented from background and outlined. The watershed function was used in more confluent samples if cells were touching. Next, the '*Analyse particles'* command was applied to the mask with minimum particle area set at 20μM^2 to exclude background noise. As such, the outline of individual cells were assigned as regions of interest (ROIs). The binary mask was overlay on the Cell Mask channel to verify "true" cells identified by the automatic analysis, and area, feret, diameter and circularity measurements were computed.

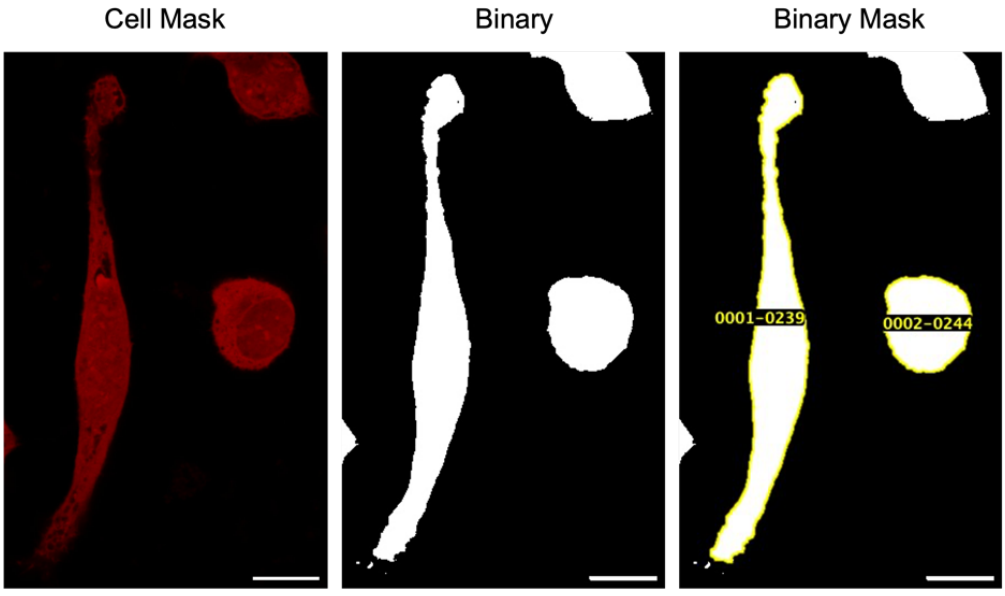


Figure 2.4 Creating binary masks that were representative of cellular outlines on ImageJ. Representative images of NCI-H716 used morphology measurements by ImageJ. NCI-H716 cells were fixed and permeabilised before staining with HCS CellMask™ Deep Red

Stain and DAPI and mounting on glass slides. Slides were imaged by confocal microscopy. Scale bar= 10μM. Conditions were imaged across 120 cells captured in 3 independent experiments. Images were input into ImageJ and split into respective channels. The Deep Red channel was thresholded and converted to a binary mask. Automated particle analysis was then carried out on binary masks, and measurements of area, feret diameter, and circularity.

2.2.8.6 Quantitative analysis of fluorescent organoids

Organoids were imaged on an All-in-One Fluorescence microscope (Keyence) and images were used for quantitative analysis. Microscope settings were kept consistent for individual organoids between timepoints. Temporal profiles of GFP fluorescence intensity were quantified in HES1-GFP organoids. On ImageJ, the outlines of individual organoids were manually traced such that the lumen was excluded and ROIs were created (*Figure 2.5A)*. Images were then split into respective GFP and brightfield (BF) channels. The ROI was projected onto the GFP channel and the 'Histogram' function. Grey values were divided into 256 bins and the distribution of pixels were plotted (*Figure 2.5B)*. Mean grey values were obtained per organoid at each time point. ROIs were also used to determine organoid area and % GFP-positive area was computed by manual thresholding of positive regions. This method was also used to compute % LGR5-positive area in the Lgr5-lineage tracer system.

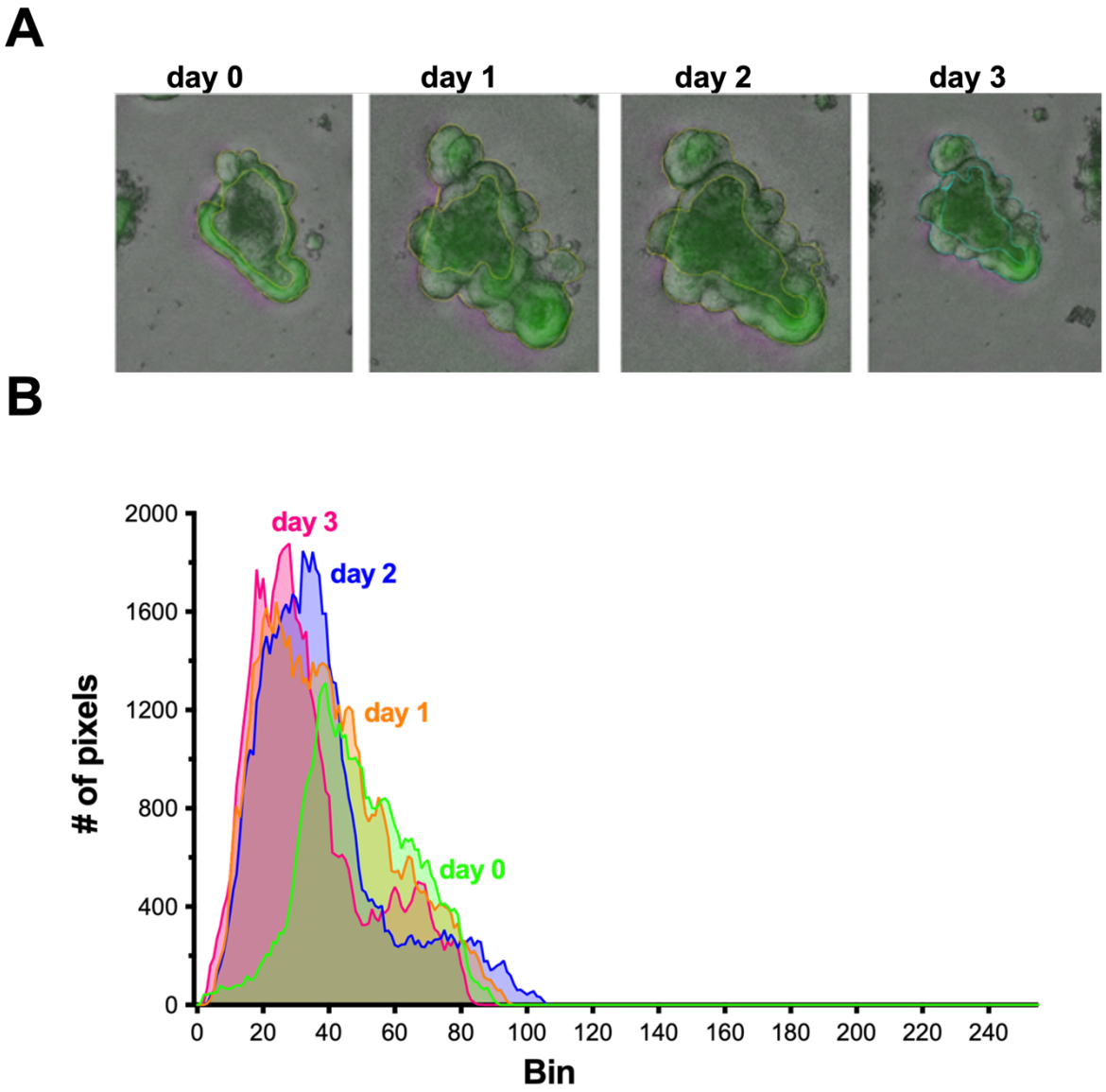


Figure 2.5 Quantification of fluorescence in HES1-GFP organoids by ImageJ. Individual HES1-GFP organoids were imaged by a fluorescence microscope across 0 to 72h (day 0 to day 3) which captured GFP fluorescence in addition to brightfield (BF) images. (A) Representative images of a single HES1-GFP routinely imaged every 24h across a 72h period. Composite GFP/BF images were input into ImageJ and organoid outlines were manually traced such that the luminal area was excluded. (B) Representative Histogram of ROIs generated from tracing in (A) and applied to GFP channels at respective timepoints.

2.2.8.7 TIRF microscopy

Total internal reflection fluorescence microscopy was conducted on a NanoImager S from ONI (Oxford Nanoimaging; ONI). NCI-H716 cells (5 x 10^4) were plated on an ibidi µ-Slide 8 well Glass Bottom and grown to 40-50% confluency for 48h. 15 minutes before imaging, cell media was changed to phenol red-free secretion buffer. The nanoimager was pre-warmed to 37℃. Frames were captured on a close-loop piezo stage with a 100x NA 1.4 oil immersion objective and SCmos camera with excitation 405nm, 488nm, 561nm and 640nm lasers. Samples were brought into TIRF mode by adjustment of the angle of incidence of laser excitation. Frames were captured every 100ms (10 frames per second) for 5 minutes per sample.

2.2.9 Immunoassays

Gut peptide hormone concentrations were detected by various immunoassays in the supernatants and lysates of NCI-H716 cells. NCI-H716 cells were grown on 24 well plates (5 x 10^5 cells/well) for 48 hours till 80-90% confluency. Prior to ligand treatments, wells were washed twice with pre-warmed sterile Krebs buffer. Cells were incubated for 2 hours with ligand diluted in sterile Krebs buffer with 0.2% BSA added at 37℃. Plates were immediately placed on ice and supernatants were collected into pre-chilled 1.5ml eppendorfs. Tubes were spun at *800 x g* for 10 mins at 4℃ to pellet any remaining cells and/or debris and supernatants were aliquoted and transferred into fresh tubes at stored at -80℃ for up to 1 year. For collection of cell lysates, wells were washed with ice-cold PBS, and 50µl RIPA lysis buffer was added per well. Wells were then scraped and incubated for 10min at 4℃ before lysates were transferred to 1.5ml eppendorfs and spun down at *16000 x g* for 15 min. Lysates were stored at -80℃ for up to 1 year.

2.2.9.1 Radioimmunoassays

An in-house radioimmunoassay was used to measured GLP-1 secretion. (Kreymann et al., 1987). The GLP-1 7-36 antibody utilised in this assay shows 100% cross-reactivity with all amidated GLP-1 forms but not glycine-extended forms of GLP-1 or any other proglucagon-derived gut peptides. Iodinate-125 labelled GLP-1 7-36 peptide was iodinated by the chloramine T method by Professor Kevin Murphy and purified by high-performance liquid chromatography (Hunter & Greenwood, 1962). 20μl of supernatant or 20μl of diluted lysate (1:500 in phosphate buffer) was incubated with 230μl of phosphate buffer, 50μl of iodinated label (12 counts/second) and 50μl of anti-GLP-1 antibody for 3 days at 4℃. Standard curve samples containing 1, 2, 3, 5, 10, 15, 20, 30, 50 and 100 μl of 0.125 pmol/ml were included. 250μl of dextran-coated charcoal buffer was added to each tube before centrifuging at 150g for 30 mins at to separate free labelled peptide and antibody-bound labelled peptide. A NEI1600 γ scintillation counter was used to measure radioactivity of supernatants containing bound peptide and pellet containing bound peptide. The intra-assay and inter-assay coefficients of variation were 5.6% and 9.2% respectively and R^2 values of standard curves were above 0.95.

2.2.9.2 ELISA

GLP-2 (Abcam) and PYY (Merck) secretion were measured by enzyme-linked immunosorbent assay (ELISA) kits. All steps were carried out at room temperature. To measure GLP-2 secretion, 50μl of supernatant was added to GLP-2 antibody-coated wells and the plate was sealed and incubated for 2 hours. Wells were washed five times with 200μl of wash buffer. 50μl of biotinylated GLP-2 detection antibody was added to each well and the plate was incubated for 1 hour. Washing was repeated before 50μl of Streptavidin-Peroxidase Conjugate was added per well and incubation for 30 minutes. Wells were washed again and 50μl of chromogen substrate was added. After incubation for 25 minutes, 50μl of stop solution was added per well and plates were read immediately at 450nm. Background readings at 570nm were subtracted from readings and values were interpolated from a standard curve.

To measure PYY secretion, 100μl of sample was added to PYY antibody-coated wells and the plate was sealed and incubated overnight at 4℃ with gentle shaking. All subsequent steps were carried out at room temperature. Wells were washed four times with 300μl of wash buffer. 100μl of biotinylated PYY detection antibody was added to each well and the plate was incubated for 1 hour with gentle shaking. Washing steps were repeated. 100μl of Streptavidin-Peroxidase Conjugate were added per well and the plate was incubated for 45 minutes with gentle shaking. Wells were washed again and 100μl of colorimetric reagent were added per well. The plate was incubated for 30 minutes in the dark with gentle shaking. 50μl of stop solution was added per well and absorbance was read immediately at 450nm. Background readings at 570nm were subtracted and concentrations were interpolated from a standard curve. Detection limits were 0.14ng/ml and 0.15ng/ml for GLP-2 and PYY respectively.

2.2.9.3 Measurement of SEP-PYY release

The fluorescence intensity of supernatants of SEP-PYY-transfected NCI-H716 cells was determine as a measure of SEP-PYY secretion. During reverse transfection (*2.2.3.1)* NCI-H716 cells were seeded into 24-well plates (5 x 10^5 cells/well) 48 hours prior to assaying and grown to 70-80% confluency. Butyrate pre-treatments were added to respective wells at indicated time points prior to assaying. Wells were rinsed twice with pre-warmed sterile Krebs buffer. Next, cells were incubated with respective ligands in sterile Krebs buffer with 0.2% BSA for 2 hours at 37℃. The plate was immediately put on ice at 4℃ in the dark, and supernatants were transferred to fresh pre-chilled 1.5ml Eppendorf tubes and then spun at *800 x g* for 10 mins at 4℃. Whilst maintaining dark conditions, 100μl of each supernatant was transferred added to individual wells of a 96 well white-opaque plate. Treatment control wells containing 100μl of Krebs buffer-diluted ligand were also included. Plates were read using a LUMIstar OPTIMA microplate reader (BMG Labtech) with optical filters for excitation and emission set to 485nm and 520nm respectively. Fluorescent gain was manually adjusted to avoid detector saturation. Per each condition, measurements were corrected for background signal and values of SEP-PYY-transfected cells were normalised to values of untransfected cells:

$$\text{Normalised fluorescence intensity} = \frac{\text{fluorescence intensity}_{\text{SEP-PYY transfected cell}} - \text{fluorescence intensity}_{\text{treatment control}}}{\text{fluorescence intensity}_{\text{untransfected cell}} - \text{fluorescence intensity}_{\text{treatment control}}}$$

2.2.10 Flow cytometry

HEK-293 were plated on 6 well plates (1 x 10^6 cells/well) and grown for 48 hours to 80-90% confluency. To determine transfection efficiency of FLAG-hFFAR2 in HEK-293 cells, cells were stained with anti-FLAG M1 antibody at for 20 minutes at 37℃ in -/- DMEM. NCI-H716 cells were seeded (6 x 10^5/well of a 12 well plate) for flow cytometry during SEP-PYY reverse transfections and grown for 48 hours to 80-90% confluency. SCFA pre-treatments were added at respective timepoints.

On the day of assaying, cells were washed twice with cold PBS-Ca2+ and harvested in FACs buffer in 1.5ml Eppendorf tubes. Tubes were spun down at *1118 x g* at 4℃. Supernatants were removed and pellets were resuspended in AlexaFluor 488-conjugated anti-mouse secondary antibody and incubated on ice in the dark for one hour. Cells were centrifuged at *1118 x* g at 4℃ twice more, with two cold PBS-Ca^{2+} washes between each spin. Pellets were resuspended to a final volume of 300µl in FACs buffer and transferred to polyprolene round bottom FACs tubes. Samples were analysed on a FACS Calibur Flow cytometer. The parameter of the gating region of interest for assays with HEK-293 or NCI-H716 cells was adjusted based on; readings with untransfected HEK-293 cells exposed to M1 and secondary antibodies or readings with untransfected NCI-H716 cells respectively. Mean fluorescence intensity (MFI) was normalised to readings of untransfected cells:

$$\text{Normalised MFI} = \frac{\text{MFI}_{\text{transfected}}}{\text{MFI}_{\text{untransfected}}}$$

2.2.11 NanoBit

NanoLuc Binary Technology (NanoBiT) was used to probe the Interaction between Gαq/11 and endofin, a marker of early endosomes, using the Nano-Glo Live Cell Assay system (Promega). The engineered luciferase NanoLuc (NLuc) generates luminescence in the presence of its substrate furimazine when its two separate subunits form an active enzymatic complex based on the interaction of separate binding partners to which they are fused (Dixon et al., 2016). The following constructs were kindly gifted by Prof Aska Inoue *(Tohoku University*); The 18-kDa Large BiT fragment of NLuc fused to the C-terminus of Gαq/11 (Gαq/11-Lgbit); The 1.3kDa Small BiT fragment of NLuc fused to the C-terminus of the FVYE zinc finger domain of endofin (endofin-Smbit). 48h prior to assays, NCI-H716 cells were seeded (5 x 10^5 cells/well of a 12 well plate) during reverse transfection (500ng each of Gαq/11-Lgbit and endofin-Smbit) and grown for 48h to 80-90% confluency.

Media was removed and wells were each washed with pre-warmed PBS before harvesting by manual pipetting and suspension in 1ml of pre-warmed PBS. 100µl of cell suspension were added per well of a white flat-bottomed 96 well plate. Immediately, 25µl of Nano-Glo Live Cell Substrate furimazine, which has been equilibrated to room temperature and diluted according to manufacturer's instructions in Nano-Glo Live Cell Reagent, was added per well under dark conditions. Luminescence was measured using a LUMIstar OPTIMA microplate reader (BMG Labtech), and cycles were 27 seconds long. Measurements were taken for 5 minutes (12 cycles) at baseline. Quickly, 10µl of 130mM NaCl or propionate diluted in pre-warmed PBS, or PBS alone (vehicle) were added to wells in the dark to give a final concentration of 10mM using a multichannel pipette. Luminescence was then measured for another 40 minutes. Ligand-induced changes in luminescence were represented as a fold change of average basal (0-5min) luminescence and normalised to vehicle.

2.2.12 Bioinformatics analysis

2.2.12.1 Single-cell RNA-seq (scRNAseq) analysis

Raw counts and meta-data for the 'Large intestine' was obtained from the single-cell RNA-seq (scRNA-seq) *Tabula Muris* dataset and analysed using the Seurat package on R (Tabula Muris Consortium, 2018; Hao et al., 2024). Expression data across 23, 433 genes from 3950 large intestinal cells, each expressing at least 500 genes and at least 50,000 UMI counts, passed standard quality-control (QC) processing**.** Counts were normalised using the Seurat '*LogNormalise'* function which computes gene expression values by dividing feature counts by total feature counts per cell, multiplies by scale factor 1,000,000, and computes the natural logarithm of log(1+X). Pre-defined ontologies were assigned to cells by merging meta-data: epithelial cell, enterocytes, goblet cells, brush cells, and EECs (Tabula Muris Consortium, 2018). Characteristic marker genes of each cell ontology class are indicated in (*Appendix 1)*

2.2.12.2 Protein structure prediction

The Alphafold2 pipeline, which integrates the Mmseq2 software to perform automated multiple sequence alignment, was used to predict three-dimensional (3D) structures of SEP-PYY constructs based on input amino acid sequences (Jumper et al., 2021; Steinegger & Söding, 2017). The open source code for Alphafold2 was accessed and run on GitHub. The number or recycles ("num_recycles" function) was set to **3**, meaning that structural predictions were fed and refined thrice through the model. Prediction outputs were ranked based on average predicted local distance difference test (pLDDT) scores. Amino acid sequences were also input to SignalP 5.0 to identify potential cleavage sites of signal peptidase I (Spase I) (Almagro Armenteros et al., 2019). PDB files output from AlphaFold2 were visualised and annotated on PyMOL. (Schrödinger & DeLano, 2020).

2.2.13 Statistical analysis

Quantitative data are presented as the means ± standard error of the mean (SEM) from independent experiments. All statistical significance was determined by

parametric tests on GraphPad Prism 9 for normally-distributed data; unpaired Student's T test for two groups; one sample T-test for comparison to a single value; one-way ANOVA for comparison of >2 groups; two-way ANOVA for considering 2 independent variables between >2 groups. Post-hoc tests used were Bonferroni (when comparing all groups to one another) or Dunnett's (when comparing multiple treatment groups to a single control group). Significance was considered at $p < 0.05$ *; $p < 0.01$ **; $p < 0.001$ ***; $p < 0.0001$ ****.

3. FFAR2 signalling and trafficking profiles activated by short chain fatty acids in human EECs

3.1 Introduction

Free fatty acid receptors (FFAR) are a family of class A GPCRs which are activated by free fatty acids (FFAs) and differ in their specificity based on FFA carbon chain length (Briscoe et al., 2003; Brown et al., 2003; Le Poul et al., 2003; Hirasawa et al., 2005). FFAR2 and FFAR3 are both sensors to the products of gut microbial fermentation of dietary fibre called short chain fatty acids (SCFAs), mediating a multitude of metabolic and immune effects (Kimura et al., 2020). FFAR2 is pleiotropic in its G-protein coupling and can couple both Gαi and Gαq pathways, whereas FFAR3 prefers signalling via Gαi (Le Poul et al., 2003; Brown et al., 2003). There is much clinical interest in the mechanistic role of FFAR2 in SCFA-induced secretion of the anorectic gut peptide hormones GLP-1 and PYY. Both Gαi and Gαq mechanisms have been implicated in FFAR2-dependent GLP-1 and PYY release, however previous studies have been limited to mouse models (Psichas et al., 2015; Caengprasath et al., 2020).

The classic paradigms of GPCR activation have evolved in the last two decades, extending the role of the endocytic pathway beyond terminating plasma membrane signalling and subsequent receptor recycling or degradation, to facilitating the signalling of internalised receptors from diverse endomembrane hubs (Hanyaloglu & Von Zastrow, 2008). The introduction of fluorescence resonance energy transfer (FRET)- based techniques was able to capture a temporal complexity in GPCR-activated cAMP responses, encoded by cellular location (Calebiro et al., 2009). As such, several endocrine-relevant GPCRs ligands have been shown to activate prolonged and pharmacologically-unique G protein-dependent and independent responses from endomembrane platforms which can outlast transient GPCR signals from the plasma membrane (Caengprasath & Hanyaloglu, 2019). A further development to this tenet of intracellular GPCR signalling emerged in the case of the parathyroid hormone receptor (PTHR), in which such spatiotemporally-pleiotropic Gαs responses are induced from the single receptor by activation with two functionally divergent endogenous agonists, PTH and PTHrP (Ferrandon et al., 2009). The demonstration that agonist-directed spatial encryption of GPCR signalling can be decoded to specific cellular functions in both physiological and pathophysiological

systems, holds therapeutic benefit in the development compartment-specific GPCR ligands.

Previous work from our lab has uncovered a spatial complexity to mouse FFAR2 signalling pathways that drives anorectic gut hormone release (Caengprasath et al., 2020). This chapter aims to characterise and compare the SCFA-activated signalling pathways of the human ortholog of FFAR2 (hFFAR2) in a system where it is endogenously expressed; the NCI-H716 EEC line, and in a heterologous expression system; HEK-293 cells transiently transfected with hFFAR2.
In addition, I question the identity of specific endosomal compartments to which hFFAR2 might traffic to downstream of SCFA activation and investigate the integration of human FFAR2 endocytic trafficking in Gαi and Gαq signalling profiles.

3.2 Results

3.2.1 Propionate activates both human FFAR2-Gαi and -Gαq pathways in a heterologous expression system

The Gαi and Gαq signalling profiles of the human ortholog of FFAR2 were first characterised in a heterologous expression system. A human FFAR2 construct bearing an N-terminal FLAG tag (FLAG-hFFAR2) was transiently transfected into the HEK-293 cells line which lacks endogenous expression of the receptor**.** Transfected cells were stimulated with endogenous SCFA ligand of FFAR2, propionate (C3), and Gαi and Gαq signalling responses were measured and compared with wild-type cells.

Activation of the Gαq pathway results in the stimulation of phospholipase C- β which cleaves phosphatidylinositol phosphate (PIP_2) to diacylglycerol (DAG) and inositol triphosphate (IP_3) facilitating the activation of protein kinase A and mobilisation of calcium from IP_3 receptor-gated channels respectively. Gαq activation was quantified by measuring the accumulation of a more stable downstream metabolite of IP3, inositol monophosphate (IP1). Propionate stimulated an increase in intracellular IP1 levels in transfected cells (*Figure 3.1A)*. In contrast, propionate IP1 responses were comparable to NaCl control in WT HEK-293 cells, confirming a hFFAR2-dependence.

Next, propionate-stimulated Gαi activation was investigated in FLAG-hFFAR2 HEK-293 cells. The Gαi pathway inhibits the enzyme adenyl cyclase, thereby dampening the conversion of ATP to cAMP and activity of cAMP-dependent protein kinase (PKA). FLAG-hFFAR2^{+} HEK-293 cells were pre-treated with phosphodiesterase inhibitor 3-isobutyl-1-methylxanthanine (IBMX) to raise intracellular cAMP. Cells were then co-treated with adenyl cyclase activator forskolin and propionate or NaCl control, and inhibition of forskolin-mediated cAMP accumulation was measured (*Figure 3.1D)*. Propionate significantly inhibited forskolin-mediated accumulation of cAMP in a concentration-dependent manner (logIC_{50}= -4.224 ± 0.258) in FLAG-FFAR2^{+} but not WT HEK-293 cells (*Figure 3.1B).*

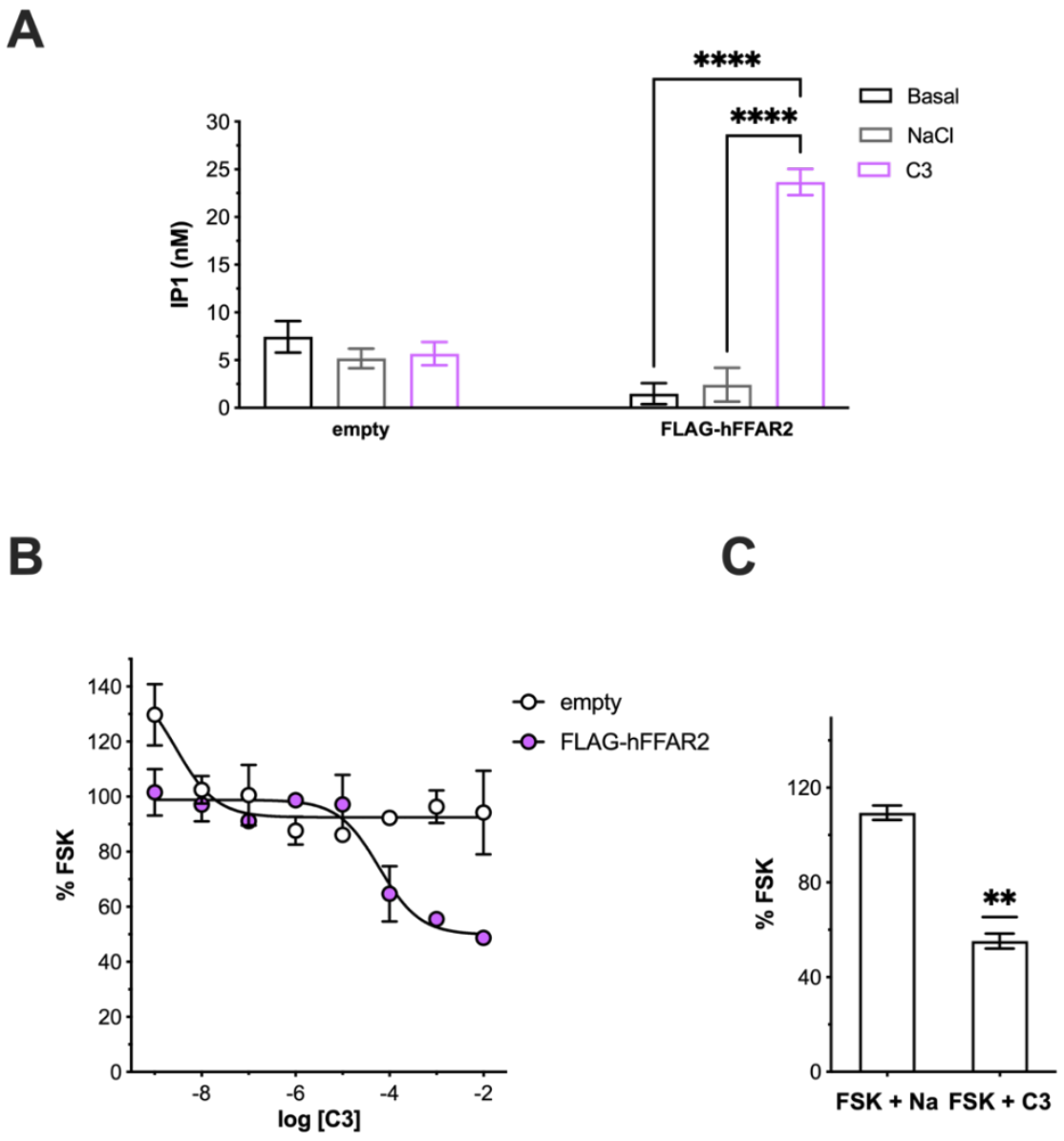


Figure 3.1 Propionate activates Gαi and Gαq signalling in HEK-293 cells transiently transfected with FLAG-hFFAR2. (A) Intracellular accumulation of inositol monophosphate (IP1) measured in untransfected (*empty)* and HEK-293 cells transiently transfected with FLAG-hFFAR2 at baseline (basal) or following treatment with NaCl (1mM, 2hr) or C3 (1mM, 2hr). Data are presented as mean ± SEM of at least triplicates, n=3 independent experiments. Two-way ANOVA; Basal vs NaCl vs C3 in untransfected or transfected cells (****p<0.001). **(B)** Intracellular cAMP accumulation measured in FLAG-hFFAR2 transfected HEK-293 cells. Cells were treated with IBMX (500 nM, 5 min), followed by FSK (3μM, 5 min) or a combination of FSK (3μM, 5min) and NaCl (1mM, 5 min) and C3 (1mM, 5 min). Responses are shown as % change to FSK. Data are presented as mean ± SEM of at least triplicates, n=3 independent experiments. t-test vs FSK (**p>0.01). (**C)** Intracellular cAMP accumulation in untransfected HEK-293 cells and FLAG-hFFAR2 transfected HEK-293 cells following treatment with IBMX (500 nM, 5 min) and then treatment with FSK (3μM, 5 min) or FSK (3μM, 5 min) and C3 (1nM-10mM, 5 min). Responses are shown as % change to FSK. Data are presented as mean ± SEM of at least triplicates, n=3 independent experiments.

3.2.2 NCI-H716 cells as a model for investigating FFAR2 signalling in human colonic L-cells

L-cells exhibit unique functionalities based on their macro-anatomical location and microenvironment along the gastrointestinal tract. As such, duodenal and jejunal L-cells are more responsive to absorbed meal-derived nutrients than colonic L-cells, whereas colonic L-cells largely modulate secretory responses to metabolites of the gut microbiome (Kuhre et al., 2021). Therefore, in studying the FFAR2 signalling responses to SCFAs on L-cells human gastrointestinal tract, it seemed appropriate to consider a colon- rather than a small intestine-derived model. NCI-H716 is a suspension cell line derived from a colorectal adenocarcinoma and has been characterised as a model for studying GLP-1 and PYY secretion in human enteroendocrine L-cells (Park et al., 1987; Reimer et al., 2001). The expression of FFAR2 and FFAR3 in NCI-H716 cells was quantified alongside expression of GLP-1 precursor proglucagon (*Gcg*) and *Pyy (Figure 3.2).* Single cell RNA sequencing (scRNAseq) analyses have further resolved specific L-cell transcriptome signatures of distinct regions within the colonic epithelium (Burclaff et al., 2022). Expression of *Pyy*

in NCI-H716 cells was much lower than *Gcg*, similar to L-cell transcriptomes specific to the ascending colon. *Ffar2* expression was ~400 fold higher than *Ffar3* , which is endogenously characteristic of native human L-cells *in vivo* (Tazoe et al., 2009). Together these findings suggested NCI-H716 cells to as a suitable model to SCFA-driven FFAR2 signalling mechanisms that might drive anorectic gut hormone production in human colonic L-cells.

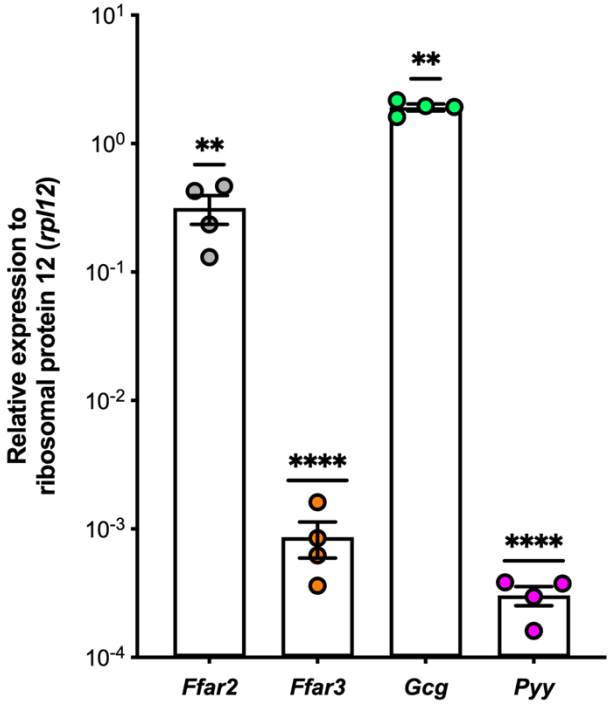


Figure 3.2 The human colonic NCI-H716 cell line express nutrient-sensing machinery and hormone products characteristic of L-cells. Relative gene expression of *Ffar2*, *Ffar3*, *Gcg* and *Pyy* in NCI-H716 cells to housekeeping gene ribosomal protein 12 (*rpl12*) obtained by the 2-ΔCt method. Data are represented as mean ± SEM of triplicates, n=4 independent experiments. T-test to 1 (****p>0.001, ***p>0.001, **p>0.01).

3.2.3 SCFAs activate heterogeneous Gαi and Gαq signalling profiles in NCI-H716 cells

Despite the coupling of FFAR2 to both Gαi and Gαq signalling pathways, previous data from our lab has found propionate to activate Gαi but not Gαq in mouse EECs (Caengprasath et al., 2020). I questioned whether propionate-stimulated hFFAR2

signallinag mechanisms might be conserved across mouse and human receptor orthologs in EECs. Gαi activation with increasing concentration of NaCl treatment control in NCI-H716 cells showed large variation and no likeness to an inhibitory trend *(Figure 3.3A)*. Propionate-activated Gαi responses in NCI-H716 cells were compared alongside those of two other endogenous SCFA ligands of hFFAR2, acetate (C2) and butyrate (C4). *(Figure 3.3B).*

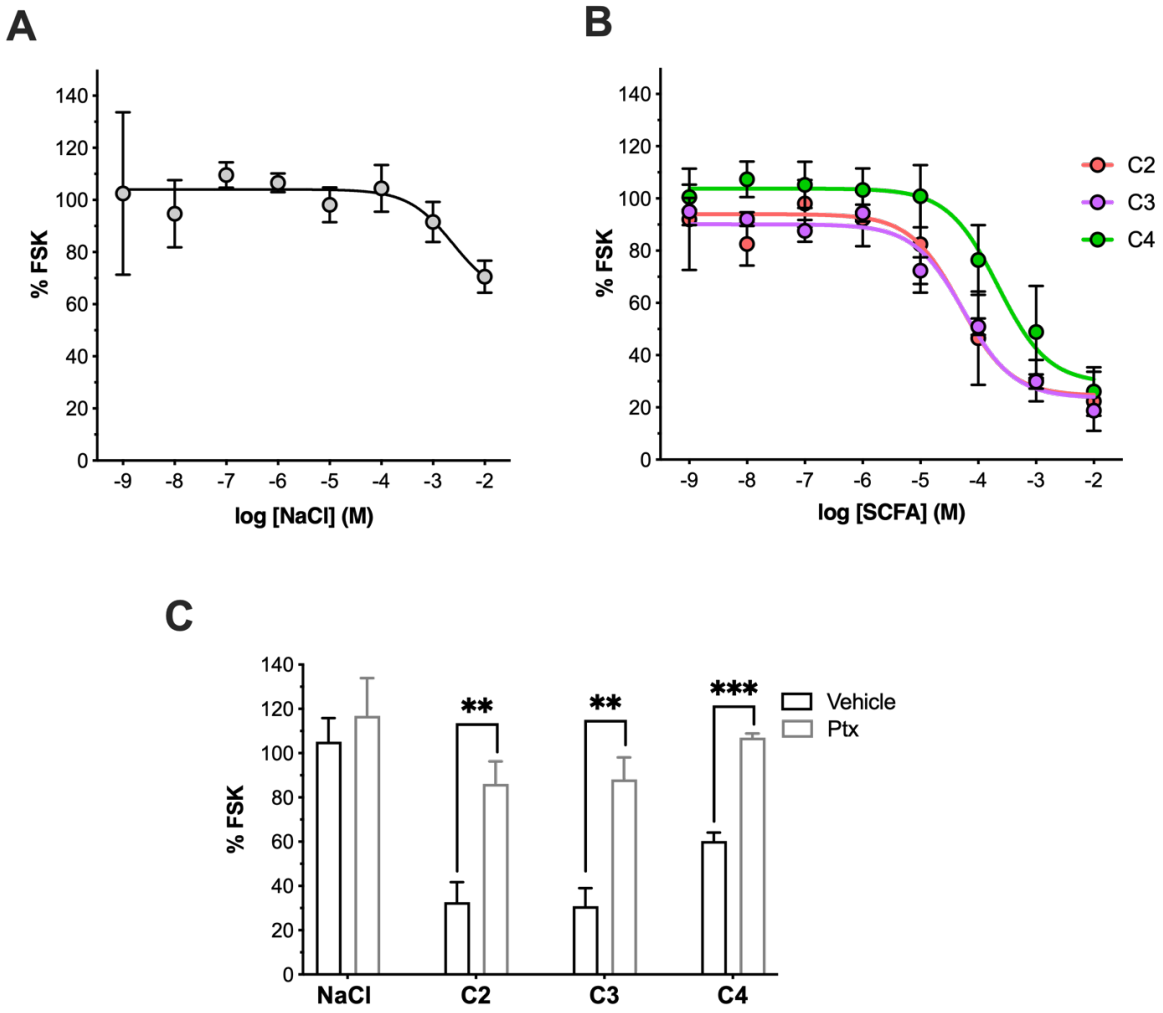
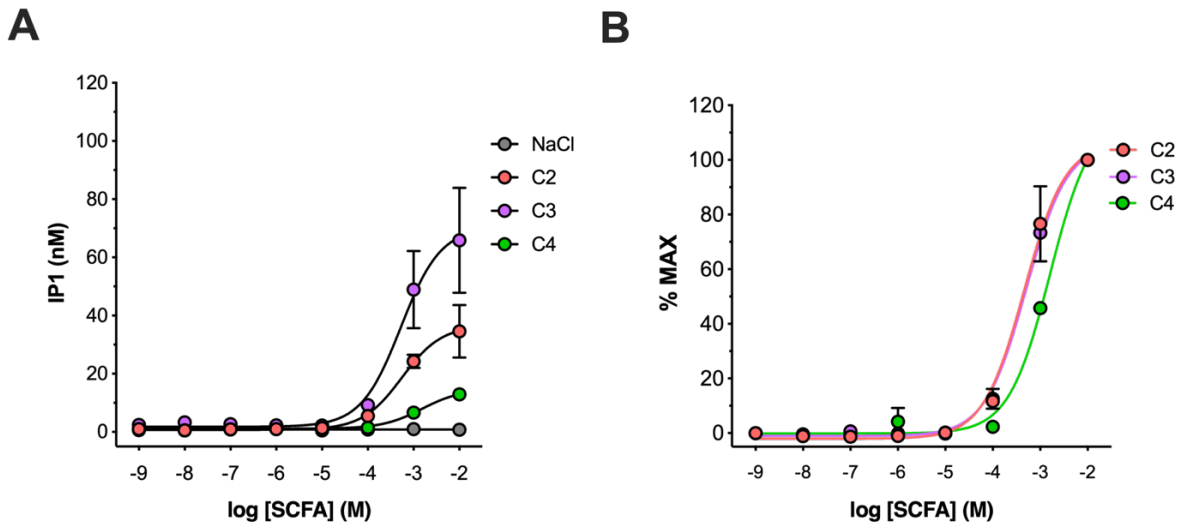


Figure 3.3 SCFAs activate Gαi signalling in NCI-H716 cells in a concentration dependent manner. Intracellular FSK-mediated cAMP accumulation in NCI-H716 cells. Cells were treated with IBMX (500 nM, 5 min), followed by FSK (3μM, 5 min) or a **(A)** combination of FSK (3μM, 5min) and NaCl (100nM-10mM 5 min) (**B)** or a combination of FSK and SCFA (1nM-10mM, 5 min); NaCl *(grey),* C2 *(red),* C3 *(purple),* C4 *(green).* Responses are shown as % change to FSK. Data are presented as mean ± SEM of at least triplicates, n=6 independent experiments. (**C)** NCI-H716 cells were pre-treated with Pertussis toxin (PTX) (250ng/ml) or vehicle for 20 hours, and subsequently IBMX (500 nM, 5 min), followed by FSK (3μM, 5 min) or a combination of FSK (3μM, 5min) and NaCl/SCFA (1mM, 5 min); H20 vehicle *(white)*, PTX

(dark grey). Data are presented as mean ± SEM of at least triplicates, n=3 independent experiments. t-test Vehicle vs PTX (***p<0.001, **p<0.01).

Propionate, butyrate, and acetate significantly inhibited forskolin-mediated cAMP accumulation in a concentration dependent manner, ranking first, second and third in potency amongst the SCFAs respectively (*Table 3.1).* SCFA-mediated inhibition of cAMP accumulation in NCI-H716 cells was confirmed to be a Gαi-specific effect using Pertussis toxin (PTX) *(Figure 3.3C)*. PTX catalyses the transfer of an ADP-ribose moiety to Gαi proteins, inhibiting receptor coupling (Bokoch et al., 1983). 20-hour pre-treatment of NCI-H716 cells with 250ng/ml PTX significantly blunted SCFA-mediated decreases in cAMP, confirming an underlying Gαi mechanism.

SCFAs were also able to activate Gαq signalling in NCI-H716 cells. Acetate, propionate, and butyrate increased IP1 accumulation in a concentration-dependent manner, ranking in identical order to their Gαi potencies (*Table 1)*. Propionate demonstrated maximal efficacy in stimulating IP1 accumulation, followed by acetate and butyrate (*Figure 3.4A).* Butyrate-driven IP1 accumulation was modest, only slightly exceeding NaCl control response. To confirm an underlying Gαq-specific effect in SCFA IP1 profiles, selective Gαq inhibitor YM-254890 was employed, which mechanistically inhibits the GDP/GTP exchange of Gαq (Nishimura et al., 2010). Pre-treatment of cells with YM-254890 significantly inhibited SCFA-mediated accumulation of IP1 in NCI-H716 cells, confirming a Gαq-mediated effect (*Figure 3.4B)*.



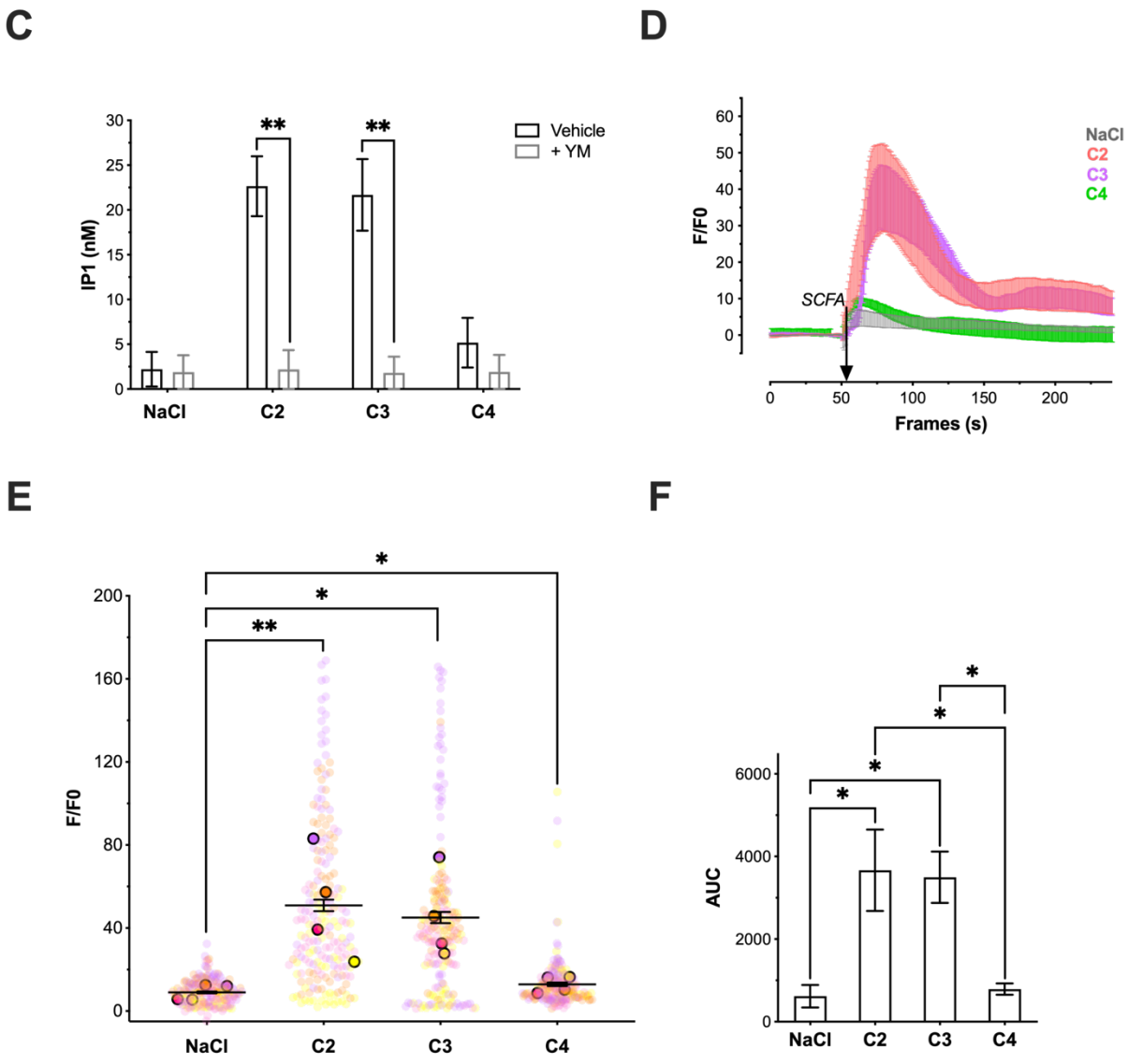


Figure 3.4 SCFAs activate Gαq signalling in NCI-H716 cells. (A, B & C) Intracellular IP1 accumulation in NCI-H716 cells following (A) 2hr treatment with increasing concentrationss (1nM-10mM) of NaCl (*grey),* or C2 *(red),* or C3 *(purple),* or C4 *(green)*. Data is shown as **(B)** normalised curves by defining minimum and maximum responses for each SCFA (or NaCl) defined as 0% and 100% respectively. **(C)** SCFA-mediated IP1 accumulation (1mM, 2hr) measured after pre-treatment with YM-254890 or DMSO vehicle; DMSO (*white),* YM-254890 *(grey).* Data are presented as mean ± SEM of at least triplicates, n=3 independent experiments. t-test Vehicle vs YM (**p<0.01). (D, E & F) SCFA-mediated intracellular calcium mobilisation measured by Fluo-4 fluorescent calcium indicator in NCI-H716 cells. Cells were incubated with FLuo4-AM for 1 hour, and imaged by confocal microscopy for 1 minute (50 frames) before the addition of NaCl (10mM) or SCFA (10mM). **(D)** Maximal change in fluorescence intensity over baseline(F/F0) in individual cells. Opaque circles represent the

mean ± SEM of n=40 cells counted per experiment, n=4 independent experiments. One-way ANOVA; NaCl vs CS vs C3 vs C4 (**p<0.01, *p<0.05). (**E)** Representative F/F0 trace averaged across n=40 cells per experiment, n=3 independent experiments. (**F)** Area-under-curve (AUC) measurements of F/F0 traces from beginning of baseline (0s) to the end of imaging (270s). Data are presented as mean ± SEM of at least triplicates, n=3 independent experiments. One-way ANOVA; NaCl vs CS vs C3 vs C4 (*p<0.05).

Additionally, in investigating SCFA-mediated Gαq signalling in NCI-H716 cells, an intracellular calcium mobilisation assay was employed. Cells were incubated with fluorescent Fluo-4AM indicator and calcium mobilisation captured by confocal microscopy. In agreement with IP1 profiles, acetate and propionate exhibit a greater maximal increase than butyrate in stimulating Ca^{2+} mobilisation (*Figure 3.4C).* Cell fluorescence (F/F0) exhibited a immediate monophasic increase after addition with acetate or propionate which began to decay within ~60 seconds and remained in a plateau for the remaining assay duration (*Figure 3.4D)*. In contrast, butyrate-mediated calcium responses were not significantly different from NaCl-treated cells (*Figure 3.4D)*. Area-under-the-curve (AUC) measurements of SCFA F/F0 temporal profiles indicated similar magnitudes of C2 and C3 responses in the given time window (*Figure 3.4E)*.

SCFA	pIC50 (M)	pEC50 (M)
C2	-4.313 ± 0.299	-3.255 ± 0.459
C3	-4.251 ± 0.286	-3.277 ± 0.496
C4	-3.660 ± 0.298	-2.814 ± 0.354

Table 3.1 pIC50 and pEC50 values of SCFAs in NCI-H716 cells. Cells were treated as in Figure 3.3B and 3.4A to obtain pIC50s and pEC50s respectively for each SCFA. Data are presented as mean ± SEM of three technical triplicates per experiment, n=3 independent experiments.

3.2.4 SCFA-activated Gαi responses are mediated by FFAR2 in NCI-H716 cells

Although FFAR3 is expressed in much lower abundance than FFAR2 in NCI-H716 cells, which has been both previously reported and confirmed in my qPCR analysis (3.2.2), SCFA-mediated Gαi responses may not be solely mediated by FFAR2 (Larraufie et al., 2018). Moreover, prior studies have reported FFAR3-mediated GLP-1 secretion in NCI-H716 cells in response to the synthetic FFAR3-selective ligand AR420626 (Ducastel et al., 2020). Therefore, to investigate the involvement of FFAR2-independent mechanisms of Gαi activation downstream of SCFA treatment, NCI-H716 cells were pre-treated with GLPG0974, a synthetic orthosteric antagonist of human FFAR2 (Pizzonero et al., 2014). A significant concentration-dependent reversal of propionate-induced GαI signalling was observed with GLPG0974 pre-treatment (logIC50 = -7.37 ± 0.501) *(Figure 5A).* A 1μM treatment of GLPG0974, which was >logIC50 and coinciding with maximal antagonist efficacy, was chosen for subsequent assays. Pre-treatment with 1μM of GLPG0974 significantly inhibited Gαi signalling downstream of all three SCFAs, suggesting the involvement of FFAR2 rather than FFAR3 in activating Gαi responses in NCI-H716 cells (*Figure 5B)*.

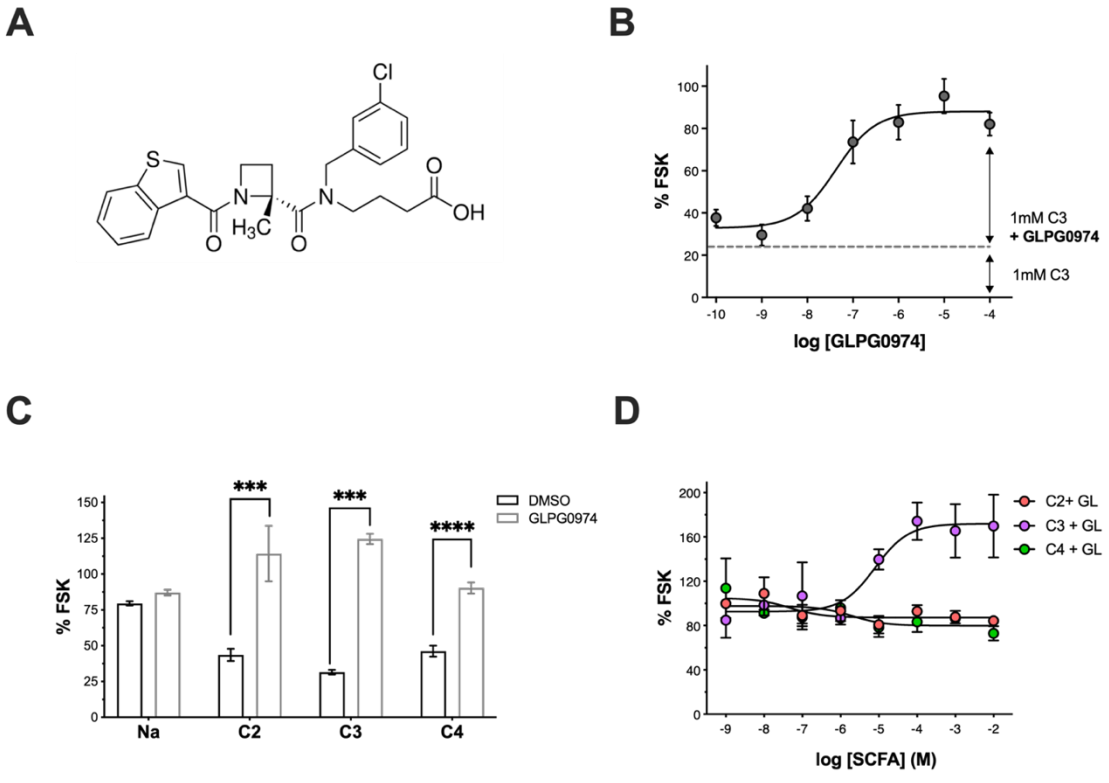


Figure 3.5 FFAR2 mediates SCFA-activated Gαi signalling in NCI-H716 cells. (A, B, and C) Inhibition of Gαi signalling downstream of C3 activation by antagonist for human FFAR2, GLPG0974. **(A)** Cells were pre-treated with increasing concentrations of GLPG0974 (100pM - 100μM, 15 min) or DMSO vehicle, followed by IBMX (500nM, 5 min), and then FSK (3μM, 5min), or a combination of FSK (3μM, 5min) and C3 (1mM, 5 min). Responses are shown as % change to forskolin. The dotted line represents the average % FSK response of C3. Data are presented as mean ± SEM of triplicates, n=3 independent repeats. **(B)** Intracellular cAMP accumulation following pre-treatment with GLPG0974 (1μM, 15 min) or vehicle, IBMX (500nM, 5 min) and then FSK (3μM, 5min) or a combination of FSK (3μM, 5min) and NaCl/SCFA (1mM, 5 min). Responses are shown as % change to forskolin. Data are presented as mean ± SEM of at triplicates, n=3 independent repeats. t-test vehicle vs GLPG0974 (***p<0.001) **(C)** Intracellular cAMP accumulation n following pre-treatment with GLPG0974 (1μM, 15 min) or vehicle, IBMX (500nM, 5 min) and then FSK (3μM, 5min) or a combination of FSK (3μM, 5min) and **(D)** increasing concentrations of C2/C3/C4 (100nM-10mM, 5 min). Responses are shown as % change to forskolin. Data are presented as mean ± SEM of triplicates, n=3 independent repeats.

A GLPG0974-mediated inhibition of Gαi responses was evident for all three SCFAs *(Figure 5C)* and was consistent across increasing SCFA concentrations of SCFAs (*Figure 5D).* Above 10nM of propionate, stimulation in the presence of GLPG0974 even led to an increase in cAMP levels above forskolin positive control (*Figure 5D)*.

3.2.5 SCFA promote phosphorylation of ERK 1/2 in NCI-H716 cells

The ERK/Mitogen-activated protein kinase (MAPK) cascade, a regulator of pivotal cellular functions, is a downstream signalling effector common to numerous GPCRs (Eishingdrelo, 2013). Agonism of both mouse and human FFAR2 have been shown to activate phosphorylation of ERK 1/2 *in vitro* (Bolognini et al., 2016; Chun et al., 2019; Negari, Keshari & Huang, 2021). I aimed to elucidate whether SCFAs induce ERK1/2 phosphorylation in human EECs, and compare potential differences in temporal patterns of activation. NCI-H716 cells were treated with 1mM of SCFA or 1mM NaCl control for 5, 15 or 30 minutes, and Western Blot analysis was used to measure protein expression levels of phospho- and total-ERK1/2 (*Figure 3.6A).* A fold-change increase in phospho-ERK1/2 relative to NaCl control was evident after & C 5-minute treatment

with C2, C3 or C4 (*Figure 3.6B).* Interestingly C4-stimulated phosphorylation of ERK1/2 demonstrated a time-dependent decrease, whereas C2- and C3-stimulated phosphorylation remained elevated at both 15 and 30 minutes.

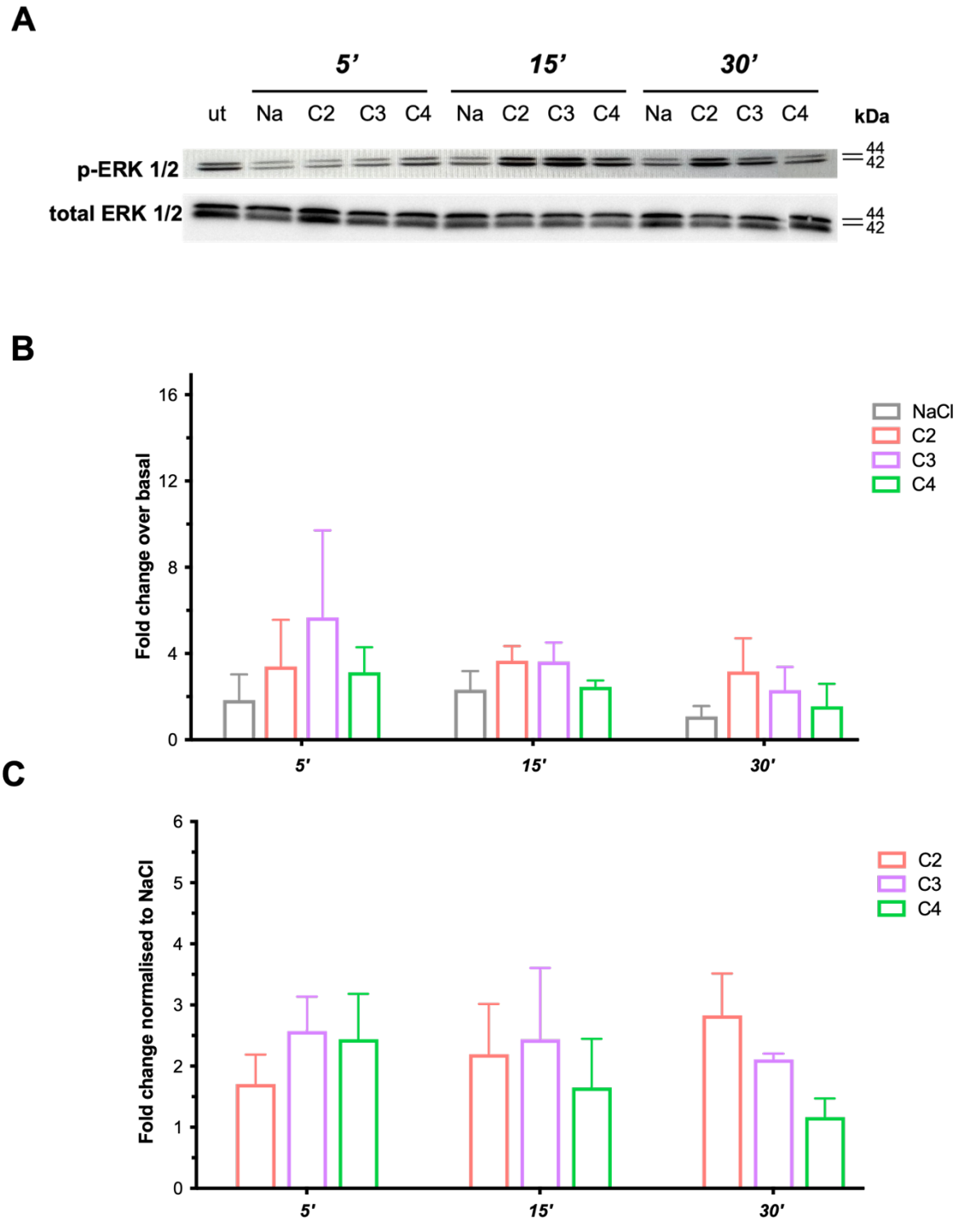


Figure 3.6 SCFAs promote phosphorylation of ERK 1/2 in NCI-H716 cells. (A) Representative Western Blot measuring the protein expression of phosphorylated ERK 1/2 (p-ERK 1/2) and total ERK 1/2. NCI-H716 cells were serum starved for 24h prior to treatment

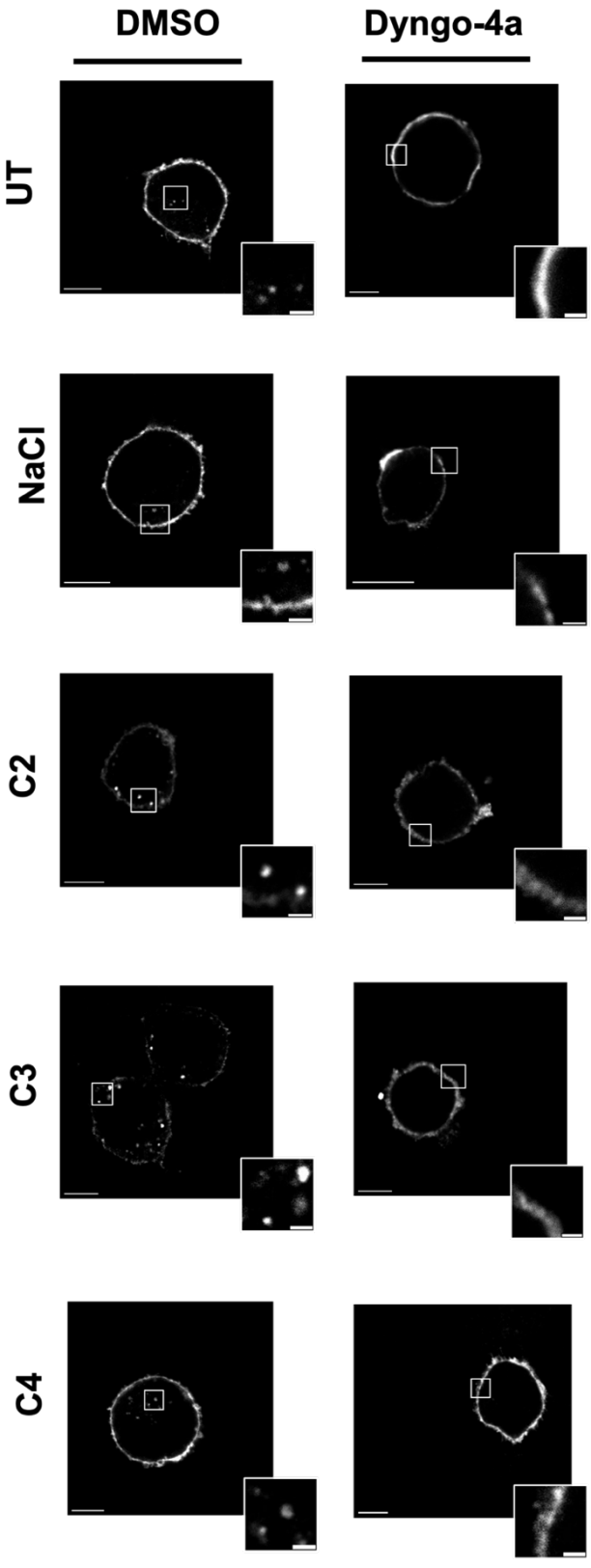
with 1mM NaCl control or 1mM SCFA for 5, 15 or 30 minutes. Lysates were collected for Western Blot analysis and expression of p-ERK 1/2 was probed. Membranes were then stripped and re-probed for total ERK 1/2 which served as a loading control. ut= untreated basal control. **(B)** Densitometry analysis of p-ERK 1/2 normalised to total-ERK 1/2 in lysates at each timepoint represented as a fold change over basal or **(C)** fold change over NaCl control; NaCl *(grey),* C2 *(red),* C3 *(purple),* C4 *(green).* Data are expressed as mean ± SEM, n=3 independent experiments.

3.2.6 FFAR2 undergoes constitutive and SCFA-induced internalisation in NCI-H716 cells and FLAG-hFFAR2 HEK-293 cells *via* a dynamin-dependent mechanism

Research from our lab has shown propionate-induced internalisation and intracellular signalling of mouse FFAR2 to be vital in GLP-1 secretion (Caengprasath et al., 2020). Aside from agonist-dependent internalisation, many GPCRs undergo ligand-independent endocytosis, a process known as constitutive internalisation, which functions in the regulation of basal receptor activity and subcellular receptor targeting (Schmidt et al., 2020). Both constitutive and propionate-induced internalisation of mouse FFAR2 proceeds *via* a dynamin-dependent mechanism, in which the GTPase dynamin facilitates the intracellular scission of receptor-populated clathrin-coated pits at the plasma membrane.

To determine whether human FFAR2 undergoes constitutive and/or agonist-dependent internalisation, NCI-H716 and HEK-293 cells were transiently transfected with FLAG-hFFAR2 construct, and receptor internalisation was qualitatively assessed by confocal microscopy. In addition, the role of dynamin-dependent endocytosis in human FFAR2 trafficking was assessed by pre-treatment with dynamin inhibitor Dyngo-4a. In both NCI-H716 and transiently-transfected FLAG-hFFAR2 HEK-293 cells, few receptor endosomes could be observed under basal conditions, and increased in abundance following treatment with acetate, propionate or butyrate but not NaCl (*Figure 3.7)*. A strong inhibition of constitutive and SCFA-induced internalisation was observed with Dyngo-4a in both cell lines, suggesting a dynamin-

mediated mechanism of ligand-independent and -dependent endocytosis of human FFAR2.



HEK-293

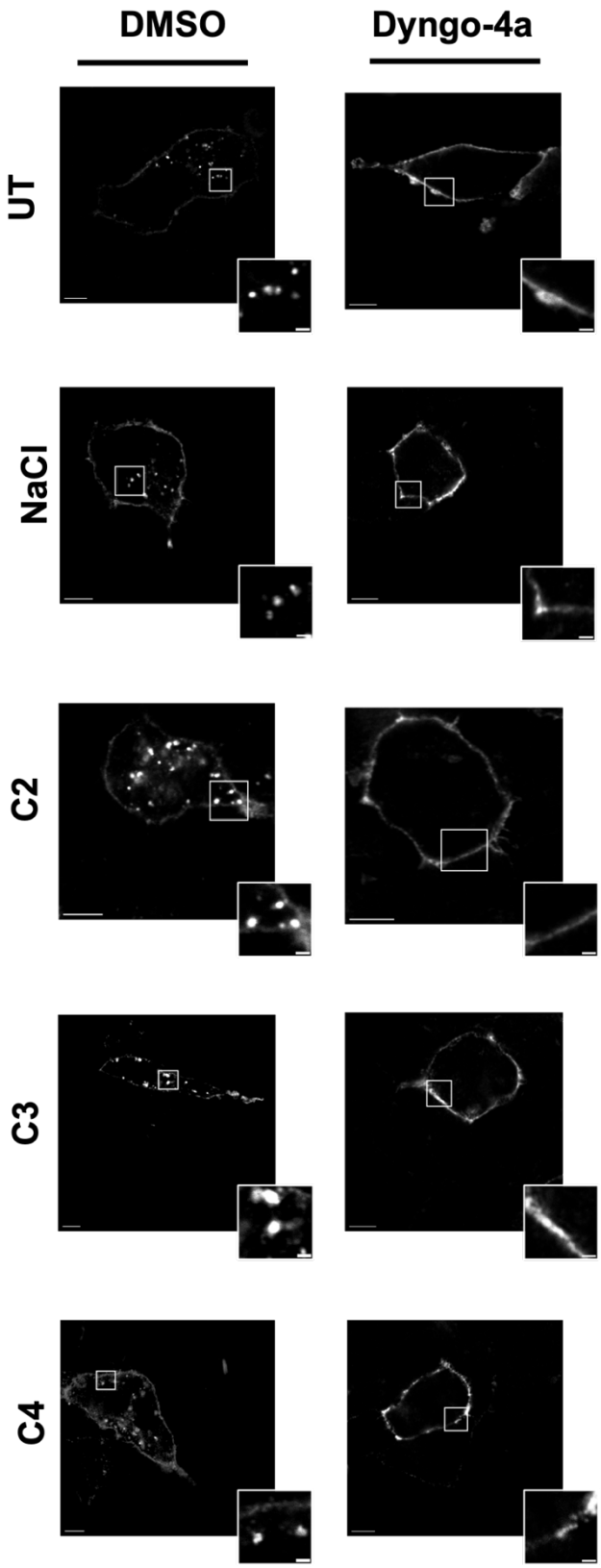


Figure 3.7 FFAR2 undergoes both constitutive and SCFA-induced dynamin-dependent endocytosis in NCI-H716 cells and HEK-293 cells transiently transfected HEK-293 cells. NCI-H716 cells and HEK-293 cells transiently transfected with FLAG-hFFAR2 were treated with DMSO vehicle or inhibitor of dynamin-dependent endocytosis Dyngo-4a (45 min, 50μM), followed by incubation with anti-FLAG M1 primary antibody (30 min) which included NaCl/SCFA treatments (1mM, 20 min). Subsequently, cells were permeabilised, labelled with AlexFluor 555 secondary antibody and mounted onto glass slides. Slides were imaged by confocal microscopy using the Leica super-resolution 'Lightning' module. n=5 cells captured per experiment, n=3 independent experiments.

3.2.7 hFFAR2 demonstrates constitutive Gαq but not Gαi activity in NCI-H716 cells

Due to hFFAR2 exhibiting considerable constitutive internalisation, I explored whether these trafficking patterns correlated with basal activity of the receptor. To determine basal Gαq and Gαi activity that was specific to hFFAR2, I measured the effect of GLPG0974 antagonism on IP1 and cAMP levels in the absence of SCFAs. Notably, Gαq but not Gαi responses were slightly yet significantly diminished in the presence of GLPG0974, indicating a basal Gαq activity of FFAR2 in NCI-H716 cells *(Figure 3.8)*.

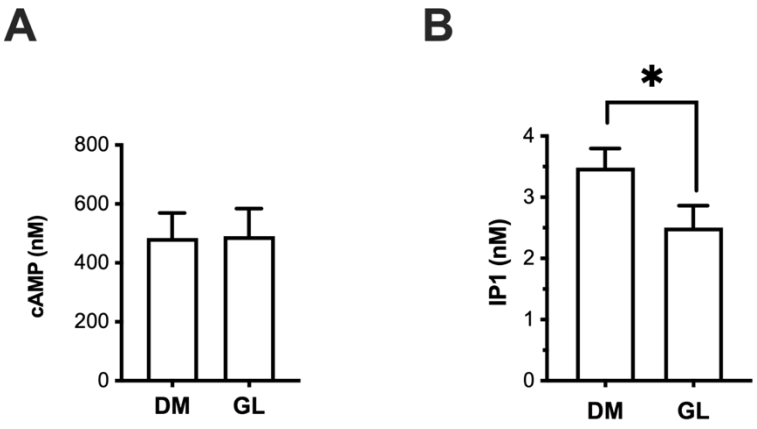


Figure 3.8 hFFAR2 exhibits basal Gαq but not Gαi activity in NCI-H716 cells. (A) Intracellular forskolin-mediated cAMP accumulation in cells pre-treated with GLPG0974 (*GL)* (1μM, 15 min) or DMSO vehicle (*DM)* (15 min) followed by IBMX (500nM, 5 min) and then FSK (3μM, 5 min). Data represents mean ± SEM of triplicates, n=3 independent experiments. (**B)** IP1 accumulation in cells pre-treated with GLPG0974 (1μM, 15 min) or DMSO vehicle (15

min) across 2 hours. Data represents mean ± SEM of triplicates, n=3 independent experiments. Unpaired t-test; DM vs GL (*p<0.05).

3.2.8 SCFA-mediated FFAR2 signalling responses show differential dependence on receptor internalisation in NCI-H716 cells

Next, it was investigated whether SCFA-activated signalling profiles of FFAR2 were dependent on internalisation of the receptor by use of Dyngo-4a. First, the effect of Dyngo-4a on SCFA-driven Gαi signalling profiles in NCI-H716 cells was measured. Pre-treatment with Dyngo-4a appeared to increase forskolin-induced cAMP measurements NaCl treatment in three out of four independent repeats (*Figure 3.9A)*. However following normalisation to NaCl, no significant inhibition of SCFA responses by Dyngo-4a could be observed (*Figure 3.9B).*

The effect of Dyngo-4a on SCFA-mediated Gαq activation was investigated by measuring levels of intracellular IP1. Similar to the effect on Gαi, levels of IP1 in the presence of NaCl were increased by Dyngo-4a pre-treatment although remained low in comparison to SCFA-induced responses (*Figure 3.9C).* Acetate and propionate-stimulated IP1 accumulation exhibited a strong dependence on receptor internalisation (*Figure 3.9D)*. Moreover, although butyrate activates a much weaker FFAR2-Gαq response compared to acetate and propionate, inhibition of butyrate Gαq responses with Dyngo-4a is still evident. Lastly, I confirmed the inhibitory effect of Dyngo-4a on propionate-Gαq responses to be evident across a range of propionate concentrations (*Figure 3.9E).*

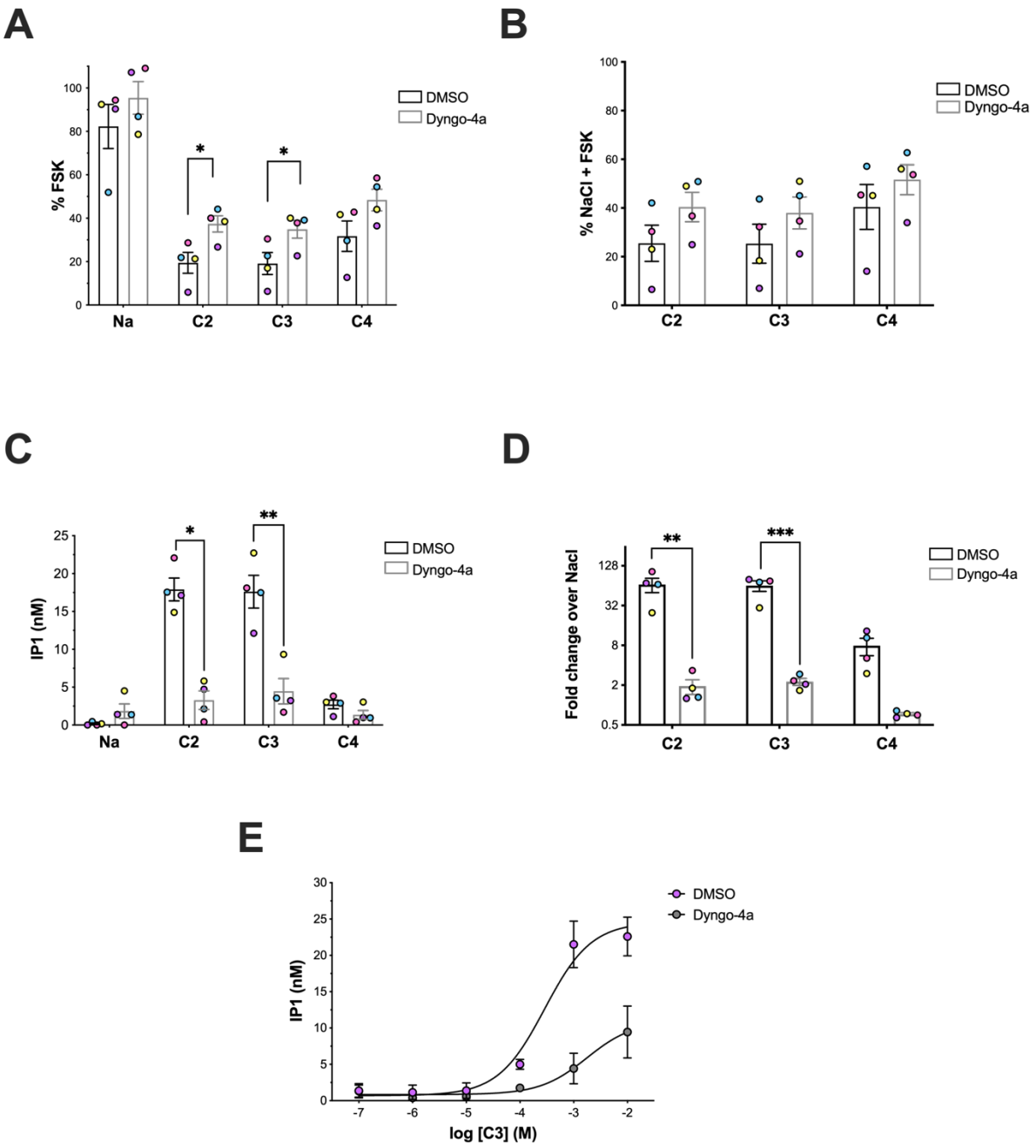


Figure 3.9 SCFA-mediated signalling responses show differential dependencies on receptor internalisation in NCI-H716 cells. Effect of Dyngo-4a on (**A & B)** SCFA-mediated Gαi responses and (C, D & E) SCFA-mediated Gαq activation in NCI-H716 cells. **(A & B)** Intracellular cAMP accumulation following pre-treatment with Dyngo-4a (50μM, 45 min) or DMSO vehicle, IBMX (500nM, 5 min) and then FSK (3μM, 5min) or a combination of FSK (3μM, 5min) and NaCl/SCFA (1mM, 5 min). Data are shown as **(A)** % change to FSK or (**B)** normalised as % change to normalised to NaCl + FSK. Symbols represent the mean ± SEM of triplicates per independent repeat, n=4 independent repeats. t-test DMSO vs Dyngo-4a

(*p<0.05). (**C & D)** Intracellular IP1 accumulation after treatment with Dyngo-4a (50μM, 45 min) or DMSO vehicle followed by treatment with NaCl or SCFAs (1mM). (**D)** Data are normalised as fold change over NaCl response. Symbols represent the mean ± SEM of triplicates per independent repeat, n=4 independent repeats. t-test DMSO vs Dyngo-4a (***p<0.001, **p<0.01, *p<0.05) **(E)** Intracellular accumulation of IP1 stimulated by increasing concentrations of C3 (100nM-10mM, 2hr) following pre-treatment with DMSO vehicle or Dyngo-4a (50μM, 45 min). Data are shown as the mean ± SEM of triplicates per independent experiment, n=3 independent experiments.

Significant differences in the signalling profiles of mouse FFAR2 between EECs and heterologous expression systems have been identified by our lab. My results thus far demonstrated that Gαq responses of hFFAR2 were evident in both NCI-H716 and transfected HEK-293 cells, but I questioned whether a system bias might impose unique spatial control of receptor signalling. I assessed the impact of Dyngo-4a pre-treatment on propionate-driven Gαi and Gαq signalling in FLAG-hFFAR2 transiently-transfected HEK-293 cells. In contrast to NCI-H716 cells, neither Gαq or Gαi responses stimulated by propionate were sensitive to inhibition by Dyngo-4a in FLAG-hFFAR2+ HEK-293 cells *(Figure 3.10)*.

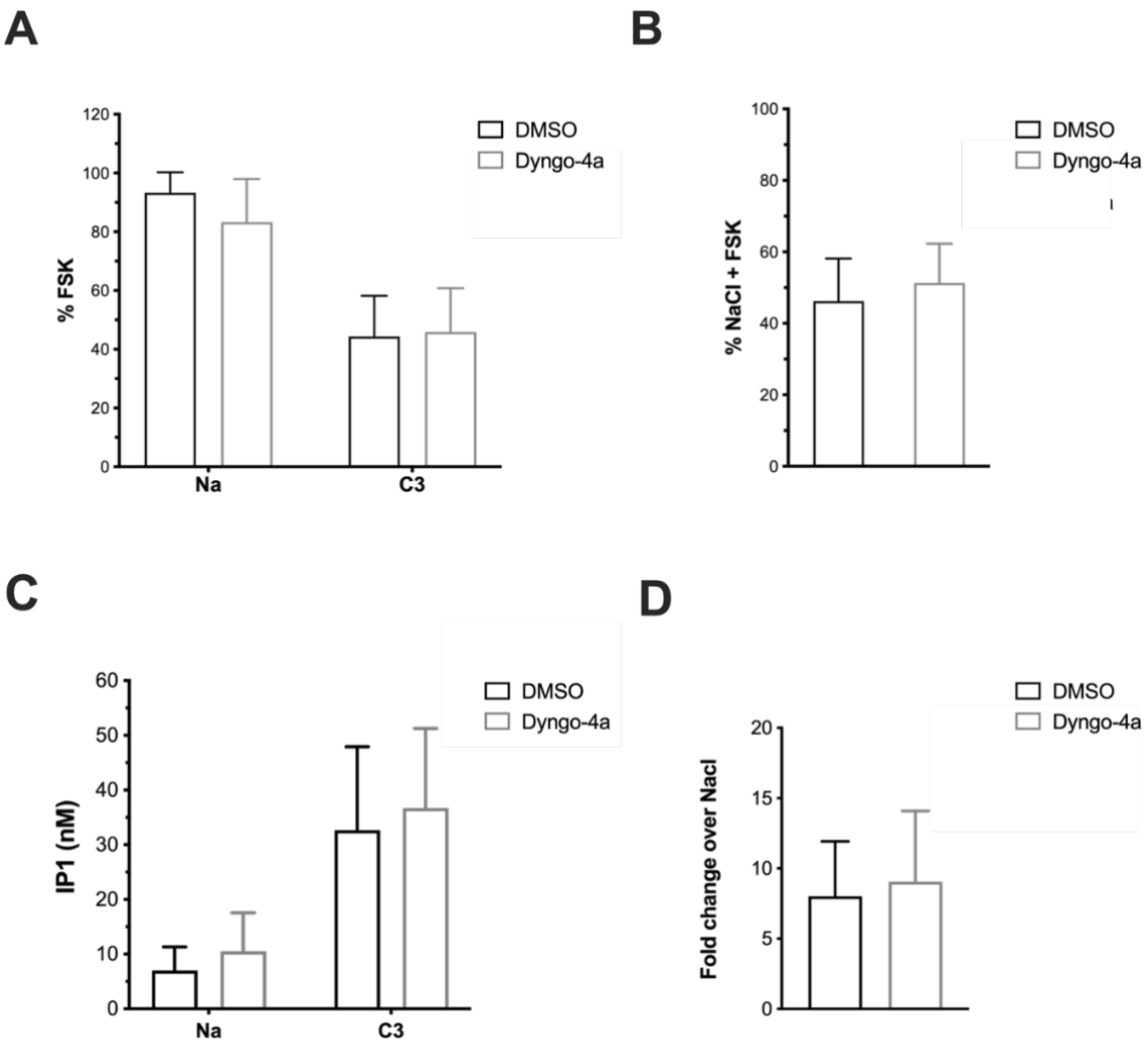


Figure 3.10 Propionate-activated Gαi and Gαq signalling in HEK-293 cells transiently transfected FLAG-hFFAR2 cells are restricted to the plasma membrane. The effect of Dyngo-4a on C3-activated **(A & B)** Gαl responses and (**C & D)** Gαq responses in HEK-293 cells transiently transfected with FLAG-hFFAR2. (**A & B)** Intracellular cAMP accumulation measured after pre-treatment with DMSO vehicle (*white bars)* or Dyngo-4a (50μM, 45 min) *(grey bars)* followed by treatment with IBMX (500nM, 5 min) and then FSK or a combination of FSK and NaCl or C3 (1mM, 5 min). Data are shown as (A) % change to FSK or (B) normalised as % change to FSK. Data is mean ± SEM of triplicates, n=3 independent experiment. (**C & D)** Intracellular IP1 accumulation measured after pre-treatment with DMSO vehicle *(white bars)* or Dyngo-4a (50μM, 45 min) *(grey bars)* followed by 2hr treatment with NaCl (1mM) or C3 (1mM). (**D)** C3 response as fold change over NaCl response. Data is mean ± SEM of triplicates, n=4 independent experiment.

3.2.9 Propionate-activated FFAR2 Gαi and Gαq responses are insensitive to knockdown of very early endosomal marker APPL1 in NCI-H716 cells

Our lab has reported FFAR2 traffics to the very early endosomes (VEEs) following receptor endocytosis in mouse EECs (Caengprasath et al., 2020). Mouse FFAR2 intracellularly occupies a subpopulation of VEEs marked with the protein APPL1, which functions as a positive regulator of receptor recycling and negative regulator of intracellular Gαi signalling. Following my observations in FFAR2 signalling profiles following Dyngo-4a treatment, I assessed whether SCFA-driven Gαi responses might be active in APPL1-positive VEEs by employing a siRNA knockdown. Western blotting confirmed a mean APPL1 knockdown of ~87% across biological repeats (*Figure 3.11A)* No significant differences could be observed in NaCl or propionate-mediated Gαi or Gαq signalling responses upon APPL1 knockdown *(Figure 3.11C; 3.11D).* Preliminary data also suggests that APPL1 knockdown similarly might have no effect on acetate- and butyrate-stimulating FFAR2 signalling profiles in NCI-H716 cells *(Figure 3.11E; 3.11F).*

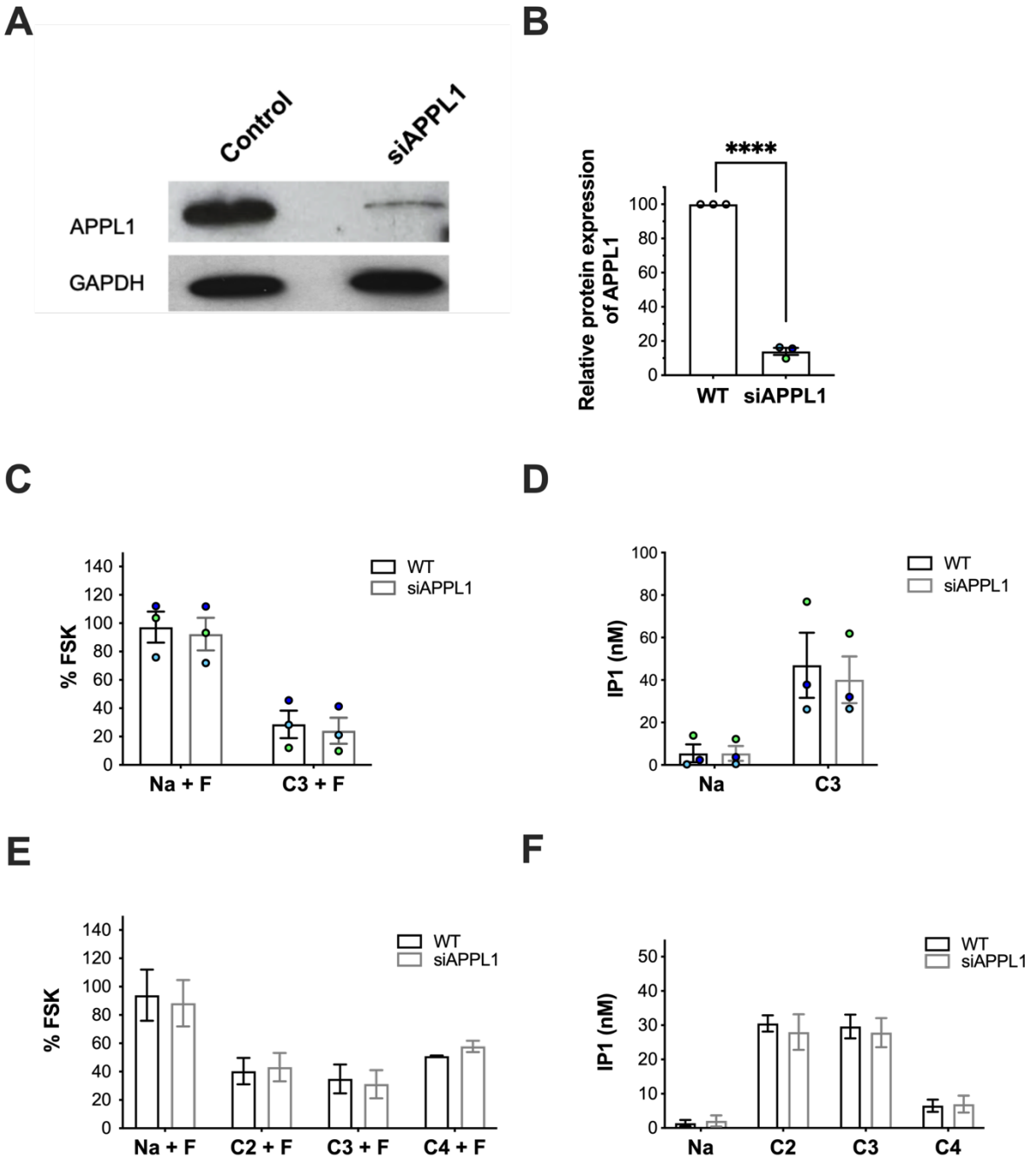


Figure 3.11 SCFA-activated Gαi and Gαq signalling responses appear to be insensitive to knockdown of very early endosomal marker APPL1. (A) Representative image of western blot probing for expression of APPL1 and GAPDH loading control in lysates of NCI-H716 cells transfected with siAPPL1 *vs* control cells. **(B)** Densitometry analysis showing APPL1 protein expression relative to GAPDH in siAPPL1-treated cells as % APPL1 expression relative to GAPDH in control cells. Symbols represent APPL1 protein expression in singlet per independent experiment, n=3 independent experiments. t-test Control vs siAPPL1 (****p<0.0001). (**C & D)** Effect of siAPPL1 knockdown on intracellular cAMP

accumulation measured after treatment with IBMX (500nM, 5 min) followed by FSK (3μM, 5 min) or a combination of FSK (3μM, 5 min) and NaCl or SCFAs (1mM, 5 min), control *(white bars)* and siAPPL1 *(grey bars).* Data are shown as % to FSK response and symbols represents the mean ± SEM of triplicates per independent experiment**, (C)** n=3 independent experiments**, (D)** n=2 independent experiments. **(E & F)** Effect of siAPPL1 knockdown on intracellular IP1 accumulation following 2hr treatment with NaCl (1mM) or SCFA (1mM) control *(white bars)* and siAPPL1 *(grey bars).* Symbols represents the mean ± SEM of triplicates per independent experiment, (**E)** n=3 independent experiments, **(F)** n=2 independent experiments.

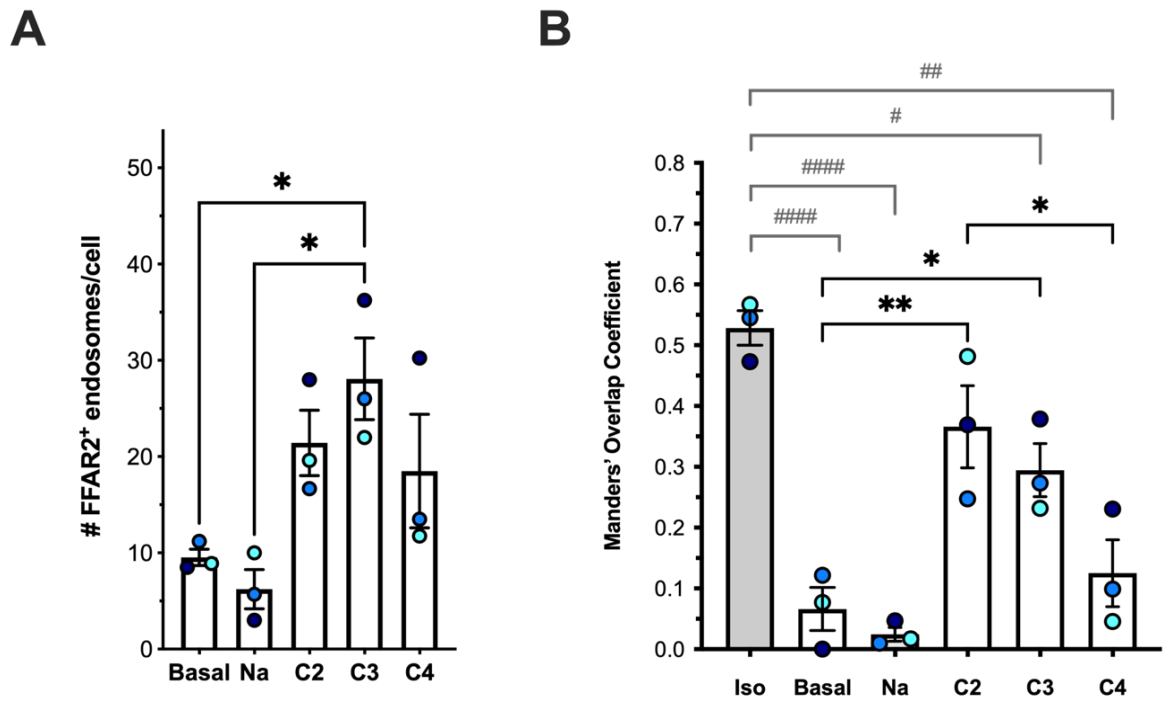
3.2.10 SCFAs encourage FFAR2 trafficking to EEs in NCI-H716 cells

Next, I considered whether SCFA-driven FFAR2 responses might be driven from intracellular compartments other than VEEs in human EECs. The early endosomes (EEs) are a major hub for the trafficking and sorting of internalised membrane cargo and serve as intracellular signalling platforms for diverse GPCRs such as PTHR and the beta-2 adrenergic receptor (β2AR) (Irannejad et al., 2013; Ferrandon et al., 2009). To determine whether human FFAR2 might be trafficked to EEs, colocalisation of hFFAR2 with Early endosomal antigen-1 protein (EEA1), a well-characterised marker of EEs, was measured (Mu et al., 1995).

NCI-H716 cells transiently transfected with FLAG-hFFAR2 were co-stained with anti-FLAG M1 antibody prior to ligand treatment. Anti-FLAG M1 antibody bound to receptor was removed by EDTA wash as this antibody is calcium-dependent and facilitates visualisation of internalised receptor in endosomes. Number of total receptor endosomes was equivalent in basal and NaCl-treated cells, yet increased by treatment with acetate, propionate or butyrate (*Figure 3.12A).*

To quantify the abundance of EEA1-positive FLAG-hFFAR2 endosomes, Manders Overlap Coefficient (MOC) values were determined by automated colocalization analysis on ImageJ (*Figure 3.12B).* The β2AR was employed as a positive control as it is well established to rapidly internalise to EEA1 endosomes following stimulation with its agonist isoproterenol (Sposini et al., 2017). FLAG-FFAR2 endosomes in untreated- and NaCl-treated cells exhibited limited co-localisation with EEA1.

Trafficking of FFA2 to EEA1 positive endosomes was significantly increased from basal in acetate- or propionate-treated but not butyrate-treated cells *(Figure 3.12B & C)*. Moreover, acetate-driven colocalization of FFAR2/EEA1 was not significantly different to levels observed with isoproterenol-activated β2AR. Together these findings suggest a unique functionality of acetate and propionate in driving FFAR2 internalisation and trafficking to the early endosomes in NCI-H716 cells. Moreover, further studies might uncover butyrate-mediated receptor internalisation directs FFAR2 trafficking to a unique intracellular compartment other than the early endosomes, and the functional outcomes of the heterogeneous receptor trafficking profiles elicited amongst the three SCFAs.



C

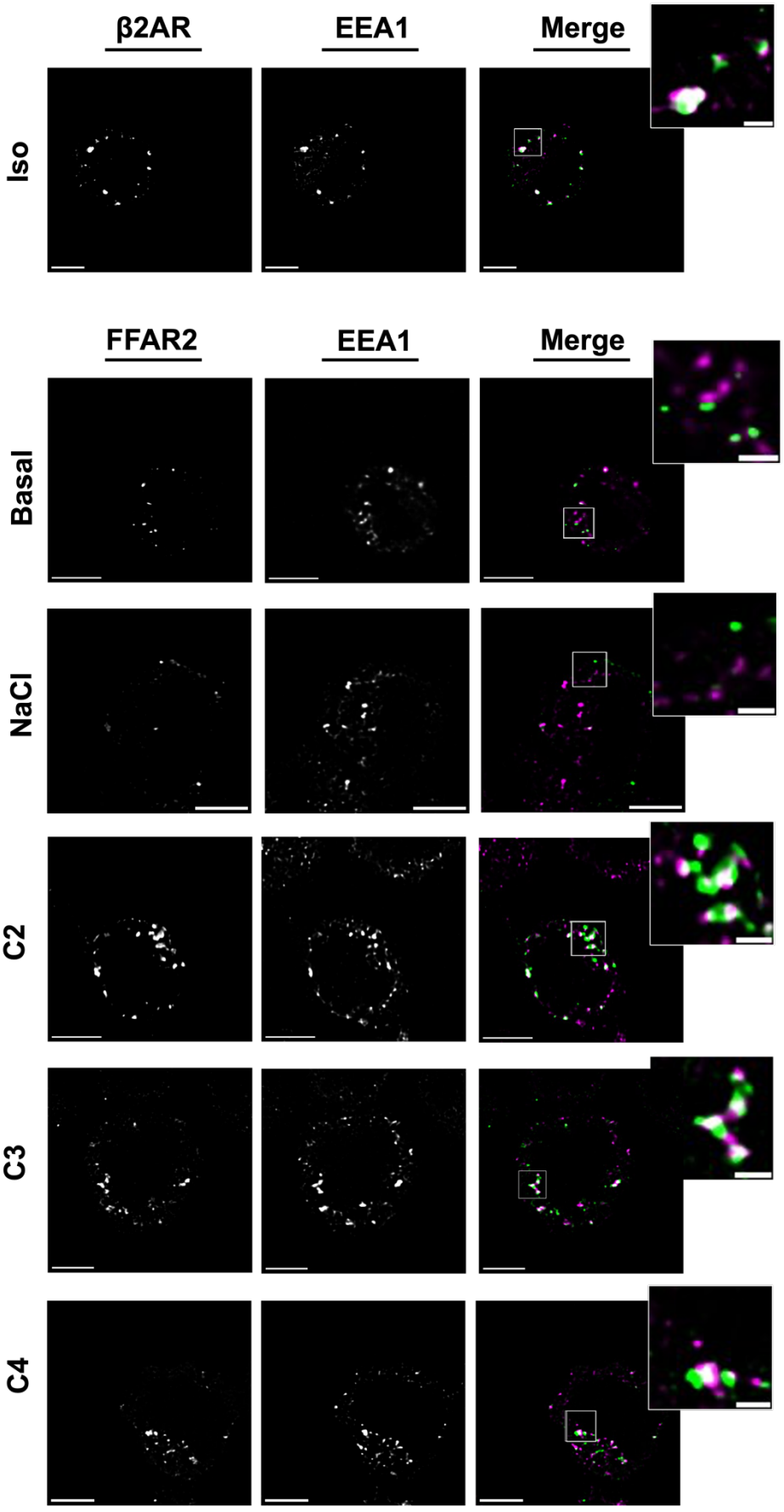


Figure 3.12 Acetate and propionate drive FFAR2 internalisation to early endosomes in NCI-H716 cells. (A, B & C) NCI-H716 cells transiently transfected with FLAG-hFFAR2 or FLAG-β2AR were incubated with anti-FLAG M1 antibody, and then treated with NaCl/SCFA (1mM, 20 min) or Isoproterenol (Iso) (10μM, 20 min). Cells were fixed, permeabilised and then labelled with anti-EEA1 and AlexaFluor 488 secondary antibody before mounting on glass slides. Slides were imaged by confocal microscopy using the Leica super-resolution 'Lightning' module. **(A)** Number of FLAG-hFFAR2 endosomes internalised in a constitutive manner and following NaCl/SCFA treatment determined by manual counting and **(B)** Mander's Overlap coefficient of FLAG-β2AR endosomes internalised following Iso treatment, and FLAG-hFFAR2 endosomes internalised constitutively and following NaCl/SCFA treatment with early endosomal marker EEA1, determined by automated colocalisation analysis of confocal images on ImageJ. Data represented as mean ± SEM. n=20 cells collected across three independent experiments. One-way ANOVA; Basal vs Na vs C2 vs C3 vs C4 (*p<0.05. B). One-way ANOVA; Isoproterenol vs Basal/Na/C2/C3 or C4 ($^{###}$p<0.001, $^{##}$p<0.01, $^{#}$p<0.05). (**C)** Representative images of internalised FLAG-β2AR or FLAG-hFFAR2 endosomes co-localised with EEA1. Scale bar = 5μm, Inset scale bar=2μm.

3.2.11 Propionate promotes sustained Gαq recruitment from the early endosomal compartment in NCI-H716 cells

The strong dependence of propionate-mediated IP1 responses on receptor internalisation and FFAR2-EEA1 co-localisation observed after propionate treatment motivated me to investigate the possibility propionate-induced hFFAR2-Gαq signalling from the early endosomes. The NanoLuc Binary Technology (Nanobit) split-luciferase system was employed to measure interaction between Gαq and the PI(3)P-binding FYVE domain of early endosomal marker endofin. NCI-H716 cells were co-transfected with miniGs/q protein fused to luciferase "Large BiT" fragment (mGsq-LgBit) and endofin fused to "Small BiT" fragment (endofin-Smbit). Upon interaction of the respective tagged proteins, complementation of Lgbit and Smbit fragments reconstitute active luciferase, producing luminescence in the presence of furimazine substrate. Luminescence was recorded for 5 minutes prior to the addition of propionate, measured over the course of 45 minutes.

Within seconds of addition of propionate, but not NaCl, a rapid decreased in luminescence was observed, potentially suggesting the trafficking of constitutively EE-residing Gαq proteins for plasma membrane activation (*Figure 3.13B, C).* No noticeable trend could be observed in luminescence in NaCl-treated cells. Notably, luminescence in propionate-treated cells was observed to continuously increase before plateauing at 25 minutes. These results might suggest a model in which propionate-induced hFFAR2-Gαq responses, initially activated at the plasma membrane, are prolonged by Gαq signalling from the early endosomes (*Figure 3.13A)*.

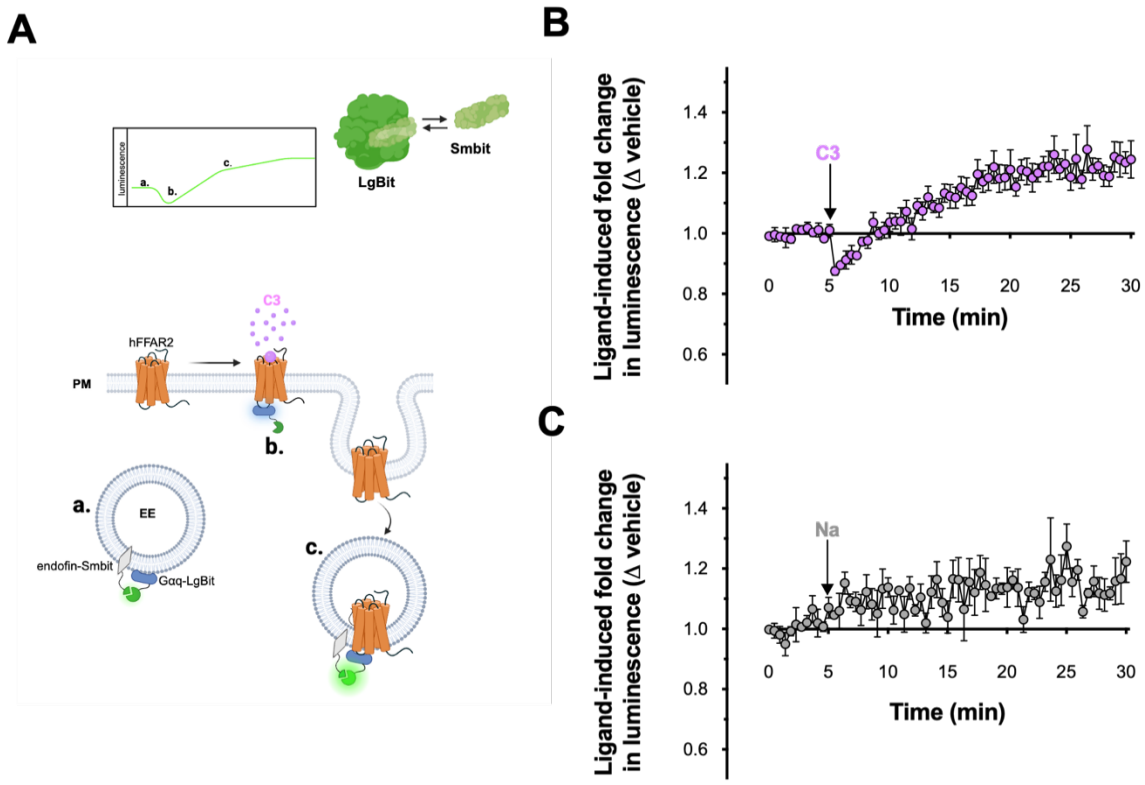


Figure 3.13 Propionate activates sustained Gαq responses localised to the early endosome in NCI-H716 cells. (A) Schematic representation of the proposed model of the spatial regulation of propionate-activated hFFAR2-Gαq signalling profiles between the plasma membrane and early endosomes reflected by trends in data from the Nano-Glo Live Cell Assays using mGsq-LgBit and endofin-Smbit); a. Luminescence prior to ligand addition is derived Gαq is constitutively residing in early endosomes b. Gαq is redirected to the plasma membrane following activation of hFFAR2 with propionate causing a drop in luminescence. c. Plasma membrane propionate-mediated Gαq activation is followed by a sustained Gαq response from early endosomes that leads to a sustained elevation in luminescence. **(B & C)**

NCI-H716 cells were transiently transfected with mGsq-LgBit and endofin-Smbit. Cells were harvested and treated with the Nano-Glo substrate furamizine. Luminescence was measured every 17s. Basal luminescence was measured for 5 mins prior to the addition of 10mM (**B)** propionate or **(C)** NaCl, after which measurements were continued for another 25 minutes. Data represented as mean ± SEM of triplicated collected across three independent experiments (n=3).

3.3 Discussion

The findings presented in this chapter delineate the diverse signalling behaviours of hFFAR2 in a human EEC line elicited by its three primary endogenous SCFA agonists, and identify novel species- and system-specific complexities in respective pathways. Moreover, I explore the role of receptor trafficking and location bias in diversifying SCFA-mediated hFFAR2 responses.

Following on from previous work in our lab characterising and comparing the Gαi and Gαq responses of mFFAR2 activated by propionate in EECs, I intended to investigate the equivalent mechanisms of its human ortholog in EECs and identify potential overlap and differences between species. The heterologous expression system comprising HEK-293 cells transiently transfected with a FLAG-tagged hFFAR2 construct (FLAG-hFFAR2) provided a simple and effective foundation for studying SCFA-mediated hFFAR2 activation in isolation from hFFAR3 and/or any other off-target receptor activation. Propionate-mediated activation of hFFAR2-Gαi signalling was detected, with a logIC50 akin to previously reported values, discounting a potential compromised functionality of receptor due to the FLAG tag (Le Poul et al., 2003; Brown et al., 2003; Hudson et al., 2012; Nilsson et al., 2003). Likewise, robust hFFAR2-specific propionate-mediated Gαq responses were detected in these cells.

Mechanistic insights into FFAR2-mediated anorectic gut hormone release are limited to mouse EECs (Tolhurst et al., 2012; Caengprasath et al., 2020; Psichas et al., 2015). As significant interspecies differences have been observed in the hormonal repertoires, the regulation of secretory functions, and even the GPCR-omes of EECs, studies using a human model is favourable. (Kuhre, Albrechtsen, et al., 2016; Reimer

et al., 2001; Roberts et al., 2019). As such, I employed the human NCI-H716 cell line and observed both Gαq and Gαi pathway activation downstream of treatment of all three SCFAs in NCI-H716 cells. These signal profiles seem to be mediated by hFFAR2 activation, rather than via hFFAR3, as SCFA-mediated Gαi responses were inhibited with a hFFAR2-selective antagonist (Pizzonero et al., 2014). The ability of SCFAs to activate Gαq signalling in NCI-H716 EECs are in contrast to the previous functional characterisation of mFFAR2 by our lab in which only Gαi but not a Gαq response could be detected in the mouse enteroendocrine STC-1 cell line as well as primary mouse colonic crypts, but activation of both G-protein pathways by propionate could be detected in mFFAR2-expressing HEK-293 cells (Caengprasath et al., 2020). This disparity may be due to a difference between relative FFAR2 and FFAR3 expression in these models. mFFAR3 is expressed in only ~3-4 fold less abundant than mFFAR2 in STC-1 cells, mouse colonic crypts, and primary mouse colonic and ileal tissue (Caengprasath, 2019). In contrast, I quantified hFFAR2 mRNA expression to be 400-fold more abundant than hFFAR3 expression in the NCI-H716 cell line, which mirrors results from previous immunohistochemical (IHC) staining of the human colon (Tazoe et al., 2009). It is possible that SCFA-mediated activation of FFAR3 may predominate or regulate FFAR2-Gαq responses in mouse but not human EECs and their respective models. Mechanistically, this may also be due to receptor crosstalk from the formation of mFFAR3-mFFAR2 heteromers with unique signalling capabilities, and/or downstream inhibitory crosstalk between both receptor pathways (Ang et al., 2018). Aside from FFAR3, mouse EECs might express a different complement of nutrient-sensing receptors from human enteroendocrine and/or NCI-H716 cells that may also modulate FFAR2-Gαq signalling.

I have extensively characterised the different potencies and efficacies of acetate, propionate and butyrate in driving Gαq and Gαi pathway activation in NCI-H716 cells. In both pathways, propionate and acetate exhibited equal potency which outperformed butyrate (C2=C3 > C4). These findings are in agreement with the reported from seminal de-orphanisation studies of hFFAR2 (Brown et al., 2003; Nilsson et al., 2003; Le Poul et al., 2003). However, the SCFA potencies of both Gαi and Gαq signalling in NCI-H716 cells are also lower than the values reported in these studies. A crucial difference is the exclusive use of heterologous overexpression systems in these

previous reports, compared to an endogenous FFAR2 expression model which is likely subject to lower receptor expression levels, as well as cell system-specific regulatory mechanisms that might influence signalling.

However, both the IC_{50} and EC_{50} values of SCFAs measured in NCI-H716 cells, and the previously mentioned de-orphanisation studies, are of 10-fold lower magnitutude than the known concentrations of SCFAs in the human gut lumen (Topping & Clifton, 2001). It remains unknown whether FFAR2 binds to SCFAs at the apical or basolateral surface of L-cells, however it is likely that apical receptor desensitisation would occur if these SCFA potency values are representative of their respective values within the human gut lumen. In contrast, SCFA concentrations in the circulation are in the micromolar range which aligns with potencies (Cummings et al., 1987). It is also important to consider the expression of other SCFA-binding GPCRs and/or channels (eg MCT1) on endogeneous EECs that compete with FFAR2 for SCFA binding on apical and basolateral surfaces and might considerably diminish the available SCFA pool. By use of Ussing chambers, propionate and the FFAR2-selective agonist Compound 1 (Cpd 1) have been shown to evoke responses in mouse colonic mucosae from both the apical or basolateral side; these findings suggest that FFAR2 might be expressed on both epithelial domains in mice, however cellular distribution of the receptor in the human colon remains unknown (Forbes et al, 2015; Tough et al, 2018).

Previous studies have demonstrated that the ERK1/2 signalling cascade is involved in mediating GLP-1 secretion in NCI-H716 cells in response to diverse nutrient stimuli (Lim et al., 2009; Ma et al., 2020; Reimer, 2006). ERK1/2 activation is also mechanistically imperative in glucose-stimulated insulin secretion (GSIS) of pancreatic β-cells, *via* activating the phosphorylation of specific cytoplasmic exocytic machinery and insulin promoter-binding nuclear transcription factors (Lawrence et al., 2005; Longuet et al., 2005; Ikushima et al., 2021; Ren & Guo, 2012). Importantly, numerous pathophysiologically-relevant effects elicited downstream of SCFA-mediated mFFAR2 activation in adipocytes, macrophages, and kidney podocytes have also been linked to upregulation of the ERK1/2 signalling pathway (Hu et al., 2016; Lu et al., 2022; Shi et al., 2014). I have characterised the activation profiles of ERK1/2 of acetate, propionate, and butyrate in NCI-H716 cells. Phosphorylation of ERK1/2 by acetate and propionate but not butyrate was evident at later time-points, which might correlate

with a spatiotemporal diversity in the hFFAR2 signalling mechanisms each SCFA activates. Our lab has previously characterised sustained ligand-induced MAPK signalling profiles of FSHR, LHR, β1AR and mFFAR2 which requires receptor internalisation and sorting to very early endosomes (VEEs) (Jean-Alphonse et al., 2014; Caengprasath et al., 2020). In the case of mFFAR2, findings in mouse STC-1 cells and colonic crypts have demonstrated that intracellular Gαi-dependent activation of the MAPK p38 is essential to propionate-mediated GLP-1 release (Caengprasath et al., 2020). A potential involvement of SCFA-mediated activation of ERK1/2 signalling in hFFAR2-mediated anorectic hormone release and/or other physiological responses in human EECs warrants further studies, in addition to spatiotemporal characterisation of underlying signalling pathways.

hFFAR2 exhibited both constitutive and ligand-induced internalisation in NCI-H716 and HEK-293 cells. Constitutive internalisation of several GPCRs across class A, B and C have been observed, however its functional significance remains largely unknown albeit for few (Hendrik Schmidt et al., 2020; Møller et al., 2024). In neurons, the polarised distribution of the axonal type 1 cannabinoid receptor (CB1R) and the serotonin 5-HT1B receptor, relies specifically on constitutive receptor endocytosis from the somatodendritic membrane followed by delivery to the axonal domain (McDonald et al., 2007; Leterrier et al., 2006; Carrel et al., 2011).

Constitutive internalisation of GPCRs has been shown to correlate with constitutive activity and is most prominent for Gαq-coupled GPCRs (Hendrik Schmidt et al., 2020). The extracellular distribution of FFAR2 is yet to be confirmed in the mouse and human colon and will be imperative to characterising both constitutive and/or ligand induced trafficking of the receptor Interestingly, the FFAR2-selective antagonist GLPG0974 demonstrated a significant inhibition of basal Gαq, but not Gαi activity of hFFAR2 in NCI-H716 cells. In contrast, Miyasato et al., have recently demonstrated a constitutive activity of the FFAR2-Gαi pathway, also by employing GLPG0974, which is imperative to FFAR2-mediated G0/G1 growth phase arrest in human leukocytes *in vitro.* The functional implication(s) of basal hFFAR2- Gαq activity in human EECs is yet to be uncovered.

This chapter explores a novel pleiotropy to SCFA-mediated hFFAR2 signalling in human EECs which might be encoded by subcellular spatial compartmentalisation. My results highlighted a significant dependence on receptor internalisation of SCFA-mediated Gαq, but not Gαi signalling in NCI-H716 cells. Other dually coupled GPCRs have been shown to engage in signalling with each of their two G-protein coupling partners from discrete subcellular locations (Jensen et al., 2017; Yarwood et al., 2017). Interestingly, neither Gαq nor Gαi propionate-mediated responses were sensitive to inhibition by Dyngo-4a in FLAG-hFFAR2 transfected HEK-293 cells. suggesting a plasma-membrane-restricted signalling mechanism in this system. Recently, characterisation of basal and ligand-induced phosphorylation patterns at the C-terminus hFFAR2, a concept in the GPCR world known as “phosphorylation bar-coding”, have also identified tissue-specific variations (Barki et al., 2023). Overlapping profiles of agonist-stimulated hFFAR2 phosphorylation were captured in immune and colonic EECs but not white adipocytes, which might suggest a tissue-selective recruitment of distinct downstream signalling networks to activated FFAR2 (Barki et al., 2023).

hFFAR2 signalling profiles exhibited a differential dependence on receptor internalisation between NCI-H716 cells and HEK-293 cells. In NCI-H716 cells, SCFA-mediated Gαq but not Gαi responses were sensitive to inhibition by the dynamin inhibitor Dyngo-4a, whereas neither of these pathways were affected by Dyngo-4a in in hFFAR2-transfected HEK-293 cells. This context-dependency is in contrast previously reported findings on spatial regulation of mFFAR2 by our lab; propionate-mediated Gαi responses of mFFAR2 are sensitive to inhibition by Dyngo-4a and have been proposed to derive from endosomal VEE populations which are positive for the marker APPL1 (Caengprasath et al., 2020). Interestingly, neither Gαi nor Gαq responses in NCI-H716 cells were unaffected by knockdown of APPL1, suggesting that signalling compartmentalisation to the VEE compartment might be unique to the mouse ortholog. Divergent spatial localisation of hFFAR2- and mFFAF2-mediated Gαi responses in EECs may be encoded by structural differences. Structure-based functional studies on FFAR2 are all but few and have identified key residue networks which mediate receptor agonism and antagonism, along with G-protein coupling selectivity (Bolognini et al., 2016; Sergeev et al., 2017; Stoddart et al., 2008; Sergeev

et al., 2016). Notably, GLPG0974 is a selective antagonist for human but not mouse FFAR2; this is due to a stabilising hydrogen bond which forms between and extracellular-facing lysine (Lys^{65}) at the top of TMDII exclusively in hFFAR2, which is replaced by an arginine in mFFAR2, with an amide-carbonyl group of GLPG0974 (Sergeev et al., 2017; Srivastava et al., 2014). In addition, mutational studies also revealed that substitution of Lys^{65} or Arg^{65}, in hFFAR2 and mFFAR2 respectively, with a negatively charged or neutral amino acid, could impose a significant receptor-G-protein coupling bias which favours Gαi over Gαq (Sergeev et al., 2017). The aforementioned studies have relied on the crystal structure of FFAR1 to guide the characterisation of FFAR2 by homology modelling. The recently solved cryo-EM structure of human FFAR2, in complex with an engineered miniGq protein, might further help to map differences in signalling between orthologs to intracellular and extracellular specific sites (Zhang et al., 2024). In particular, TM5 and ICL3 of FFAR2 have been found to engage with miniGq differently than other members of the FFAR family and might also be areas of interest in deducing interspecies complexities.

Interestingly the sequences of mouse and human FFAR2, although exhibiting over 80% similarity on the protein level, are most different at the C-terminal ends (Mishra et al., 2020). The C-terminal tail region of GPCRs is embedded with several target motifs for post-translational modifications (PTMs), including phosphorylation, ubiquitination, glycosylation and palmitoylation. By promoting interactions with specific intracellular effectors, GPCR PTMs have prominent influence on receptor trafficking, heteromerization, compartmentalised signalling, and even biased signalling (Patwardhan, Cheng & Trejo, 2021). Future studies should assess C-tail-mediated interactions of mFFAR2 and hFFAR2, such as by the engineering of chimeric constructs by exchange of C-tails to determine functional implications (Tohgo et al., 2003). In particular, future studies should assess the recruitment of β-arrestins, which largely bind to phosphorylated C-tail residues of GPCRs, in promoting the internalisation and/or endosomal signalling of mFFAR2 and hFFAR2. Previous studies employing heterologous overexpression systems have demonstrated a robust recruitment of β-arrestin 2 to hFFAR2 in response to ligand treatment, and the inhibition of propionate-stimulated mFFAR2 internalisation and Gαi signalling in β-arrestin knockout cells (Bolognini et al., 2019; Mårtensson et al., 2023; Caengprasath et al., 2020).

From my findings on APPL1, I also questioned whether internalisation-dependent Gαq signalling of hFFAR2 might be compartmentalised to a distinct endosomal platform other than the VEEs. I explored localisation of FFAR2 with the primary GPCR sorting platform and a hub for intracellular responses of numerous GPCRs, the early endosome. Notably, stimulation with SCFAs promoted an increased co-localisation of hFFAR2 with the canonical marker of EEs, EEA1. Interestingly, SCFAs exhibited a distinct rank potency in stimulating receptor internalisation (C3 > C2 > C4). My findings suggested butyrate to be a significantly weaker activator of receptor signalling and internalisation than acetate and propionate. As such, the divergent signalling profiles of SCFAs might indeed stem from their propensity to promote receptor endocytosis and spatially defined signalling activity of FFAR2. Alternatively, ligand bias at FFAR2 might arise due to stabilisation of unique active receptor conformational states by individual SCFAs that mediates receptor affinity for specific intracellular signalling transducers and/or effectors (Smith, Lefkowitz & Rajagopal, 2018). This phenomenon has been leveraged in the structure-based drug design of spatially biased GPCR agonists, including the μ-OR agonist TRV130 and the κ-OR agonist triazole 1.1 analgesics, which exhibit enhanced clinical efficacy and reduced side-effects compared to their conventional receptor agonists counterparts (Smith, Lefkowitz & Rajagopal, 2018).

Given that propionate-mediated Gαq responses exhibited the most significant sensitivity to receptor internalisation, and propionate also promoted the highest degree of hFFAR2 internalisation to the EE, the NanoBit system was used to assess the existence and temporal profile of propionate-mediated Gαq activation from the EE in NCI-H716 cells. Gαq signalling responses from the early endosome are characteristic of GPCRs involved in pain transmission such as the NK1 receptor and the receptor for the calcitonin gene-related peptide (CGPR) δ-opioid receptor (DOPr) (Latorre et al., 2022; Jensen et al., 2017; Yarwood et al., 2017). In these instances, the early endosome serves as a platform for Gαq signalling following receptor internalisation which outlives transient Gαq responses from the plasma membrane. In recent years, the nanoluciferease (Nanobit) protein complementation system has been widely used in profiling the kinetics and subcellular location of GPCRs activation profiles in live

cells (Laschet, Dupuis & Hanson, 2019; Inoue et al., 2019). Interestingly, propionate stimulation initially caused an acute reduction in ∆Luminescence which I proposed might derive from a re-routing of Gαq from the early endosome to the plasma membrane upon activation. As I have also observed constitutive hFFAR2 Gαq signalling in my findings, whether this response is localised specifically to the early endosome will provide further depth to this proposed model. Subsequently, I observed a sustained increase in propionate-treated cells. Moreover, no consistent trend was measured in NaCl-treated cells, suggesting the specific involvement of hFFAR2 in mediating this effect. Admittedly, an outstanding limitation to my findings using is the failure to detect an adequate signal from the plasma membrane reporter CAAX-Smbit construct despite several attempts, which would provide a fair comparison to Gαq-endofin responses as well as a spatially- and temporally resolved profile of hFFAR2-Gαq activation.

The temporal profiles of the Gαq responses of NK1 and CGPR imposed by location bias are reflected in downstream physiological consequences; prolonged endosomal Gαq signals have been shown to underlie the hyperexcitablity of nociceptors which characteristic of chronic pain and has spurred the development of endosomally-targeted antagonists which provide prolonged analgesia *in vivo* (Latorre et al., 2022). Despite the phenomenon of Gαq-signalling from the early endosome has been reported for numerous GPCRs, these findings have been mechanistically challenged based on the preferential enrichment of the PLCβ phosphoinositide substrate phosphatidylinositol 4,5-bisphosphate (PIP2) at the plasma membrane (Daly & Plouffe, 2023). Briefly, PIP2 is converted to the phosphatidylinositol-3-phosphate (PI3P) during the multi-step process of endocytosis and vesicle fission from the plasma membrane. Consistent with this fact, Wright et al., demonstrated the production of DAG to be unique to plasma-membrane Gαq and not early endosomal Gαq signalling downstream of AT1R. Two PLC-β-independent effector pathways that have previously been linked to Gαq signalling, are the activation of the RhoGEF proteins such as p63RhoGEF, Trio and Duet, and the phosphorylation of the MAPK ERK5 (García-Hoz et al., 2010; Lutz et al., 2007). The cellular outcomes of both plasma membrane and endosomal Gαq signalling profiles of hFFAR2 in human EECs are yet to be uncovered and might provide novel pharmacological targets. However

further studies should assess the candidate effectors of hFFAR2-Gαq endosomal signalling such as using appropriate fluorescent reporters of PLC-β-dependent and PLC-β-independent pathways. In addition, that I exclusively interrogated SCFA-mediated hFFAR2-Gαq signalling from EEs and not other compartments should be noted; future studies should investigate hFFAR2 localisation other subcellular organelles such as the Golgi, the E.R and the nucleus from which functionally diverse GPCR responses have been detected (Barrios-Rodiles et al., 2005; O'Malley et al., 2003; Valdehita et al., 2010; Hebert-Chatelain et al., 2016; Purgert et al., 2014; Wright et al., 2023; Godbole et al., 2017; Irannejad et al., 2017; Nash et al., 2019).

In summary, this chapter has characterised the G-protein signalling profiles of hFFAR2 activated by SCFAs in a human L-cell model. In addition, findings from this chapter also uncovered the spatial regulation of hFFAR2-mediated signalling responses in human L-cells and demonstrated a dependence of Gαq responses on dynamin-dependent internalisation which was context-dependent. Finally, intracellular Gαq responses activated by propionate were mapped to the early endosome, and exhibited a prolonged temporal profile of activation which might be harnessed for the development of therapeutic agents with sustained clinical outcomes.

4. Canonical roles of short chain fatty acids in acutely driving anorectic hormone release in human EECs

4.1 Introduction

Obesity poses a growing public health problem to almost every country worldwide, with 1.2 billion adults predicted to be obese in the world by 2030 (Kelly et al., 2008). Originally developed as pharmacological agents for T2D based on their incretin effects, agonists of the glucagon-like peptide 1 (GLP-1) receptor (GLP1-RAs) have rapidly dominated the obesity market in recent years (Gores & Rickwood, 2024). GLP-1 is an endogenous product of EECs of the “L cell” subtype and stimulates the central regulation of satiety and blood glucose optimisation *via* paracrine, endocrine and neural mechanisms. Apart from GLP-1, enteroendocrine L-cells of the “L-cell” subtype also secrete PYY which has similar anorexigenic effects to GLP-1; PYY analogues have newly entered the anti-obesity pharmacotherapy pipeline and demonstrated promising clinical benefits in early phase trials (ClinicalTrials.gov, 2018; Tan et al., 2021). Despite their clinical efficacy, many gut peptide hormone RAs still are limited by their adverse side effects and laborious routes of administration (Melson et al., 2024).

In Chapter 3, I characterised the G-protein signalling profiles of the GPCR FFAR2 in human EECs that are activated downstream of stimulation by its endogenous ligands, short chain fatty acids (SCFAs). SCFA-mediated activation of FFAR2 has been shown to stimulate the co-secretion of GLP-1 and PYY from mouse L-cells (Psichas et al., 2015). Moreover, previous reports have indicated that colonic SCFA concentrations are increased following Roux-en-Y Gastric Bypass (RYGB) surgery, and this phenomenon has been suggested to underlie the elevated GLP-1 and PYY secretory profiles that is characteristic of post-operative patients (Borg et al., 2006; Ilhan et al., 2017; Martínez-Sánchez et al., 2023). Our lab has developed a fermentable inulin-propionate ester (iPE), which ensures delivery of propionate to the colon; iPE has exhibited promising clinical effects in acutely stimulating GLP-1 and PYY release and suppressing weight gain in pilot studies, and a large-scale trial (iPREVENT) is currently ongoing (Chambers et al., 2015; Frost, 2018).

Characterising the intracellular signalling pathways activated downstream of FFAR2 in driving SCFA-mediated GLP-1 and PYY release could uncover druggable anti-

obesity targets. However, mechanistic insights in these FFAR2 axes are limited to mouse systems (Tolhurst et al., 2012; Psichas et al., 2015; Caengprasath et al., 2020). Considering the interspecies variability in ligand potency of FFAR2 orthologs, as well as reported functional differences in agonist-induced responses between mouse and human FFAR2, there remain outstanding mechanistic questions on decoding the FFAR2 pathways specific to human L-cell-driven GLP-1 release (Hudson et al., 2012; Priyadarshini et al., 2015).

In this chapter, I optimise and employ NCI-H716 cells as a model to investigate the dynamic secretory responses of human enteroendocrine L cells. I characterise and compare the effectiveness of SCFAs and an FFAR2-Gαi-specific allosteric agonist in acutely stimulating GLP-1 in this model. In addition, I assess whether GLP-1 and PYY are co-secreted in response to acute stimuli in NCI-H716 cells, and the subcellular co-localisation of these enterohormones.

4.2 Results

4.2.1 SCFAs acutely stimulate GLP-1 secretion in NCI-H716 cells

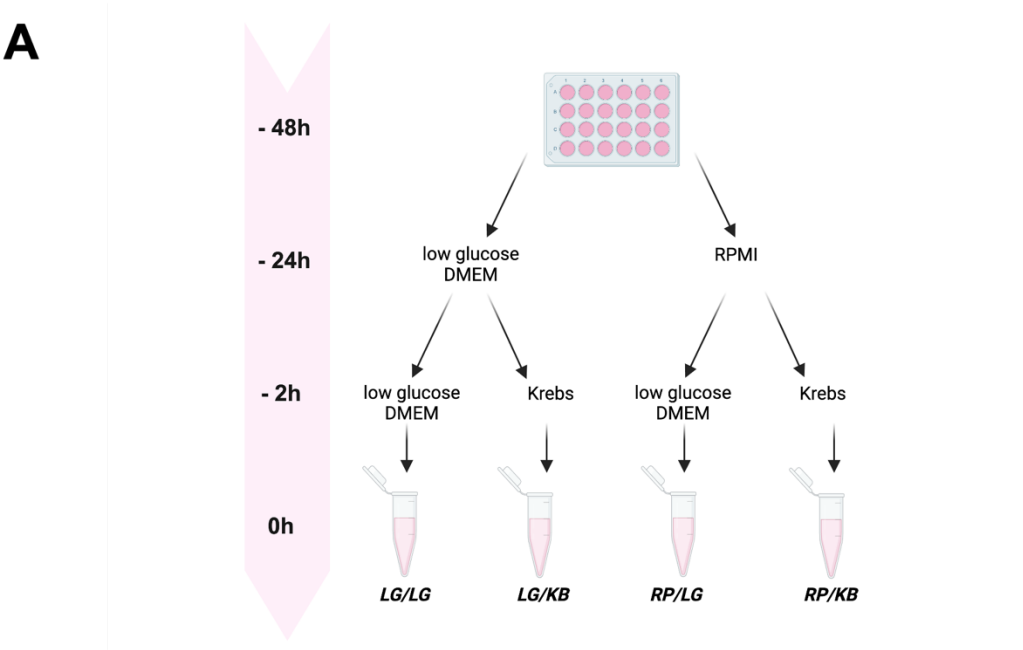
NCI-H716 cells tonically secrete GLP-1 in high concentrations, and secretion is greatly responsive to ligands of nutrient-sensing receptors GPCRs in enteroendocrine L-cells (Kuhre et al., 2016; Jang et al., 2007; Larraufie et al., 2018; Reimer et al., 2001; Tian et al., 2021; Lee et al., 2023). An in-house radioimmunoassay (RIA) was used to measure GLP-1 secretion in NCI-H716 cells (Kreymann et al., 1987). Prior to investigating the effects of acute stimuli on GLP-1 secretion, it was necessary to optimise treatment conditions to achieve results within the detection limits of the assay.

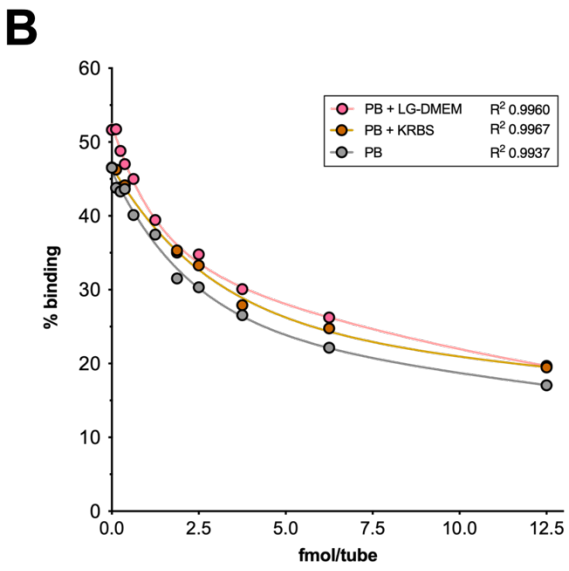
In previous studies employing NCI-H716 cells, there is inconsistency in the formulation of buffers used to investigate basal- and ligand-induced GLP-1 secretion, particularly in glucose concentration (Ducastel et al., 2020; Kuhre et al., 2016; Ang et al., 2018; Lee et al., 2023). Hence, I sought to assess the effect of two secretion buffer parameters in order to optimise downstream immunoassays in this cell line *(Table 4.1)*. The first parameter I investigated was the effect of glucose starvation on GLP-1 secretion; cells were either glucose-starved for 24 hours prior to assaying by incubation in low glucose (5.5mM) serum-free DMEM (*LG*), or incubated in routinely-used culturing media *(RPMI)* in this time-frame. Secondly, I also compared the effect of two buffer formulations to be used during the assay to directly measure GLP-1 levels; Krebs buffer containing no glucose (*KB*), or *LG.* Basal GLP-1 secretion was compared from cells across 4 culturing conditions (*Figure 4.1A).* GLP-1 concentrations were interpolated from a standard exponential decay curve in which the x and y axis represent known concentrations of a GLP-1 standard (range 0 – 12.5 fmol/tube) and % binding of radioactive iodinate-125 labelled $GLP1_{(7\text{-}36)}$ peptide to anti-GLP1 antibody respectively (*Figure 4.1B)*. Optimal sensitivity and precision range of the assay falls within the exponential region of the curve.

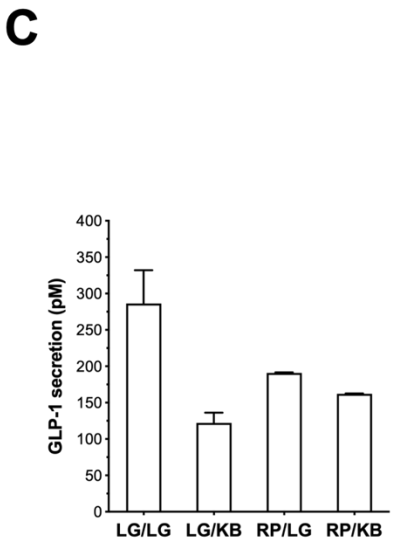
	Culturing media 24 hours prior to assay	**Assay secretion buffer**
RPMI/KB	Total RPMI-1640 (11mM glucose)	Krebs (0mM glucose)
LG/KB	Low-glucose DMEM (5.5mM)	Krebs (0mM glucose)
RPMI/LG	Total RPMI-1640 (11mM glucose)	Low-glucose DMEM (5.5mM)
LG/LG	Low-glucose DMEM (5.5mM)	Low-glucose DMEM (5.5mM)

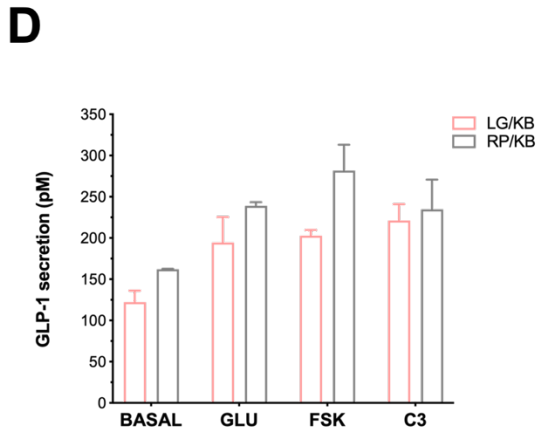
Table 4.1 Culturing conditions used for 24 hours prior to assaying and secretion buffer used to measure GLP-1 in NCI-H716 cell supernatants by RIA. Cells were incubated for 2 hours with respective buffers in the absence of acute stimuli, and supernatants were collected for RIA quantification of GLP-1. NCI-H716 exhibited a high responsiveness to differences in glucose concentrations in the low millimolar range *(Figure 4.1C).* Glucose starvation did not appear to have a prominent effect of GLP-1 levels. However, basal GLP-1 measurements were higher in the cellular supernatants when the assay secretion buffer was a glucose-containing buffer (*RPMI/LG* and *LG/LG)*, in comparison to a glucose-free Krebs buffer (*RPMI/KB* and *LG/KB)*.

Next, I assessed the secretagogue effects of three previously characterised acute GLP-1 stimuli, forskolin, glucose and propionate, under these 4 different conditions. Notably when acute ligand-induced GLP-1 release was assayed in glucose-containing buffer (*RPMI/LG* and *LG/LG*, hormone concentrations could not be interpolated as raw values as it surpassed the upper detection limit (12.5 fmol/tube) of the assay (*data not shown).* Acute ligand stimulation in glucose-free Krebs buffer (RPMI/KB and LG/LB) induced measurable GLP-1 increases over basal which did not appear to differ with prior glucose starvation (*Figure 4.1D, E)*. I decided to proceed with *RP/KB* conditions in measuring secretory profiles in NCI-H716 cells to bypass any confounding effects of metabolic shifts that have previously been linked to glucose starvation in cancer cells (Tsai et al., 2021).


A
- 48h
- 24h
- 2h
0h
low glucose DMEM
RPMI
low glucose DMEM
Krebs
low glucose DMEM
Krebs
LG/LG
LG/KB
RP/LG
RP/KB


B
PB + LG-DMEM R² 0.9960
PB + KRBS R² 0.9967
PB R² 0.9937
% binding
fmol/tube
0
10
20
30
40
50
60
0.0
2.5
5.0
7.5
10.0
12.5


C
GLP-1 secretion (pM)
0
50
100
150
200
250
300
350
400
LG/LG
LG/KB
RP/LG
RP/KB


D
GLP-1 secretion (pM)
LG/KB
RP/KB
0
50
100
150
200
250
300
350
BASAL
GLU
FSK
C3

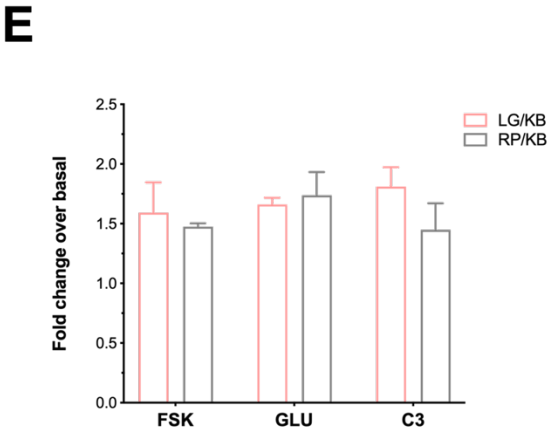

E
Fold change over basal
LG/KB
RP/KB
0.0
0.5
1.0
1.5
2.0
2.5
FSK
GLU
C3

Figure 4.1 Basal and ligand-induced acute GLP-1 secretion by NCI-H716 cells may be affected by glucose content of secretion buffer and culturing media. NCI-H716 cells were cultured in total RPMI-1640 (RP) or low-glucose DMEM (LG) for 24 hours, incubated in LG media or Krebs (KB) in the presence or absence of ligand for 2 hours, and supernatants were collected. GLP-1 concentration was measured by RIA. **(A)** Schematic of culturing conditions and assay buffers used. (**B)** Standard curves representing % bound ^{125}I-labelled GLP-1 peptide measured in samples containing GLP-1 standard, label, and antibody, with either phosphate buffer (PB), phosphate buffer adjusted with KRBS (PB + KRBS), or phosphate buffer adjusted with LG (PB + LG). Curves were fit by non-linear regression analyses and R^2 values were computed on GraphPad Prism. Data represents mean of triplicates, n=1 independent experiment. **(C)** Basal GLP-1 secretion of NCI-H716 cells by under 4 different assay culturing conditions. Data represents mean ± SE of triplicates, n=1 independent experiment. **(D&E)** GLP-1 secretion at basal and in response to 2h incubation with 10μM FSK, 10mM glucose (GLU) or 1mM C3 under 2 different assay culturing conditions. Data represents mean ± SE of triplicates, n=1 independent experiment. **(E)** The effect of 2h treatments on GLP-1 secretion represented as a fold change over respective basal.

Next, I aimed to characterise and compare the GLP-1 secretory profiles elicited by SCFAs in NCI-H716 cells in the selected secretion conditions. Cells were incubated with 1mM of respective SCFA for 2 hours in KRB, and GLP-1 secretion and content were measured in cell supernatants *(Figure 4.2A)* and lysates (*Figure 4.2C)*. Treatment with either 1mM propionate or 1mM butyrate significantly increased GLP-1 secretion by ~ 2-fold and ~1.5 fold over baseline respectively, whereas a limited effect is evident following 1mM acetate treatment *(Figure 4.2B)*. When content of GLP-1 was measured in cell lysates, no significant changes could be observed with SCFA treatment *(Figure 4.2D).*

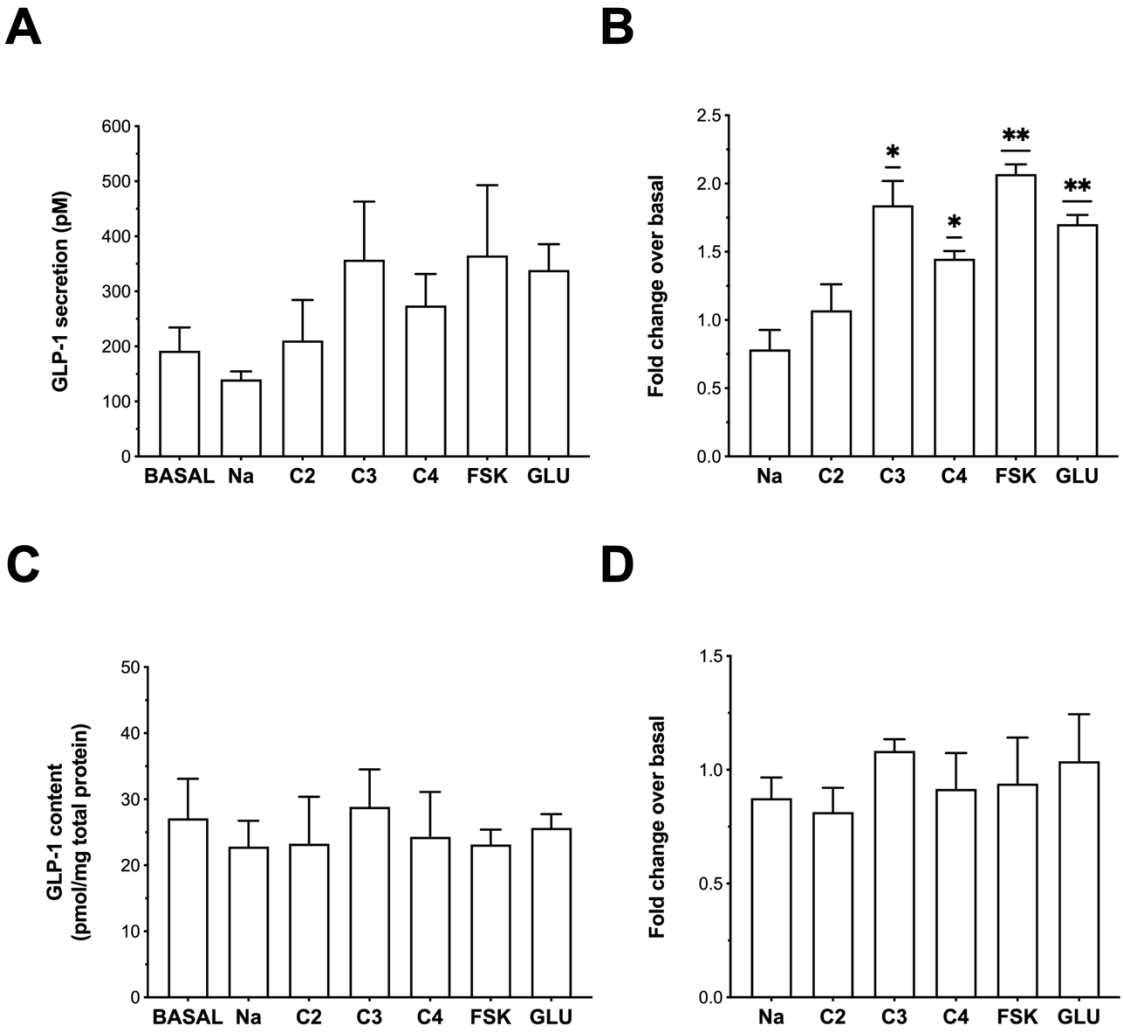
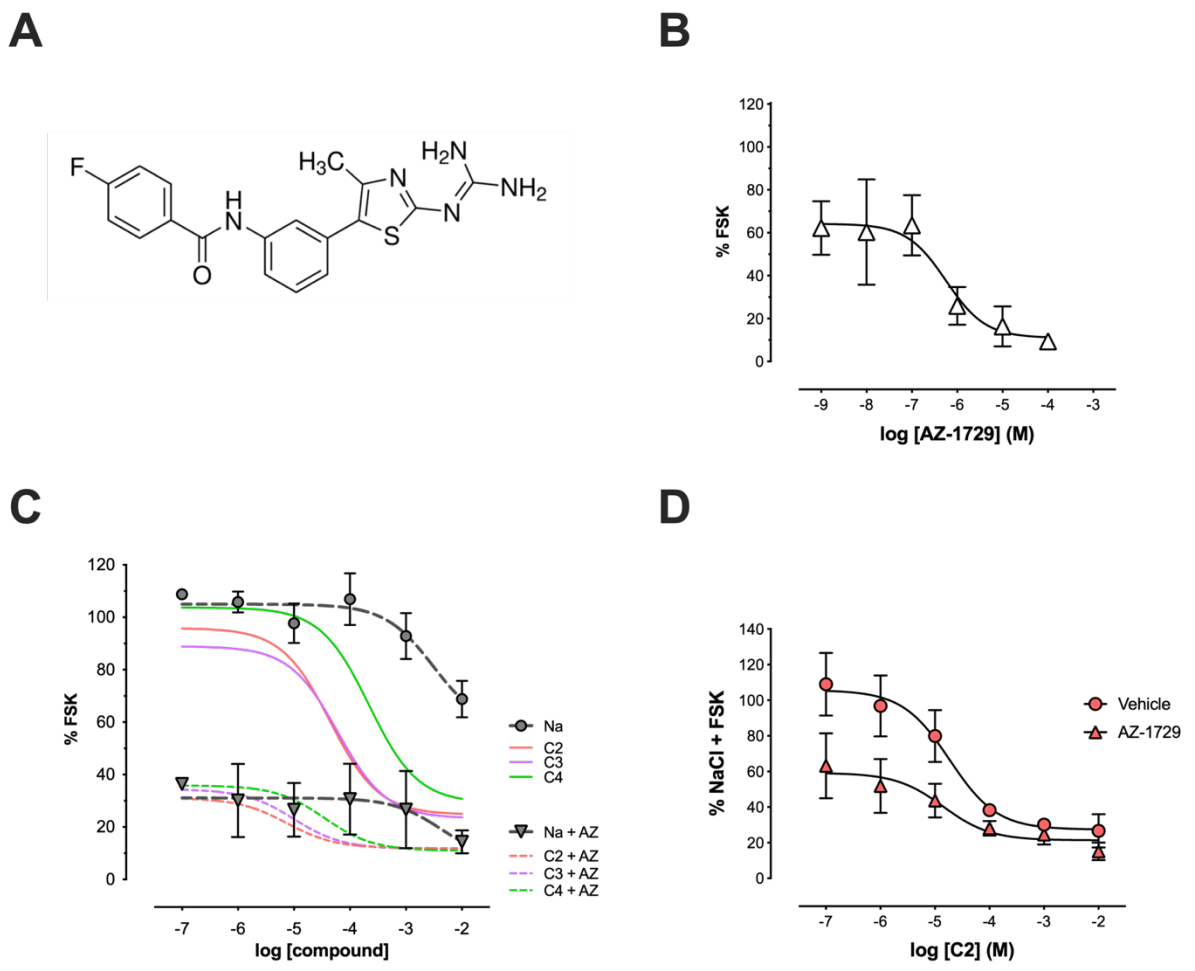


Figure 4.2 SCFAs acutely stimulate GLP-1 secretion in NCI-H716 cells. NCI-H716 cells were cultured in total RPMI-1640 (RP) for 24 hours, and then incubated with KB or KB with Na,C2, C3 or C4 (1mM), FSK (10μM) or Glu (10mM) for 2 hours. GLP-1 concentration was measured in supernatants (**A & B)** or lysates (**C & D**) by RIA. Data represents mean ± SEM of triplicates per independent experiments, n=3 independent experiment. (B & D) Effect of acute stimuli are represented as fold change over basal. One-sample t test *vs* 1 (**p<0.01, *p<0.05).

4.2.2 FFAR2-Gαi agonist AZ 1729 stimulates acute GLP-1 release

AZ-1729 is a potent allosteric agonist of human FFAR2 that displays a functional bias for signalling via Gαi (Bolognini et al., 2016a). Inhibition of forskolin-mediated cAMP accumulation by AZ-1729 was measured in NCI-H716 cells. AZ1729 inhibited forskolin-stimulated cAMP accumulation in a concentration-dependent manner with significantly greater potency and efficacy than acetate, propionate or butyrate (LogIC50 = -6.442 ± 0.187) (*Figure 4.3A).* When cells were co-treated with SCFAs and AZ-1729, AZ1729 produced a significant leftward and downward shift in concentration curves of all three SCFAs, confirming a cooperative allosteric activity in addition to its intrinsic allosteric function (*Figure 4.3B; Table 4.2).* Curves were normalised to NaCl/vehicle or NaCl/AZ-1729 to specifically assess the effect of AZ-1729 on the potency of SCFA-induced Gαi signalling in NCI-H716 cells (*Figure 4.3C; Table 4.2).*



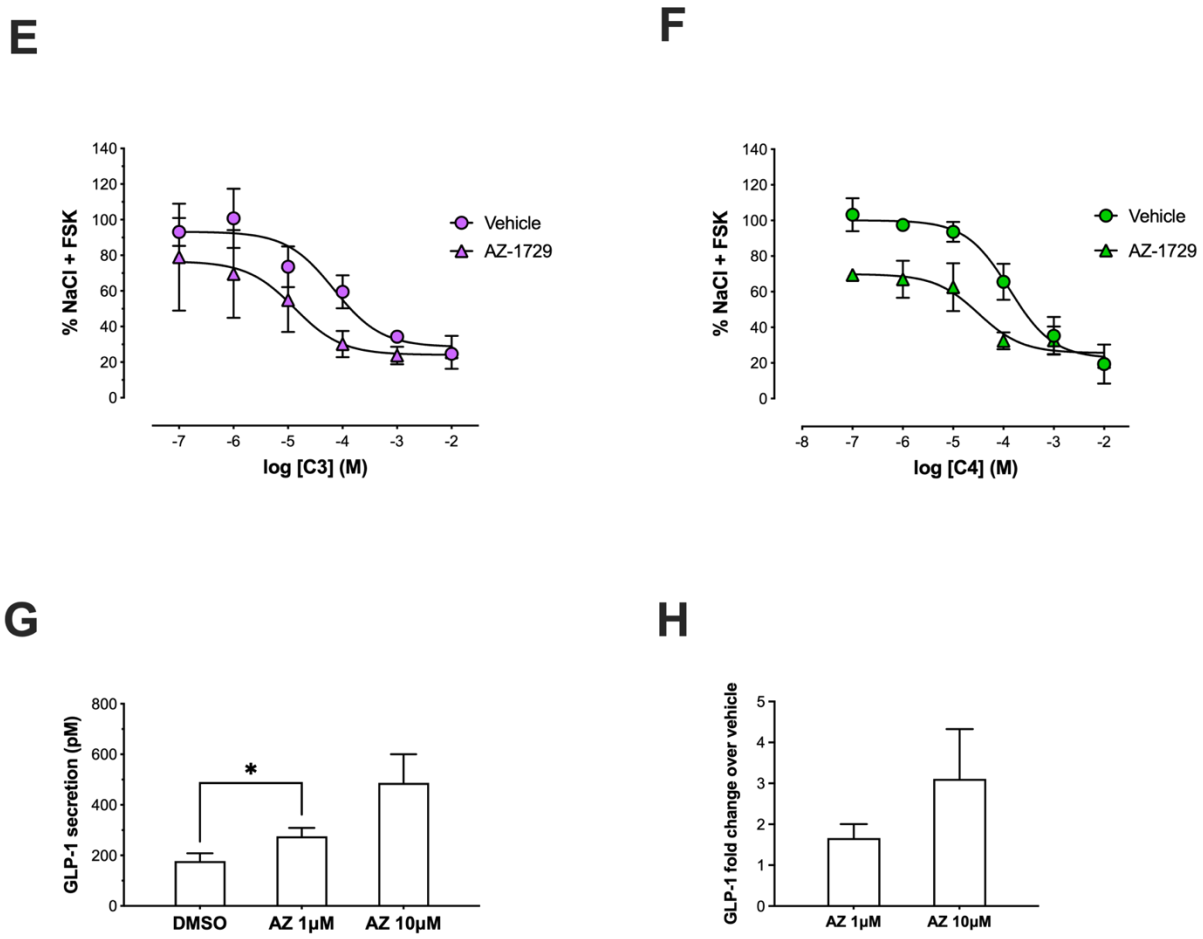


Figure 4.3 AZ-1729 is an allosteric FFAR2-Gαi agonist and GLP-1 secretagogue in NCI-H716 cells. (A) Chemical structure of AZ-1729 (Bolognini et al., 2016b). **(B)** Inhibition of intracellular FSK-mediated cAMP accumulation by AZ-1729 in NCI-H716 cells. Cells were treated with IBMX (500nM, 5 min), followed by forskolin (FSK) (3μM, 5 min) or combination of FSK (3μM, 5min) and increasing concentrations of AZ-1729 (1nM-100μM, 5 min), Responses are shown as % change to FSK. Data represents mean ± SEM of triplicates per independent experiments, n=3 independent experiment. **(C, D, E & F)** Positive allosteric agonism of SCFA-mediated Gαi responses in NCI-H716 cells by AZ-1729. Cells were treated with IBMX (500nM, 5 min), followed by forskolin (FSK) (3μM, 5 min) or combination of FSK (3μM, 5min) and NaCl/SCFA (1mM, 5 min) and DMSO vehicle, or a combination of FSK (3μM, 5min), and NaCl/SCFA (1mM, 5 min), and AZ-1729 (1μM, 5 min). (**C)** Responses are shown as % change to FSK. Data represents mean ± SEM (for NaCl) or mean (for SCFAs) of triplicates per independent experiments, n=3 independent experiments. (**D, E & F)** SCFA responses are normalised to NaCl responses in the presence of 1μM AZ-1729 or DMSO and represented as % change of NaCl + FSK. Data represents mean ± SEM (for NaCl) of triplicates per independent experiments, n=3 independent experiment. **(G & H)** GLP-1 secretion measured

in NCI-H716 supernatants by RIA following 2-hour incubation with 1μM or 10μM AZ-1279 or DMSO vehicle. (**G)** Symbols represent the mean of triplicates per independent experiment, n=3 independent experiments. Unpaired t-test; DMSO vs AZ-1729 1μM (*p<0.05). **(H)** The effect of AZ-1729 acute stimuli is shown as fold change over DMSO vehicle. Data are represented as the mean ± SEM of triplicates per independent experiment, n=3 independent experiments.

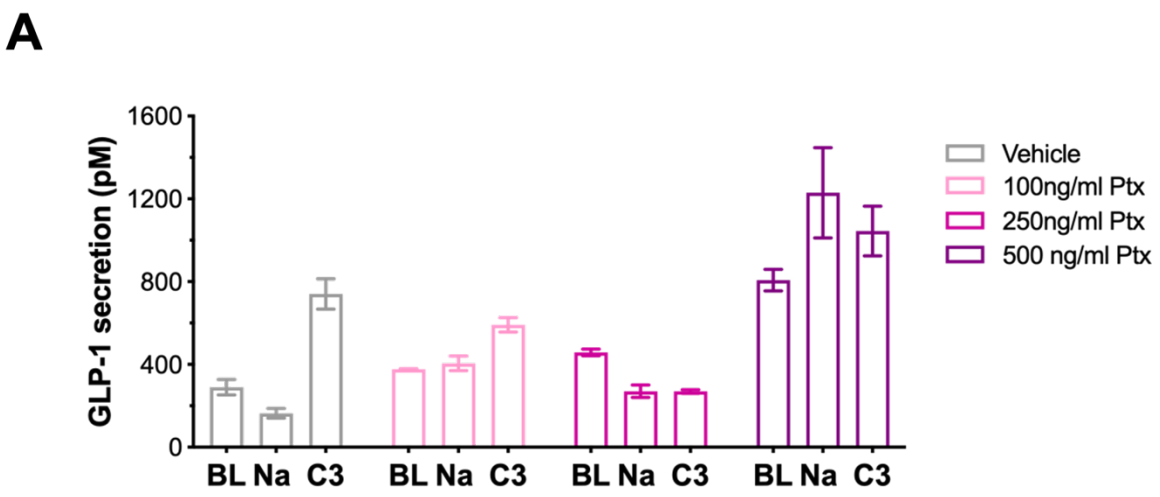
SCFA	pIC50 (M)	
	DMSO Vehicle	AZ-1729
C2	-4.354± 0.257	-5.127 ± 0.409
C3	-4.216 ± 0.292	-5.354± 0.236
C4	-3.658 ± 0.376	-4.609 ± 0.298

Table 4.2 pIC50 values of SCFA concentration-responses in the presence of 1μM AZ-1729 or DMSO vehicle NCI-H716 cells. Cells were treated as in Figure 4.3C with SCFAs in the presence of AZ-1729 (1μM) or DMSO vehicle. Data are presented as mean ± SEM of at least triplicates, n=3 independent experiments

Previous reports from our lab have indicated that propionate-driven GLP-1 release is mediated by an FFAR2-Gαi pathway in mouse EECs (Caengprasath et al., 2020). Next, I employed AZ-1729 to assess a similar involvement of the FFAR2-Gαi axis in GLP-1 secretion in NCI-H716 cells. A significant upregulation in GLP-1 secretion was observed following treatment with 1μM AZ1-1729 (*Figure 4.3D)*. Moreover, a concentration-dependent trend of AZ-1729-mediated GLP-1 release was apparent, however significance was limited by inter-repeat variability.

4.2.3 Is Propionate-stimulated GLP-1 release mediated by a FFAR2-Gαi pathway in human EECs

Following on from the stimulatory effects observed with AZ1729, I interrogated the involvement of the Gαi pathway in propionate-mediated GLP-1 release in NCI-H716 cells. Preliminary data *(not shown)* indicated that 20h pre-treatment with 500ng/ml of the inhibitor of Gαi Pertussis toxin (PTX), the concentration used for characterising SCFA-mediated Gαi signalling profiles in *3.2.3,* increased basal GLP-1 secretion by 3.5-fold. To investigate this further, GLP-1 secretion was measured after pre-treatment with 100ng/ml, 250ng/ml and 500ng/ml PTX. Interestingly, PTX appeared to increase basal GLP-1 secretion in a concentration-dependent manner (*Figure 4.4A)*. At all three concentrations of PTX, propionate-stimulated fold changes in GLP-1 levels, normalised to basal, was diminished in comparison to the effect of the SCFA in cells treated with H_20 vehicle. NaCl-mediated GLP-1-fold changes appeared to be unchanged with PTX treatment. These preliminary findings suggest a potential involvement of an FFAR2-GαI axis in mediating propionate-stimulated GLP-1 release in NCI-H716 cells.



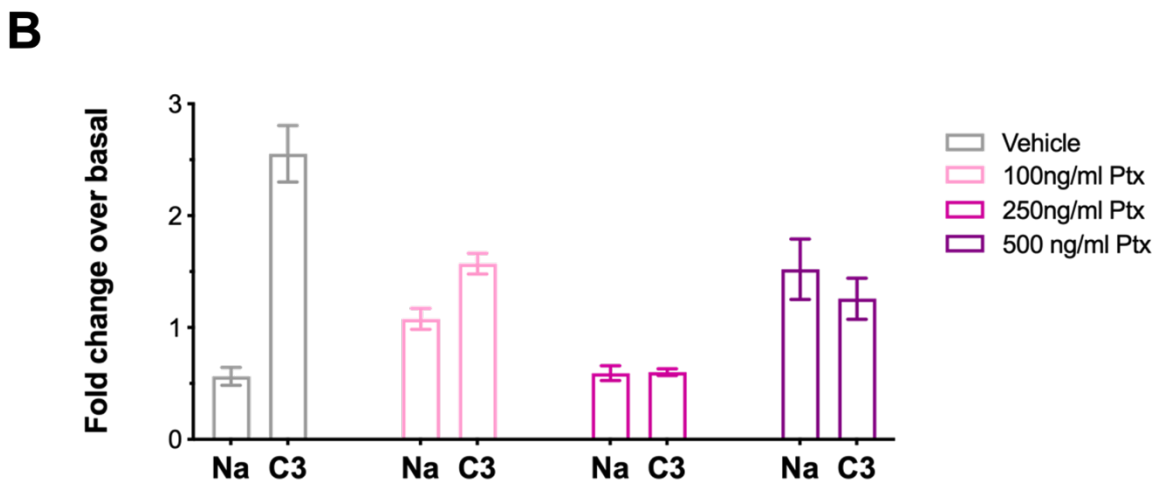


Figure 4.4 Propionate may acutely stimulate GLP-1 release in a Gαi-dependent manner in NCI-H716 cells. (A & B) Cells were pre-treated with 100, 250 or 500ng/ml of Gαi-inhibitor Pertussis toxin (Ptx) (20 hours) or H2O vehicle. GLP-1 secretion was measured in supernatants by RIA following incubation with NaCl (Na, 1mM, 2h) or C3 (1mM, 2h) or ligand-free buffer (Baseline, BL). Data represents mean ± SEM of triplicates per independent experiments, n=1 independent experiment. **(B)** The acute effects of Na and C3 on GLP-1 secretion are represented as fold changes over respective basal values.

4.2.3 SCFAs may not acutely stimulate PYY secretion in NCI-H716 cells

Given that SCFAs are known to stimulate the release of both GLP-1 and PYY *via* FFAR2 in mouse L-cells, I next aimed to characterise the acute secretion profiles of the latter in NCI-H716 cells (Psichas et al., 2015). PYY could not be detected by radioimmunoassay in NCI-H716 cell supernatants or lysates (data not shown). In contrast, basal PYY secretion of NCI-H716 cells was detected in preliminary ELISA assays (*Figure 4.5A)*. However, ELISA findings indicated that acute stimulation with neither SCFA(s) nor forskolin increased PYY secretion (*Figure 4.5B).*

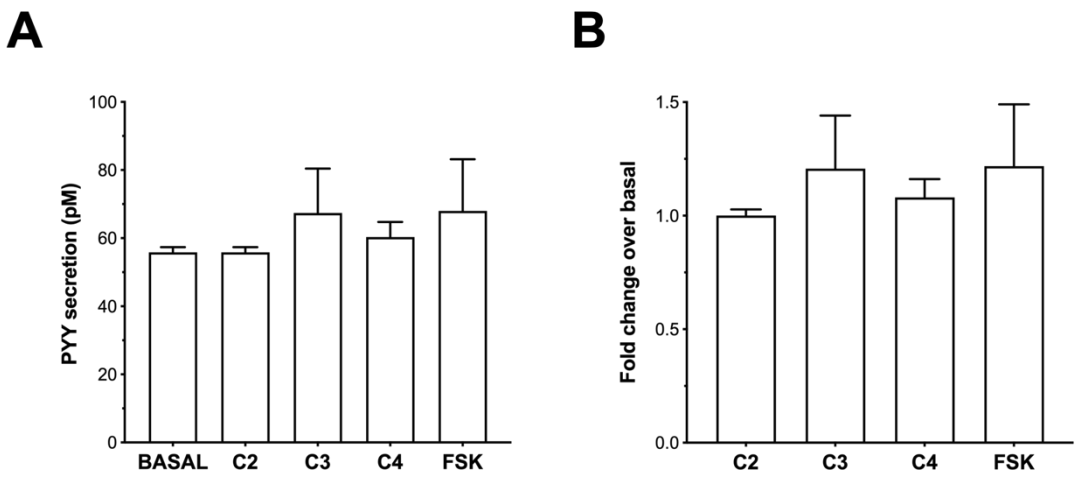
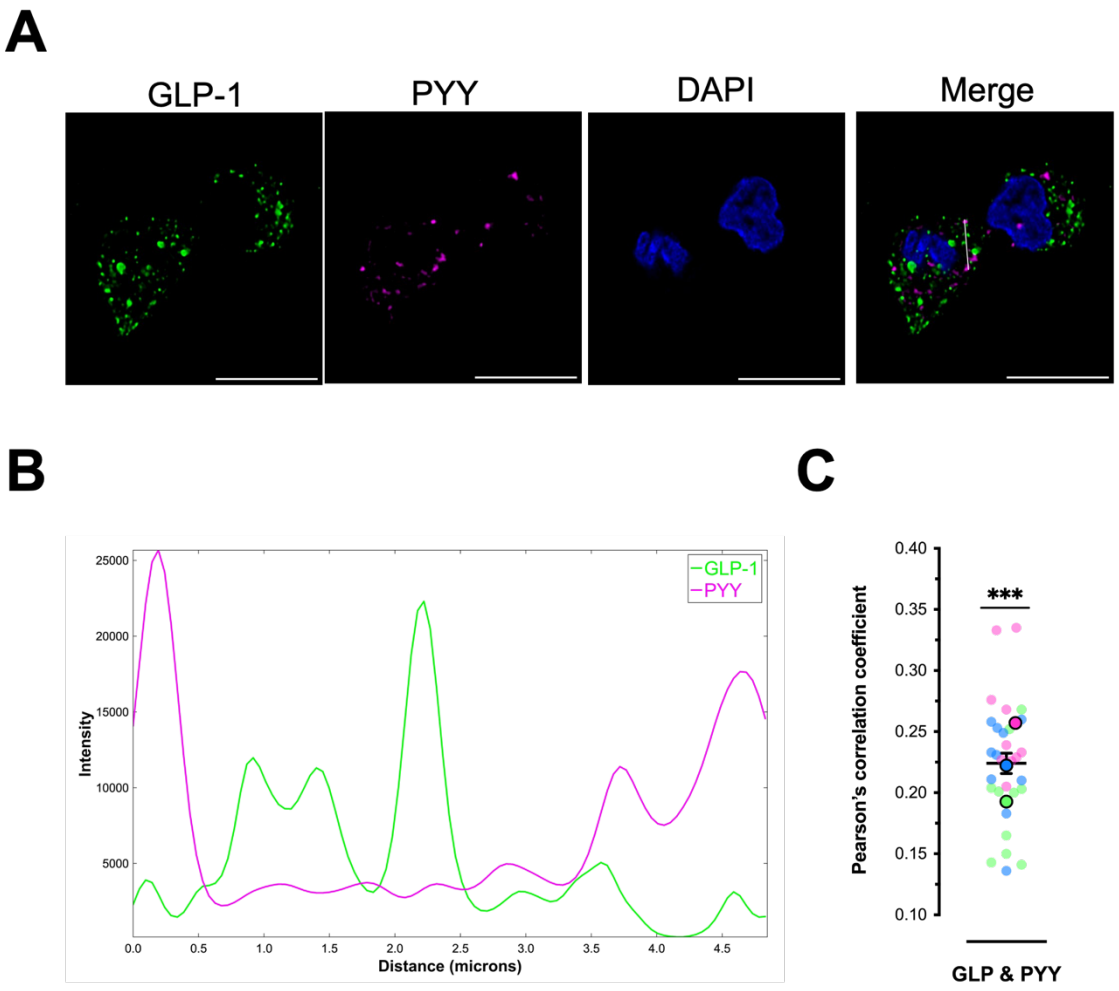


Figure 4.5 SCFAs may not acutely stimulate PYY secretion in NCI-H716 cells. (A & B) PYY secretion measured by ELISA in NCI-H716 cell supernatants following incubation with C2, C3 or C4 (1mM, 2h), FSK (10μM, 2h), or ligand-free buffer (Basal). Data represents mean ± SE of triplicates per independent experiments, n=1 independent experiment. **(B)** The effects of acute stimuli on PYY secretion are represented as fold changes over basal.

4.2.4 GLP-1 and PYY are poorly co-localised in NCI-H716 cells

Previous reports are conflicting as to whether GLP-1 and PYY are co-secreted from L-cells, or if their release profiles are regulated by distinct stimuli (Anini et al., 1999; Böttcher et al., 1984; Gerspach et al., 2011; Habib et al., 2013; Nilsson et al., 1991; Pironi et al., 1993). My findings thus far suggested that SCFAs might selectively act as acute GLP-1 but not PYY secretagogues in NCI-H716 cells; it is possible that these two hormones exist in separate vesicles or subcellular organelles that are mobilised in response to distinct stimuli. By employing confocal fluorescence microscopy paired with the adaptive deconvolution modality 'Lightning', the subcellular spatial distribution of GLP-1 and PYY in NCI-H716 cells could be imaged with ~120nm resolution (Reymann, 2018). A granular structure of both hormones was observed, and a higher abundance of GLP-1 than PYY granules was evident across cells (*Figure 4.6A)*. There appeared to be a distinct subcellular separation between GLP-1 and PYY granule

populations, exhibited by a representative intensity profile line plot (*Figure 4.6B).* Co-localisation analysis indicated ~22% GLP-1/PYY co-localisation across cells (*Figure 4.6C).* Volume occupancy of granule populations were visualised in three dimensions (*Figure 4.6D) and* reinforced the distinct compartmentalisation of both hormones.



D

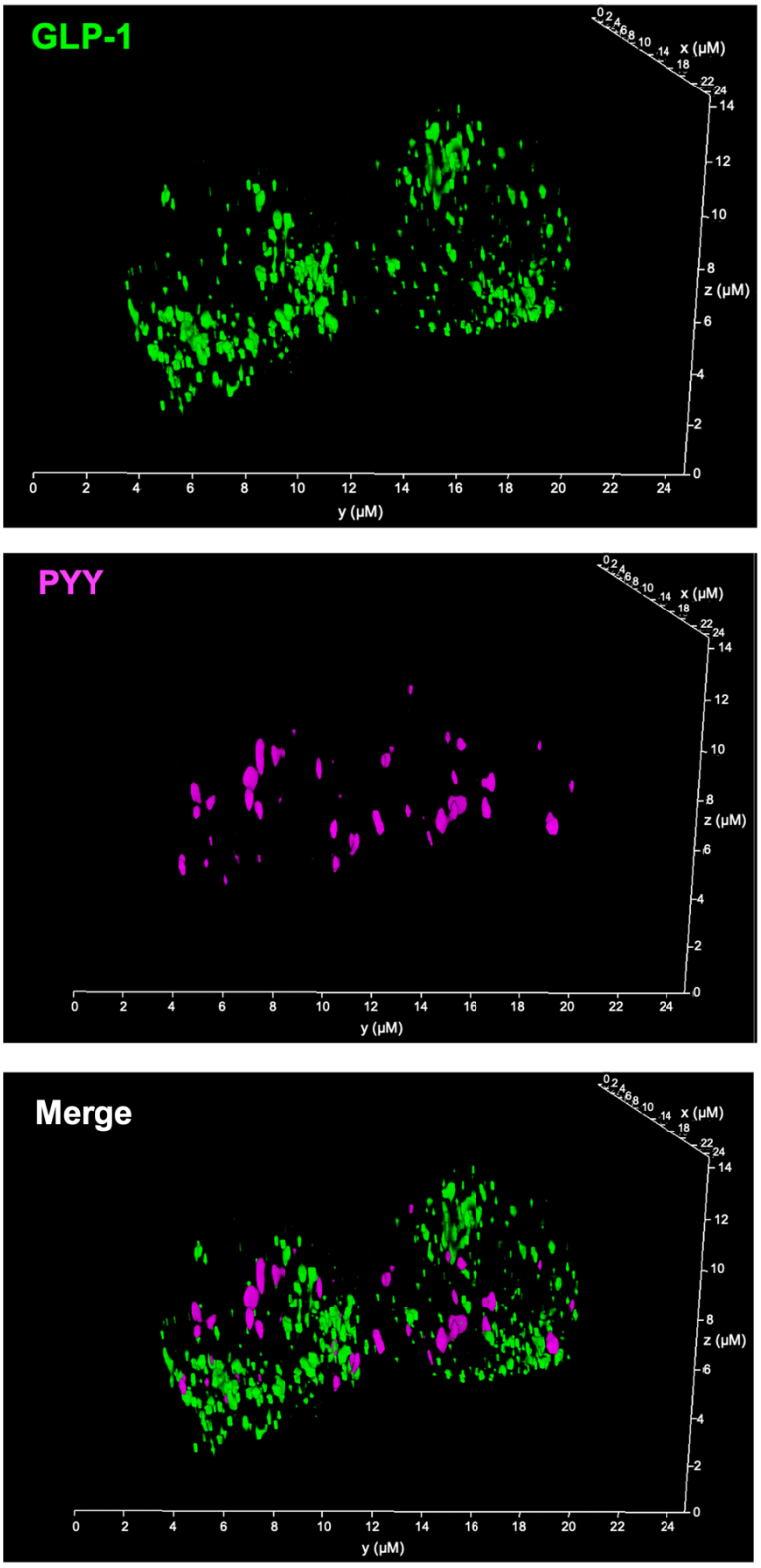


Figure 4.6 GLP-1 and PYY poorly co-localise in NCI-H716 cells. Immunofluorescent analysis of GLP-1 and PYY staining in NCI-H716 cells by confocal microscopy paired with 'LIGHTNING' adaptive deconvolution processing (LEICA). Cells were fixed and permeabilised before primary antibody labelling with anti-GLP1 and anti-PYY antibodies followed by labelling with Alexa Fluor 488 and 647 secondary antibodies. Subsequently, cells were stained with DAPI, mounted onto glass slides and imaged. **(A)** Confocal images of anti-GLP-1 and anti-PYY staining in NCI-H716 cells Scale bar= 10μm. Images are representative of 40 cells imaged across 6 independent experiments**. (B)** Line plot of GLP-1 and PYY intensity profiles across a ROI (indicated by a white line in (A) of 5μm length computed on ImageJ. **(C)** Pearson's correlation coefficient of GLP-1 and PYY channel overlap determined by automated colocalisation analysis of confocal images on ImageJ. Data represented as mean ± SEM of n=30 cells collected across three independent experiments. One sample t-test; Pearsons vs 1 (***$p<0.001$). (**D)** 3D visualisation of GLP-1 and PYY granule volume occupancy in (A), on the LAS X 3D Visualization software (LEICA).

4.3 Discussion

In this chapter I aimed to characterise the effects of SCFAs as acute secretagogues of the anorectic gut peptide hormones GLP-1 and PYY from the human EEC line, NCI-H716. My findings propose the involvement of a hFFAR2-Gαi pathway in mediating GLP-1 secretion. In addition, this chapter explores a selectivity of SCFAs in regulating the acute release profiles of GLP-1 and not PYY release.

As I confirmed in described in Chapter 3 (*3.2.2),* the colonic NCI-H716 cell line recapitulates key nutrient-sensing functionalities of the human L-cell (Kuhre et al., 2021; Kuhre et al., 2016; Reimer et al., 2001). Prior to assaying the acute effects of SCFAs on hormone secretion, buffer formulations from previous studies were compared and optimised for use, and basal GLP-1 secretion in NCI-H716 cells was observed to be highly sensitive to glucose. Previous *ex vivo* studies with human L-cells have also characterised a dose-dependency in glucose-mediated GLP-1 secretion which is mediated by the glucose transporters SGLT1 and GLUT2 (Sun et al, 2017). Postprandial GLP-1 secretion in the human gut cannot be ascribed to one class of nutrient given the complexity of the human diet and the vast repertoire of nutrient-sensing receptors on EECs. However, for the sake of isolating the effects of SCFAs and their cognate GPCRs, glucose-free buffers were chosen for these secretion studies.

In comparing the GLP-1 secretagogue potency of all three SCFAs in NCI-H716 cells, I observed propionate to stimulate the largest increase in secreted GLP-1, ~2 fold over basal, which agrees with previous studies in mouse EECs (Tolhurst et al., 2012). Butyrate also significantly increased GLP-1 secretion, yet the effect of acetate was slight. In a study by Christiansen et al., employing an *ex vivo* perfused rat colon model, butyrate and acetate exhibited higher GLP-1 secretagogue potency of propionate. It is possible that there are species-dependent complexities in the actions of SCFAs on acute GLP-1 release in L-cells that derive from differences in the intracellular effector machinery that they engage. The low potency of acetate in driving acute GLP-1 release from NCI-H716 cells is conflicting to its performance as a FFAR2-Gαi and -Gαq activator and instead might be representative of a compensatory mechanism in

native human L-cells. Acetate is the most abundant SCFA in the colonic lumen, existing in a 60:20:20 ratio with propionate and butyrate (C2:C3:C4) (Cummings et al., 1987; Topping & Clifton, 2001). As such, intracellular mechanisms in some or many of the stages involved in propeptide production, maturation and exocytosis might be fine-tuned downstream of acetate to prevent an overstimulation of GLP-1 release.

In vivo studies have previously demonstrated a mechanistic role of FFAR2 in mediating SCFA-stimulated colonic GLP-1 and PYY release, however these findings are limited to rodent models (Tolhurst et al., 2012; Psichas et al., 2015). Downstream of FFAR2 activation, the activation of Gαi and/or Gαq in mediating this response is conflicted between reports (Tolhurst et al., 2012; Caengprasath et al., 2020). I observed a concentration-dependent increase in acute GLP-1 secretion in NCI-H716 cells by treatment with the selective FFAR2-Gαi allosteric agonist AZ-1729. In contrast to my findings, a previous study has demonstrated an inability of AZ-1729 to stimulate GLP-1 secretion from mouse colonic crypts (Bolognini et al., 2016). Notably, AZ-1729 exhibited a lower potency at mouse FFAR2 compared to FFAR2, and signalling assays in this study were limited to heterologous expression systems (Bolognini et al., 2016b). In general, allosteric binding pockets of GPCRs are less conserved between orthologs than orthosteric ligand-binding sites (Grundmann et al., 2021). Furthermore, structure-based functional studies between human and mouse FFAR2 orthologs in the future might also uncover species-dependent specificities in AZ-1729 binding. Moreover, this discrepancy might be due to the differences between assay methods used; Bolognini et al., used ELISAs to measure GLP-1 secretion which is limited to detection of “active” or “intact” forms of GLP-1 and only accounts for 10-15% of the total secreted pool (Holst, 2007). In contrast, radioimmunoassays are able to detect the active GLP-1 as well as metabolites which are formed after rapid degradation by enzyme dipeptiyl peptidase-4 (DPP-IV) and are the major circulating forms of the hormone (Deacon & Holst, 2009).

As AZ-1729 is a selective activator of FFAR2-Gαi and not -Gαq signalling, my findings suggested the involvement of the former in mediating GLP-1 secretion from human EECs. Hormone secretion by EECs is driven by Ca^{2+}-dependent exocytosis, which has canonically been linked to elevations in intracellular calcium levels downstream of

Gαq-coupled GPCRs (Goldspink et al., 2018). In addition, several Gαs-coupled GPCRs have been shown to stimulate Ca^{2+}-dependent exocytosis of EEC peptide hormones due to the modulation of voltage- and/or ligand-gated Ca^{2+} channels by cAMP (Goldspink et al., 2018). As such, the involvement of Gαi pathway in GLP-1 release from human and/or mouse EECs seems somewhat paradoxical. Next, I questioned whether involvement of the Gαi pathway was required for SCFA-stimulated GLP-1 secretion in NCI-H716 cells. My preliminary results indicated a significant decrease in propionate-stimulated GLP-1 secretion following pre-treatment with the Gαi inhibitor Pertussis toxin (PTX). These findings are in agreement with previous reports from our lab which demonstrated propionate to stimulate GLP-1 release from the mouse enteroendocrine STC-1 cell line and colonic crypts *via* activation of Gαi (Caengprasath et al., 2020). Notably, I observed a concentration-dependent increase in basal GLP-1 secretion following PTX treatment; this phenomenon has previously been demonstrated in murine pancreatic β cells, which is suggested to arise due to an increase in intracellular cAMP following PTX-mediated inactivation of Gαi-mediated inhibition of adenylate cyclase (Toyota et al., 1978; Sim et al., 2014). The potential involvement of a Gαi mechanism in driving FFAR2-mediated GLP-1 secretion is strengthened by numerous examples of the functionality of numerous Gαi-coupled GPCRs across EEC subtypes. For example, activation of the permeable transient receptor potential canonical (TRPC) channels TRPC4 by Gαi-coupled adrenoreceptor α2 (Adrα2) has been shown to be central to serotonin release from mouse EECs (Bellono et al., 2017). In addition, a synthetic agonist of Gαi-coupled FFAR3, AR420626, is a significant stimulator of GLP-1 secretion from both mouse and human EEC lines (Ducastel et al., 2020).

An outstanding limitation to my findings is that experiments only assessed the inhibition of Gαi. Given that FFAR2 is a dual-coupled GPCR and I observed SCFA-mediated activation of both Gαi and Gαq, which I described in Chapter 3 (*3.2.3)* future studies should employ inhibitors of both G-protein pathways. Importantly, a study by Tolhurst et al. (2012) which associated SCFA-mediated GLP-1 release with elevations in intracellular Ca^{2+} and proposed an underlying FFAR2-Gαq mechanism, a considerable inhibition of propionate-mediated GLP-1 release was also detected after treatment with pertussis toxin. Activation of a Gαi pathway downstream of FFAR2

might mediate the intracellular Ca^{2+} flux linked to hormone release in L-cells, such as by a mechanism described above for Adrα2, which might explain the contrasting findings from previous studies (Tolhurst et al., 2012; Caengprasath et al., 2020). My findings on SCFA-mediated mobilisation of intracellular calcium (*3.2.3*) did not assess the effect of pertussis toxin, which will be a valuable starting point for assessing the possibility and functional implications of such a non-canonical FFAR2-Gαi-Ca^{2+} cascade in the human L-cell. The action of FFAR2 in regulating insulin sensitivity in adipocyte tissue has been linked to the activity of the receptor's Gβγ subunit (Kimura et al., 2013). In NCI-H716 cells, Gβɣ-mediated signalling cascades have been linked to the stimulation of GLP-1 secretion downstream of the human bitter taste receptor hTAS2R50 (Lee et al., 2023). Uncovering the synergy between Gαi-dependent and potential Gαi-independent pathways involved in FFAR2-mediated L-cell hormone release might uncover novel pharmacologically-targetable axes.

Enteroendocrine L-cells cells exhibit marked proximo-distal variation in the repertoire of hormones found co-expressed with GLP-1; this should be considered when reasoning the 'GLP-1-bias' I observed in the acute secretory profiles of NCI-H716 cell line (Habib et al., 2012, 2013; Billing et al., 2019; Burclaff et al., 2022). The origin of the NCI-H716 cell line is the ascites fluid of carcinoma specifically localised to the cecum (Park et al., 1987). Notably, previous characterisation of NCI-H716 cells by Kuhre et al., reported that neither CCK or GIP were expressed in this cell line, both of which have been found to be enriched in L-cell subclusters in the upper small intestine and proximal colon in mice (Habib et al., 2012; Billing et al., 2019). On the other hand, scRNA-seq analysis has reported PYY to predominate in colonic and not small intestinal L-cells in mice, and PYY expression has also been found to increase longitudinally from ascending to descending colon in humans (Habib et al., 2012; Burclaff et al., 2022). Due to inconsistency in the expression of PYY in NCI-H716 cells amongst reports, neither a distal colon-like nor proximal colon-like L-cell identity is agreed upon for this cell line (Kuhre et al., 2016). Given the well-characterised heterogeneity of L-cells along the GI tract, the use of region-specific primary L-cell cultures based on the hormone product in question, might be most suitable for future studies on nutrient-sensing GPCRs.

Contrasting to my findings on GLP-1 in NCI-H716 cells, I was unable to detect PYY in supernatants or lysates by radioimmunoassays in this cell line. Indeed, previous studies in this cell line have also failed to detect PYY by radioimmunoassay yet the use of ELISAs has been successful in some instances (Kim et al., 2014; Kuhre et al., 2016; Larraufie et al., 2018; Wang et al., 2022). This disparity might derive from the laborious handling required for performing radioimmunoassays that could elicit random errors. However, I did successfully measure basal PYY secretion of NCI-H716 cells, by use of ELISA assays, albeit in ~5 fold lower abundance than GLP-1. Moreover, PYY secretion did not appear to be enhanced by acute stimulation with SCFAs or the cAMP elevating agent Forskolin. SCFA-mediated FFAR2 activation has been implicated in driving the co-secretion of both GLP-1 and PYY from mouse L-cells (Psichas et al., 2015). Moreover, previous reports have visualised a subcellular co-localisation of both these hormones in human L-cells by conventional microscopy techniques. Notably, ultrastructural characterisations of L-cells by electron microscopy have indicated that their secretory granules range from ~80 to ~300nM in size (Böttcher et al., 1986; Dobbins & Austin, 1991; Nishimura et al., 2013). Therefore, considering the ~200nm resolution limit of conventional confocal microscopy techniques, it is possible that a separate compartmentalisation of GLP-1 and PYY granules, particularly at the lower end of this size range, might be masked. GLP-1 and PYY granules were visualised in NCI-H716 cells by the use of super-resolution confocal microscopy. A low degree of overlap was evident between GLP-1 and PYY granules in NCI-H716 cells. This spatial distribution may underlie the selective release of a single hormone from L-cells upon acute nutrient stimulus which I observed in my own findings and has also been reported in a number of previous studies (; Böttcher et al., 1984; Nilsson et al., 1991; Pironi et al., 1993; Anini et al., 1999; Gerspach et al., 2011; Habib et al., 2013).

In summary, this chapter explored the roles of SCFAs as acute secretagogues of the peptide hormones GLP-1 and PYY in a human colonic L-cell model. SCFAs and a selective FFAR2-Gαi agonist promoted the acute secretion of GLP-1, and a FFAR2-Gαi axis was also implicated in driving propionate-mediated GLP-1 acute release was also suggested. In contrast to GLP-1, PYY secretion was not promoted by similar acute stimuli in this system. Super-resolution immunofluorescence analyses were able to uncover a subcellular separation in the distribution of GLP-1 and PYY granules,

further suggesting the existence of distinct regulatory mechanisms driving their secretion.

5. Non-canonical actions of short chain fatty acids on human EECs

5.1 Introduction

The intestinal epithelium is completely turned over every 4-5 days, fuelled by the continuous proliferation of $Lgr5^{+}$ intestinal stem cells (ISCs) that reside at the base of crypts of Lieberkühn (Barker et al., 2007). ISCs give rise to transit amplifying (TA) cells which further differentiate to absorptive or secretory intestinal epithelial cell (IEC) fates as they migrate up along the crypt-villus axis (Cheng & Leblond, 1974). As such, homeostasis along this epithelial 'conveyor belt' necessitates a stringent balance between maintaining stemness *via* ISC populations for self-renewal and repair, and achieving specialised functions *via* lineage-specific differentiation of IEC populations (Cheng & Leblond, 1974). Commitment of mature IEC to specific lineages is mediated by a complex network of transcriptional regulators and juxtracrine signalling mechanisms (Sanchez, Enriquez & Wells, 2022). The NOTCH pathway is responsible for mediating cell fate commitment and spatiotemporal patterning in developing and several adult tissues (Kageyama & Nakanishi, 1997). Early stages of enteroendocrine differentiation require an inhibition of Notch signalling in secretory progenitors, releasing the hairy/enhancer-of-split (*Hes1*)-mediated repression of proendocrine bHLH transcriptional factor cascades (Jensen et al., 2000). Gene inactivation studies in mice and single cell transcriptomics have identified sequential gene expression cascades which drive enterohormone transcription and specify maturation of EEC precursors into hormone-secreting enteroendocrine subtypes (Gehart et al., 2019).

The intestinal lumen is laden with nutrient and non-nutrient signals which can reflect exogeneous macronutrient intake, as well as endogenous metabolite production by the gut microbiome. There is much interest in understanding how behaviours along the intestinal epithelial 'conveyor belt' adapt maintain gut homeostasis in response to various dietary factors (Wang et al., 2022). For example, Cheng et al., 2019 have reported opposing Notch-mediated effects of ketogenic diets and glucose-rich diets in mice in favouring ISC proliferation or differentiation respectively. Notably, expansion of enteroendocrine L-cell populations in the rodent intestine *in vivo* has been shown to increase following ingestion of fermentable carbohydrates (Kaji et al., 2011; Brooks et al., 2017). SCFAs themselves have also been shown to increase the expression of markers specific to L-cell differentiation in human colonic cell lines and organoids *in*

vitro (Petersen et al., 2014; Larraufie et al., 2018; Pearce et al., 2020; Grouls et al., 2022). Importantly, a decreased intestinal density of GLP-1- and PYY-positive cells is signature of morbidly obese individuals, yet has been found to be reversible with bariatric surgery (Wölnerhanssen et al., 2017). In addition, transcriptomic analyses have identified aberrations specific to Notch-sensitive L-cell differentiation cascades in the intestinal biopsies of obese individuals with and without T2D (Wölnerhanssen et al., 2017; Osinski et al., 2021). These include reduced expression of the L-cell specific differentiation factors *NeuroD1* and *Pax6*, and increased expression of the inhibitor of EEC cell fate, *Hes1* (Wölnerhanssen et al., 2017; Osinski et al., 2021). As such, enhancing the abundance of anorectic gut hormone-secreting EECs is emerging as a novel, but likely powerful, therapeutic avenue in treating metabolic disease (Wölnerhanssen et al., 2017; Osinski et al., 2021).

In this chapter, I explore the effect of SCFAs in NCI-H716 cells on morphology and gene expression of transcription factor cascades that regulate markers of L-cell differentiation. At millimolar concentrations, comparable to the endogenous luminal environment, butyrate exhibited particularly prominent effects on enterohormone repertoire, morphological parameters and Notch-regulated markers of L-cell development that suggested the induction of differentiation to a ‘PYY-bias’ mature L-cell phenotype. Finally, mouse colonic organoid systems were employed to investigate the effects of butyrate on Notch activity across heterogeneous intestinal epithelial cells types, and the maintenance or inhibition of ‘stemness’ in immature ISCs.

5.2 Results

5.2.1 SCFAs upregulate the gene expression of PYY but not GCG in human EECs

Apart from being potent GLP-1 and PYY secretagogues, SCFAs have also been implicated in the transcriptional regulation of genes involved in the nutrient-sensing functions of L cells (Larraufie et al., 2018; Petersen et al., 2014; Shackley et al., 2020). To assess whether SCFAs might affect the expression of *Pyy* and GLP-1 precursor (*Gcg)*, NCI-H716 cells were treated for 24 hours with 2mM of each SCFA; a physiologically relevant concentration at which SCFAs activate FFAR2 (> EC50) and exerts transcriptional effects (Larraufie et al., 2018). The abundance of *Gcg* and *Pyy* mRNA transcripts was compared in SCFA-treated and untreated NCI-H716 cells. Trypan Blue staining confirmed cell viability after chronic SCFA treatment (*data not shown)* but revealed extensive cell death after incubation with NaCl. As such, 24-hour treatments with NaCl were excluded from subsequent assays.

The addition of short chain fatty acids stimulated a decrease in *Gcg* expression in NCI-H716 cells *(Figure 5.1A)*. This effect was specific with butyrate and propionate, stimulating a ~4- and ~2-fold decrease respectively, whereas expression of *Gcg* in acetate-treated was not different to untreated control. In contrast**,** *Pyy* mRNA abundance was robustly upregulated after incubation with all three SCFAs, and this effect was positively correlated with chain length (C2 < C3 < C4) (*Figure 5.1B)*. Butyrate induced a large increase (~122 mean fold) in transcript level, while acetate and propionate both upregulated expression by ~7 fold. Next, cells were treated with a combined treatment of all three SCFAs, formulated to mimic the 60:20:20 physiological ratio of the gut lumen, at a concentration which was still tolerable by cells (6mM C2: 2mM C3, 2mM C4). GCG and PYY responses to the SCFA cocktail were not significantly different to butyrate-mediated effects in NCI-H716 cells(*Figure 5.1A; Figure 5.1B).*

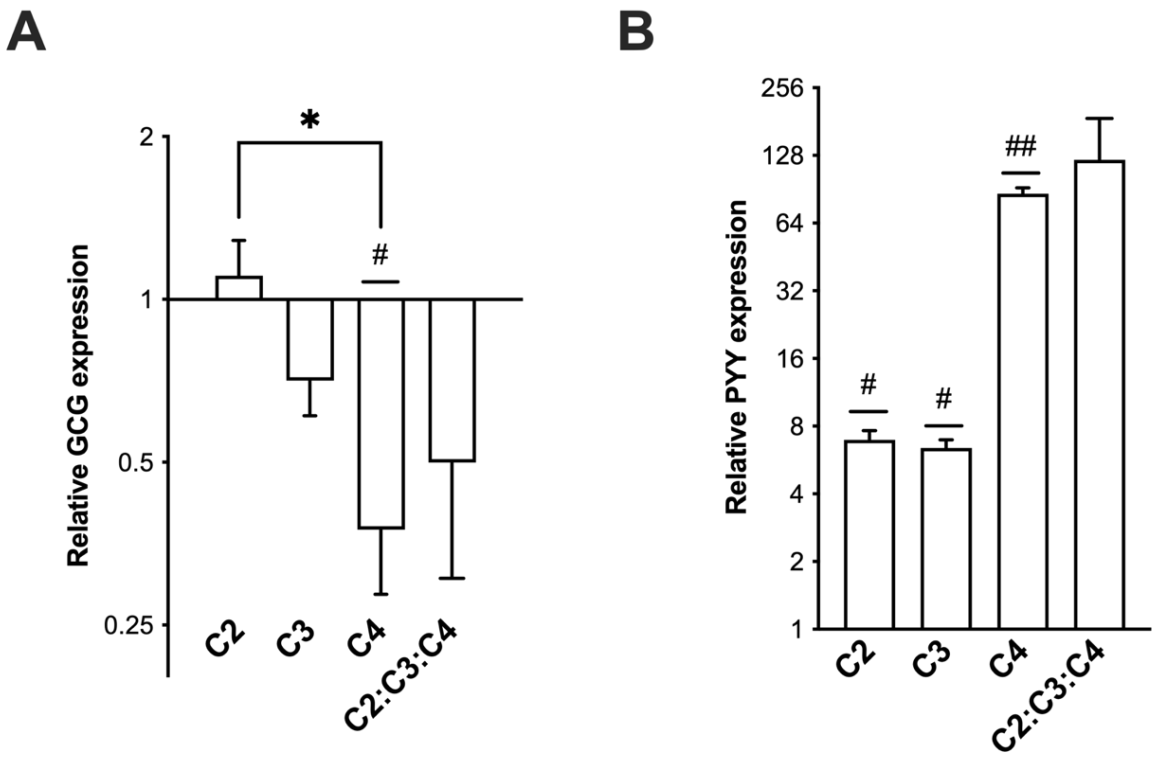


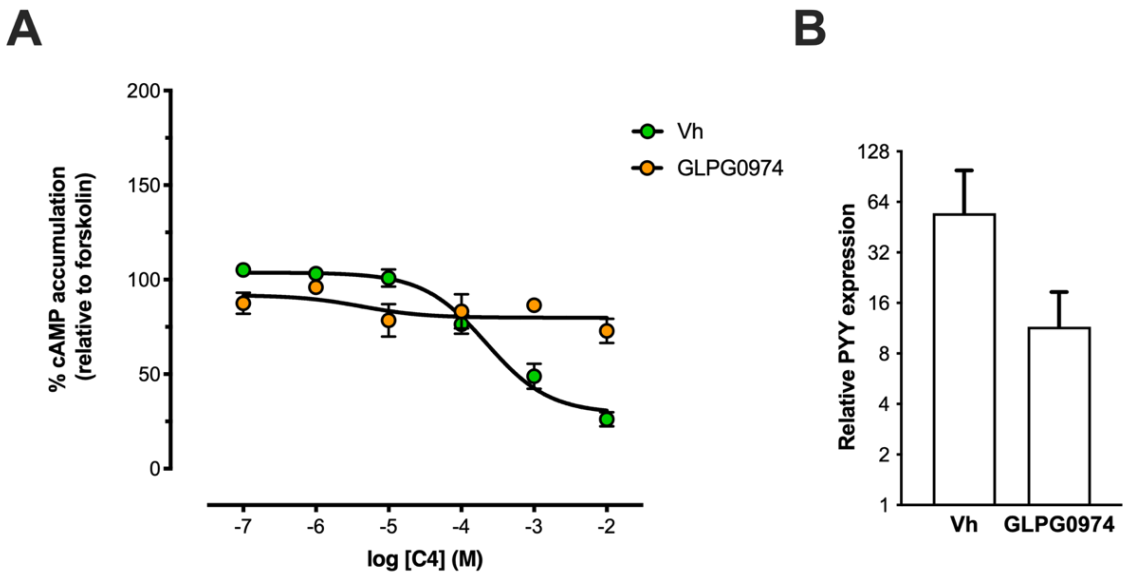
Figure 5.1 Chronic SCFA treatments affect the expression of *Gcg* and *Pyy* in NCI-H716 cells. Relative gene expression of **(A)** *Gcg* or **(B)** *Pyy* in NCI-H716 cells treated with 2mM of C2,C3, C4 or C2:C3:C4 (6mM C2, 2mM C3, 2mM C4) for 24h. RNA was extracted from treated and untreated cells and converted to cDNA. *Gcg* or *Pyy* transcript levels were detected alongside *Rpl12* housekeeping gene by RT-qPCR. Relative gene expression was determined using the 2--ΔCt method. Data are mean ± SEM, n=3 and conditions were run in at least triplicate per independent experiment. Unpaired t-test vs untreated (UT): ($^{\#\#}p<0.01$; $^{\#}p<0.05$). One-way ANOVA: C2 vs C3 vs C4 (*p<0.05). Unpaired T-Test: C4 vs C2:C3:C4.

5.2.2 Butyrate upregulates *Pyy* expression *via* FFAR2-Gαi signalling at the plasma membrane

Dietary supplementation with non-digestible carbohydrates have been reported to increase mouse colonic populations of PYY^{+} cells in an FFAR2-dependent manner (Brooks et al., 2017). I next questioned whether the pronounced effect of butyrate on PYY expression in NCI-H716 cells might mechanistically involve the activation of human FFAR2 expressed in these cells. 1μM of GLPG0974 was confirmed to inhibit the G-protein signalling capabilities of butyrate across 1nM-10mM (*Figure 5.3A)*. When cells were pre-treated with 1μM GLPG0974 prior to measuring butyrate-

mediated upregulation of *Pyy* expression, the antagonist caused a ~ 57% reduction in response compared to vehicle, indicating an important contribution of FFAR2 (*Figure 5.3B)*.

Next, I assessed whether these FFAR2-dependent effects on *Pyy* were mediated downstream by a Gαi pathway, considering butyrate is a stronger activator of Gαi than Gαq in NCI-H716 cells (Chapter 3). Pre-treatment with 500ng/ml of pertussis toxin (Ptx) effectively inhibited butyrate-mediated Gαi signalling *(Figure 5.3C)*, and significantly blunted butyrate-mediated *Pyy* upregulation by over 50% (*Figure 5.3D)*. In contrast, pre-treatment with inhibitors of Gαq (YM-254890) or dynamin-dependent internalisation **(**Dyngo 4a) did not produce any significant inhibitory effects on butyrate-mediated *Pyy* regulation (*Figure 5.3E)*. Together, these findings suggest that butyrate-mediated effects on *Pyy* mRNA expression are partially mediated by an FFAR2- Gαi rather than a Gαq pathway which operates primarily at the plasma membrane.



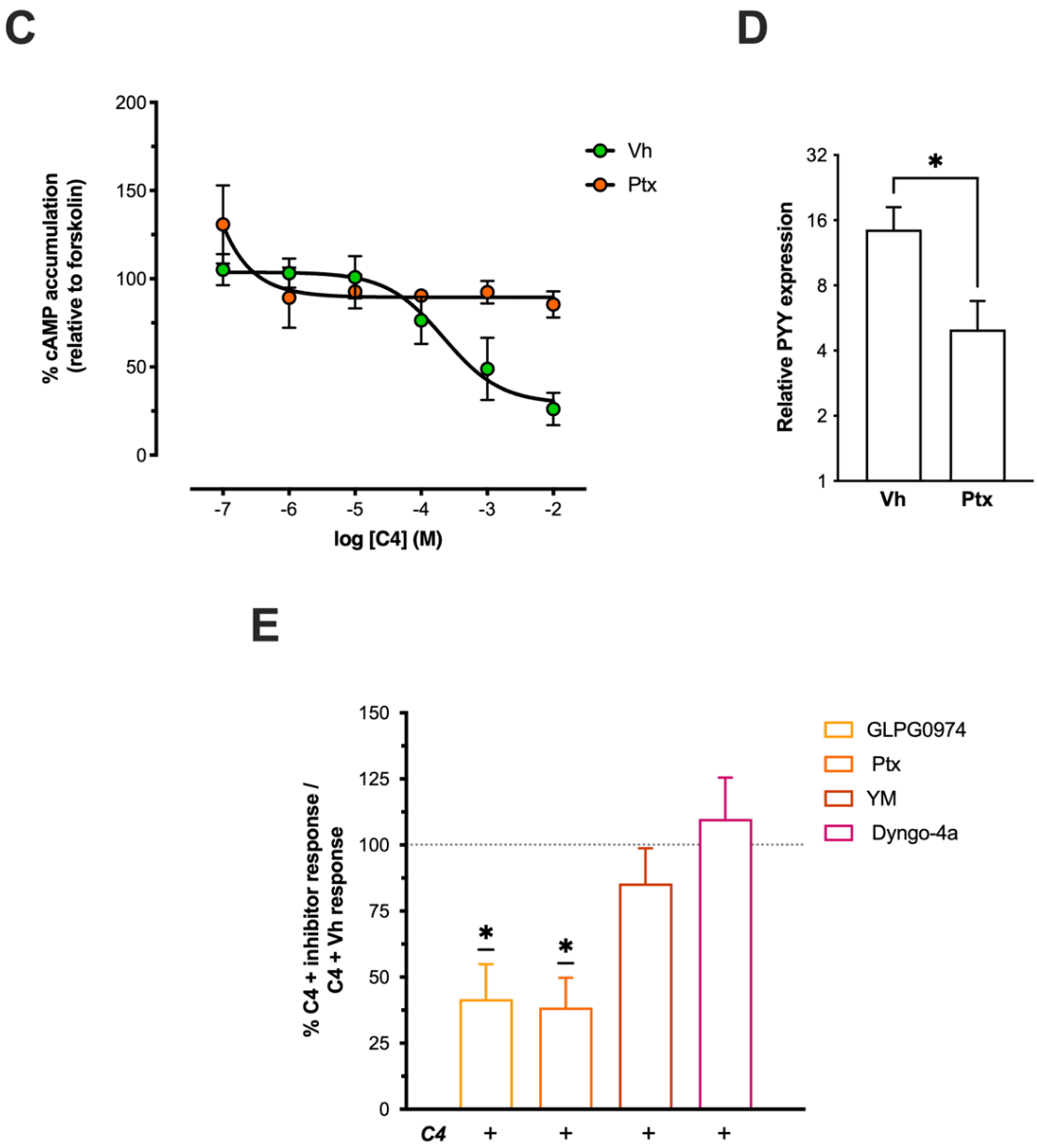


Figure 5.2 Butyrate upregulates *Pyy* expression *via* activation of a FFAR2-Gαi pathway at the plasma membrane. (A) NCI-H716 cells were incubated with FFAR2-specific antagonist GLPG0974 (*green)* (1μM, 15 min) or DMSO vehicle (*black)* prior to treatment with IBMX (500μM, 5 min) , and then forskolin (3μM, 5 min) or a combination of forskolin (3μM, 5 min) and C4 (1nM-100mM, 5 min). Intracellular cAMP levels were measured in cell lysates and expressed as a % of the forskolin response. Data are mean ± SEM, n=3 and conditions were run in at least triplicate per independent experiment. **(B)** *Pyy* transcript levels determined in cells treated with GLPG0974 (1μM, 15 min) or DMSO vehicle prior to incubation with C4 (2mM, 24h). Relative *Pyy* expression was determined using the 2--ΔCt method using *Rpl12* housekeeping gene. Data are mean ± SEM, n=3 and conditions were run in at least triplicate

per independent experiment. **(C)** Inhibition of FSK-mediated cAMP accumulation by butyrate in NCI-H716 cells pre-treated with Pertussis toxin (Ptx) (500ng/ml, 20h) or H_20 vehicle. Data are mean ± SEM, n=3 and conditions were run in at least triplicate per independent experiment. (**D)** *Pyy* transcript levels determined in cells treated with Ptx (500ng/ml, 20h) or H_20 vehicle prior to incubation with C4 (2mM, 24h). Relative *Pyy* expression was determined using the 2--ΔCt method using *Rpl12* housekeeping gene. Data are mean ± SEM, n=3 and conditions were run in at least triplicate per independent experiment. Unpaired T Test C4 + DMSO vs C4 + Ptx (*p<0.05). (**E)** Relative *Pyy* expression in cells pre-treated with DMSO vehicle (Vh) or GLPG0974 (1μM, 15 min) or PTX (500ng/ml, 20h) or YM-254890 (10μM, 15 min) or Dyngo-4a (50μM, 15 min) followed by C4 (2mM, 24h). Data are normalised as a % of change of C4 + inhibitor / C4 + DMSO vehicle response. Data are mean ± SEM, n=3 and conditions were run in at least triplicate per independent experiment. Unpaired T Test C4 + inhibitor vs C4 response (100%) (*p<0.05).

To further investigate the involvement of a Gαi mechanism in the transcriptional regulation of *Pyy*, NCI-H716 cells were incubated with the FFAR2-selective Gαi biased allosteric agonist, AZ-1729. Interestingly, 24-hour treatment with 1μM of AZ-1729 induced a ~2-fold increase in *Pyy* expression relative to baseline (*Figure 5.3A)*. However, the effect of butyrate-mediated upregulation of *Pyy* was increased by ~2 fold when cells were treated with a combination of 1μM AZ-1729 and butyrate, suggesting a synergistic response involving FFAR2-Gαi (*Figure 5.3B)*.

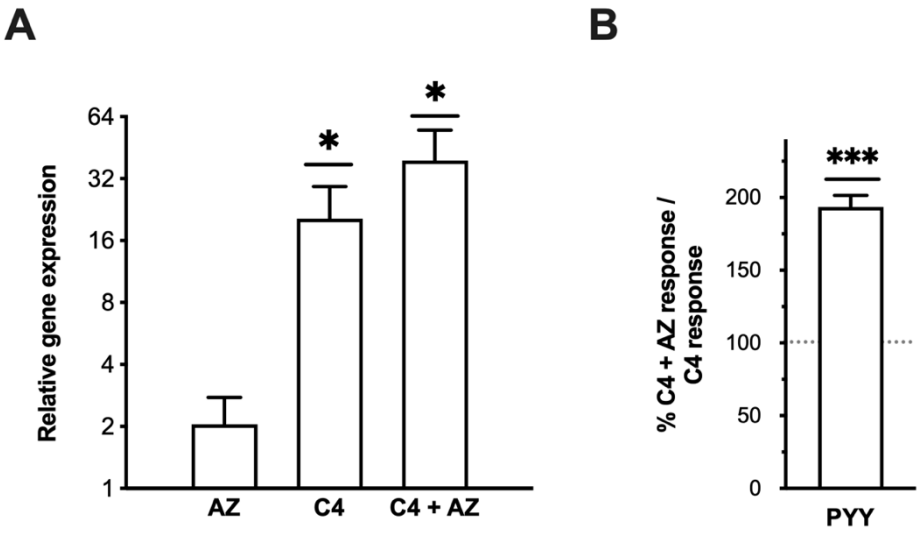


Figure 5.3 The biased FFAR2-Gαiactivator AZ-1729 enhances the effect of butyrate on *Pyy* expression. (A) Relative PYY expression in NCI-H716 cells treated with C4 (2mM, 24h), FFAR2 biased agonist AZ-1729 (1μM, 24h) or a combination of C4 (2mM, 24h) and AZ-1729 (1μM, 24h). Relative PYY expression was determined using the 2--ΔCt method using *Rpl12* housekeeping gene. **(B)** Relative *Pyy* expression normalised as a % change of C4 + AZ/ C4 response. Data are mean ± SEM, n=3 and conditions were run in at least triplicate per independent experiment. Unpaired T Test C4 + AZ-1729 vs C4 (100%) (***p<0.001).

5.2.3 SCFAs appear to downregulate the gene expression of *Gcg* in human EECs in an FFAR2-independent manner

Given that SCFAs have previously been shown to stimulate GLP-1 secretion by FFAR2-dependent mechanisms in EECs (Psichas et al., 2015; Caengprasath et al., 2020), that SCFAs did not support the transcriptional activation of proglucagon was surprising. However, aberrant regulatory mechanisms of proglucagon expression, in which the proglucagon gene promoter is functionally redundant, have been previously reported in NCI-H716 cells (Cao et al., 2003). As I previously characterised that SCFA-induced signalling responses are selectively mediated by FFAR2 in NCI-H716 cells (*3.2.4),* it was important to ascertain the role of FFAR2 in mediating these changes in gene expression. Cells were pre-treated with an FFAR2 antagonist GLPG0974, at a concentration (1μM) which effectively inhibits the Gαi and Gαq responses of all three SCFAs (*3.2.4).* Preliminary data indicated that GLPG0974 pre-treatment did not affect SCFA-mediated decreases compared to vehicle, suggesting an FFAR2-independent mechanism (*Figure 5.4A). Gcg* expression was also measured following treatment with AZ-1729. Interestingly, AZ-1729 did not stimulate any significant changes in *Gcg* transcript levels compared to vehicle, suggesting a mechanistic pathway independent of FFAR2-Gαi (*Figure 5.4B).* C4-mediated downregulation of *Gcg* was not enhanced by co-incubation with C4 and AZ-1729.

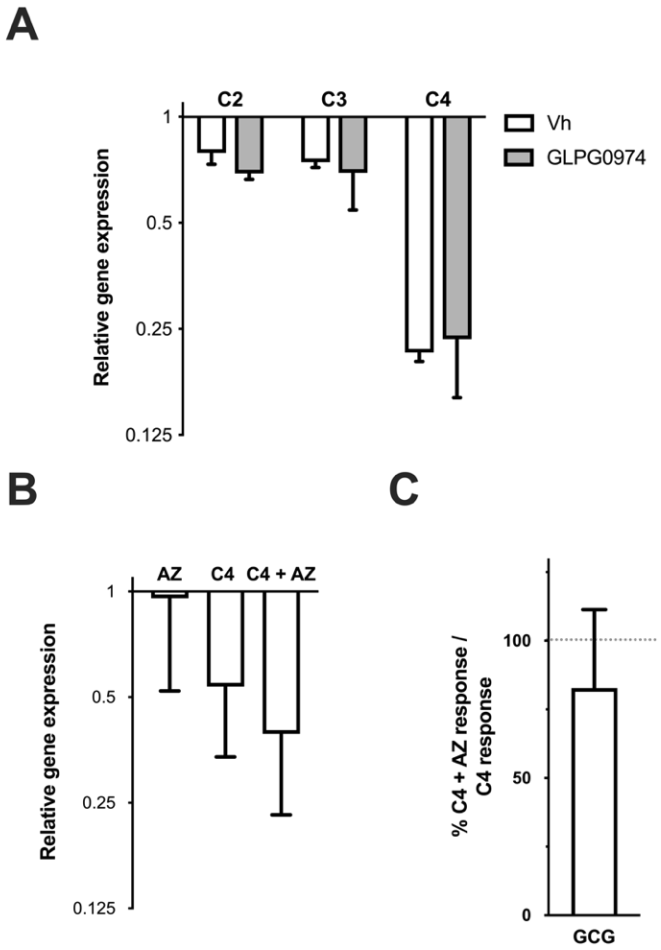


Figure 5.4 SCFAs appears to downregulate *Gcg* expression in an FFAR2-independent manner. **(A)** NCI-H716 cells were pre-treated with FFAR2-specific antagonist GLPG0974 (1μM) or DMSO vehicle for 15 minutes. Subsequently, cells were incubated with respective SCFAs (2mM, 24h). Relative expression of *Gcg* in SCFA-treated cells compared to untreated cells was determined using the 2--ΔCt method using *rpl12* housekeeping gene for both DMSO (*white bars)* and GLPG0974 (*black* bars) conditions. Data are mean ± SEM, n=2 and conditions were run in at least triplicate per independent experiment. **(B)** *Gcg* transcript levels were measured in NCI-H716 cells treated with C4 (2mM, 24h), FFAR2 biased agonist AZ-1729 (1μM, 24h) or a combination of C4 (2mM, 24h) and AZ-1729 (1μM, 24h). Relative *Gcg* expression was determined using the 2--ΔCt method using *Rpl12* housekeeping gene. Data are mean ± SEM, n=3 and conditions were run in at least triplicate per independent experiment. (**C)** Relative *Gcg* expression normalised as a % change of C4 + AZ/ C4 response. Data are mean ± SEM, n=3 and conditions were run in at least triplicate per independent experiment.

5.2.4 Butyrate might selectively enhance PYY secretory tone in NCI-H716 cells

To understand whether butyrate's prominent transcriptional effects on hormone gene expression would also be reflected in enhanced cellular secretory capacity, NCI-H716 cells were pre-treated with butyrate for 24 hours and changes in basal PYY and GLP-1 secretion were measured in supernatants by ELISA and radioimmunoassays respectively. Preliminary ELISA data suggests that cells pre-treated with butyrate exhibited a mean ~1.3-fold increase in basal PYY secretion compared to wild-type, however no change in PYY peptide content was observed (*Figure 5.5A, 5.5B)*. When GLP-1 secretion was measured by radioimmunoassay, a mean ~1.4-fold increase was observed following chronic butyrate treatment, with the caveat of variability between biological repeats. As I previously reported in *2.2.2,* variation in signalling responses between passage numbers and/or age is not uncommon in NCI-H716 cells. GLP-1 content between butyrate-treated and untreated cells was not significantly different (*Figure 5.5C)*.

Having previously characterised GLP-1 secretion in NCI-H716 in response to acute SCFA treatment, I sought to investigate whether these acute responses might differ after cells were pre-treated with butyrate for 24 hours (*Figure 5.5E).* Elevated GLP-1 secretion in response to acute treatment with C2 and C4 as well as NaCl negative control was apparent in cells pre-treated for 24h with butyrate. Although no significant trends were evident, the data did suggest that chronic pre-treatment with butyrate might in fact saturate basal GLP-1 secretion such that the effect of acute stimulation with potent GLP-1 secretagogues (*ie* C3 and C4) is equivalent to weaker stimuli (*ie NA* and C2), however significance is again limited by biological variability.

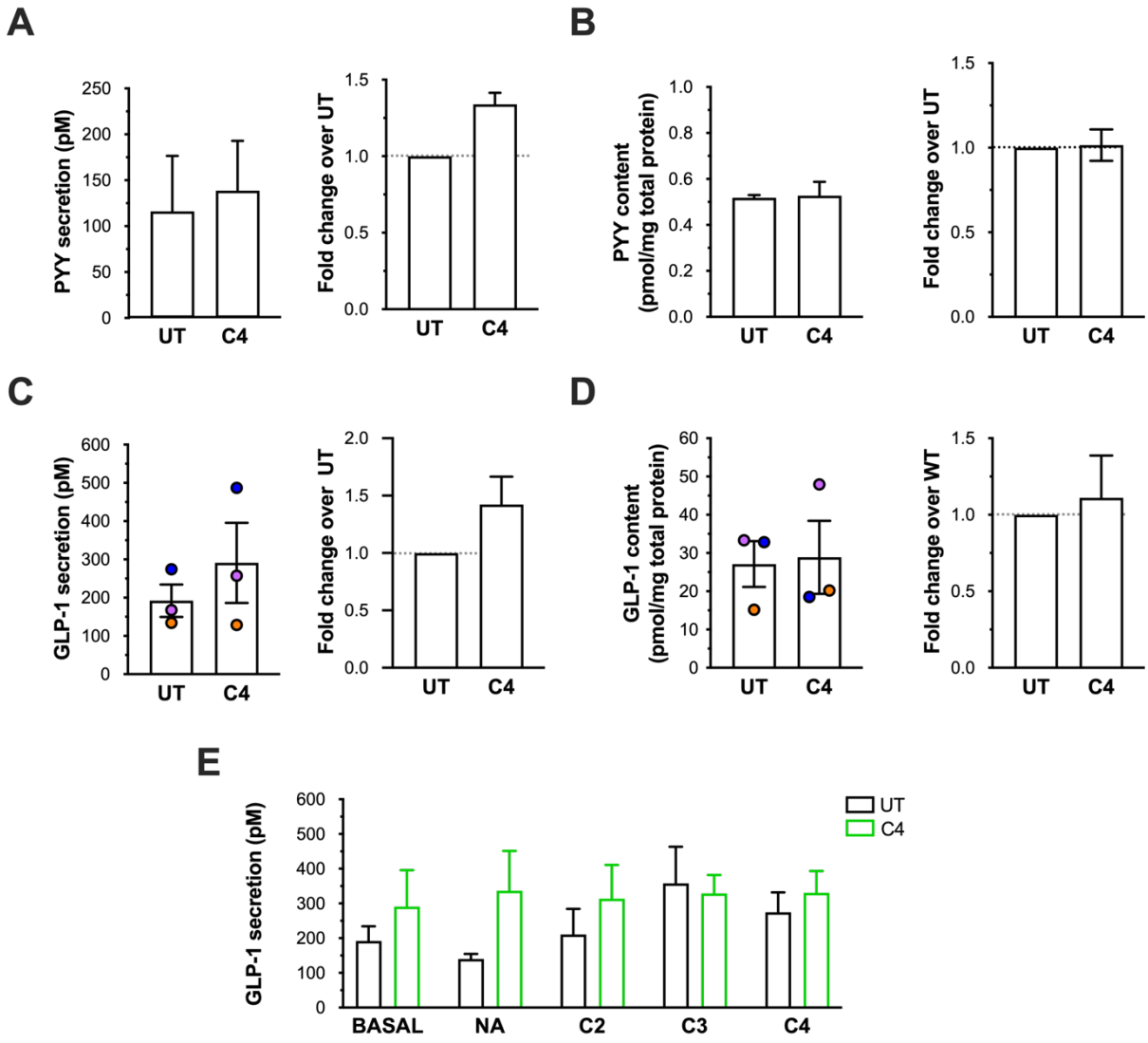


Figure 5.5 Chronic SCFA treatments may induce distinct effects on PYY and GLP-1 production and secretion. (A) PYY secretion in supernatants or **(B)** PYY content in lysates in NCI-H716 cells treated with C4 (2mM, 24h) or untreated (UT). Data is also represented as C4 fold change over UT. Symbols represent the mean ± SEM of two independent experiments (n=2) run in technical duplicates per experiment. (**C)** GLP-1 secretion and content **(D)** measured by radioimmunoassay (RIA) in NCI-H716 cells treated with C4 (2mM, 24h) or untreated (UT). Coloured symbols represent the mean ± SEM of each independent experiment (n=3) run in triplicates. (E) GLP-1 secretion in supernatants measured by RIA in response to acute NaCl or SCFA treatment (1mM, 2h) in cells pre-treated with C4 *(green)* (2mM, 24h) or not *(black).* Data represent the mean ± SEM of each independent experiment (n=3) run in triplicates.

5.2.5 Butyrate causes cells to adopt a spindle-like shape characteristic of colonic EECs

A drastic change in the morphology of NCI-H716 cells was observed following chronic incubation in butyrate. In bright-field images, there was a prominent increase in length and change from spherical to spindle-shape in almost all cells when treated with butyrate (*Figure 5.6A)*. These observations were also apparent with propionate, however 'transformed' cells represented a smaller fraction of the population, which was largely occupied by cells with the expected spherical shape of NCI-H716. Acetate-treated cells did not appear different to untreated cells. Native EECs have long been described to exhibit a bottle-like shape, possessing apical cytoplasmic processes that allow for close proximity with the gut lumen (Buffa et al., 1978). However, a specific anatomic difference has been reported for PYY-positive L-cells in the ileum and the colon, with the latter adopting an elongated spindle-shaped morphology akin to my observations (*Figure 5.6B)* (Bohórquez et al., 2011). Prolonged incubation with C2, C3 or C4 did not appear to increase cell count compared to untreated conditions (*data not shown).*

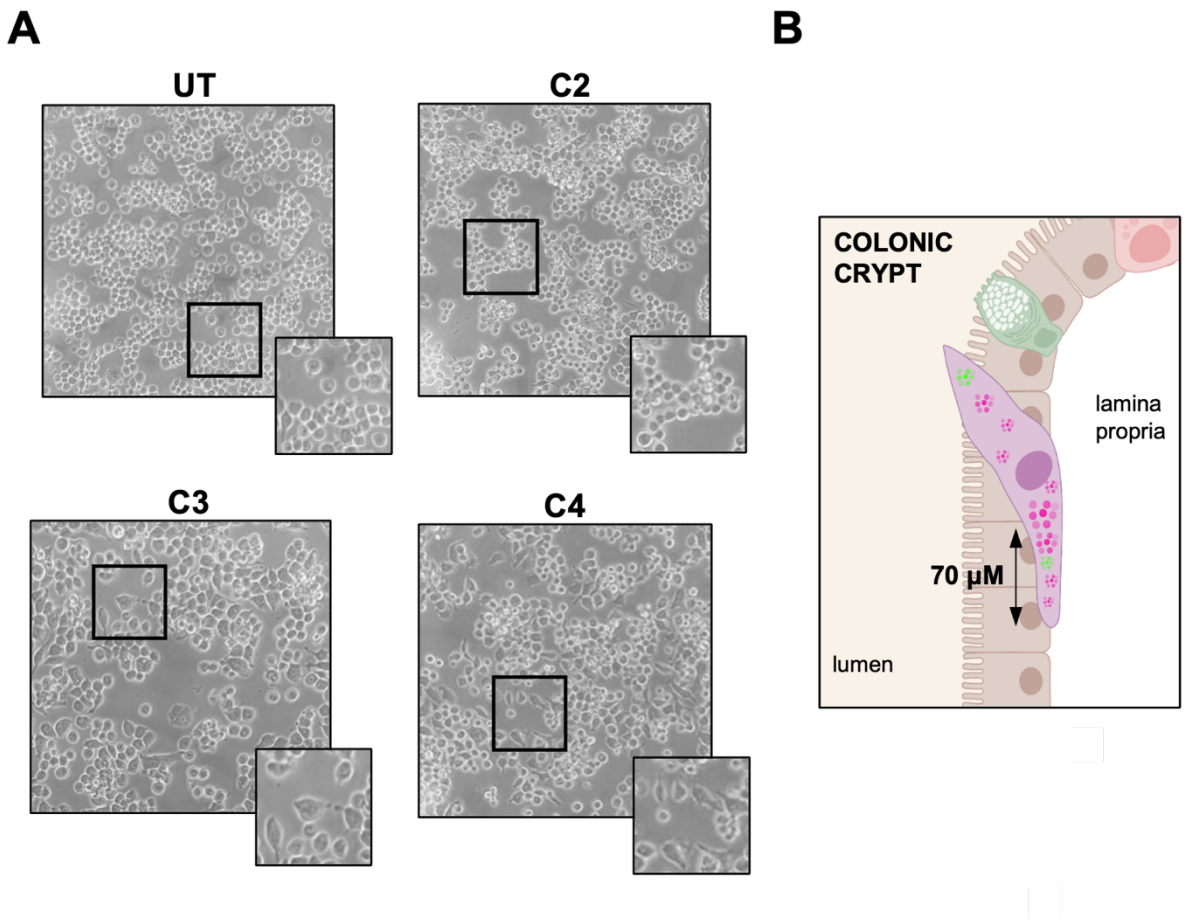
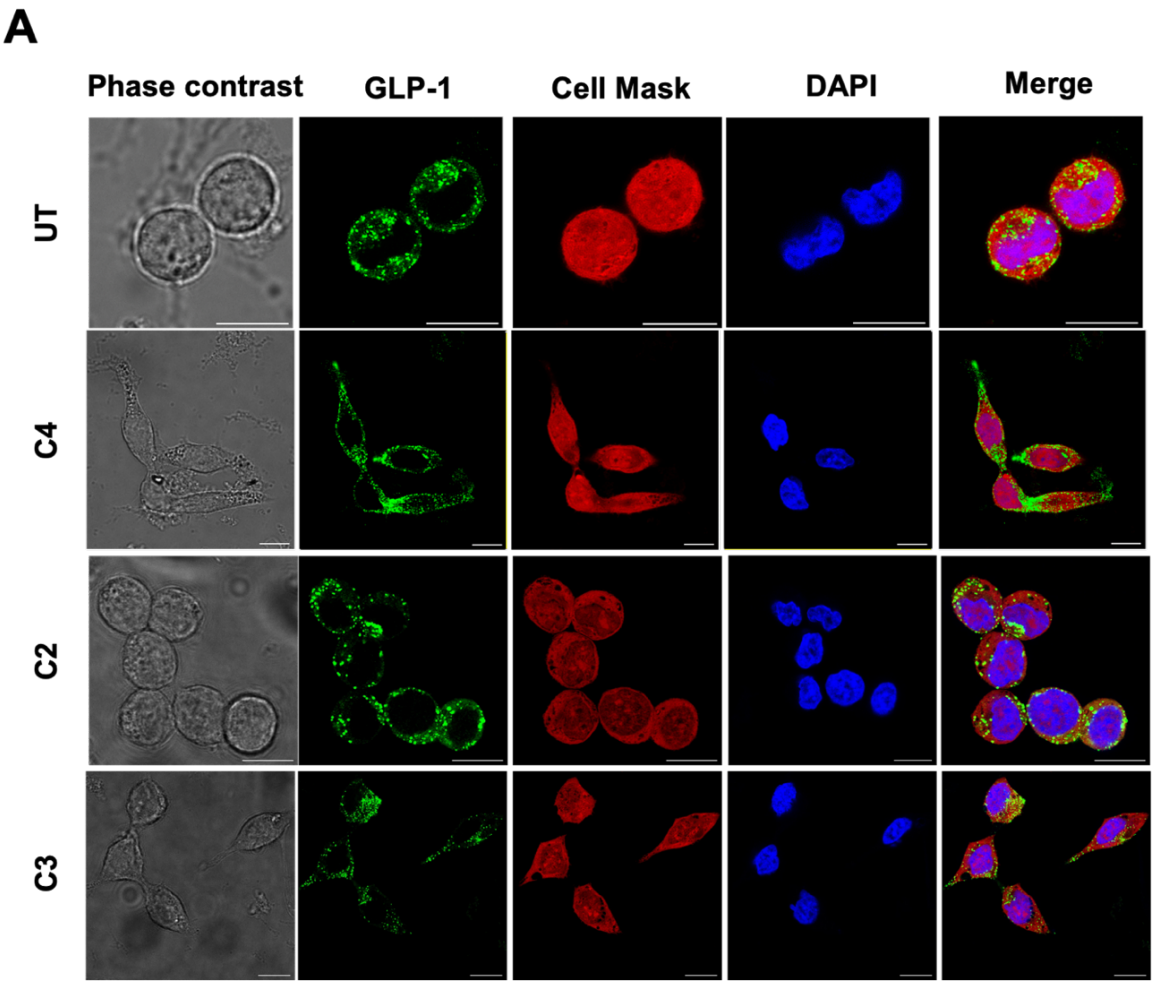


Figure 5.6 Chronic incubation with propionate and butyrate cause unique morphological changes characteristic of colonic L-cells. (A) Observations by Brightfield microscopy, captured by a smartphone, of untreated (UT) NCI-H716 cells or cells following incubation with respective SCFA (2mM, 24h). **(B)** Cartoon of the unique spindle shape of PYY-positive L-cells in the colon characterised by (Bohórquez et al., 2011).

Next, I investigated these morphological changes via confocal microscopy. Cellular morphologies were visualised by staining with HCS CellMask™ Deep Red Stain which labels the cytoplasm (Figure *5.7A*). Cells were also co-stained for GLP-1, which exhibited a uniform vesicular and ubiquitous distribution in both SCFA-treated and untreated cells that was also indicative of cellular shape. In order to quantify SCFA-mediated morphological changes, binary masks were generated from thresholded images in which the outline of individual cells were represented as separate ROIs. Using this methodology, the area, feret diameter (defined as the longest distance

between any two points along the ROI also known as the caliper length) and circularity of cells could be measured and compared in untreated and SCFA-treated cells.

Butyrate treatment caused a significant ~2- fold and ~1.8-fold increase in cell area and feret respectively (*Figure 5.7B, 5.7C)*. Moreover, circularity (Perimeter^2/4π x Area) measurements, recorded on a scale of 0.0-1.0 with 0.0 representing a polygonal shape and 1.0 representing a perfect circle, indicated a slight reduction of "roundness" in butyrate-treated cells (*Figure 5.7D)*. In comparison to butyrate, 24h treatment with acetate did not induce any significantly different effects on cell size or shape from wild type cells. Propionate-treated cells did in fact display increased areas and ferets, and reduced circularity, though these effects were more modest than with butyrate.



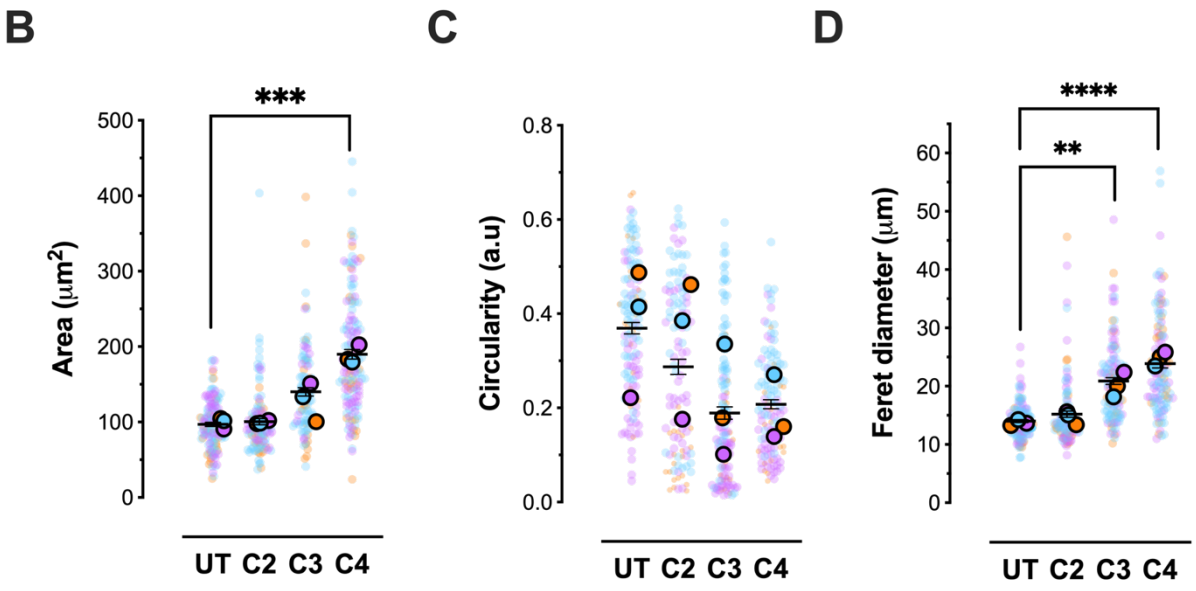


Figure 5.7 Chronic incubation with butyrate increase cell area and feret diameter. (A) Images of untreated (UT) NCI-H716 cells or after treatment with respective SCFA (2mM, 24h) by phase contrast microscopy and confocal microscopy. Cells were fixed and permeabilised before primary antibody labelling with anti-GLP1 antibody followed by labelling with Alexa Fluor 488 secondary antibody. Subsequently, cells were stained with HCS CellMask™ Deep Red Stain and DAPI. Scale bar= 10μm. Conditions were imaged in at least quadruplicates across 3 independent experiments. **(B)** Measurements of Area, (**C)** Feret Diameter, and (**D**) Circularity obtained by automatic particle analysis on thresholded images by ImageJ. Data represent the mean ± SEM of n=120 cells collected across 3 independent experiments. One-way ANOVA: UT vs C2 vs C3 vs C4 (****p<0.0001; ***p<0.001; **p<0.01).

5.2.6 PYY granules are enriched in the cytoplasmic processes of cells chronically treated with butyrate

Considering the 'PYY-bias' in transcriptional and secretory effects of chronic butyrate treatment, I next compared PYY and GLP-1 expression by immunofluorescence in SCFA-treated and untreated cells. Co-staining with anti-PYY and anti-GLP1 antibodies revealed PYY^+ cells were in much lower abundance than $GLP\text{-}1^+$ cells, even after SCFA treatment (*Figure 5.8).* Notably, PYY^+ cells in untreated conditions were spherical, whereas butyrate-treated PYY+ cells were exclusively spindle-shaped. PYY staining also demonstrated presence of the hormone in secretory granules, and

enrichment exclusively in the extending pseudopods of butyrate- but not propionate-treated cells. 100% of PYY^+ cells were also positive for GLP-1 across all conditions (PYY^+ cell = PYY^+ GLP^+ cell).

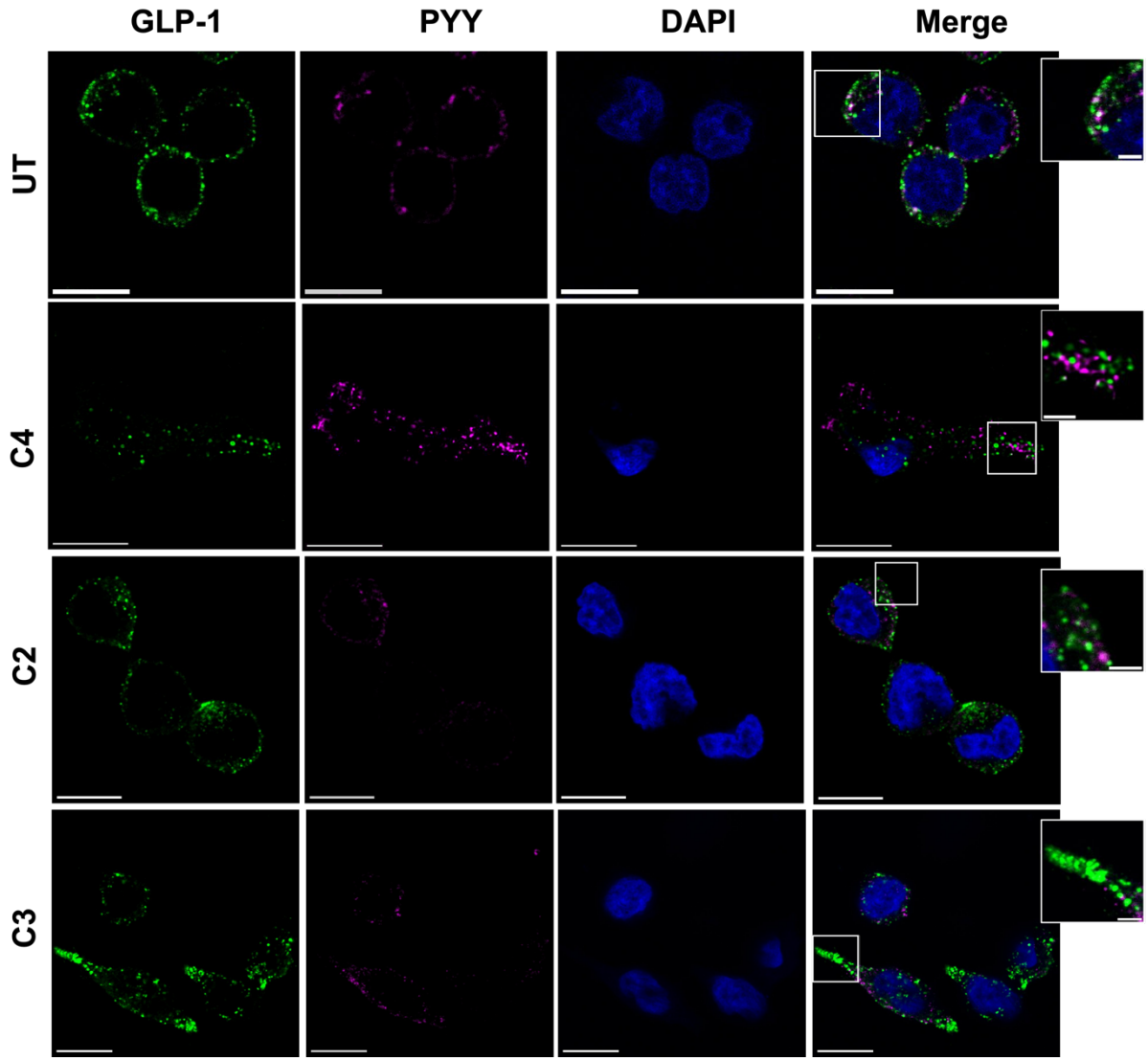


Figure 5.8 PYY granules are enriched in the cytoplasmic processes of cells chronically treated with butyrate. Representative confocal images of untreated (UT) NCI-H716 cells or after treatment with respective SCFA (2mM, 24h). Cells were fixed and permeabilised before primary antibody labelling with anti-GLP1 and anti-PYY antibodies, followed by labelling with Alexa Fluor 488 and 647 secondary antibodies and staining with DAPI. Scale bar= 10μm. Inset scale bar= 2μm. Conditions were imaged in at least triplicates across 5 independent experiments.

5.2.7 Chronic butyrate treatment may not stimulate secretion of intestinotrophic GLP-2

Glucagon peptide-like 2 (GLP-2) is a proglucagon-derived peptide hormone secreted by EECs, with distinct functions from GLP-1. GLP-2 behaves as a paracrine intestinotrophic factor, stimulating cell proliferation and anti-apoptotic effects in the intestinal epithelium (Drucker et al., 1996). Given the upregulatory effects of butyrate on parameters of cell size that I had observed, I questioned a mechanistic involvement of upregulated GLP-2 secretion. As per previous reports, acute stimulation with glucose and forskolin were first investigated as positive controls for GLP-2 secretion, measured by ELISA assays, in NCI-H716 cells (Kuhre et al., 2016) (*Figure 5.9A).* Forskolin was chosen as a positive control for subsequent assays, with acute forskolin stimulation inducing a mean ~ 1.8-fold increase over basal (*Figure 5.9A).* Next, I investigated the effect of prolonged butyrate treated on basal GLP-2 secretory tone as well as on acute responses to forskolin. Preliminary data suggests that chronic treatment with butyrate may not enhance basal nor acute forskolin-stimulated GLP-2 secretion in NCI-H716 cells (*Figure 5.9B)*.

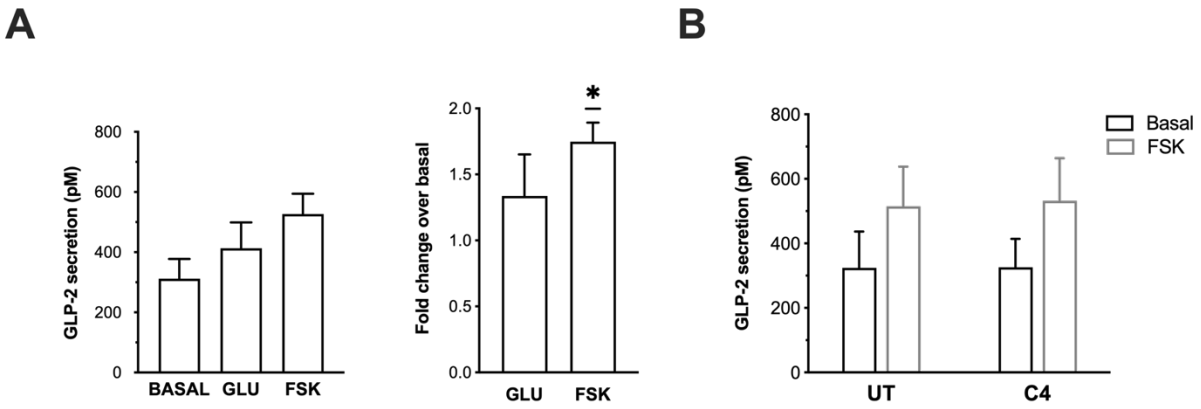


Figure 5.9 Chronic SCFA treatments may not affect GLP-2 secretion. (A) GLP-2 secretion measured in supernatants NCI-H716 cells by ELISA at baseline (basal) or following acute stimulation with glucose (10mM, 2hr) or FSK (50μM, 2hr). Data are also represented as fold change over basal. Data represent the mean ± SEM across three independent experiments run in duplicates. One-sample t-test to 1 (*p<0.05). **(B)** Acute GLP-2 secretion measured by ELISA following treatment with DMSO vehicle (2hr) or FSK (50μM, 2hr) without (UT) or with C2, C3 or C4 pre-treatment (2mM, 24h). Data are also represented as fold change of acute

vehicle or FSK response in SCFA pre-treated cells over the correlating acute response in cells without pre-treatment. Data represent the mean ± SEM across two independent experiments run in duplicates.

5.2.8 SCFAs modulate the gene expression of markers of L-cell differentiation in NCI-H716 cells

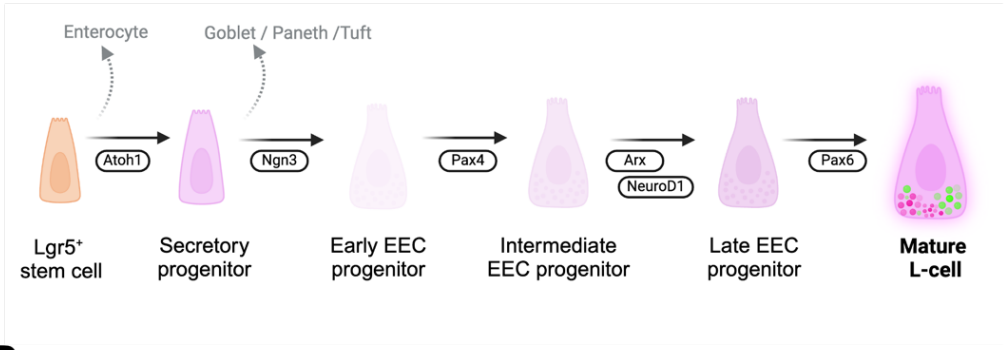
Apart from modulating the endocrine functionalities of EECs within the intestinal milieu, SCFAs have also been shown to influence the differentiation of EECs (Petersen et al., 2014; Brooks et al., 2017; Wang et al., 2022). My observations thus far had implicated chronic butyrate in NCI-H716 cells in promoting an EEC-like morphology and enhancing several parameters of L-cell function. In considering that butyrate might be re-programming NCI-H716 cells towards an exaggerated L-cell like identity, I interrogated the gene expression of key regulators of cell fate checkpoints along the differentiation pathway of L-cells from ISCs.

The canonical pathway by which $Lgr5^{+}$ intestinal stem cells differentiate into EECs comprises of a Notch-sensitive and highly choreographed cascade of the basic helix-loop-helix transcription factors *Atoh1*, *Neurog3* and *NeuroD1* (*Figure 5.10A)* (Schonhoff et al., 2004). *Atoh1*, or *Math1*, is the master transcriptional factor in promoting cell cycle exit and differentiation of multipotent Lgr5+ stem cells in intestinal crypts to a secretory rather than an absorptive lineage (Yang et al., 2001; Kim & Shivdasani, 2011). 24-hour incubation with propionate or butyrate induced a modest decrease in *Atoh1* expression in NCI-H716 cells whereas no change was observed with acetate *(Figure 5.10B).* Downstream of regulation by *Atoh1*, secretory progenitors can divergently progress into Paneth cell, goblet cell or EEC cell fates. (Yang et al., 2001). The transcription factor *Neurog3* is transiently expressed in common secretory progenitors, guiding differentiation into early EEC precursors (Jenny et al., 2002). Butyrate induces a modest ~25% decrease in *Neurog3* expression *(Figure 5.10B).* No conclusive trends can be observed in *Neurog3* expression in acetate- or propionate-treated cells and this target consistently demonstrated a high-degree of inter-repeat/inter-passage variation in basal and SCFA-treated conditions. Next, I investigated the effect of chronic butyrate on the expression of *NeuroD1*, the

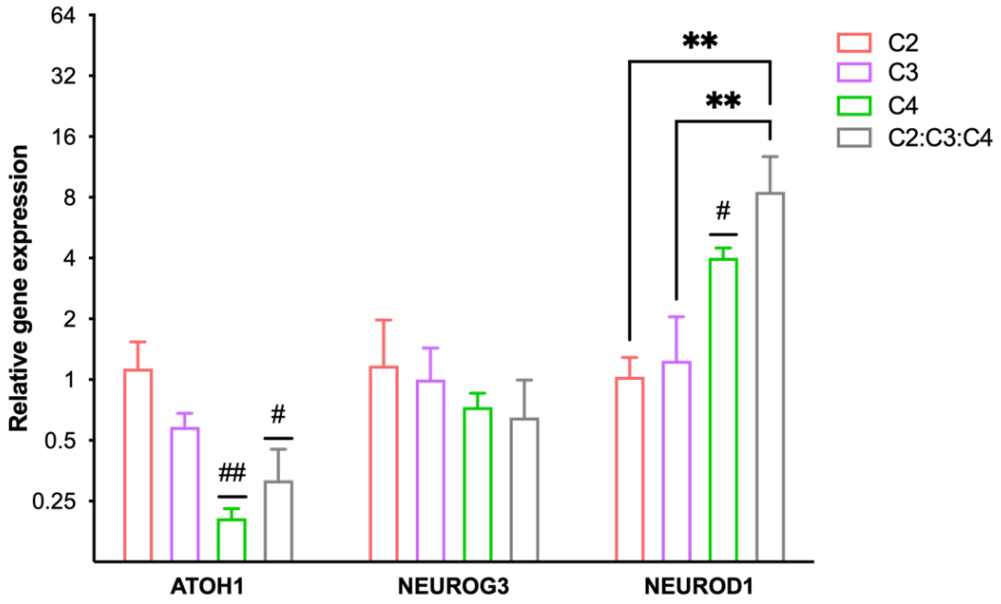
downstream target of *Neurog3* which has been implicated in the terminal differentiation into specific enteroendocrine lineages (Naya et al., 1997; Gehart et al., 2019). Notably, *NeuroD1* expression was significantly increased by ~4 fold in butyrate-treated cells compared to untreated cells, however no changes were observed with acetate or propionate treatment *(Figure 5.10B).* No significant differences in gene expression of the *Atoh1-Neurog3-NeuroD1* cascade between C4 and C2:C3:C4 treatment were evident.

Downstream of the *Atoh1-Neurog3-NeuroD1* cascade, other transcription factors participate in specifying the differentiation into EEC sub-lineages *(Figure 5.10A*). The activity of the homeodomain transcription factors *Pax4, Arx* and *Pax6* have specifically been mapped to the production of GLP^+ and/or PYY^+ EECs *in vivo* and *in vitro* (Hill et al., 1999; Beucher et al., 2012; Brooks et al., 2017; Gehart et al., 2019). Prolonged butyrate treatment significantly downregulated the expression of *Arx* but more so *Pax4*, whereas data suggested acetate might upregulate levels of these both transcripts *(Figure 5.10C).* In contrast, expression of the transcription factor *Pax6*, which has previously been characterised as a direct downstream target *NeuroD1*, was significantly upregulated ~10 fold by butyrate (Marsich et al., 2003). A much more modest increase in *Pax6* expression, ~ 2-fold, was observed in propionate-treated cells, and no change could be measured with acetate. Incubation with C2:C3:C4 induced similar effects to butyrate on *Arx* and *Pax6* expression however did not decrease *Pax4* transcript abundance (*Figure 5.10C).*

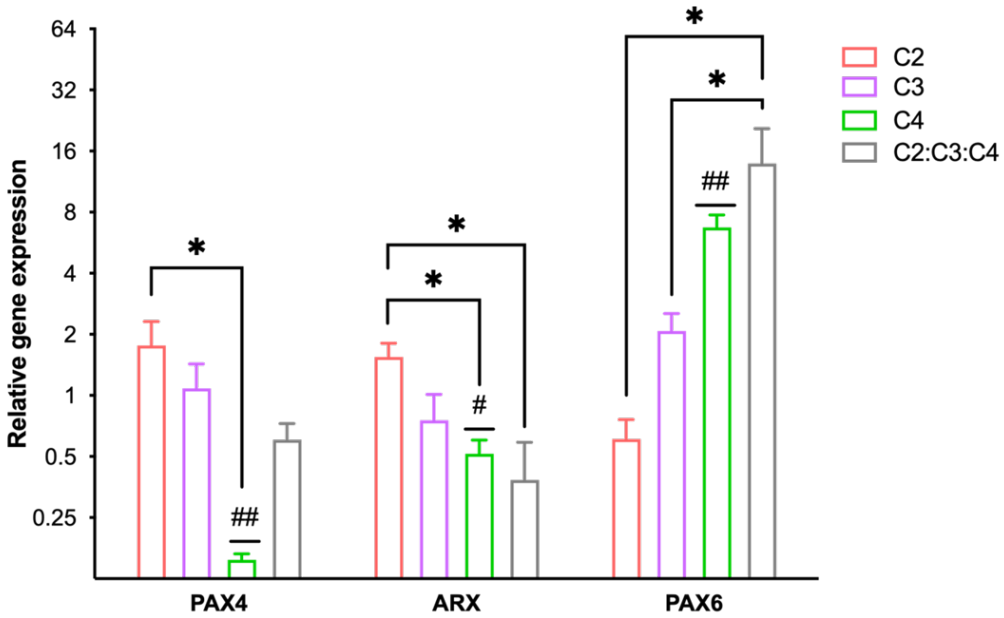
A


Enterocyte
Goblet / Paneth /Tuft
Atoh1
Ngn3
Pax4
Arx
NeuroD1
Pax6
Lgr5⁺ stem cell
Secretory progenitor
Early EEC progenitor
Intermediate EEC progenitor
Late EEC progenitor
Mature L-cell

B


Relative gene expression
64
32
16
8
4
2
1
0.5
0.25
C2
C3
C4
C2:C3:C4
**
**
#
#
##
ATOH1
NEUROG3
NEUROD1

C


Relative gene expression
64
32
16
8
4
2
1
0.5
0.25
C2
C3
C4
C2:C3:C4
*
*
*
*
#
##
##
PAX4
ARX
PAX6

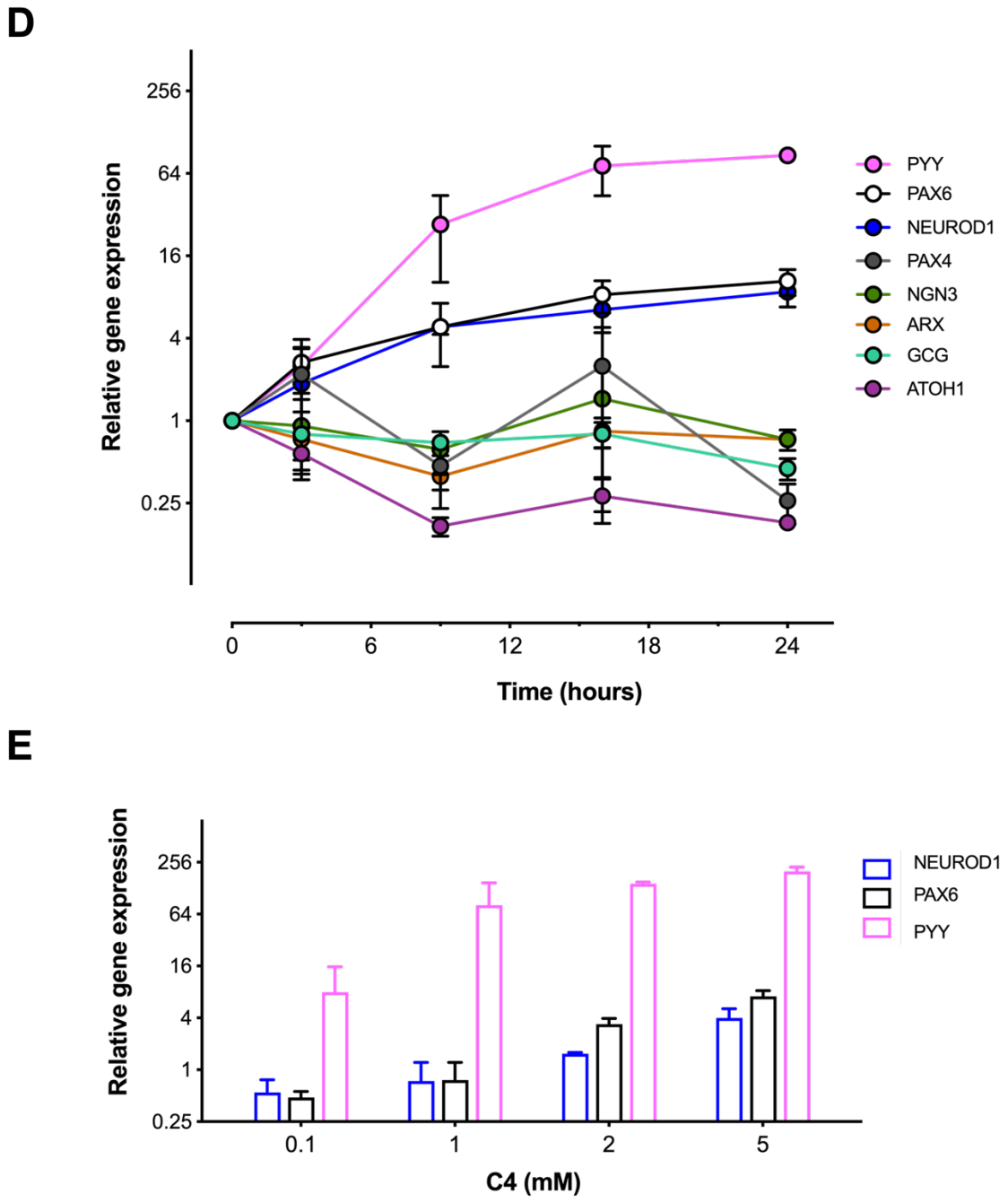


Figure 5.10 Chronic butyrate treatment affects the expression of L-cell differentiation markers. (A) Schematic depicting the pathways underlying the differentiation of intestinal Lrg5^{+} stem cells to absorptive or secretory lineages. (**B)** Relative gene expression of master regulators of enteroendocrine (EEC) cell differentiation, *Atoh1, Neurog3* and *NeuroD1* or (**C)** regulators of L-cell specific differentiation, *Pax4, Arx,* and *Pax6*, in NCI-H716 cells treated with C2, C3, or C4 (2mM, 24h) or C2:C3:C4 (6mM C2, 2mM C3, 2mM C4, 24h) determined by the 2--ΔCt method using *Rpl12* housekeeping gene. One-way ANOVA: C2 vs C3 vs C4 vs C2:C3:C4 (**p<0.01; *p<0.05). Unpaired t-test vs UT: ($^{\#\#}$p<0.01; $^{\#}$p<0.05). **(D)** Relative gene

expression of *Pyy, Pax6, NeuroD1, Pax4, Neurog3, Arx, Gcg* and *Atoh1* in NCI-H716 cells incubated with C4 (2mM) measured from 3h-24h after ligand treatment. Relative gene expression was determined by the 2--ΔCt method using *Rpl12* housekeeping gene Data are mean ± SEM, n=3 (B) and conditions were run in at least triplicate per independent experiment. **(E)** Relative gene expression of *NeuroD1*, *Pax6* and *Pyy* in NCI-H716 cells incubated with varying of concentrations of C4 (0.1-5mM) for 24h. Relative gene expression was determined by the 2--ΔCt method using *Rpl12* housekeeping gene. Data are mean ± SEM, n=2 and conditions were run in at least triplicate per independent experiment.

Next, butyrate-mediated transcriptomic changes on markers of master EEC differentiation, in addition to L-cell specific markers were temporally characterised (*Figure 5.10D).* Butyrate appeared to upregulate the expression of *NeuroD1, Pax6 and Pyy* in a time-dependent manner whereas no prominent trends were apparent in the temporal profiles of other differentiation markers. In addition, butyrate-mediated downregulation of GCG transcript levels increased over time. The upregulation of butyrate on *NeuroD1, Pax6 and Pyy* was also assessed at varying concentrations of the SCFA (*Figure 5.10E).* My preliminary findings suggested a concentration-dependency in the effects of butyrate on all three genes.

Overexpression of the canonical stem cell marker *Lgr5* is characteristic of human colorectal cancers and has been implicated in the proliferative behaviours of CRC cells in primary tumour growth (de Sousa e Melo et al., 2017; Hirsch et al., 2014; B. G. Jang et al., 2018). Unsurprisingly, *Lgr5* is also expressed in several CRC cell lines, including NCI-H716 (Uhlén et al., 2015). Given that I had observed a significant modulation of the expression of key transcription factors involved in the ISC to EEC differentiation cascade by butyrate, it was important to assess whether the SCFA might also affect *Lgr5* expression in this cell line (*Figure 5.11)*. *Lgr5* transcripts were detected in NCI-H716 cells; butyrate did cause a mean ~ 6-fold increase in *Lgr5* gene expression however significance was limited due to biological variability.

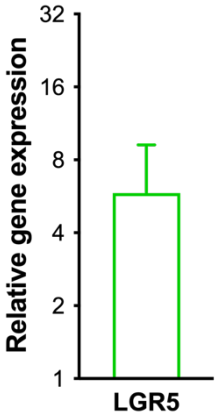


Figure 5.11 Butyrate upregulates the gene expression of *Lgr5* in NCI-H716 cells. Relative LGR5 expression in NCI-H716 cells treated with C4 (2mM, 24h). Relative gene expression was determined using the 2--ΔCt method using *rpl12* housekeeping gene. Data are mean ± SEM, n=3 and conditions were run in at least triplicate per independent experiment.

5.2.9 The FFAR2-Gαi agonist AZ-1729 upregulates *Pax6* expression in NCI-H716 cells

Next, I questioned whether AZ-1729 might recapitulate the upregulatory effects of butyrate I had observed on *NeuroD1* and *Pax6*. AZ-1729 induced a significant upregulation of *Pax6* but not *NeuroD1* (*Figure 5.12A).* Moreover, co-treatment with C4 and AZ-1729 appeared to have a synergistic effect on *Pax6* expression, significantly enhancing the response of C4 (*Figure 5.12B).* These findings suggested an involvement of the FFAR2-Gαi axis in the transcriptomic regulation of *Pax6* in NCI-H716 cells.

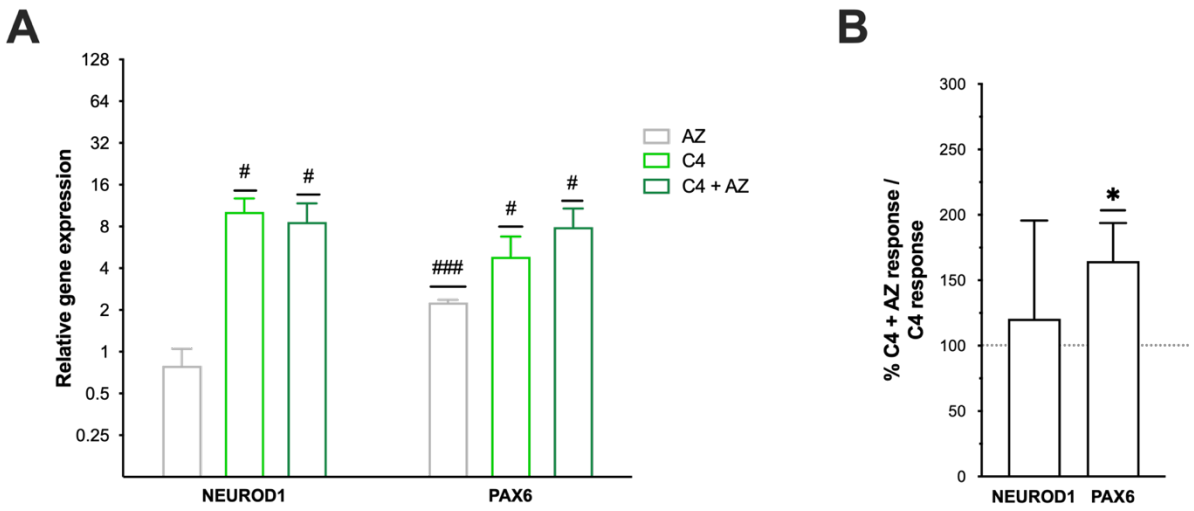


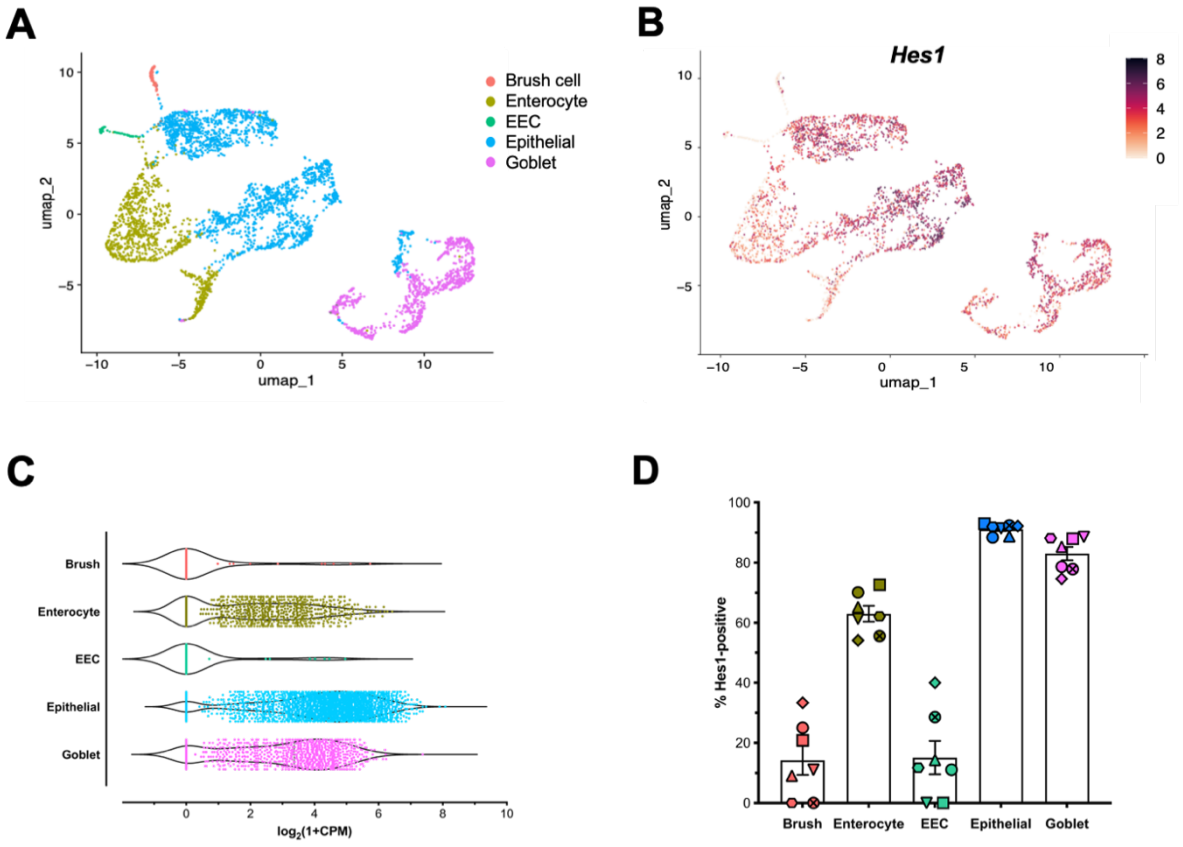
Figure 5.12 AZ-1729 upregulates the gene expression of *Pax6* but not *NeuroD1* in NCI-H716 cells. (**A)** Relative *NeuroD1* and *Pax6* expression in NCI-H716 cells treated with FFAR2 biased agonist AZ-1729 (1μM, 24h), C4 (2mM, 24h), or a combination of C4 (2mM, 24h) and AZ-1729 (1μM, 24h). Relative gene expression was determined using the 2--ΔCt method using *Rpl12* housekeeping gene. Unpaired t-test vs untreated (UT): ($^{###}$p<0.01; $^{#}$p<0.05). (**B)** Relative gene expression normalised as a % change of C4+ AZ / C4 response. Data are mean ± SEM, n=3 and conditions were run in at least triplicate per independent experiment. Unpaired T Test C4 + AZ-1729 response vs C4 response (100%) (*p<0.05).

5.2.10 Monitoring butyrate-mediated Notch activity using Hes1-GFP mouse colonic organoids

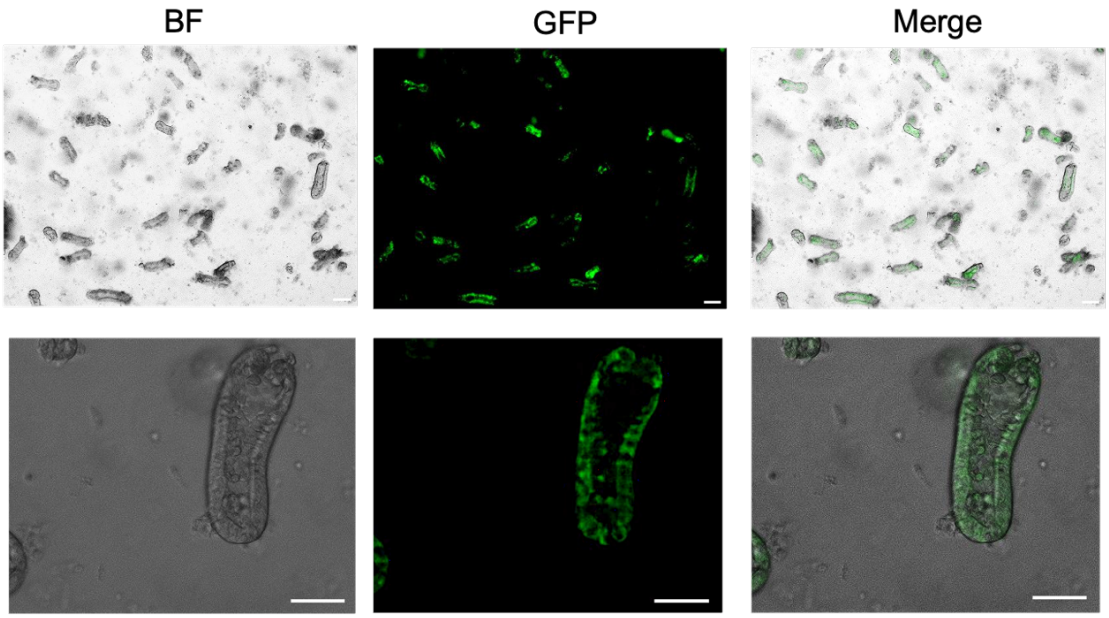
My *in vitro* findings thus far show that butyrate exerts significant effects on the gene expression of transcription factors which have been implicated in Notch-sensitive EEC differentiation cascades *in vivo.* However, the NCI-H716 cell line is undoubtedly disadvantaged in its physiological relevance to the human colon due to a) its cancerous origin b) its immortalised nature. In comparison, organoid cultures grown from isolated colonic ISCs promise a more relevant representation of the colon due to their retention of cellular heterogeneity and function, as well their 3D structures which resembles *in vivo* tissue architecture (Corrò, Novellasdemunt & Li, 2020)**.** Next, I investigateD the effects of butyrate on intestinal epithelial secretory lineage differentiation in colonic organoid models. Organoids were to be established from a previously described Notch reporter mouse, Hes1-GFP (Fre et al., 2011). The expression of GFP in this model under the control of the endogenous promoter of the Notch-target gene *Hes1*, thereby allowing the detection of transcriptional activity of Notch in situ. Briefly, *Hes1* is highly expressed in ISCs and is important in maintaining their proliferative status (Fre et al., 2011; Ueo et al., 2012). In addition, *Hes1* antagonises secretory lineage differentiation in ISCs and proliferating transit-amplifying (TA) cells with 'high-Notch' activity by directly repression of *Atoh1* expression. Notch activation suppresses the production of cell surface Notch ligands, and thereby the juxtacrine activation of Notch in neighbouring cells, known as lateral inhibition (Sancho, Cremona & Behrens, 2015). The de-repression of Atoh1 in 'low-Notch' neighbours permits NEUROG3-mediated secretory lineage commitment.

First, I aimed to validate the expression of *Hes1* across the mouse large intestinal epithelium at single-cell resolution using the publically-available *Tabula Muris* database (Tabula Muris Consortium, 2018; Hao et al., 2024). Data was categorised into five pre-defined cellular ontology classes *(Figure 5.13A)* which were visualised by gene expression enrichment of classical markers; *Lgr5* and *Mki67* in the epithelial class, *Slc26a3* in enterocytes, *Dclk1* in brush cells, *Spdef* in goblet cells, and *Chga* in EECs *(Appendix 1)* (Tabula Muris Consortium, 2018). *Hes1* expression was ubiquitous amongst the epithelial cell class as well as enterocytes, and low amongst the secretory

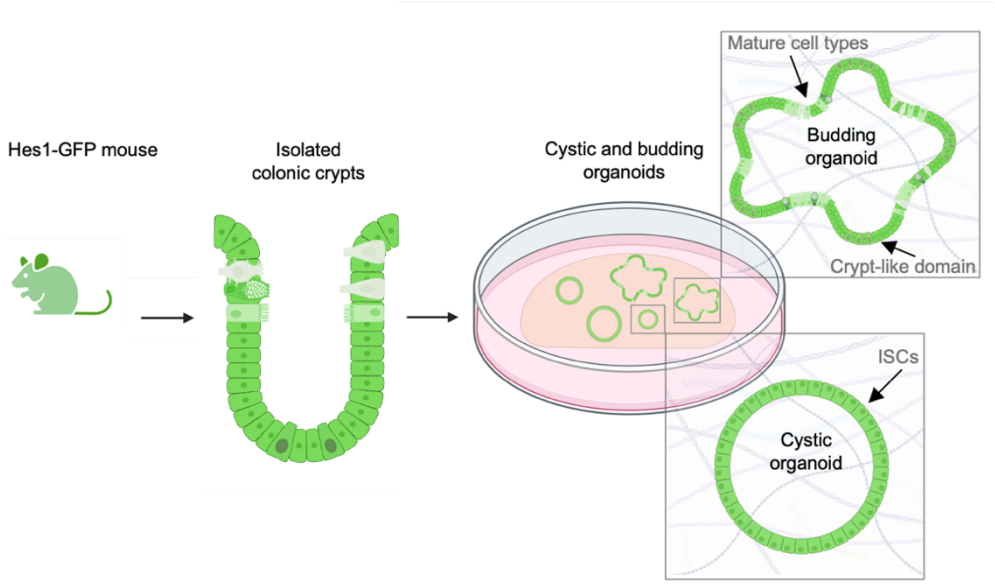
lineages, EEC and brush cells. *Hes1*-positive cells were counted and separated by cell ontology identities (*Figure 5.13B, C)*. *Hes1* expression was also computed as % of cells positive per ontology class. ~20% of brush and EEC populations were positive for *Hes1*, whereas *Hes1* expression was detected in ~70% and ~90% of enterocytes and epithelial cells respectively *(Figure 5.13D)*. Surprisingly, ~80% of goblet cells were positive for *Hes-1*. Notably, non-canonical Hes1 expressing goblet cells specific to the colonic epithelium have recently been characterised (Nyström et al., 2021).



E


BF
GFP
Merge

F


Hes1-GFP mouse
Isolated colonic crypts
Cystic and budding organoids
Mature cell types
Budding organoid
Crypt-like domain
ISCs
Cystic organoid

G

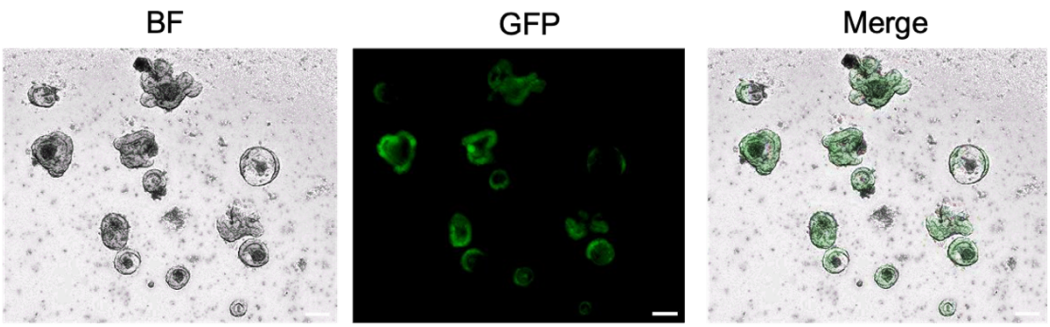

BF
GFP
Merge

Figure 5.13 Employing a Hes1-GFP reporter mouse model. Uniform Manifold Approximation and Projection (UMAP) visualisation of the Large Intestine *Tabula Muris* single-cell RNA-seq (scRNA-seq) dataset with cells coloured by **(A)** ontology class; Brush (*red)*, Enterocyte (*khaki),* EEC (*turquoise),* Epithelial (*blue),* Goblet (*pink)* **or (B)** log_2CPM-normalised Hes1 expression level. (**C)** Violin plot depicting log_2CPM-normalised Hes1 expression between cell ontology classes. Data points represent individual cells. **(D)** Percentage of cells per ontology class with log2CPM-normalised Hes1 expression > 0. Distinct symbol shapes represent mean % per cell ontology class in individual mice, n=7 mice**. (E)** Representative brightfield (BF), GFP channel and merged images (at 4x and 20x) of isolated crypts from Hes1-GFP mice imaged live on a fluorescent microscope. Scale bar = 100µm. **(F)** Schematic of pipeline of establishment of Hes1-GFP organoid cultures. **(G)** Representative images of Hes1-GFP organoids at passage 2 (P2) imaged live on a fluorescent microscope. Scale bar = 200µm. n=100 organoids from n=3 mice captured.

Isolated Hes1-GFP colonic crypts exhibited a mosaic-like GFP expression at both the ISC-rich crypt base, and the upper-crypt where differentiated IEC populations reside *(Figure 5.13E)*. Crypts were grown in Matrigel and within a week formed a mixture of two organoid populations with distinct morphologies typical of mouse intestinal organoid cultures were observed; 'cystic' population and a 'budding' population *(Figure 5.13F)*. "Cystic" organoids consist of a lumen surrounded by a thin epithelial monolayer of stem cells akin to populations of continuously dividing ISCs at that occupy the base of crypts and support homeostatic renewal in the intestinal stem cell niche *(Figure 5.13G)* (Barker et al., 2007). Mature "budding" organoids consist of projections of crypt-base-like domains, enriched in proliferative stem cells, which are separated from upper-crypt-like domains in which late-stage progenitors and mature differentiated cells of both absorptive and secretory lineages reside *(Figure 5.13G)*. As such, budding organoids recapitulate the *in vivo* architecture and functional compartmentalisation of stem cell and differentiated zones in the intestinal colonic crypt (Dou et al., 2022; Sato, Stange, et al., 2011). As scRNAseq analysis indicated that *Hes1* is expressed across stem and some differentiated populations in the mouse colonic epithelium, the patterns of GFP expression observed in crypts, cystic and budding organoids was affirming.

To confirm the validity of the Hes1-GFP reporter system and measuring GFP fluorescence as a readout of Notch activity, organoids were pulse-treated with a diazepine inhibitor of ɣ-secretase (DBZ) (*Figure 5.14).* Within 48 hours of DBZ treatment, GFP signal was completely depleted from the cellular domains of both cystic and budding organoids indicating successful blockade of Notch activity.

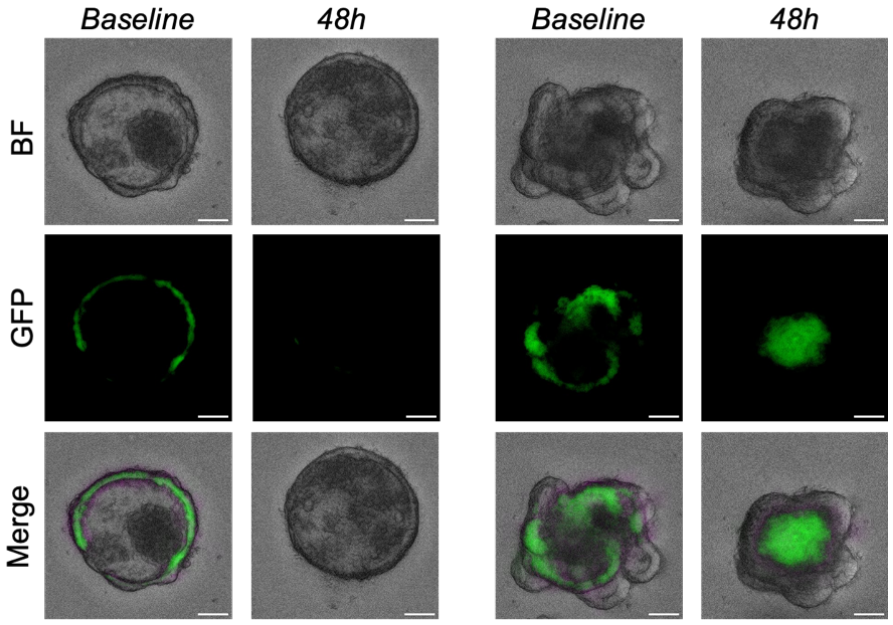


Figure 5.14 A ɣ-secretase inhibitor diminished GFP fluorescence in Hes1-GFP reporter mice. Representative brightfield (BF), GFP channel and merged images of a cystic (left) and a budding (right) organoid at baseline, and 48h after a 3hr pulse-chase treatment with 5μM of the diazepine DBZ inhibitor DBZ imaged live on a fluorescence microscope. n=10 cystic and budding organoids captured from n=2 mice. Scale bar = 50μm.

To investigate the effects of butyrate on Notch-dependent differentiation in the intestinal epithelium, Hes1-GFP organoid cultures were incubated with 2mM butyrate for 72 hours and GFP fluorescence was monitored periodically on a single organoid basis. Mean GFP-fluorescence of cystic untreated organoids significantly increased in a time-dependent manner across 0 to 72 hours *(Figure 5.15A)*. In contrast, no significant change in mean fluorescence from baseline was measured in butyrate-treated organoids. When fluorescent changes over time are mapped per organoid *(Figure 5.15B)*, three outcomes summarise trends in untreated cystic populations; (a.) a decrease in fluorescence which accompanied a tendency to transition to a budding morphology (b.) a moderate fold ~1.2-1.3 change increase in fluorescence or

morphology or the most common outcome (c.) which was a large (> 1.5) fold change increase in fluorescence and no change from cystic morphology *(Figure 5.15C)*. In contrast, the most common outcome in butyrate-treated cystic organoids was a (d.) time-dependent decrease in fluorescence to as low as ~ 0.2 fold change over baseline, followed by a (e.) moderate ~0.8 fold change decrease or no change from baseline,

and thirdly (f.) a moderate time-dependent increase in fluorescence which does not exceed ~1.5 fold change over baseline (*Figure 5.15D).*

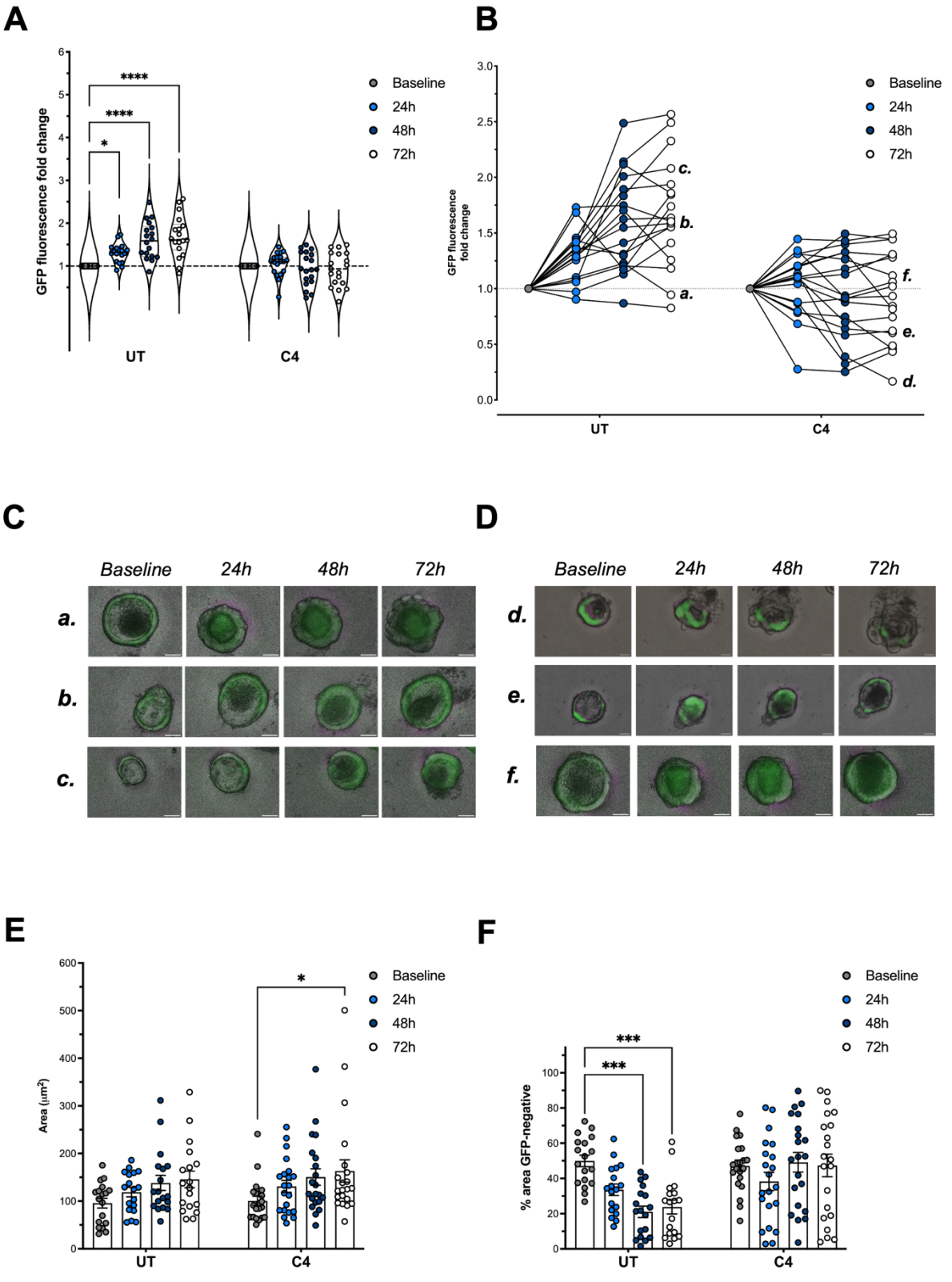


Figure 5.15 Butyrate modulates the GFP fluorescence and area of Hes1-GFP cystic organoids. Individual cystic organoids were imaged by a fluorescence microscope across 0 to 72h in untreated (UT) conditions and following treatment with 2mM butyrate (C4) at 24hrs; Baseline/0h *(grey),* 24h (*blue),* 48h (*navy),* 72h *(white).* Individual organoids represented by individual symbols. Data are represented as mean ± SEM of total n=19 organoids at each time point per condition which were established from n=4 mice. Two-way ANOVA: 0h vs 24h vs 48h vs 72h in UT or C4 conditions (*p<0.05; ***p< 0.001; ****p<0.00001). (**A & B**) GFP fluorescence represented as fold change over baseline on an individual organoid basis. Lines in B represent time-dependent trends of individual organoid fluorescence. Representative UT outcomes (a. b. & c) and C4-treated outcomes (d. e. and f) are indicated in (**C**) and (**D**) respectively. Brightfield (BF), GFP channel (GFP) and merged images are shown per organoid. Scale bar= 50μm. (**E**) Area per organoid and (**F**) area GFP-negative represented as a % of area per organoid are shown.

Moreover, area per organoid was measured for individual organoids at each time point and was not significantly different in untreated cystic populations, however butyrate significantly increased organoid area 72h after treatment *(Figure 5.15E)*. In parallel to the observed trends in fluorescence fold changes, untreated organoids exhibited a time-dependent decrease in mean % negative area, which was significant at 48 and 72h, however no significant changes were evident in butyrate-treated cystic populations *(Figure 5.15F).*

Next, corresponding analyses were carried out on budding organoids. The mean fluorescence fold change over basal was not significantly different in untreated organoids at any time-point, however it significantly decreased in time-dependent manner in butyrate-treated budding organoid populations *(Figure 5.16A)*. Three time-dependent trends were observed amongst the untreated budding population of organoids (*Figure 5.15B)*; (a) a modest decrease to ~0.8-fold change over baseline or no change from baseline b. a moderate ~1.2-fold change increase or c. a large ~1.5-fold change increase (*Figure 5.15C)*. In contrast, most butyrate-treated budding organoids exhibited a decrease in fluorescence fold change from baseline which was d. large (dropping to ~0.2-fold change over baseline) or e. moderate (dropping to ~0.7-0.8 fold change over baseline), or exhibited (f.) next to no change from baseline (*Figure 5.16D).* No qualitative or quantitative differences in morphology or area measurements

respectively were evident between untreated- and butyrate-treated budding populations *(Figure 5.15E)*. However, % GFP-negative area significantly increased in a time-dependent manner in butyrate-treated but not untreated budding organoids *(Figure 5.15F)*.

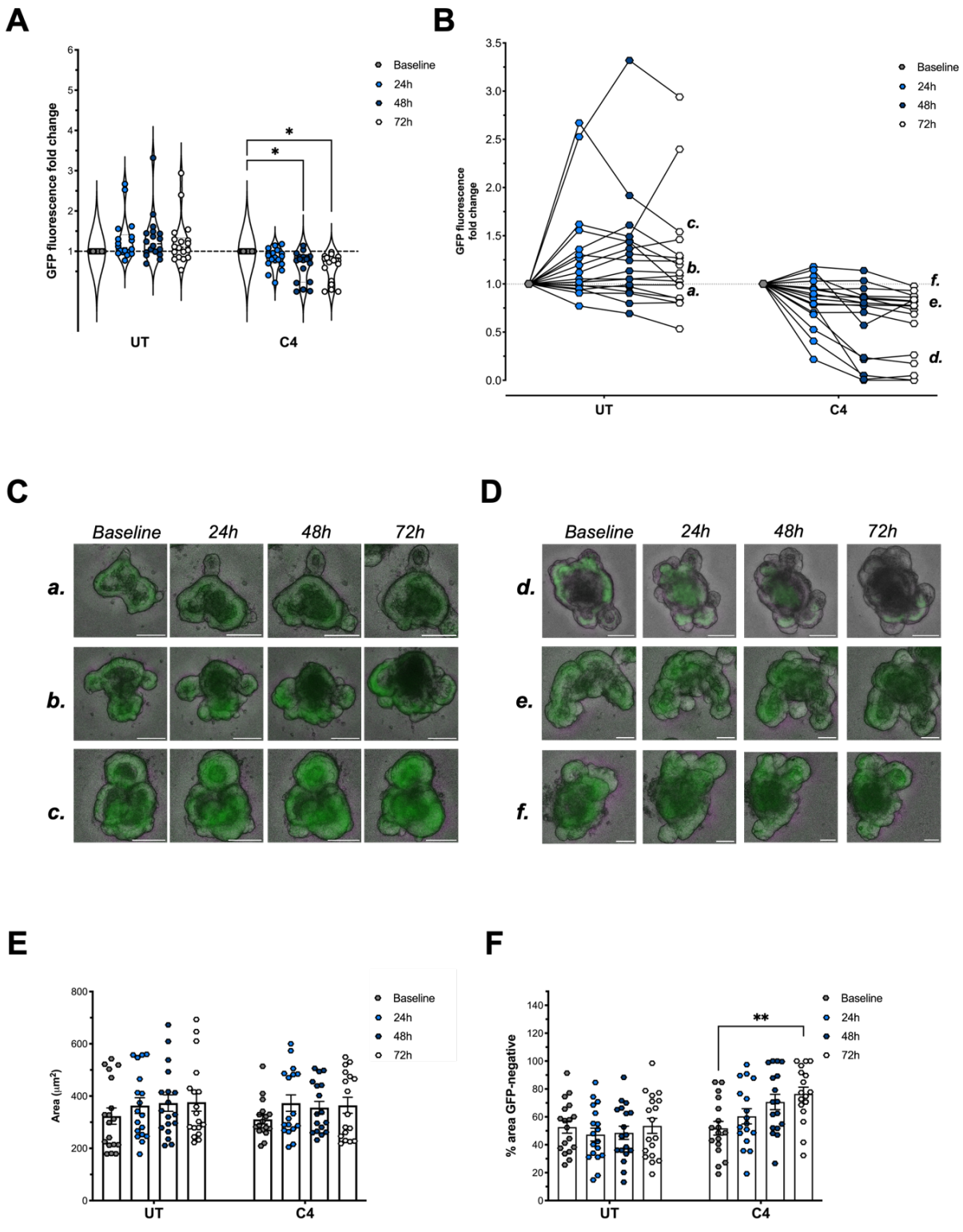


Figure 5.16 Butyrate downregulates the GFP fluorescence of budding Hes1-GFP organoids in a time-dependent manner. Budding organoids were imaged by a fluorescence microscope across 0 to 72h in untreated (UT) conditions and following treatment with 2mM butyrate (C4) at 24hrs; Baseline/0h *(grey),* 24h (*blue),* 48h (*navy),* 72h *(white).* Individual organoids represented by individual symbols. Data are represented as mean ± SEM of total n=18 organoids at each time point per condition which were established from n=2 mice. Two-way ANOVA: 0h vs 24h vs 48h vs 72h in UT or C4 conditions (*p<0.05; ***p< 0.01). (**A & B)** GFP fluorescence represented as fold change over baseline on an individual organoid basis. Lines in B represent time-dependent trends of individual organoid fluorescence. Representative UT outcomes (a. b. & c) and C4-treated outcomes (d. e. and f) are indicated in **(C)** and (**D)** respectively. Brightfield (BF), GFP channel (GFP) and merged images are shown per organoid. Scale bar= 50μM. (E) Area per organoid and (F) area GFP-negative represented as a % of area per organoid are shown.

Preliminary immunostaining analyses indicated an upregulation of PYY in butyrate-treated budding organoids *(Figure 5.17).* PYY-immunoreactivity was predominantly localised to GFP-negative regions. These findings suggest that butyrate might promote the differentiation of intestinal epithelial cells to PYY-positive ‘low-Notch’ cell fates in the mouse colon.

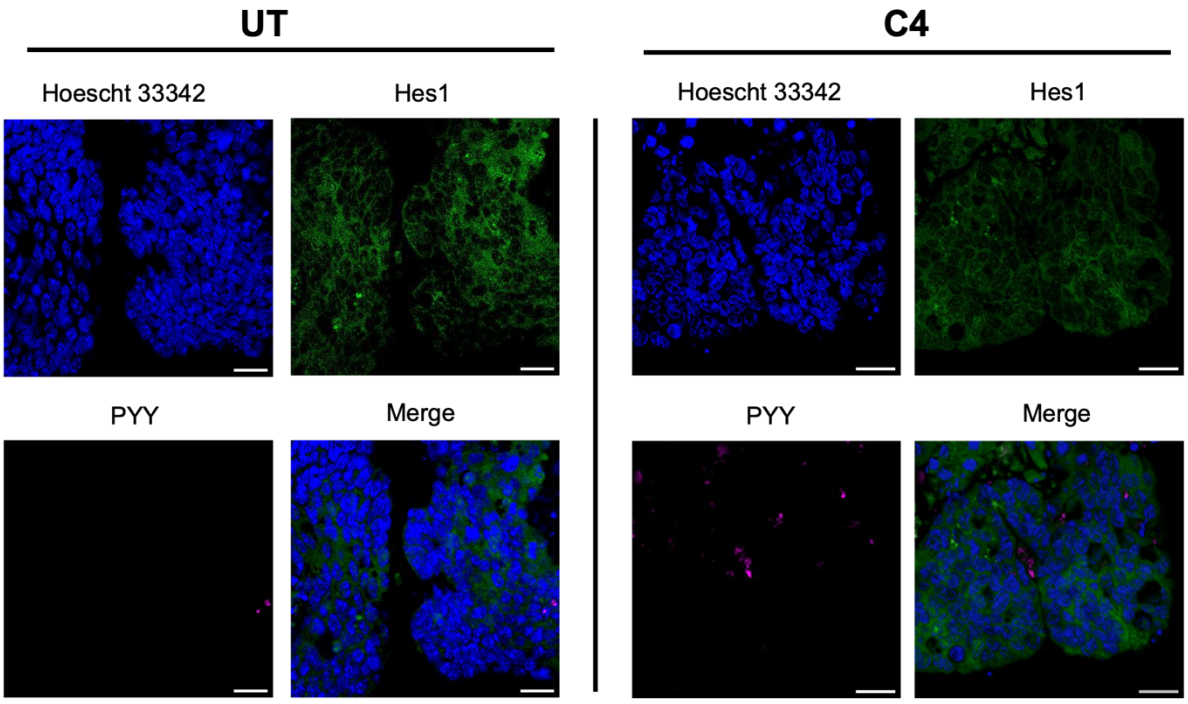


Figure 5.17 Butyrate appears to upregulate the expression of PYY in mouse Hes1-GFP colonic organoids. Representative confocal images of untreated (UT) mouse colonic organoids, or after 48h treatment with 2mM C4. Organoids were fixed onto chamber slides, permeabilised and labelled with primary anti-PYY antibody. Secondary antibody labelling was carried out with Alexa Fluor 647 in the presence of Hoescht 33342 stain. Glass coverslips were mounted using ProLong Gold AntiFade Mountant. Scale bar= 20μm. 6 organoids were imaged per condition, n=1 independent experiment.

5.2.11 Butyrate downregulates the expression of Lgr5 in Lgr5 lineage-tracing mouse colonic organoids

Since I had observed significant butyrate-driven changes in the Notch activity of cystic organoids, which are enriched in ISCs, my next experiment aimed to isolate the effects of butyrate on Lgr5+ ISCs in particular. Organoids were established from primary crypts of an Lgr5 lineage tracer mouse (Lgr5$^{+/-}$, Rosa26-tdTomato$^{+/-}$); in this model, treatment with 4-OH tamoxifen (4-OHT) induces recombination and permanent tdtTomato labelling of all Lgr5+ stem cells and their progeny within 24h. Organoids were treated with butyrate, and then treated with 4-OHT 24 hours later to label Lgr5-positive cells *(Figure 5.17A)*. Labelling with 4-OHT revealed that 40-80% of the area

(excluding the lumen) of untreated organoids were positive for Lgr5 *(Figure 5.17B)*. In comparison, butyrate-treated exhibited a significantly lower Td-tomato positive-area per organoid on average, however there was an indication of two kinds of responders; half of the butyrate-treated population exhibited 20% or less of Lgr5-positive labelling, whereas the other half mirrored the results of the untreated population with >40% labelling. These results suggest that butyrate might encourage a loss of stemness and potentially subsequent initiation of differentiation in a subset of Lgr5+ ISCs.

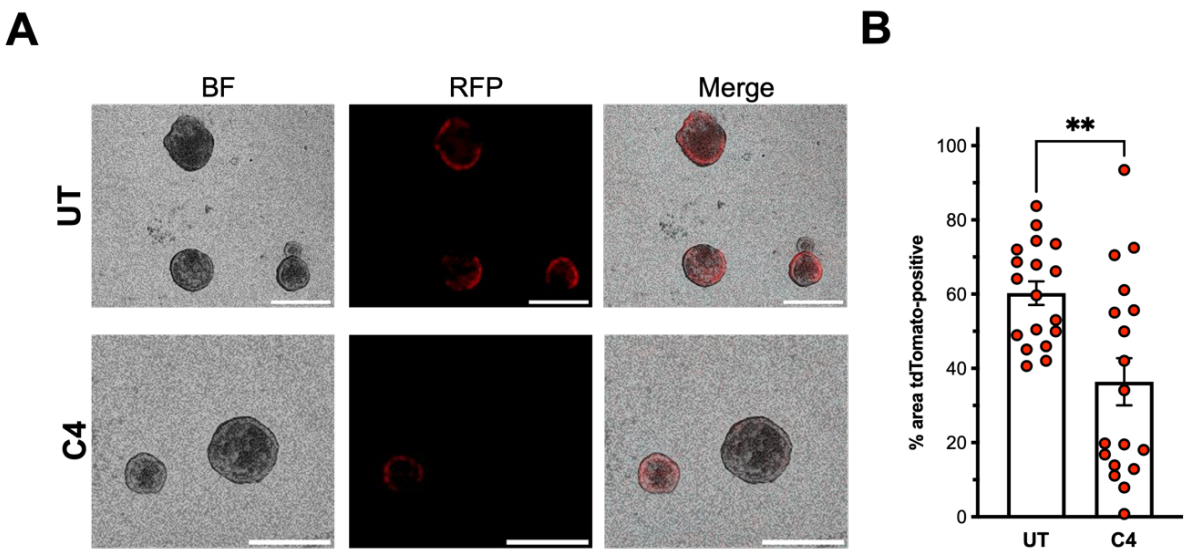


Figure 5.18 Butyrate decreases the abundance of Lgr5+ cells in cystic organoids. Organoids were established from a Lgr5-lineage tracer mouse. Organoids were treated with 2mM butyrate (C4) was added for 48 hours, or left untreated (UT), and 4-OH tamoxifen was added to the culture medium at 24 hours. (**A)** Representative brightfield (BF), RFP channel (RFP) and merged (merge) images of Lrg5-lineage tracer organoid imaged on a fluorescence microscope. Scale bar = 50µm. **(B)** % of area tdTomato-positive in untreated (UT) or butyrate-treated (C4) cystic organoids 24 hours after tamoxifen treatment. Data represent mean ± SEM of n=18 organoids per condition derived from n=1 mouse. Symbols represent individual organoids. t-test: UT vs C4 (**p<0.01).

5.3 Discussion

In this chapter, I explored the effects of SCFAs on EEC differentiation in the intestinal stem cell niche using two model systems. In NCI-H716, I demonstrated unique effects of SCFAs and the pharmacological FFAR2-Gαi agonist AZ-1729 on the expression of enterohormone, markers of EEC differentiation, and on cellular morphology. In mouse colonic organoids, I assessed the effect of butyrate on the differentiation of both immature (ISC) and mature (differentiated) cell-types, focusing particularly on transcriptional activity of Notch, using a Hes1-GFP reporter line, and the expression of Lgr5, using a Lgr5-lineage tracing line.

5.3.1 NCI-H716 cells

The effects of prolonged SCFA incubations on *Pyy* and *Gcg* expression in NCI-H716 cells were strikingly different to the respective secretory profiles induced by acute SCFA stimulation in *Chapter 4.* In contrast to their potency as acute GLP-1 secretagogues, propionate and butyrate in fact downregulated *Gcg* mRNA expression. In comparison, all three SCFAs stimulated a significant increase in PYY gene expression, in contrast to their ineffectiveness as acute PYY secretagogues. A previous report by Cao et al. have demonstrated a downregulatory effect of canonical GLP-1 secretagogues such as forskolin on *Gcg* expression in this cell line. Despite detecting the expression of several transcription factors that modulate *Gcg* transcription, Cao et al. observed a total transcriptional inactivity of promoter sequences implicated in the control of *Gcg* expression in NCI-H716 cells; it is possible that the regulation of *Gcg* expression in NCI-H716 cells may not be reflective of mechanisms in the healthy colon. Butyrate stimulated the largest decrease and increase in *Gcg* and *Pyy* expression respectively out of all 3 SCFAs. For both enterohormones, co-incubation with all three SCFAs (C2:C3:C4) at concentrations to mimic the physiological luminal ratio (60:20:20, C2:C3:C4) did not significantly outperform butyrate treatment, further emphasising the role of butyrate in these effects.

The ‘PYY-bias’ of transcriptional effects following prolonged butyrate treatment was also reflected in secretory profiles; my preliminary ELISA findings suggested an upregulation in basal PYY secretion of NCI-H716 cells following 24h of butyrate treatment, however no significant effect of this treatment was evident on basal or acute ligand-induced profiles of RIA-detected GLP-1 secretion. Beyond its functionality as a ligand of FFAR2, butyrate has been widely shown to affect gene expression in several cell types *via* histone deacetylase (HDAC) inhibition (Rada-Iglesias et al., 2007; Ozkan et al., 2023; Chriett et al., 2019; Bridgeman et al., 2021; Davie, 2003). Notably, a previous study in the NCI-H716 cell line has reported that class I and II HDAC inhibitors (HDACi) such as trichostatin A and valproic acid recapitulate the strong upregulatory effect of butyrate on *Pyy* expression (Larraufie et al., 2018). However, this study also reported a partial inhibitory effect of CRISPR/Cas9-mediated FFAR2-depletion in NCI-H716 cells on butyrate-mediated *Pyy* upregulation, suggesting a mechanistic involvement of the receptor (Larraufie et al., 2018). In my findings, exposure to the FFAR2-selective antagonist GLPG0974 induced 50% reduction in butyrate-mediated *Pyy* upregulation which is comparable to the inhibitory effect of FFAR2 knockout reported by Larraufie et al., (2018). However, the concentration of antagonist employed inhibited ~80% of the Gαi signalling response, which may suggest that at millimolar concentrations of the SCFAs some residual FFAR2 activity still remains. Further studies could employ a higher concentration of the antagonist in order to achieve complete inhibition of receptor activity and investigate FFAR2-dependence in butyrate-mediated *Pyy* transcriptional upregulation as well as secretion of the hormone.

This is the first report to uncover the involvement of an FFAR2-Gαi axis in regulation of gut hormone expression in EECs. I observed a significant reduction in the butyrate-mediated *Pyy* response with the Gαi inhibitor, Pertussis toxin, but not with inhibition of Gαq by YM-254890. Notably, butyrate is a more potent and efficacious activator of Gαi (pIC50= -3.660 ± 0.298) over Gαq (pEC50= -2.814 ± 0.354) signalling (*3.2.2)*. My previous findings (*3.2.8)* also suggested a plasma-membrane**,** rather than an intracellular localisation, of butyrate-mediated Gαi and Gαq activation. This spatial dimension in butyrate-FFAR2-Gαi signalling was also reflected by the insensitivity of butyrate-mediated upregulation of *Pyy* expression to the dynamin inhibitor Dyngo-4a.

Nevertheless, as the FFAR2 antagonist and Gαi inhibition only partially impacted butyrate-mediated increases in *Pyy*, the mechanistic involvement of butyrate HDACi action still cannot be discounted. The involvement of an FFAR2-Gαi axis in the regulation of PYY mRNA expression was further corroborated by use of the selective FFAR2 Gαi biased allosteric agonist AZ-1729, which induced a synergistic effect with butyrate. Butyrate-mediated upregulation of *Pyy* mRNA expression did occur in a time-dependent manner. However, it will be valuable to compare these findings to the temporal profile of AZ-1729-mediated effects in order to precisely map potential FFAR2-dependent and FFAR2-independent mechanisms.

My preliminary findings indicate that SCFA-mediated downregulation of *Gcg* occurs via an FFAR2-independent mechanism. Notably, a previous study has reported a selective FFAR2-dependence in increasing the density of PYY- but not GCG-positive EEC *in vivo* following supplementation with the fermentable fiber inulin (Brooks et al., 2017). It is possible that FFAR2 may mediate acute secretion of both GLP-1 and PYY from L-cells, which has been indicated by previous reports and by my findings in *4.2.2,* however activation of the receptor on a longer timescale might exert unique effects on the transcription and production of PYY (Tolhurst et al., 2012; Psichas et al., 2015; Caengprasath et al., 2020). Further characterisation and comparison of the signalling pathways activated downstream of acute or prolonged stimulation FFAR2 with SCFA(s), including the spatial regulation of these pathways, will be valuable.

Butyrate has been shown to exert prominent effects on the overall morphology of the intestinal mucosa; oral supplementation with butyrate significantly increases the villus height to crypt depth ratio in several juvenile animal models including chicks, calves and piglets (Bartholome et al., 2004; Y. Han et al., 2022; Koch et al., 2019; Kotunia et al., 2004; H. Zhao et al., 2022). In addition, several *in vivo* studies investigating either the effects of direct SCFA supplementation or increased intestinal or fecal SCFA content as a result of a high-fibre diet, have reported SCFA-mediated increases in the rates of crypt cell proliferation (Mathers, Kennard & James, 1993; Lupton & Kurtz, 1993; Zhang & Lupton, 1994; Ichikawa et al., 2002; Sakata & Engelhardt, 1983; Sakata, 1987; Edwards et al., 1992). However, in contrast to these studies, butyrate has been shown to specifically inhibit the proliferation of several CRC cell lines by

HDACi-mediated upregulation of negative cell cycle regulators (Archer et al., 1998; Donohoe et al., 2012; Gamet et al., 1992; S. Hu et al., 2011; Oncel et al., 2024; Orchel et al., 2005; Siavoshian et al., 1997; Tailor et al., 2014; Xi et al., 2021). In fact, the protective effect of dietary fiber consumption in decreasing the risk of colorectal cancer (CRC) which has been widely reported across epidemiological studies, is often attributed to this tumor-suppressive effect that butyrate has on CRC cells (Ma et al., 2017; Arayici et al., 2022; Dahm et al., 2010; Schwingshackl et al., 2018; Oh et al., 2019; Liu et al., 2021. The NCI-H716 cell line does originate from a human colorectal adenocarcinoma (Park et al., 1987). Notably, I did not observe any changes in the rate of proliferation of NCI-H716 cells, assessed by Trypan blue staining, following 24 hours of acetate, propionate or butyrate treatment (*data not shown).* However, I observed a prominent elongation in NCI-H716 cells following prolonged incubation with butyrate that I confirmed by quantitative measurements of cellular area and feret distance, that significantly differed from the 'normal' lymphoblast-like morphology of this cell line (Reimer et al., 2001). A similar yet less potent effect was observed with propionate. To my knowledge, this is the first report of intestinal SCFA-mediated morphological effects on EECs and/or EEC-committed cells at a single-cell resolution. It is important to note that multiple lines of evidence have demonstrated significant effects on the morphology of butyrate on cancer cell lines of diverse tissue origins *in vitro* (Kim et al., 1980; Amoêdo et al., 2011; Klepinina et al., 2021; Kruh, 1981; Mori et al., 1979; Hargreaves et al., 1989; Zhang et al., 2007; Witt, Sand & Pekrun, 2000; Witt et al., 2001). Some reports have mechanistically associated these effects with the induction of cellular differentiation to more benign and functionally mature phenotype by butyrate (Witt, Sand & Pekrun, 2000; Witt et al., 2001; Amoêdo et al., 2011; Klepinina et al., 2021; Kruh, 1981). In addition, butyrate-mediated morphological shifts have also been linked to regulation of various parameters of cellular mechanics and metabolism including: the regulation of cytoskeletal elements, glycolipid biosynthesis, and activation of MAPK cascades which could be explored further in future studies (Kim et al., 1980; Witt, Sand & Pekrun, 2000; Witt et al., 2001; Hargreaves et al., 1989).

In contrast to the anorexigenic effects of GLP-1 which continue to gain sprawling pharmaceutical interest, its proglucagon-derived peptide counterpart GLP-2 has long been recognised as an intestinotrophic mediator (Drucker, 2019; Drucker et al., 1996; Brubaker et al., 1997). Exogeneous GLP-2 administration has been shown to

significant increase the length of villi in both normal and injured intestinal epithelium *in vivo via* a mechanism that involves downstream mediators such as insulin-like growth factor-1 (IGF-1) and its cognate receptor, intestinal epithelial insulin-like growth factor-1 receptor (IE-IGF-1R) (Drucker, 2002; Chen et al., 2022; Fesler, Mitova & Brubaker, 2020; Markovic & Brubaker, 2019). I considered the possibility that the morphological effects I had observed following SCFA treatment might stem from stimulation of GLP-2 secretion. In fact, SCFAs have previously been shown to enhance intestinal structure and absorptive functions in rats following bowel resection *via* upregulated secretion of GLP-2 (Tappenden et al., 1998). Although basal GLP-2 secretion was detected in NCI-H716 cells, preliminary findings suggested that neither basal nor acute forskolin-induced GLP-2 secretion were enhanced by prolonged SCFA treatments.

Interestingly, I observed an enriched localisation of PYY granules at the elongated cytoplasmic processes of butyrate-'transformed' cells compared to cells treated with other SCFAs or left untreated. These findings, in combination with the aforementioned studies on differentiation, raise the question of whether morphological changes by butyrate in NCI-H716 cells were reflective of cellular differentiation into a 'PYY-biased' phenotype. The classical view on the polarised flask-like morphology of enteroendocrine L-cells, comprising of a broad base and a single apical-facing cytoplasmic extension, is specific to immunohistochemical examinations of GLP-1-positive EECs in the small intestine (Buffa et al., 1978). In contrast, equivalent studies on PYY-immunoreactivity reported the existence of PYY-positive EECs enriched in the distal intestine of humans and rodents which possessed both apical- and basal-facing cytoplasmic processes (Böttcher et al., 1984; El-Salhy et al., 1983; Lundberg et al., 1982; Sjölund et al., 1983; Buffa et al., 1978). Although NCI-H716 cells lack the polarised configuration of EECs *in vivo,* incubation with butyrate stimulated the formation of long and tapering PYY-rich processes and a striking resemblance to such PYY-positive EECs. In the recent decade, these characteristic basal processes of PYY-EECs have been termed 'neuropods' due to their anatomical similarity to axonal boutons and facilitate a direct physical and functional connectivity between EECs and nerve fibers innervating the colon *in vivo* (Bohórquez et al., 2011, 2014, 2015; Kaelberer et al., 2018). The occurrence and functionality of neuropod EECs in the human colonic epithelium are yet to be characterised and might represent a unique

paradigm of gut-brain communication by specific EEC subtype(s) and/or enterohormones that is under the regulation of luminal SCFAs.

My findings in this chapter uncovered distinct transcriptional effects of SCFAs on the transcript levels of three hierarchical bHLH transcription factors (TFs) that are imperative to EEC differentiation across various EEC subtypes; *Atoh1*, *Neurog3* and *NeuroD1* (Yang et al., 2001; Jenny et al., 2002; Beumer et al., 2020; Rindi et al., 1999). Importantly, comprehensive single-cell RNA-seq (scRNAseq) data sets in recent years have provided invaluable temporal resolution to developmental TF cascades of EEC lineages which I will frequently refer to in this discussion (*Appendix 2)* (The Tabula Sapiens Consortium* et al., 2022; Elmentaite et al., 2021; Wang et al., 2020; Burclaff et al., 2022; Gehart et al., 2019).

Atoh1 is the primary gatekeeper for ISC commitment to a secretory (goblet, Paneth, Tuft, EEC) rather than an absorptive lineage within the intestinal milieu (The Tabula Sapiens Consortium* et al., 2022; Elmentaite et al., 2021; Wang et al., 2020; Burclaff et al., 2022; Gehart et al., 2019; Yang et al., 2001). I observed a significant downregulation in the mRNA expression of *Atoh1* in NCI-H716 cells following 24h incubation with butyrate, but not acetate or propionate. Looking further down the cascade, no significant effects of SCFA treatment were observed on SCFA treatment on expression on the *Atoh1*-target and early EEC progenitor marker, *Neurog3*; *Neurog3* restricts the differentiation of multipotent secretory progenitors to an EEC, rather than a goblet, Paneth or Tuft cell fate (Jenny et al., 2002; Gehart et al., 2019; López-Díaz et al., 2007). The final bHLH in question was the *Neurog3*-target *NeuroD1*, which is expressed when cells progress to intermediate EEC progenitors (Schwitzgebel et al., 2000; Gasa et al., 2008; Huang et al., 2000; Naya et al., 1997; Gehart et al., 2019). A significant increase in *NeuroD1* expression was observed downstream of butyrate but not acetate or propionate treatment. Interestingly, C2:C3:C4 co-incubation appeared to have a summative effect on expression of this TF, however significance of this effect was limited by variation. It is important to note that the expression of *NeuroD1* persists in progenitor cells as they continue to differentiate and has been detected across most mature EEC subtypes; in contrast, the expression of *Atoh1* and *Neurog3* is transient and enriched in secretory and EEC progenitors respectively, but diminishes as differentiation progresses (*Appendix 2)*

(The Tabula Sapiens Consortium* et al., 2022; Elmentaite et al., 2021; Wang et al., 2020; Burclaff et al., 2022; Gehart et al., 2019; Rindi et al., 1999). It is tempting to speculate that the concurrent downregulation of *Atoh1* and upregulation of *NeuroD1* following butyrate treatment might be reflective of NCI-H716 cellular differentiation towards a more mature EEC fate. At this juncture however, it is important to regard the origin and cellular identity of NCI-H716 cells themselves.

NCI-H716 cells are widely regarded as a model system for EECs due to their enrichment in EEC markers and enterohormone products, as well as nutrient-sensing functionalities which are comparable to L-cells (Kuhre et al., 2021, 2016). However, observations from early reports on this cell line do preclude a strict enteroendocrine designation of this cell line (Park et al., 1987; de Bruïne et al., 1993; Bruïne et al., 1992). When establishing this line in the 1980s, Park et al., described NCI-H716 cells to 'retain epithelial cell features' and be representative of a 'poorly differentiated' line based on their amorphous phenotype compared to other CRC lines which formed prominent glandular or dome structures. Other studies indicated limited endocrine properties of this cell line during routine culturing in suspension; the induction of *in vitro* endocrine differentiation was strongly dependent on the presence of native extracellular matrix (ECM) (or fibroblast feeder layers) and still only scarce in comparison to the robust differentiation observed *in vivo* in tumor xenografts (de Bruïne et al., 1993; Bruïne et al., 1992). Moreover, staining for Chromagranin A (ChgA), which was used as a marker of endocrine differentiation, appeared to be highly heterogeneous amongst ECM-cultured NCI-H716 populations and ChgA-negative cells were evident (Bruïne et al., 1992). In addition, Bruïne et al., *also* demonstrated increased exocrine properties such as mucin production following their culturing on ECM, suggesting the possibility of an 'amphicrine' identity of this cell line. In my own findings, I observed that growing NCI-H716 cells on Matrigel ECM substrate for assaying, *vs* culturing in suspension, did not significantly affect the mRNA expression of the enterohormones GCG and PYY, or EEC differentiation markers *(Appendix 3).* It remains unclear as to which stage(s) of the *in vivo* EEC differentiation cascade of EECs that NCI-H716 cells might be comparable to, and/or if they represent an inherently abnormal epithelial identity which reflects their cancerous background.

Chronic SCFA treatments also modulated the expression of the homeodomain transcription factors *Pax4, Arx* and *Pax6*, which have been implicated in instructing the differentiation of EEC progenitors specifically to an L-cell subtype (Beucher et al., 2012; Brooks et al., 2017; Fujita et al., 2008; Hill et al., 1999). Brooks et al., specifically implicated a role for *Pax4* in the FFAR2-dependent expansion of the colonic PYY-positive EEC density following inulin supplementation. Considering the 'PYY-bias' of butyrate-mediated transcriptomic and secretory effects that I had observed in NCI-H716 cells, it was surprising that butyrate appeared to stimulate a significant decrease in *Pax4* expression. However, another study has reported a *Pax4*-dependence in driving the differentiation of small-intestinal somasostatin-positive (D cells) lineages *in vivo*, which in fact operated in an antagonistic manner to the allocation of GLP-1 and PYY-positive L-cells by *Arx* (Beucher et al., 2012). Notably, butyrate treatment also appeared to stimulate a significant decrease in *Arx* expression in NCI-H716 cells, whereas no significant effects were observed with the other SCFAs. The significance of butyrate-mediated decreases in *Arx* and *Pax4* expression in guiding EEC differentiation in NCI-H716 cells is uncertain. The expression of *Pax4* and *Arx* have been mapped to Neurog3+ early EEC progenitors and intermediate EEC progenitors respectively *in vivo* (Gehart et al., 2019). However, these time-resolved findings on *Pax4* and *Arx*, as well as on the aforementioned bHLH cascade, are from the mouse small intestine (Gehart et al., 2019). In addition, scRNAseq analyses have mapped the expression of both factors amongst mature human EECs in addition to EEC progenitors, contrasting to their transient profiles observed in mice (*Appendix 2)* (The Tabula Sapiens Consortium* et al., 2022; Elmentaite et al., 2021; Wang et al., 2020; Burclaff et al., 2022; Gehart et al., 2019). Moreover, it remains unclear on the involvement in specifically guiding the development of PYY-positive EEC subtypes in the human colon.

Expression of the homeodomain transcription factor and downstream target of *NeuroD1*, *Pax6*, has been shown to be particularly enriched in late-stage EEC progenitors and mature EECs *in vivo* in the mouse small intestine (Marsich et al., 2003; Gehart et al., 2019). All three SCFAs stimulated an upregulation in the transcript levels of *Pax6*, with butyrate being the most potent activator, followed by propionate and then acetate. In addition, SCFA co-incubation (C2:C3:C4 cocktail) appeared to have a summative effect, stimulating a *Pax6* upregulation of double the magnitude to that of

butyrate. Given the 'PYY-bias' I had observed in the transcriptomic and secretory effects of prolonged SCFA incubations, these findings are particularly surprising. *In vitro* studies have identified *Pax6* as a direct activator of proglucagon gene expression through binding to G1 and G3 promoter elements. Moreover, *Pax6* depletion has been shown to diminish populations of proglucagon-derived-peptide-expressing EECs across the small and large intestine of mice, without affect the abundance of PYY-expressing EECs (Larsson et al., 1998; Hill, Asa & Drucker, 1999). As such, SCFA-mediated upregulation of *Pax6* in NCI-H716 cells is somewhat contradictory to the downregulation of GCG transcript levels and GLP-1 secretory profiles that I observed of Pax6 expression by the agonist AZ-1729. Aside from the upregulatory effect of AZ-1729 on *Pax6* expression by itself, AZ-1729 co-treatment with butyrate led to a synergistic effect on the expression of this gene. Whether an FFAR2-Gαi axis is instrumental to this regulatory node in the intestinal stem cell niche e.g in switching on Pax6 expression in late-stage EEC progenitors and guiding terminal differentiation to L-cells, could be studied in the future in appropriate transgenic *in vitro* models (eg FFAR2-knockout organoids) in complement with G-protein inhibitors (*Figure 5.19)*.

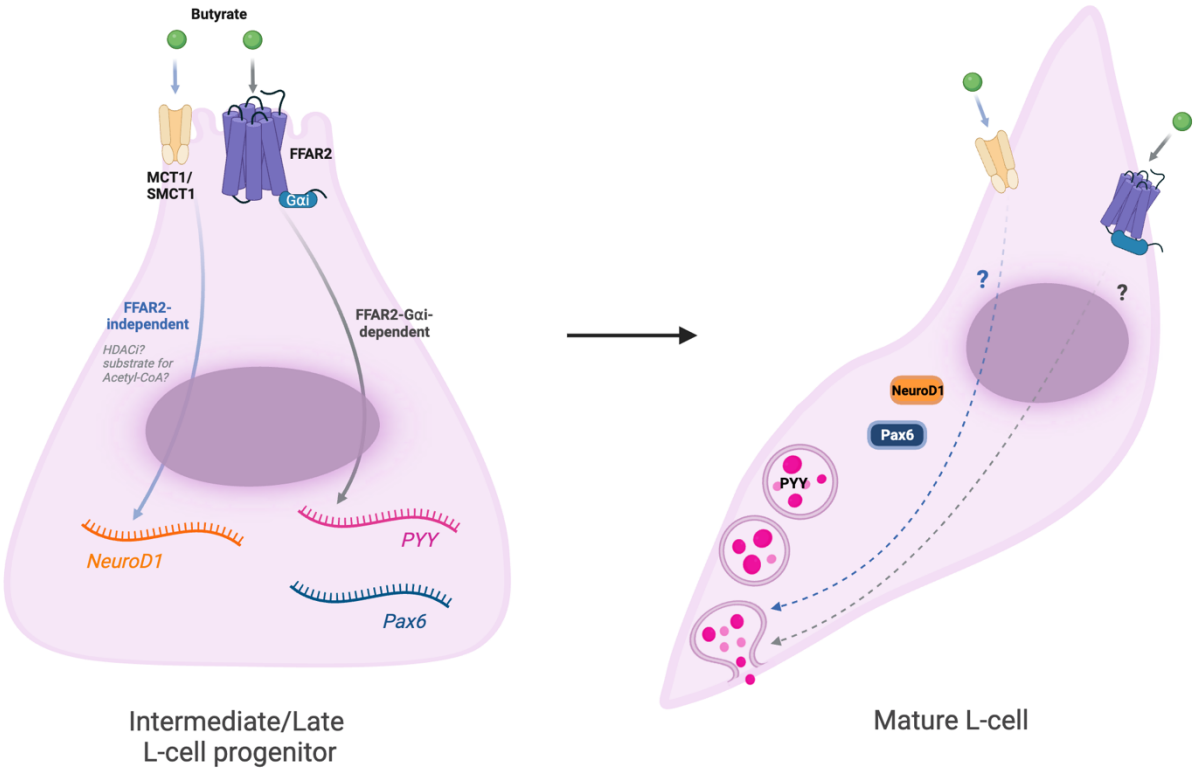


Figure 5.19 Schematic illustrating potential FFAR2-independent and FFAR2-Gαi-dependent pathways underlying butyrate's effects on the maturation and endocrine function of human L-cells based on findings in NCI-H716 cells. Butyrate might upregulate the expression of transcription factors involved in maturation of late-stage L-cell progenitors to mature L-cells *via* activation of an FFAR2-Gαi pathway (*eg PYY and Pax6)* or *via* FFAR2-independent pathways having been transported intracellularly by monocarboxylate transporter 1 (MCT1) or sodium-coupled MCT1 (MCT1). In mature L-cells, butyrate might enhance basal PYY secretory tone; the mechanistic involvement of FFAR2 in this effect also warrants further study.

Interestingly, small-molecule agonists of FFAR2 have directly recapitulated the effects of SCFAs in promoting the growth of mouse intestinal organoid cultures *in vitro,* and multiple lines of evidence in recent years have indicated a functionality of GPCRs in regulating stem cell proliferation and cell fate decisions in the intestinal stem cell niche (Park et al., 2016; Ho et al., 2024). Unlike butyrate, AZ-1729 did not affect the expression of *NeuroD1* that may indicate FFAR2-independent pathways underlying its transcriptional regulation (*Figure 5.19)*. Further studies should aim to provide a comprehensive and time-resolved map of FFAR2 activity in the ISC-to-EEC differentiation cascade by use of AZ-1729 in combination with non-G-protein biased FFAR2 allosteric agonists such as 4-CMTB (Schofield et al., 2018).

Butyrate exhibited differential temporal profiles in levels of the distinct genes analysed. Considering the heterogeneity in endocrine differentiation induction of this cell line, which I described above, the use of single-cell sequencing approaches would provide more detail on the complexities of butyrate-mediated transcriptomic changes, compared to the bulk approaches in my assays. Given that several of these differentiation targets are transient in their expression, future studies might employ a combination of scRNAseq and lineage tracing similar to that reported by the Clevers group whereby the use of multiple fluorescent reporters of EEC markers with varying half-lives allows for precise transcriptional mapping of specific progenitor populations over time (Gehart et al., 2019). Moreover, I also observed a concentration-dependent effect of butyrate on *NeuroD1*, *Pax6* and *Pyy* in my preliminary findings. In addition to the proximal to distal gradient of butyrate concentration that exists across the intestinal lumen, studies have reported the existence of a second butyrate gradient within

colonic crypts; the metabolite exists in millimolar concentrations at the upper crypt, however, is present at lower levels (50-800μM) at the crypt base (Donohoe et al., 2012; Kaiko et al., 2016). As such, the effects of butyrate on gene expression in differentiating EECs *in vivo* might vary concentration-dependently and thus positioning of target cell(s) along the crypt. Importantly, Donohoe et al., also demonstrated a significant concentration-dependency in dictating the effects of butyrate on the proliferative dynamics and transcriptome of CRC cells in *vitro*; lower concentrations (0.5mM) of butyrate favoured cell growth, whereas higher concentrations (2-5mM) had a contrasting anti-proliferative effect. Not only was butyrate-mediated HDACi activity found to increase concentration-dependently, but unique gene sets were found to be upregulated at different concentrations (Donohoe et al., 2012). Whether a similar concentration-dependency of butyrate's action(s) operates in native luminal crypt microenvironments of the human colonic epithelium is unknown and might encode physiological and/or pathophysiological functional diversity.

In addition to butyrate acting via FFAR2 and potentially as an HDACi in modulating the effects on EEC differentiation markers in NCI-H716 cells, butyrate is also known to serve as a primary energy source for intestinal epithelial cells by undergoing mitochondrial β-oxidation to acetyl-CoA, which is particularly important in the context of CRC lines (Donohoe et al., 2011; Roediger, 1980; Roediger, 1982). Cancer cells are notoriously recognised for preferentially favouring high rates of glycolytic metabolism even under normoxic conditions, known as the "Warburg effect"; apart from the catabolism of butyrate itself in fuelling ATP production, the SCFA has been shown to also re-equilibrate this abnormal energetic profile of CRC cells *in vitro* towards oxidative phosphorylation via the epigenetic modulation of crucial metabolic enzymes (Klepinina et al., 2021; Amoêdo et al., 2011; Boren et al., 2003). It will be valuable to further investigate a mechanistic involvement of an energetic and metabolic reprogramming by butyrate NCI-H716 cells in driving its morphological and transcriptomic effects.

Surprisingly, the expression of the canonical stem-cell marker *Lgr5* in NCI-H716 cells was increased following prolonged treatment with butyrate. *Lgr5* expression is characteristic of ISCs but not progenitor or mature EEC populations *in vivo* (The Tabula Sapiens Consortium* et al., 2022; Elmentaite et al., 2021; Wang et al., 2020;

Burclaff et al., 2022; Gehart et al., 2019; Barker et al., 2007). As such, this finding is somewhat paradoxical to butyrate-mediated upregulation of intermediate-stage (*NeuroD1*) and late-stage (*Pax6*) EEC progenitor transcription factors that I had observed in this cell line. However, expression of *Lgr5* has been found to be enriched in both human and mouse CRC cells and implicated in driving clonogenicity and tumour progression *in vitro* and *in vivo* (Kemper et al., 2012; de Sousa e Melo et al., 2017; Hirsch et al., 2014; Jang et al., 2018). The significance of *Lgr5* expression in the growth and/or differentiation of NCI-H716 cell line is yet to be uncovered.

5.3.2 Mouse intestinal organoid systems

Intestinal organoid culture systems recapitulate the 3D architecture and cell-type heterogeneity of the intestinal epithelium *in vivo* (Sato et al., 2009; Sato, Stange, et al., 2011). By using a variety of strategies to enrich EEC abundance in both human and murine intestinal organoids, such as the overexpression of *Neurog3* and the manipulation of growth factors and small molecule inhibitors, previous studies have demonstrated a strong resemblance of the development and function of EECs in organoids with native EECs in the gut (Basak et al., 2017; Beumer et al., 2020; Gehart et al., 2019; Ohki et al., 2020; Petersen et al., 2018; Sanchez et al., 2022). In NCI-H716 cells, the EEC differentiation markers upon which butyrate exerted significant transcriptional control, exhibit a direct or indirect dependence on Notch signalling in the intestinal milieu *in vivo*. *Atoh1* is directly repressed by the Notch effector HES1 in ISCs and TA cells, which instructs their continuous proliferation or differentiation to an absorptive phenotype (Sancho, Cremona & Behrens, 2015; Fre et al., 2005, 2011; Li et al., 2012; van Es et al., 2005). As per the mechanism of lateral inhibition, neighbouring cells with low Notch activity reciprocally express *Atoh1*, and can thereby commit to the induction of secretory lineage differentiation (Sancho, Cremona & Behrens, 2015). Li et al., have also demonstrated a direct responsiveness of early EEC Neurog3^{+} progenitors to Notch activation *in vivo*, whereby Notch favours a cell-fate switching to enterocyte or goblet fates over EEC differentiation. Using a HES1-GFP reporter line of colonic organoids, I observed significant modulation of butyrate on cellular Notch activity in a time-dependent manner on distinct organoid populations.

Prolonged incubation with SCFA in colonic organoids indicates an inhibitory effect of butyrate on the transcriptional activity of Notch *in vitro* which may demonstrate the induction of EEC differentiation. In 'mature' budding organoids, which harbour several differentiated cell types and progenitor populations, I also observed a time-dependent decrease in fluorescence following butyrate treatment. Mechanistically, these observations in budding organoids might be explained by butyrate stimulating a transdifferentiation of 'Notch-high' epithelial cell fates to 'Notch-low' lineages. Numerous reports have demonstrated inherent plasticity of mature lineages in the intestinal epithelium, such as the capacity for dedifferentiation to ISC identity particularly under epithelial injury, as well as a transdifferentiation between mature lineages (van Es et al., 2005; Yan et al., 2017; Li et al., 2021; Kurokawa, Hayakawa & Koike, 2020). However, further studies are necessary to validate if the downregulation of Notch activity by butyrate is actually indicative of the induction of EEC differentiation, and if this is specific to a PYY-positive subtype. For example, low Hes1 expression may also be representative of brush cell populations. In my preliminary findings, PYY immunoreactivity appeared to be upregulated in Hes1-negative cells of butyrate-treated organoids. Future studies could leverage the application of scRNA-seq analysis on Hes1-GFP-positive and -negative populations sorted by flow-cytometry to characterise the precise cellular fate of 'butyrate-responders'.

In my findings from the Lgr5 lineage-tracing system, I reported a downregulation of Lgr5 expression in cystic organoids following prolonged butyrate treatment. These observations may in fact provide a causative explanation for the suppressed fluorescence in butyrate-treated Hes1-GFP cystic organoids Butyrate may be encouraging a loss of 'stemness' in ISCs, reflected by downregulation of both Lgr5 and Hes1 which are enriched in ISCs in vivo, upon which post-mitotic differentiation is induced. Previous *in vitro* studies have characterised the transcriptomic effect of butyrate on mouse and human organoid cultures and demonstrated a downregulation of Lgr5, as well as an upregulation in markers of EEC differentiation in both human and mouse systems. (Grouls et al., 2022; Pearce et al., 2020; Petersen et al., 2014). A model may be proposed whereby butyrate induces EEC differentiation in the ISC niche by acting at two regulatory nodes. The first node would comprise butyrate-mediated effect of differentiation induction in immature ISCs; The second node could encompass the responsiveness of progenitors and/or mature lineages to butyrate and

restriction to an EEC-fate. It is important to consider the limitations of mouse colonic organoid systems due to potential species-dependent nuances. For example, the Clevers group have identified several species-dependent transcriptomic differences between mouse and human EECs such as in hormonal repertoires, developmental transcription factors and nutrient-sensing membrane receptors (Beumer et al., 2020). These findings emphasise the need for high order human models, *i.e* human patient-derived or iPSC-derived intestinal organoids, to characterise the influence of butyrate on the development and function of EECs.

In summary, this chapter demonstrated significant effects of SCFAs on transcriptional and morphological parameters of L-cell differentiation. In a human L-cell model, butyrate in particular stimulated the transcriptional upregulation of PYY as well as Notch-sensitive transcription factors implicated in the terminal stages of native L-cell differentiation, and an underlying FFAR2-dependent Gαi mechanism was implicated in driving some of these effects. In parallel to these transcriptional changes, butyrate-treated human L-cells exhibited mature morphological phenotypes that resembled native colonic PYY-positive EECs. By use of fluorescent reporter mouse colonic organoid cultures, butyrate-mediated modulation of Notch-sensitive differentiation was also observed, and an effect of butyrate on the cell fate of both immature and mature intestinal epithelial populations was uncovered.

6. Employing a pH-sensitive fluorescent biosensor of PYY secretion in human L-cells

6.1 Introduction

Fluorescent protein (FP) tags have provided an avenue for the real-time tracking of hormone exocytosis, at single-granule resolution in live cells. Studies applying this approach have largely focused on dynamics of insulin granules in β-cells, with a smaller number reporting GLP-1 exocytosis in intestinal L-cells (Harada et al., 2023; Li et al., 2014; Nagamatsu, 2006; Ohara-Imaizumi et al., 2002; Ohara-Imaizumi et al., 2004; Schifferer et al., 2017; Tsuzuki et al., 2022; Wheeler et al., 2017).

In Chapters 4 and 5, I explored the effects of SCFAs on the transcription and secretion of PYY in NCI-H716 cells. However, measuring PYY secretion in this cell line remains elusive because it was not detected by RIA, and its release was minimal compared to GLP-1 when detected by ELISA (Kim et al., 2014; Kuhre et al., 2016; Larraufie et al., 2018; Wang et al., 2022). In order to overcome this barrier, I designed a novel fluorescent protein (FP)-tagged version of human PYY which I describe in this chapter. Overexpression of this construct in NCI-H716 cells allowed for the detection of SCFA-mediated effects on the biosynthesis and secretion of the peptide hormone which might otherwise be masked. Finally, by leveraging the pH sensitivity of the chosen FP tag in combination with Total internal reflection fluorescence microscopy (TIRFM), exocytosis of the FP-tagged PYY from NCI-H716 cells could be captured at single-event resolution.

6.2 Results

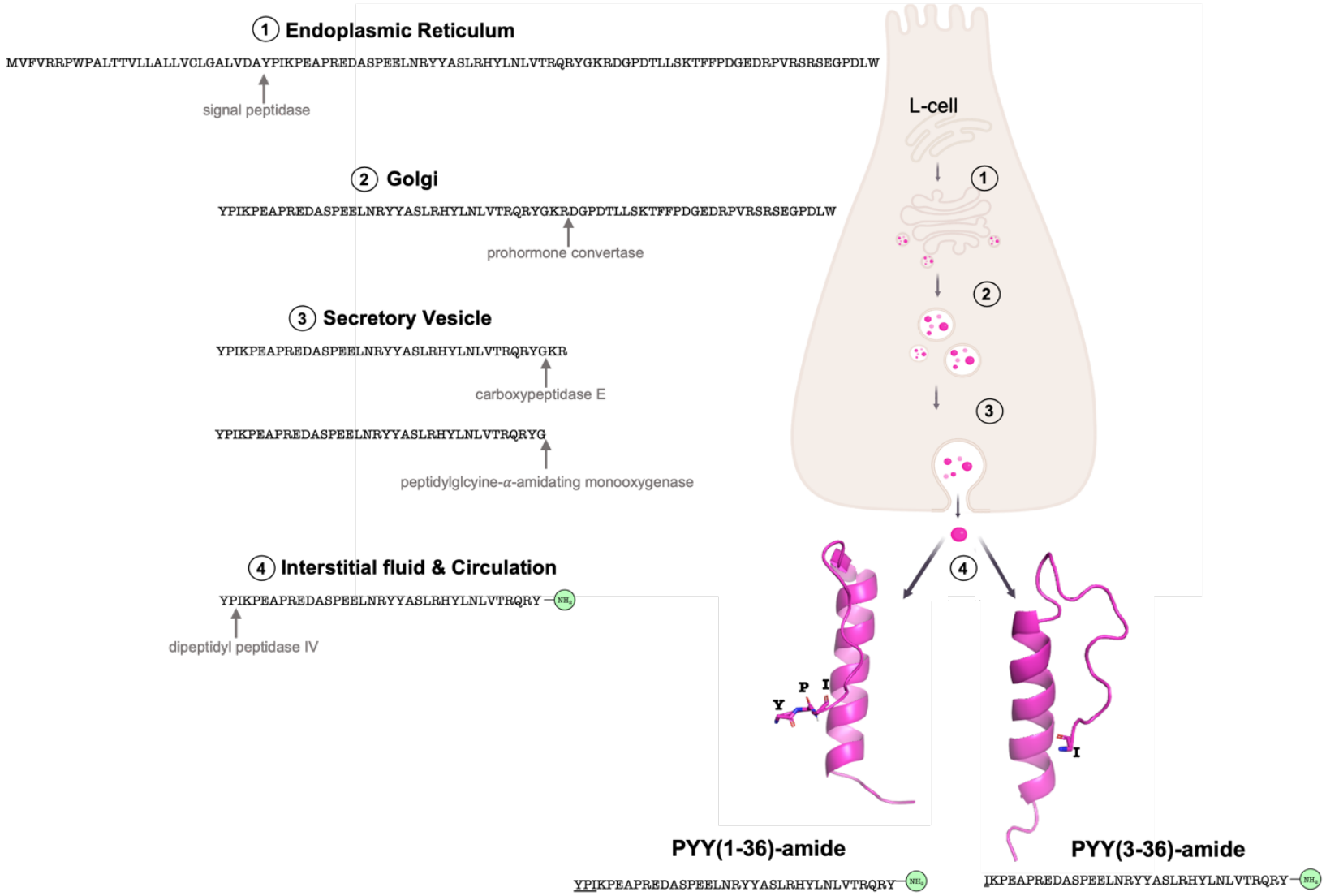
6.2.1 Cloning a pH sensitive fluorescent PYY biosensor

Previous studies engineering fluorescent protein (FP)-tagged versions of peptide hormones, such as insulin, NPY and GLP-1, have considered the complex cascades of post-translational processing steps bridging the production of nascent prepropolypeptide precursors and their maturation to secretory granules, and how insertion of an FP might compromise this (El Meskini et al., 2001; Matsuno et al., 2005; Schifferer et al., 2017; Tsuzuki et al., 2022).The prepropeptide of human PYY (preproPYY), is a 98 amino acid sequence that is highly conserved amongst

mammalian and non-mammalian species and consists of: an N-terminal 29 amino acid long signal peptide, a 36 amino acid sequence representing the mature 1-36 and 3-36 peptide forms, a Gly-Lys-Arg cleavage-amidation sequence, and 30 amino acid propeptide sequence at its C-terminus (Tatemoto et al., 1988; Keire et al., 2002; Eberlein et al., 1989; Tatemoto, 1982). The proposed processing of preproPYY along the characteristic eukaryotic secretory pathway into its active PYY(1-36)-amide and PYY(3-36)-amide forms (*Figure 6.1A)* is as follows; formation of the N-terminus of PYY by co-translational targeting to the endoplasmic reticulum and action of signal peptidase I (SPase I); formation of the C-terminus by sequential endopeptidase processing in the Golgi and within secretory vesicles by the actions of prohormone convertase and carboxypeptidase E; C-terminal alpha-amidation by peptidylglycine-a-amidating monooxygenase (PAM); extracellular cleavage by dipeptidyl peptidase IV (DPP-IV) (Keire et al., 2010).

The pH-sensitive variant of green fluorescent protein (GFP), super-ecliptic phluorin (SEP), was chosen due to its optimal pKa value (7.6) for reporting pH change upon fusion of exocytic vesicles with the plasma membrane (Miesenböck, De Angelis & Rothman, 1998). Previous studies have uncovered the indispensability of the N-terminal signal peptide sequence of prepropeptide hormone precursors in instructing maturation into secretory granules (Magoulas et al., 2000; Liu et al., 2012; Tsuzuki et al., 2022; El Meskini et al., 2001). I chose to position the SEP sequence directly at the C-terminus of the signal peptide sequence, before Tyrosine29 (Y29) of preproPYY (Tyrosine 1 (Y1)) of mature PYY and hypothesised that this positioning would not impede the crucial proteolytic trimming and processing of N- or C-terminal ends (*Figure 6.1B)*.

A


1 Endoplasmic Reticulum
MVFVRRPWPALTTVLLALLVCLGALVDAYPIKPEAPREDASPEELNRYYASLRHYLNLVTRQRYGKRDGPDTLLSKTFFPDGEDRPVRSRSEGPDLW
signal peptidase
2 Golgi
YPIKPEAPREDASPEELNRYYASLRHYLNLVTRQRYGKRDGPDTLLSKTFFPDGEDRPVRSRSEGPDLW
prohormone convertase
3 Secretory Vesicle
YPIKPEAPREDASPEELNRYYASLRHYLNLVTRQRYGKR
carboxypeptidase E
YPIKPEAPREDASPEELNRYYASLRHYLNLVTRQRYG
peptidylglcyine-α-amidating monooxygenase
4 Interstitial fluid & Circulation
YPIKPEAPREDASPEELNRYYASLRHYLNLVTRQRY
dipeptidyl peptidase IV
L-cell
1
2
3
4
PYY(1-36)-amide
YPIKPEAPREDASPEELNRYYASLRHYLNLVTRQRY
PYY(3-36)-amide
IKPEAPREDASPEELNRYYASLRHYLNLVTRQRY

B

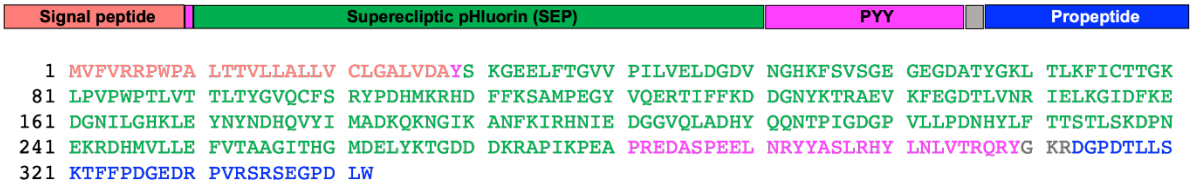


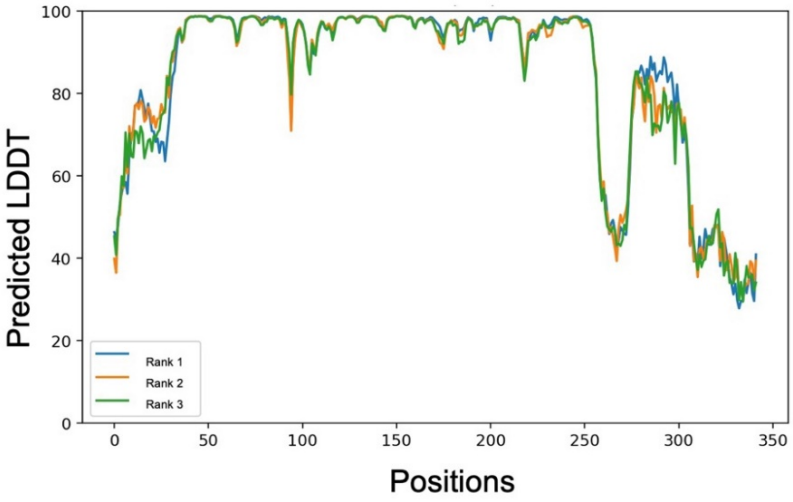
Figure 6.1 Schematic of post-translational processing cascade of PYY in EECs. (A) Diagram of the proposed post-translational processing of preproPYY along the eukaryotic secretory pathway in EECs. **(B)** Diagram of the amino-acid sequence of SEP-PYY consisting of N-Terminal signal PYY peptide (*red*), PYY *(pink),* super-ecliptic phluorin sequence *(green,)* linker *(grey),* PYY C-terminal propeptide sequence *(blue).*

Next, I used the AI-powered protein structural prediction software AlphaFold2 to produce a 3D structural prediction of the SEP-PYY construct (Jumper et al., 2021). The computational architecture of AlphaFold, which has been trained by the genetic sequences and determined structures of over 150,000 proteins, is able to predict the 3D coordinates of residues using the primary amino acid sequence and aligned homologs as inputs (Jumper et al., 2021). The AlphaFold2 output for the amino acid sequences of SEP-PYY version was confined to 3 models which were ranked based on the average predicted local distance difference test (pLDDT) score (*Figure 6.2A),* representative of a per-residue measure of confidence of local structural accuracy. Mean pLDDT scores across all three of the top three ranked models scored above 80 (*Figure 6.2B)* which correspond to a model with reasonably high confidence (Varadi et al., 2022).

In particular, per-residue pLDDT scores were highest in the regions that encode for the conserved hairpin structure of mature PYY(1-36/3-36) (residues 276-310 of SEP-PYY) and characteristic GFP β-barrel of SEP (residues 30-257 of SEP-PYY*) (Figure 6.2C & D).* The N-terminal signal peptide region (1-28) scored moderately, which might be indicative of the highly conserved membrane-anchoring α-helix conformation adopted by the preproPYY signal peptide (von Heijne, 1990). AlphaFold2 assigns pLDDT scores below 50 to regions that the algorithm recognised as intrinsically disordered. A region of low-confidence prediction (low pLDDT scores) was the C-

terminal end of the SEP tag (258-275 of SEP-PYY), which overlaps with the characteristically disordered but functionally important C-terminal tail of GFP (Lassalle & Kondou, 2016). The C-terminal PYY propeptide sequence of SEP-PYY (313-342) also exhibited low pLDDT scores. Notably, an experimentally solved PYY-specific propeptide atomic structure, or one that is conserved across secreted proteins, has not yet been reported.

A



B

Rank	Mean pLDDT score
1	84.17
2	83.98
3	83.55

C

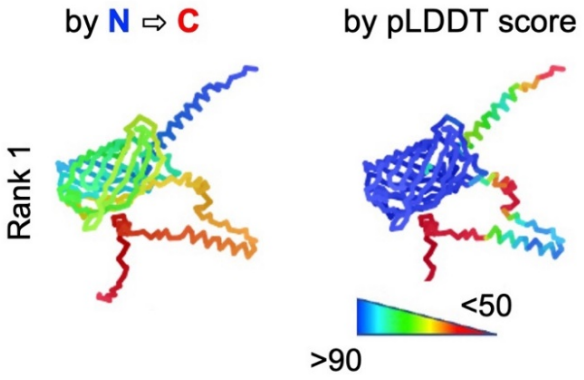


Figure 6.2 In silico structural predictions of SEP-PYY by AlphaFold2 (A) 2D cartoon representation of the AlphaFold2 model of SEP-PYY structural predictions, 'Rank 1', which obtained the highest average predicted local distance difference test (pLDDT) score. Cartoons are coloured by N to C terminus, or by pLDDT score (>90 to >50). (**B)** Per-residue pLDDT scores of SEP-PYY models Ranks 1-3. (**C)** AlphaFold2-generated cartoon of the Rank 1 3D prediction of SEP-PYY, coloured by N to C terminus (*left)* or by pLDDT score

*(right).*AlphaFold2 scoring system; ‘Very high’ (pLDDT > 90) (*cobalt),* ‘High’ (90 > pLDDT > 70) *(turquoise),* ‘Low’ (70 > pLDDT > 50) (*yellow),* ‘Very low’ (pLDDT < 50) (Jumper et al., 2021).

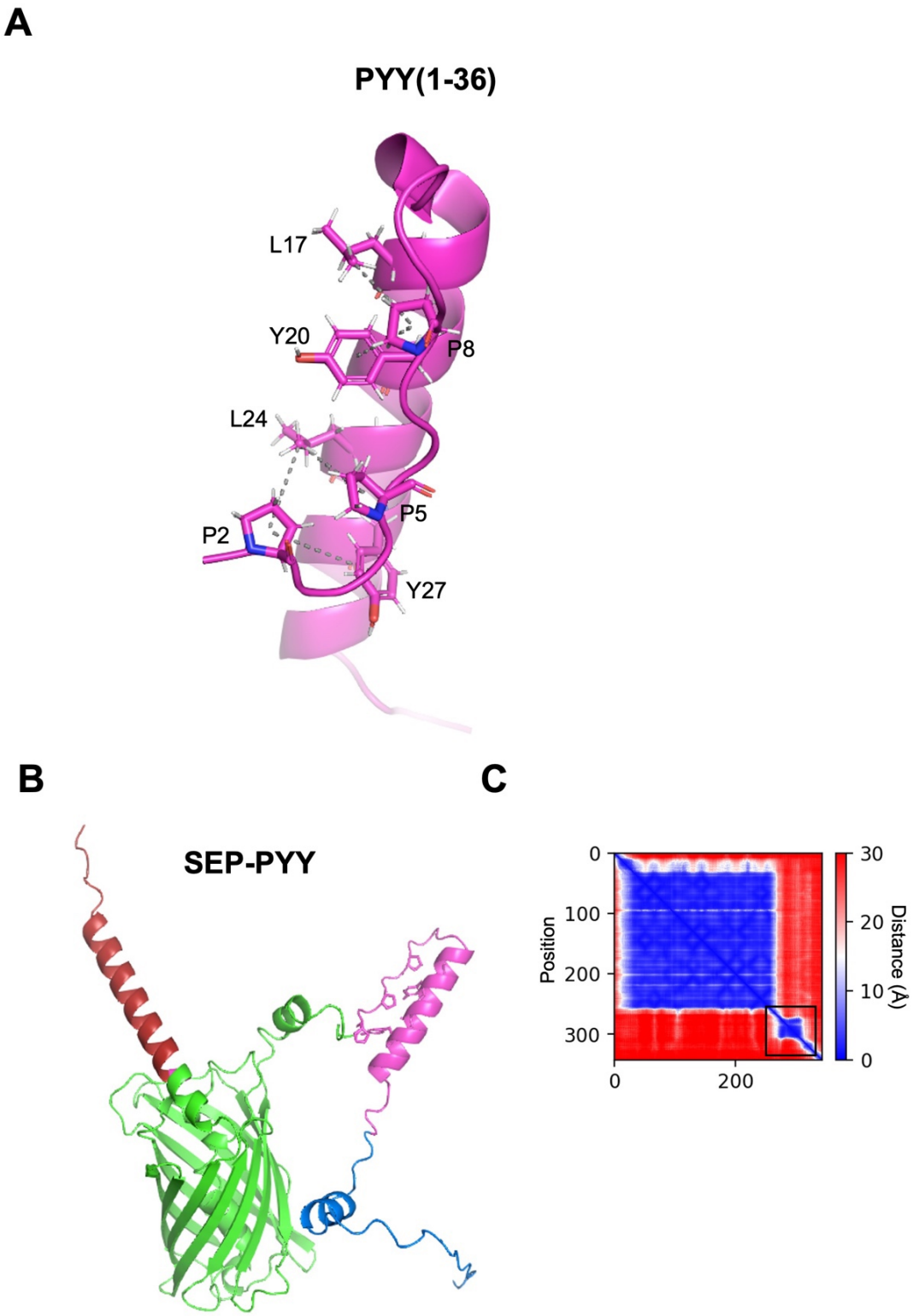


Figure 6.3 Structures of human PYY(1-36) and SEP-PYY visualised on PyMOL. PyMOL visualisation of the (A) NMR structure of human PYY(1-36) (PDB: 2DEZ) and the (B) AlphaFold2 3D structural prediction of SEP-PYY. Conserved PP-fold residues are depicted as sticks in both structures. (C) Predicted aligned error (PAE) plot of SEP-PYY prediction computed by AlphaFold2. Residue positions run along the x- and left-y axes. Colouring from blue to red indicates the expect distance error between a pair of residues between 0 and 30 Å respectively.

The 3D structure prediction of the highest scoring 'Rank 1' model of SEP-PYY were visualised on Pymol (Schrödinger & DeLano, 2020). Endogenous human PYY (PYY(1-36) and (3-36) possesses a stable 3D structure in solution common to other PP family members, which have previously been established by X-ray crystallography and NMR, formed of an N-terminal polyproline helix connected via β-turn to a C-terminal amphipathic α-helix (*Figure 6.3A)* (Nygaard et al., 2006; Langley et al., 2022).This is known as the PP-fold and involves three conserved proline residues (P2,P5,P8) folded back down the length of the α-helix with their pyrrolidine rings interdigitating with side chains of a hydrophobic stretch of residues (L17, Y20, L24, Y27) in the α-helix. Importantly, the PP-fold was not compromised in AlphaFold2-predicted structures of SEP-PYY (*Figure 6.3B & C).* The average distance between the rings of P2, P5 and P8 and the sidechains of the aforementioned hydrophobic residues was computed as a surrogate measure of structural consistency to the structure of endogenous PYY(1-36) structure. Average distances were within 0.5 Å of each other (5.14 Å for PYY(1-36); 5.15 Å for SEP-PYY). The residues of interest within the PP-fold also scored low prediction alignment error scores (PAE) in AlphaFold2 outputs (*Figure 6.3B & C).*

Finally, the SEP-PYY sequence was inputted into the signal peptide prediction software SignalP5.0 to verify SPase I cleavage sites (CS) alongside the sequence of preproYY as a reference (Almagro Armenteros et al., 2019) (*Figure 6.4).* The predicted location of SPase I cleavage was after the last signal peptide residue (A28) of SEP-PYY*,* with high but slightly lower probability than preproPYY (*SEP-PYY* p=0.8003;; *preproPYY* p=0.9501). In the analysis of the SEP-PYY sequence, there was an unexpected increase in CS and 'other' scores from L22-A24 of the sequence. However, this was overlooked given the comparatively low values to the desired A28 cleavage interface. Based on the results from the aforementioned bioinformatics

analysis, I anticipated SEP-PYY to undergo similar post-translational processing to endogenous PYY, and faithful targeting to secretory vesicles.

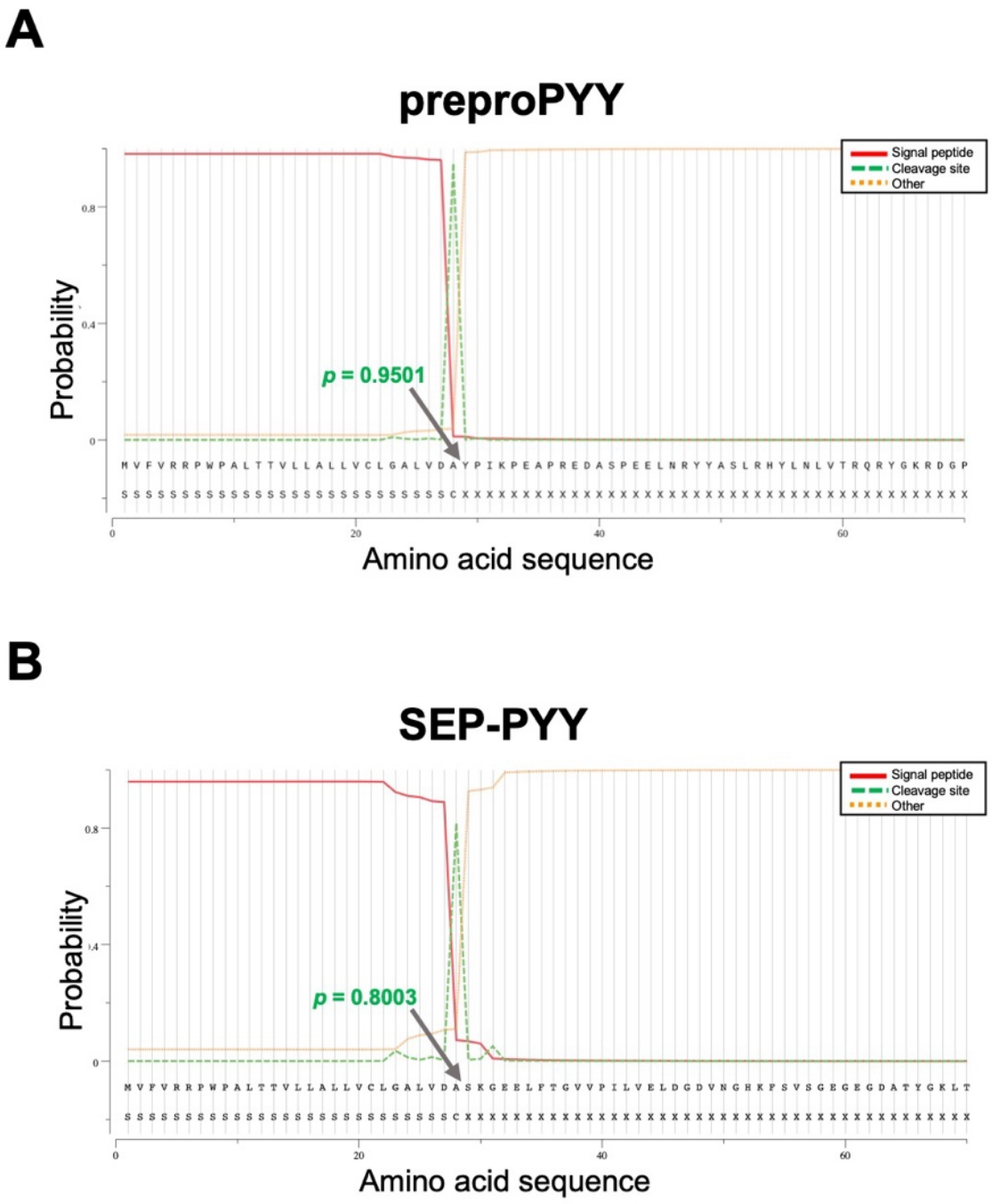


Figure 6.4 *In silico* predictions of signal peptide cleavage sites in endogenous preproPYY and SEP-PYY by SignalP5.0. Predictions of the signal peptidase I (SPase (I) cleavage site of **(A)** preproPYY sequence and **(B)** SEP-PYY sequence computed by the SignalP5.0 server. x- and y-axes indicate amino acid residue position and probability of signal peptide likelihood *(red),* SPase I cleave (*green*) or likelihood of a non-signal peptide sequence

region *(yellow).* Predicted location of cleavage site is indicated by an arrow *(grey)* with cleavage probability also printed.

6.2.2 SEP-PYY exhibits a granular structure in NCI-H716 but not HEK-293 cells

After successful cloning of SEP-PYY, the construct was transfected into both HEK-293 cells and NCI-H716 cells in equimolar quantities, and expression was subsequently probed by flow cytometry by measurement of GFP fluorescence *(Figure 6.5A)*. A functional SEP-tagged LHR construct (SEP-LHR), previously characterised by our group, was used as a positive control for protein expression and detection (Sposini et al., 2017). In HEK-293 cells, both the % of GFP+-gated cells *(Figure 6.5B)* and GFP fluorescence intensity *(Figure 6.5C)* were lower in SEP-PYY transfected cells compared to cells transfected with SEP-LHR. In contrast, SEP-PYY-transfected NCI-H716 cells exhibited higher % gating and GFP fluorescence intensity than SEP-LHR-positive NCI-H716 populations. Next, confocal microscopy was used to visualise SEP-PYY expression in both cell lines. SEP-PYY appeared diffusely distributed in the cytoplasm of transfected HEK-293 cells. However, SEP-PYY appeared as distinct vesicular structures in NCI-H716 cells which closely resembled that of endogenous peptide hormone granules in this cell line (*5.2.6).* These findings suggested that SEP-PYY might undergo similar processes of maturation and targeting to secretory vesicles to endogenous PYY, and that this is cell-dependent *i.e* might depend on L-cell specific machinery which are present in NCI-H716 but not HEK-293 cells.

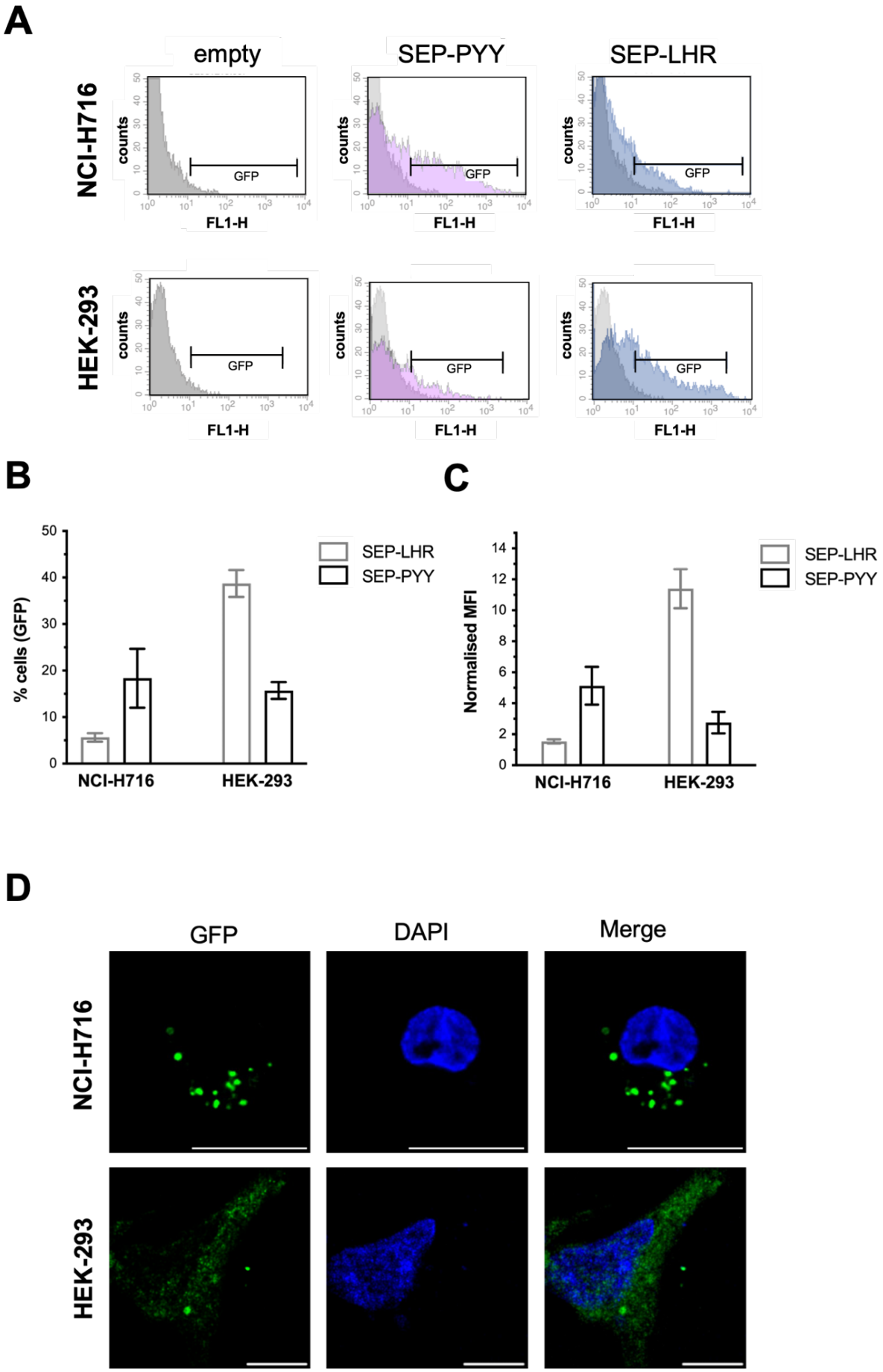

A
empty
SEP-PYY
SEP-LHR
NCI-H716
HEK-293
counts
GFP
FL1-H
B
% cells (GFP)
SEP-LHR
SEP-PYY
NCI-H716
HEK-293
C
Normalised MFI
SEP-LHR
SEP-PYY
NCI-H716
HEK-293
D
GFP
DAPI
Merge
NCI-H716
HEK-293

Figure 6.5 SEP-PYY may be packaged into secretory granules in NCI-H716 but not HEK-293 cells. HEK-293 or NCI-H716 cells were transiently transfected with 1µg of SEP-PYY or SEP-LHR for 48 hours. (**A)** Representative flow cytometric histograms of untransfected/'empty' cells (*grey),* SEP-PYY-transfected (*purple),* or SEP-LHR-transfected (*blue)* HEK-293 or NCI-H716 cells. (**B)** Measurement of SEP-PYY protein expression by detection of % cells gated for GFP-expression, and the mean fluorescence intensity (MFI) in the GFP-positive gate. MFI is represented as a fold change over GFP-positive MFI amongst *empty* cells. Data represent mean ± SEM of duplicates, n=3 independent experiments. **(C)** SEP-PYY-transfected HEK-293 or NCI-H716 cells were fixed and mounted onto glass slides before imaging by confocal microscopy. Scale bar = 50µm. Images shown are representative of n=10 cells taken across 2 independent experiments.

6.2.3 Chronic butyrate treatment upregulates the production and secretion of SEP-PYY in NCI-H716 cells

Having observed prominent effects of SCFA on PYY mRNA expression *(5.2.1*I questioned whether the production of FP-tagged hormone SEP-PYY might be sensitive to prolonged SCFA treatments. Interestingly, 24-hour treatment with butyrate, but not acetate or propionate, significantly enhanced the mean GFP fluorescence intensity of SEP-PYY-transfected cells, suggesting upregulated production of the fusion protein (*Figure 6.6A & B)*. Butyrate also increased the % of cells within the GFP-positive region, indicating that the SCFA might stimulate production and expression of the SEP-PYY above a detectable threshold (*Figure 6.6C)*. Interestingly, co-incubation with all three SCFAs to represent the 3:1:1 physiological ratio (6mM C2, 2mM C3, 2mM C4) also increased both parameters but not to a greater extent than butyrate alone (*Figure 6.6B & C).* Butyrate-mediated upregulation of SEP-PYY production was also confirmed by confocal microscopy. Fluorescent granules were much more abundant after butyrate treatment in SEP-PYY-transfected cells (Figure 6.6D). Moreover, the previously described effects of chronic butyrate treatment on NCI-H716 morphology *(5.2.5)* was evident in SEP-PYY-

transfected cells, and fluorescent granules appeared to be enriched in cellular pseudopods similar to the distribution pattern of endogenous PYY (*5.2.6).*

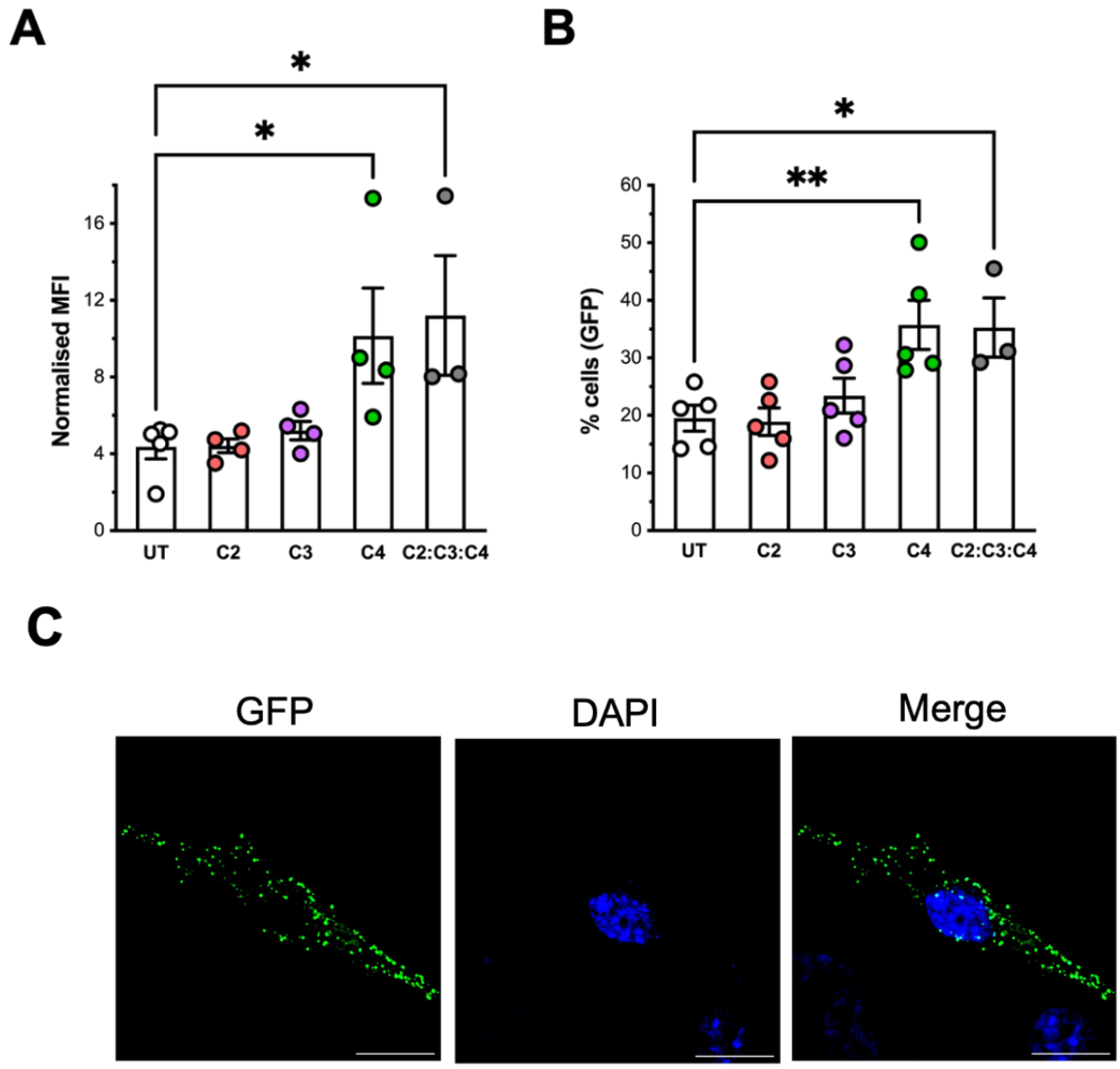


Figure 6.6 Chronic butyrate treatment enhances the production of SEP-PYY in NCI-H716 cells. NCI-H716 cells transiently-transfected with 1µg of SEP-PYY were treated with either 2mM acetate (C2), 2mM propionate (C3), 2mM butyrate (C4), 6mM acetate, 2mM propionate and 2mM butyrate (C2:C3:C4) or left untreated (UT) for 24 hours. (**A)** Measurement of SEP-PYY protein expression by detection of % cells gated for GFP-expression, and **(B)** mean fluorescence intensity (MFI) in the GFP-positive gate normalised to untransfected cells across untreated and SCFA-treated conditions Data represent mean ± SEM of duplicates, n=3 independent experiments. One-way ANOVA; UT vs C2/C3/C4/C2:C3:C4 (*p<0.05, **p<0.01). **(C)** Confocal images of SEP-PYY transiently-transfected cells treated with 2mM butyrate for

24h, fixed and mounted onto glass slides. Images are representative of n=17 cells imaged across n=3 repeats, scale bar=10μm.

Next, the secretion of SEP-PYY was quantified by measuring the fluorescence intensity of cell culture medium, Culture supernatants were collected and fluorescence intensity was measured. Supernatant fluorescence intensity of SEP-PYY-transfected cells was equivalent to that of untransfected cells *(Figure 6.7A).* However, chronic butyrate pre-treatment significantly upregulated the levels of fluorescence in the culture medium of SEP-PYY-transfected cells by ~ 2.5-fold and preliminary data suggested that this might occur in a time-dependent manner (*Figure 6.7B**).***

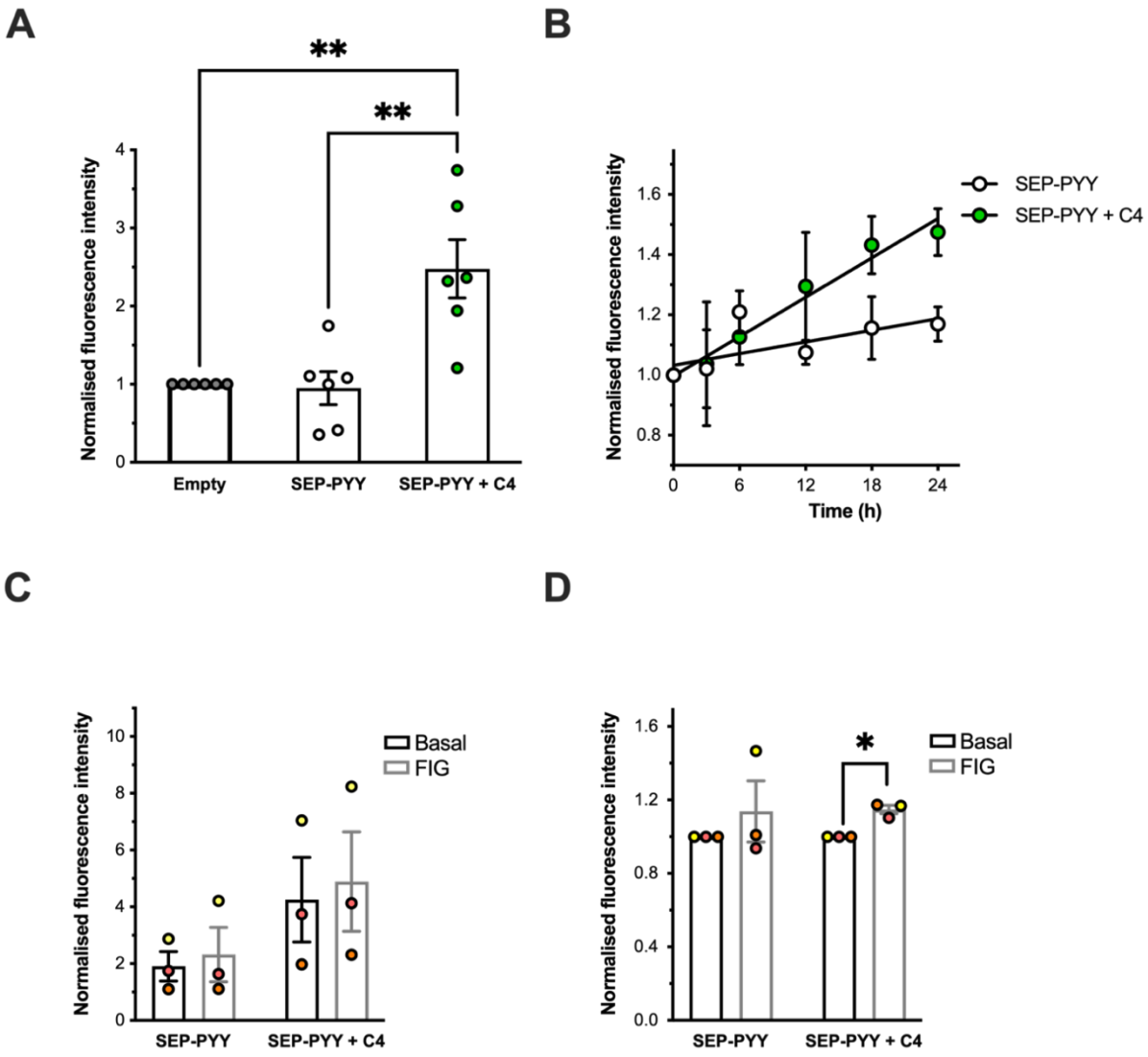


Figure 6.7 Chronic butyrate treatment promotes SEP-PYY secretion in NCI-H716 cells. NCI-H716 cells transiently transfected with 1µg SEP-PYY for 48 hours were **(A)** pre-treated with 2mM butyrate (C4) for 24 hours (SEP-PYY + C4) or left untreated (SEP-PYY). Cell supernatants were collected, centrifuged to pellet and separate from remaining cells, and GFP fluorescence was read. Fluorescence intensity is normalised as fold change to untransfected (Empty) cells. Data represent mean ± SEM of duplicates, n=4 independent experiments. One-way ANOVA; Empty vs SEP-PYY vs SEP-PYY + C4 (**p<0.01). (**B)** Transfected cells were treated with 2mM butyrate (C4) for 6, 12, 18 or 24 hours and cell supernatants were collected, centrifuged and assayed for GFP fluorescence at respective timepoints. Fluorescence intensity is normalised as fold change to untransfected/empty cells. Data represent mean ± SEM of triplicates, n=2 independent experiments. (**C & D)** Transfected cells were treated with 2mM butyrate for 24 hours or left untreated before 2-hour incubation with Vehicle (DMSO) or 'FIG' (10µM Forskolin, 10µM IBMX, 10mM glucose). Fluorescence intensity is normalised as fold change to untransfected/empty cells. Data represent mean ± SEM of triplicates, n=3 independent experiments. **(D)** Supernatant fluorescence of FIG-treated cells normalised to supernatant fluorescence of Vehicle-treated cells.

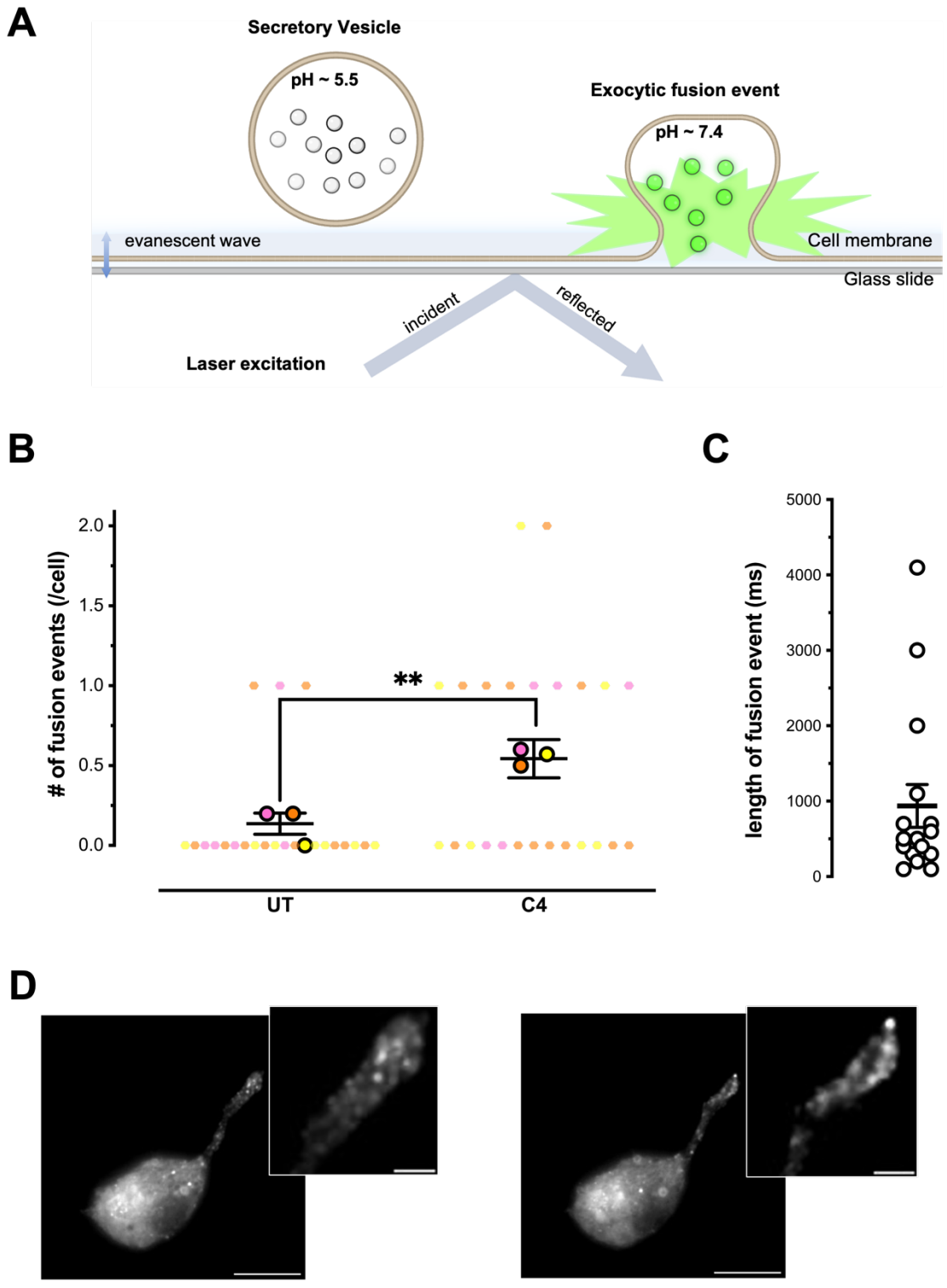
I also assessed whether SEP-PYY secretion might be responsive to a cocktail of the cAMP elevators forskolin and IBMX, and glucose (FIG) which has been shown to acutely stimulate the secretion of PYY release from mouse and human EECs: (Larraufie et al., 2018; Billing et al., 2018). No significant effect of acute FIG treatment was observed in SEP-PYY transfected cells. However, in cells pre-treated with butyrate, acute treatment with FIG promoted a significant ~1.2-fold change in fluorescence intensity over basal only in cells. These data suggests that prolonged incubation with butyrate enhances both basal and acute ligand-induced SEP-PYY secretion in NCI-H716 cells.

6.2.4 Chronic butyrate treatment stimulates SEP-PYY exocytosis observed by total internal reflection fluorescence microscopy (TIRFM)

The bimodal excitation spectra of wild-type green fluorescent protein (GFP) absorb light at both 395nm and 475nm due to the protonation and deprotonation of a conserved tyrosine residue (Y66) within the fluorophore (Ward, 1981). SEP represents an optimised variant of GFP for pH measurement, whereby introduction of specific amino acid substitutions within the local proton-relay network of Y66 endowed a loss of 475nm fluorescence at pH values <6.0 (Miesenböck, De Angelis & Rothman, 1998).

The expression of SEP-tagged PYY provides a tool for capturing PYY secretion at single event resolution in real time, as the exocytic fusion of the acidic interior of secretory granules (pH ~5.2 – 5.5) with the slightly alkaline (pH ~7.3-7.4) extracellular environment is concomitant with an increase in the phluorin brightness *(Figure 6.8A)* (Paroutis, Touret & Grinstein, 2004; Miesenböck, De Angelis & Rothman, 1998). TIRFM exploits the properties of an evanescent field that selectively illuminates fluorophores within a restricted distance (less than ~100nm) from the solid-liquid interface (Axelrod, 1981). Therefore, TIRFM is a ideal tool in capturing membrane-associated dynamics at single-event resolution (Burchfield et al., 2010). Flash events were measured by TIR-FM in SEP-PYY-transfected cells and were significantly.. in butyrate-treated conditions *(Figure 6.8B)*. Flash events were ~ 1000 ms long on average *(Figure 6.8C)* and all flash events consisted of a elevation in fluorescence of at least ~2.5 fold change magnitude from basal *(Figure 6.8D)*. These findings further

substantiate the effect of butyrate in the basal secretion of endogenous PYY in NCI-H716 cells that I reported in *5.2.4.*



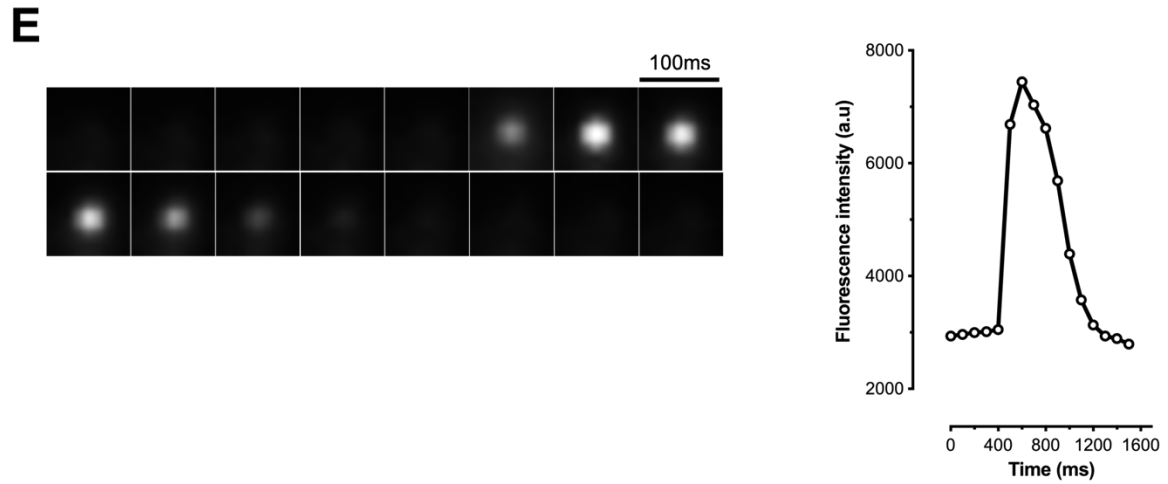


Figure 6.8 Visualisation of SEP-PYY exocytosis with single event resolution by TIR-FM. (**A)** Schematic of a characteristic single-vesicle exocytic fusion event at the plasma membrane imaged by TIR-FM in real time. (B & C) NCI-H716 cells transiently-transfected with SEP-PYY were pre-treated with butyrate (2mM) or left untreated (UT) for 24 hours. Cells were imaged by TIR-FM at 100ms intervals for 5 minutes in Krebs secretion buffer **(B)** The number of fusion events per cell (/5min). t-test; UT vs C4 **p<0.01). *Pink, orange* and *yellow* symbols represent the mean ± SEM of each biological repeat. Faded hexagons represent individual cells, coloured according to respective repeat. n=22-24 cells imaged per condition across n=3 independent experiments (**C)** The length of each fusion event. Symbols represent individual cells. n=22-24 cells imaged per condition across n=3 independent experiments. **(D)** Representative TIR-FM images of SEP-PYY-expressing NCI-H716 cells (scale bar=10μm, inset = 1μm) and sequential images (1μm x 1μm) of single-vesicle fusion events captured at 100ms intervals. **(E)** Intensity traces of single-vesicle fusion events were also plotted from measurements of fluorescence in sequential images taken every 100ms and normalised to background.

6.3 Discussion

In this chapter, I have reported the a) successful design of a novel pH-sensitive fluorescently tagged PYY construct that functionally recapitulates its endogenous counterpart and b) its utility in reporting the effects of nutrient-sensing stimuli, particularly butyrate, on enterohormone production and secretion in human enteroendocrine L-cells *in vitro.*

To validate that addition of the FP would not compromise the folding and post-translational processing of the peptide construct, I ran a series of *in silico* analyses. My results from structural predictions of SEP-PYY by AlphaFold2 achieved high confidence scores, and also exhibited high similarity to the atomic structure of PYY when visualised on PyMOL. The revolutionary impact that computational prediction methods such as AlphaFold2 have had on speed, cost and ease in the field of protein structural biology cannot be overemphasised (Bertoline et al., 2023). Despite this, such methods also have limitations which should be considered. For example, AlphaFold2 is limited in the prediction of novel structures, due to its template-based modelling approach, which is based on multiple sequence alignments (MSA) (Bertoline et al., 2023). Moreover, intrinsically disordered regions or proteins, which exhibit low conservation across orthologs, are predicted by AlphaFold2 with limited accuracy (Ruff & Pappu, 2021). The AlphaFold2 output of the SEP-PYY construct scored lowest confidence in the C-terminal pro-peptide region (of SEP-PYY, of endogenous PYY). Previous studies have identified precise motifs in the sequences of other hormone propeptides and prohormone convertase (PC 1/3) that specify cleavage, however structural determinants remain unknown (Holst, 2022; Ozawa, Peinado & Lindberg, 2010; Hoshino et al., 2011). As of now, published structures of PYY are limited to the 36-residue-long region which encodes the conserved PP-fold of the hormone (Langley et al., 2022; Nygaard et al., 2006) As such, it is important to note that the *in silico* analyses of SEP-PYY could only be partially validated by experimentally-solved data and would profit from structure-based functional studies on the full-length peptide hormone form in the future.

Certainly, the findings in this chapter should be interpreted with caution due to the recombinant nature of the SEP-PYY transfection model. However, the striking difference in the distribution of the SEP-PYY protein that I observed between HEK-293 and NCI-H716 cells by fluorescence microscopy was affirming. The HEK-293 cell line lacks the integral prohormone processing machinery such as prohormone convertase 1/3 (PC1/3) and carboxypeptidase E which are predominant in neuroendocrine and endocrine systems (Ji et al., 2017; McGirr, Guizzetti & Dhanvantari, 2013; Stijnen et al., 2016). SEP-PYY resembled distinct granular structures in NCI-H716 but not HEK-293 cells, which is likely indicative of prohormone

maturation along the regulated secretory pathway in the former system. However, faithful packaging of SEP-PYY into granules could be further validated in future studies by assessing co-localisation with canonical secretory granule markers such as tissue-plasminogen activator (tPA) (Harada et al., 2018; Oya et al., 2013; Tsuzuki et al., 2022)

My previous findings *(5.2.4)* suggested that chronic butyrate treatment upregulated the basal secretion, but not content, of PYY in NCI-H716 cells. However, flow cytometric measurements of GFP expression in SEP-PYY transfected cells in this chapter indicated a significant upregulation of SEP-PYY content in butyrate-treated but not acetate- or propionate-treated populations. This disparity between ELISA-detected PYY and flow cytometry-detected SEP-PYY could be due to the low concentrations of the endogenous hormone that were detected *(5.2.4)* which have previously been reported to be characteristic of this cell line (Kuhre, Albrechtsen, et al., 2016). Notably, the SCFA rank potency of upregulation of SEP-PYY content mirrors that of SCFA-mediated regulation of endogenous PYY transcripts in NCI-H716 cells *(5.2.1).* Moreover, SEP-PYY cells pre-treated with butyrate did appear to be enriched in SEP-PYY granules when visualised by fluorescence microscopy, which further suggested an underlying upregulation and faithful packaging of SEP-PYY *vs* an unspecific upregulation of the fluorescent tag. Although I did not assess the effect of butyrate on the gene expression SEP-PYY, it is possible that the boosted production of the FP-construct might indeed be an after effect of a positive transcriptional regulation by butyrate which operates similarly on SEP-tagged and endogenous PYY. Alternatively, the SCFA might exert a distinct regulatory mechanism on translation of the peptide. Notably, the activation of a number of GPCRs including the α_{1A} adrenergic receptor (ADRA1A) and FSHR has been linked to enhanced phosphorylation and subsequent assembly of the rate-limiting translational effector, the eukaryotic initiation factor 4F complex (eIF4F) (Musnier et al., 2012; León et al., 2014; Musnier et al., 2010). Future studies might assess the possibility of a FFAR2-dependence, as I identified in the gene expression of PYY (*5.2.2),,* or an FFAR2-independence in the potential effects of butyrate on PYY production.

In a recent study, Tsuzuki et al., described a novel method of quantification of the secretion of fluorescently tagged GLP-1 that involved direct measurement of cellular supernatant fluorescence, importantly, canonical GLP-1 secretagogues stimulated

fold change increases in FP-tagged GFP fluorescence in supernatants that were equivalent to their respective fold changes in endogenous GLP-1 secretion detected by ELISA. A similar protocol has previously been validated for fluorescence-based quantification of HIV particle release (Hermle et al., 2010). When I quantified SEP-PYY exocytosis in a similar manner, I observed a significant increase in supernatant fluorescence of SEP-PYY in butyrate-treated compared to untreated SEP-PYY-transfected cells. The magnitude of this effect (~2.5-fold change over basal) was considerably higher than the effect elicited by butyrate on endogenous PYY secretion (~1.5-fold change over basal) in preliminary ELISA assays (*cite section).* Although the SEP-PYY system was invaluable in that it aided to overcome the low abundance of PYY in this NCI-H716 cells, ultimately it is a system of overexpression which does thwart its direct comparability to endogenous secretion.

I also explored the impact of a previously characterised PYY secretagogue cocktail, 'FIG', on SEP-PYY secretion (Billing et al., 2018; Larraufie et al., 2018). Interestingly, acute treatment with FIG significantly increased supernatant fluorescence only in SEP-PYY-transfected cells pre-treated with butyrate. Indeed, it could be concluded that chronic incubation with butyrate has a selective endocrine 'priming' effect on NCI-H716 cells, whereby both the basal PYY secretion as well as responsiveness of PYY secretion to acute stimuli is augmented. Mechanistically, these findings might simply be explained by the larger pool of available PYY mRNA and translated protein following butyrate treatment. However, prior to the exocytosis of secretory vesicles at the plasma membrane is a cascade of tightly regulated trafficking and priming steps that attend to newly-synthesis hormone vesicles in the Golgi (Park & Loh, 2008). Several studies have identified essential roles of isoforms of the Soluble N-ethylmaleimide-sensitive factor activating protein receptor (SNARE) vesicle-fusing proteins in mediating GLP-1 secretion from intestinal L-cells (Campbell et al., 2020; Gustavsson et al., 2011; Li et al., 2014; Biancolin et al., 2020; Wheeler et al., 2017). Interestingly, comprehensive analyses of the β-cell phosphoproteome have identified the phosphorylation dynamics of SNAREs and other secretory pathway effectors to be directly modulated by the insulin secretagogues glucose and GLP-1 (Tang et al., 2017). Phosphoproteomic analyses in butyrate-treated NCI-H716 cells might uncover novel pharmacological targets for harnessing endogenous PYY secretion from intestinal L-cells. Numerous studies support the involvement of distinct GPCR

signalling modes, beyond increases in Gαq-mediated Ca^{2+} and Gαs-mediated cAMP, in modulating secretory vesicle exocytosis**.** For example, unique pathways comprising of Gβγ-mediated regulation of SNARE complex activity have been identified downstream of GPCRs on neuronal and endocrine cells (Bauer et al., 2007; X.-K. Chen et al., 2005; Ferdaoussi et al., 2012; Photowala et al., 2006; Rives et al., 2018; Yim et al., 2021; Yoon et al., 2007; Zhao et al., 2010; Zurawski et al., 2017, 2019). In addition, an allosteric agonist of Gαi- and Gαq-coupled FFAR1, called 'Compound A', has been shown to potentiate GSIS from human islets by stimulating promiscuous coupling to Gα12/13 (Rives et al., 2018). The precise role of Gα12 in insulin secretion is unclear yet has previously been linked to Protein kinase D (PKD) activation in β cells; PKD mediates actin depolymerisation which is central to the mobilisation of intracellular vesicle pools to the plasma membrane (Rives et al., 2018; Ferdaoussi et al., 2012; Kalwat & Thurmond, 2013; Siehler, 2007). Interestingly, a ligand of the bitter taste TAS2R receptor, quinine, has been shown to specifically hinder GLP-1 exocytosis from mouse enteroendocrine L-cells by stimulating actin polymerisation at the plasma membrane (Harada et al., 2018). In future studies, it will be highly informative to unravel the allocation of FFAR2-dependence and –independence to specific stages along the enterohormone maturation pathway in intestinal L-cells.

The use of TIR-FM in the last two decades has provided immense spatiotemporal resolution to the dynamics of neurotransmitter and hormone exocytosis in neurons and endocrine cells respectively (Lu et al., 2019; Ohara-Imaizumi et al., 2004; Steyer et al., 1997; Tsuzuki et al., 2022). Fluorescent tags with pH sensitivity have provided a further specificity in discerning exocytic events at the plasma membrane (Miesenböck, De Angelis & Rothman, 1998). To my knowledge, this is the first report of a fluorescent pH-sensitive biosensor of PYY and real-time imaging of its exocytosis at single-event resolution.

TIR-FM-captured fusion events in SEP-PYY transfected cells were greater in butyrate-treated cells compared to untreated conditions. Notably, the magnitude of this butyrate-mediated secretory effect (~2.5-fold change over untreated), agrees with that observed by fluorometric measurements of culture supernatants. Although the pH-sensitivity of SEP is highly advantageous in reporting the dynamics of hormone

granule exocytosis, SEP is limited in the visualisation of pre-exocytic docking steps due to its lower fluorescence in the acidic pH environment of vesicles. In β-cells , previous studies have reported the availability of two separate intracellular pools of insulin granules with distinct dynamics that mechanistically underlie the biphasic profile of GSIS; pre-docked ('old face') insulin granules which immediately fuse with the plasma membrane upon glucose stimulation underlie the first phase, whereas the second phase predominantly derives from the secretion of more-distantly located granules that are and recruited, docked and fused at the plasma membrane upon stimulation ('resting' newcomer') (Ohara-Imaizumi et al., 2007). Defects in the first phase of insulin secretion are a hallmark of T2D, and several T2D pharmacological agents, such as DPP4 inhibitors and GLP-1 receptor agonists, do exhibit direct improvements on the first-phase response (Di Giuseppe et al., 2023; Del Prato & Tiengo, 2001). However, this abnormal β-cell first-phase response has been shown to only be partially reversed in T2D patients in 'remission' and thus a more phase-selective approach of pharmacological inhibition may help to fully recover β-cell function (Zhyzhneuskaya et al., 2020). The availability and dynamics of functionally distinct intracellular pools of GLP-1 and PYY granules in human L-cells is yet to be uncovered. Future studies might benefit from use of a novel red pH-sensitive FP to tag enterohormone constructs, known as pHmscarlet, with optimised pH sensitivity that facilitates the detection of docking as well as fusion events by TIRFM (Liu et al., 2021). Ultimately, the characterisation of L-cell hormone dynamics and their potential pathophysiological regulation in metabolic disease may be promising in the development of high-selective and efficacious therapeutic agents.

In summary, this chapter has demonstrated the successful use of a novel pH-sensitive fluorescent construct, SEP-PYY, to report the regulatory mechanisms of PYY in human L-cells. The design of SEP-PYY accounted for the post-translational processing cascades undertaken by preproPYY in native L-cells, and the construct appeared to recapitulate the maturation of endogeneous PYY into granular structures. In addition, the induction of a 'PYY-bias' phenotype by butyrate which I reported in Chapter 5 was mirrored by an upregulatory effect of the SCFA on both the production and secretion of SEP-PYY was upregulated by butyrate. Finally, the use of TIR-FM enabled the detection of SEP-PYY exocytosis at single-event resolution.

7. General Discussion

This thesis aimed to decode the signalling profiles of the GPCR FFAR2 elicited by short-chain fatty acids in human enteroendocrine L-cells, and their functional implications in regulating key paradigms of cellular development and endocrine function(s). The main findings are: i) SCFA-activated signalling pathways of human FFAR2 (hFFAR2) in human enteroendocrine L-cells display ligand- and context-dependent complexities and are spatially regulated, ii) the effects of SCFAs on the L-cell enterohormone products GLP-1 and PYY are not equal, iii) a hFFAR2-Gαi axis mediates SCFA-mediated secretory functions in a human L-cell model; iv) the SCFA butyrate drives human EEC differentiation towards a 'PYY' biased phenotype which is reflected in the transcriptional modulation of Notch-sensitive differentiation cascades and striking morphological changes, and this may also be conserved in mouse colonic organoids.

To my knowledge, the findings in this thesis are the first to report a dependence of hFFAR2-Gαq responses on receptor internalisation. In contrast, our lab has previously demonstrated an intracellular compartmentalisation of propionate-mediated FFAR2-Gαi signalling in mouse EECs (Caengprasath et al., 2020); SCFA-activated Gαi responses did not demonstrate a dependence on receptor internalisation in human L-cells. Previous transcriptomic and peptidomic characterisations of mouse and human EECs have highlighted significant differences in their nutrient-sensing repertoires including GPCRs (Roberts et al., 2019; Beumer et al., 2020). Future analyses might illuminate species-dependent differences in the downstream effectors that instruct the distinct spatial regulatory mechanisms of mouse and human FFAR2-Gαi responses in EECs.

The findings in this thesis uncovered temporal complexities of the effects of SCFAs on the endocrine functions of human enteroendocrine L cells. Acute treatments with SCFAs appeared to stimulate effective GLP-1 but not PYY secretion in NCI-H716 cells. In contrast, an upregulation in the transcriptional and secretory responses of PYY but not GLP-1 was evident after prolonged SCFA incubations. Mechanistically, activation of an FFAR-Gαi axis was implicated in both GLP-1 and PYY release by acute and prolonged treatment with the selective FFAR2-Gαi agonist AZ-1729 respectively. Previous studies by our lab have also characterised an underlying

FFAR2-Gαi pathway in driving propionate-mediated GLP-1 release from mouse EECs (Caengprasath et al., 2020) . However, future experiments should employ a wider set of receptor agonists and G-protein inhibitors to further validate if this pathway is conserved in human EECs.

This thesis also identified a novel pathway of sustained FFAR2-Gαq activation in human EECs which is localised to the early endosome. Although a role of the Gαi functionality of this receptor was demonstrated for both acute and chronic secretory profiles in this system, the functional implications of its Gαq counterpart, and its intracellular localisation, remains unclear. As evidenced by the analgesic benefits of targets antagonists of the sustained endosomal responses of GPCRs on nociceptors, the prolonged nature of this response might also be pharmacologically harnessed to provide sustained clinical efficacy. (Jensen et al., 2017; Jimenez-Vargas et al., 2018; Hegron et al., 2023; Jiménez-Vargas et al., 2022; Jimenez-Vargas et al., 2020; Latorre et al., 2022). With the cryo-EM structure of FFAR2 successfully published earlier this year, there is much opportunity for structure-based functional characterisation and drug development in the future (Zhang et al., 2024). A recent study has illuminated a protective role of EECs in relaying the nutritional status of the intestinal lumen to crypt ISCs *via* modulation of ISC metabolic profiles (McCauley et al., 2023). The intracellular mechanisms in EECs and specific paracrine factors that might mediate this response have not yet been characterised; the activation of prolonged hFFAR2-Gαq responses downstream of luminal SCFA sensing may stimulate a sustained production of appropriate metabolites and/or peptides by EECs that maintain homeostasis in the intestinal stem cell niche.

This study focused on FFAR2 as a candidate GPCR for SCFA-mediated effects on human EECs, as FFAR2 was the primary SCFA-responsive receptor in our human L-cell model, and that prior published data has supported a role for FFAR2 in acute gut hormone secretion (REFS). Although Gαi responses in this system were effectively inhibited by FFAR2 antagonist GLPG0974, FFAR3 mRNA was detected. Moreover, the functionality of this receptor in mediating GLP-1 release from this cell line has previously been demonstrated by use of an FFAR3-selective agonist (Ducastel et al., 2020). As butyrate acts at hFFAR2 and hFFAR3 with equal potency, it is plausible that

the partial inhibition of butyrate-mediated transcriptional effects by GLPG0974 is indicative of co-activation of both FFAR2 and FFAR3 in mediating this response. Moreover, a previous *in vitro* study by Ang et al., have characterised the formation of FFAR2/FFAR3 heterodimers in human leukocytes with enhance signalling capacities to their respective monomers. The occurrence of this phenomenon in human EECs warrants further study and might underlie specificities in SCFA-mediated FFAR2 signalling profiles.

Apart from FFAR3, the expression of three other SCFA-binding GPCRs have been characterised in EECs thus far. One is the Gαi-coupled receptor GPR109A that recognises butyrate in addition to ketone-body metabolites such as β-OHB and the B vitamin niacin (Mao et al., 2023; Wallenius et al., 2020). The two other SCFA-binding candidates on EECs are the olfactory receptors OR51E1 (mouse Olfr558) which also exhibits a SCFA preference for butyrate and OR51E2 (mouse Olfr78) which is activated by acetate and propionate but not butyrate (Wang et al., 2023; Nishida et al., 2021; Han et al., 2018; Fleischer et al., 2015; Bellono et al., 2017). In fact, each of these three GPCRs has previously have been implicated in GLP-1 and/or PYY release from L-cells *in vitro* (Wang et al., 2023; Nishida et al., 2021; Kotlo et al., 2020; Han et al., 2018). The inherent diversity of the macronutrient and micronutrient composition of the human diet is complex and is amplified by the multitude of postprandial digestive- and microbiome-derived metabolites that it can produce. As such, a 'one ligand: one GPCR' model of L-cell-mediated anorectic peptide hormone release may not be representative of the interactions between the extensive complement of nutrient-sensing machinery on the surface of L-cells and their nutrient-rich microenvironment *in vivo*. There is an immense potential for crosstalk between nutrient sensing GPCRs on EECs in co-ordinating postprandial hormone release in response to complex luminal stimuli: a number of these synergies have already been reported *e.g.* between GPR84 and FFAR4, and between GPR119, FFAR1 and GPBAR1 (Peiris et al., 2022; Hauge et al., 2017). FFAR2 and other nutrient-sensing GPCR(s) in human EECs may synergistically converge at the level of the receptor, G-proteins and/or secondary messengers. To investigate this further, future studies might employ appropriate pharmacological inhibitors of candidate GPCRs for FFAR2 crosstalk, in

combination with bioluminescence resonance energy transfer (BRET) based approaches to measure direct receptor-receptor interactions in live cells.

This thesis demonstrates the prominent transcriptional effects of SCFAs on hierarchical EEC differentiation cascades in human L-cells. In particular, the effects of butyrate on these targets were observed to be more efficacious compared to acetate and propionate. In addition, butyrate also stimulated the induction of mature EEC-like morphological phenotypes in human L-cells. Whether the differentiation and/or morphology of native L-cells in the human colonic epithelium are tonically or postprandially regulated by SCFAs is not known and might be a clinically relevant area of study in the future. Moreover, the 'PYY-bias' phenotype observed in NCI-H716 cells might be indicative of a selective fine-tuning in EEC lineage differentiation *in vivo*. These PYY-rich EECs might exert unique metabolic functions in the colonic epithelium. This may include neuronal-like properties that facilitate direct synaptic transmission with neighbouring nerves and rapid communication with central appetite centres, which has previously been described for similarly elongated and PYY-positive EECs in the mouse colon (Bohórquez et al., 2011, 2014, 2015; Kaelberer et al., 2018). Moreover, characterising the influence of SCFAs on the differentiation of L-cells might illuminate novel strategies to replenish depleted L-cell abundance which is a patient characteristic in a number of metabolic and gastrointestinal diseases *e.g.,* obesity, T2D and irritable bowel syndrome (IBS) (El-Salhy, Hatlebakk & Hausken, 2020; Osinski et al., 2021; Wölnerhanssen et al., 2017).

In comparison to the growing interest in GLP-1 RAs as weight-loss agents, PYY-based assets in the anti-obesity pipeline are scarce. Beyond its similar anorectic actions to GLP-1, PYY exerts several other beneficial gastrointestinal effects that are yet to be therapeutically harnessed. For example, PYY functions to optimise the dynamics of postprandial nutrient absorption by modulating the mechanics of digestion (Karra, Chandarana & Batterham, 2009). Moreover, PYY has been shown to exert several intestinotrophic effects in stimulating colonic epithelial proliferation (Mannon et al., 1999; Mannon & Mele, 2000). Selectively targeting PYY release from colonic L-cells *in vivo* might deploy some of these benefits, whilst simultaneously reducing the incidence of gastrointestinal side effects that could potentially occur with co-release of both GLP-1 and PYY due to overstimulation of central and peripheral pathways.

The findings in this thesis also explored butyrate-mediated effects on EEC differentiation in the mouse colonic organoids, from which two conclusions can be deduced; firstly, butyrate induces a loss of 'stemness' in colonic ISCs, and secondly that butyrate restricts the differentiation of post-mitotic colonic progenitor populations towards 'Notch-low' lineage(s). Further studies are warranted to characterise the identity and functionality of enriched 'Notch-low' populations in butyrate-treated organoid cultures. However, considering these findings in combination with the Notch-sensitivity of butyrate-regulated L-cell developmental cascades in NCI-H716 cells might be indicative of a conserved action of butyrate in inducing EEC differentiation in the mouse and human colonic epithelium.

Future studies could interrogate the stage-specific and/or blanket underlying intracellular mechanisms that mediate the interactions of SCFAs with developing EECs. This includes the study of GPCR-independent axes modulated by SCFAs in EECs, such as HDACi and mitochondrial energy metabolism, which were beyond the scope of this project. In addition, transcription analyses indicated a significant regulatory effect of AZ-7129 on the late-stage marker of L-cell differentiation, PAX6. These findings could be indicative of FFAR2-Gαi involvement in the terminal differentiation of late-stage EEC-committed progenitors into a mature L-cell phenotype *in vivo*. Future studies could explore this hypothesis further by employing CRISPR/Cas9-mediated knockdown of the receptor in NCI-H716 cells and/or human organoid models.

Previous studies on FFAR2 in the intestinal stem cell niche are limited to the functional characterisation of the receptor in EECs (Lu, Gribble & Reimann, 2018). However, multiple sc-RNAseq analyses in recent years have shown that FFAR2 expression is in fact evident in secretory progenitor stem cell populations in the mouse and human colonic epithelium (Smillie et al., 2019; Domínguez Conde et al., 2022; Elmentaite et al., 2021; Wang et al., 2020; The Tabula Sapiens Consortium* et al., 2022; Schaum et al., 2018). Several approaches could be employed to further delineate the function(s) of FFAR2 in EEC differentiation *in vivo.* The first could involve the development of an appropriate FFAR2 reporter mouse line *e.g.* FFAR2-GFP; this approach would allow for discriminate transcriptomic and/or proteomic profiling of

intestinal epithelial cells enriched in the expression of FFAR2 at the protein level, *via* flow cytometric sorting of GFP-positive and negative populations. In addition, employing *in situ* hybridisation in mouse and/or human colonic tissues will provide a spatial resolution to FFAR2 expression along the crypt axis, which might also be indicative of its role(s) in differentiation of various progenitor populations located along the intestinal epithelial 'conveyor belt'.

As of now, no genetic variants of human FFAR2 have been related to the incidence or prognosis of obesity. However, the relative abundance of FFAR2-expressing EECs compared to the total EEC population has been shown to be inversely correlated with BMI in obese and morbidly obese individuals (Burclaff et al., 2022). Moreover, further investigations into the precise influences of FFAR2 in mediating the development and functions of human L-cells *in vivo* might emphasise its potential as an anti-obesity target. Currently, two agonists of L-cell-localised nutrient-sensing GPCRs are already in phase II clinical trial, however their precise targets remain undisclosed (Clinicaltrials.gov, 2023).

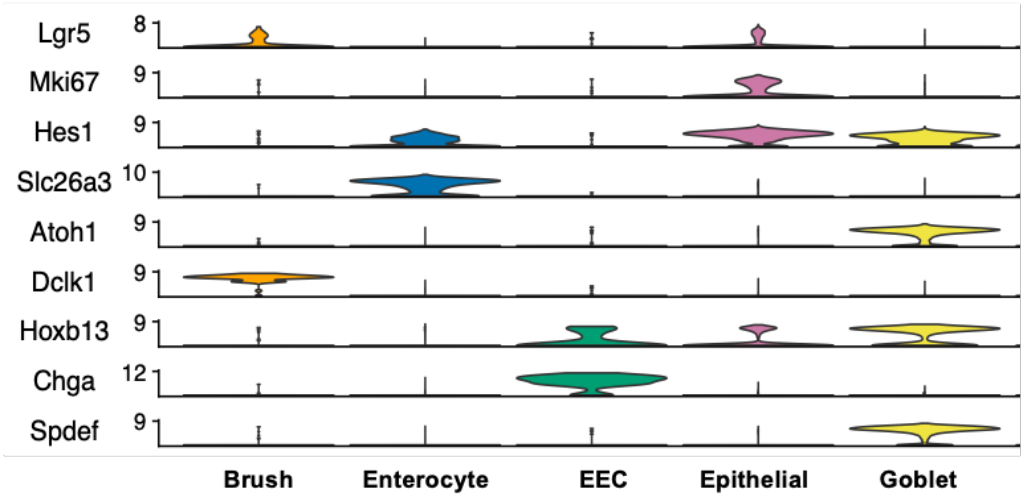
In addition, future anti-obesity therapeutic strategies might consider the possibility of enhancing the abundance of hormone-producing L-cells by manipulating the expression of transcription factors implicated in their development. Previous studies have indicated a downregulation of EEC-generic and/or L-cell specific developmental transcription factors in patients with obesity; these factors might serve as novel targets for the development of anti-obesity gene therapies (Wölnerhanssen et al., 2017; Osinski et al., 2021). SCFAs themselves might also emerge as anti-obesity agents; the specific delivery of orally supplemented SCFAs to the colon has been achieved by their conjugation to fermentable dietary fibre (Chambers et al., 2015; Frost, 2018). Thus far, an inulin-propionate (iPE) has demonstrated clinical efficacy in improving weight gain, appetite and blood glucose control; the iPREVENT trial has investigated the long-term effects of iPE across a 12-month period, and its results are expected to be released later this year (Frost, 2018). Based on the findings in this thesis, a novel SCFA-based therapeutic approach can be proposed. A pre-treatment phase of butyrate, such as with a inulin-butyrate ester or colon-targeted drug delivery system such as EUDRATEC® COL, might be benefical in 'priming' the endocrine functionalities colonic L-cells (Evonik, 2018). This approach might promote a longevity

in the effects of subsequent treatment with iPE and/or commercial GLP-1 RAs. A current bottleneck in anti-obesity therapies like GLP-1 RAs are the reversibility of effects; following treatment withdrawal, weight re-gain and declining metabolic functions are common to patients. It will be interesting to investigate whether the effects of butyrate administration on PYY hormonal profiles are more long-lasting, particularly if a modulation of cellular differentiation is evident. As we enter the era of personalised medicine, we can also expect the emergence of precision probiotics as anti-obesity agents (Veiga et al., 2020). Dysregulations in microbiota composition have been mapped to a number of pathophysiological conditions, and a downregulation of butyrate-producing strains in particular is evident in obese individuals (Brahe, Astrup & Larsen, 2013). By leveraging in-depth metagenomic sequencing approaches, the development of probiotics will effectively replenish and/or maintain specific microbiome-derived functions with personalised physiological and pathophysiological value.

In conclusion, this thesis uncovers the functions of the microbial metabolites SCFAs in modulating the endocrine profiles of enteroendocrine L-cells, as well as in regulating crucial cell-fate checkpoints implicated in native L-cell differentiation in the intestinal stem cell niche. The activity of the SCFA-binding GPCR FFAR2 was central in mediating these diverse effects, and a functional diversity in cellular outcomes was encoded by ligand- and spatial-bias in receptor signalling profiles. Together, the findings in this thesis could galvanise the development of novel pharmacological and non-pharmacological approaches, such as dietary regimes and/or probiotic supplementation, which leverage the myriad effects of SCFA-mediated FFAR2 activation in human colonic L-cells.

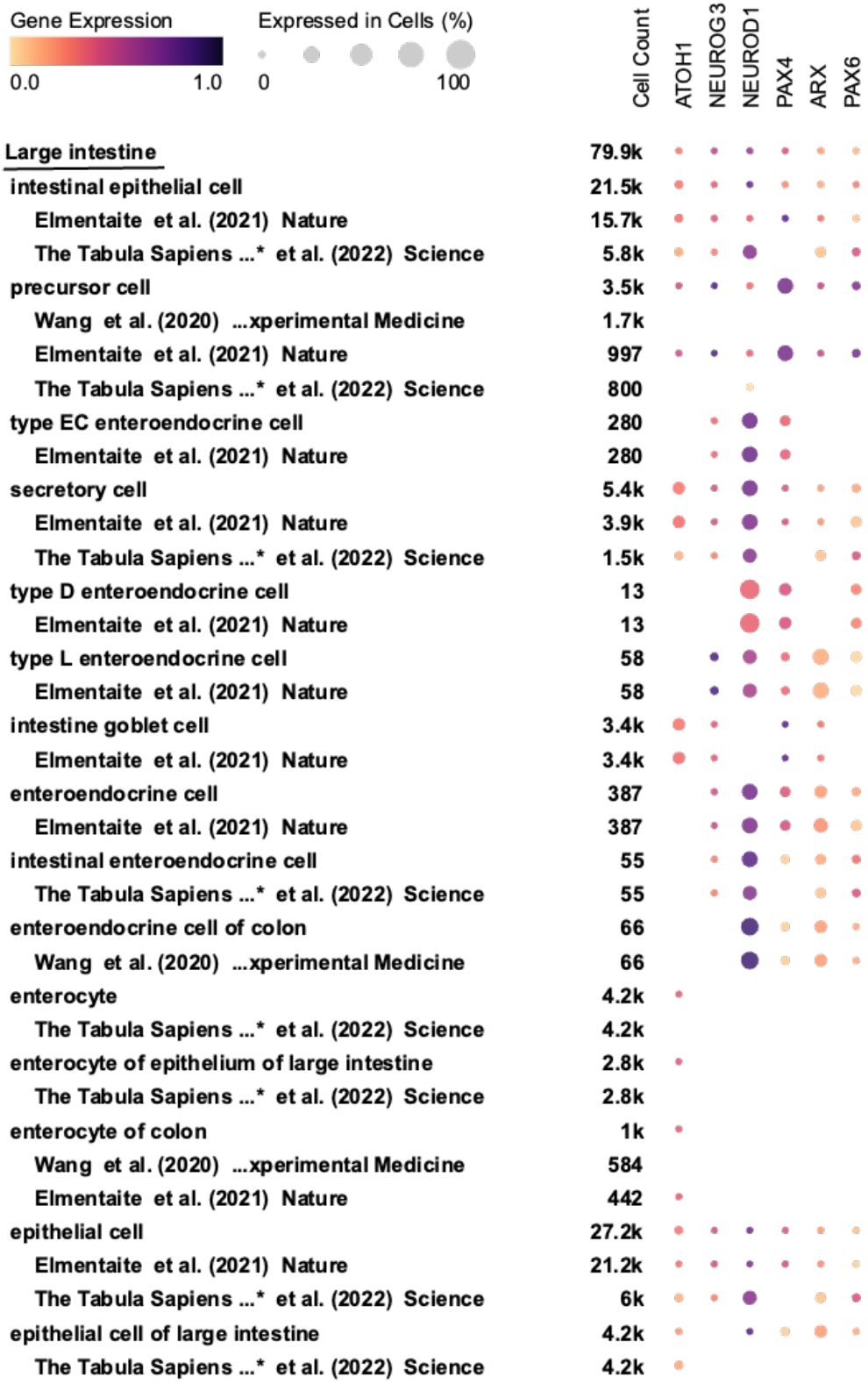
8. Appendix

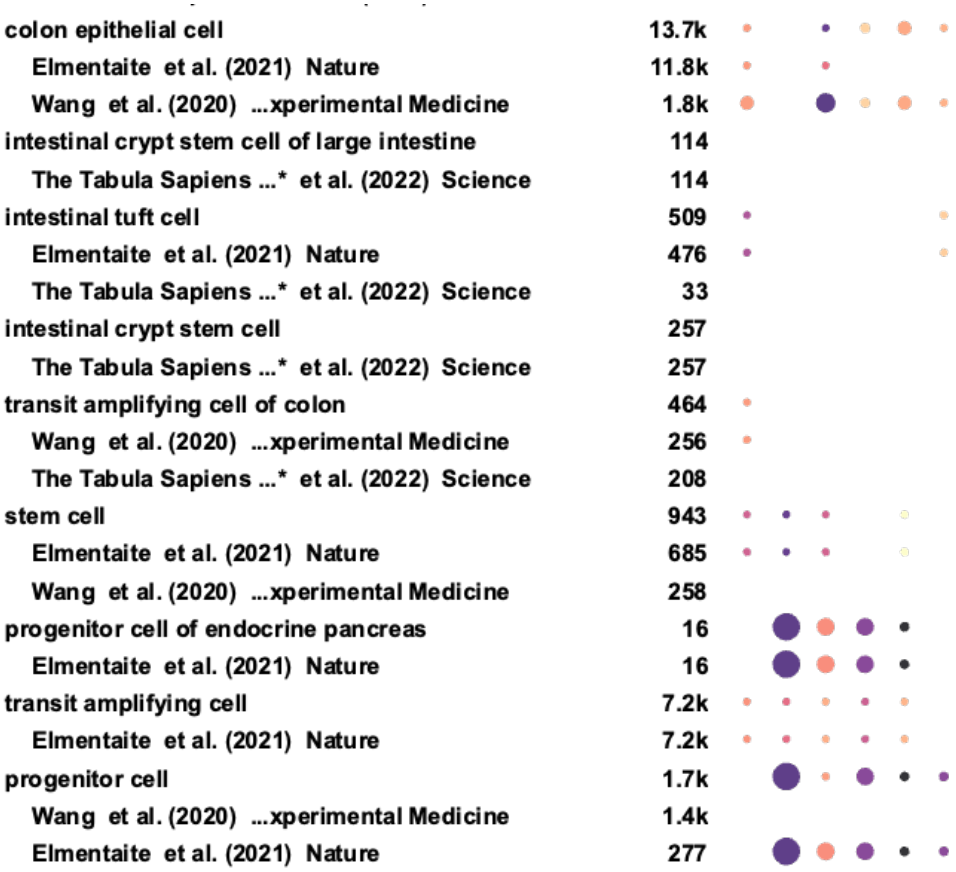
8.1 Appendix 1. Marker genes of pre-defined Cell ontology classifications in the sc-RNAseq database ‘Tabula Muris’

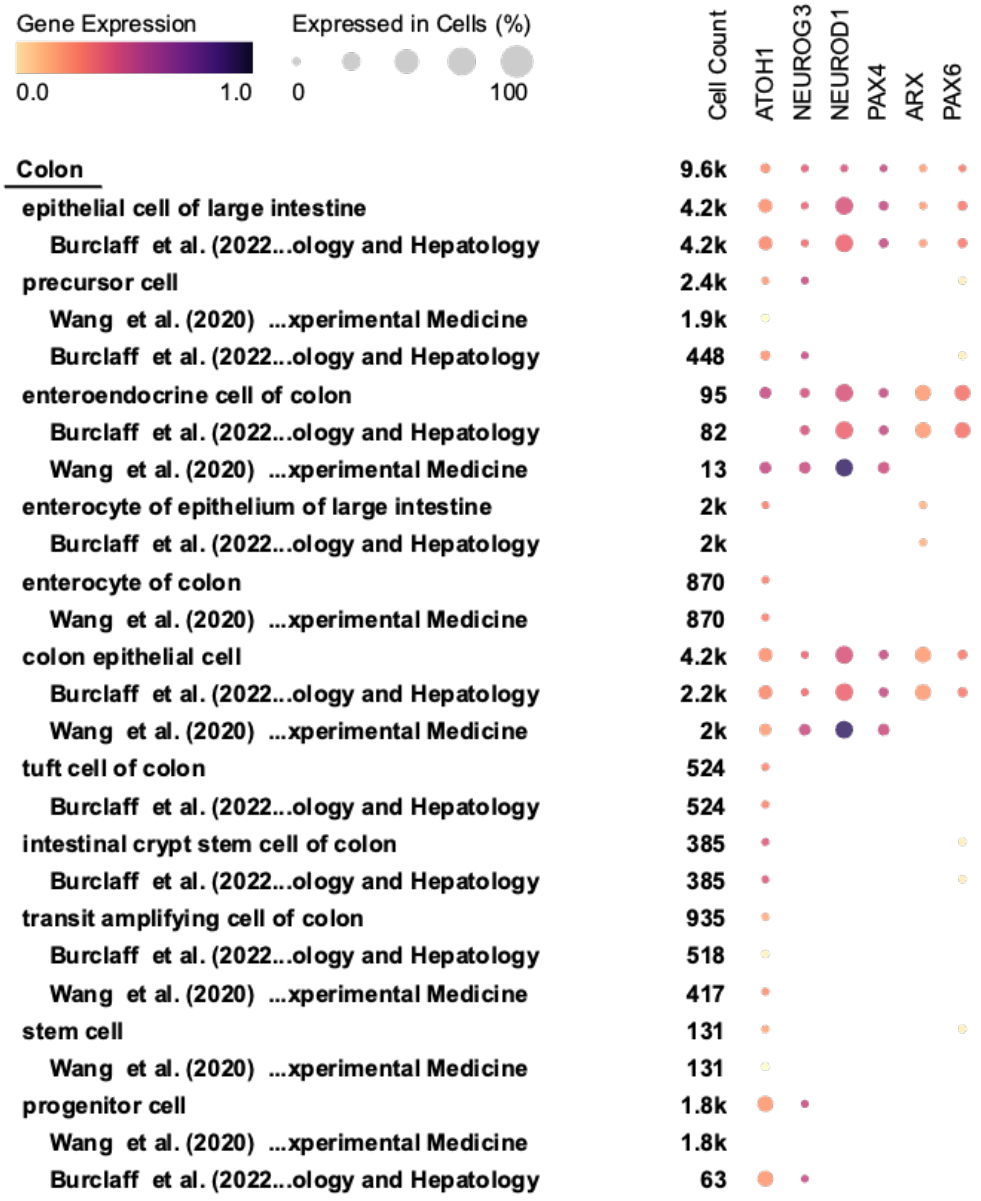


Plot generated by the ‘Seurat ‘package on R (Hao et al., 2024).

8.2 Appendix 2. Expression of candidate transcription factors from scRNA-seq datasets of the human ‘Large Intestine’ or ‘Colon’ grouped by publication

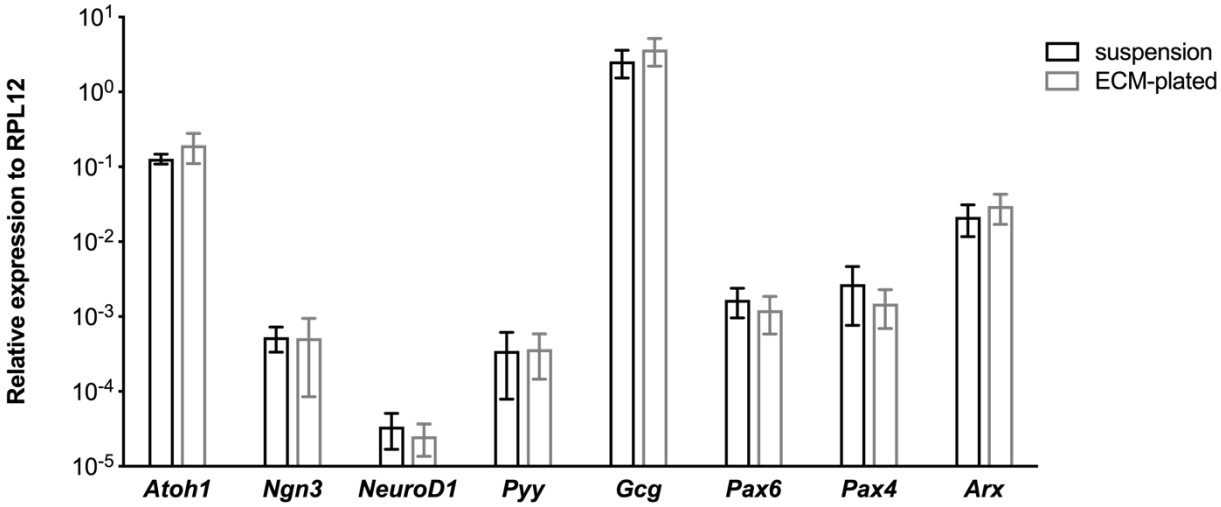



colon epithelial cell 13.7k
Elmentaite et al. (2021) Nature 11.8k
Wang et al. (2020) ...xperimental Medicine 1.8k
intestinal crypt stem cell of large intestine 114
The Tabula Sapiens ...* et al. (2022) Science 114
intestinal tuft cell 509
Elmentaite et al. (2021) Nature 476
The Tabula Sapiens ...* et al. (2022) Science 33
intestinal crypt stem cell 257
The Tabula Sapiens ...* et al. (2022) Science 257
transit amplifying cell of colon 464
Wang et al. (2020) ...xperimental Medicine 256
The Tabula Sapiens ...* et al. (2022) Science 208
stem cell 943
Elmentaite et al. (2021) Nature 685
Wang et al. (2020) ...xperimental Medicine 258
progenitor cell of endocrine pancreas 16
Elmentaite et al. (2021) Nature 16
transit amplifying cell 7.2k
Elmentaite et al. (2021) Nature 7.2k
progenitor cell 1.7k
Wang et al. (2020) ...xperimental Medicine 1.4k
Elmentaite et al. (2021) Nature 277



Data downloaded from the CELLxGENE platform.

8.3 Appendix 3 – Expression of L-cell differentiation markers in NCI-H716 cells in suspension and following plating on extracellular matrix (ECM) substrate.



mRNA transcript levels were quantified by RT-qPCR and normalised to expression of *rpl12* housekeeping gene.

9. References

Acuna-Goycolea, C. & van den Pol, A.N. (2005) Peptide YY $_{3-36}$ Inhibits Both Anorexigenic Proopiomelanocortin and Orexigenic Neuropeptide Y Neurons: Implications for Hypothalamic Regulation of Energy Homeostasis. *The Journal of Neuroscience*. 25 (45), 10510–10519. doi:10.1523/JNEUROSCI.2552-05.2005.

Adrian, T.E., Ferri, G.-L., Bacarese-Hamilton, A.J., Fuessl, H.S., Polak, J.M. & Bloom, S.R. (1985) Human distribution and release of a putative new gut hormone, peptide YY. *Gastroenterology*. 89 (5), 1070–1077. doi:10.1016/0016-5085(85)90211-2.

Agus, A., Denizot, J., Thévenot, J., Martinez-Medina, M., Massier, S., Sauvanet, P., Bernalier-Donadille, A., Denis, S., Hofman, P., Bonnet, R., Billard, E. & Barnich, N. (2016) Western diet induces a shift in microbiota composition enhancing susceptibility to Adherent-Invasive E. coli infection and intestinal inflammation. *Scientific Reports*. 6 (1), 19032. doi:10.1038/srep19032.

Aizawa, F., Nishinaka, T., Yamashita, T., Nakamoto, K., Kurihara, T., Hirasawa, A., Kasuya, F., Miyata, A. & Tokuyama, S. (2016) GPR40/FFAR1 deficient mice increase noradrenaline levels in the brain and exhibit abnormal behavior. *Journal of Pharmacological Sciences*. 132 (4), 249–254. doi:10.1016/j.jphs.2016.09.007.

Aliluev, A., Tritschler, S., Sterr, M., Oppenländer, L., Hinterdobler, J., Greisle, T., Irmler, M., Beckers, J., Sun, N., Walch, A., Stemmer, K., Kindt, A., Krumsiek, J., Tschöp, M.H., Luecken, M.D., Theis, F.J., Lickert, H. & Böttcher, A. (2021) Diet-induced alteration of intestinal stem cell function underlies obesity and prediabetes in mice. *Nature Metabolism*. 3 (9), 1202–1216. doi:10.1038/s42255-021-00458-9.

Almagro Armenteros, J.J., Tsirigos, K.D., Sønderby, C.K., Petersen, T.N., Winther, O., Brunak, S., von Heijne, G. & Nielsen, H. (2019) SignalP 5.0 improves signal peptide predictions using deep neural networks. *Nature Biotechnology*. 37 (4), 420–423. doi:10.1038/s41587-019-0036-z.

Amoêdo, N.D., Rodrigues, M.F., Pezzuto, P., Galina, A., da Costa, R.M., de Almeida, F.C.L., El-Bacha, T. & Rumjanek, F.D. (2011) Energy Metabolism in H460 Lung Cancer Cells: Effects of Histone Deacetylase Inhibitors. *PLoS ONE*. 6 (7), e22264. doi:10.1371/journal.pone.0022264.

Ang, Z., Er, J.Z., Tan, N.S., Lu, J., Liou, Y.-C., Grosse, J. & Ding, J.L. (2016) Human and mouse monocytes display distinct signalling and cytokine profiles upon stimulation with FFAR2/FFAR3 short-chain fatty acid receptor agonists. *Scientific Reports*. 6 (1), 34145. doi:10.1038/srep34145.

Anini, Y., Fu-Cheng, X., Cuber, J.C., Kervran, A., Chariot, J. & Roz□, C. (1999) Comparison of the postprandial release of peptide YY and proglucagon-derived peptides in the rat. *Pfl□gers Archiv European Journal of Physiology*. 438 (3), 299–306. doi:10.1007/s004240050913.

Apelqvist, Å., Li, H., Sommer, L., Beatus, P., Anderson, D.J., Honjo, T., de Angelis, M.H., Lendahl, U. & Edlund, H. (1999) Notch signalling controls

pancreatic cell differentiation. *Nature*. 400 (6747), 877–881. doi:10.1038/23716.
Aranias, T., Grosfeld, A., Poitou, C., Omar, A.A., Le Gall, M., Miquel, S., Garbin, K., Ribeiro, A., Bouillot, J.L., Bado, A., Brot-Laroche, E., Clément, K., Leturque, A., Guilmeau, S. & Serradas, P. (2015) Lipid-rich diet enhances L-cell density in obese subjects and in mice through improved L-cell differentiation. *Journal of Nutritional Science*. 4. doi:10.1017/jns.2015.11.
Arayici, M.E., Mert-Ozupek, N., Yalcin, F., Basbinar, Y. & Ellidokuz, H. (2022) Soluble and Insoluble Dietary Fiber Consumption and Colorectal Cancer Risk: A Systematic Review and Meta-Analysis. *Nutrition and Cancer*. 74 (7), 2412–2425. doi:10.1080/01635581.2021.2008990.
Archer, S.Y., Meng, S., Shei, A. & Hodin, R.A. (1998) p21 ^{WAF1} is required for butyrate-mediated growth inhibition of human colon cancer cells. *Proceedings of the National Academy of Sciences*. 95 (12), 6791–6796. doi:10.1073/pnas.95.12.6791.
Axelrod, D. (1981) Cell-substrate contacts illuminated by total internal reflection fluorescence. *The Journal of cell biology*. 89 (1), 141–145. doi:10.1083/jcb.89.1.141.
Baik, J.H. (2021) Dopaminergic control of the feeding circuit. *Endocrinology and Metabolism*.36 (2) pp.229–239. doi:10.3803/ENM.2021.979.
Ballantyne, G. (2006) Peptide YY(1-36) and Peptide YY(3-36): Part I. Distribution, Release and Actions. *Obesity Surgery*. 16 (5), 651–658. doi:10.1381/096089206776944959.
Balthasar, N., Dalgaard, L.T., Lee, C.E., Yu, J., Funahashi, H., et al. (2005) Divergence of melanocortin pathways in the control of food intake and energy expenditure. *Cell*. 123 (3), 493–505. doi:10.1016/j.cell.2005.08.035.
Barker, N., van Es, J.H., Kuipers, J., Kujala, P., van den Born, M., Cozijnsen, M., Haegebarth, A., Korving, J., Begthel, H., Peters, P.J. & Clevers, H. (2007) Identification of stem cells in small intestine and colon by marker gene Lgr5. *Nature*. 449 (7165), 1003–1007. doi:10.1038/nature06196.
Barki, N., Bolognini, D., Börjesson, U., Jenkins, L., Riddell, J., Hughes, D.I., Ulven, T., Hudson, B.D., Ulven, E.R., Dekker, N., Tobin, A.B. & Milligan, G. (2022) Chemogenetics defines a short-chain fatty acid receptor gut–brain axis. *eLife*. 11. doi:10.7554/eLife.73777.
Barki, N., Jenkins, L., Marsango, S., Dedeo, D., Bolognini, D., Dwomoh, L., Abdelmalik, A.M., Nilsen, M., Stoffels, M., Nagel, F., Schulz, S., Tobin, A.B. & Milligan, G. (2023) Phosphorylation bar-coding of free fatty acid receptor 2 is generated in a tissue-specific manner. *eLife*. 12. doi:10.7554/eLife.91861.3.
Barrios-Rodiles, M., Brown, K.R., Ozdamar, B., Bose, R., Liu, Z., Donovan, R.S., Shinjo, F., Liu, Y., Dembowy, J., Taylor, I.W., Luga, V., Przulj, N., Robinson, M., Suzuki, H., Hayashizaki, Y., Jurisica, I. & Wrana, J.L. (2005) High-throughput mapping of a dynamic signaling network in mammalian cells. *Science*. 307 (5715), 1621–1625. doi:10.1126/science.1105776.
Bartholome, A., Albin, D., Baker, D., Holst, J. & Tappenden, K. (2004) Supplementation of total parenteral nutrition with butyrate acutely increases structural aspects of intestinal adaptation after an 80%

jejunoileal resection in neonatal piglets. *Journal of Parenteral and Enteral Nutrition*. 28 (4), 210–222. doi:10.1177/0148607104028004210.
Basak, O., Beumer, J., Wiebrands, K., Seno, H., van Oudenaarden, A. & Clevers, H. (2017) Induced Quiescence of Lgr5+ Stem Cells in Intestinal Organoids Enables Differentiation of Hormone-Producing Enteroendocrine Cells. *Cell Stem Cell*. 20 (2), 177-190.e4. doi:10.1016/j.stem.2016.11.001.
Batterham, R.L., Cowley, M.A., Small, C.J., Herzog, H., Cohen, M.A., Dakin, C.L., Wren, A.M., Brynes, A.E., Low, M.J., Ghatei, M.A., Cone, R.D. & Bloom, S.R. (2002) Gut hormone PYY3-36 physiologically inhibits food intake. *Nature*. 418 (6898), 650–654. doi:10.1038/nature00887.
Batterham, R.L., Ffytche, D.H., Rosenthal, J.M., Zelaya, F.O., Barker, G.J., Withers, D.J. & Williams, S.C.R. (2007) PYY modulation of cortical and hypothalamic brain areas predicts feeding behaviour in humans. *Nature*. 450 (7166), 106–109. doi:10.1038/nature06212.
Bauer, C.S., Woolley, R.J., Teschemacher, A.G. & Seward, E.P. (2007) Potentiation of Exocytosis by Phospholipase C-Coupled G-Protein-Coupled Receptors Requires the Priming Protein Munc13-1. *The Journal of Neuroscience*. 27 (1), 212–219. doi:10.1523/JNEUROSCI.4201-06.2007.
Bellahcene, M., O'Dowd, J.F., Wargent, E.T., Zaibi, M.S., Hislop, D.C., Ngala, R.A., Smith, D.M., Cawthorne, M.A., Stocker, C.J. & Arch, J.R.S. (2013) Male mice that lack the G-protein-coupled receptor GPR41 have low energy expenditure and increased body fat content. *British Journal of Nutrition*. 109 (10), 1755–1764. doi:10.1017/S0007114512003923.
Bellono, N.W., Bayrer, J.R., Leitch, D.B., Castro, J., Zhang, C., O'Donnell, T.A., Brierley, S.M., Ingraham, H.A. & Julius, D. (2017) Enterochromaffin Cells Are Gut Chemosensors that Couple to Sensory Neural Pathways. *Cell*. 170 (1), 185-198.e16. doi:10.1016/j.cell.2017.05.034.
Berthoud, H.-R. & Neuhuber, W.L. (2000) Functional and chemical anatomy of the afferent vagal system. *Autonomic Neuroscience: Basic and Clinical*.85. www.elsevier.com/locate/autneu.
Bertoline, L.M.F., Lima, A.N., Krieger, J.E. & Teixeira, S.K. (2023) Before and after AlphaFold2: An overview of protein structure prediction. *Frontiers in Bioinformatics*. 3. doi:10.3389/fbinf.2023.1120370.
Den Besten, G., Van Eunen, K., Groen, A.K., Venema, K., Reijngoud, D.J. & Bakker, B.M. (2013) The role of short-chain fatty acids in the interplay between diet, gut microbiota, and host energy metabolism. *Journal of Lipid Research*.54 (9) pp.2325–2340. doi:10.1194/jlr.R036012.
Beumer, J., Artegiani, B., Post, Y., Reimann, F., Gribble, F., Nguyen, T.N., Zeng, H., Van den Born, M., Van Es, J.H. & Clevers, H. (2018) Enteroendocrine cells switch hormone expression along the crypt-to-villus BMP signalling gradient. *Nature Cell Biology*. 20 (8), 909–916. doi:10.1038/s41556-018-0143-y.
Beumer, J. & Clevers, H. (2021) Cell fate specification and differentiation in the adult mammalian intestine. *Nature Reviews Molecular Cell Biology*. 22 (1), 39–53. doi:10.1038/s41580-020-0278-0.
Beumer, J., Puschhof, J., Bauzá-Martinez, J., Martínez-Silgado, A., Elmentaite, R., et al. (2020) High-Resolution mRNA and Secretome Atlas of Human

Enteroendocrine Cells. *Cell*. 181 (6), 1291-1306.e19. doi:10.1016/j.cell.2020.04.036.
Beyaz, S., Mana, M.D., Roper, J., Kedrin, D., Saadatpour, A., et al. (2016) High-fat diet enhances stemness and tumorigenicity of intestinal progenitors. *Nature*. 531 (7592), 53–58. doi:10.1038/nature17173.
Biancolin, A.D., Martchenko, A., Mitova, E., Gurges, P., Michalchyshyn, E., Chalmers, J.A., Doria, A., Mychaleckyj, J.C., Adriaenssens, A.E., Reimann, F., Gribble, F.M., Gil-Lozano, M., Cox, B.J. & Brubaker, P.L. (2020) The core clock gene, Bmal1, and its downstream target, the SNARE regulatory protein secretagogin, are necessary for circadian secretion of glucagon-like peptide-1. *Molecular Metabolism*. 31, 124–137. doi:10.1016/j.molmet.2019.11.004.
Billing, L.J., Larraufie, P., Lewis, J., Leiter, A., Li, J., Lam, B., Yeo, G.SH., Goldspink, D.A., Kay, R.G., Gribble, F.M. & Reimann, F. (2019) Single cell transcriptomic profiling of large intestinal enteroendocrine cells in mice – Identification of selective stimuli for insulin-like peptide-5 and glucagon-like peptide-1 co-expressing cells. *Molecular Metabolism*. 29, 158–169. doi:10.1016/j.molmet.2019.09.001.
Billing, L.J., Smith, C.A., Larraufie, P., Goldspink, D.A., Galvin, S., Kay, R.G., Howe, J.D., Walker, R., Pruna, M., Glass, L., Pais, R., Gribble, F.M. & Reimann, F. (2018) Co-storage and release of insulin-like peptide-5, glucagon-like peptide-1 and peptideYY from murine and human colonic enteroendocrine cells. *Molecular Metabolism*. 16, 65–75. doi:10.1016/j.molmet.2018.07.011.
Blythe, E.E. & von Zastrow, M. (2023) β-Arrestin-independent endosomal cAMP signaling by a polypeptide hormone GPCR. *Nature Chemical Biology*. doi:10.1038/s41589-023-01412-4.
Boese, E.A., Tollefson, M.R., Schnieders, M.J., Darbro, B.W., Alward, W.L.M. & Fingert, J.H. (2020) Novel Intragenic *PAX6* Deletion in a Pedigree with Aniridia, Morbid Obesity, and Diabetes. *Current Eye Research*. 45 (1), 91–96. doi:10.1080/02713683.2019.1649704.
Boffa, L.C., Lupton, J.R., Mariani, M.R., Ceppi, M., Newmark, H.L., Scalmati, A. & Lipkin, M. (1992) Modulation of colonic epithelial cell proliferation, histone acetylation, and luminal short chain fatty acids by variation of dietary fiber (wheat bran) in rats. *Cancer research*. 52 (21), 5906–5912.
Bohórquez, D. V., Chandra, R., Samsa, L.A., Vigna, S.R. & Liddle, R.A. (2011) Characterization of basal pseudopod-like processes in ileal and colonic PYY cells. *Journal of Molecular Histology*. 42 (1), 3–13. doi:10.1007/s10735-010-9302-6.
Bohórquez, D. V., Samsa, L.A., Roholt, A., Medicetty, S., Chandra, R. & Liddle, R.A. (2014) An Enteroendocrine Cell – Enteric Glia Connection Revealed by 3D Electron Microscopy. *PLoS ONE*. 9 (2), e89881. doi:10.1371/journal.pone.0089881.
Bohórquez, D. V., Shahid, R.A., Erdmann, A., Kreger, A.M., Wang, Y., Calakos, N., Wang, F. & Liddle, R.A. (2015) Neuroepithelial circuit formed by innervation of sensory enteroendocrine cells. *Journal of Clinical Investigation*. 125 (2), 782–786. doi:10.1172/JCI78361.
Bolognini, D., Barki, N., Butcher, A.J., Hudson, B.D., Sergeev, E., Molloy, C., Moss, C.E., Bradley, S.J., Le Gouill, C., Bouvier, M., Tobin, A.B. & Milligan, G. (2019) Chemogenetics defines receptor-mediated functions

of short chain free fatty acids. *Nature Chemical Biology*. 15 (5), 489–498. doi:10.1038/s41589-019-0270-1.
Boren, J., Lee, W.-N.P., Bassilian, S., Centelles, J.J., Lim, S., Ahmed, S., Boros, L.G. & Cascante, M. (2003) The Stable Isotope-based Dynamic Metabolic Profile of Butyrate-induced HT29 Cell Differentiation. *Journal of Biological Chemistry*. 278 (31), 28395–28402. doi:10.1074/jbc.M302932200.
Borg, C.M., Le Roux, C.W., Ghatei, M.A., Bloom, S.R., Patel, A.G. & Aylwin, S.J.B. (2006) Progressive rise in gut hormone levels after Roux-en-Y gastric bypass suggests gut adaptation and explains altered satiety. *British Journal of Surgery*. 93 (2), 210–215. doi:10.1002/bjs.5227.
Böttcher, G., Alumets, J., Håkanson, R. & Sundler, F. (1986) Co-existence of glicentin and peptide YY in colorectal L-cells in cat and man. An electron microscopic study. *Regulatory Peptides*. 13 (3–4), 283–291. doi:10.1016/0167-0115(86)90046-7.
Böttcher, G., Sjölund, K., Ekblad, E., Håkanson, R., Schwartz, T.W. & Sundler, F. (1984) Coexistence of peptide YY and glicentin immunoreactivity in endocrine cells of the gut. *Regulatory Peptides*. 8 (4), 261–266. doi:10.1016/0167-0115(84)90034-X.
Boucrot, E., Ferreira, A.P.A., Almeida-Souza, L., Debard, S., Vallis, Y., Howard, G., Bertot, L., Sauvonnet, N. & McMahon, H.T. (2015) Endophilin marks and controls a clathrin-independent endocytic pathway. *Nature*. 517 (7535), 460–465. doi:10.1038/nature14067.
Brahe, L.K., Astrup, A. & Larsen, L.H. (2013) Is butyrate the link between diet, intestinal microbiota and obesity-related metabolic diseases? *Obesity Reviews*. 14 (12), 950–959. doi:10.1111/obr.12068.
Bray, S.J. (2016) Notch signalling in context. *Nature Reviews Molecular Cell Biology*. 17 (11), 722–735. doi:10.1038/nrm.2016.94.
Breit, A., Wolff, K., Kalwa, H., Jarry, H., Büch, T. & Gudermann, T. (2006) The Natural Inverse Agonist Agouti-related Protein Induces Arrestin-mediated Endocytosis of Melanocortin-3 and -4 Receptors. *Journal of Biological Chemistry*. 281 (49), 37447–37456. doi:10.1074/jbc.M605982200.
Bridgeman, S., Ellison, G., Newsholme, P. & Mamotte, C. (2021) The HDAC Inhibitor Butyrate Impairs β Cell Function and Activates the Disallowed Gene Hexokinase I. *International Journal of Molecular Sciences*. 22 (24), 13330. doi:10.3390/ijms222413330.
Brighton, C.A., Rievaj, J., Kuhre, R.E., Glass, L.L., Schoonjans, K., Holst, J.J., Gribble, F.M. & Reimann, F. (2015) Bile Acids Trigger GLP-1 Release Predominantly by Accessing Basolaterally Located G Protein–Coupled Bile Acid Receptors. *Endocrinology*. 156 (11), 3961–3970. doi:10.1210/en.2015-1321.
Briscoe, C.P., Tadayyon, M., Andrews, J.L., Benson, W.G., Chambers, J.K., et al. (2003) The Orphan G Protein-coupled Receptor GPR40 Is Activated by Medium and Long Chain Fatty Acids. *Journal of Biological Chemistry*. 278 (13), 11303–11311. doi:10.1074/jbc.M211495200.
Brown, A.J., Goldsworthy, S.M., Barnes, A.A., Eilert, M.M., Tcheang, L., et al. (2003) The orphan G protein-coupled receptors GPR41 and GPR43 are activated by propionate and other short chain carboxylic acids. *Journal of Biological Chemistry*. 278 (13), 11312–11319. doi:10.1074/jbc.M211609200.

Brown, N.A., Schrevens, S., van Dijck, P. & Goldman, G.H. (2018) Fungal G-protein-coupled receptors: mediators of pathogenesis and targets for disease control. *Nature Microbiology*. 3 (4), 402–414. doi:10.1038/s41564-018-0127-5.

Brubaker, P.L., Izzo, A., Hill, M. & Drucker, D.J. (1997) Intestinal function in mice with small bowel growth induced by glucagon-like peptide-2. *American Journal of Physiology-Endocrinology and Metabolism*. 272 (6), E1050–E1058. doi:10.1152/ajpendo.1997.272.6.E1050.

Bruïne, A.P., Dinjens, W.N., van der Linden, E.P., Pijls, M.M., Moerkerk, P.T. & Bosman, F.T. (1993) Extracellular matrix components induce endocrine differentiation in vitro in NCI-H716 cells. *The American journal of pathology*. 142 (3), 773–782.

Bruïne, A.P., Dinjens, W.N.M., Pijls, M.M.J., Linden, E.P.M., Rousch, M.J.M., Moerkerk, P.T., Goeij, A.F.P.M. & Bosnian, F.T. (1992) NCI-H716 cells as a model for endocrine differentiation in colorectal cancer. *Virchows Archiv B Cell Pathology Including Molecular Pathology*. 62 (1), 311–320. doi:10.1007/BF02899698.

Brüning, J.C., Gautam, D., Burks, D.J., Gillette, J., Schubert, M., Orban, P.C., Klein, R., Krone, W., Müller-Wieland, D. & Kahn, C.R. (2000) Role of Brain Insulin Receptor in Control of Body Weight and Reproduction. *Science*. 289 (5487), 2122–2125. doi:10.1126/science.289.5487.2122.

Bryant MG, Bloom SR, Polak JM, Hobbs S, Domschke W, Domschke S, Mitznegg, P., Ruppin, H. & Demling, L. (1983)Measurement of gut hormonal peptides in biopsies from human stomach and proximal small intestine. *Gut.* 24(2):114-9. doi: 10.1136/gut.24.2.114.

Buczacki, S.J.A., Zecchini, H.I., Nicholson, A.M., Russell, R., Vermeulen, L., Kemp, R. & Winton, D.J. (2013) Intestinal label-retaining cells are secretory precursors expressing Lgr5. *Nature*. 495 (7439), 65–69. doi:10.1038/nature11965.

Buffa, R., Capella, C., Fontana, P., Usellini, L. & Solcia, E. (1978) Types of endocrine cells in the human colon and rectum. *Cell and Tissue Research*. 192 (2). doi:10.1007/BF00220741.

Buffa, R., Solcia, E. & Go, V.L. (1976) Immunohistochemical identification of the cholecystokinin cell in the intestinal mucosa. *Gastroenterology*. 70 (4), 528–532.

Bünemann, M. & Hosey, M.M. (1999) G-protein coupled receptor kinases as modulators of G-protein signalling. *The Journal of Physiology*. 517 (1), 5–23. doi:10.1111/j.1469-7793.1999.0005z.x.

Burchfield, J.G., Lopez, J.A., Mele, K., Vallotton, P. & Hughes, W.E. (2010) Exocytotic Vesicle Behaviour Assessed by Total Internal Reflection Fluorescence Microscopy. *Traffic*. 11 (4), 429–439. doi:10.1111/j.1600-0854.2010.01039.x.

Burclaff, J., Bliton, R.J., Breau, K.A., Ok, M.T., Gomez-Martinez, I., Ranek, J.S., Bhatt, A.P., Purvis, J.E., Woosley, J.T. & Magness, S.T. (2022) A Proximal-to-Distal Survey of Healthy Adult Human Small Intestine and Colon Epithelium by Single-Cell Transcriptomics. *CMGH*. 13 (5), 1554–1589. doi:10.1016/j.jcmgh.2022.02.007.

Cabrele, C. & Beck-Sickinger, A.G. (2000), Molecular characterization of the ligand–receptor interaction of the neuropeptide Y family. J. Peptide Sci.,

6: 97-122. https://doi.org/10.1002/(SICI)1099-1387(200003)6:3<97::AID-PSC236>3.0.CO;2-E
Caengprasath, N. (2019) *Understanding the mechanisms regulating SCFA mediated release of anorectic gut hormones*. London, Imperial College London.
Caengprasath, N., Gonzalez-Abuin, N., Shchepinova, M., Ma, Y., Inoue, A., Tate, E.W., Frost, G. & Hanyaloglu, A.C. (2020) Internalization-Dependent Free Fatty Acid Receptor 2 Signaling Is Essential for Propionate-Induced Anorectic Gut Hormone Release. *iScience*. 23 (9). doi:10.1016/j.isci.2020.101449.
Caengprasath, N. & Hanyaloglu, A.C. (2019) Hardwiring wire-less networks: spatially encoded GPCR signaling in endocrine systems. *Current Opinion in Cell Biology*.57 pp.77–82. doi:10.1016/j.ceb.2018.12.009.
Cahill, T.J., Thomsen, A.R.B., Tarrasch, J.T., Plouffe, B., Nguyen, A.H., et al. (2017) Distinct conformations of GPCR-β-arrestin complexes mediate desensitization, signaling, and endocytosis. *Proceedings of the National Academy of Sciences of the United States of America*. 114 (10), 2562–2567. doi:10.1073/pnas.1701529114.
Calabrò, S., Kankowski, S., Cescon, M., Gambarotta, G., Raimondo, S., Haastert-Talini, K. & Ronchi, G. (2023) Impact of Gut Microbiota on the Peripheral Nervous System in Physiological, Regenerative and Pathological Conditions. *International Journal of Molecular Sciences*.24 (9). doi:10.3390/ijms24098061.
Campbell, J.R., Martchenko, A., Sweeney, M.E., Maalouf, M.F., Psichas, A., Gribble, F.M., Reimann, F. & Brubaker, P.L. (2020) Essential Role of Syntaxin-Binding Protein-1 in the Regulation of Glucagon-Like Peptide-1 Secretion. *Endocrinology*. 161 (5). doi:10.1210/endocr/bqaa039.
Cani, P.D., Hoste, S., Guiot, Y. & Delzenne, N.M. (2007) Dietary non-digestible carbohydrates promote L-cell differentiation in the proximal colon of rats. *British Journal of Nutrition*. 98 (1), 32–37. doi:10.1017/S0007114507691648.
Cao, X., Flock, G., Choi, C., Irwin, D.M. & Drucker, D.J. (2003) Aberrant regulation of human intestinal proglucagon gene expression in the NCI-H716 cell line. *Endocrinology*. 144 (5), 2025–2033. doi:10.1210/en.2002-0049.
Carabotti, M., Scirocco, A., Maselli, M.A. & Severi, C. (2015) The gut-brain axis: interactions between enteric microbiota, central and enteric nervous systems. *Annals of gastroenterology*. 28 (2), 203–209.
Carrel, D., Simon, A., Emerit, M.B., Rivals, I., Leterrier, C., Biard, M., Hamon, M., Darmon, M. & Lenkei, Z. (2011) Axonal Targeting of the 5-HT $_{1B}$ Serotonin Receptor Relies on Structure-Specific Constitutive Activation. *Traffic*. 12 (11), 1501–1520. doi:10.1111/j.1600-0854.2011.01260.x.
Castillo-Badillo, J.A., Molina-Muñoz, T., Romero-Ávila, M.T., Vázquez-Macías, A., Rivera, R., Chun, J. & García-Sáinz, J.A. (2012) Sphingosine 1-phosphate-mediated α1B-adrenoceptor desensitization and phosphorylation. Direct and paracrine/autocrine actions. *Biochimica et Biophysica Acta (BBA) - Molecular Cell Research*. 1823 (2), 245–254. doi:10.1016/j.bbamcr.2011.10.002.
Chambers, E.S., Viardot, A., Psichas, A., Morrison, D.J., Murphy, K.G., et al. (2015) Effects of targeted delivery of propionate to the human colon on

appetite regulation, body weight maintenance and adiposity in overweight adults. *Gut*. 64 (11), 1744–1754. doi:10.1136/gutjnl-2014-307913.
Chaudhri, O., Small, C. & Bloom, S. (2006) Gastrointestinal hormones regulating appetite. *Philosophical Transactions of the Royal Society B: Biological Sciences*. 361 (1471), 1187–1209. doi:10.1098/rstb.2006.1856.
Chen, M.E., Naeini, S.M., Srikrishnaraj, A., Drucker, D.J., Fesler, Z. & Brubaker, P.L. (2022) Glucagon-Like Peptide-2 Stimulates S-Phase Entry of Intestinal Lgr5+ Stem Cells. *Cellular and Molecular Gastroenterology and Hepatology*. 13 (6), 1829–1842. doi:10.1016/j.jcmgh.2022.02.011.
Chen, X.-K., Wang, L.-C., Zhou, Y., Cai, Q., Prakriya, M., Duan, K.-L., Sheng, Z.-H., Lingle, C. & Zhou, Z. (2005) Activation of GPCRs modulates quantal size in chromaffin cells through Gβγ and PKC. *Nature Neuroscience*. 8 (9), 1160–1168. doi:10.1038/nn1529.
Cheng, C.W., Biton, M., Haber, A.L., Gunduz, N., Eng, G., et al. (2019) Ketone Body Signaling Mediates Intestinal Stem Cell Homeostasis and Adaptation to Diet. *Cell*. 178 (5), 1115-1131.e15. doi:10.1016/j.cell.2019.07.048.
Cheng, L., Xia, F., Li, Z., Shen, C., Yang, Z., Hou, H., Sun, S., Feng, Y., Yong, X., Tian, X., Qin, H., Yan, W. & Shao, Z. (2023) Structure, function and drug discovery of GPCR signaling. *Molecular Biomedicine*. 4 (1), 46. doi:10.1186/s43556-023-00156-w.
Cho, H.-J., Robinson, E.S., Rivera, L.R., McMillan, P.J., Testro, A., Nikfarjam, M., Bravo, D.M. & Furness, J.B. (2014) Glucagon-like peptide 1 and peptide YY are in separate storage organelles in enteroendocrine cells. *Cell and Tissue Research*. 357 (1), 63–69. doi:10.1007/s00441-014-1886-9.
Chriett, S., Dąbek, A., Wojtala, M., Vidal, H., Balcerczyk, A. & Pirola, L. (2019) Prominent action of butyrate over β-hydroxybutyrate as histone deacetylase inhibitor, transcriptional modulator and anti-inflammatory molecule. *Scientific Reports*. 9 (1), 742. doi:10.1038/s41598-018-36941-9.
Christensen, L.W., Kuhre, R.E., Janus, C., Svendsen, B. & Holst, J.J. (2015) Vascular, but not luminal, activation of FFAR1 (GPR40) stimulates GLP-1 secretion from isolated perfused rat small intestine. *Physiological Reports*. 3 (9), e12551. doi:10.14814/phy2.12551.
Christiansen, C.B., Gabe, M.B.N., Svendsen, B., Dragsted, L.O., Rosenkilde, M.M. & Holst, J.J. (2018) The impact of short-chain fatty acids on GLP-1 and PYY secretion from the isolated perfused rat colon. *American Journal of Physiology-Gastrointestinal and Liver Physiology*. 315 (1), G53–G65. doi:10.1152/ajpgi.00346.2017.
Chun, E., Lavoie, S., Fonseca-Pereira, D., Bae, S., Michaud, M., Hoveyda, H.R., Fraser, G.L., Gallini Comeau, C.A., Glickman, J.N., Fuller, M.H., Layden, B.T. & Garrett, W.S. (2019) Metabolite-Sensing Receptor Ffar2 Regulates Colonic Group 3 Innate Lymphoid Cells and Gut Immunity. *Immunity*. 51 (5), 871-884.e6. doi:10.1016/j.immuni.2019.09.014.
Clément, K., Vaisse, C., Lahlou, N., Cabrol, S., Pelloux, V., Cassuto, D., Gourmelen, M., Dina, C., Chambaz, J., Lacorte, J.-M., Basdevant, A., Bougnères, P., Lebouc, Y., Froguel, P. & Guy-Grand, B. (1998) A mutation in the human leptin receptor gene causes obesity and pituitary dysfunction. *Nature*. 392 (6674), 398–401. doi:10.1038/32911.

Clevers, H. (2013) The Intestinal Crypt, A Prototype Stem Cell Compartment. *Cell*. 154 (2), 274–284. doi:10.1016/j.cell.2013.07.004.
ClinicalTrials.gov (2018) *A Research Study of NNC0165-1875 Alone or Together With Semaglutide in People Who Are Overweight or Obese*. 2018.
Clinicaltrials.gov (2023) *NCT06019559: A Study to Evaluate the Safety, Tolerability, and Weight Loss Efficacy of K-757 Alone and in Combination With K-833*. 2023.
Cohen, M.A., Ellis, S.M., Le Roux, C.W., Batterham, R.L., Park, A., Patterson, M., Frost, G.S., Ghatei, M.A. & Bloom, S.R. (2003) Oxyntomodulin Suppresses Appetite and Reduces Food Intake in Humans. *The Journal of Clinical Endocrinology & Metabolism*. 88 (10), 4696–4701. doi:10.1210/jc.2003-030421.
Cone, R., Cowley, M., Butler, A., Fan, W., Marks, D. & Low, M. (2001) The arcuate nucleus as a conduit for diverse signals relevant to energy homeostasis. *International Journal of Obesity*. 25 (S5), S63–S67. doi:10.1038/sj.ijo.0801913.
Cook, T.M., Gavini, C.K., Jesse, J., Aubert, G., Gornick, E., Bonomo, R., Gautron, L., Layden, B.T. & Mansuy-Aubert, V. (2021) Vagal neuron expression of the microbiota-derived metabolite receptor, free fatty acid receptor (FFAR3), is necessary for normal feeding behavior. *Molecular Metabolism*. 54, 101350. doi:10.1016/j.molmet.2021.101350.
Corrêa, R.O., Castro, P.R., Fachi, J.L., Nirello, V.D., El-Sahhar, S., et al. (2023) Inulin diet uncovers complex diet-microbiota-immune cell interactions remodeling the gut epithelium. *Microbiome*. 11 (1), 90. doi:10.1186/s40168-023-01520-2.
Corrò, C., Novellasdemunt, L. & Li, V.S.W. (2020) A brief history of organoids. *American Journal of Physiology-Cell Physiology*. 319 (1), C151–C165. doi:10.1152/ajpcell.00120.2020.
Cryan, J.F., O, K.J., M Cowan, C.S., Sandhu, K. V, S Bastiaanssen, T.F., et al. (2019) The Microbiota-Gut-Brain Axis. *Physiol Rev*. 99, 1877–2013. doi:10.1152/physrev.00018.2018.-The.
Cui, H., López, M. & Rahmouni, K. (2017) The cellular and molecular bases of leptin and ghrelin resistance in obesity. *Nature Reviews Endocrinology*. 13 (6), 338–351. doi:10.1038/nrendo.2016.222.
Cummings, D.E. & Overduin, J. (2007) Gastrointestinal regulation of food intake. *Journal of Clinical Investigation*.117 (1) pp.13–23. doi:10.1172/JCI30227.
Cummings, J.H. (1981) Short chain fatty acids in the human colon. *Gut*.22 (9) pp.763–779. doi:10.1136/gut.22.9.763.
Cummings, J.H. & Macfarlane, G.T. (1997) Role of intestinal bacteria in nutrient metabolism. *Journal of Parenteral and Enteral Nutrition*. 21 (6), 357–365. doi:10.1177/0148607197021006357.
Cummings, J.H., Pomare, E.W., Branch, H.W.J., Naylor, C.P.E. & MacFarlane, G.T. (1987) Short chain fatty acids in human large intestine, portal, hepatic and venous blood. *Gut*. 28 (10), 1221–1227. doi:10.1136/gut.28.10.1221.
Cummings, J.H. & Stephen, A.M. (2007) Carbohydrate terminology and classification. *European Journal of Clinical Nutrition*. 61 (S1), S5–S18. doi:10.1038/sj.ejcn.1602936.

Dahm, C.C., Keogh, R.H., Spencer, E.A., Greenwood, D.C., Key, T.J., Fentiman, I.S., Shipley, M.J., Brunner, E.J., Cade, J.E., Burley, V.J., Mishra, G., Stephen, A.M., Kuh, D., White, I.R., Luben, R., Lentjes, M.A.H., Khaw, K.T. & Rodwell (Bingham), S.A. (2010) Dietary Fiber and Colorectal Cancer Risk: A Nested Case-Control Study Using Food Diaries. *JNCI Journal of the National Cancer Institute*. 102 (9), 614–626. doi:10.1093/jnci/djq092.

Dalvi, P.S. & Belsham, D.D. (2012) Glucagon-Like Peptide-2 Directly Regulates Hypothalamic Neurons Expressing Neuropeptides Linked to Appetite Control in Vivo and in Vitro. *Endocrinology*. 153 (5), 2385–2397. doi:10.1210/en.2011-2089.

Daly, C., Guseinov, A.A., Hahn, H., Wright, A., Tikhonova, I.G., Thomsen, A.R.B. & Plouffe, B. (2023) β-Arrestin-dependent and -independent endosomal G protein activation by the vasopressin type 2 receptor. *eLife*. 12. doi:10.7554/eLife.87754.3.

Daly, C. & Plouffe, B. (2023) $G\alpha_q$ signalling from endosomes: A new conundrum. *British Journal of Pharmacology*. doi:10.1111/bph.16248.

Davie, J.R. (2003) Inhibition of Histone Deacetylase Activity by Butyrate. *The Journal of Nutrition*. 133 (7), 2485S-2493S. doi:10.1093/jn/133.7.2485S.

Davies, M.J., Bergenstal, R., Bode, B., Kushner, R.F., Lewin, A., Skjøth, T.V., Andreasen, A.H., Jensen, C.B. & DeFronzo, R.A. (2015) Efficacy of Liraglutide for Weight Loss Among Patients With Type 2 Diabetes. *JAMA*. 314 (7), 687. doi:10.1001/jama.2015.9676.

Deacon, C.F. & Holst, J.J. (2009) Immunoassays for the incretin hormones GIP and GLP-1. *Best Practice & Research Clinical Endocrinology & Metabolism*. 23 (4), 425–432. doi:10.1016/j.beem.2009.03.006.

Delaney, K.A., Murph, M.M., Brown, L.M. & Radhakrishna, H. (2002) Transfer of M2 Muscarinic Acetylcholine Receptors to Clathrin-derived Early Endosomes following Clathrin-independent Endocytosis. *Journal of Biological Chemistry*. 277 (36), 33439–33446. doi:10.1074/jbc.M205293200.

Demby, A. & Zaccolo, M. (2024) Investigating G-protein coupled receptor signalling with light-emitting biosensors. *Frontiers in Physiology*. 14. doi:10.3389/fphys.2023.1310197.

Dewulf, E.M., Ge, Q., Bindels, L.B., Sohet, F.M., Cani, P.D., Brichard, S.M. & Delzenne, N.M. (2013) Evaluation of the relationship between GPR43 and adiposity in human. *Nutrition & Metabolism*. 10 (1), 11. doi:10.1186/1743-7075-10-11.

Diakogiannaki, E., Pais, R., Tolhurst, G., Parker, H.E., Horscroft, J., Rauscher, B., Zietek, T., Daniel, H., Gribble, F.M. & Reimann, F. (2013) Oligopeptides stimulate glucagon-like peptide-1 secretion in mice through proton-coupled uptake and the calcium-sensing receptor. *Diabetologia*. 56 (12), 2688–2696. doi:10.1007/s00125-013-3037-3.

Dinsart, G., Leprovots, M., Lefort, A., Libert, F., Quesnel, Y., Veithen, A., Vassart, G., Huysseune, S., Parmentier, M. & Garcia, M.-I. (2023) The olfactory receptor Olfr78 promotes differentiation of enterochromaffin cells in the mouse colon. *EMBO Reports*. 25 (1), 304–333. doi:10.1038/s44319-023-00013-5.

Dixon, A.S., Schwinn, M.K., Hall, M.P., Zimmerman, K., Otto, P., Lubben, T.H., Butler, B.L., Binkowski, B.F., Machleidt, T., Kirkland, T.A., Wood, M.G.,

Eggers, C.T., Encell, L.P. & Wood, K. V. (2016) NanoLuc Complementation Reporter Optimized for Accurate Measurement of Protein Interactions in Cells. *ACS Chemical Biology*. 11 (2), 400–408. doi:10.1021/acschembio.5b00753.

Diz-Chaves, Y., Herrera-Pérez, S., González-Matías, L.C. & Mallo, F. (2022) *Effects of Glucagon-like peptide 1 (GLP-1) analogs in the hippocampus*. In: pp. 457–478. doi:10.1016/bs.vh.2021.12.005.

Dobbins, W.O. & Austin, L.L. (1991) Electron Microscopic Definition of Intestinal Endocrine Cells: Immunogrold Localization and Review. *Ultrastructural Pathology*. 15 (1), 15–39. doi:10.3109/01913129109021301.

Domínguez Conde, C., Xu, C., Jarvis, L.B., Rainbow, D.B., Wells, S.B., et al. (2022) Cross-tissue immune cell analysis reveals tissue-specific features in humans. *Science*. 376 (6594). doi:10.1126/science.abl5197.

Dong, C.X., Zhao, W., Solomon, C., Rowland, K.J., Ackerley, C., Robine, S., Holzenberger, M., Gonska, T. & Brubaker, P.L. (2014) The Intestinal Epithelial Insulin-Like Growth Factor-1 Receptor Links Glucagon-Like Peptide-2 Action to Gut Barrier Function. *Endocrinology*. 155 (2), 370–379. doi:10.1210/en.2013-1871.

Donohoe, D.R., Garge, N., Zhang, X., Sun, W., O'Connell, T.M., Bunger, M.K. & Bultman, S.J. (2011) The microbiome and butyrate regulate energy metabolism and autophagy in the mammalian colon. *Cell Metabolism*. 13 (5), 517–526. doi:10.1016/j.cmet.2011.02.018.

Dores, M.R. & Trejo, J. (2019) Endo-lysosomal sorting of G-protein-coupled receptors by ubiquitin: Diverse pathways for G-protein-coupled receptor destruction and beyond. *Traffic*. 20 (2), 101–109. doi:10.1111/tra.12619.

Dou, Y., Pizarro, T. & Zhou, L. (2022) Organoids as a Model System for Studying Notch Signaling in Intestinal Epithelial Homeostasis and Intestinal Cancer. *The American Journal of Pathology*. 192 (10), 1347–1357. doi:10.1016/j.ajpath.2022.06.008.

Downes, G.B. & Gautam, N. (1999) The G Protein Subunit Gene Families. *Genomics*. 62 (3), 544–552. doi:10.1006/geno.1999.5992.

Drucker, D.J. (2002) Gut adaptation and the glucagon-like peptides. *Gut*. 50 (3), 428–435. doi:10.1136/gut.50.3.428.

Drucker, D.J. (2018) Mechanisms of Action and Therapeutic Application of Glucagon-like Peptide-1. *Cell Metabolism*. 27 (4), 740–756. doi:10.1016/j.cmet.2018.03.001.

Drucker, D.J. (2019) The Discovery of GLP-2 and Development of Teduglutide for Short Bowel Syndrome. *ACS Pharmacology & Translational Science*. 2 (2), 134–142. doi:10.1021/acsptsci.9b00016.

Du, A., McCracken, K.W., Walp, E.R., Terry, N.A., Klein, T.J., Han, A., Wells, J.M. & May, C.L. (2012) Arx is required for normal enteroendocrine cell development in mice and humans. *Developmental Biology*. 365 (1), 175–188. doi:10.1016/j.ydbio.2012.02.024.

Duah, M., Zhang, K., Liang, Y., Ayarick, V.A., Xu, K. & Pan, B. (2023) Immune regulation of poly unsaturated fatty acids and free fatty acid receptor 4. *Journal of Nutritional Biochemistry*.112. doi:10.1016/j.jnutbio.2022.109222.

Ducastel, S., Touche, V., Trabelsi, M.S., Boulinguiez, A., Butruille, L., et al. (2020) The nuclear receptor FXR inhibits Glucagon-Like Peptide-1

secretion in response to microbiota-derived Short-Chain Fatty Acids. *Scientific Reports*. 10 (1). doi:10.1038/s41598-019-56743-x.
Eberlein, G.A., Eysselein, V.E., Schaeffer, M., Layer, P., Grandt, D., Goebell, H., Niebel, W., Davis, M., Lee, T.D., Shively, J.E. & Reeve, J.R. (1989) A new molecular form of PYY: Structural characterization of human PYY(3–36) and PYY(1–36). *Peptides*. 10 (4), 797–803. doi:10.1016/0196-9781(89)90116-2.
Edfalk, S., Steneberg, P. & Edlund, H. (2008) Gpr40 Is Expressed in Enteroendocrine Cells and Mediates Free Fatty Acid Stimulation of Incretin Secretion. *Diabetes*. 57 (9), 2280–2287. doi:10.2337/db08-0307.
Egerod, K.L., Engelstoft, M.S., Grunddal, K. V., Nøhr, M.K., Secher, A., Sakata, I., Pedersen, J., Windeløv, J.A., Füchtbauer, E.-M., Olsen, J., Sundler, F., Christensen, J.P., Wierup, N., Olsen, J. V., Holst, J.J., Zigman, J.M., Poulsen, S.S. & Schwartz, T.W. (2012) A Major Lineage of Enteroendocrine Cells Coexpress CCK, Secretin, GIP, GLP-1, PYY, and Neurotensin but Not Somatostatin. *Endocrinology*. 153 (12), 5782–5795. doi:10.1210/en.2012-1595.
Eishingdrelo, H. (2013) Minireview: Targeting GPCR Activated ERK Pathways for Drug Discovery. *Current Chemical Genomics and Translational Medicine*. 7, 9–15. doi:10.2174/2213988501307010009.
Eissele, R., Göke, R., Willemer, S., Harthus, H. -P., Vermeer, H., Arnold, R. & Göke, B. (1992) Glucagon-like peptide-1 cells in the gastrointestinal tract and pancreas of rat, pig and man. *European Journal of Clinical Investigation*. 22 (4), 283–291. doi:10.1111/j.1365-2362.1992.tb01464.x.
Ekberg, J.H., Hauge, M., Kristensen, L. V., Madsen, A.N., Engelstoft, M.S., Husted, A.-S., Sichlau, R., Egerod, K.L., Timshel, P., Kowalski, T.J., Gribble, F.M., Reiman, F., Hansen, H.S., Howard, A.D., Holst, B. & Schwartz, T.W. (2016) GPR119, a Major Enteroendocrine Sensor of Dietary Triglyceride Metabolites Coacting in Synergy With FFA1 (GPR40). *Endocrinology*. 157 (12), 4561–4569. doi:10.1210/en.2016-1334.
Elebring, E., Casselbrant, A., Persson, S.M.T., Fändriks, L. & Wallenius, V. (2023) βHB inhibits glucose-induced GLP-1 secretion in GLUTag and human jejunal enteroids. *Journal of Molecular Endocrinology*. 70 (4). doi:10.1530/JME-22-0115.
Elias, C.F., Aschkenasi, C., Lee, C., Kelly, J., Ahima, R.S., Bjorbæk, C., Flier, J.S., Saper, C.B. & Elmquist, J.K. (1999) Leptin Differentially Regulates NPY and POMC Neurons Projecting to the Lateral Hypothalamic Area. *Neuron*. 23 (4), 775–786. doi:10.1016/S0896-6273(01)80035-0.
Elmentaite, R., Kumasaka, N., Roberts, K., Fleming, A., Dann, E., et al. (2021) Cells of the human intestinal tract mapped across space and time. *Nature*. 597 (7875), 250–255. doi:10.1038/s41586-021-03852-1.
Elmquist, J.K., Elias, C.F. & Saper, C.B. (1999) From Lesions to Leptin: Review Hypothalamic Control of Food Intake and Body Weight. *Nueron*. 22, 221–232.
El-Salhy, M., Grimelius, L., Wilander, E., Ryberg, B., Terenius, L., Lundberg, J.M. & Tatemoto, K. (1983) Immunocytochemical identification of polypeptide YY (PYY) cells in the human gastrointestinal tract. *Histochemistry*. 77 (1), 15–23. doi:10.1007/BF00496632.

El-Salhy, M., Hatlebakk, J.G. & Hausken, T. (2020) Possible role of peptide YY (PYY) in the pathophysiology of irritable bowel syndrome (IBS). *Neuropeptides*. 79, 101973. doi:10.1016/j.npep.2019.101973.

Emery, E.C., Diakogiannaki, E., Gentry, C., Psichas, A., Habib, A.M., Bevan, S., Fischer, M.J.M., Reimann, F. & Gribble, F.M. (2015) Stimulation of GLP-1 Secretion Downstream of the Ligand-Gated Ion Channel TRPA1. *Diabetes*. 64 (4), 1202–1210. doi:10.2337/db14-0737.

Engelstoft, M.S., Park, W., Sakata, I., Kristensen, L. V., Husted, A.S., et al. (2013) Seven transmembrane G protein-coupled receptor repertoire of gastric ghrelin cells. *Molecular Metabolism*. 2 (4), 376–392. doi:10.1016/j.molmet.2013.08.006.

van Es, J.H., van Gijn, M.E., Riccio, O., van den Born, M., Vooijs, M., Begthel, H., Cozijnsen, M., Robine, S., Winton, D.J., Radtke, F. & Clevers, H. (2005) Notch/γ-secretase inhibition turns proliferative cells in intestinal crypts and adenomas into goblet cells. *Nature*. 435 (7044), 959–963. doi:10.1038/nature03659.

van Es, J.H., Sato, T., van de Wetering, M., Lyubimova, A., Yee Nee, A.N., Gregorieff, A., Sasaki, N., Zeinstra, L., van den Born, M., Korving, J., Martens, A.C.M., Barker, N., van Oudenaarden, A. & Clevers, H. (2012) Dll1+ secretory progenitor cells revert to stem cells upon crypt damage. *Nature Cell Biology*. 14 (10), 1099–1104. doi:10.1038/ncb2581.

Evonik (2018) *EUDRATEC® COL : Sustained release delivery of drugs to the colon*. 2018.

Fachi, J.L., Sécca, C., Rodrigues, P.B., Mato, F.C.P. de, Di Luccia, B., et al. (2020) Acetate coordinates neutrophil and ILC3 responses against *C. difficile* through FFAR2. *Journal of Experimental Medicine*. 217 (3). doi:10.1084/jem.20190489.

Farooqi, I.S., Yeo, G.S.H., Keogh, J.M., Aminian, S., Jebb, S.A., Butler, G., Cheetham, T. & O'Rahilly, S. (2000) Dominant and recessive inheritance of morbid obesity associated with melanocortin 4 receptor deficiency. *Journal of Clinical Investigation*. 106 (2), 271–279. doi:10.1172/JCI9397.

Feinstein, T.N., Wehbi, V.L., Ardura, J.A., Wheeler, D.S., Ferrandon, S., Gardella, T.J. & Vilardaga, J.-P. (2011) Retromer terminates the generation of cAMP by internalized PTH receptors. *Nature Chemical Biology*. 7 (5), 278–284. doi:10.1038/nchembio.545.

Feinstein, T.N., Yui, N., Webber, M.J., Wehbi, V.L., Stevenson, H.P., King, J.D., Hallows, K.R., Brown, D., Bouley, R. & Vilardaga, J.-P. (2013) Noncanonical Control of Vasopressin Receptor Type 2 Signaling by Retromer and Arrestin. *Journal of Biological Chemistry*. 288 (39), 27849–27860. doi:10.1074/jbc.M112.445098.

Ferdaoussi, M., Bergeron, V., Zarrouki, B., Kolic, J., Cantley, J., Fielitz, J., Olson, E.N., Prentki, M., Biden, T., MacDonald, P.E. & Poitout, V. (2012) G protein-coupled receptor (GPR)40-dependent potentiation of insulin secretion in mouse islets is mediated by protein kinase D1. *Diabetologia*. 55 (10), 2682–2692. doi:10.1007/s00125-012-2650-x.

Ferrandon, S., Feinstein, T.N., Castro, M., Wang, B., Bouley, R., Potts, J.T., Gardella, T.J. & Vilardaga, J.P. (2009) Sustained cyclic AMP production by parathyroid hormone receptor endocytosis. *Nature Chemical Biology*. 5 (10), 734–742. doi:10.1038/nchembio.206.

Fesler, Z., Mitova, E. & Brubaker, P.L. (2020) GLP-2, EGF, and the Intestinal Epithelial IGF-1 Receptor Interactions in the Regulation of Crypt Cell Proliferation. *Endocrinology*. 161 (4). doi:10.1210/endocr/bqaa040.

Filipek, S., Teller, D.C., Palczewski, K. & Stenkamp, R. (2003) The Crystallographic Model of Rhodopsin and Its Use in Studies of Other G Protein–Coupled Receptors. *Annual Review of Biophysics and Biomolecular Structure*. 32 (1), 375–397. doi:10.1146/annurev.biophys.32.110601.142520.

Fleischer, J., Bumbalo, R., Bautze, V., Strotmann, J. & Breer, H. (2015) Expression of odorant receptor Olfr78 in enteroendocrine cells of the colon. *Cell and Tissue Research*. 361 (3), 697–710. doi:10.1007/s00441-015-2165-0.

van der Flier, L.G. & Clevers, H. (2009) Stem Cells, Self-Renewal, and Differentiation in the Intestinal Epithelium. *Annual Review of Physiology*. 71 (1), 241–260. doi:10.1146/annurev.physiol.010908.163145.

Forbes, S., Stafford, S., Coope, G., Heffron, H., Real, K., Newman, R., Davenport, R., Barnes, M., Grosse, J. & Cox, H. (2015) Selective FFA2 Agonism Appears to Act via Intestinal PYY to Reduce Transit and Food Intake but Does Not Improve Glucose Tolerance in Mouse Models. *Diabetes.* 64(11):3763-3771. doi: 10.2337/db15-0481.

Foster, S.R., Hauser, A.S., Vedel, L., Strachan, R.T., Huang, X.-P., Gavin, A.C., Shah, S.D., Nayak, A.P., Haugaard-Kedström, L.M., Penn, R.B., Roth, B.L., Bräuner-Osborne, H. & Gloriam, D.E. (2019) Discovery of Human Signaling Systems: Pairing Peptides to G Protein-Coupled Receptors. *Cell*. 179 (4), 895-908.e21. doi:10.1016/j.cell.2019.10.010.

Fothergill, L.J., Callaghan, B., Hunne, B., Bravo, D.M. & Furness, J.B. (2017) Costorage of Enteroendocrine Hormones Evaluated at the Cell and Subcellular Levels in Male Mice. *Endocrinology*. 158 (7), 2113–2123. doi:10.1210/en.2017-00243.

Fothergill, L.J. & Furness, J.B. (2018) Diversity of enteroendocrine cells investigated at cellular and subcellular levels: the need for a new classification scheme. *Histochemistry and Cell Biology*. 150 (6), 693–702. doi:10.1007/s00418-018-1746-x.

Fre, S., Hannezo, E., Sale, S., Huyghe, M., Lafkas, D., Kissel, H., Louvi, A., Greve, J., Louvard, D. & Artavanis-Tsakonas, S. (2011) Notch Lineages and Activity in Intestinal Stem Cells Determined by a New Set of Knock-In Mice. *PLoS ONE*. 6 (10), e25785. doi:10.1371/journal.pone.0025785.

Frost, G. (2018) *iPREVENT: Increase in colonic PRopionate as a method of prEVENTing weight gain in adults aged 20-40 years*.

Frost, G., Cai, Z., Raven, M., Otway, D.T., Mushtaq, R. & Johnston, J.D. (2014) Effect of short chain fatty acids on the expression of free fatty acid receptor 2 (Ffar2), Ffar3 and early-stage adipogenesis. *Nutrition & Diabetes*. 4 (8), e128–e128. doi:10.1038/nutd.2014.25.

Fujita, Y., Y Chui, J.W., King, D.S., Zhang, T., Seufert, J., Pownall, S., Cheung, A.T. & Kieffer, T.J. (2008) Pax6 and Pdx1 are required for production of glucose-dependent insulinotropic polypeptide in proglucagon-expressing L cells Cheung AT, Kieffer TJ. Pax6 and Pdx1 are required for production of glucose-dependent insulinotropic polypeptide in proglucagon-expressing L cells. *Am J Physiol Endocrinol Metab*. 295, 648–657. doi:10.1152/ajpendo.90440.2008.-Glu.

Gagnon, L., Leduc, M., Thibodeau, J.-F., Zhang, M.-Z., Grouix, B., et al. (2018) A Newly Discovered Antifibrotic Pathway Regulated by Two Fatty Acid Receptors. *The American Journal of Pathology*. 188 (5), 1132–1148. doi:10.1016/j.ajpath.2018.01.009.

Gamet, L., Daviaud, D., Denis-Pouxviel, C., Remesy, C. & Murat, J. (1992) Effects of short-chain fatty acids on growth and differentiation of the human colon-cancer cell line HT29. *International Journal of Cancer*. 52 (2), 286–289. doi:10.1002/ijc.2910520222.

García-Cáceres, C., Quarta, C., Varela, L., Gao, Y., Gruber, T., et al. (2016) Astrocytic Insulin Signaling Couples Brain Glucose Uptake with Nutrient Availability. *Cell*. 166 (4), 867–880. doi:10.1016/j.cell.2016.07.028.

García-Hoz, C., Sánchez-Fernández, G., Díaz-Meco, M.T., Moscat, J., Mayor, F. & Ribas, C. (2010) Gαq Acts as an Adaptor Protein in Protein Kinase Cζ (PKCζ)-mediated ERK5 Activation by G Protein-coupled Receptors (GPCR). *Journal of Biological Chemistry*. 285 (18), 13480–13489. doi:10.1074/jbc.M109.098699.

Gasa, R., Mrejen, C., Lynn, F.C., Skewes-Cox, P., Sanchez, L., Yang, K.Y., Lin, C.-H., Gomis, R. & German, M.S. (2008) Induction of pancreatic islet cell differentiation by the neurogenin–neuroD cascade. *Differentiation*. 76 (4), 381–391. doi:10.1111/j.1432-0436.2007.00228.x.

Gaus, B., Brüning, D., Groß, S., Müller, M. & Rustenbeck, I. (2022) The changing view of insulin granule mobility: From conveyor belt to signaling hub. *Frontiers in Endocrinology*. 13. doi:10.3389/fendo.2022.983152.

Ge, H., Li, X., Weiszmann, J., Wang, P., Baribault, H., Chen, J.-L., Tian, H. & Li, Y. (2008) Activation of G Protein-Coupled Receptor 43 in Adipocytes Leads to Inhibition of Lipolysis and Suppression of Plasma Free Fatty Acids. *Endocrinology*. 149 (9), 4519–4526. doi:10.1210/en.2008-0059.

Gehart, H. & Clevers, H. (2019) Tales from the crypt: new insights into intestinal stem cells. *Nature Reviews Gastroenterology & Hepatology*. 16 (1), 19–34. doi:10.1038/s41575-018-0081-y.

Gehart, H., van Es, J.H., Hamer, K., Beumer, J., Kretzschmar, K., Dekkers, J.F., Rios, A. & Clevers, H. (2019) Identification of Enteroendocrine Regulators by Real-Time Single-Cell Differentiation Mapping. *Cell*. 176 (5), 1158-1173.e16. doi:10.1016/j.cell.2018.12.029.

Gerspach, A.C., Steinert, R.E., Schönenberger, L., Graber-Maier, A. & Beglinger, C. (2011) The role of the gut sweet taste receptor in regulating GLP-1, PYY, and CCK release in humans. *American Journal of Physiology-Endocrinology and Metabolism*. 301 (2), E317–E325. doi:10.1152/ajpendo.00077.2011.

Ghislain, J. & Poitout, V. (2021) Targeting lipid GPCRs to treat type 2 diabetes mellitus — progress and challenges. *Nature Reviews Endocrinology*. 17 (3), 162–175. doi:10.1038/s41574-020-00459-w.

Di Giuseppe, G., Ciccarelli, G., Soldovieri, L., Capece, U., Cefalo, C.M.A., Moffa, S., Nista, E.C., Brunetti, M., Cinti, F., Gasbarrini, A., Pontecorvi, A., Giaccari, A. & Mezza, T. (2023) First-phase insulin secretion: can its evaluation direct therapeutic approaches? *Trends in Endocrinology & Metabolism*. 34 (4), 216–230. doi:10.1016/j.tem.2023.02.001.

Glass, L.L., Calero-Nieto, F.J., Jawaid, W., Larraufie, P., Kay, R.G., Göttgens, B., Reimann, F. & Gribble, F.M. (2017) Single-cell RNA-sequencing reveals a distinct population of proglucagon-expressing cells specific to

the mouse upper small intestine. *Molecular Metabolism*. 6 (10), 1296–1303. doi:10.1016/j.molmet.2017.07.014.
Godbole, A., Lyga, S., Lohse, M.J. & Calebiro, D. (2017) Internalized TSH receptors en route to the TGN induce local Gs-protein signaling and gene transcription. *Nature Communications*. 8 (1), 443. doi:10.1038/s41467-017-00357-2.
Goldspink, D.A., Lu, V.B., Billing, L.J., Larraufie, P., Tolhurst, G., Gribble, F.M. & Reimann, F. (2018) Mechanistic insights into the detection of free fatty and bile acids by ileal glucagon-like peptide-1 secreting cells. *Molecular Metabolism*. 7, 90–101. doi:10.1016/j.molmet.2017.11.005.
Goldspink, D.A., Reimann, F. & Gribble, F.M. (2018) Models and Tools for Studying Enteroendocrine Cells. *Endocrinology*. 159 (12), 3874–3884. doi:10.1210/en.2018-00672.
Goodman, O.B., Krupnick, J.G., Santini, F., Gurevich, V. V., Penn, R.B., Gagnon, A.W., Keen, J.H. & Benovic, J.L. (1996) β-Arrestin acts as a clathrin adaptor in endocytosis of the β2-adrenergic receptor. *Nature*. 383 (6599), 447–450. doi:10.1038/383447a0.
Gores, M. & Rickwood, S. (2024) *2024: The obesity market's inflection point?* 22 February 2024. IQVIA.
Gorvin, C.M., Rogers, A., Hastoy, B., Tarasov, A.I., Frost, M., Sposini, S., Inoue, A., Whyte, M.P., Rorsman, P., Hanyaloglu, A.C., Breitwieser, G.E. & Thakker, R. V. (2018) AP2σ Mutations Impair Calcium-Sensing Receptor Trafficking and Signaling, and Show an Endosomal Pathway to Spatially Direct G-Protein Selectivity. *Cell Reports*. 22 (4), 1054–1066. doi:10.1016/j.celrep.2017.12.089.
Gribble, F.M. & Reimann, F. (2016) Enteroendocrine Cells: Chemosensors in the Intestinal Epithelium. *Annual Review of Physiology*. 78 (1), 277–299. doi:10.1146/annurev-physiol-021115-105439.
Gribble, F.M. & Reimann, F. (2019) Function and mechanisms of enteroendocrine cells and gut hormones in metabolism. *Nature Reviews Endocrinology*.15 (4) pp.226–237. doi:10.1038/s41574-019-0168-8.
Gropp, E., Shanabrough, M., Borok, E., Xu, A.W., Janoschek, R., Buch, T., Plum, L., Balthasar, N., Hampel, B., Waisman, A., Barsh, G.S., Horvath, T.L. & Brüning, J.C. (2005) Agouti-related peptide-expressing neurons are mandatory for feeding. *Nature Neuroscience*. 8 (10), 1289–1291. doi:10.1038/nn1548.
Grunddal, K. V., Ratner, C.F., Svendsen, B., Sommer, F., Engelstoft, M.S., Madsen, A.N., Pedersen, J., Nøhr, M.K., Egerod, K.L., Nawrocki, A.R., Kowalski, T., Howard, A.D., Poulsen, S.S., Offermanns, S., Bäckhed, F., Holst, J.J., Holst, B. & Schwartz, T.W. (2016) Neurotensin Is Coexpressed, Coreleased, and Acts Together With GLP-1 and PYY in Enteroendocrine Control of Metabolism. *Endocrinology*. 157 (1), 176–194. doi:10.1210/en.2015-1600.
Grundmann, M., Bender, E., Schamberger, J. & Eitner, F. (2021) Pharmacology of Free Fatty Acid Receptors and Their Allosteric Modulators. *International Journal of Molecular Sciences*. 22 (4), 1763. doi:10.3390/ijms22041763.
Grüter, T., Mohamad, N., Rilke, N., Blusch, A., Sgodzai, M., Demir, S., Pedreiturria, X., Lemhoefer, K., Gisevius, B., Haghikia, A., Fisse, A.L., Motte, J., Gold, R. & Pitarokoili, K. (2023) Propionate exerts

neuroprotective and neuroregenerative effects in the peripheral nervous system. *Proceedings of the National Academy of Sciences*. 120 (4). doi:10.1073/pnas.2216941120.

Guan, X., Karpen, H.E., Stephens, J., Bukowski, J.T., Niu, S., Zhang, G., Stoll, B., Finegold, M.J., Holst, J.J., Hadsell, D.L., Nichols, B.L. & Burrin, D.G. (2006) GLP-2 Receptor Localizes to Enteric Neurons and Endocrine Cells Expressing Vasoactive Peptides and Mediates Increased Blood Flow. *Gastroenterology*. 130 (1), 150–164. doi:10.1053/j.gastro.2005.11.005.

Gurevich, V. V., Dion, S.B., Onorato, J.J., Ptasienski, J., Kim, C.M., Sterne-Marr, R., Hosey, M.M. & Benovic, J.L. (1995) Arrestin Interactions with G Protein-coupled Receptors. *Journal of Biological Chemistry*. 270 (2), 720–731. doi:10.1074/jbc.270.2.720.

Gustavsson, N., Wang, Y., Kang, Y., Seah, T., Chua, S., Radda, G.K. & Han, W. (2011) Synaptotagmin-7 as a positive regulator of glucose-induced glucagon-like peptide-1 secretion in mice. *Diabetologia*. 54 (7), 1824–1830. doi:10.1007/s00125-011-2119-3.

Haber, A.L., Biton, M., Rogel, N., Herbst, R.H., Shekhar, K., et al. (2017) A single-cell survey of the small intestinal epithelium. *Nature*. 551 (7680), 333–339. doi:10.1038/nature24489.

Habib, A.M., Richards, P., Cairns, L.S., Rogers, G.J., Bannon, C.A.M., Parker, H.E., Morley, T.C.E., Yeo, G.S.H., Reimann, F. & Gribble, F.M. (2012) Overlap of Endocrine Hormone Expression in the Mouse Intestine Revealed by Transcriptional Profiling and Flow Cytometry. *Endocrinology*. 153 (7), 3054–3065. doi:10.1210/en.2011-2170.

Habib, A.M., Richards, P., Rogers, G.J., Reimann, F. & Gribble, F.M. (2013) Co-localisation and secretion of glucagon-like peptide 1 and peptide YY from primary cultured human L cells. *Diabetologia*. 56 (6), 1413–1416. doi:10.1007/s00125-013-2887-z.

Han, Y., Tang, C., Zhao, Q., Fan, S., Yang, P. & Zhang, J. (2022) Butyrate Mitigates Lipopolysaccharide-Induced Intestinal Morphological Changes in Weanling Piglets by Regulating the Microbiota and Energy Metabolism, and Alleviating Inflammation and Apoptosis. *Microorganisms*. 10 (10), 2001. doi:10.3390/microorganisms10102001.

Hanyaloglu, A.C. & von Zastrow, M. (2007) A Novel Sorting Sequence in the β2-Adrenergic Receptor Switches Recycling from Default to the Hrs-dependent Mechanism. *Journal of Biological Chemistry*. 282 (5), 3095–3104. doi:10.1074/jbc.M605398200.

Hanyaloglu, A.C. & Von Zastrow, M. (2008) Regulation of GPCRs by endocytic membrane trafficking and its potential implications. *Annual Review of Pharmacology and Toxicology*.48 pp.537–568. doi:10.1146/annurev.pharmtox.48.113006.094830.

Hao, Y., Stuart, T., Kowalski, M.H., Choudhary, S., Hoffman, P., Hartman, A., Srivastava, A., Molla, G., Madad, S., Fernandez-Granda, C. & Satija, R. (2024) Dictionary learning for integrative, multimodal and scalable single-cell analysis. *Nature Biotechnology*. 42 (2), 293–304. doi:10.1038/s41587-023-01767-y.

Harada, K., Sakaguchi, H., Sada, S., Ishida, R., Hayasaka, Y. & Tsuboi, T. (2018) Bitter tastant quinine modulates glucagon-like peptide-1 exocytosis from clonal GLUTag enteroendocrine L cells via actin

reorganization. *Biochemical and Biophysical Research Communications*. 500 (3), 723–730. doi:10.1016/j.bbrc.2018.04.143.
Harada, K., Takashima, M., Kitaguchi, T. & Tsuboi, T. (2023) F-actin determines the time-dependent shift in docking dynamics of glucagon-like peptide-1 granules upon stimulation of secretion. *FEBS Letters*. 597 (5), 657–671. doi:10.1002/1873-3468.14580.
Hargreaves, A.J., Yusta, B., Avila, J., Hesketh, J.E., Aranda, A. & Pascual, A. (1989) Sodium butyrate induces major morphological changes in C6 glioma cells that are correlated with increased synthesis of a spectrin-like protein. *Developmental Brain Research*. 45 (2), 291–295. doi:10.1016/0165-3806(89)90047-3.
Harris, H., Edwards, C. & Morrison, D. (2017) Impact of Glycosidic Bond Configuration on Short Chain Fatty Acid Production from Model Fermentable Carbohydrates by the Human Gut Microbiota. *Nutrients*. 9 (1), 26. doi:10.3390/nu9010026.
Hauge, M., Ekberg, J.P., Engelstoft, M.S., Timshel, P., Madsen, A.N. & Schwartz, T.W. (2017) Gq and Gs signaling acting in synergy to control GLP-1 secretion. *Molecular and Cellular Endocrinology*. 449, 64–73. doi:10.1016/j.mce.2016.11.024.
Hauser, A.S., Kooistra, A.J., Munk, C., Heydenreich, F.M., Veprintsev, D.B., Bouvier, M., Babu, M.M. & Gloriam, D.E. (2021) GPCR activation mechanisms across classes and macro/microscales. *Nature Structural & Molecular Biology*. 28 (11), 879–888. doi:10.1038/s41594-021-00674-7.
Hebert-Chatelain, E., Desprez, T., Serrat, R., Bellocchio, L., Soria-Gomez, E., et al. (2016) A cannabinoid link between mitochondria and memory. *Nature*. 539 (7630), 555–559. doi:10.1038/nature20127.
Hegron, A., Peach, C.J., Tonello, R., Seemann, P., Teng, S., Latorre, R., Huebner, H., Weikert, D., Rientjes, J., Veldhuis, N.A., Poole, D.P., Jensen, D.D., Thomsen, A.R.B., Schmidt, B.L., Imlach, W.L., Gmeiner, P. & Bunnett, N.W. (2023) Therapeutic antagonism of the neurokinin 1 receptor in endosomes provides sustained pain relief. *Proceedings of the National Academy of Sciences*. 120 (22). doi:10.1073/pnas.2220979120.
von Heijne, G. (1990) The signal peptide. *The Journal of Membrane Biology*. 115 (3), 195–201. doi:10.1007/BF01868635.
Heppner, K.M., Kirigiti, M., Secher, A., Paulsen, S.J., Buckingham, R., Pyke, C., Knudsen, L.B., Vrang, N. & Grove, K.L. (2015) Expression and Distribution of Glucagon-Like Peptide-1 Receptor mRNA, Protein and Binding in the Male Nonhuman Primate (*Macaca mulatta*) Brain. *Endocrinology*. 156 (1), 255–267. doi:10.1210/en.2014-1675.
Hermle, J., Anders, M., Heuser, A.-M. & Müller, B. (2010) A simple fluorescence based assay for quantification of human immunodeficiency virus particle release. *BMC Biotechnology*. 10 (1), 32. doi:10.1186/1472-6750-10-32.
Heydenreich, F.M., Plouffe, B., Rizk, A., Milic, D., Zhou, J., Breton, B., Le Gouill, C., Inoue, A., Bouvier, M. & Veprintsev, D. (2022) Michaelis-Menten quantification of ligand signalling bias applied to the promiscuous Vasopressin V2 receptor. *Molecular Pharmacology*. MOLPHARM-AR-2022-000497. doi:10.1124/molpharm.122.000497.
Hilger, D. (2021) The role of structural dynamics in GPCR-mediated signaling. *The FEBS Journal*. 288 (8), 2461–2489. doi:10.1111/febs.15841.

Hill, M.E., Asa, S.L. & Drucker, D.J. (1999) *Essential Requirement for Pax6 in Control of Enteroendocrine Proglucagon Gene Transcription*. https://academic.oup.com/mend/article/13/9/1474/2747887.
Hirasawa, A., Tsumaya, K., Awaji, T., Katsuma, S., Adachi, T., Yamada, M., Sugimoto, Y., Miyazaki, S. & Tsujimoto, G. (2005) Free fatty acids regulate gut incretin glucagon-like peptide-1 secretion through GPR120. *Nature Medicine*. 11 (1), 90–94. doi:10.1038/nm1168.
Hirsch, D., Barker, N., McNeil, N., Hu, Y., Camps, J., McKinnon, K., Clevers, H., Ried, T. & Gaiser, T. (2014) LGR5 positivity defines stem-like cells in colorectal cancer. *Carcinogenesis*. 35 (4), 849–858. doi:10.1093/carcin/bgt377.
Ho, J., Hirdaramani, A., Puoplo, N., Pokharel, N., Cheng, C.W. & Hanyalolgu, A. (2024) Nutrigenomic underpinnings of intestinal stem cells in inflammatory bowel disease and 2 colorectal cancer development. *Frontiers of Genetics.* 15:1349717. doi: 10.3389/fgene.2024.1349717.
Hodge, D., Glass, L.L., Diakogiannaki, E., Pais, R., Lenaghan, C., Smith, D.M., Wedin, M., Bohlooly-Y, M., Gribble, F.M. & Reimann, F. (2016) Lipid derivatives activate GPR119 and trigger GLP-1 secretion in primary murine L-cells. *Peptides*. 77, 16–20. doi:10.1016/j.peptides.2015.06.012.
Holst, J.J. (2022) Glucagon and other proglucagon-derived peptides in the pathogenesis of obesity. *Frontiers in Nutrition*. 9. doi:10.3389/fnut.2022.964406.
Holst, J.J. (2007) The Physiology of Glucagon-like Peptide 1. *Physiological Reviews*. 87 (4), 1409–1439. doi:10.1152/physrev.00034.2006.
Holst, J.J., Ørskov, C., Vagn Nielsen, O. & Schwartz, T.W. (1987) Truncated glucagon-like peptide I, an insulin-releasing hormone from the distal gut. *FEBS Letters*. 211 (2), 169–174. doi:10.1016/0014-5793(87)81430-8.
Holt, M.K., Richards, J.E., Cook, D.R., Brierley, D.I., Williams, D.L., Reimann, F., Gribble, F.M. & Trapp, S. (2019) Preproglucagon Neurons in the Nucleus of the Solitary Tract Are the Main Source of Brain GLP-1, Mediate Stress-Induced Hypophagia, and Limit Unusually Large Intakes of Food. *Diabetes*. 68 (1), 21–33. doi:10.2337/db18-0729.
Hong, Y.-H., Nishimura, Y., Hishikawa, D., Tsuzuki, H., Miyahara, H., Gotoh, C., Choi, K.-C., Feng, D.D., Chen, C., Lee, H.-G., Katoh, K., Roh, S.-G. & Sasaki, S. (2005) Acetate and Propionate Short Chain Fatty Acids Stimulate Adipogenesis via GPCR43. *Endocrinology*. 146 (12), 5092–5099. doi:10.1210/en.2005-0545.
Horwitz, M.J., Tedesco, M.B., Sereika, S.M., Syed, M.A., Garcia-Ocaña, A., Bisello, A., Hollis, B.W., Rosen, C.J., Wysolmerski, J.J., Dann, P., Gundberg, C. & Stewart, A.F. (2005) Continuous PTH and PTHrP Infusion Causes Suppression of Bone Formation and Discordant Effects on 1,25(OH)2Vitamin D. *Journal of Bone and Mineral Research*. 20 (10), 1792–1803. doi:10.1359/JBMR.050602.
Hoshino, A., Kowalska, D., Jean, F., Lazure, C. & Lindberg, I. (2011) Modulation of PC1/3 Activity by Self-Interaction and Substrate Binding. *Endocrinology*. 152 (4), 1402–1411. doi:10.1210/en.2010-1170.
Hoyles, L., Snelling, T., Umlai, U.-K., Nicholson, J.K., Carding, S.R., Glen, R.C. & McArthur, S. (2018) Microbiome–host systems interactions: protective effects of propionate upon the blood–brain barrier. *Microbiome*. 6 (1), 55. doi:10.1186/s40168-018-0439-y.

Hu, J., Kyrou, I., Tan, B.K., Dimitriadis, G.K., Ramanjaneya, M., Tripathi, G., Patel, V., James, S., Kawan, M., Chen, J. & Randeva, H.S. (2016) Short-Chain Fatty Acid Acetate Stimulates Adipogenesis and Mitochondrial Biogenesis via GPR43 in Brown Adipocytes. *Endocrinology*. 157 (5), 1881–1894. doi:10.1210/en.2015-1944.

Hu, S., Dong, T.S., Dalal, S.R., Wu, F., Bissonnette, M., Kwon, J.H. & Chang, E.B. (2011) The Microbe-Derived Short Chain Fatty Acid Butyrate Targets miRNA-Dependent p21 Gene Expression in Human Colon Cancer. *PLoS ONE*. 6 (1), e16221. doi:10.1371/journal.pone.0016221.

Hudson, B.D., Due-Hansen, M.E., Christiansen, E., Hansen, A.M., Mackenzie, A.E., Murdoch, H., Pandey, S.K., Ward, R.J., Marquez, R., Tikhonova, I.G., Ulven, T. & Milligan, G. (2013) Defining the Molecular Basis for the First Potent and Selective Orthosteric Agonists of the FFA2 Free Fatty Acid Receptor. *Journal of Biological Chemistry*. 288 (24), 17296–17312. doi:10.1074/jbc.M113.455337.

Hugon, P., Dufour, J.C., Colson, P., Fournier, P.E., Sallah, K. & Raoult, D. (2015) A comprehensive repertoire of prokaryotic species identified in human beings. *The Lancet Infectious Diseases*.15 (10) pp.1211–1219. doi:10.1016/S1473-3099(15)00293-5.

HUNTER, W.M. & GREENWOOD, F.C. (1962) Preparation of Iodine-131 Labelled Human Growth Hormone of High Specific Activity. *Nature*. 194 (4827), 495–496. doi:10.1038/194495a0.

Ichimura, A., Hirasawa, A., Poulain-Godefroy, O., Bonnefond, A., Hara, T., et al. (2012) Dysfunction of lipid sensor GPR120 leads to obesity in both mouse and human. *Nature*. 483 (7389), 350–354. doi:10.1038/nature10798.

Ikushima, Y.M., Awazawa, M., Kobayashi, N., Osonoi, S., Takemiya, S., Kobayashi, H., Suwanai, H., Morimoto, Y., Soeda, K., Adachi, J., Muratani, M., Charron, J., Mizukami, H., Takahashi, N. & Ueki, K. (2021) MEK/ERK Signaling in β-Cells Bifunctionally Regulates β-Cell Mass and Glucose-Stimulated Insulin Secretion Response to Maintain Glucose Homeostasis. *Diabetes*. 70 (7), 1519–1535. doi:10.2337/db20-1295.

Ilhan, Z.E., DiBaise, J.K., Isern, N.G., Hoyt, D.W., Marcus, A.K., Kang, D.-W., Crowell, M.D., Rittmann, B.E. & Krajmalnik-Brown, R. (2017) Distinctive microbiomes and metabolites linked with weight loss after gastric bypass, but not gastric banding. *The ISME Journal*. 11 (9), 2047–2058. doi:10.1038/ismej.2017.71.

Inoue, A., Raimondi, F., Kadji, F.M.N., Singh, G., Kishi, T., Uwamizu, A., Ono, Y., Shinjo, Y., Ishida, S., Arang, N., Kawakami, K., Gutkind, J.S., Aoki, J. & Russell, R.B. (2019) Illuminating G-Protein-Coupling Selectivity of GPCRs. *Cell*. 177 (7), 1933-1947.e25. doi:10.1016/j.cell.2019.04.044.

Inoue, D., Tsujimoto, G. & Kimura, I. (2014) Regulation of Energy Homeostasis by GPR41. *Frontiers in Endocrinology*. 5. doi:10.3389/fendo.2014.00081.

Inui, A., Asakawa, A., Y. Bowers, C., Mantovani, G., Laylano, A., M. Meguid, M. & Fujimiya, M. (2004) Ghrelin, appetite, and gastric motility: the emerging role of the stomach as an endocrine organ. *The FASEB Journal*. 18 (3), 439–456. doi:10.1096/fj.03-0641rev.

Irannejad, R., Pessino, V., Mika, D., Huang, B., Wedegaertner, P.B., Conti, M. & von Zastrow, M. (2017) Functional selectivity of GPCR-directed drug

action through location bias. *Nature Chemical Biology*. 13 (7), 799–806. doi:10.1038/nchembio.2389.
Irannejad, R., Tomshine, J.C., Tomshine, J.R., Chevalier, M., Mahoney, J.P., Steyaert, J., Rasmussen, S.G.F., Sunahara, R.K., El-Samad, H., Huang, B. & Von Zastrow, M. (2013) Conformational biosensors reveal GPCR signalling from endosomes. *Nature*. 495 (7442), 534–538. doi:10.1038/nature12000.
Itoh, Y., Kawamata, Y., Harada, M., Kobayashi, M., Fujii, R., et al. (2003) Free fatty acids regulate insulin secretion from pancreatic β cells through GPR40. *Nature*. 422 (6928), 173–176. doi:10.1038/nature01478.
Iván, J., Major, E., Sipos, A., Kovács, K., Horváth, D., Tamás, I., Bay, P., Dombrádi, V. & Lontay, B. (2017) The Short-Chain Fatty Acid Propionate Inhibits Adipogenic Differentiation of Human Chorion-Derived Mesenchymal Stem Cells Through the Free Fatty Acid Receptor 2. *Stem Cells and Development*. 26 (23), 1724–1733. doi:10.1089/scd.2017.0035.
Jang, B.G., Kim, H.S., Chang, W.Y., Bae, J.M., Kim, W.H. & Kang, G.H. (2018) Expression Profile of LGR5 and Its Prognostic Significance in Colorectal Cancer Progression. *The American Journal of Pathology*. 188 (10), 2236–2250. doi:10.1016/j.ajpath.2018.06.012.
Jastreboff, A.M., Aronne, L.J., Ahmad, N.N., Wharton, S., Connery, L., Alves, B., Kiyosue, A., Zhang, S., Liu, B., Bunck, M.C. & Stefanski, A. (2022) Tirzepatide Once Weekly for the Treatment of Obesity. *New England Journal of Medicine*. 387 (3), 205–216. doi:10.1056/NEJMoa2206038.
Jean-Alphonse, F., Bowersox, S., Chen, S., Beard, G., Puthenveedu, M.A. & Hanyaloglu, A.C. (2014) Spatially restricted G protein-coupled receptor activity via divergent endocytic compartments. *Journal of Biological Chemistry*. 289 (7), 3960–3977. doi:10.1074/jbc.M113.526350.
Jenny, M., Uhl, C., Roche, C., Duluc, I., Guillermin, V., Guillemot, F., Jensen, J., Kedinger, M. & Gradwohl, G. (2002) Neurogenin3 is differentially required for endocrine cell fate specification in the intestinal and gastric epithelium. *The EMBO Journal*. 21 (23), 6338–6347.
Jensen, D.D., Lieu, T., Halls, M.L., Veldhuis, N.A., Imlach, W.L., et al. (2017) Neurokinin 1 receptor signaling in endosomes mediates sustained nociception and is a viable therapeutic target for prolonged pain relief. *Science Translational Medicine*. 9 (392). doi:10.1126/scitranslmed.aal3447.
Ji, L., Wu, H.-T., Qin, X.-Y. & Lan, R. (2017) Dissecting carboxypeptidase E: properties, functions and pathophysiological roles in disease. *Endocrine Connections*. 6 (4), R18–R38. doi:10.1530/EC-17-0020.
Jimenez-Vargas, N.N., Gong, J., Wisdom, M.J., Jensen, D.D., Latorre, R., et al. (2020) Endosomal signaling of delta opioid receptors is an endogenous mechanism and therapeutic target for relief from inflammatory pain. *Proceedings of the National Academy of Sciences*. 117 (26), 15281–15292. doi:10.1073/pnas.2000500117.
Jimenez-Vargas, N.N., Pattison, L.A., Zhao, P., Lieu, T., Latorre, R., et al. (2018) Protease-activated receptor-2 in endosomes signals persistent pain of irritable bowel syndrome. *Proceedings of the National Academy of Sciences*. 115 (31). doi:10.1073/pnas.1721891115.
Jiménez-Vargas, N.N., Yu, Y., Jensen, D.D., Bok, D.D., Wisdom, M., et al. (2022) Agonist that activates the μ-opioid receptor in acidified

microenvironments inhibits colitis pain without side effects. *Gut*. 71 (4), 695–704. doi:10.1136/gutjnl-2021-324070.
Jin, G., Ramanathan, V., Quante, M., Baik, G.H., Yang, X., Wang, S.S.W., Tu, S., Gordon, S.A.K., Pritchard, D.M., Varro, A., Shulkes, A. & Wang, T.C. (2009) Inactivating cholecystokinin-2 receptor inhibits progastrin-dependent colonic crypt fission, proliferation, and colorectal cancer in mice. *Journal of Clinical Investigation*. doi:10.1172/JCI38918.
Jin, G., Sakitani, K., Wang, H., Jin, Y., Dubeykovskiy, A., Worthley, D.L., Tailor, Y. & Wang, T.C. (2017) The G-protein coupled receptor 56, expressed in colonic stem and cancer cells, binds progastrin to promote proliferation and carcinogenesis. *Oncotarget*. 8 (25), 40606–40619. doi:10.18632/oncotarget.16506.
Jin, S.-L.C., Han, V.K.M., Simmons, J.G., Towle, A.C., Lauder, J.M. & Lund, P.K. (1988) Distribution of glucagonlike peptide I (GLP-I), glucagon, and glicentin in the rat brain: An immunocytochemical study. *The Journal of Comparative Neurology*. 271 (4), 519–532. doi:10.1002/cne.902710405.
Jones, L.A., Sun, E.W., Lumsden, A.L., Thorpe, D.W., Peterson, R.A., De Fontgalland, D., Sposato, L., Rabbitt, P., Hollington, P., Wattchow, D.A. & Keating, D.J. (2023) Alterations in GLP-1 and PYY release with aging and body mass in the human gut. *Molecular and Cellular Endocrinology*. 578, 112072. doi:10.1016/j.mce.2023.112072.
Jumper, J., Evans, R., Pritzel, A., Green, T., Figurnov, M., et al. (2021) Highly accurate protein structure prediction with AlphaFold. *Nature*. 596 (7873), 583–589. doi:10.1038/s41586-021-03819-2.
Kaelberer, M.M., Buchanan, K.L., Klein, M.E., Barth, B.B., Montoya, M.M., Shen, X. & Bohórquez, D. V. (2018) A gut-brain neural circuit for nutrient sensory transduction. *Science*. 361 (6408). doi:10.1126/science.aat5236.
Kageyama, R. & Nakanishi, S. (1997) Helix-loop-helix factors in growth and differentiation of the vertebrate nervous system. *Current Opinion in Genetics & Development*. 7 (5), 659–665. doi:10.1016/S0959-437X(97)80014-7.
Kaiko, G.E., Ryu, S.H., Koues, O.I., Collins, P.L., Solnica-Krezel, L., Pearce, E.J., Pearce, E.L., Oltz, E.M. & Stappenbeck, T.S. (2016) The Colonic Crypt Protects Stem Cells from Microbiota-Derived Metabolites. *Cell*. 165 (7), 1708–1720. doi:10.1016/j.cell.2016.05.018.
Kaji, I., Karaki, S.I., Tanaka, R. & Kuwahara, A. (2011) Density distribution of free fatty acid receptor 2 (FFA2)-expressing and GLP-1-producing enteroendocrine L cells in human and rat lower intestine, and increased cell numbers after ingestion of fructo-oligosaccharide. *Journal of Molecular Histology*. 42 (1), 27–38. doi:10.1007/s10735-010-9304-4.
Kalwat, M.A. & Thurmond, D.C. (2013) Signaling mechanisms of glucose-induced F-actin remodeling in pancreatic islet β cells. *Experimental & Molecular Medicine*. 45 (8), e37–e37. doi:10.1038/emm.2013.73.
Karaki, S., Mitsui, R., Hayashi, H., Kato, I., Sugiya, H., Iwanaga, T., Furness, J.B. & Kuwahara, A. (2006) Short-chain fatty acid receptor, GPR43, is expressed by enteroendocrine cells and mucosal mast cells in rat intestine. *Cell and Tissue Research*. 324 (3), 353–360. doi:10.1007/s00441-005-0140-x.
Karaki, S.I., Tazoe, H., Hayashi, H., Kashiwabara, H., Tooyama, K., Suzuki, Y. & Kuwahara, A. (2008) Expression of the short-chain fatty acid receptor,

GPR43, in the human colon. *Journal of Molecular Histology*. 39 (2), 135–142. doi:10.1007/s10735-007-9145-y.
Karra, E., Chandarana, K. & Batterham, R.L. (2009) The role of peptide YY in appetite regulation and obesity. *The Journal of Physiology*. 587 (1), 19–25. doi:10.1113/jphysiol.2008.164269.
Kechele, D.O., Blue, R.E., Zwarycz, B., Espenschied, S.T., Mah, A.T., Siegel, M.B., Perou, C.M., Ding, S., Magness, S.T., Lund, P.K. & Caron, K.M. (2017) Orphan Gpr182 suppresses ERK-mediated intestinal proliferation during regeneration and adenoma formation. *Journal of Clinical Investigation*. 127 (2), 593–607. doi:10.1172/JCI87588.
Keire, D.A., Bowers, C.W., Solomon, T.E. & Reeve, J.R. (2002) Structure and receptor binding of PYY analogs. *Peptides*. 23 (2), 305–321. doi:10.1016/S0196-9781(01)00602-7.
Keire, D.A., Whitelegge, J.P., Souda, P., Faull, K.F., Bassilian, S., Reidelberger, R.D., Haver, A.C. & Reeve, J.R. (2010) PYY(1-36) is the major form of PYY in rat distal small intestine: Quantification using high-resolution mass spectrometry. *Regulatory Peptides*. 165 (2–3), 151–157. doi:10.1016/j.regpep.2010.06.006.
Kelly, E., Bailey, C.P. & Henderson, G. (2008) Agonist-selective mechanisms of GPCR desensitization. *British Journal of Pharmacology*. 153 (S1). doi:10.1038/sj.bjp.0707604.
Kelly, T., Yang, W., Chen, C.S., Reynolds, K. & He, J. (2008) Global burden of obesity in 2005 and projections to 2030. *International Journal of Obesity*. 32 (9), 1431–1437. doi:10.1038/ijo.2008.102.
Kemper, K., Prasetyanti, P.R., De Lau, W., Rodermond, H., Clevers, H. & Medema, J.P. (2012) Monoclonal Antibodies Against Lgr5 Identify Human Colorectal Cancer Stem Cells. *Stem Cells*. 30 (11), 2378–2386. doi:10.1002/stem.1233.
Khan, S.M., Sleno, R., Gora, S., Zylbergold, P., Laverdure, J.-P., Labbé, J.-C., Miller, G.J. & Hébert, T.E. (2013) The Expanding Roles of G *βγ* Subunits in G Protein–Coupled Receptor Signaling and Drug Action. *Pharmacological Reviews*. 65 (2), 545–577. doi:10.1124/pr.111.005603.
Kim, K.-S., Lee, I.-S., Kim, K.-H., Park, J., Kim, Y., Choi, J.-H., Choi, J.-S. & Jang, H.-J. (2017) Activation of intestinal olfactory receptor stimulates glucagon-like peptide-1 secretion in enteroendocrine cells and attenuates hyperglycemia in type 2 diabetic mice. *Scientific Reports*. 7 (1), 13978. doi:10.1038/s41598-017-14086-5.
Kim, M.H., Kang, S.G., Park, J.H., Yanagisawa, M. & Kim, C.H. (2013) Short-Chain Fatty Acids Activate GPR41 and GPR43 on Intestinal Epithelial Cells to Promote Inflammatory Responses in Mice. *Gastroenterology*. 145 (2), 396-406.e10. doi:10.1053/j.gastro.2013.04.056.
Kim, Y.S., Tsao, D., Siddiqui, B., Whitehead, J.S., Arnstein, P., Bennett, J. & Hicks, J. (1980) Effects of sodium butyrate and dimethylsulfoxide on biochemical properties of human colon cancer cells. *Cancer*. 45 (5 Suppl), 1185–1192. doi:10.1002/1097-0142(19800315)45:5+<1185::aid-cncr2820451324>3.0.co;2-w.
Kimura, I., Ichimura, A., Ohue-Kitano, R. & Igarashi, M. (2020) Free fatty acid receptors in health and disease. *Physiological Reviews*. 100 (1), 171–210. doi:10.1152/physrev.00041.2018.

Kimura, I., Inoue, D., Maeda, T., Hara, T., Ichimura, A., Miyauchi, S., Kobayashi, M., Hirasawa, A. & Tsujimoto, G. (2011) Short-chain fatty acids and ketones directly regulate sympathetic nervous system via G protein-coupled receptor 41 (GPR41). *Proceedings of the National Academy of Sciences*. 108 (19), 8030–8035. doi:10.1073/pnas.1016088108.

King, K., Dohlman, H.G., Thorner, J., Caron, M.G. & Lefkowitz, R.J. (1990) Control of Yeast Mating Signal Transduction by a Mammalian β_2-adrenergic Receptor and $G_s\alpha$ Subunit. *Science*. 250 (4977), 121–123. doi:10.1126/science.2171146.

Klauer, M.J., Willette, B.K.A. & Tsvetanova, N.G. (2024) Functional diversification of cell signaling by GPCR localization. *Journal of Biological Chemistry*. 105668. doi:10.1016/j.jbc.2024.105668.

Klepinina, L., Klepinin, A., Truu, L., Chekulayev, V., Vija, H., Kuus, K., Teino, I., Pook, M., Maimets, T. & Kaambre, T. (2021) Colon cancer cell differentiation by sodium butyrate modulates metabolic plasticity of Caco-2 cells via alteration of phosphotransfer network. *PLOS ONE*. 16 (1), e0245348. doi:10.1371/journal.pone.0245348.

Koch, C., Gerbert, C., Frieten, D., Dusel, G., Eder, K., Zitnan, R. & Hammon, H.M. (2019) Effects of ad libitum milk replacer feeding and butyrate supplementation on the epithelial growth and development of the gastrointestinal tract in Holstein calves. *Journal of Dairy Science*. 102 (9), 8513–8526. doi:10.3168/jds.2019-16328.

Koda, S., Date, Y., Murakami, N., Shimbara, T., Hanada, T., Toshinai, K., Niijima, A., Furuya, M., Inomata, N., Osuye, K. & Nakazato, M. (2005) The Role of the Vagal Nerve in Peripheral PYY3–36-Induced Feeding Reduction in Rats. *Endocrinology*. 146 (5), 2369–2375. doi:10.1210/en.2004-1266.

Kotlo, K., Anbazhagan, A.N., Priyamvada, S., Jayawardena, D., Kumar, A., Chen, Y., Xia, Y., Finn, P.W., Perkins, D.L., Dudeja, P.K. & Layden, B.T. (2020) The olfactory G protein-coupled receptor (Olfr-78/OR51E2) modulates the intestinal response to colitis. *American Journal of Physiology-Cell Physiology*. 318 (3), C502–C513. doi:10.1152/ajpcell.00454.2019.

Kotowski, S.J., Hopf, F.W., Seif, T., Bonci, A. & von Zastrow, M. (2011) Endocytosis Promotes Rapid Dopaminergic Signaling. *Neuron*. 71 (2), 278–290. doi:10.1016/j.neuron.2011.05.036.

Kotunia, A., Woliński, J., Laubitz, D., Jurkowska, M., Romé, V., Guilloteau, P. & Zabielski, R. (2004) Effect of sodium butyrate on the small intestine development in neonatal piglets fed [correction of feed] by artificial sow. *Journal of physiology and pharmacology : an official journal of the Polish Physiological Society*. 55 Suppl 2, 59–68.

Krautkramer, K.A., Kreznar, J.H., Romano, K.A., Vivas, E.I., Barrett-Wilt, G.A., Rabaglia, M.E., Keller, M.P., Attie, A.D., Rey, F.E. & Denu, J.M. (2016) Diet-Microbiota Interactions Mediate Global Epigenetic Programming in Multiple Host Tissues. *Molecular Cell*. 64 (5), 982–992. doi:10.1016/j.molcel.2016.10.025.

Kreymann, B., Williams, G., Ghatei, M.A. & Bloom, S.R. (1987) GLUCAGON-LIKE PEPTIDE-1 7-36; A PHYSIOLOGICAL INCRETIN IN MAN. *Lancet*. 1300–1303.

Krieger, J.-P., Arnold, M., Pettersen, K.G., Lossel, P., Langhans, W. & Lee, S.J. (2016) Knockdown of GLP-1 Receptors in Vagal Afferents Affects Normal Food Intake and Glycemia. *Diabetes*. 65 (1), 34–43. doi:10.2337/db15-0973.

Kroeze, W.K., Sassano, M.F., Huang, X.-P., Lansu, K., McCorvy, J.D., Giguère, P.M., Sciaky, N. & Roth, B.L. (2015) PRESTO-Tango as an open-source resource for interrogation of the druggable human GPCRome. *Nature Structural & Molecular Biology*. 22 (5), 362–369. doi:10.1038/nsmb.3014.

Kruh, J. (1981) Effects of sodium butyrate, a new pharmacological agent, on cells in culture. *Molecular and Cellular Biochemistry*. 42 (2). doi:10.1007/BF00222695.

Kuhre, R.E., Deacon, C.F., Holst, J.J. & Petersen, N. (2021) What Is an L-Cell and How Do We Study the Secretory Mechanisms of the L-Cell? *Frontiers in Endocrinology*.12. doi:10.3389/fendo.2021.694284.

Kuhre, R.E., Frost, C.R., Svendsen, B. & Holst, J.J. (2015) Molecular Mechanisms of Glucose-Stimulated GLP-1 Secretion From Perfused Rat Small Intestine. *Diabetes*. 64 (2), 370–382. doi:10.2337/db14-0807.

Kullmann, S., Heni, M., Hallschmid, M., Fritsche, A., Preissl, H. & Häring, H.-U. (2016) Brain Insulin Resistance at the Crossroads of Metabolic and Cognitive Disorders in Humans. *Physiological Reviews*. 96 (4), 1169–1209. doi:10.1152/physrev.00032.2015.

Kurokawa, K., Hayakawa, Y. & Koike, K. (2020) Plasticity of Intestinal Epithelium: Stem Cell Niches and Regulatory Signals. *International Journal of Molecular Sciences*. 22 (1), 357. doi:10.3390/ijms22010357.

L. Veech, B.C.Y.R. (2001) Ketone Bodies, Potential Therapeutic Uses. *IUBMB Life (International Union of Biochemistry and Molecular Biology: Life)*. 51 (4), 241–247. doi:10.1080/152165401753311780.

Langley, D.B., Schofield, P., Jackson, J., Herzog, H. & Christ, D. (2022) Crystal structures of human neuropeptide Y (NPY) and peptide YY (PYY). *Neuropeptides*. 92, 102231. doi:10.1016/j.npep.2022.102231.

Laporte, S.A., Oakley, R.H., Zhang, J., Holt, J.A., Ferguson, S.S.G., Caron, M.G. & Barak, L.S. (1999) The β_2-adrenergic receptor/βarrestin complex recruits the clathrin adaptor AP-2 during endocytosis. *Proceedings of the National Academy of Sciences*. 96 (7), 3712–3717. doi:10.1073/pnas.96.7.3712.

Larraufie, P., Martin-Gallausiaux, C., Lapaque, N., Dore, J., Gribble, F.M., Reimann, F. & Blottiere, H.M. (2018) SCFAs strongly stimulate PYY production in human enteroendocrine cells. *Scientific Reports*. 8 (1). doi:10.1038/s41598-017-18259-0.

Larsson, L.I., Holst, J., Håkanson, R. & Sundler F. (1975) Distribution and properties of glucagon immunoreactivity in the digestive tract of various mammals: an immunohistochemical and immunochemical study. Histochemistry. 44(4):281-90. doi: 10.1007/BF00490364.

Larsson, L-I., St-Onge, L., Hougaard, D.M., Sosa-Pineda, B. & Gruss, P. (1998) Pax 4 and 6 regulate gastrointestinal endocrine cell development. *Mechanisms of Development.* 79 (1) 153-159. doi: 10.1016/S0925-4773(98)00182-8.

Laschet, C., Dupuis, N. & Hanson, J. (2019) A dynamic and screening-compatible nanoluciferase-based complementation assay enables

profiling of individual GPCR–G protein interactions. *Journal of Biological Chemistry*. 294 (11), 4079–4090. doi:10.1074/jbc.RA118.006231.
Lassalle, M.W. & Kondou, S. (2016) Uncovering the role of the flexible C-terminal tail: A model study with Strep-tagged GFP. *Biochimie Open*. 2, 1–8. doi:10.1016/j.biopen.2015.11.004.
Latorre, R., Ramírez-Garcia, P.D., Hegron, A., Grace, J.L., Retamal, J.S., Shenoy, P., Tran, M., Aurelio, L., Flynn, B., Poole, D.P., Klein-Cloud, R., Jensen, D.D., Davis, T.P., Schmidt, B.L., Quinn, J.F., Whittaker, M.R., Veldhuis, N.A. & Bunnett, N.W. (2022) Sustained endosomal release of a neurokinin-1 receptor antagonist from nanostars provides long-lasting relief of chronic pain. *Biomaterials*. 285, 121536. doi:10.1016/j.biomaterials.2022.121536.
Latorre, R., Sternini, C., De Giorgio, R. & Greenwood-Van Meerveld, B. (2016) Enteroendocrine cells: a review of their role in brain–gut communication. *Neurogastroenterology & Motility*. 28 (5), 620–630. doi:10.1111/nmo.12754.
Lawrence, M.C., McGlynn, K., Park, B.-H. & Cobb, M.H. (2005) ERK1/2-dependent Activation of Transcription Factors Required for Acute and Chronic Effects of Glucose on the Insulin Gene Promoter. *Journal of Biological Chemistry*. 280 (29), 26751–26759. doi:10.1074/jbc.M503158200.
Lee, N.H. & Fraser, C.M. (1993) Cross-talk between m1 muscarinic acetylcholine and beta 2-adrenergic receptors. cAMP and the third intracellular loop of m1 muscarinic receptors confer heterologous regulation. *Journal of Biological Chemistry*. 268 (11), 7949–7957. doi:10.1016/S0021-9258(18)53050-7.
Lee, S.U., In, H.J., Kwon, M.S., Park, B., Jo, M., Kim, M.-O., Cho, S., Lee, S., Lee, H.-J., Kwak, Y.S. & Kim, S. (2013) β-Arrestin 2 Mediates G Protein-Coupled Receptor 43 Signals to Nuclear Factor-κB. *Biological and Pharmaceutical Bulletin*. 36 (11), 1754–1759. doi:10.1248/bpb.b13-00312.
Lee, Y.-S., Kim, T.-Y., Kim, Y., Lee, S.-H., Kim, S., Kang, S.W., Yang, J.-Y., Baek, I.-J., Sung, Y.H., Park, Y.-Y., Hwang, S.W., O, E., Kim, K.S., Liu, S., Kamada, N., Gao, N. & Kweon, M.-N. (2018) Microbiota-Derived Lactate Accelerates Intestinal Stem-Cell-Mediated Epithelial Development. *Cell host & microbe*. 24 (6), 833-846.e6. doi:10.1016/j.chom.2018.11.002.
León, K., Boulo, T., Musnier, A., Morales, J., Gauthier, C., Dupuy, L., Heyne, S., Backofen, R., Poupon, A., Cormier, P., Reiter, E. & Crepieux, P. (2014) Activation of a GPCR leads to eIF4G phosphorylation at the 5′ cap and to IRES-dependent translation. *Journal of Molecular Endocrinology*. 52 (3), 373–382. doi:10.1530/JME-14-0009.
Leterrier, C., Lainé, J., Darmon, M., Boudin, H., Rossier, J. & Lenkei, Z. (2006) Constitutive Activation Drives Compartment-Selective Endocytosis and Axonal Targeting of Type 1 Cannabinoid Receptors. *The Journal of Neuroscience*. 26 (12), 3141–3153. doi:10.1523/JNEUROSCI.5437-05.2006.
Li, H.J., Kapoor, A., Giel-Moloney, M., Rindi, G. & Leiter, A.B. (2012) Notch signaling differentially regulates the cell fate of early endocrine precursor cells and their maturing descendants in the mouse pancreas and

intestine. *Developmental Biology*. 371 (2), 156–169. doi:10.1016/j.ydbio.2012.08.023.
Li, H.J., Ray, S.K., Kucukural, A., Gradwohl, G. & Leiter, A.B. (2021) Reduced Neurog3 Gene Dosage Shifts Enteroendocrine Progenitor Towards Goblet Cell Lineage in the Mouse Intestine. *Cellular and Molecular Gastroenterology and Hepatology*. 11 (2), 433–448. doi:10.1016/j.jcmgh.2020.08.006.
Li, S.K., Zhu, D., Gaisano, H.Y. & Brubaker, P.L. (2014) Role of vesicle-associated membrane protein 2 in exocytosis of glucagon-like peptide-1 from the murine intestinal L cell. *Diabetologia*. 57 (4), 809–818. doi:10.1007/s00125-013-3143-2.
Liddle, R.A. (1997) CHOLECYSTOKININ CELLS. *Annual Review of Physiology*. 59 (1), 221–242. doi:10.1146/annurev.physiol.59.1.221.
Lim, G.E., Huang, G.J., Flora, N., LeRoith, D., Rhodes, C.J. & Brubaker, P.L. (2009) Insulin Regulates Glucagon-Like Peptide-1 Secretion from the Enteroendocrine L Cell. *Endocrinology*. 150 (2), 580–591. doi:10.1210/en.2008-0726.
Lincoff, A.M., Brown-Frandsen, K., Colhoun, H.M., Deanfield, J., Emerson, S.S., Esbjerg, S., Hardt-Lindberg, S., Hovingh, G.K., Kahn, S.E., Kushner, R.F., Lingvay, I., Oral, T.K., Michelsen, M.M., Plutzky, J., Tornøe, C.W. & Ryan, D.H. (2023) Semaglutide and Cardiovascular Outcomes in Obesity without Diabetes. *New England Journal of Medicine*. 389 (24), 2221–2232. doi:10.1056/NEJMoa2307563.
Liou, A.P., Lu, X., Sei, Y., Zhao, X., Pechhold, S., Carrero, R.J., Raybould, H.E. & Wank, S. (2011) The G-Protein−Coupled Receptor GPR40 Directly Mediates Long-Chain Fatty Acid−Induced Secretion of Cholecystokinin. *Gastroenterology*. 140 (3), 903-912.e4. doi:10.1053/j.gastro.2010.10.012.
Liu, M., Lara-Lemus, R., Shan, S., Wright, J., Haataja, L., Barbetti, F., Guo, H., Larkin, D. & Arvan, P. (2012) Impaired Cleavage of Preproinsulin Signal Peptide Linked to Autosomal-Dominant Diabetes. *Diabetes*. 61 (4), 828–837. doi:10.2337/db11-0878.
Liu, X., Zhang, Z., Song, Y., Xie, H. & Dong, M. (2023) An update on brown adipose tissue and obesity intervention: Function, regulation and therapeutic implications. *Frontiers in Endocrinology*. 13. doi:10.3389/fendo.2022.1065263.
Liu, Y., Yang, Y., Ward, R., An, S., Guo, X.-X., Li, W. & Xu, T.-R. (2015) Biased signalling: the instinctive skill of the cell in the selection of appropriate signalling pathways. *Biochemical Journal*. 470 (2), 155–167. doi:10.1042/BJ20150358.
Livak, K.J. & Schmittgen, T.D. (2001) Analysis of Relative Gene Expression Data Using Real-Time Quantitative PCR and the 2−ΔΔCT Method. *Methods*. 25 (4), 402–408. doi:10.1006/meth.2001.1262.
Longuet, C., Broca, C., Costes, S., Hani, E.H., Bataille, D. & Dalle, S. (2005) Extracellularly Regulated Kinases 1/2 (p44/42 Mitogen-Activated Protein Kinases) Phosphorylate Synapsin I and Regulate Insulin Secretion in the MIN6 β-Cell Line and Islets of Langerhans. *Endocrinology*. 146 (2), 643–654. doi:10.1210/en.2004-0841.
López-Díaz, L., Jain, R.N., Keeley, T.M., VanDussen, K.L., Brunkan, C.S., Gumucio, D.L. & Samuelson, L.C. (2007) Intestinal Neurogenin 3 directs differentiation of a bipotential secretory progenitor to endocrine cell rather

than goblet cell fate. *Developmental Biology*. 309 (2), 298–305. doi:10.1016/j.ydbio.2007.07.015.
Lorza-Gil, E., Kaiser, G., Rexen Ulven, E., König, G.M., Gerst, F., Oquendo, M.B., Birkenfeld, A.L., Häring, H.-U., Kostenis, E., Ulven, T. & Ullrich, S. (2020) FFA2-, but not FFA3-agonists inhibit GSIS of human pseudoislets: a comparative study with mouse islets and rat INS-1E cells. *Scientific Reports*. 10 (1), 16497. doi:10.1038/s41598-020-73467-5.
Louis, P., Duncan, S.H., McCrae, S.I., Millar, J., Jackson, M.S. & Flint, H.J. (2004) Restricted Distribution of the Butyrate Kinase Pathway among Butyrate-Producing Bacteria from the Human Colon. *Journal of Bacteriology*. 186 (7), 2099–2106. doi:10.1128/JB.186.7.2099-2106.2004.
Louis, P. & Flint, H.J. (2017) Formation of propionate and butyrate by the human colonic microbiota. *Environmental Microbiology*.19 (1) pp.29–41. doi:10.1111/1462-2920.13589.
Lovshin, J., Estall, J., Yusta, B., Brown, T.J. & Drucker, D.J. (2001) Glucagon-like Peptide (GLP)-2 Action in the Murine Central Nervous System Is Enhanced by Elimination of GLP-1 Receptor Signaling. *Journal of Biological Chemistry*. 276 (24), 21489–21499. doi:10.1074/jbc.M009382200.
Lu, J., Chen, P.P., Zhang, J.X., Li, X.Q., Wang, G.H., Yuan, B.Y., Huang, S.J., Liu, X.Q., Jiang, T.T., Wang, M.Y., Liu, W.T., Ruan, X.Z., Liu, B.C. & Ma, K.L. (2022) GPR43 activation-mediated lipotoxicity contributes to podocyte injury in diabetic nephropathy by modulating the ERK/EGR1 pathway. *International Journal of Biological Sciences*. 18 (1), 96–111. doi:10.7150/ijbs.64665.
Lu, K.-Y., Primus Dass, K.T., Tsai, S.-F., Chuang, H.-M., Lin, S.-Z., Liu, S.-P. & Harn, H.-J. (2020) Clinical Application Potential of Small Molecules that Induce Brown Adipose Tissue Thermogenesis by Improving Fat Metabolism. *Cell Transplantation*. 29, 096368972092739. doi:10.1177/0963689720927394.
Lu, V.B., Rievaj, J., O'Flaherty, E.A., Smith, C.A., Pais, R., Pattison, L.A., Tolhurst, G., Leiter, A.B., Bulmer, D.C., Gribble, F.M. & Reimann, F. (2019) Adenosine triphosphate is co-secreted with glucagon-like peptide-1 to modulate intestinal enterocytes and afferent neurons. *Nature Communications*. 10 (1), 1029. doi:10.1038/s41467-019-09045-9.
Lund, M.L., Sorrentino, G., Egerod, K.L., Kroone, C., Mortensen, B., Knop, F.K., Reimann, F., Gribble, F.M., Drucker, D.J., De Koning, E.J.P., Schoonjans, K., Bäckhed, F., Schwartz, T.W. & Petersen, N. (2020) L-cell differentiation is induced by bile acids through GpBAR1 and paracrine GLP-1 and serotonin signaling. *Diabetes*. 69 (4), 614–623. doi:10.2337/db19-0764.
Lundberg, J.M., Tatemoto, K., Terenius, L., Hellström, P.M., Mutt, V., Hökfelt, T. & Hamberger, B. (1982) Localization of peptide YY (PYY) in gastrointestinal endocrine cells and effects on intestinal blood flow and motility. *Proceedings of the National Academy of Sciences*. 79 (14), 4471–4475. doi:10.1073/pnas.79.14.4471.
Lutz, S., Shankaranarayanan, A., Coco, C., Ridilla, M., Nance, M.R., Vettel, C., Baltus, D., Evelyn, C.R., Neubig, R.R., Wieland, T. & Tesmer, J.J.G. (2007) Structure of Gα $_q$ -p63RhoGEF-RhoA Complex Reveals a

Pathway for the Activation of RhoA by GPCRs. *Science*. 318 (5858), 1923–1927. doi:10.1126/science.1147554.
Ma, L., Cao, X., Ye, X., Ye, J. & Sun, Y. (2020) Sennoside A Induces GLP-1 Secretion Through Activation of the ERK1/2 Pathway in L-Cells . *Diabetes, Metabolic Syndrome and Obesity: Targets and Therapy*. Volume 13, 1407–1415. doi:10.2147/DMSO.S247251.
Ma, Y., Huang, P., Hu, M., Ling, S., Li, Y., Chen, B. & Xu, Y. (2017) Dietary fiber intake and risks of proximal and distal colon cancers: A systematic review and meta-analysis. *Journal of Clinical Oncology*. 35 (15_suppl), e15080–e15080. doi:10.1200/JCO.2017.35.15_suppl.e15080.
Mace, O.J., Schindler, M. & Patel, S. (2012) The regulation of K- and L-cell activity by GLUT2 and the calcium-sensing receptor CasR in rat small intestine. *The Journal of Physiology*. 590 (12), 2917–2936. doi:10.1113/jphysiol.2011.223800.
Macia, L., Tan, J., Vieira, A.T., Leach, K., Stanley, D., et al. (2015) Metabolite-sensing receptors GPR43 and GPR109A facilitate dietary fibre-induced gut homeostasis through regulation of the inflammasome. *Nature Communications*. 6 (1), 6734. doi:10.1038/ncomms7734.
Magoulas, C., McGuinness, L., Balthasar, N., Carmignac, D.F., Sesay, A.K., Mathers, K.E., Christian, H., Candeil, L., Bonnefont, X., Mollard, P. & Robinson, I.C.A.F. (2000) A Secreted Fluorescent Reporter Targeted to Pituitary Growth Hormone Cells in Transgenic Mice. *Endocrinology*. 141 (12), 4681–4689. doi:10.1210/endo.141.12.7828.
Mah, A.T., Van Landeghem, L., Gavin, H.E., Magness, S.T. & Lund, P.K. (2014) Impact of Diet-Induced Obesity on Intestinal Stem Cells: Hyperproliferation but Impaired Intrinsic Function That Requires Insulin/IGF1. *Endocrinology*. 155 (9), 3302–3314. doi:10.1210/en.2014-1112.
Al Mahri, S., Malik, S.S., Al Ibrahim, M., Haji, E., Dairi, G. & Mohammad, S. (2022) Free Fatty Acid Receptors (FFARs) in Adipose: Physiological Role and Therapeutic Outlook. *Cells*. 11 (4), 750. doi:10.3390/cells11040750.
Majumdar, S., Chiu, Y.-T., Pickett, J.E. & Roth, B.L. (2024) Illuminating the understudied GPCR-ome. *Drug Discovery Today*. 29 (3), 103848. doi:10.1016/j.drudis.2023.103848.
Mannon, P.J., Kanungo, A., Mannon, R.B. & Ludwig, K.A. (1999) Peptide YY/neuropeptide Y Y1 receptor expression in the epithelium and mucosal nerves of the human colon. *Regulatory Peptides*. 83 (1), 11–19. doi:10.1016/S0167-0115(99)00035-X.
Mannon, P.J. & Mele, J.M. (2000) Peptide YY Y1 receptor activates mitogen-activated protein kinase and proliferation in gut epithelial cells via the epidermal growth factor receptor. *Biochemical Journal*. 350 (3), 655–661. doi:10.1042/bj3500655.
Mao, C., Gao, M., Zang, S.-K., Zhu, Y., Shen, D.-D., Chen, L.-N., Yang, L., Wang, Z., Zhang, H., Wang, W.-W., Shen, Q., Lu, Y., Ma, X. & Zhang, Y. (2023) Orthosteric and allosteric modulation of human HCAR2 signaling complex. *Nature Communications*. 14 (1), 7620. doi:10.1038/s41467-023-43537-z.
Markovic, M.A. & Brubaker, P.L. (2019) The roles of glucagon-like peptide-2 and the intestinal epithelial insulin-like growth factor-1 receptor in regulating

microvillus length. *Scientific Reports*. 9 (1), 13010. doi:10.1038/s41598-019-49510-5.
Marshman, E., Booth, C. & Potten, C.S. (2002) The intestinal epithelial stem cell. *BioEssays*. 24 (1), 91–98. doi:10.1002/bies.10028.
Marsich, E., Vetere, A., Di Piazza, M., Tell, G. & Paoletti, S. (2003) The PAX6 gene is activated by the basic helix-loop-helix transcription factor NeuroD/BETA2. *Biochem. J*.376.
Martin, C.R., Osadchiy, V., Kalani, A. & Mayer, E.A. (2018) The Brain-Gut-Microbiome Axis. *Cellular and Molecular Gastroenterology and Hepatology*. 6 (2), 133–148. doi:10.1016/j.jcmgh.2018.04.003.
Martínez-Sánchez, M.A., Balaguer-Román, A., Fernández-Ruiz, V.E., Almansa-Saura, S., García-Zafra, V., Ferrer-Gómez, M., Frutos, M.D., Queipo-Ortuño, M.I., Ruiz-Alcaraz, A.J., Núñez-Sánchez, M.Á. & Ramos-Molina, B. (2023) Plasma short-chain fatty acid changes after bariatric surgery in patients with severe obesity. *Surgery for Obesity and Related Diseases*. 19 (7), 727–734. doi:10.1016/j.soard.2022.12.041.
Martins, P., Fakhry, J., de Oliveira, E.C., Hunne, B., Fothergill, L.J., Ringuet, M., Reis, D. d'Ávila, Rehfeld, J.F., Callaghan, B. & Furness, J.B. (2017) Analysis of enteroendocrine cell populations in the human colon. *Cell and Tissue Research*. 367 (2), 161–168. doi:10.1007/s00441-016-2530-7.
Masuda, M., Tomita, H., Okubo, K. & Miyasaka, K. (1994) Vagal efferent nerve-dependent inhibitory action of pancreatic polypeptide and peptide YY in conscious rats: comparison with somatostatin. *Journal of the Autonomic Nervous System*. 50 (2), 131–138. doi:10.1016/0165-1838(94)90003-5.
Masuho, I., Kise, R., Gainza, P., Von Moo, E., Li, X., Tany, R., Wakasugi-Masuho, H., Correia, B.E. & Martemyanov, K.A. (2023) Rules and mechanisms governing G protein coupling selectivity of GPCRs. *Cell Reports*. 42 (10), 113173. doi:10.1016/j.celrep.2023.113173.
Mathers, J.C., Kennard, J. & James, O.F.W. (1993) Gastrointestinal responses to oats consumption in young adult and elderly rats: digestion, large bowel fermentation and crypt cell proliferation rates. *British Journal of Nutrition*. 70 (2), 567–584. doi:10.1079/BJN19930149.
Matsuno, A., Mizutani, A., Itoh, J., Takekoshi, S., Nagashima, T., Okinaga, H., Takano, K. & Osamura, R.Y. (2005) Establishment of Stable GH3 Cell Line Expressing Enhanced Yellow Fluorescein Protein-Growth Hormone Fusion Protein. *Journal of Histochemistry & Cytochemistry*. 53 (9), 1177–1180. doi:10.1369/jhc.5B6708.2005.
McCauley, H.A., Riedman, A.M., Enriquez, J.R., Zhang, X., Watanabe-Chailland, M., Sanchez, J.G., Kechele, D.O., Paul, E.F., Riley, K., Burger, C., Lang, R.A. & Wells, J.M. (2023) Enteroendocrine Cells Protect the Stem Cell Niche by Regulating Crypt Metabolism in Response to Nutrients. *Cellular and Molecular Gastroenterology and Hepatology*. 15 (6), 1293–1310. doi:10.1016/j.jcmgh.2022.12.016.
McDonald, N.A., Henstridge, C.M., Connolly, C.N. & Irving, A.J. (2007) An Essential Role for Constitutive Endocytosis, but Not Activity, in the Axonal Targeting of the CB_1 Cannabinoid Receptor. *Molecular Pharmacology*. 71 (4), 976–984. doi:10.1124/mol.106.029348.
McGirr, R., Guizzetti, L. & Dhanvantari, S. (2013) The sorting of proglucagon to secretory granules is mediated by carboxypeptidase E and intrinsic

sorting signals. *Journal of Endocrinology*. 217 (2), 229–240. doi:10.1530/JOE-12-0468.
McNelis, J.C., Lee, Y.S., Mayoral, R., van der Kant, R., Johnson, A.M.F., Wollam, J. & Olefsky, J.M. (2015) GPR43 Potentiates β-Cell Function in Obesity. *Diabetes*. 64 (9), 3203–3217. doi:10.2337/db14-1938.
Melson, E., Ashraf, U., Papamargaritis, D. & Davies, M.J. (2024) What is the pipeline for future medications for obesity? *International Journal of Obesity*. doi:10.1038/s41366-024-01473-y.
Mentlein, R. (1999) Dipeptidyl-peptidase IV (CD26)-role in the inactivation of regulatory peptides. *Regulatory Peptides*. 85 (1), 9–24. doi:10.1016/S0167-0115(99)00089-0.
Merchenthaler, I., Lane, M. & Shughrue, P. (1999) Distribution of pre-pro-glucagon and glucagon-like peptide-1 receptor messenger RNAs in the rat central nervous system. *The Journal of Comparative Neurology*. 403 (2), 261–280. doi:10.1002/(SICI)1096-9861(19990111)403:2<261::AID-CNE8>3.0.CO;2-5.
El Meskini, R., Jin, L., Marx, R., Bruzzaniti, A., Lee, J., Emeson, R.B. & Mains, R.E. (2001) A Signal Sequence Is Sufficient for Green Fluorescent Protein to Be Routed to Regulated Secretory Granules**This work was supported by NIH Grants DK-32948, DA-00266 (to R.E.M.), and NS-35891 (to R.B.E.). *Endocrinology*. 142 (2), 864–873. doi:10.1210/endo.142.2.7929.
Midorikawa, M. (2018) Real-time imaging of synaptic vesicle exocytosis by total internal reflection fluorescence (TIRF) microscopy. *Neuroscience Research*. 136, 1–5. doi:10.1016/j.neures.2018.01.008.
Miesenböck, G., De Angelis, D.A. & Rothman, J.E. (1998) Visualizing secretion and synaptic transmission with pH-sensitive green fluorescent proteins. *Nature*. 394 (6689), 192–195. doi:10.1038/28190.
Milligan, G., Shimpukade, B., Ulven, T. & Hudson, B.D. (2017) Complex pharmacology of free fatty acid receptors. *Chemical Reviews*.117 (1) pp.67–110. doi:10.1021/acs.chemrev.6b00056.
Millington, G.W. (2007) The role of proopiomelanocortin (POMC) neurones in feeding behaviour. *Nutrition & Metabolism*. 4 (1), 18. doi:10.1186/1743-7075-4-18.
Mishra, S.P., Karunakar, P., Taraphder, S. & Yadav, H. (2020) Free fatty acid receptors 2 and 3 as microbial metabolite sensors to shape host health: Pharmacophysiological view. *Biomedicines*.8 (6). doi:10.3390/BIOMEDICINES8060154.
Miyamoto, J., Ohue-Kitano, R., Mukouyama, H., Nishida, A., Watanabe, K., Igarashi, M., Irie, J., Tsujimoto, G., Satoh-Asahara, N., Itoh, H. & Kimura, I. (2019) Ketone body receptor GPR43 regulates lipid metabolism under ketogenic conditions. *Proceedings of the National Academy of Sciences*. 116 (47), 23813–23821. doi:10.1073/pnas.1912573116.
Miyasato, S., Iwata, K., Mura, R., Nakamura, S., Yanagida, K., Shindou, H., Nagata, Y., Kawahara, M., Yamaguchi, S., Aoki, J., Inoue, A., Nagamune, T., Shimizu, T. & Nakamura, M. (2023) Constitutively active GPR43 is crucial for proper leukocyte differentiation. *The FASEB Journal*. 37 (1). doi:10.1096/fj.202201591R.
Modvig, I.M., Kuhre, R.E., Jepsen, S.L., Xu, S.F.S., Engelstoft, M.S., Egerod, K.L., Schwartz, T.W., Ørskov, C., Rosenkilde, M.M. & Holst, J.J. (2021)

Amino acids differ in their capacity to stimulate GLP-1 release from the perfused rat small intestine and stimulate secretion by different sensing mechanisms. *American Journal of Physiology-Endocrinology and Metabolism*. 320 (5), E874–E885. doi:10.1152/ajpendo.00026.2021.

Mohammad, S., Baldini, G., Granell, S., Narducci, P., Martelli, A.M. & Baldini, G. (2007) Constitutive Traffic of Melanocortin-4 Receptor in Neuro2A Cells and Immortalized Hypothalamic Neurons. *Journal of Biological Chemistry*. 282 (7), 4963–4974. doi:10.1074/jbc.M608283200.

Mojsov, S., Weir, G.C. & Habener, J.F. (1987) Insulinotropin: glucagon-like peptide I (7-37) co-encoded in the glucagon gene is a potent stimulator of insulin release in the perfused rat pancreas. *Journal of Clinical Investigation*. 79 (2), 616–619. doi:10.1172/JCI112855.

Møller, T.C., Moo, E. Von, Inoue, A., Pedersen, M.F. & Bräuner-Osborne, H. (2024) Characterization of the real-time internalization of nine GPCRs reveals distinct dependence on arrestins and G proteins. *Biochimica et Biophysica Acta (BBA) - Molecular Cell Research*. 1871 (1), 119584. doi:10.1016/j.bbamcr.2023.119584.

Mori, Y., Akedo, H., Tanaka, K., Tanigaki, Y. & Okada, M. (1979) Effect of sodium butyrate on the granulopoiesis of mastocytoma cells. *Experimental Cell Research*. 118 (1), 15–22. doi:10.1016/0014-4827(79)90578-0.

Mu, F.T., Callaghan, J.M., Steele-Mortimer, O., Stenmark, H., Parton, R.G., Campbell, P.L., McCluskey, J., Yeo, J.P., Tock, E.P.C. & Toh, B.H. (1995) EEA1, an early endosome-associated protein. EEA1 is a conserved α- helical peripheral membrane protein flanked by cysteine 'fingers' and contains a calmodulin-binding IQ motif. *Journal of Biological Chemistry*. 270 (22), 13503–13511. doi:10.1074/jbc.270.22.13503.

Müller, T.D., Finan, B., Bloom, S.R., D'Alessio, D., Drucker, D.J., et al. (2019) Glucagon-like peptide 1 (GLP-1). *Molecular Metabolism*. 30, 72–130. doi:10.1016/j.molmet.2019.09.010.

Müller, T.D., Nogueiras, R., Andermann, M.L., Andrews, Z.B., Anker, S.D., et al. (2015) Ghrelin. *Molecular Metabolism*. 4 (6), 437–460. doi:10.1016/j.molmet.2015.03.005.

Mullershausen, F., Zecri, F., Cetin, C., Billich, A., Guerini, D. & Seuwen, K. (2009) Persistent signaling induced by FTY720-phosphate is mediated by internalized S1P1 receptors. *Nature Chemical Biology*. 5 (6), 428–434. doi:10.1038/nchembio.173.

Musnier, A., Blanchot, B., Reiter, E. & Crépieux, P. (2010) GPCR signalling to the translation machinery. *Cellular Signalling*. 22 (5), 707–716. doi:10.1016/j.cellsig.2009.10.012.

Musnier, A., León, K., Morales, J., Reiter, E., Boulo, T., Costache, V., Vourc'h, P., Heitzler, D., Oulhen, N., Poupon, A., Boulben, S., Cormier, P. & Crépieux, P. (2012) mRNA-Selective Translation Induced by FSH in Primary Sertoli Cells. *Molecular Endocrinology*. 26 (4), 669–680. doi:10.1210/me.2011-1267.

Mutoh, H., Fung, B.P., Naya, F.J., Tsai, M.-J., Nishitani, J. & Leiter, A.B. (1997) The basic helix–loop–helix transcription factor BETA2/NeuroD is expressed in mammalian enteroendocrine cells and activates secretin gene expression. *Proceedings of the National Academy of Sciences*. 94 (8), 3560–3564. doi:10.1073/pnas.94.8.3560.

Nagamatsu, S. (2006) TIRF Microscopy Analysis of the Mechanism of Insulin Exocytosis. *Endocrine Journal*.53 (4).
Nakamoto, K., Aizawa, F., Miyagi, K., Yamashita, T., Mankura, M., Koyama, Y., Kasuya, F., Hirasawa, A., Kurihara, T., Miyata, A. & Tokuyama, S. (2017) Dysfunctional GPR40/FFAR1 signaling exacerbates pain behavior in mice. *PLOS ONE*. 12 (7), e0180610. doi:10.1371/journal.pone.0180610.
Nash, C.A., Wei, W., Irannejad, R. & Smrcka, A. V (2019) Golgi localized β1-adrenergic receptors stimulate Golgi PI4P hydrolysis by PLCε to regulate cardiac hypertrophy. *eLife*. 8. doi:10.7554/eLife.48167.
NCD Risk Factor Collaboration (NCD-RisC) (2016) Trends in adult body-mass index in 200 countries from 1975 to 2014: a pooled analysis of 1698 population-based measurement studies with 19·2 million participants. *The Lancet*. 387 (10026), 1377–1396. doi:10.1016/S0140-6736(16)30054-X.
Negari, I.P., Keshari, S. & Huang, C.-M. (2021) Probiotic Activity of Staphylococcus epidermidis Induces Collagen Type I Production through FFaR2/p-ERK Signaling. *International Journal of Molecular Sciences*. 22 (3), 1414. doi:10.3390/ijms22031414.
Nergård, B.J., Lindqvist, A., Gislason, H.G., Groop, L., Ekelund, M., Wierup, N. & Hedenbro, J.L. (2015) Mucosal glucagon-like peptide-1 and glucose-dependent insulinotropic polypeptide cell numbers in the super-obese human foregut after gastric bypass. *Surgery for Obesity and Related Diseases*. 11 (6), 1237–1246. doi:10.1016/j.soard.2015.03.021.
Nguyen, A.H. & Lefkowitz, R.J. (2021) Signaling at the endosome: cryo-EM structure of a GPCR–G protein–beta-arrestin megacomplex. *The FEBS Journal*. 288 (8), 2562–2569. doi:10.1111/febs.15773.
Nilsson, N.E., Kotarsky, K., Owman, C. & Olde, B. (2003) Identification of a free fatty acid receptor, FFA2R, expressed on leukocytes and activated by short-chain fatty acids. *Biochemical and Biophysical Research Communications*. 303 (4), 1047–1052. doi:10.1016/S0006-291X(03)00488-1.
Nilsson, O., Bilchik, A.J., Goldenring, J.R., Ballantyne, G.H., Adrian, T.E. & Modlin, I.M. (1991) Distribution and Immunocytochemical Colocalization of Peptide YY and Enteroglucagon in Endocrine Cells of the Rabbit Colon*. *Endocrinology*. 129 (1), 139–148. doi:10.1210/endo-129-1-139.
Nishida, A., Miyamoto, J., Shimizu, H. & Kimura, I. (2021) Gut microbial short-chain fatty acids-mediated olfactory receptor 78 stimulation promotes anorexigenic gut hormone peptide YY secretion in mice. *Biochemical and Biophysical Research Communications*. 557, 48–54. doi:10.1016/j.bbrc.2021.03.167.
Nishimura, A., Kitano, K., Takasaki, J., Taniguchi, M., Mizuno, N., Tago, K., Hakoshima, T., Itoh, H. & Gilman, A.G. (n.d.) *Structural basis for the specific inhibition of heterotrimeric G q protein by a small molecule*. doi:10.1073/pnas.1003553107/-/DCSupplemental.
Nishimura, K., Hiramatsu, K., Monir, M.M., Takemoto, C. & Watanabe, T. (2013) Ultrastructural Study on Colocalization of Glucagon-Like Peptide (GLP)-1 with GLP-2 in Chicken Intestinal L-Cells. *Journal of Veterinary Medical Science*. 75 (10), 1335–1339. doi:10.1292/jvms.13-0106.
Nøhr, M.K., Egerod, K.L., Christiansen, S.H., Gille, A., Offermanns, S., Schwartz, T.W. & Møller, M. (2015) Expression of the short chain fatty

acid receptor GPR41/FFAR3 in autonomic and somatic sensory ganglia. *Neuroscience*. 290, 126–137. doi:10.1016/j.neuroscience.2015.01.040.
Nøhr, M.K., Pedersen, M.H., Gille, A., Egerod, K.L., Engelstoft, M.S., Husted, A.S., Sichlau, R.M., Grunddal, K. V., Seier Poulsen, S., Han, S., Jones, R.M., Offermanns, S. & Schwartz, T.W. (2013) GPR41/FFAR3 and GPR43/FFAR2 as Cosensors for Short-Chain Fatty Acids in Enteroendocrine Cells vs FFAR3 in Enteric Neurons and FFAR2 in Enteric Leukocytes. *Endocrinology*. 154 (10), 3552–3564. doi:10.1210/en.2013-1142.
Nonaka, N., Shioda, S., Niehoff, M.L. & Banks, W.A. (2003) Characterization of Blood-Brain Barrier Permeability to PYY $_{3-36}$ in the Mouse. *Journal of Pharmacology and Experimental Therapeutics*. 306 (3), 948–953. doi:10.1124/jpet.103.051821.
Nunn, E., Jaiswal, N., Gavin, M., Uehara, K., Stefkovich, M., Drareni, K., Calhoun, R., Lee, M., Holman, C.D., Baur, J.A., Seale, P. & Titchenell, P.M. (2024) Antibody blockade of activin type II receptors preserves skeletal muscle mass and enhances fat loss during GLP-1 receptor agonism. *Molecular Metabolism*. 80, 101880. doi:10.1016/j.molmet.2024.101880.
Nygaard, R., Nielbo, S., Schwartz, T.W. & Poulsen, F.M. (2006) The PP-Fold Solution Structure of Human Polypeptide YY and Human PYY3-36 As Determined by NMR ›. *Biochemistry*. 45 (27), 8350–8357. doi:10.1021/bi060359l.
Nyström, E.E.L., Martinez-Abad, B., Arike, L., Birchenough, G.M.H., Nonnecke, E.B., Castillo, P.A., Svensson, F., Bevins, C.L., Hansson, G.C. & Johansson, M.E. V. (2021) An intercrypt subpopulation of goblet cells is essential for colonic mucus barrier function. *Science*. 372 (6539). doi:10.1126/science.abb1590.
Oakley, R.H., Laporte, S.A., Holt, J.A., Barak, L.S. & Caron, M.G. (1999) Association of β-Arrestin with G Protein-coupled Receptors during Clathrin-mediated Endocytosis Dictates the Profile of Receptor Resensitization. *Journal of Biological Chemistry*. 274 (45), 32248–32257. doi:10.1074/jbc.274.45.32248.
Obradovic, M., Sudar-Milovanovic, E., Soskic, S., Essack, M., Arya, S., Stewart, A.J., Gojobori, T. & Isenovic, E.R. (2021) Leptin and Obesity: Role and Clinical Implication. *Frontiers in Endocrinology*. 12. doi:10.3389/fendo.2021.585887.
Oh, D.Y., Walenta, E., Akiyama, T.E., Lagakos, W.S., Lackey, D., et al. (2014) A Gpr120-selective agonist improves insulin resistance and chronic inflammation in obese mice. *Nature Medicine*. 20 (8), 942–947. doi:10.1038/nm.3614.
Oh, H., Kim, H., Lee, D.H., Lee, A., Giovannucci, E.L., Kang, S.-S. & Keum, N. (2019) Different dietary fibre sources and risks of colorectal cancer and adenoma: a concentration–response meta-analysis of prospective studies. *British Journal of Nutrition*. 122 (6), 605–615. doi:10.1017/S0007114519001454.
Ohara-Imaizumi, M., Fujiwara, T., Nakamichi, Y., Okamura, T., Akimoto, Y., Kawai, J., Matsushima, S., Kawakami, H., Watanabe, T., Akagawa, K. & Nagamatsu, S. (2007) Imaging analysis reveals mechanistic differences

between first- and second-phase insulin exocytosis. *The Journal of Cell Biology*. 177 (4), 695–705. doi:10.1083/jcb.200608132.
Ohara-Imaizumi, M., Nakamichi, Y., Tanaka, T., Ishida, H. & Nagamatsu, S. (2002) Imaging exocytosis of single insulin secretory granules with evanescent wave microscopy: Distinct behavior of granule motion in biphasic insulin release. *Journal of Biological Chemistry*. 277 (6), 3805–3808. doi:10.1074/jbc.C100712200.
Ohara-Imaizumi, M., Nishiwaki, C., Kikuta, T., Nagai, S., Nakamichi, Y. & Nagamatsu, S. (2004) TIRF imaging of docking and fusion of single insulin granule motion in primary rat pancreatic β-cells: different behaviour of granule motion between normal and Goto–Kakizaki diabetic rat β-cells. *Biochemical Journal*. 381 (1), 13–18. doi:10.1042/BJ20040434.
Ohki, J., Sakashita, A., Aihara, E., Inaba, A., Uchiyama, H., Matsumoto, M., Ninomiya, Y., Yamane, T., Oishi, Y. & Iwatsuki, K. (2020) Comparative analysis of enteroendocrine cells and their hormones between mouse intestinal organoids and native tissues. *Bioscience, Biotechnology, and Biochemistry*. 84 (5), 936–942. doi:10.1080/09168451.2020.1713043.
Okamoto, Y., Ninomiya, H., Miwa, S. & Masaki, T. (2000) Cholesterol Oxidation Switches the Internalization Pathway of Endothelin Receptor Type A from Caveolae to Clathrin-coated Pits in Chinese Hamster Ovary Cells. *Journal of Biological Chemistry*. 275 (9), 6439–6446. doi:10.1074/jbc.275.9.6439.
Olsen, R.H.J., DiBerto, J.F., English, J.G., Glaudin, A.M., Krumm, B.E., Slocum, S.T., Che, T., Gavin, A.C., McCorvy, J.D., Roth, B.L. & Strachan, R.T. (2020) TRUPATH, an open-source biosensor platform for interrogating the GPCR transducerome. *Nature Chemical Biology*. 16 (8), 841–849. doi:10.1038/s41589-020-0535-8.
O'Malley, K.L., Jong, Y.J.I., Gonchar, Y., Burkhalter, A. & Romano, C. (2003) Activation of metabotropic glutamate receptor mGlu5 on nuclear membranes mediates intranuclear Ca2+ changes in heterologous cell types and neurons. *Journal of Biological Chemistry*. 278 (30), 28210–28219. doi:10.1074/jbc.M300792200.
Oncel, S., Safratowich, B.D., Lindlauf, J.E., Liu, Z., Palmer, D.G., Briske-Anderson, M. & Zeng, H. (2024) Efficacy of Butyrate to Inhibit Colonic Cancer Cell Growth Is Cell Type-Specific and Apoptosis-Dependent. *Nutrients*. 16 (4), 529. doi:10.3390/nu16040529.
Ookawara, M., Matsuda, K., Watanabe, M. & Moritoh, Y. (2020) The GPR40 Full Agonist SCO-267 Improves Liver Parameters in a Mouse Model of Nonalcoholic Fatty Liver Disease without Affecting Glucose or Body Weight. *Journal of Pharmacology and Experimental Therapeutics*. 375 (1), 21–27. doi:10.1124/jpet.120.000046.
Orchel, A., Dzierżewicz, Z., Parfiniewicz, B., Weglarz, L. & Wilczok, T. (2005) Butyrate-Induced Differentiation of Colon Cancer Cells Is PKC and JNK Dependent. *Digestive Diseases and Sciences*. 50 (3), 490–498. doi:10.1007/s10620-005-2463-6.
Oteng, A.-B. & Liu, L. (2023) GPCR-mediated effects of fatty acids and bile acids on glucose homeostasis. *Frontiers in Endocrinology*. 14. doi:10.3389/fendo.2023.1206063.

Oya, M., Kitaguchi, T., Pais, R., Reimann, F., Gribble, F. & Tsuboi, T. (2013) The G Protein-coupled Receptor Family C Group 6 Subtype A (GPRC6A) Receptor Is Involved in Amino Acid-induced Glucagon-like Peptide-1 Secretion from GLUTag Cells. *Journal of Biological Chemistry*. 288 (7), 4513–4521. doi:10.1074/jbc.M112.402677.

Ozawa, A., Peinado, J.R. & Lindberg, I. (2010) Modulation of Prohormone Convertase 1/3 Properties Using Site-Directed Mutagenesis. *Endocrinology*. 151 (9), 4437–4445. doi:10.1210/en.2010-0296.

Ozkan, A.D., Eskiler, G.G., Kazan, N. & Turna, O. (2023) Histone deacetylase inhibitor sodium butyrate regulates the activation of toll-like receptor 4/interferon regulatory factor-3 signaling pathways in prostate cancer cells. *Journal of Cancer Research and Therapeutics*. 19 (7), 1812–1817. doi:10.4103/jcrt.jcrt_2032_21.

Palczewski, K., Kumasaka, T., Hori, T., Behnke, C.A., Motoshima, H., Fox, B.A., Trong, I. Le, Teller, D.C., Okada, T., Stenkamp, R.E., Yamamoto, M. & Miyano, M. (2000) Crystal Structure of Rhodopsin: A G Protein-Coupled Receptor. *Science*. 289 (5480), 739–745. doi:10.1126/science.289.5480.739.

Panaro, B.L., Tough, I.R., Engelstoft, M.S., Matthews, R.T., Digby, G.J., Møller, C.L., Svendsen, B., Gribble, F., Reimann, F., Holst, J.J., Holst, B., Schwartz, T.W., Cox, H.M. & Cone, R.D. (2014) The Melanocortin-4 Receptor Is Expressed in Enteroendocrine L Cells and Regulates the Release of Peptide YY and Glucagon-like Peptide 1 In Vivo. *Cell Metabolism*. 20 (6), 1018–1029. doi:10.1016/j.cmet.2014.10.004.

Park, J., Kotani, T., Konno, T., Setiawan, J., Kitamura, Y., Imada, S., Usui, Y., Hatano, N., Shinohara, M., Saito, Y., Murata, Y. & Matozaki, T. (2016) Promotion of Intestinal Epithelial Cell Turnover by Commensal Bacteria: Role of Short-Chain Fatty Acids. *PLOS ONE*. 11 (5), e0156334. doi:10.1371/journal.pone.0156334.

Park, J.J. & Loh, Y.P. (2008) Minireview: How Peptide Hormone Vesicles Are Transported to the Secretion Site for Exocytosis. *Molecular Endocrinology*. 22 (12), 2583–2595. doi:10.1210/me.2008-0209.

Parker, H.E., Adriaenssens, A., Rogers, G., Richards, P., Koepsell, H., Reimann, F. & Gribble, F.M. (2012) Predominant role of active versus facilitative glucose transport for glucagon-like peptide-1 secretion. *Diabetologia*. 55 (9), 2445–2455. doi:10.1007/s00125-012-2585-2.

Paroutis, P., Touret, N. & Grinstein, S. (2004) The pH of the Secretory Pathway: Measurement, Determinants, and Regulation. *Physiology*. 19 (4), 207–215. doi:10.1152/physiol.00005.2004.

Patwardhan, A., Cheng, N. & Trejo, J. (2021) Post-Translational Modifications of G Protein–Coupled Receptors Control Cellular Signaling Dynamics in Space and Time. *Pharmacological Reviews*. 73 (1), 120–151. doi:10.1124/pharmrev.120.000082.

Peiris, M., Aktar, R., Reed, D., Cibert-Goton, V., Zdanaviciene, A., Halder, W., Robinow, A., Corke, S., Dogra, H., Knowles, C.H. & Blackshaw, A. (2022) Decoy bypass for appetite suppression in obese adults: role of synergistic nutrient sensing receptors GPR84 and FFAR4 on colonic endocrine cells. *Gut*. 71 (5), 928–937. doi:10.1136/gutjnl-2020-323219.

Pellegrinet, L., Rodilla, V., Liu, Z., Chen, S., Koch, U., Espinosa, L., Kaestner, K.H., Kopan, R., Lewis, J. & Radtke, F. (2011) Dll1- and Dll4-Mediated

Notch Signaling Are Required for Homeostasis of Intestinal Stem Cells. *Gastroenterology*. 140 (4), 1230-1240.e7. doi:10.1053/j.gastro.2011.01.005.
Pera, T. & Penn, R.B. (2014) Crosstalk between beta-2-adrenoceptor and muscarinic acetylcholine receptors in the airway. *Current Opinion in Pharmacology*. 16, 72–81. doi:10.1016/j.coph.2014.03.005.
Petersen, M.C. & Shulman, G.I. (2018) Mechanisms of Insulin Action and Insulin Resistance. *Physiological Reviews*. 98 (4), 2133–2223. doi:10.1152/physrev.00063.2017.
Petersen, N., Frimurer, T.M., Terndrup Pedersen, M., Egerod, K.L., Wewer Albrechtsen, N.J., Holst, J.J., Grapin-Botton, A., Jensen, K.B. & Schwartz, T.W. (2018) Inhibiting RHOA Signaling in Mice Increases Glucose Tolerance and Numbers of Enteroendocrine and Other Secretory Cells in the Intestine. *Gastroenterology*. 155 (4), 1164-1176.e2. doi:10.1053/j.gastro.2018.06.039.
Petersen, N., Reimann, F., Bartfeld, S., Farin, H.F., Ringnalda, F.C., Vries, R.G.J., Van Den Brink, S., Clevers, H., Gribble, F.M. & De Koning, E.J.P. (2014) Generation of l cells in mouse and human small intestine organoids. *Diabetes*. 63 (2), 410–420. doi:10.2337/db13-0991.
Photowala, H., Blackmer, T., Schwartz, E., Hamm, H.E. & Alford, S. (2006) G protein βγ-subunits activated by serotonin mediate presynaptic inhibition by regulating vesicle fusion properties. *Proceedings of the National Academy of Sciences*. 103 (11), 4281–4286. doi:10.1073/pnas.0600509103.
Pigeyre, M., Yazdi, F.T., Kaur, Y. & Meyre, D. (2016) Recent progress in genetics, epigenetics and metagenomics unveils the pathophysiology of human obesity. *Clinical Science*. 130 (12), 943–986. doi:10.1042/CS20160136.
Pingitore, A., Gonzalez-Abuin, N., Ruz-Maldonado, I., Huang, G.C., Frost, G. & Persaud, S.J. (2019) Short chain fatty acids stimulate insulin secretion and reduce apoptosis in mouse and human islets in vitro: Role of free fatty acid receptor 2. *Diabetes, Obesity and Metabolism*. 21 (2), 330–339. doi:10.1111/dom.13529.
Piper, R.C. & Luzio, J.P. (2007) Ubiquitin-dependent sorting of integral membrane proteins for degradation in lysosomes. *Current Opinion in Cell Biology*. 19 (4), 459–465. doi:10.1016/j.ceb.2007.07.002.
Pi-Sunyer, F.X. (1999) Comorbidities of overweight and obesity: current evidence and research issues. *Medicine & Science in Sports & Exercise*. 31 (Supplement 1), S602. doi:10.1097/00005768-199911001-00019.
Pizzonero, M., Dupont, S., Babel, M., Beaumont, S., Bienvenu, N., et al. (2014) Discovery and optimization of an azetidine chemical series as a free fatty acid receptor 2 (FFA2) antagonist: From hit to clinic. *Journal of Medicinal Chemistry*. 57 (23), 10044–10057. doi:10.1021/jm5012885.
Pocai, A. (2012) Unraveling oxyntomodulin, GLP1's enigmatic brother. *Journal of Endocrinology*. 215 (3), 335–346. doi:10.1530/JOE-12-0368.
Pon`kina, D., Kuranov, S., Khvostov, M., Zhukova, N., Meshkova, Y., Marenina, M., Luzina, O., Tolstikova, T. & Salakhutdinov, N. (2023) Hepatoprotective Effect of a New FFAR1 Agonist—N-Alkylated Isobornylamine. *Molecules*. 28 (1). doi:10.3390/molecules28010396.

Popoola-Akinola, O.O., Raji, T.J. & Olawoye, B. (2022) Lignocellulose, dietary fibre, inulin and their potential application in food. *Heliyon*. 8 (8), e10459. doi:10.1016/j.heliyon.2022.e10459.
Le Poul, E., Loison, C., Struyf, S., Springael, J.Y., Lannoy, V., Decobecq, M.E., Brezillon, S., Dupriez, V., Vassart, G., Van Damme, J., Parmentier, M. & Detheux, M. (2003) Functional characterization of human receptors for short chain fatty acids and their role in polymorphonuclear cell activation. *Journal of Biological Chemistry*. 278 (28), 25481–25489. doi:10.1074/jbc.M301403200.
Prabhu, Y. & Eichinger, L. (2006) The Dictyostelium repertoire of seven transmembrane domain receptors. *European Journal of Cell Biology*. 85 (9–10), 937–946. doi:10.1016/j.ejcb.2006.04.003.
Del Prato, S. & Tiengo, A. (2001) The importance of first-phase insulin secretion: implications for the therapy of type 2 diabetes mellitus. *Diabetes/Metabolism Research and Reviews*. 17 (3), 164–174. doi:10.1002/dmrr.198.
Priyadarshini, M. & Layden, B.T. (2015) FFAR3 modulates insulin secretion and global gene expression in mouse islets. *Islets*. 7 (2), e1045182. doi:10.1080/19382014.2015.1045182.
Psichas, A., Larraufie, P.F., Goldspink, D.A., Gribble, F.M. & Reimann, F. (2017) Chylomicrons stimulate incretin secretion in mouse and human cells. *Diabetologia*. 60 (12), 2475–2485. doi:10.1007/s00125-017-4420-2.
Psichas, A., Sleeth, M.L., Murphy, K.G., Brooks, L., Bewick, G.A., Hanyaloglu, A.C., Ghatei, M.A., Bloom, S.R. & Frost, G. (2015) The short chain fatty acid propionate stimulates GLP-1 and PYY secretion via free fatty acid receptor 2 in rodents. *International Journal of Obesity*. 39 (3), 424–429. doi:10.1038/ijo.2014.153.
Puhl, H.L., Won, Y.J., Lu, V.B. & Ikeda, S.R. (2015) Human GPR42 is a transcribed multisite variant that exhibits copy number polymorphism and is functional when heterologously expressed. *Scientific Reports*. 5. doi:10.1038/srep12880.
Purgert, C.A., Izumi, Y., Jong, Y.-J.I., Kumar, V., Zorumski, C.F. & O'Malley, K.L. (2014) Intracellular mGluR5 Can Mediate Synaptic Plasticity in the Hippocampus. *The Journal of Neuroscience*. 34 (13), 4589–4598. doi:10.1523/JNEUROSCI.3451-13.2014.
Puthenveedu, M.A., Lauffer, B., Temkin, P., Vistein, R., Carlton, P., Thorn, K., Taunton, J., Weiner, O.D., Parton, R.G. & von Zastrow, M. (2010) Sequence-Dependent Sorting of Recycling Proteins by Actin-Stabilized Endosomal Microdomains. *Cell*. 143 (5), 761–773. doi:10.1016/j.cell.2010.10.003.
Qi, K.K., Wu, J., Deng, B., Li, Y.M. & Xu, Z.W. (2015) PEGylated porcine glucagon-like peptide-2 improved the intestinal digestive function and prevented inflammation of weaning piglets challenged with LPS. *Animal*. 9 (9), 1481–1489. doi:10.1017/S1751731115000749.
Qin, J., Li, R., Raes, J., Arumugam, M., Burgdorf, K.S., et al. (2010) A human gut microbial gene catalogue established by metagenomic sequencing. *Nature*. 464 (7285), 59–65. doi:10.1038/nature08821.
Rada-Iglesias, A., Enroth, S., Ameur, A., Koch, C.M., Clelland, G.K., Respuela-Alonso, P., Wilcox, S., Dovey, O.M., Ellis, P.D., Langford, C.F., Dunham, I., Komorowski, J. & Wadelius, C. (2007) Butyrate mediates decrease of

histone acetylation centered on transcription start sites and down-regulation of associated genes. *Genome Research*. 17 (6), 708–719. doi:10.1101/gr.5540007.
Rajagopal, S. & Shenoy, S.K. (2018) GPCR desensitization: Acute and prolonged phases. *Cellular Signalling*. 41, 9–16. doi:10.1016/j.cellsig.2017.01.024.
Raybould, H.E. (2007) Mechanisms of CCK signaling from gut to brain. *Current Opinion in Pharmacology*. 7 (6), 570–574. doi:10.1016/j.coph.2007.09.006.
Reichardt, N., Duncan, S.H., Young, P., Belenguer, A., McWilliam Leitch, C., Scott, K.P., Flint, H.J. & Louis, P. (2014) Phylogenetic distribution of three pathways for propionate production within the human gut microbiota. *ISME Journal*. 8 (6), 1323–1335. doi:10.1038/ismej.2014.14.
Reimer, R.A. (2006) Meat hydrolysate and essential amino acid-induced glucagon-like peptide-1 secretion, in the human NCI-H716 enteroendocrine cell line, is regulated by extracellular signal-regulated kinase1/2 and p38 mitogen-activated protein kinases. *Journal of Endocrinology*. 191 (1), 159–170. doi:10.1677/joe.1.06557.
Reimer, R.A., Darimont, C., Gremlich, S., Rie, V., Tral, N.-M., Ru¨egg, U.T., Ru¨egg, R. & Macé, K. (2001) *A Human Cellular Model for Studying the Regulation of Glucagon-Like Peptide-1 Secretion*. https://academic.oup.com/endo/article/142/10/4522/2989125.
Ren, J. & Guo, W. (2012) ERK1/2 Regulate Exocytosis through Direct Phosphorylation of the Exocyst Component Exo70. *Developmental Cell*. 22 (5), 967–978. doi:10.1016/j.devcel.2012.03.005.
Reymann, J. (2018) *Lightning - image information extraction by adaptive deconvolution*. 2018. Leica Microsystems.
Rhee, N.A., Wahlgren, C.D., Pedersen, J., Mortensen, B., Langholz, E., Wandall, E.P., Friis, S.U., Vilmann, P., Paulsen, S.J., Kristiansen, V.B., Jelsing, J., Dalbøge, L.S., Poulsen, S.S., Holst, J.J., Vilsbøll, T. & Knop, F.K. (2015) Effect of Roux-en-Y gastric bypass on the distribution and hormone expression of small-intestinal enteroendocrine cells in obese patients with type 2 diabetes. *Diabetologia*. 58 (10), 2254–2258. doi:10.1007/s00125-015-3696-3.
Richards, P., Pais, R., Habib, A.M., Brighton, C.A., Yeo, G.S.H., Reimann, F. & Gribble, F.M. (2016) High fat diet impairs the function of glucagon-like peptide-1 producing L-cells. *Peptides*. 77, 21–27. doi:10.1016/j.peptides.2015.06.006.
Rindi, G., Ratineau, C., Ronco, A., Candusso, M.E., Tsai, M.-J. & Leiter, A.B. (1999) Targeted ablation of secretin-producing cells in transgenic mice reveals a common differentiation pathway with multiple enteroendocrine cell lineages in the small intestine. *Development*. 126 (18), 4149–4156. doi:10.1242/dev.126.18.4149.
Rives, M.-L., Rady, B., Swanson, N., Zhao, S., Qi, J., Arnoult, E., Bakaj, I., Mancini, A., Breton, B., Lee, S.P., Player, M.R. & Pocai, A. (2018) GPR40-Mediated G *α* 12 Activation by Allosteric Full Agonists Highly Efficacious at Potentiating Glucose-Stimulated Insulin Secretion in Human Islets. *Molecular Pharmacology*. 93 (6), 581–591. doi:10.1124/mol.117.111369.

Roberge, J.N. & Brubaker, P.L. (1993) Regulation of intestinal proglucagon-derived peptide secretion by glucose-dependent insulinotropic peptide in a novel enteroendocrine loop. *Endocrinology*. 133 (1), 233–240. doi:10.1210/endo.133.1.8319572.

Rocca, A.S. & Brubaker, P.L. (1999) Role of the Vagus Nerve in Mediating Proximal Nutrient-Induced Glucagon-Like Peptide-1 Secretion*. *Endocrinology*. 140 (4), 1687–1694. doi:10.1210/endo.140.4.6643.

Roediger, W.E. (1980) Role of anaerobic bacteria in the metabolic welfare of the colonic mucosa in man. *Gut*. 21 (9), 793–798. doi:10.1136/gut.21.9.793.

Roediger, W.E.W. (1982) Utilization of Nutrients by Isolated Epithelial Cells of the Rat Colon. *Gastroenterology*. 83 (2), 424–429. doi:10.1016/S0016-5085(82)80339-9.

Romero, G., von Zastrow, M. & Friedman, P.A. (2011) *Role of PDZ Proteins in Regulating Trafficking, Signaling, and Function of GPCRs: Means, Motif, and Opportunity*. In: pp. 279–314. doi:10.1016/B978-0-12-385952-5.00003-8.

Ruff, K.M. & Pappu, R. V. (2021) AlphaFold and Implications for Intrinsically Disordered Proteins. *Journal of Molecular Biology*. 433 (20), 167208. doi:10.1016/j.jmb.2021.167208.

Sakar, Y., Duca, F.A., Langelier, B., Devime, F., Blottiere, H., Delorme, C., Renault, P. & Covasa, M. (2014) Impact of high-fat feeding on basic helix–loop–helix transcription factors controlling enteroendocrine cell differentiation. *International Journal of Obesity*. 38 (11), 1440–1448. doi:10.1038/ijo.2014.20.

Sakata, T. (1987) Stimulatory effect of short-chain fatty acids on epithelial cell proliferation in the rat intestine: a possible explanation for trophic effects of fermentable fibre, gut microbes and luminal trophic factors. *British Journal of Nutrition*. 58 (1), 95–103. doi:10.1079/BJN19870073.

Sakata, T. & Engelhardt, W. Von (1983) Stimulatory effect of short chain fatty acids on the epithelial cell proliferation in rat large intestine. *Comparative Biochemistry and Physiology Part A: Physiology*. 74 (2), 459–462. doi:10.1016/0300-9629(83)90631-X.

Samuel, B.S., Shaito, A., Motoike, T., Rey, F.E., Backhed, F., Manchester, J.K., Hammer, R.E., Williams, S.C., Crowley, J., Yanagisawa, M. & Gordon, J.I. (2008) Effects of the gut microbiota on host adiposity are modulated by the short-chain fatty-acid binding G protein-coupled receptor, Gpr41. *Proceedings of the National Academy of Sciences*. 105 (43), 16767–16772. doi:10.1073/pnas.0808567105.

Sancho, R., Cremona, C.A. & Behrens, A. (2015) Stem cell and progenitor fate in the mammalian intestine: Notch and lateral inhibition in homeostasis and disease. *EMBO reports*. 16 (5), 571–581. doi:10.15252/embr.201540188.

de Santa Barbara, P., van den Brink, G.R. & Roberts, D.J. (2003) Development and differentiation of the intestinal epithelium. *Cellular and Molecular Life Sciences (CMLS)*. 60 (7), 1322–1332. doi:10.1007/s00018-003-2289-3.

Sasaki, N., Sachs, N., Wiebrands, K., Ellenbroek, S.I.J., Fumagalli, A., Lyubimova, A., Begthel, H., van den Born, M., van Es, J.H., Karthaus, W.R., Li, V.S.W., López-Iglesias, C., Peters, P.J., van Rheenen, J., van Oudenaarden, A. & Clevers, H. (2016) Reg4+ deep crypt secretory cells function as epithelial niche for Lgr5 $^{+}$ stem cells in colon. *Proceedings of*

the National Academy of Sciences. 113 (37). doi:10.1073/pnas.1607327113.
Sassone-Corsi, P. (2012) The Cyclic AMP Pathway. *Cold Spring Harbor Perspectives in Biology*. 4 (12), a011148–a011148. doi:10.1101/cshperspect.a011148.
Sato, T., Vries, R.G., Snippert, H.J., Van De Wetering, M., Barker, N., Stange, D.E., Van Es, J.H., Abo, A., Kujala, P., Peters, P.J. & Clevers, H. (2009) Single Lgr5 stem cells build crypt-villus structures in vitro without a mesenchymal niche. *Nature*. 459 (7244), 262–265. doi:10.1038/nature07935.
Sawzdargo, M., George, S.R., Nguyen, T., Xu, S., Kolakowski, L.F. & O'dowd, B.F. (1997) A Cluster of Four Novel Human G Protein-Coupled Receptor Genes Occurring in Close Proximity to CD22 Gene on Chromosome 19q13.1. *Biochemical and Biophysical Research Communications*. 239 (2), 543–547. doi:10.1006/bbrc.1997.7513.
Schaum, N., Karkanias, J., Neff, N.F., May, A.P., Quake, S.R., et al. (2018) Single-cell transcriptomics of 20 mouse organs creates a Tabula Muris. *Nature*. 562 (7727), 367–372. doi:10.1038/s41586-018-0590-4.
Scherer, T., Sakamoto, K. & Buettner, C. (2021) Brain insulin signalling in metabolic homeostasis and disease. *Nature Reviews Endocrinology*. 17 (8), 468–483. doi:10.1038/s41574-021-00498-x.
Schifferer, M., Yushchenko, D.A., Stein, F., Bolbat, A. & Schultz, C. (2017) A Ratiometric Sensor for Imaging Insulin Secretion in Single β Cells. *Cell Chemical Biology*. 24 (4), 525-531.e4. doi:10.1016/j.chembiol.2017.03.001.
Schmidt, P.T., Näslund, E., Grybäck, P., Jacobsson, H., Hartmann, B., Holst, J.J. & Hellström, P.M. (2003) Peripheral administration of GLP-2 to humans has no effect on gastric emptying or satiety. *Regulatory Peptides*. 116 (1–3), 21–25. doi:10.1016/S0167-0115(03)00175-7.
Schofield, Z. V., Croker, D., Robertson, A.A.B., Massey, N.L., Donovan, C., Tee, E., Edwards, D., Woodruff, T.M., Halai, R., Hansbro, P.M. & Cooper, M.A. (2018) Characterisation of small molecule ligands 4CMTB and 2CTAP as modulators of human FFA2 receptor signalling. *Scientific Reports*. 8 (1), 17819. doi:10.1038/s41598-018-36242-1.
Schönfeld, P. & Wojtczak, L. (2016) Short- and medium-chain fatty acids in energy metabolism: the cellular perspective. *Journal of Lipid Research*. 57 (6), 943–954. doi:10.1194/jlr.R067629.
Schonhoff, S.E., Giel-Moloney, M. & Leiter, A.B. (2004) Minireview: Development and differentiation of gut endocrine cells. *Endocrinology*.145 (6) pp.2639–2644. doi:10.1210/en.2004-0051.
Schrödinger, L., & DeLano, W. (2020) *Pymol*.
Schulingkamp, R.J., Pagano, T.C., Hung, D. & Raffa, R.B. (2000) Insulin receptors and insulin action in the brain: review and clinical implications. *Neuroscience and biobehavioral reviews*. 24 (8), 855–872. doi:10.1016/s0149-7634(00)00040-3.
Schwingshackl, L., Schwedhelm, C., Hoffmann, G., Knüppel, S., Laure Preterre, A., Iqbal, K., Bechthold, A., De Henauw, S., Michels, N., Devleesschauwer, B., Boeing, H. & Schlesinger, S. (2018) Food groups and risk of colorectal cancer. *International Journal of Cancer*. 142 (9), 1748–1758. doi:10.1002/ijc.31198.

Sealy, L. & Chalkley, R. (1978) The effect of sodium butyrate on histone modification. *Cell*. 14 (1), 115–121. doi:10.1016/0092-8674(78)90306-9.
Sedki, D., Cho, A., Cao, Y., Nikolajev, L., Atmuri, N.D.P., Lubell, W.D. & Laporte, S.A. (2022) Prostaglandin F2α and angiotensin II type 1 receptors exhibit differential cognate G protein coupling regulation. *Journal of Biological Chemistry*. 298 (9), 102294. doi:10.1016/j.jbc.2022.102294.
Seljeset, S. & Siehler, S. (2012) Receptor-specific regulation of ERK1/2 activation by members of the “free fatty acid receptor” family. *Journal of Receptors and Signal Transduction*. 32 (4), 196–201. doi:10.3109/10799893.2012.692118.
Sergeev, E., Hansen, A.H., Bolognini, D., Kawakami, K., Kishi, T., Aoki, J., Ulven, T., Inoue, A., Hudson, B.D. & Milligan, G. (2017) A single extracellular amino acid in Free Fatty Acid Receptor 2 defines antagonist species selectivity and G protein selection bias. *Scientific Reports*. 7 (1), 13741. doi:10.1038/s41598-017-14096-3.
Sergeev, E., Hansen, A.H., Pandey, S.K., MacKenzie, A.E., Hudson, B.D., Ulven, T. & Milligan, G. (2016) Non-equivalence of Key Positively Charged Residues of the Free Fatty Acid 2 Receptor in the Recognition and Function of Agonist Versus Antagonist Ligands. *Journal of Biological Chemistry*. 291 (1), 303–317. doi:10.1074/jbc.M115.687939.
Shackley, M., Ma, Y., Tate, E.W., Brown, A.J.H., Frost, G. & Hanyaloglu, A.C. (2020) Short Chain Fatty Acids Enhance Expression and Activity of the Umami Taste Receptor in Enteroendocrine Cells via a Gαi/o Pathway. *Frontiers in Nutrition*. 7. doi:10.3389/fnut.2020.568991.
Shankar, S.S., Shankar, R.R., Mixson, L.A., Miller, D.L., Pramanik, B., O’Dowd, A.K., Williams, D.M., Frederick, C.B., Beals, C.R., Stoch, S.A., Steinberg, H.O. & Kelley, D.E. (2018) Native Oxyntomodulin Has Significant Glucoregulatory Effects Independent of Weight Loss in Obese Humans With and Without Type 2 Diabetes. *Diabetes*. 67 (6), 1105–1112. doi:10.2337/db17-1331.
Shi, G., Sun, C., Gu, W., Yang, M., Zhang, X., Zhai, N., Lu, Y., Zhang, Z., Shou, P., Zhang, Z. & Ning, G. (2014) Free fatty acid receptor 2, a candidate target for type 1 diabetes, induces cell apoptosis through ERK signaling. *Journal of Molecular Endocrinology*. 53 (3), 367–380. doi:10.1530/JME-14-0065.
Shimizu, H., Masujima, Y., Ushiroda, C., Mizushima, R., Taira, S., Ohue-Kitano, R. & Kimura, I. (2019) Dietary short-chain fatty acid intake improves the hepatic metabolic condition via FFAR3. *Scientific Reports*. 9 (1), 16574. doi:10.1038/s41598-019-53242-x.
Shroyer, N.F., Helmrath, M.A., Wang, V.Y. –C., Antalffy, B., Henning, S.J. & Zoghbi, H.Y. (2007) Intestine-Specific Ablation of Mouse atonal homolog 1 (Math1) Reveals a Role in Cellular Homeostasis. *Gastroenterology*. 132 (7), 2478–2488. doi:10.1053/j.gastro.2007.03.047.
Siavoshian, S., Blottiere, H.M., Cherbut, C. & Galmiche, J.-P. (1997) Butyrate Stimulates Cyclin D and p21 and Inhibits Cyclin-Dependent Kinase 2 Expression in HT-29 Colonic Epithelial Cells. *Biochemical and Biophysical Research Communications*. 232 (1), 169–172. doi:10.1006/bbrc.1997.6255.

Sibley, D.R., Peters, J.R., Nambi, P., Caron, M.G. & Lefkowitz, R.J. (1984) Desensitization of turkey erythrocyte adenylate cyclase. Beta-adrenergic receptor phosphorylation is correlated with attenuation of adenylate cyclase activity. *The Journal of biological chemistry*. 259 (15), 9742–9749.

Sibley, D.R., Strasser, R.H., Caron, M.G. & Lefkowitz, R.J. (1985) Homologous desensitization of adenylate cyclase is associated with phosphorylation of the beta-adrenergic receptor. *The Journal of biological chemistry*. 260 (7), 3883–3886.

Siehler, S. (2007) $G_{12/13}$ -dependent signaling of G-protein-coupled receptors: disease context and impact on drug discovery. *Expert Opinion on Drug Discovery*. 2 (12), 1591–1604. doi:10.1517/17460441.2.12.1591.

Siehler, S. (2009) Regulation of RhoGEF proteins by $G_{12/13}$ -coupled receptors. *British Journal of Pharmacology*. 158 (1), 41–49. doi:10.1111/j.1476-5381.2009.00121.x.

Sierra-Fonseca, J.A., Bracamontes, C., Saldecke, J., Das, S. & Roychowdhury, S. (2018) Activation of β- and α2-adrenergic receptors stimulate tubulin polymerization and promote the association of Gβγ with microtubules in cultured NIH3T3 cells. *Biochemical and Biophysical Research Communications*. 503 (1), 102–108. doi:10.1016/j.bbrc.2018.05.188.

De Silva, A., Salem, V., Matthews, P.M. & Dhillo, W.S. (2012) The use of functional MRI to study appetite control in the CNS. *Experimental Diabetes Research*.2012. doi:10.1155/2012/764017.

Sim, Y.B., Park, S.H., Kim, S.S., Lim, S.M., Jung, J.S., Lee, J.K. & Suh, H.W. (2014) Pertussis toxin administered spinally induces a hypoglycemic effect on normal and diabetic mice. *Pharmacology*. 94, 29–40. doi:10.1159/000363578.

Sina, C., Gavrilova, O., Förster, M., Till, A., Derer, S., et al. (2009) G Protein-Coupled Receptor 43 Is Essential for Neutrophil Recruitment during Intestinal Inflammation. *The Journal of Immunology*. 183 (11), 7514–7522. doi:10.4049/jimmunol.0900063.

Sivaprakasam, S., Gurav, A., Paschall, A. V, Coe, G.L., Chaudhary, K., et al. (2016) An essential role of Ffar2 (Gpr43) in dietary fibre-mediated promotion of healthy composition of gut microbiota and suppression of intestinal carcinogenesis. *Oncogenesis*. 5 (6), e238–e238. doi:10.1038/oncsis.2016.38.

Sloth, B., Holst, J.J., Flint, A., Gregersen, N.T. & Astrup, A. (2007) Effects of $PYY_{1–36}$ and $PYY_{3–36}$ on appetite, energy intake, energy expenditure, glucose and fat metabolism in obese and lean subjects. *American Journal of Physiology-Endocrinology and Metabolism*. 292 (4), E1062–E1068. doi:10.1152/ajpendo.00450.2006.

Smillie, C.S., Biton, M., Ordovas-Montanes, J., Sullivan, K.M., Burgin, G., et al. (2019) Intra- and Inter-cellular Rewiring of the Human Colon during Ulcerative Colitis. *Cell*. 178 (3), 714-730.e22. doi:10.1016/j.cell.2019.06.029.

Smith, E.A. & Macfarlane, G.T. (1997) *Dissimilatory Amino Acid Metabolism in Human Colonic Bacteria*.

Smith, J.S., Lefkowitz, R.J. & Rajagopal, S. (2018) Biased signalling: from simple switches to allosteric microprocessors. *Nature Reviews Drug Discovery*. 17 (4), 243–260. doi:10.1038/nrd.2017.229.

Smith, P.M., Howitt, M.R., Panikov, N., Michaud, M., Gallini, C.A., Bohlooly-Y, M., Glickman, J.N. & Garrett, W.S. (2013) The Microbial Metabolites, Short-Chain Fatty Acids, Regulate Colonic T $_{reg}$ Cell Homeostasis. *Science*. 341 (6145), 569–573. doi:10.1126/science.1241165.

Smith, S.B., Gasa, R., Watada, H., Wang, J., Griffen, S.C. & German, M.S. (2003) Neurogenin3 and Hepatic Nuclear Factor 1 Cooperate in Activating Pancreatic Expression of Pax4. *Journal of Biological Chemistry*. 278 (40), 38254–38259. doi:10.1074/jbc.M302229200.

Soret, R., Chevalier, J., De Coppet, P., Poupeau, G., Derkinderen, P., Segain, J.P. & Neunlist, M. (2010) Short-Chain Fatty Acids Regulate the Enteric Neurons and Control Gastrointestinal Motility in Rats. *Gastroenterology*. 138 (5), 1772-1782.e4. doi:10.1053/j.gastro.2010.01.053.

Sorkin, A. & von Zastrow, M. (2002) Signal transduction and endocytosis: close encounters of many kinds. *Nature Reviews Molecular Cell Biology*. 3 (8), 600–614. doi:10.1038/nrm883.

Souli, A., Chariot, J., Voisin, T., Presset, O., Tsocas, A., Balasubramaniam, A., Laburthe, M. & Rozé, C. (1997) Several Receptors Mediate the Antisecretory Effect of Peptide YY, Neuropeptide Y, and Pancreatic Polypeptide on VIP-Induced Fluid Secretion in the Rat Jejunum In Vivo. *Peptides*. 18 (4), 551–557. doi:10.1016/S0196-9781(97)00069-7.

de Sousa e Melo, F., Kurtova, A. V., Harnoss, J.M., Kljavin, N., Hoeck, J.D., Hung, J., Anderson, J.E., Storm, E.E., Modrusan, Z., Koeppen, H., Dijkgraaf, G.J.P., Piskol, R. & de Sauvage, F.J. (2017) A distinct role for Lgr5+ stem cells in primary and metastatic colon cancer. *Nature*. 543 (7647), 676–680. doi:10.1038/nature21713.

Sposini, S. & Hanyaloglu, A.C. (2017) Spatial encryption of G protein-coupled receptor signaling in endosomes; Mechanisms and applications. *Biochemical Pharmacology*.143 pp.1–9. doi:10.1016/j.bcp.2017.04.028.

Sposini, S., Jean-Alphonse, F.G., Ayoub, M.A., Oqua, A., West, C., Lavery, S., Brosens, J.J., Reiter, E. & Hanyaloglu, A.C. (2017) Integration of GPCR Signaling and Sorting from Very Early Endosomes via Opposing APPL1 Mechanisms. *Cell Reports*. 21 (10), 2855–2867. doi:10.1016/j.celrep.2017.11.023.

Sposini, S., De Pascali, F., Richardson, R., Sayers, N.S., Perrais, D., Yu, H.N., Palmer, S., Nataraja, S., Reiter, E. & Hanyaloglu, A.C. (2020) Pharmacological Programming of Endosomal Signaling Activated by Small Molecule Ligands of the Follicle Stimulating Hormone Receptor. *Frontiers in Pharmacology*. 11. doi:10.3389/fphar.2020.593492.

Spreckley, E. & Murphy, K.G. (2015) The L-Cell in Nutritional Sensing and the Regulation of Appetite. *Frontiers in Nutrition*.2. doi:10.3389/fnut.2015.00023.

Srivastava, A., Yano, J., Hirozane, Y., Kefala, G., Gruswitz, F., Snell, G., Lane, W., Ivetac, A., Aertgeerts, K., Nguyen, J., Jennings, A. & Okada, K. (2014) High-resolution structure of the human GPR40 receptor bound to allosteric agonist TAK-875. *Nature*. 513 (7516), 124–127. doi:10.1038/nature13494.

Stanasila, L., Abuin, L., Dey, J. & Cotecchia, S. (2008) Different Internalization Properties of the α1a- and α1b-Adrenergic Receptor Subtypes: The Potential Role of Receptor Interaction with β-Arrestins and AP50. *Molecular Pharmacology*. 74 (3), 562–573. doi:10.1124/mol.107.043422.

Steinegger, M. & Söding, J. (2017) MMseqs2 enables sensitive protein sequence searching for the analysis of massive data sets. *Nature Biotechnology*. 35 (11), 1026–1028. doi:10.1038/nbt.3988.
Sternini, C., Wong, H., Pham, T., de Giorgio, R., Miller, L.J., Kuntz, S.M., Reeve, J.R., Walsh, J.H. & Raybould, H.E. (1999) Expression of cholecystokinin a receptors in neurons innervating the rat stomach and intestine. *Gastroenterology*. 117 (5), 1136–1146. doi:10.1016/S0016-5085(99)70399-9.
Steyer, J.A., Horstmann, H. & Almers, W. (1997) Transport, docking and exocytosis of single secretory granules in live chromaffin cells. *Nature*. 388 (6641), 474–478. doi:10.1038/41329.
Stijnen, P., Ramos-Molina, B., O'Rahilly, S. & Creemers, J.W.M. (2016) PCSK1 Mutations and Human Endocrinopathies: From Obesity to Gastrointestinal Disorders. *Endocrine Reviews*. 37 (4), 347–371. doi:10.1210/er.2015-1117.
Stoeber, M., Jullié, D., Lobingier, B.T., Laeremans, T., Steyaert, J., Schiller, P.W., Manglik, A. & von Zastrow, M. (2018) A Genetically Encoded Biosensor Reveals Location Bias of Opioid Drug Action. *Neuron*. 98 (5), 963-976.e5. doi:10.1016/j.neuron.2018.04.021.
Su, Z., Alhadeff, A.L. & Betley, J.N. (2017) Nutritive, Post-ingestive Signals Are the Primary Regulators of AgRP Neuron Activity. *Cell Reports*. 21 (10), 2724–2736. doi:10.1016/j.celrep.2017.11.036.
Sun, Y., Wang, P., Zheng, H. & Smith, R.G. (2004) Ghrelin stimulation of growth hormone release and appetite is mediated through the growth hormone secretagogue receptor. *Proceedings of the National Academy of Sciences*. 101 (13), 4679–4684. doi:10.1073/pnas.0305930101.
Sun, E.W., de Fontgalland, D., Rabbitt, P., Hollington, P., Sposato, L., Due, S.L., Wattchow, D.A., Rayner, C.K., Deane, A.M., Young, R.L. & Keating, D.J. (2017) Mechanisms Controlling Glucose-Induced GLP-1 Secretion in Human Small Intestine. *Diabetes.* 66(8):2144-2149. doi: 10.2337/db17-0058. Epub 2017 Apr 6. PMID: 28385801; PMCID: PMC5860185.
Suzuki, K., Fukui, H., Kayahara, T., Sawada, M., Seno, H., Hiai, H., Kageyama, R., Okano, H. & Chiba, T. (2005) Hes1-deficient mice show precocious differentiation of Paneth cells in the small intestine. *Biochemical and Biophysical Research Communications*. 328 (1), 348–352. doi:10.1016/j.bbrc.2004.12.174.
Suzuki, K., Iwasaki, K., Murata, Y., Harada, N., Yamane, S., Hamasaki, A., Shibue, K., Joo, E., Sankoda, A., Fujiwara, Y., Hayashi, Y. & Inagaki, N. (2018) Distribution and hormonal characterization of primary murine L cells throughout the gastrointestinal tract. *Journal of Diabetes Investigation*. 9 (1), 25–32. doi:10.1111/jdi.12681.
Sveiven, S.N., Anesko, K., Morgan, J., Nair, M.G. & Nordgren, T.M. (2023) Lipid-Sensing Receptor FFAR4 Modulates Pulmonary Epithelial Homeostasis following Immunogenic Exposures Independently of the FFAR4 Ligand Docosahexaenoic Acid (DHA). *International Journal of Molecular Sciences*. 24 (8), 7072. doi:10.3390/ijms24087072.
Syrovatkina, V., Alegre, K.O., Dey, R. & Huang, X.-Y. (2016) Regulation, Signaling, and Physiological Functions of G-Proteins. *Journal of Molecular Biology*. 428 (19), 3850–3868. doi:10.1016/j.jmb.2016.08.002.

Szwabowski, G.L., Baker, D.L. & Parrill, A.L. (2023) Application of computational methods for class A GPCR Ligand discovery. *Journal of Molecular Graphics and Modelling*. 121, 108434. doi:10.1016/j.jmgm.2023.108434.
Tabula Muris Consortium (2018) Single-cell transcriptomics of 20 mouse organs creates a Tabula Muris. *Nature*. 562 (7727), 367–372. doi:10.1038/s41586-018-0590-4.
Tailor, D., Hahm, E.-R., Kale, R.K., Singh, S. V. & Singh, R.P. (2014) Sodium butyrate induces DRP1-mediated mitochondrial fusion and apoptosis in human colorectal cancer cells. *Mitochondrion*. 16, 55–64. doi:10.1016/j.mito.2013.10.004.
Tan, T., Minnion, J., Eu Khoo, B.C., Ball, L.-J., Malviya, R., Day, E., Fiorentino, F., Brindley, C., Bush, J. & Bloom, S.R. (2021) Weight Loss With a Novel Peptide YY Analogue for Obesity: A Randomised, Placebo-Controlled Phase I Trial. *Journal of the Endocrine Society*. 5 (Supplement_1), A32–A32. doi:10.1210/jendso/bvab048.061.
Tang, C., Ahmed, K., Gille, A., Lu, S., Gröne, H.-J., Tunaru, S. & Offermanns, S. (2015) Loss of FFA2 and FFA3 increases insulin secretion and improves glucose tolerance in type 2 diabetes. *Nature Medicine*. 21 (2), 173–177. doi:10.1038/nm.3779.
Tang, J., Li, Q., Li, J., Wu, J. & Zeng, R. (2017) Systematic Synergy of Glucose and GLP-1 to Stimulate Insulin Secretion Revealed by Quantitative Phosphoproteomics. *Scientific Reports*. 7 (1), 1018. doi:10.1038/s41598-017-00841-1.
Tanowitz, M. & von Zastrow, M. (2003) A Novel Endocytic Recycling Signal That Distinguishes the Membrane Trafficking of Naturally Occurring Opioid Receptors. *Journal of Biological Chemistry*. 278 (46), 45978–45986. doi:10.1074/jbc.M304504200.
Tappenden, K.A., Drozdowski, L.A., Thomson, A.B. & McBurney, M.I. (1998) Short-chain fatty acid–supplemented total parenteral nutrition alters intestinal structure, glucose transporter 2 (GLUT2) mRNA and protein, and proglucagon mRNA abundance in normal rats. *The American Journal of Clinical Nutrition*. 68 (1), 118–125. doi:10.1093/ajcn/68.1.118.
Tatemoto, K. (1982) Isolation and characterization of peptide YY (PYY), a candidate gut hormone that inhibits pancreatic exocrine secretion. *Proceedings of the National Academy of Sciences*. 79 (8), 2514–2518. doi:10.1073/pnas.79.8.2514.
Tatemoto, K., Nakano, I., Makk, G., Angwin, P., Mann, M., Schilling, J. & Go, V.L.W. (1988) Isolation and primary structure of human peptide YY. *Biochemical and Biophysical Research Communications*. 157 (2), 713–717. doi:10.1016/S0006-291X(88)80308-5.
Terry, N.A., Walp, E.R., Lee, R.A., Kaestner, K.H. & May, C.L. (2014) Impaired enteroendocrine development in intestinal-specific *Islet1* mouse mutants causes impaired glucose homeostasis. *American Journal of Physiology-Gastrointestinal and Liver Physiology*. 307 (10), G979–G991. doi:10.1152/ajpgi.00390.2013.
Thangaraju, M., Cresci, G.A., Liu, K., Ananth, S., Gnanaprakasam, J.P., Browning, D.D., Mellinger, J.D., Smith, S.B., Digby, G.J., Lambert, N.A., Prasad, P.D. & Ganapathy, V. (2009) GPR109A Is a G-protein–Coupled Receptor for the Bacterial Fermentation Product Butyrate and Functions

as a Tumor Suppressor in Colon. *Cancer Research*. 69 (7), 2826–2832. doi:10.1158/0008-5472.CAN-08-4466.
The Tabula Sapiens Consortium*, Jones, R.C., Karkanias, J., Krasnow, M.A., Pisco, A.O., et al. (2022) The Tabula Sapiens: A multiple-organ, single-cell transcriptomic atlas of humans. *Science*. 376 (6594). doi:10.1126/science.abl4896.
Thomsen, A.R.B., Jensen, D.D., Hicks, G.A. & Bunnett, N.W. (2018) Therapeutic Targeting of Endosomal G-Protein-Coupled Receptors. *Trends in Pharmacological Sciences*.39 (10) pp.879–891. doi:10.1016/j.tips.2018.08.003.
Thomsen, A.R.B., Plouffe, B., Cahill, T.J., Shukla, A.K., Tarrasch, J.T., Concentrationy, A.M., Kahsai, A.W., Strachan, R.T., Pani, B., Mahoney, J.P., Huang, L., Breton, B., Heydenreich, F.M., Sunahara, R.K., Skiniotis, G., Bouvier, M. & Lefkowitz, R.J. (2016) GPCR-G Protein-β-Arrestin Super-Complex Mediates Sustained G Protein Signaling. *Cell*. 166 (4), 907–919. doi:10.1016/j.cell.2016.07.004.
Tian, F., Wang, X., Ni, H., Feng, X., Yuan, X. & Huang, Q. (2021) The ginsenoside metabolite compound K stimulates glucagon-like peptide-1 secretion in NCI–H716 cells by regulating the RhoA/ROCKs/YAP signaling pathway and cytoskeleton formation. *Journal of Pharmacological Sciences*. 145 (1), 88–96. doi:10.1016/j.jphs.2020.11.005.
Timper, K. & Brüning, J.C. (2017) Hypothalamic circuits regulating appetite and energy homeostasis: Pathways to obesity. *DMM Disease Models and Mechanisms*. 10 (6), 679–689. doi:10.1242/dmm.026609.
Tohgo, A., Choy, E.W., Gesty-Palmer, D., Pierce, K.L., Laporte, S., Oakley, R.H., Caron, M.G., Lefkowitz, R.J. & Luttrell, L.M. (2003) The Stability of the G Protein-coupled Receptor-β-Arrestin Interaction Determines the Mechanism and Functional Consequence of ERK Activation. *Journal of Biological Chemistry*. 278 (8), 6258–6267. doi:10.1074/jbc.M212231200.
Tolhurst, G., Heffron, H., Lam, Y.S., Parker, H.E., Habib, A.M., Diakogiannaki, E., Cameron, J., Grosse, J., Reimann, F. & Gribble, F.M. (2012) Short-chain fatty acids stimulate glucagon-like peptide-1 secretion via the G-protein-coupled receptor FFAR2. *Diabetes*. 61 (2), 364–371. doi:10.2337/db11-1019.
Tong, Q., Ye, C.-P., Jones, J.E., Elmquist, J.K. & Lowell, B.B. (2008) Synaptic release of GABA by AgRP neurons is required for normal regulation of energy balance. *Nature Neuroscience*. 11 (9), 998–1000. doi:10.1038/nn.2167.
Tough, I.R, Forbes, S. & Cox, H.M. (2018) Signaling of free fatty acid receptors 2 and 3 differs in colonic mucosa following selective agonism or coagonism by luminal propionate. *Neurogastroenterology Motility*. 30(12):e13454. doi: 10.1111/nmo.13454.
Tough, I.R., Schwartz, T.W. & Cox H.M. (2020) Synthetic G protein-coupled bile acid receptor agonists and bile acids act via basolateral receptors in ileal and colonic mucosa. *Neurogastroenterology Motility.* 32(12):e13943. doi: 10.1111/nmo.13943.
Toyota, T., Kakizaki, M., Kimura, K., Yajima, M., Okamoto, T. & Ui, M. (1978) Islet Activating Protein (IAP) Derived from the Culture Supernatant Fluid

of Bordeteila Pertussis: Effect on Spontaneous Diabetic Rats. *Diabetologia*.14.

Trabelsi, M.-S., Daoudi, M., Prawitt, J., Ducastel, S., Touche, V., et al. (2015) Farnesoid X receptor inhibits glucagon-like peptide-1 production by enteroendocrine L cells. *Nature Communications*. 6 (1), 7629. doi:10.1038/ncomms8629.

Trapp, S. & Brierley, D.I. (2022) Brain GLP-1 and the regulation of food intake: GLP-1 action in the brain and its implications for GLP-1 receptor agonists in obesity treatment. *British Journal of Pharmacology*. 179 (4), 557–570. doi:10.1111/bph.15638.

Traub, L.M. (2009) Tickets to ride: selecting cargo for clathrin-regulated internalization. *Nature Reviews Molecular Cell Biology*. 10 (9), 583–596. doi:10.1038/nrm2751.

Trzaskowski, B., Latek, D., Yuan, S., Ghoshdastider, U., Debinski, A. & Filipek, S. (2012) Action of Molecular Switches in GPCRs - Theoretical and Experimental Studies. *Current Medicinal Chemistry*. 19 (8), 1090–1109. doi:10.2174/092986712799320556.

Tsai, P.Y., Lee, M.S., Jadhav, U., Naqvi, I., Madha, S., et al. (2021) Adaptation of pancreatic cancer cells to nutrient deprivation is reversible and requires glutamine synthetase stabilization by mTORC1. *Proceedings of the National Academy of Sciences of the United States of America*. 118 (10). doi:10.1073/pnas.2003014118.

Tsuchiya, Y., Hayashi, M., Nagamatsu, K., Ono, T., Kamakura, M., Iwata, T. & Nakashima, T. (2020) The key royal jelly component 10-hydroxy-2-decenoic acid protects against bone loss by inhibiting NF-κB signaling downstream of FFAR4. *Journal of Biological Chemistry*. 295 (34), 12224–12232. doi:10.1074/jbc.RA120.013821.

Tsuzuki, A., Fujioka, Y., Yoshida, A., Kashiwagi, S., Amano, M., Hira, T., Nakamura, A., Miyoshi, H., Atsumi, T. & Ohba, Y. (2022) Direct visualization of glucagon-like peptide-1 secretion by fluorescent fusion proteins. *Journal of Diabetes Investigation*. 13 (7), 1134–1139. doi:10.1111/jdi.13800.

Tsvetanova, N.G., Trester-Zedlitz, M., Newton, B.W., Peng, G.E., Johnson, J.R., Jimenez-Morales, D., Kurland, A.P., Krogan, N.J. & von Zastrow, M. (2021) Endosomal cAMP production broadly impacts the cellular phosphoproteome. *Journal of Biological Chemistry*. 297 (1), 100907. doi:10.1016/j.jbc.2021.100907.

Tsvetanova, N.G. & von Zastrow, M. (2014) Spatial encoding of cyclic AMP signaling specificity by GPCR endocytosis. *Nature Chemical Biology*. 10 (12), 1061–1065. doi:10.1038/nchembio.1665.

Ueo, T., Imayoshi, I., Kobayashi, T., Ohtsuka, T., Seno, H., Nakase, H., Chiba, T. & Kageyama, R. (2012) The role of Hes genes in intestinal development, homeostasis and tumor formation. *Development*. 139 (6), 1071–1082. doi:10.1242/dev.069070.

Uhlén, M., Fagerberg, L., Hallström, B.M., Lindskog, C., Oksvold, P., et al. (2015) Tissue-based map of the human proteome. *Science*. 347 (6220). doi:10.1126/science.1260419.

Ursell, L.K., Metcalf, J.L., Parfrey, L.W. & Knight, R. (2012) Defining the human microbiome. *Nutrition Reviews*. 70 (SUPPL. 1). doi:10.1111/j.1753-4887.2012.00493.x.

Valdehita, A., Bajo, A.M., Fernández-Martínez, A.B., Arenas, M.I., Vacas, E., Valenzuela, P., Ruíz-Villaespesa, A., Prieto, J.C. & Carmena, M.J. (2010) Nuclear localization of vasoactive intestinal peptide (VIP) receptors in human breast cancer. *Peptides*. 31 (11), 2035–2045. doi:10.1016/j.peptides.2010.07.024.

Varadi, M., Anyango, S., Deshpande, M., Nair, S., Natassia, C., et al. (2022) AlphaFold Protein Structure Database: massively expanding the structural coverage of protein-sequence space with high-accuracy models. *Nucleic Acids Research*. 50 (D1), D439–D444. doi:10.1093/nar/gkab1061.

Veiga, P., Suez, J., Derrien, M. & Elinav, E. (2020) Moving from probiotics to precision probiotics. *Nature Microbiology*. 5 (7), 878–880. doi:10.1038/s41564-020-0721-1.

Villarreal, D., Pradhan, G., Zhou, Y., Xue, B. & Sun, Y. (2022) Diverse and Complementary Effects of Ghrelin and Obestatin. *Biomolecules*. 12 (4), 517. doi:10.3390/biom12040517.

Vilsbøll, T., Krarup, T., Sonne, J., Madsbad, S., Vølund, A., Juul, A.G. & Holst, J.J. (2003) Incretin Secretion in Relation to Meal Size and Body Weight in Healthy Subjects and People with Type 1 and Type 2 Diabetes Mellitus. *The Journal of Clinical Endocrinology & Metabolism*. 88 (6), 2706–2713. doi:10.1210/jc.2002-021873.

Wachsmuth, H.R., Weninger, S.N. & Duca, F.A. (2022) Role of the gut–brain axis in energy and glucose metabolism. *Experimental and Molecular Medicine*.54 (4) pp.377–392. doi:10.1038/s12276-021-00677-w.

Wadden, T.A., Hollander, P., Klein, S., Niswender, K., Woo, V., Hale, P.M. & Aronne, L. (2013) Weight maintenance and additional weight loss with liraglutide after low-calorie-diet-induced weight loss: The SCALE Maintenance randomized study. *International Journal of Obesity*. 37 (11), 1443–1451. doi:10.1038/ijo.2013.120.

Wadden, T.A., Webb, V.L., Moran, C.H. & Bailer, B.A. (2012) Lifestyle Modification for Obesity. *Circulation*. 125 (9), 1157–1170. doi:10.1161/CIRCULATIONAHA.111.039453.

Wallenius, V., Elias, E., Elebring, E., Haisma, B., Casselbrant, A., Larraufie, P., Spak, E., Reimann, F., le Roux, C.W., Docherty, N.G., Gribble, F.M. & Fändriks, L. (2020) Suppression of enteroendocrine cell glucagon-like peptide (GLP)-1 release by fat-induced small intestinal ketogenesis: a mechanism targeted by Roux-en-Y gastric bypass surgery but not by preoperative very-low-calorie diet. *Gut*. 69 (8), 1423–1431. doi:10.1136/gutjnl-2019-319372.

Wang, J., Cortina, G., Wu, S.V., Tran, R., Cho, J.-H., Tsai, M.-J., Bailey, T.J., Jamrich, M., Ament, M.E., Treem, W.R., Hill, I.D., Vargas, J.H., Gershman, G., Farmer, D.G., Reyen, L. & Martín, M.G. (2006) Mutant Neurogenin-3 in Congenital Malabsorptive Diarrhea. *New England Journal of Medicine*. 355 (3), 270–280. doi:10.1056/NEJMoa054288.

Wang, L., Gourcerol, G., Yuan, P.-Q., Wu, S.V., Million, M., Larauche, M. & Taché, Y. (2010) Peripheral peptide YY inhibits propulsive colonic motor function through Y_2 receptor in conscious mice. *American Journal of Physiology-Gastrointestinal and Liver Physiology*. 298 (1), G45–G56. doi:10.1152/ajpgi.00349.2009.

Wang, Y., Li, M., Guo, J., Kang, S., Huang, K. & Tong, T. (2023) Olfr78, a novel short-chain fatty acid receptor, regulates glucose homeostasis and gut GLP-1 secretion in mice. *Food Frontiers*. 4 (4), 1893–1912. doi:10.1002/fft2.301.

Ward, W.W. (1981) PROPERTIES OF THE COELENTERATE GREEN-FLUORESCENT PROTEINS. In: *Bioluminescence and Chemiluminescence*. Elsevier. pp. 235–242. doi:10.1016/B978-0-12-208820-9.50035-5.

Watson, S.-J., Brown, A.J.H. & Holliday, N.D. (2012) Differential Signaling by Splice Variants of the Human Free Fatty Acid Receptor GPR120. *Molecular Pharmacology*. 81 (5), 631–642. doi:10.1124/mol.111.077388.

Wehbi, V.L., Stevenson, H.P., Feinstein, T.N., Calero, G., Romero, G. & Vilardaga, J.-P. (2013) Noncanonical GPCR signaling arising from a PTH receptor–arrestin–Gβγ complex. *Proceedings of the National Academy of Sciences*. 110 (4), 1530–1535. doi:10.1073/pnas.1205756110.

Wen, J., Phillips, S.F., Sarr, M.G., Kost, L.J. & Holst, J.J. (1995) PYY and GLP-1 contribute to feedback inhibition from the canine ileum and colon. *American Journal of Physiology-Gastrointestinal and Liver Physiology*. 269 (6), G945–G952. doi:10.1152/ajpgi.1995.269.6.G945.

Wen, X., Zhang, B., Wu, B., Xiao, H., Li, Z., Li, R., Xu, X. & Li, T. (2022) Signaling pathways in obesity: mechanisms and therapeutic interventions. *Signal Transduction and Targeted Therapy*. 7 (1), 298. doi:10.1038/s41392-022-01149-x.

West, C. & Hanyaloglu, A.C. (2015) Minireview: Spatial programming of g protein-coupled receptor activity: Decoding signaling in health and disease. *Molecular Endocrinology*.29 (8) pp.1095–1106. doi:10.1210/ME.2015-1065.

Wettschureck, N. & Offermanns, S. (2005) Mammalian G Proteins and Their Cell Type Specific Functions. *Physiological Reviews*. 85 (4), 1159–1204. doi:10.1152/physrev.00003.2005.

Wharton, J., Gordon, L., Byrne, J., Herzog, H., Selbie, L.A., Moore, K., Sullivan, M.H., Elder, M.G., Moscoso, G. & Taylor, K.M. (1993) Expression of the human neuropeptide tyrosine Y1 receptor. *Proceedings of the National Academy of Sciences*. 90 (2), 687–691. doi:10.1073/pnas.90.2.687.

Wheeler, S.E., Stacey, H.M., Nahaei, Y., Hale, S.J., Hardy, A.B., Reimann, F., Gribble, F.M., Larraufie, P., Gaisano, H.Y. & Brubaker, P.L. (2017) The SNARE Protein Syntaxin-1a Plays an Essential Role in Biphasic Exocytosis of the Incretin Hormone Glucagon-Like Peptide 1. *Diabetes*. 66 (9), 2327–2338. doi:10.2337/db16-1403.

White, A.D., Peña, K.A., Clark, L.J., Maria, C.S., Liu, S., et al. (2021) Spatial bias in cAMP generation determines biological responses to PTH type 1 receptor activation. *Science Signaling*. 14 (703). doi:10.1126/scisignal.abc5944.

Williams, D.L. (2022) The diverse effects of brain glucagon-like peptide 1 receptors on ingestive behaviour. *British Journal of Pharmacology*. 179 (4), 571–583. doi:10.1111/bph.15535.

Williams, E.K.K., Chang, R.B.B., Strochlic, D.E.E., Umans, B.D.D., Lowell, B.B.B. & Liberles, S.D.D. (2016) Sensory Neurons that Detect Stretch and Nutrients in the Digestive System. *Cell*. 166 (1), 209–221. doi:10.1016/j.cell.2016.05.011.

Wingler, L.M. & Lefkowitz, R.J. (2020) Conformational Basis of G Protein-Coupled Receptor Signaling Versatility. *Trends in Cell Biology*. 30 (9), 736–747. doi:10.1016/j.tcb.2020.06.002.
Witt, O., Sand, K. & Pekrun, A. (2000) Butyrate-induced erythroid differentiation of human K562 leukemia cells involves inhibition of ERK and activation of p38 MAP kinase pathways. *Blood*. 95 (7), 2391–2396.
Witt, O., Schulze, S., Kanbach, K., Roth, C. & Pekrun, A. (2001) Tumor cell differentiation by butyrate and environmental stress. *Cancer Letters*. 171 (2), 173–182. doi:10.1016/S0304-3835(01)00628-0.
Wolfe, B.L., Marchese, A. & Trejo, J. (2007) Ubiquitination differentially regulates clathrin-dependent internalization of protease-activated receptor-1. *The Journal of Cell Biology*. 177 (5), 905–916. doi:10.1083/jcb.200610154.
Wölnerhanssen, B.K., Moran, A.W., Burdyga, G., Meyer-Gerspach, A.C., Peterli, R., Manz, M., Thumshirn, M., Daly, K., Beglinger, C. & Shirazi-Beechey, S.P. (2017) Deregulation of transcription factors controlling intestinal epithelial cell differentiation; a predisposing factor for reduced enteroendocrine cell number in morbidly obese individuals. *Scientific Reports*. 7 (1), 8174. doi:10.1038/s41598-017-08487-9.
Woods, S.C., Lotter, E.C., McKay, L.D. & Porte, D. (1979) Chronic intracerebroventricular infusion of insulin reduces food intake and body weight of baboons. *Nature*. 282 (5738), 503–505. doi:10.1038/282503a0.
Wootten, D., Christopoulos, A., Marti-Solano, M., Babu, M.M. & Sexton, P.M. (2018) Mechanisms of signalling and biased agonism in G protein-coupled receptors. *Nature Reviews Molecular Cell Biology*. 19 (10), 638–653. doi:10.1038/s41580-018-0049-3.
World Health Organisation (2000) Obesity: preventing and managing the global epidemic. Report of a WHO consultation. *World Health Organization technical report series*. 894, i–xii, 1–253.
World Obesity Federation (2023) *World Obesity Atlas*.
Wright, S.C., Lukasheva, V., Le Gouill, C., Kobayashi, H., Breton, B., Mailhot-Larouche, S., Blondel-Tepaz, É., Antunes Vieira, N., Costa-Neto, C., Héroux, M., Lambert, N.A., Tabajara Parreiras-e-Silva, L. & Bouvier, M. (n.d.) *BRET-based effector membrane translocation assay monitors GPCR-promoted and endocytosis-mediated G q activation at early endosomes*. doi:10.1073/pnas.2025846118/-/DCSupplemental.
Wright, S.C., Motso, A., Koutsilieri, S., Beusch, C.M., Sabatier, P., Berghella, A., Blondel-Tepaz, É., Mangenot, K., Pittarokoilis, I., Sismanoglou, D.-C., Le Gouill, C., Olsen, J. V., Zubarev, R.A., Lambert, N.A., Hauser, A.S., Bouvier, M. & Lauschke, V.M. (2023) GLP-1R signaling neighborhoods associate with the susceptibility to adverse drug reactions of incretin mimetics. *Nature Communications*. 14 (1), 6243. doi:10.1038/s41467-023-41893-4.
Wu, W., Sun, M., Chen, F., Cao, A.T., Liu, H., Zhao, Y., Huang, X., Xiao, Y., Yao, S., Zhao, Q., Liu, Z. & Cong, Y. (2017) Microbiota metabolite short-chain fatty acid acetate promotes intestinal IgA response to microbiota which is mediated by GPR43. *Mucosal Immunology*. 10 (4), 946–956. doi:10.1038/mi.2016.114.
Wynne, K., Park, A.J., Small, C.J., Patterson, M., Ellis, S.M., Murphy, K.G., Wren, A.M., Frost, G.S., Meeran, K., Ghatei, M.A. & Bloom, S.R. (2005)

Subcutaneous Oxyntomodulin Reduces Body Weight in Overweight and Obese Subjects. *Diabetes*. 54 (8), 2390–2395. doi:10.2337/diabetes.54.8.2390.
Xi, Y., Jing, Z., Wei, W., Chun, Z., Quan, Q., Qing, Z., Jiamin, X. & Shuwen, H. (2021) Inhibitory effect of sodium butyrate on colorectal cancer cells and construction of the related molecular network. *BMC Cancer*. 21 (1), 127. doi:10.1186/s12885-021-07845-1.
Yan, K.S., Chia, L.A., Li, X., Ootani, A., Su, J., Lee, J.Y., Su, N., Luo, Y., Heilshorn, S.C., Amieva, M.R., Sangiorgi, E., Capecchi, M.R. & Kuo, C.J. (2012) The intestinal stem cell markers Bmi1 and Lgr5 identify two functionally distinct populations. *Proceedings of the National Academy of Sciences*. 109 (2), 466–471. doi:10.1073/pnas.1118857109.
Yan, S., Conley, J.M., Reilly, A.M., Stull, N.D., Abhyankar, S.D., Ericsson, A.C., Kono, T., Molosh, A.I., Kubal, C.A., Evans-Molina, C. & Ren, H. (2022) Intestinal Gpr17 deficiency improves glucose metabolism by promoting GLP-1 secretion. *Cell Reports*. 38 (1), 110179. doi:10.1016/j.celrep.2021.110179.
Yang, D., Zhou, Q., Labroska, V., Qin, S., Darbalaei, S., Wu, Y., Yuliantie, E., Xie, L., Tao, H., Cheng, J., Liu, Q., Zhao, S., Shui, W., Jiang, Y. & Wang, M.-W. (2021) G protein-coupled receptors: structure- and function-based drug discovery. *Signal Transduction and Targeted Therapy*. 6 (1), 7. doi:10.1038/s41392-020-00435-w.
Yang, Q., Bermingham, N.A., Finegold, M.J. & Zoghbi, H.Y. (2001) Requirement of Math1 for Secretory Cell Lineage Commitment in the Mouse Intestine. *Science*. 294, 2155–2158.
Yarwood, R.E., Imlach, W.L., Lieu, T., Veldhuis, N.A., Jensen, D.D., Klein Herenbrink, C., Aurelio, L., Cai, Z., Christie, M.J., Poole, D.P., Porter, C.J.H., McLean, P., Hicks, G.A., Geppetti, P., Halls, M.L., Canals, M. & Bunnett, N.W. (2017) Endosomal signaling of the receptor for calcitonin gene-related peptide mediates pain transmission. *Proceedings of the National Academy of Sciences*. 114 (46), 12309–12314. doi:10.1073/pnas.1706656114.
Ye, D.Z. & Kaestner, K.H. (2009) Foxa1 and Foxa2 Control the Differentiation of Goblet and Enteroendocrine L- and D-Cells in Mice. *Gastroenterology*. 137 (6), 2052–2062. doi:10.1053/j.gastro.2009.08.059.
Ye, J., Coulouris, G., Zaretskaya, I., Cutcutache, I., Rozen, S. & Madden, T.L. (2012) Primer-BLAST: A tool to design target-specific primers for polymerase chain reaction. *BMC Bioinformatics*. 13 (1), 134. doi:10.1186/1471-2105-13-134.
Yim, Y.Y., McDonald, W.H., Betke, K.M., Kaya, A., Hyde, K., Erreger, K., Gilsbach, R., Hein, L. & Hamm, H.E. (2021) Specificities of Gβγ subunits for the SNARE complex before and after stimulation of α_{2a} -adrenergic receptors. *Science Signaling*. 14 (714). doi:10.1126/scisignal.abc4970.
Yoon, E.-J., Gerachshenko, T., Spiegelberg, B.D., Alford, S. & Hamm, H.E. (2007) Gβγ Interferes with Ca^{2+} -Dependent Binding of Synaptotagmin to the Soluble *N* -Ethylmaleimide-Sensitive Factor Attachment Protein Receptor (SNARE) Complex. *Molecular Pharmacology*. 72 (5), 1210–1219. doi:10.1124/mol.107.039446.
Zaibi, M.S., Stocker, C.J., O'Dowd, J., Davies, A., Bellahcene, M., Cawthorne, M.A., Brown, A.J.H., Smith, D.M. & Arch, J.R.S. (2010) Roles of GPR41

and GPR43 in leptin secretory responses of murine adipocytes to short chain fatty acids. *FEBS Letters*. 584 (11), 2381–2386. doi:10.1016/j.febslet.2010.04.027.
von Zastrow, M. & Sorkin, A. (2007) Signaling on the endocytic pathway. *Current Opinion in Cell Biology*. 19 (4), 436–445. doi:10.1016/j.ceb.2007.04.021.
Zhang, H., Feng, Z., Wu, J., Wang, Y., Guo, X., Liang, N., Zhu, Z. & Ma, J. (2007) Sodium butyrate-induced death-associated protein kinase expression promote Raji cell morphological change and apoptosis by reducing FAK protein levels. *Acta Pharmacologica Sinica*. 28 (11), 1783–1790. doi:10.1111/j.1745-7254.2007.00660.x.
Zhang, L., Bijker, M.S. & Herzog, H. (2011) The neuropeptide Y system: Pathophysiological and therapeutic implications in obesity and cancer. *Pharmacology & Therapeutics*. 131 (1), 91–113. doi:10.1016/j.pharmthera.2011.03.011.
Zhang, X., Guseinov, A.-A., Jenkins, L., Li, K., Tikhonova, I.G., Milligan, G. & Zhang, C. (2024) Structural basis for the ligand recognition and signaling of free fatty acid receptors. *Science Advances*. 10 (2). doi:10.1126/sciadv.adj2384.
Zhang, Y., Proenca, R., Maffei, M., Barone, M., Leopold, L. & Friedman, J.M. (1994) Positional cloning of the mouse obese gene and its human homologue. *Nature*. 372 (6505), 425–432. doi:10.1038/372425a0.
Zhao, H., Bai, H., Deng, F., Zhong, R., Liu, L., Chen, L. & Zhang, H. (2022) Chemically Protected Sodium Butyrate Improves Growth Performance and Early Development and Function of Small Intestine in Broilers as One Effective Substitute for Antibiotics. *Antibiotics*. 11 (2), 132. doi:10.3390/antibiotics11020132.
Zhao, J., Wang, H., Shi, P., Wang, W. & Sun, Y. (2017) GPR120, a potential therapeutic target for experimental colitis in IL-10 deficient mice. *Oncotarget*. 8 (5), 8397–8405. doi:10.18632/oncotarget.14210.
Zhao, Y., Fang, Q., Straub, S.G., Lindau, M. & Sharp, G.W.G. (2010) Noradrenaline inhibits exocytosis via the G protein βγ subunit and refilling of the readily releasable granule pool via the $\alpha_{i1/2}$ subunit. *The Journal of Physiology*. 588 (18), 3485–3498. doi:10.1113/jphysiol.2010.190090.
Zhyzhneuskaya, S. V., Al-Mrabeh, A., Peters, C., Barnes, A., Aribisala, B., Hollingsworth, K.G., McConnachie, A., Sattar, N., Lean, M.E.J. & Taylor, R. (2020) Time Course of Normalization of Functional β-Cell Capacity in the Diabetes Remission Clinical Trial After Weight Loss in Type 2 Diabetes. *Diabetes Care*. 43 (4), 813–820. doi:10.2337/dc19-0371.
Zurawski, Z., Page, B., Chicka, M.C., Brindley, R.L., Wells, C.A., Preininger, A.M., Hyde, K., Gilbert, J.A., Cruz-Rodriguez, O., Currie, K.P.M., Chapman, E.R., Alford, S. & Hamm, H.E. (2017) Gβγ directly modulates vesicle fusion by competing with synaptotagmin for binding to neuronal SNARE proteins embedded in membranes. *Journal of Biological Chemistry*. 292 (29), 12165–12177. doi:10.1074/jbc.M116.773523.
Zurawski, Z., Thompson Gray, A.D., Brady, L.J., Page, B., Church, E., Harris, N.A., Dohn, M.R., Yim, Y.Y., Hyde, K., Mortlock, D.P., Jones, C.K., Winder, D.G., Alford, S. & Hamm, H.E. (2019) Disabling the Gβγ-SNARE interaction disrupts GPCR-mediated presynaptic inhibition, leading to

physiological and behavioral phenotypes. *Science Signaling*. 12 (569). doi:10.1126/scisignal.aat8595.